PARAMETERIZATION OF N_2O_5 REACTION PROBABILITIES FOR INCLUSION IN CMAQ

Jerry M. Davis*
U.S. Environmental Protection Agency, Research Triangle Park, NC, USA

Prakash V. Bhave and Kristen M. Foley
National Oceanic and Atmospheric Administration, Research Triangle Park, NC, USA
In partnership with the National Exposure Research Laboratory, U.S. Environmental Protection Agency

1. INTRODUCTION

Heterogeneous reactions of N_2O_5 have a substantial influence on gaseous and particulate pollutant concentrations. To accurately simulate nighttime nitrogen chemistry and the resulting impacts on ozone, particulate nitrate, and nitrogen oxides, air quality models must contain a reliable parameterization of the heterogeneous reaction probability, γ, which is defined as the fraction of collisions between gaseous N_2O_5 molecules and particle surfaces that lead to the production of HNO_3.

Bhave et al. (2006) updated the parameterization of γ in the Community Multiscale Air Quality (CMAQ) model v4.6 based on an equation by Evans and Jacob (2005), referred to hereafter as EJ05. Later, we discovered a typographical error in that equation. The form of their equation should read $\gamma = \alpha \times 10^{-\beta}$ but the negative sign was accidentally omitted from the publication (Mathew Evans, personal communication). Correction of that typographical error led to a substantial degradation in wintertime model performance for particulate NO_3^-. In the process of diagnosing this problem, we found a few other shortcomings in EJ05 so we began an effort to derive a new parameterization of γ. Results of our efforts are described on this poster.

Our work has several advantages over previous studies: (1) our parameterization uses all published laboratory measurements of γ on ammoniated sulfate and nitrate particles; (2) rigorous statistical methods are employed (e.g., significance test of each independent variable, weighting of each data point by the measurement uncertainty, defining extrapolation limits) leading to a simple formula that captures the most important features in the laboratory data; (3) the effect of particulate nitrate to suppress γ is quantified using measurements that are representative of continental, rather than marine, conditions; (4) the effect of particle acidity to enhance γ is accounted for; and (5) phase changes are considered explicitly in our parameterization such that γ on aqueous particles exceeds that on solid particles.

2. LABORATORY DATA

All the data used for our examination of γ with respect to T, RH, and particle composition come from laboratory work documented in the following publications: Mozurkewich and Calvert (1988); Hu and Abbatt (1997); Folkers (2001); Kane et al. (2001); Folkers et al. (2003); Hallquist et al. (2003); Badger et al. (2006). For brevity, these documents will be referred to hereafter as MOZ88, HU97, FOL01, KAN01, FOL03, HAL03, and BAD06, respectively. To our knowledge, these seven publications contain all of the published laboratory measurements of γ on ammoniated sulfate and nitrate particles at conditions relevant to the troposphere. We focus on these particle compositions because they constitute a substantial portion of the aerosol surface area in continental air masses and because laboratory measurements of γ on these surfaces are relatively abundant.

Figure 2 on the poster summarizes all 78 of the laboratory measurements used to develop our statistical parameterization, and illustrates the dependence of γ on RH, T, particle composition, and phase state. For all four particle types studied here, the most prominent feature, with a few exceptions, is that γ increases with RH. For a fixed RH and T, γ is highest on aqueous NH_4HSO_4 (see Fig. 2a), relatively high on aqueous $(NH_4)_2SO_4$ (Fig. 2b), quite low on aqueous NH_4NO_3 (Fig. 2c), and lowest on the dry ammoniated sulfate particles (Fig. 2d). A successful statistical model must capture these features of the laboratory data.

**Corresponding author:* Jerry M. Davis, Visiting Scientist, Atmospheric Modeling Division, U.S. Environmental Protection Agency, Research Triangle Park, NC 27711; e-mail: davisj@ncsu.edu

3. METHODS

3.1 Statistical Models for Aqueous Particles

Prior to our regression analyses, the laboratory data were transformed using the logit function: $\lambda = \ln(\gamma/(1-\gamma))$. This transformation ensures that all model estimates of γ lie between zero and one, which is consistent with the relative-frequency definition of γ. One regression equation was estimated from the union of aqueous NH_4HSO_4 and $(NH_4)_2SO_4$ data for which observations are most abundant. A second regression equation based on the NH_4NO_3 data was fit separately since those measurements were reported in a separate study (FOL01) from all the ammoniated sulfate data and include only four unique combinations of T and RH values.

On aqueous NH_4HSO_4 and $(NH_4)_2SO_4$ particles, a dependence of γ on temperature is difficult to observe in the measurements. The only cross sections of data where temperature was varied over a large range are at 50% RH (see Fig. 2a and 2b). Along those cross sections, the γ values do not change monotonically with temperature. Based on HAL03, EJ05, and our own data analyses, a temperature threshold, *j*, was applied within our statistical model. The threshold temperature variable is defined as:

$$T_j = \begin{cases} T - j & T > j \\ 0 & T \le j \end{cases}$$

Our initial form of the statistical model for aqueous NH_4HSO_4 and $(NH_4)_2SO_4$ particles, denoted λ_1 and λ_2, respectively, is given by:

$$\lambda_1 = \beta_{10} + \beta_{11}RH + \beta_{12}T_j + \beta_{13}RH \times T_j + \beta_{14}RH^2 + \beta_{15}RH^3 + \varepsilon_1 \quad (1)$$

$$\lambda_2 = (\beta_{10} + \beta_{20}) + (\beta_{11} + \beta_{21})RH + (\beta_{12} + \beta_{22})T_j + (\beta_{13} + \beta_{23})RH \times T_j + (\beta_{14} + \beta_{24})RH^2 + (\beta_{15} + \beta_{25})RH^3 + \varepsilon_2 \quad (2)$$

The model errors were assumed to be normally and independently distributed. Higher order polynomial terms were considered for *RH*, but not T_j, based on our inspection of plots of λ versus RH and T. Note that during the regression analysis, Eqs. (1) and (2) were solved simultaneously using the combination of aqueous NH_4HSO_4 and $(NH_4)_2SO_4$ data. The extra coefficients – β_{20}, β_{21}, β_{22}, β_{23}, β_{24}, and β_{25} – in Eq. (2) were included to test whether the linear relationship between λ, *RH*, and T_j, differs significantly for different particle compositions.

Coefficients of the linear model were estimated using weighted least squares (Kutner et al. 2005). Each observation was assigned a weight, *w*, that is a function of the standard error values, σ, reported with each laboratory measurement of γ:

$$w = [\gamma(1-\gamma)]^2 / \sigma^2 \quad (3)$$

These weights were derived based on a Taylor approximation for the estimate of the variance of λ (Casella and Berger, 2002, pg 241).

Stepwise model selection for regression analysis was used to determine which of the variables in Eqs. (1) and (2) are statistically significant. At each stage of the model selection process, the Akaike Information Criterion (AIC) was used to decide whether linear terms, cross product terms, and higher order terms should be included or excluded. This process was repeated for each integer value of *j* between 275 K and 295 K as well as for a model with no temperature threshold (i.e. *j* = 0 K). The AIC value was used to determine the most parsimonious statistical model that best fits the data with a minimum number of covariates (Akaike, 1973). This procedure yielded a model with four statistically significant terms and a threshold temperature of *j* = 287 K. The individual equations for aqueous NH_4HSO_4 and $(NH_4)_2SO_4$ differ only in the intercept term.

$$\lambda_1 = \beta_{10} + \beta_{11}RH + \beta_{12}T_{287} \quad (4)$$

$$\lambda_2 = (\beta_{10} + \beta_{20}) + \beta_{11}RH + \beta_{12}T_{287} \quad (5)$$

The best-fit values and standard errors of each coefficient are given in Table 1 on the poster.

For aqueous NH_4NO_3 particles, all data were collected in a narrow temperature range so it was not possible to identify a temperature trend. The model for NH_4NO_3 was selected to match the form of Eq. (1), and is given by the following equation:

$$\lambda_3 = \beta_{30} + \beta_{31}RH \quad (6)$$

The estimated coefficients for this model are also given in Table 1.

Equations (4– 6) are back transformed to compute the reaction probability values for the three aqueous particle compositions.

$$\gamma_i = \frac{1}{1 + e^{-\lambda_i}} \quad i = 1, 2, 3 \quad (7)$$

In the upper panel of Fig. 3, the parameterized functions for γ are plotted on a log scale versus

RH for a selected set of temperatures. The lower panel of Fig. 3 shows contour plots of the estimated γ values spanning the ranges of T and RH encountered in the lower troposphere. Each laboratory measurement is shown as a discrete point in the lower panel. Laboratory data are not available over the entire range of tropospheric conditions, so caution must be exercised when extrapolating parameterizations derived from the available data. For example, extrapolation of the regression equations to the regime of low T and high RH yields γ values which exceed all of the lab measurements (e.g., $\gamma_1 > 0.15$). To prevent erroneous extrapolations when these functions are used in air quality models, the estimated γ values were constrained to be no greater than the maximum observed γ:

$$\gamma_1^* = \min(\gamma_1, 0.08585)$$
$$\gamma_2^* = \min(\gamma_2, 0.053) \quad (8)$$
$$\gamma_3^* = \min(\gamma_3, 0.0154)$$

These upper limits are depicted by horizontal gray lines in Fig. 3a-c, and the lightly-shaded pentagons in the lower-right portions of Fig. 3d-f.

Extrapolation of Eqs. (4–7) must also be limited by thermodynamic considerations. At RH < 32.8%, $(NH_4)_2SO_4$ crystallizes to form a solid phase (Martin et al., 2003) and γ_2 is not expected to decline smoothly with decreasing RH across this phase boundary. The regions of Fig. 2b and 2e with RH lower than the crystallization relative humidity (CRH) are shaded to illustrate this limit. In contrast, aqueous droplets containing pure NH_4HSO_4 or pure NH_4NO_3 do not crystallize (Martin et al., 2003) so our equations for γ_1 and γ_3 may be applicable at very low RH.

Under the conditions of very high RH and low T encountered occasionally in the lower troposphere, particle-bound water will freeze to form ice. The point at which this phase change occurs is determined by the ratio of the saturation vapor pressure over ice (pw_{ice}) to that over water (pw_{water}). This portion of the phase diagram is shaded in the lower panel of Fig. 3, using the Goff-Gratch equations to compute pw_{ice} and pw_{water} (Goff and Gratch, 1946). As RH increases across this phase boundary, we expect γ to differ from the upper limits imposed by Eq. (8).

3.2 Statistical Model for Dry Particles

When the ambient RH is below the deliquescence relative humidity (DRH), ammoniated sulfate and nitrate can exist as dry particles that are devoid of liquid water. For dry particles, a separate parameterization is needed for γ. The statistical methodology outlined in Section 3.1 was repeated using the 15 dry particle data points in Fig. 2d except, this time, higher order polynomial terms of *RH* were not considered due to the very limited sample size. The variable selection procedure yielded a model with three statistically significant terms and a threshold temperature of 293 K. Analogous to Eq. (2), extra coefficients were included to test whether the linear relationship between λ, *RH*, and T_j, differs for different particle compositions, but none of those coefficients were deemed significant. The model for dry particles (denoted with subscript "d" for dry) is given by

$$\lambda_d = \beta_{d0} + \beta_{d1} RH + \beta_{d2} T_{293} \quad (9)$$

The best-fit values and standard errors of each coefficient are given in Table 1. The estimated values of λ_d can be back transformed using Eq. (7). As with the aqueous parameterizations, estimated γ values were constrained to be no greater than the maximum observed γ:

$$\gamma_d^* = \min(\gamma_d, 0.0124) \quad (10)$$

Recall that no laboratory measurements of γ on dry NH_4NO_3 were found, so Eqs. (9–10) are intended primarily for dry ammoniated sulfate particles.

3.3 Model for Internally-Mixed Particles

In the CMAQ model, inorganic fine particles are often assumed to exist as an internal mixture of SO_4^{2-}, NO_3^-, NH_4^+, and H_2O. To date, laboratory measurements of γ on such mixtures have not been reported. As a provisional measure, it is useful to express γ as a molar-weighted average of the single-component parameterizations provided above. Assuming all of the NO_3^- is present as NH_4NO_3 and the leftover NH_4^+ is distributed between $(NH_4)_2SO_4$ and NH_4HSO_4, we computed mole fractions

$$x_1 = 1 - (x_2 + x_3)$$
$$x_2 = \max\left(0, \min\left(1 - x_3, \frac{A}{N+S} - 1\right)\right) \quad (11)$$
$$x_3 = \frac{N}{N+S}$$

where x_i represents the molar concentration of component *i* normalized by the summed concentrations of NH_4HSO_4, $(NH_4)_2SO_4$, and NH_4NO_3; and *A*, *N*, and *S*, represent the molar concentra-

tions of particle-phase NH_4^+, NO_3^-, and SO_4^{2-}, respectively. The limiting values of x_2 correspond to mixtures that are more acidic than NH_4HSO_4 or more alkaline than $(NH_4)_2SO_4$. Such compositions are rarely found in tropospheric fine particles, but were considered in Eq. (11) for completeness.

Using the above mole fractions as weighting factors, the reaction probability of N_2O_5 on mixed aqueous particles, $\gamma_{aq,mix}$, can be computed as

$$\gamma_{aq,mix} = \sum_{i=1}^{3} x_i \gamma_i^* \quad (12)$$

where γ_i^* is defined in Eq. (8). The corresponding expression for mixed dry particles is

$$\gamma_{d,mix} = (x_1 + x_2)\gamma_d^* + x_3 \cdot \min(\gamma_d^*, \gamma_3^*) \quad (13)$$

In the absence of laboratory measurements on dry NH_4NO_3 particles, the min function is used in Eq. (13) to reflect our expectation that γ on dry NH_4NO_3 particles is similar to γ on dry ammoniated sulfate particles, but should not exceed γ on aqueous NH_4NO_3 particles.

No laboratory measurements of γ on particles containing a mixture of ice and ammoniated sulfate or nitrate were found, but γ on pure ice has been studied extensively for stratospheric applications. A representative γ value of 0.02 was selected from those data (IUPAC, 2006). This fixed value was applied to all ice-containing particles in the present study.

$$\gamma_{ice,mix} = 0.02 \quad (14)$$

4. RESULTS

Among the 78 data points reported in seven different laboratory studies, our parameterizations (i.e., Eqs. (4 – 7, 9) reproduce 53% within a factor of 1.25 and 79% within a factor of two. For comparison, we contrasted this performance with the EJ05 parameterization. When compared against all 40 $(NH_4)_2SO_4$ data points (dry and wet), EJ05 underestimates half of them by 15% or more whereas our parameterization exhibits a smaller median relative bias (+5%). The EJ05 parameterization is not intended for NH_4HSO_4 particles and an erroneous application of EJ05 to such acidic particle surfaces would underestimate most of the NH_4HSO_4 data points by nearly a factor of 2. Similarly, EJ05 should not be applied to NH_4NO_3 particles because it was not designed to capture the nitrate effect on γ.

To illustrate the atmospheric relevance of this work, we applied our parameterizations to conditions representative of the eastern United States using 3-dimensional fields of T, RH, SO_4^{2-}, NO_3^-, and NH_4^+, obtained from a recent CMAQ model simulation with 12 km horizontal grid spacing (Appel et al., 2007). In that model application, transitions in the aerosol phase state were not simulated. To utilize all of the parameterizations developed in this study, we assume here that the modeled particles are wet above their CRH and dry below their CRH. The CRH for an internally mixed particle composed of SO_4^{2-}, NO_3^-, and NH_4^+ was calculated using the equation for complete crystallization by Martin et al. (2003). Although that equation was only validated at 293 K, we applied it at all T because there currently exists very little data to justify a temperature-dependent CRH. To compute γ over the full range of conditions encountered in the atmosphere, $\gamma_{ambient}$, we applied Eqs. (12–14) as follows:

$$\gamma_{ambient} = \begin{cases} \gamma_{d,mix} & \text{RH} < \text{CRH} \\ \gamma_{ice,mix} & \text{RH} > \text{IRH} \\ \gamma_{aq,mix} & \text{otherwise} \end{cases} \quad (15)$$

where IRH is the relative humidity of ice formation, which varies with temperature (see description in Section 3.1).

Values of $\gamma_{ambient}$ were computed for each hour of January, February, July, and August 2001, using T, RH, SO_4^{2-}, NO_3^-, and NH_4^+ in each CMAQ grid cell. For comparison, we also computed hourly spatial fields of γ on NH_4HSO_4 (i.e., γ_1^*), $(NH_4)_2SO_4$ (i.e., γ_2^* when RH ≥ 32.8% and γ_d^* otherwise), and NH_4NO_3 (i.e., γ_3^*), each with the IRH constraint imposed, as well as three other parameterizations of γ that have been applied in air quality models in the past. For illustrative purposes, the hourly γ values were averaged over two-month periods representative of the winter (January – February 2001) and summer (July – August 2001). When averaging hourly values, we included only the nighttime hours of 0400 – 0900 GMT because N_2O_5 concentrations are negligible in the daylight so values of γ at those times have no practical importance. Though vertical distributions of γ were computed, we focused our attention on the model layer that is 75 – 150 m above the surface because the CMAQ results indicate that the product of N_2O_5 and aerosol surface area is highest in this layer during both the summer and winter periods. Recall that the N_2O_5 hydrolysis rate is proportional to this product (Riemer et al., 2003).

Figure 4 on our poster shows results of the above calculations for the January – February

2001 period. Across the eastern U.S., values of $\gamma_{ambient}$ range from 0.02 over the Midwest to 0.05 over Florida (see Fig. 4d). Low values over the Midwest result from high NO_3^- concentrations, typical of this region during winter, combined with below-freezing temperatures and high RH that occasionally exceeds the IRH (see Fig. 5). The high $\gamma_{ambient}$ values over Florida result from low NO_3^- concentrations coupled with relatively warm temperatures. Comparing Fig. 4d with 4e, it can be seen that our $\gamma_{ambient}$ values fall below the fixed value of 0.1 used in the early work by Dentener and Crutzen (1993) which is now recognized as an upper estimate of γ (Evans and Jacob, 2005). Comparing Fig. 4d with 4f, we see that the γ parameterization by Riemer et al. (2003) is consistently lower than $\gamma_{ambient}$. The Riemer parameterization has an upper bound of 0.02, based on measurements of γ on Na_2SO_4 and $NaHSO_4$ particles. Our parameterization is more appropriate for continental air masses because it is derived from measurements on ammoniated particles rather than sodium-containing particles. Moreover, the Riemer parameterization does not depend on T and RH due to insufficient laboratory data available at the time of that study.

The comparison between $\gamma_{ambient}$ and EJ05 is the most intriguing (compare Fig. 4d and 4g) because EJ05 is the current parameterization of choice in many regional- and global-chemistry models such as CMAQv4.6 and GEOS-CHEM. Across the northern half of the domain, EJ05 often exceeds 0.10 whereas $\gamma_{ambient}$ is between 0.02 and 0.06. At lower latitudes, EJ05 exceeds $\gamma_{ambient}$ by 0.01 to 0.02. Recognizing that $\gamma_{ambient}$ is suppressed by the nitrate effect whereas EJ05 is not, a more equitable comparison is between EJ05 and our parameterization of γ on $(NH_4)_2SO_4$ (i.e., Fig. 4g versus 4b). Surprisingly, this comparison also revealed rather large differences. The main reason for differences in the northern latitudes is that our parameterization was bounded by the maximum laboratory value of 0.053 (see Fig. 3b and 3e) whereas EJ05 yields very large values when extrapolated to low T and high RH conditions. In addition, our values of γ in the north and along the Appalachian Mountains are suppressed by ice formation (see lower-left panel of Fig. 5) whereas the effects of that phase transition are not considered in EJ05. In fact, the very highest values of γ (~0.13) are obtained when EJ05 is extrapolated to the regime where ice formation is favored. In the southern half of the domain, EJ05 exceeds γ_2^* by 0.02 to 0.03. These locations are characterized by average nighttime conditions of 80% RH and 280 K (see Fig. 5), where EJ05 yields a value of 0.08 and our parameterization reaches its upper-limit value of 0.053.

In the summer, $\gamma_{ambient}$ ranges from 0.01 over Texas and Oklahoma to 0.07 over the Appalachian Mountains (see Fig. 6d). The lowest values correspond to the portion of our domain where the nighttime average temperature was highest (302 K), RH was lowest (60%), and the particle compositions were dominated by $(NH_4)_2SO_4$ (x_2 = 0.9). Over the Appalachian Mountains, high values of $\gamma_{ambient}$ resulted from the particle compositions being dominated by NH_4HSO_4 (x_1 = 0.8) along with T < 290 K and RH > 80% (see Fig. 7). Across the entire domain, $\gamma_{ambient}$ and EJ05 are in very good agreement (compare Fig. 6d and 6g) except along the Appalachian Mountains where x_1 = 0.8. Under those acidic conditions, $\gamma_{ambient}$ exceeds EJ05 by nearly 0.02.

5. CONCLUSIONS

We have developed a comprehensive parameterization for the heterogeneous reaction probability of N_2O_5 as a function of RH, T, particle composition, and phase state, for use in advanced air quality models. We used all published measurements of γ on ammoniated sulfate and nitrate particles, which were compiled from seven different laboratory studies. The final equations are relatively simple, non-linear functions of RH and T that were selected in an objective and statistically rigorous manner. Our parameterization reproduced 79% of the laboratory data within a factor of two and 53% within a factor of 1.25. To our knowledge, this is the first parameterization in which phase changes are considered explicitly such that γ on aqueous particles exceeds that on solid particles. It is also the first parameterization to capture the ~50% enhancement of γ on NH_4HSO_4 particle surfaces relative to $(NH_4)_2SO_4$. Another important result comes from our reevaluation of the nitrate effect using laboratory data on ammoniated particles. That effect, which was previously considered to decrease γ by a factor of ten (Riemer et al., 2003), is now believed to be a factor of 1.4 to 4.4.

Our parameterization was applied under winter and summer conditions representative of the eastern United States using 3-dimensional fields of T, RH, SO_4^{2-}, NO_3^-, and NH_4^+ obtained from a recent CMAQ model simulation. The resulting spatial distributions of γ were contrasted with three other parameterizations that have been applied in

air quality models in the past. Our ambient estimates of γ fall between the upper value proposed by Dentener and Crutzen (1993) and the rather low values used by Riemer et al. (2003). Under winter conditions, large differences were found between our parameterization and that of Evans and Jacob (2005). These comparisons helped us identify critical gaps in the laboratory data that will be most valuable for future refinements of the γ parameterization.

Acknowledgements

We thank our colleagues for their help and advice. These include Dr. Hao (Helen) Zhang and Dr. Huixia (Judy) Wang, Professors of Statistics at North Carolina State University; Dr. Simon Clegg, University of East Anglia; Dr. Jenise Swall and Mr. Shawn Roselle, Atmospheric Sciences Modeling Division, Air Resources Laboratory, National Oceanic and Atmospheric Administration; and Dr. Nicole Riemer, State University of New York, Stonybrook.

The research presented here was performed under the Memorandum of Understanding between the U.S. Environmental Protection Agency (EPA) and the U.S. Department of Commerce's National Oceanic and Atmospheric Administration (NOAA) and under agreement number DW13921548. This work constitutes a contribution to the NOAA Air Quality Program. Although it has been reviewed by EPA and NOAA and approved for publication, it does not necessarily reflect their policies or views.

References

Akaike, H.: Information theory and an extension of the maximum likelihood principle. In Proc. 2nd Int. Symp. Information Theory, eds B. N. Petrov and F. Csáki, Budapest, 267 – 281, 1973.

Appel, K. W., Bhave, P. V., Gilliland, A. B., Sarwar, G., and Roselle, S. J.: Evaluation of the Community Multiscale Air Quality (CMAQ) model version 4.5: Uncertainties and sensitivities impacting model performance. Part II: Particulate matter. Atmos. Environ., 2007 (in review).

Badger, C. L., Griffiths, P. T., George, I., Abbatt, J. P. D. and Cox, R. A.: Reactive uptake of N_2O_5 by aerosol particles containing mixtures of humic acid and ammonium sulfate, J. Phys. Chem. A, 110, 6986-6994, 2006.

Bhave, P.; Sarwar, G.; Appel, W.; Dennis, R. Revised Treatment of N_2O_5 Hydrolysis in CMAQ, Models-3 Users' Conference, 1.4, Chapel Hill, October 2006.

Casella, G. and Berger, R. L.: Statistical Inference, 2nd edition, Duxbury, Pacific Grove, CA, 2002.

Dentener, F. J. and Crutzen, P. J.: Reaction of N_2O_5 on tropospheric aerosols: Impact on the global distributions of NO_x, O_3, and OH, J. Geophys.Res., 98, 7149–7163, 1993.

Evans, M. J. and Jacob, D. J.: Impact of new laboratory studies of N_2O_5 hydrolysis on global model budgets of tropospheric nitrogen oxides, ozone and OH, Geophys. Res. Lett., 32, L09813, 2005.

Folkers, M.: Bestimmung der reaktionswahrscheinlichkeit von N_2O_5 an troposhärisch relevanten aerosolen, Ph.D. Thesis, Universität Köln, 2001.

Folkers, M., Mentel, Th. F., and Wahner, A.: Influence of an organic coating on the reactivity of aqueous aerosols probed by the heterogeneous hydrolysis of N_2O_5, Geophys. Res. Lett., 30, 1644, 2003.

Goff, J. A., and Gratch, S.: Low-pressure properties of water from -160 to 212F, in Transactions of the 52nd annual meeting of the American society of heating and ventilating engineers, New York, 95-122, 1946.

Hallquist, M., Stewart, D. J., Stephenson, S. K., and Cox, R. A.: Hydrolysis of N_2O_5 on sub-micron sulfate aerosols, Phys. Chem. Chem. Phys., 5, 3453-3463, 2003.

Hu, J. H. and Abbatt, J. P. D.: Reaction probabilities for N_2O_5 hydrolysis on sulfuric acid and ammonium sulfate aerosols at room temperature, J. Phys. Chem. A, 101, 871-878, 1997.

IUPAC Subcommittee on gas kinetic data evaluation: Data sheet H23, http://www.iupac-kinetic.ch.cam.ac.uk/, revised15 August, 2006.

Kane, S. M., Caloz, F., and Leu, M.-T: Heterogeneous uptake of gaseous N_2O_5 by $(NH_4)_2SO_4$, NH_4HSO_4, and H_2SO_4 aerosols, J. Phys. Chem. A, 105, 6465-6470, 2001.

Kutner, M. H., Nachtshein, C. J., Neter, J., and Li, W.: Applied Linear Statistical Models, 5th edition, McGraw-Hill, New York, 2005.

Martin, S. T., Schlenker, J. C., Malinowski, A., Hung, H.-M., Rudich, Y.: Crystallization of atmospheric sulfate-nitrate-ammonium particles, Geophys. Res. Lett., 30, 2003.

Mozurkewich, M. and Calvert, J. G.: Reaction probability of N_2O_5 on aqueous aerosols, J. Geophys. Res., 93, 15,889-15,896, 1988.

Riemer, N., Vogel, H., Vogel, B., Schell, B., Ackermann, I., Kessler, C., and Hass, H.: Impact of the heterogeneous hydrolysis of N_2O_5 on chemistry and nitrate aerosol formation in the lower troposphere under photosmog conditions, J. Geophys. Res., 108, 4144, 2003.

Effects of Sub-Grid Scale Terrain upon CAMx Air Quality Simulation.

Carlie J. Coats, Jr.* [1,]
M. Talat Odman[2]
and Saswatti Datta[1]

[1]Baron Advanced Meteorological Systems, LLC., Raleigh NC, USA
[2]Department of Environmental Engineering, Georgia Institute of Technology, Georgia, USA

Statement of the Problem

Meteorology models typically "smooth" the underlying terrain for spatial scales of at least 3 dx, in order to avoid the formation of spurious waves due to 2 dx features interacting with advection schemes. For MM5, the minimum terrain smoothing permitted is 3 dx averaging, so that a nominal 4 KM grid spacing actually corresponds to the use of 12 KM averaged terrain height. This smoothing causes errors at the grid scale, particularly for such meteorology fields as surface temperature. Moreover, conventional meteorology models assume a laminar atmosphere that does not simulate sub-grid scale effects caused by terrain variability. In this case study, we examine some of the sub-grid scale effects upon air quality processes, particularly emissions and dry deposition. We do not study the effects of grid scale terrain height error, nor the effects of sub-grid scale terrain variability upon wet deposition. It is also beyond the scope of this study to modify meteorological model dynamics (where meteorology model drag should be enhanced to account for orographic drag, etc., as is done in ECMWF).

In this study, we implemented a sub-grid scale parameterization within the CAMx air quality model; the effects for a 4 KM California domain upon CAMx simulations are the subject of an accompanying paper with lead author Saswati Datta. We begin with a terrain preprocessor **PENFRAC** that evaluates both the grid scale error (due to smoothing in MM5's **TERRAIN** program) and the sub-grid scale terrain variability in terrain heigh. Within CAMx, we implement parameterizations for sub-grid scale terrain effects upon surface emissions, point source emissions, and dry deposition, it being outside the scope and the data-availability of the project to be able to re-run meteorologically dependent (biogenic and mobile source) emissions with corrections for the surface temperature errors due to MM5 terrain smoothing. Other studies have shown that the grid scale errors in MM5 terrain can lead to significant errors in biogenic emissions. Failure to model the sub-grid scale effects we study in "vanilla" CAMx (and other air quality models) leads to vertical mis-allocation of emissions and dry deposition. It should be noted that there are further effects due to the interaction of this mis-allocation with transport and diffusion.

Model Implementation:

Sub-Grid Terrain Analysis Pre-Processor

Terrain analysis is performed by pre-processor program **PENFRAC** that reads in 30-arc-second (approximately 0.7 KM) digital elevation model (DEM) terrain data in Models-3 I/O API format, derived from the same USGS generated DEM data used to drive *Mode 6* of program **TERRAIN**. This program creates two files:

HT_2D with these terrain related 2-D variables:

HTMIN, minimum of DEM terrain heights in grid cell (M)
HTBAR, mean of DEM terrain heights in grid cell (M)
HTMAX, maximum of DEM terrain heights in grid cell (M)
HTSIG, standard deviation of DEM terrain heights in grid cell (M)

HT_3D with 3-D variable:

> ***TFRAC,*** the fraction of each horizontal grid cell in contact with each 3-D model layer.

Note that *HTBAR* can be used to evaluate grid scale errors in meteorology model terrain, and that *HTMAX-HTMIN* and *HTSIG* are two different measures of the terrain variability within each grid cell. In this study, we used the "simple-Z" version of **PENFRAC** which uses MM5 layer thicknesses and a base elevation *HTBAR-HTSIG* to construct a 3-D layer system. Terrain penetration fraction *TFRAC* is constructed by counting how DEM elevation-points in each met-grid cell are related to this 3-D layer system, subject to the constraint that DEM-values below model-bottom are counted as being in Layer 1.

Sub-Grid Scale Terrain Effects in CAMx

We have implemented three classes of sub-grid scale terrain effects as modifications to CAMx Version 4.31:

- Dry-deposition effects
- Surface-emissions effects
- Point-source emissions effects

For the first two of these, the implementation uses *TFRAC* from **PENFRAC**'s ***HT_3D*** to deal with vertical re-allocation effects; the latter uses high resolution ***DEM_CRO_2D*** data to construct stack-height corrections (subject to the constraint that stack-top may not be below bottom-of-model). The implementation adds a new Fortran module **LPEN_MOD** that encapsulates reading and processing these files, particularly the nest management, the re-aggregation of *TFRAC* from the native MM5 layers to the variable *LFRAC* on the collapsed CAMx layers, and the adjustment of stack height for high resolution DEM terrain. These terrain parameterization effects may be turned off by means of environment variables at program-launch, following the conventions of Models-3.

Routine **DIFFUS** was modified so that it calls **LPEN_NEST** to activate **LPEN_MOD** for the current grid. Then within its internal time step loop it alternates between calling diffusion-kernel **VDIFFIMP** and computing 3-D mass exchanges from the concentration field to the deposition field, using *LFRAC* as the weights for accumulating mass from the model layers. The effect is that for significantly variable terrain, dry deposition fractionally removes mass from several layers of the atmosphere. In the day-time mixed regime, the differences are insignificant; however, during stable periods (as at night), the scheme partially scavenges multiple layers rather than completely scavenging Layer 1 only, generating greater dry deposition totals and more realistic end-of-night concentration profiles.

As we implemented this dry deposition parameterization, we discovered that the original CAMx scheme had a mass inconsistency, where first dry-deposition was treated as a bottom boundary condition sink in **VDIFFIMP** and then separately computed for output from post-**VDIFFIMP** Layer 1 concentrations. The effect of this mass inconsistency was to introduce a mild low bias into the dry deposition field relative to the modeled concentrations.

Routine **EMISS** was modified to call **LPEN_NEST**, then to allocate each grid cell's emissions in the vertical using *LFRAC* as weights. Routine **PLUMERIS** uses terrain adjusted stack heights as the basis of its plume rise computation. Again, effects are most marked in the stable nocturnal boundary layer, where vertical allocation may have substantial effects upon nocturnal precursor transport; unstable-regime effects are much smaller.

In the process, the CAMx code was extensively re-parallelized, raising the parallel efficiency on 8 SGI Origin processors from about 35% to better than 95%. The build-system was modified to support PathScale, Intel, and Sun compilers for Linux. Also, a number of additional optimizations relating to superfluous array-copy operations in **VDIFFIMP** were performed, increasing the single-processor performance of the code noticeably. However, there are still many opportunities for further code speedup. These code modifications were supplied back to the California Air Resources Board.

Terrain Analysis for the CCOS Domain

Plots for a terrain analysis based on the *MM5* **MMOUT** file for this case are given by the figures in the *Appendix* at the end of this paper. Figure 1 shows the extent of the domain, while plotting the "true mean" terrain height computed directly on this 4-KM grid from USGS 30-second digital elevation model (DEM) data. Figure 2 shows the MM5 error in terrain elevation due to smoothing in the *TERRAIN* program. Figure 3 shows the range of terrain elevation (from max to min of the DEM within each grid cell), on a "raw" PAVE scale. Figure 4 shows the maximum layer of terrain penetration, which ranges up to Layer 22 at one point (representing an elevation difference of about 1000 meters). Figures 5-8 show the fraction of each cell that *Simple-Z* regards as being in contact with Layers 1, 2, 5, and 10 of the atmospheric model, respectively. To get the fraction of the cell that interacts with a given layer $L > 1$ for purposes of emissions or dry depositions, one computes the difference

LFRAC(L) - LFRAC(L+1)

Note that terrain penetration is significant through layer 10 or so, and is quite small (particularly as regards emissions and pollutant distributions) for layers 15 or higher. Note also that the effects are insignificant in the central San Joaquin Valley, but are substantial in the foothills and the mountains that surround it-in particular, for transport between it and the San Francisco Bay area.

Acknowledgements

This work was funded under the Central California Ozone Study's request for proposals, "Improve Conservation of Mass Module in Air Quality Models".

The statements and conclusions of this report are those of tine Investigator, and not necessarily those of the California Air Resources Board, the San Joaquin Valleywide Air Pollution Study Agency, or its Policy Committee, their employees or their members. The mention of commercial products, their source, or their use in connection with material reported herein is not to be construed as actual or implied endorsement of such products.

References

Coats, C. J., A Conservative Framework for Sub-Grid Scale Terrain Effects in Air Quality Forecast Models. *7th Conference on Atmospheric Chemistry*, American Meteorology Society, San Diego CA Jan. 2005.

Coats, C. J., SMOKE R&D for Sub-Grid Scale Terrain Effects and Air Quality Forecast Modeling. Presentation for *US EPA ORD,* RTP, NC. Feb. 2005. Available at URL *http://www.baronams.com/staff/coats/EPA_feb2005.ppt*

Coats, C. J., SMOKE-RT Development for WRF-Chem and Air Quality Forecasting. *4th Annual CMAS Models-3 Users' Conference* UNC-Chapel Hill, Chapel Hill, NC, September 26-28, 2005. Available at URL *http://www.baronams.com/staff/coats/CMAS_wrf_smoke_2005.pdf*

Appendix : Terran Analysis

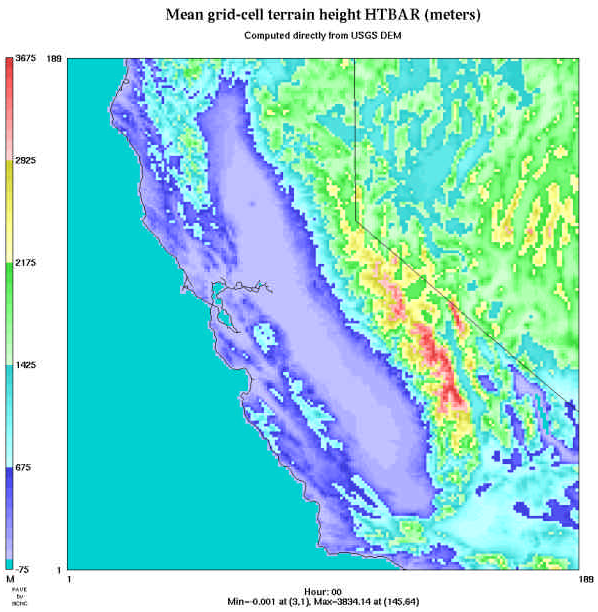

Figure 1: Terrain height computed by directly averaging USGS 30-second Digital Elevation Model (DEM; approximately 0.7 KM) terrain heights over each 4KM grid cell

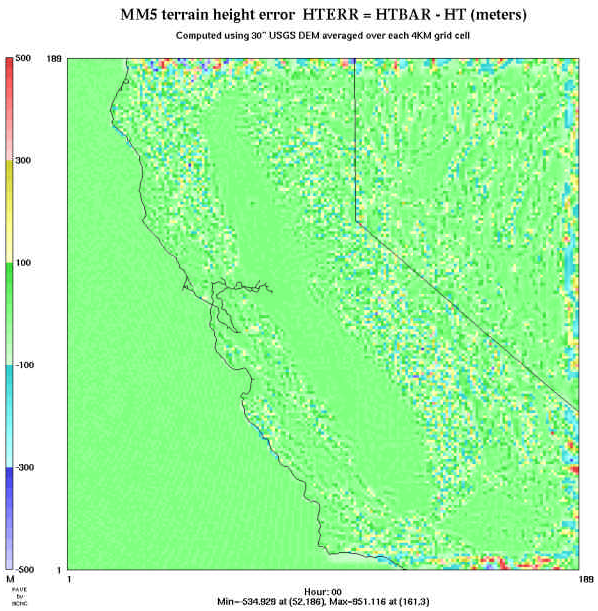

Figure 2 : Error in *MM5* terrain height due to the smoothing in the *MM5 TERRAIN* pre-processor.

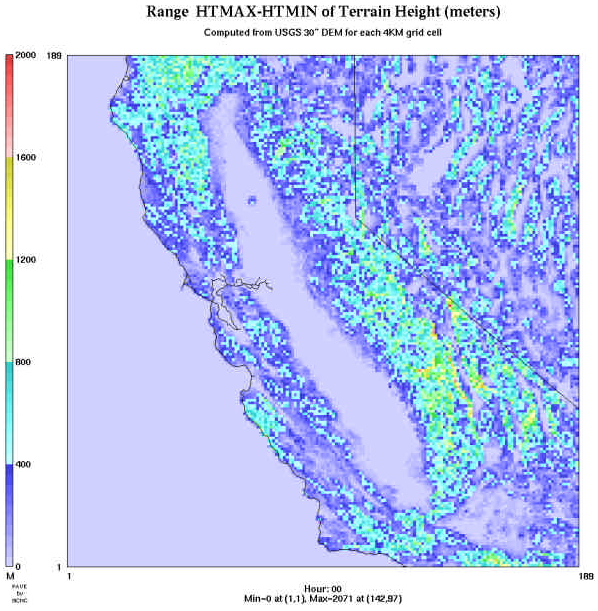

Figure 3: Range of terrain height: *HTMAX – HTMIN* for 30-second DEM elevations within each 4 KM grid cell. Note that max range is 2071 meters…

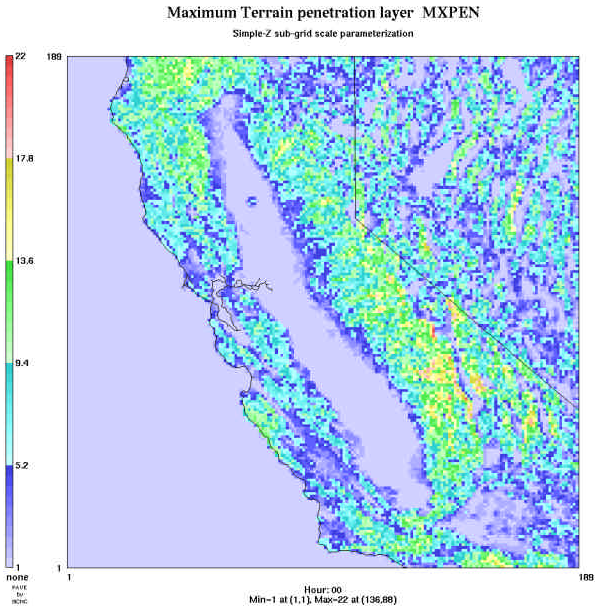

Figure 4: Maximum terrain penetration layer for the 4 KM *MM5* grid, using the Simple-Z sub-grid scale terrain parameterization. The maximum of layer 22 corresponds to an elevation of approximately 1000 meters.

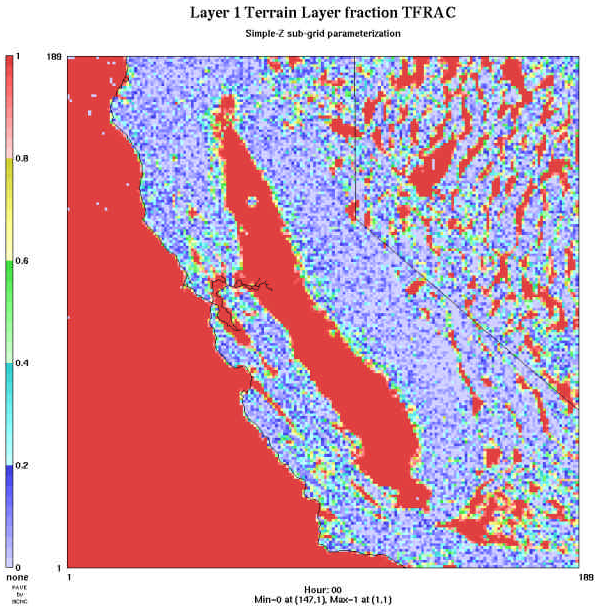

Figure 5: Fraction *TFRAC* of each 4 KM grid cell that should be regarded as being "within layer 1" as computed by the *Simple-Z* sub-grid scale terrain penetration parameterization

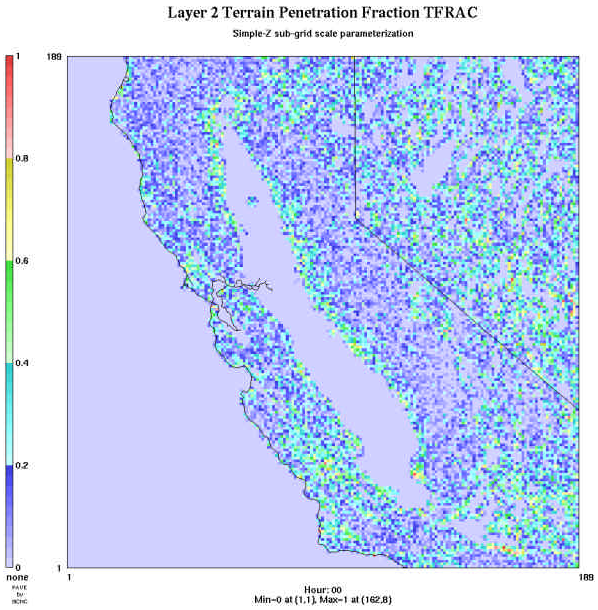

Figure 6: Layer 2 *TFRAC*

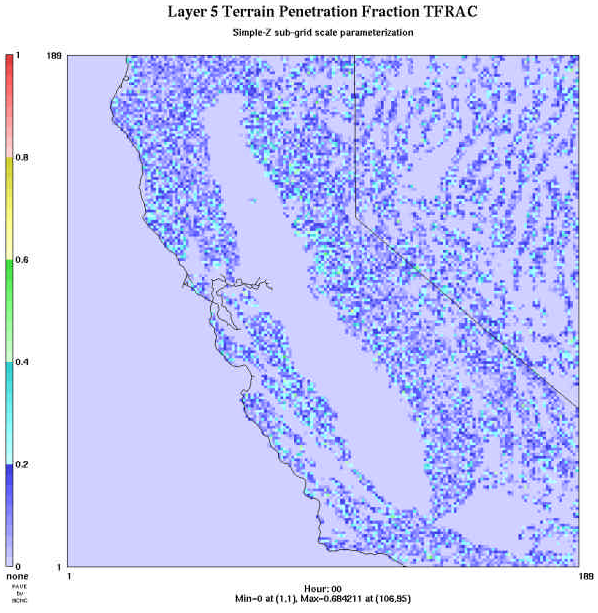

Figure 7: Layer 5 *TFRAC*

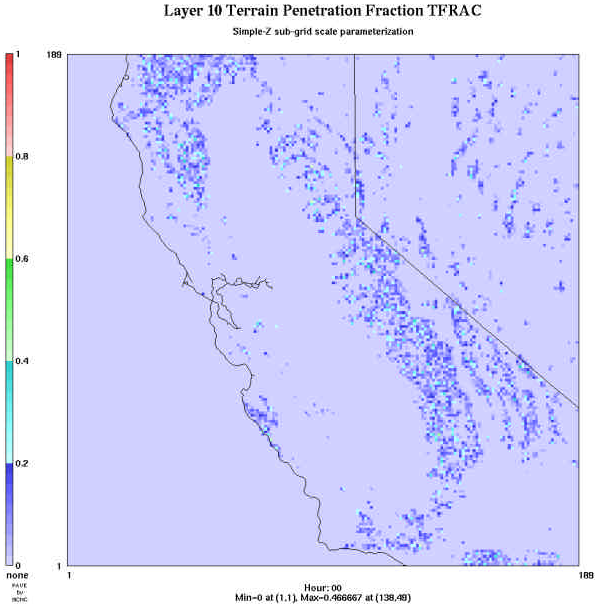

Figure 8: Layer 10 *TFRAC*

DESIGN AND DEVELOPMENT OF MAQM, AN AIR QUALITY MODEL ARCHITETCTURE WITH PROCESS-LEVEL MODULARITY

Weimin Jiang*, Helmut Roth, Qiangliang Li, Steven C. Smyth, Fuquan Yang
Institute for Chemical Process and Environmental Technology, National Research Council of Canada, Ottawa, Ontario, Canada

1. INTRODUCTION

Atmospheric processes affecting air quality are very complicated, and scientific understanding of these processes has been evolving rapidly. To successfully simulate concentration levels and changes of atmospheric pollutants, it is highly desirable to have air quality models with full and flexible modularity at the science process level. Such a modular air quality model would significantly enhance model transparency, facilitate scientific understanding, promote science algorithm development, and enable effective error checking and corrections. It would open the door for broad participation of the air quality modelling community in the model development and improvement processes, which is essential to ensure complete and robust science in the models.

Recently, we have completed the design and development of a software architecture that can be used to build modular air quality models. The architecture, named MAQM (Modular Air Quality Model), treats different processes as individual blocks. These blocks can be easily added, removed, modified, and/or reorganized, either individually or in combination. To demonstrate the MAQM concept and feasibility, a 3-D air quality model has also been developed and tested for a North American domain. The model is named MAQM/CMAQ to indicate that it is based on the MAQM architecture, and its science algorithms are mostly adapted from the Community Multiscale Air Quality (CMAQ) model developed by the United States Environmental Protection Agency (US EPA) (EPA 1999; Binkowski and Roselle, 2003).

2. CONCEPTUAL MAQM ARCHITECTURE

MAQM tries to mimic the natural environment as closely and as directly as possible within the constraints of operator-splitting. The following figure shows a simplified conceptual architecture of MAQM, which is built on the structural components and design principles discussed below.

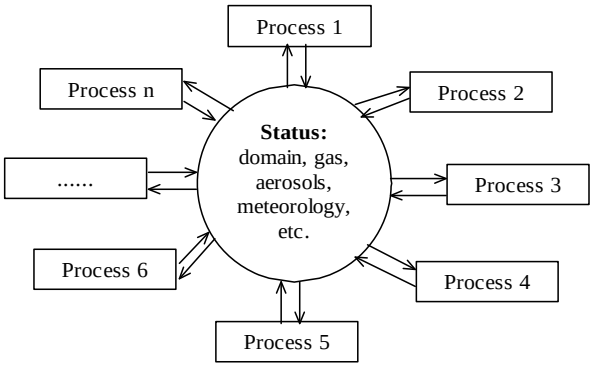

1. Status and process:

In the context of MAQM, a status (or natural status) is a numerical description of the modelled environmental situation in the modelling domain at a particular time and modelling stage. It includes quantities that change with time and location, such as concentrations of gaseous species, chemical and size-related quantities of particles, and meteorological conditions. It is also extended to include other relevant quantities and properties that do not change with time and/or location, such as model grid definition, grid cell dimensions, terrain height, molecular weights, etc.

A process is a software representation of an event or a combination of events that brings about changes in certain quantities of the natural status. Emissions, gas phase chemistry, nucleation, and advection are all examples of MAQM processes. In MAQM, the concept of a process is also extended to include a set of computer code that extracts and outputs certain status information as required.

The main objective of a process is to modify and/or output certain status quantities, based on the status information available at the beginning of

*Corresponding author: Weimin Jiang, National Research Council of Canada, Room 233, M2,1200 Montreal Road, Ottawa, Ontario, Canada K1A 0R6; e-mail: Weimin.jiang@nrc-cnrc.gc.ca

a time step through which a process progresses. It is also possible that a process may output certain other local quantities as required.

Note that the conceptual MAQM architecture does not restrict how the status will be modified by individual processes and where the new input data will come from. For example, modification of certain gaseous species concentrations by the emission process could be caused by reading in emissions from a file generated off-line, or by generating emissions directly on-line.

2. Global status data repository: uniqueness of shared status information

All status quantities in the modelling domain at a particular time that are used by multiple processes, e.g., concentrations, molecular weights, temperature, grid information, etc, are uniquely defined and represented in an on-line data repository. The data repository has a global scope and can be accessed by all relevant processes.

3. Self-contained process modules

A process module contains all the executable statements, data, and parameters required by itself, except the global status information available in the data repository mentioned above.

A process module is free to obtain any other input information through its own channels, such as specific input data files. However, any such information must not cause any conflicts with the unique status information given in the data repository. A process module is also allowed to output any quantities to its own output files with unique file names. All input or output files used by a process module are considered as integral parts of the module by MAQM.

4. Structural separation of process modules

In MAQM, each process module is an independent entity. Different process modules are treated as individual blocks, and are structurally separated. There are no direct relationships among different process modules. All data exchanges among different process modules, if any, are carried out indirectly through the global data repository. For example, a gas chemistry module needs temperature data, which are generated or obtained by a meteorology module. Instead of passing the temperature data from the meteorology module to the gas chemistry module directly, the meteorology module modifies the temperature field in the data repository, and the gas chemistry module obtains the temperature data from the data repository. As soon as the temperature field in the data repository is modified by the meteorological module, all process modules can access the same temperature data independently without repetitively calling the meteorological module and without direct data exchange with the meteorological module.

Note that a process is defined in Point 1 above as a software representation of an event or a combination of events that brings about status changes. That is to say that process modules can be organized in a flexible way. A process module can be as simple or as complicated as required. For those processes that are fundamentally un-separable, they can be combined into a single module, which is structurally separated from other modules. However, for the sake of maintaining the overall modular paradigm, the creation of these multi-process modules should be avoided if possible.

5. Structural separation and linkages of status and processes

As mentioned above, shared status quantities are stored in a uniquely defined global data repository and are structurally separated from the process code. However, the status is also closely linked to the processes through accessing the status quantities by the processes. Same status quantities can be accessed by different processes, and a process can access multiple and selective status quantities in the data repository. This is analogous to a modern computer hardware architecture, under which different devices and components carry out various functions by selectively accessing multiple data items stored in memories through bus wires.

A good implementation of the MAQM architecture would maintain relative independence of the status data repository and the process code, and minimize the need to change process code when status data are changed, and vice versa.

6. The MAQM driver and its interface with the process modules

In MAQM, all operations related to the status quantities are carried out by process modules. The MAQM driver coordinates the actions of

individual process modules by calling them in sequence according to a common user-specified time step length. The MAQM driver is kept at the simplest possible form in structure.

The interface between the MAQM driver and the process modules is also kept simple. The MAQM driver passes only the time stamp and step length information to individual process modules. There is no information passed back from the process modules to the MAQM driver. Results of the process module operations are reflected in the change of status quantities in the status data repository and/or in the output files generated by the process modules.

If needed, each process module can determine and use its own internal time step length(s). However, only the status data after the time step specified by the MAQM driver are reported back to the status data repository.

7. *Minimized usage of hardcode and repetitive code*

Whenever possible, MAQM avoids using hardcoded variable names, indices, and pointers. As a consequence, usage of repetitive code is minimized.

3. IMPLEMENTATION OF THE CONCEPTUAL MAQM ARCHITECTURE IN FORTRAN

The global status data repository can be effectively realized through a set of dedicated FORTRAN module program units, i.e., the status data are represented by a set of FORTRAN data modules.

The process modules can be implemented either through FORTRAN module program units, or through sets of FORTRAN subroutines and functions. The top level subroutine in a process module is called by the MAQM driver. It accepts the time stamp and the model step length from the driver. Subroutines at any levels of a process module can access the status data in the data modules via the USE statements. The data can be selectively accessed by including the ONLY option in the USE statements.

4. THE MAQM/CMAQ MODEL: DEMONSTRATION OF THE MAQM CONCEPT AND FEASIBILITY

MAQM/CMAQ is a model that we developed to demonstrate the MAQM concept and feasibility, although it has gone beyond our original expectation and become a fully functioning model. A preliminary evaluation for a continental North American domain over the month of July 2002 showed that in comparison with CMAQ version 4.5, MAQM/CMAQ generated almost identical spatial and temporal O_3 distribution patterns with noticeably better performance in O_3 biases and errors. The MAQM/CMAQ aerosol performance also appeared to be better.

The following sections focus on the original objective of the MAQM/CMAQ development by briefly presenting the structure, composition, functionality, and capacities of MAQM/CMAQ only. Detailed evaluation of MAQM/CMAQ will be presented elsewhere.

4.1 Overview of the MAQM/CMAQ model

MAQM/CMAQ is built on the conceptual MAQM architecture and programmed in FORTRAN. The science algorithms implemented in the model are mostly adapted from CMAQ version 4.5, along with some in-house additions and revisions. When adapting algorithms from CMAQ, we tried to use the original CMAQ code whenever possible. However, we also made substantial changes and/or recoding to correct mistakes, simplify the code, and facilitate the integration of the CMAQ code into MAQM/CMAQ.

The saprc99_ae4_aq mechanism available in the CMAQ release is used as the basis of the gas chemical mechanism in MAQM/CMAQ. It was made compatible with our revised implementation of Schell's secondary organic aerosol (SOA) algorithm (Schell et al., 2001) by adding 10 semi-volatile organic compounds (SVOCs) in appropriate reactions and removing the 6 pseudo species representing reacted amounts of organic precursors. The revised mechanism file, named saprc99_ae4_aq_SVOC.def, was reformatted by reorganizing its kinetic information and adding new information regarding some properties of the chemical species, such as molecular weights. It was then processed through a new chemical mechanism processor, PROCCHEM, developed in-house to automatically generate a list of

reactive chemical species and their molecular weights and several source code files. The species list is included in the gas_data module and the source code files are integrated into the gas_chem process module to be discussed later.

For aerosol modelling, the CMAQ approach of representing particles as three superimposed log normal size distributions, or modes, is adapted. However, the approach is structurally generalized so that it could be changed to use any number of modes. In addition, the code is generalized so that each mode contains the same 20 aerosol species. These species could be adjusted when needed. The 20 species contain all the aerosol species used by CMAQ, except that the 2 CMAQ SOA species are replaced by the 10 SVOC species partitioned in aerosols. Whenever feasible, hardcoded variable names, indices, and repetitive code specific to a given species and size mode are eliminated.

To facilitate the comparison of model results with size-resolved measurement data, MAQM/CMAQ generates and outputs not only prognostic modal aerosol quantities, but also diagnostic sectional aerosol quantities, which include total and speciated aerosol concentrations at specific size cutoffs. The size cutoffs can be easily set up by the users. At the moment, they are set up at default values of 0.01, 0.1, 1, 2.5, 5.0, and 10 μm.

The current version of MAQM/CMAQ contains 20 process modules and 5 global data modules. The data modules are shared and accessed by all the process modules.

4.2 The MAQM/CMAQ data modules

Four data modules, grid_data, gas_data, aero_data, and met_data, are used to store relevant information of the model grid, gaseous species, aerosol quantities, and meteorological variables, respectively. Another data module, const_data, contains commonly used mathematical, chemical, physical, and meteorological constants, as well as minimum concentrations of gas and aerosol quantities, which represent nominal zeros of theses quantities in MAQM/CMAQ.

4.3 The MAQM/CMAQ process modules

The 20 process modules currently implemented in MAQM/CMAQ are:

- **grid**:
  definition and set up of quantities related to model grid and model domain.
- **init_met**:
  meteorological fields initialization.
- **init_gas**:
  gas species concentration initialization.
- **init_aero**:
  aerosol quantity initialization.
- **BConc_gas**:
  gas species boundary condition.
- **BConc_aero**:
  aerosol quantity boundary condition.
- **emission**:
  gas and particle emissions.
- **gas_chem**:
  gas phase chemistry.
- **nucleation**:
  particle formation through nucleation.
- **condensation**:
  H_2SO_4 condensation on particles.
- **inor_aero**:
  inorganic gas/aerosol partitioning and equilibrium.
- **SOA**:
  secondary organic aerosol formation/evaporation through gas/aerosol partitioning.
- **coagulation**:
  particle coagulation.
- **advection**:
  gas and particle advection.
- **diffusion**:
  gas and particle diffusion.
- **cloud**:
  cloud processes affecting gas and aerosols, including wet deposition.
- **ddep_gas**:
  dry deposition of gaseous species.
- **ddep_part**:
  dry deposition of particles.
- **meteorology**:
  meteorological variable set-up and/or calculation.
- **output**:
  generation and output of required gas and aerosol quantities to output files.

4.4 The MAQM/CMAQ utilities

MAQM/CMAQ uses CMAQ pre-processors MCIP and JPROC. In addition, it uses three pre-processors that we developed in-house for

chemical mechanism processing and initial and boundary condition preparation.

MAQM/CMAQ also contains several utility subroutines that can be called by any other program units within MAQM/CMAQ for maintenance, housekeeping, and quality control purposes.

4.5 The MAQM/CMAQ input & output files

As in CMAQ, the current version of MAQM/CMAQ reads in MCIP-generated meteorological input files and SMOKE-generated emission files directly. This ensures the compatibility of MAQM/CMAQ and CMAQ in terms of using the same meteorological and emission input files. MAQM/CMAQ reads in initial (IC) and boundary (BC) conditions from a set of ASCII files, which allow more flexible set-up of initial and boundary concentration values in different grid cells. The standard CMAQ IC and BC profiles can be converted to the MAQM/CMAQ IC and BC ASCII files by using the utility programs that we developed in-house. The CMAQ IC and BC pre-processors are not used by MAQM/CMAQ.

For each day of the model run, MAQM/CMAQ generates the following three output files in I/O API format. Users can specify to use either the conventional or SI unit for the output files. In the conventional units, gas and aerosol mass concentrations are given in ppm and $\mu g/m^3$, respectively. In the SI unit, the two quantities are $mole/m^3$ and kg/m^3, respectively.

- GasConc_yyyyddd: hourly gas concentrations on the day 'yyyyddd'.

- AeroConc_yyyyddd: hourly modal aerosol quantities on the day 'yyyyddd', which include concentrations of total and speciated mass, number, and surface area of all particle modes, as well as geometric mean diameters and geometric standard deviations of all the particle number distributions.

- PMx_yyyyddd: hourly particle concentrations within specific size ranges on the day 'yyyyddd', which include total and speciated mass, number, and surface area concentrations. As mentioned in Secton 4.1, the cutoff sizes are 0.01, 0.1, 1, 2.5, 5, and 10 μm by default. The cut-off values can be easily changed by users.

5. POSSIBLE FUTURE WORK

The simple and flexible modular architecture of MAQM has laid the foundation for numerous possibilities for future work on model development, evaluation, science implementation, improvement, and applications. It opens doors for broad and effective participation in model development by the modelling community. Here, we briefly discuss some possible future work that could be done either by ourselves and/or by the community.

5.1 Develop new models or restructure current models using the MAQM architecture

The MAQM architecture, including its design principles, could be readily adapted for developing new models or restructuring current models.

The implementation of the architecture in MAQM/CMAQ could also be used as a prototype in future model development. For the modal approach of aerosol modelling, the number of modes and aerosol species in MAQM/CMAQ could be changed, along with adjustments of the current algorithms or the addition of new code. For the sectional approach, the current matrix of modes vs. species in the MAQM/CMAQ aerosol quantity definition could be readily converted to the definition of size ranges vs. species. Program code can then be developed in a similar fashion depending on the scientific formulations used.

5.2 Investigate and improve current science in individual process modules

Due to the relative structural independence of process modules, science implementation details and their embedded assumptions in any particular module in MAQM/CMAQ or other models based on the MAQM architecture can be effectively recovered, rigorously investigated and tested, and further improved. Broad participation by the modelling community in the investigation and improvement of embedded science details is the only way to ensure the correctness and robustness of the science algorithms implemented in complicated air quality models.

5.3 Add new or alternative process modules

New and/or alternative process modules can be added to MAQM/CMAQ or other models using

the MAQM architecture with minimal interference from other process modules.

5.4 Revise current meteorology and/or emission modules to use meteorology and emissions input files from alternative sources

The revision is to accept input files with different file formats, other than the I/O API currently used, and to change the status data in the data modules using the input data available in alternative input files generated by other meteorological models or emissions processors.

5.5 Implement on-line meteorology and/or emissions modules

Instead of using off-line meteorology and emission input files, on-line meteorology and/or emissions modules can be developed and implemented in MAQM/CMAQ or other models using the MAQM architecture. These modules will be structurally independent of other process modules and their implementation will be relatively straightforward. By conducting meteorological modelling and emissions modelling/processing on-line, two-way feedbacks between air quality and meteorology and between meteorology and emissions can be achieved.

5.6 Implement time-varying boundary conditions

Subject to the availability of data or algorithms, the boundary condition modules in MAQM-based models can be easily revised to update gas and aerosol concentrations in boundary cells according to time-varying boundary conditions.

5.7 Process analysis

Under MAQM, process modules can be easily added, removed, and regrouped. Process analysis can be conducted by adding, removing, and/or regrouping certain process modules, outputting quantities of interest, and comparing the results with different groupings of process modules. Alternatively, depending on the needs of specific project(s), specific process analysis module(s) can be developed and inserted into desired locations of the process module stream in a MAQM-based model in a flexible way.

6. ACKENOWLEDGEMENT

Most science algorithms implemented in the current version of MAQM/CMAQ were adapted from the CMAQ model. Early ideas of air quality model modularity and the spirit of community modelling have been built into the development of the CMAQ system, which inspired our thinking in designing and developing the MAQM architecture and the MAQM/CMAQ model presented in this paper. In addition, many organizations have contributed to the CMAQ code that was adopted and/or adapted by MAQM/CMAQ. The contributions by the CMAQ development team at the US EPA and all the other organizations are very much appreciated. We also thank the Community Modelling and Analysis (CMAS) Center at the University of North Carolina at Chapel Hill for their work in distributing and supporting CMAQ and other associated modelling tools that are used in this project.

7. REFERENCES

Binkowski, F.S., Roselle, S.J., 2003. Models–3 Community Multiscale Air Quality (CMAQ) model aerosol component, 1, Model description, *J. Geophys. Res.,* **108**(D6), 4183, doi:10.1029/2001JD001409.

EPA, 1999. Science algorithms of the EPA Models-3 Community Multiscale Air Quality (CMAQ) modeling system, edited by D.W. Byun and J.K.S. Ching, EPA/600/R-99/030, Office of Research and Development, United States Environmental Protection Agency, Washington. DC, USA, March 1999.

Schell, B., Ackermann, I.J., Hass, H., Binkowski, F.S., Ebel, A., 2001. Modeling the formation of secondary organic aerosol within a comprehensive air quality model system, *J. Geophys. Res., 106*(D22), 28,275–28,293.

SUB-GRID SCALE MODELING OF AIR TOXICS CONCENTRATIONS NEAR ROADWAYS

Prakash Karamchandani*, Kristen Lohman and Christian Seigneur
Atmospheric and Environmental Research Inc., San Ramon, CA, USA

1. INTRODUCTION

Population exposure to hazardous air pollutants (HAPs), also known as air toxics, is an important health concern. Air toxics exposure is generally higher in urban areas than in rural areas and tends to be localized around the emission sources. For example, measurements of toxic air pollution levels near a busy freeway in Los Angeles showed that exposures near the freeway were up to 10 times greater than those at background locations and dropped to background levels within 300 m downwind of the freeway (Zhu et al., 2002a). Any modeling approach used to calculate the exposure impacts of air toxics must be able to capture this variability in exposure levels.

Gaussian plume dispersion models have been used extensively in air toxics modeling to simulate the near-field impacts of emissions from point, area and mobile sources. However, these models assume steady-state conditions for calculating downwind concentrations; furthermore, they cannot treat atmospheric chemical transformations (except simple first-order decay) and, therefore, are not suitable for many air toxics, which are chemically reactive. On the other hand, three-dimensional grid models, that are often used for applications involving a large number of sources and reactive pollutants, are not able to capture the subgrid-scale variability in concentrations near a source because of their coarse resolution (typically from 4 km to tens of kilometers). Thus, simulating the atmospheric transport and fate of chemically reactive toxic air pollutants requires the use of models that can handle non-steady-state conditions and reactive pollutants as well as resolve the sub-grid scale features of emissions from point and line sources.

Several air toxics modeling studies have pointed out the possible limitations associated with a coarse spatial resolution of air toxics emissions and concentrations. For example, the Neighborhood Assessment Program of the California Air Resources Board recommends a combination of a 3-D grid model and local plume dispersion models to assess air toxics concentrations (e.g., Isakov and Venkatram, 2006). Ching and co-workers (Ching et al., 2006) have developed an approach where they account for sub-grid spatial variability using the results of simulations conducted with a finer spatial resolution. The pros and cons of each of these approaches have been discussed by Seigneur (2004) and Touma et al. (2006).

We describe here a Plume-in-Grid (PiG) modeling approach that differs from the previous approaches by combining the 3-D grid-based modeling approach with a local scale modeling approach within a single model. The PiG approach is preferable to the one where two models are used separately (a grid model for regional pollution and a dispersion model for local pollution) because issues arise for reactive pollutants when recombining the results of the two model simulations (e.g., Seigneur et al., 2002).

The PiG model used in this study consists of a reactive plume model (SCICHEM) that is embedded within a three-dimensional grid model (CMAQ), providing the capability of capturing the local variability in concentrations near a source as well as treating the chemical transformations of reactive species. The model, referred to as CMAQ-APT (CMAQ with Advanced Plume Treatment), has previously been applied to point sources for ozone (Karamchandani et al., 2002; Vijayaraghavan et al., 2006), particulate matter (Karamchandani et al., 2006a) and mercury (Karamchandani et al., 2006b).

In the proof-of-concept study presented here, we have adapted CMAQ-APT to develop a prototype model to simulate near-roadway concentrations due to mobile emissions from a busy interstate highway in New York City. We also perform a qualitative comparison of model results with measured concentration profiles available near a major highway in Los Angeles (no measurements were available for New York City). For this demonstration study, we focus only on mobile emissions of carbon monoxide (CO) and benzene.

**Corresponding author:* Prakash Karamchandani, Atmospheric and Environmental Research, Inc., 2682 Bishop Drive, Suite 120, San Ramon, CA 94583-4282; e-mail: pkaramch@aer.com

2. MODELING APPROACH

For this initial application, the chemistry and aerosol modules of CMAQ-APT were deactivated and CO and benzene were treated as chemically-inert species; this is an appropriate approximation for these chemical species at the spatial scales considered here (less than 500 m from the emission source). SCICHEM, the plume component of CMAQ-APT, has traditionally been used to simulate point source emissions, but the framework allows the use of any source, as long as the relevant source characteristics are correctly specified. For this study, the roadway emissions that were simulated with SCICHEM were specified as adjacent elongated area sources, where each source represented a road segment. The following section provides additional details on the treatment of roadway emissions.

The model outputs include both the three-dimensional grid cell concentrations, as well as the puff incremental concentrations (i.e., the fraction of the total concentration in the puff that is above background). The concentration at any receptor location is then the sum of the grid cell average concentration of the cell containing the receptor and the perturbation concentrations of the puffs impacting that receptor. Thus, the model outputs contain information to calculate concentrations at discrete receptor locations, allowing us to predict concentrations at the subgrid-scale. A post-processor was developed to calculate the modeled concentrations of CO and benzene at selected receptor points perpendicular to the roadway. Each set of receptors is located at various distances along the busiest sections of the roadway, as described in the following section.

3. MODEL APPLICATION

The model was applied to the July 11-15, 1999 period of the NARSTO/Northeast program. The NARSTO modeling domain consists of two nested grids (see Figure 1). The outer domain has a horizontal resolution of 12 km while the inner domain has a horizontal resolution of 4 km. For this study, we used the inner 4 km domain, which includes New York City, New Jersey and Washington, D.C. The domain consists of 99 x 135 grid cells in the horizontal and 13 layers with variable resolution in the vertical. The boundary conditions for the simulation were obtained from the 12 km domain results from another study (Seigneur et al., 2003).

Below, we describe how roadway emissions were developed for the plume component of the model. We also describe the selection of receptor locations near the roadway for presenting the model results.

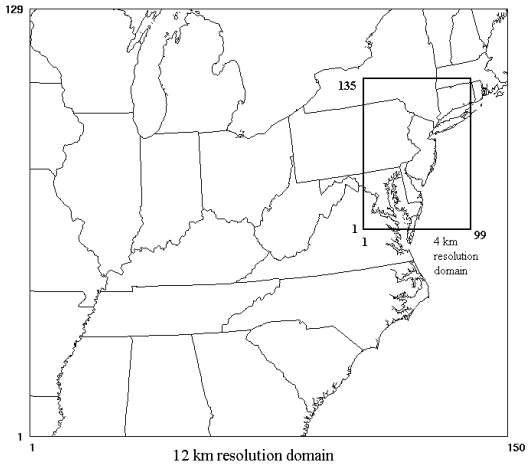

Fig. 1. Modeling domains for the NARSTO-Northeast simulation. The inner domain (4 km horizontal resolution) was used in this study.

3.1 Roadway Emissions

We selected a busy highway in the modeling domain based on the annual average daily traffic counts for various highways in the domain, Traffic count information was obtained by downloading traffic data from the Bureau of Transportation Statistics in the form of GIS files from the National Highway Planning Network (NHPN) (BTS, 2007). The data in the NHPN include both locations of the highway segments (county, latitude, longitude, and length) and also the annual average daily traffic count from the 2002 Highway Performance Monitoring System.

We chose a section of Interstate 278 (I278), which passes through all five boroughs of New York City (see Figure 2). The length of the selected section of the highway is about 50 km. This section of the highway was divided into several smaller segments, with each segment specified as a separate area source to the embedded plume model. Each segment is approximately 30 m long, based on the assumption that the highway width is 30 m and on the constraint that the initial size of the source must be less than or equal to the highway width.

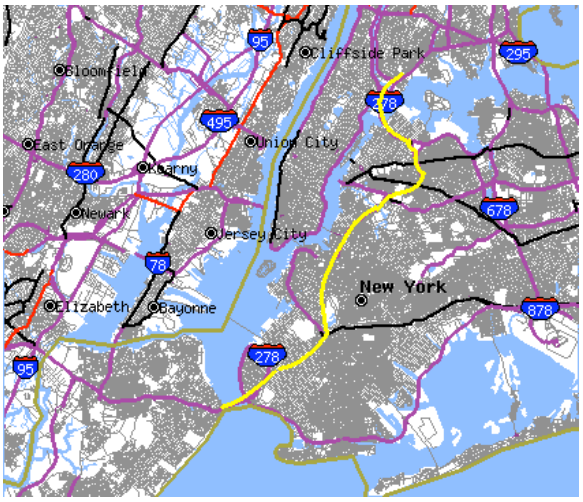

Fig. 2. Map showing section of Interstate 278 (in yellow) selected for this study.

The benzene and CO emissions data were obtained from a pre-existing SMOKE input file. Emissions from this file were available by county and Source Classification Code (SCC). The emissions for all SCC corresponding to highway traffic were summed for each county. A factor was created for I278 emissions in each county by dividing the I278 vehicle-miles (traffic count x segment length) traveled in that county by the total highway vehicle-miles traveled for the county. The vehicle-miles factor was multiplied by the highway emissions for each county to determine the total annual emissions of benzene and CO due to vehicle emissions on I278.

A list of highway segments was generated that covered the length of the selected section of I278. These segments were taken from the NHPN file. The segments were then split up by county, and each segment received a percentage of the county-wide I278 emissions calculated above. The percentage was based on the vehicle-miles traveled for that segment as compared to the total vehicle-miles traveled for I278 in that county. Once the emissions were calculated for each segment of each county, the segments were broken up into smaller (roughly 30 m) segments and the emissions were divided proportionately into each small segment. Next, the SMOKE temporal profiles were applied. There are three temporal profiles: monthly, day-of-week, and hourly. These profiles apply a fraction of the annual emissions to each hour of each day of the year. The profiles reflect changes in human activity over the course of the year, week, and day.

The total number of 30 m segments was nearly 1700. Each segment was specified as an emissions source for the plume component of the model. These emissions were subtracted from the three-dimensional emission file used by the host model to avoid double-counting of emissions. This “background” file (the file with all emissions except mobile emissions from I278) was created as follows. Each segment of I278 was assigned to its corresponding grid cell. The emissions for each grid cell for each hour were then aggregated. Then, the original gridded CMAQ emission file was read in. For each grid cell that contained some portion of I278, the roadway emissions corresponding to that grid cell were removed from the gridded CMAQ emissions.

3.2 Receptor Locations

The following considerations were used in placing the receptors for post-processing the model outputs. First, the receptors should be located along one of the busiest stretches of the roadway. Second, the receptors should be located such that the spatial variability in concentrations could be captured. The largest spatial variabilities are expected when the winds are perpendicular to the roadway. Thus, we chose a section of the roadway that was not only busy but also exhibited significant curvature, increasing the likelihood of locating receptors in the along-wind direction.

Several sets of receptors were placed along the selected section of the roadway. Figure 3 shows a line sketch of the highway with the receptor transects marked. There are 29 sets of receptors. The receptors in each transect are placed perpendicularly to the roadway at 10, 20, 30, 40, 50, 100, 200, 300, 400, and 500 m from the center of the roadway in both directions. Each transect is about 300 m apart. The section of I278 along which receptors are placed begins in Queens after the intersection of I278 with the Long Island Expressway/I495 and with Route 25. It includes the Triborough Bridge in Manhattan and the last transect is located just before I278 intersects Interstates 87 and 895 in the Bronx. Figure 3 also identifies 5 transects that are used in the discussion of results below.

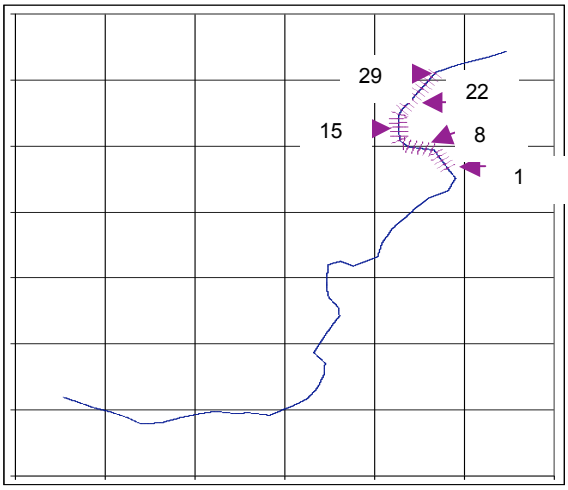

Fig. 3. Locations of 29 receptor transects along a section of I278 in Queens and Manhattan. The 5 transects identified in the figure (Transects 1, 8, 15, 22 and 29) are used for presenting the model results.

4. RESULTS

In this section, we show across-roadway concentration profiles of CO for selected hours and receptor transects. Although benzene was also simulated, the profiles for benzene are similar to those for CO and are not shown here. The results are shown for Transect 1, Transect 8, Transect 15, Transect 22 and Transect 29 (see Figure 3 for the locations of these transects) for hours during which the maximum CO perturbation (from the background or grid-cell value) was simulated for each transect. The spacing between each of these transects is about 2.1 km. Because the wind flow is not exactly perpendicular to the roadway and the freeway direction curves around (see Figure 3), there are generally no clearly defined upwind and downwind sides of the roadway; nevertheless, we define below the upwind side as the side of the roadway that has the lower concentrations and the downwind side as the one that has the greater concentrations.

Transect 1 is in Queens just after the intersection of I278 with Route 25 (Queens Boulevard). Figure 4 shows the concentration profiles across the roadway at this location at 6 pm local time (EDT) on July 12, 1995. The blue line represents the grid-cell averaged CO concentration from a grid model only simulation (i.e., in a separate CMAQ simulation, all sources, including mobile sources on I278 were treated in the grid model). All the receptor points fall in the same grid cell (each grid cell is 4 km by 4 km), so there is only one value for the grid-cell averaged concentration. The red circles are the CO concentrations from the plume-in-grid simulation in which the I278 mobile sources are treated with the embedded puff model in CMAQ.

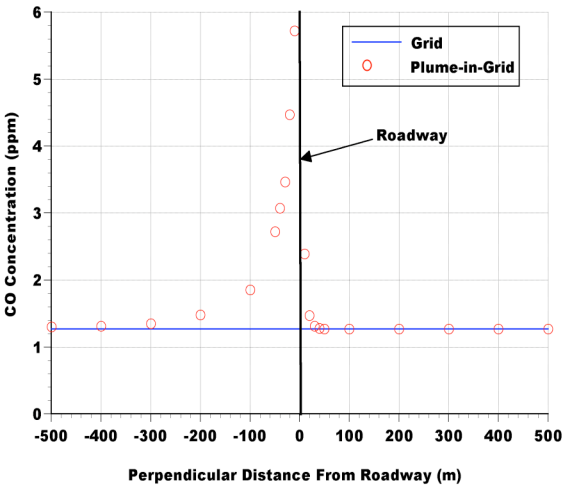

Fig. 4. Across-roadway CO concentration profile for Transect 1 at 6 pm local time on July 12, 1995.

From Figure 4, we see that the CO concentrations are greater southwest of the roadway (left side of the figure) than northeast of the roadway (right of the roadway) because the wind is blowing from the north. The peak CO concentration is nearly 6 ppm at 10 m from the center of the roadway, more than 4 times the grid-cell value of about 1.3 ppb. The concentration drops very rapidly upwind and it is about equal to the urban background concentration at 40 m from the center of the roadway; downwind, it drops rapidly to about 4.5 ppm and 3.5 ppm at 20 m and 30 m from the roadway, respectively. At 300 m from the roadway, the concentration is only slightly larger than the grid-cell value.

Figure 5 shows the results for Transect 8 at 8 am local time on July 12, 1995. This transect is approximately at the location where I278 intersects and joins the Grand Central Parkway. The results are qualitatively similar to those for Transect 1 except that the difference between the upwind (left side of the figure) and downwind (right side of the figure) sides of the roadway is not as clearly defined as in the previous case. The peak CO concentration of nearly 10 ppm at 10 m from the center of the roadway is slightly more than 4 times the grid-cell value of about 2.4 ppm. On the downwind side, the concentrations drop exponentially with increasing distance from the roadway, reaching background levels at about 300 m from the roadway. On the upwind side, the CO

concentrations drop to the urban background level within about 100 m.

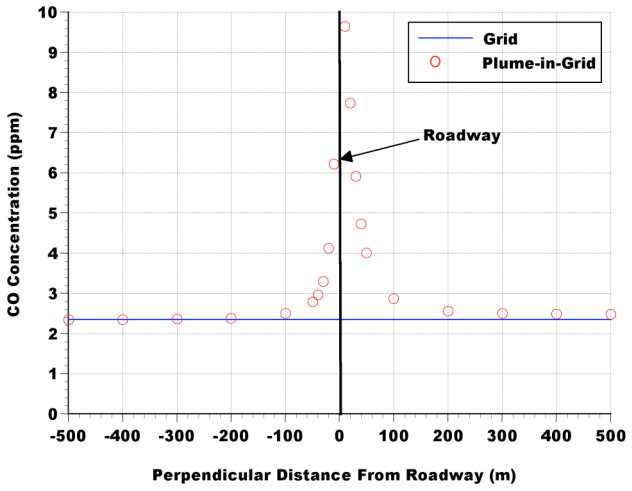

Fig. 5. Across-roadway CO concentration profile for Transcect 8 at 8 am local time on July 12, 1995.

Transect 15 is located just after I278 becomes the Triborough Bridge and enters the outskirts of Manhattan over Wards Island Park. Figure 6 shows the results for this transect at 12 noon on July 13, 1995. The peak CO concentration of 38 ppm at 10 m from the roadway is more than 7 times the grid-cell value of 5 ppm, but drops rapidly to background levels at 200 m from the roadway on the downwind side and at 100 m from the roadway on the upwind side.

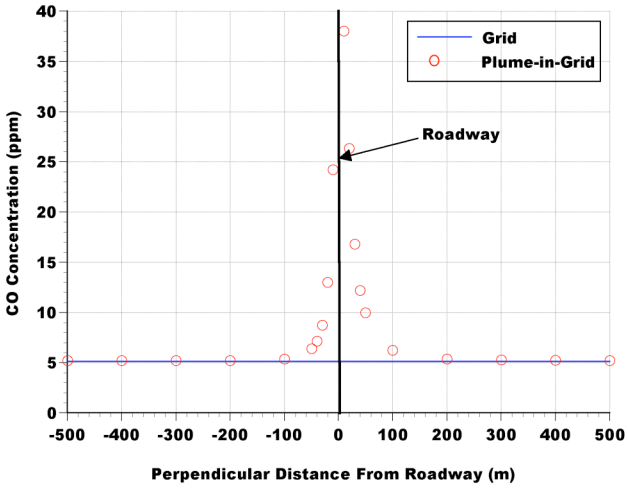

Fig. 6. Across-roadway CO concentration profile for Transect 15 at 12 pm local time on July 13, 1995.

The next transect presented here (Transect 22) is on the Triborough Bridge portion of I278 just over Randalls Island Park. Figure 7 shows the across-roadway CO concentration profile for this transect at 7 am local time on July 13, 1995. The peak CO concentration near the roadway is 26 ppm, about 5 times the grid-cell value. The concentrations drop to about 7 ppm at 500 m from the roadway center on the downwind side. It drops to the background level of 5 ppm within 200 m from the roadway center on the upwind side.

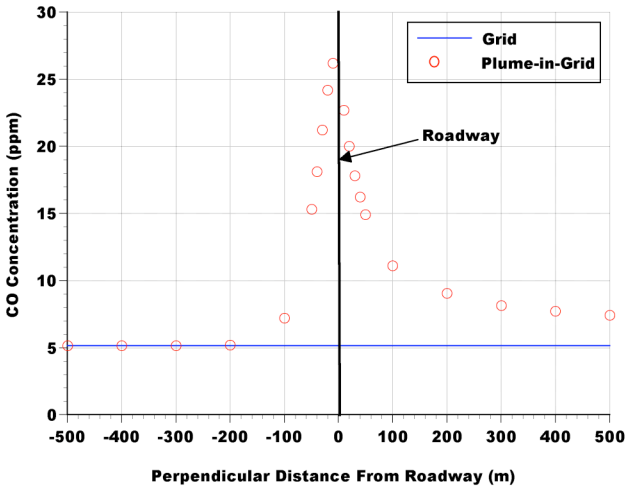

Fig. 7. Across-roadway CO concentration profile for Transect 22 at 7 am local time on July 13, 1995.

The last transect (Transect 29) is at the interchange of I278 with I87, where I278 becomes the Bruckner Expressway and enters the Bronx. The results for this transect at 8 am on July 13, 1995 are shown in Figure 8. The peak CO concentration at 10 m from the roadway is about 23 ppm, more than a factor of 4 higher than the grid-cell value. The concentration drops to the background level of 5 ppm within 200 m from the roadway center; however, the concentration drops only to 9 ppm at 500 m on the downwind side, still nearly a factor of two higher than the background level.

The results presented here are qualitatively consistent with measurements made by Zhu et al. (2002a; 2002b) on two different freeways in the Los Angeles area in the summer and fall of 2001. They found that peak CO concentration levels near the freeways were up to 10 times larger than background levels and dropped exponentially to background levels within 300 m of the roadway.

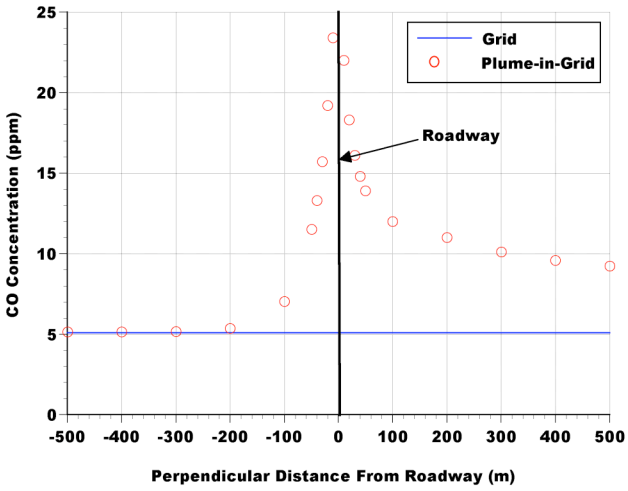

Fig. 8. Across-roadway CO concentration profile for Transect 29 at 8 am local time on July 13, 1995.

5. SUMMARY

This proof-of-concept study has shown that it is possible to adapt available modeling tools to conduct subgrid-scale modeling of toxic air pollutants for estimating population exposure to these species.

This study focused on one type of source, namely vehicles, and assumed that the emitted species (CO and benzene) were unreactive. Also, for practical reasons, the application of the model presented here used an existing data base available to us for the eastern United States. However, there were no roadway measurements available to directly evaluate the model, and we could only perform a qualitative comparison with measurements made in Southern California.

The next step is to extend this modeling approach to other sources, and to use the prototype model developed here for a variety of species with their atmospheric chemistry. The model can be applied to other regions of the country, such as Southern California, Houston, TX or the Raleigh-Durham area, NC, where measurements of air toxics are available to conduct a quantitative model performance evaluation.

6. REFERENCES

BTS, 2007. http://www.bts.gov/publications/national_transportation_atlas_database/2006

Ching, J., J. Herwehe and J. Swall, 2006. On joint deterministic grid modeling and sub-grid variability conceptual framework for model evaluation, *Atmos. Environ.*, **40**, 4935-4945.

Isakov, V. and A. Venkatram, 2006. Resolving neighborhood scale in air toxics modeling: a case study in Wilmington, CA, *J. Air Waste Manage. Assoc.*, **56**, 559-568.

Karamchandani, P., C. Seigneur, K. Vijayaraghavan and S.-Y. Wu, 2002. Development and application of a state-of-the-science plume-in-grid model, *J. Geophys. Res.*, **107**, 4403-4415.

Karamchandani, P., C. Seigneur and K. Vijayaraghavan, 2004. Development and testing of an advanced Plume-in-Grid PM model, *AWMA Visibility Specialty Conference*, October 26-29, 2004, Asheville, NC.

Karamchandani, P., K. Vijayaraghavan, S.-Y. Chen, C. Seigneur and E.S. Edgerton, 2006a. Plume-in-grid modeling for particulate matter, *Atmos. Environ.*, **40**, 7280-7297.

Karamchandani, P., K. Vijayaraghavan, S.-Y. Chen and C. Seigneur, 2006b. Plume-in-grid modeling for PM and mercury, *5th Annual CMAS Conference*, October 16-18, 2006, Chapel Hill, NC.

Seigneur, C., B. Pun, K. Lohman and S.-Y. Wu, 2002. Air Toxics Modeling, Report A-42-1, http://www.crcao.com.

Seigneur, C., B. Pun, K. Lohman and S.-Y. Wu, 2003. Regional modeling of the atmospheric fate and transport of benzene and diesel particles, *Environ. Sci. Technol.*, **37**, 5236-5246.

Seigneur, C., 2004. Air toxics modeling: state of the science, current challenges and future prospects, *Coordinating Research Council (CRC) Mobile Source Air Toxics Workshop*, 1-2 December 2004, Scottsdale, Arizona.

Touma, J.S., V. Isakov, J. Ching and C. Seigneur, 2006. Air quality modeling of hazardous pollutants: current status and future directions, *J. Air Waste Manage. Assoc.*, **56**, 547-558.

Vijayraghavan, K., P. Karamchandani and C. Seigneur, 2006. Plume-in-grid modeling of summer air pollution in Central California, *Atmos. Environ.*, **40**, 5097-5109.

Zhu, Y., W.C. Hinds, S. Kim and C. Sioutas, 2002a. Concentration and size distribution of ultrafine particles near a major highway, *J. Air Waste Manage. Assoc.*, **52**, 1032-1042.

Zhu, Y., W.C. Hinds, S. Kim, S. Shen and C. Sioutas, 2002b. Study of ultrafine particles near a major highway with heavy-duty diesel traffic, *Atmos. Environ.*, **36**, 4323-4335.

DEVELOPMENT OF LOCAL-SCALE AND SUBGRID-SCALE MODELS IN POLYPHEMUS

Irène Korsakissok*, Vivien Mallet, Bruno Sportisse
CEREA, Joint Research Laboratory, École Nationale des Ponts et Chaussées / EDF R&D, France

1 THE GAUSSIAN PLUME AND PUFF MODELS

We will briefly present the Gaussian plume and puff models that have been implemented into Polyphemus platform [Mallet et al., 2007]. An evaluation of the models was carried out thanks to comparison with Prairie Grass experiments. It will be presented with an emphasis on comparison between different parameterizations for standard deviations. In the following sections, the Gaussian plume model is described. The Gaussian puff model is based on the same equations and parameterizations, except that it also involves diffusion in the downwind direction.

1.1 Form of the Gaussian plume model

There are many underlying assumptions when using a Gaussian plume model (see Arya [1999]), particularly :

1. Continuous emission from the source so that the material is spread out in the form of a steady plume between the source and the farthest receptor.
2. Steady-state flow and constant meteorological conditions.
3. No wind shear in the vertical direction.
4. Strong enough winds to make turbulent diffusion in the downwind direction negligible in comparison to advection.

In that context, the concentration C at a given point is given by the formula:

$$C(x,y,z) = \frac{Q}{2\pi\sigma_y\sigma_z\bar{u}} \exp\left(-\frac{(y-y_s)^2}{2\sigma_y^2}\right) \times \left[\exp\left(-\frac{(z-H)^2}{2\sigma_z^2}\right) + \exp\left(-\frac{(z+H)^2}{2\sigma_z^2}\right)\right]. \quad (1)$$

Here, Q is the source emission rate, given in mass per second, $\bar{u}$ is the mean wind velocity, and σ_y and σ_z are the Gaussian plume parameters. The coordinate y refers to horizontal direction "crosswind", that is, at right angle to the plume axis which is also the wind axis, and y_s is the source coordinate in that direction. The coordinate z refers to the vertical coordinate, and H is the plume centerline height above ground.

*Corresponding author: irene.korsakissok@cerea.enpc.fr

1.2 Plume reflections

The purpose of the last term in equation 1 is to take into account the reflection of the plume on the ground. In the case of inversion, the reflection at the inversion layer can similarly be taken into account. Reflections on the ground and on the inversion layer (noted z_i) are only taken into account when the plume touches them:

- Ground reflection occurs when $\sigma_z > H$
- Reflection on the inversion height occurs when $H + \sigma_z > z_i$

where z_i is the inversion height, which is supposed to be equal to boundary height during daytime and to 0 during nighttime. If inversion height is equal to 0, there is no inversion and hence no reflection on it.

1.3 Far field model

When the plume fills the boundary layer, it is supposed to have been sufficiently mixed to be vertically homogeneous. The concentration formula is then:

$$C(x,y,z) = \frac{Q}{2\pi\sigma_y z_i \bar{u}} \exp\Big(-\frac{(y-y_s)^2}{2\sigma_y^2}\Big). \quad (2)$$

The transition to the far field model is made when $\sigma_z > 1.5\ z_i$.

1.4 Dispersion parameterization schemes

For an estimate of the dispersion parameters σ_x, σ_y and σ_z, empirical parameterization schemes are widely used. Many schemes have been proposed, most of them giving the dispersion parameters as functions of the downwind distance and stability class, and based on a few diffusion experiments. In Polyphemus, three parameterizations are proposed. Two of them are based on a discrete description of the atmospheric boundary layer: the Briggs formulae based on Pasquill stability scheme, or, alternatively, the Doury formulae. The third one is based on similarity theory. It uses functions of the wind velocity fluctuation and of other boundary layer parameters like the Monin-Obukhov length, the mixing height and the friction velocity.

1.4.1 Briggs formulae

The Briggs formulae are based on the Pasquill-Turner stability classes and on the Prairie Grass ex-

periment. This parameterization is born from an attempt to synthesize several widely used parameterization schemes by interpolating them for open country and for urban areas. These formulae apply to a distance from the source up to 10 km and may be extended up to 30 km. They are particularly recommended for urban areas.

1.4.2 Doury formulae

An alternative parameterization is the Doury model described in Doury [1976]. It is widely used in French models and recommended by the French Nuclear Energy Agency (CEA). This parameterization has been developed for the specific application of radionuclides dispersion, and fitted on radionuclides measurements. The experimental field was wider than the Prairie Grass field. The formulae use only two stability situations: one for normal dispersion, corresponding to daytime or nighttime with a wind speed greater than 3 meters per second, and one for low dispersion, corresponding to nighttime with low wind speed. The standard deviations are given in both cases in the general form:

$$\sigma_y = (A_h t)^{K_h} \sigma_z = (A_z t)^{K_z} \tag{3}$$

where t is the transfer time since release time. In the case of a steady-state plume $t = x/u$ where x is the distance from the source and u is the wind speed.

1.4.3 Similarity theory

If more accurate meteorological measurements are available, σ_x, σ_y and σ_z can be estimated using the standard deviations of wind velocity fluctuations in downwind direction σ_u, crosswind direction σ_v and in vertical direction σ_w. Whereas in the two other parameterizations, σ_x had to be taken equal to σ_y, it is here specifically computed. Following Irwin [1979] dispersion coefficients are computed in the form:

$$\left(\begin{array}{l} \sigma_x = \sigma_u \; t \; F_x \\ \sigma_y = \sigma_v \; t \; F_y \\ \sigma_z = \sigma_w \; t \; F_z \end{array} \right) \tag{4}$$

where t is the time in seconds, and F_y and F_z are functions of a set of parameters that specify the characteristics of the atmospheric boundary layer. Their forms are determined from experimental data. Various expressions of F_y and F_z have been proposed (e.g. Irwin [1979], Weil [1988]). In Polyphemus, wind standard deviations will be computed according to Hanna [1984]. For vertical standard deviation σ_w an alternative parameterization from Weil [1988] is proposed.

1.5 Other processes

Additionnal processes can be taken into account, but will not be developed here since they are not used in the presented work. One can cite:

- Plume rise,
- radioactive and biological decay,
- dry deposition with Chamberlain and Overcamp model (see Arya [1999]),
- wet scavenging,
- dispersion for particulate matter.

2 Evaluation with Prairie Grass Experiment

2.1 Presentation of the Experiment

The Prairie Grass experiment has become a standard database used for many short range models evaluation. The experiment took place in O'Neil, Nebraska, during summer 1956. The site was a flat terrain of short cut grass. A continuous plume of SO_2 was released, without plume rise, near the ground (at 0.46 m). Measurements where taken on five arcs at 50, 100, 200, 400 and 800m from the source. There were nearly 70 trials.

2.2 Comparison with other Gaussian Models

The comparisons are discussed using scatter diagrams as well as the statistical performance measures described below, which include the fractional bias (FB), the geometric mean bias (MG), the normalized mean square error (NMSE), the geometric variance (VG), the fraction of predictions within a factor two of observations (FAC2) and the correlation coefficient (Corr).

Table 1: Statistics for several Gaussian models: comparison of maximum arc concentration for simulation and observation – 43 trials in Prairie Grass Experiment. Results for ADMS, AERMOD and ISCST3 come from McHugh et al. [2001].

Model	FB	NMSE	MG	Corr	FAC2
Obs	0.00	0.00	1.00	1.00	1.00
ADMS	0.56	3.62	–	0.64	0.46
AERMOD	0.00	1.87	–	0.75	0.76
ISCST3	0.06	1.76	–	0.72	0.62
Briggs	0.0	1.83	1.23	0.78	0.74
Doury	0.46	4.47	1.05	0.42	0.27
Similarity	-0.08	1.25	0.72	0.82	0.61

Table 1 shows that all models compare very well with experimental data, except Polyphemus with Doury parameterization and ADMS. AERMOD, ISCST3 and Polyphemus with Briggs formula show good results, as the Prairie Grass results were used

directly in the formulation of their plume spread parameters. Polyphemus with similarity theory shows good results, comparable to those of AERMOD and ISCST3. All indicators are within an acceptable range, and the correlation is the highest of all models presented here (82%). Figure 1 shows the scatter diagram for Polyphemus with similarity theory.

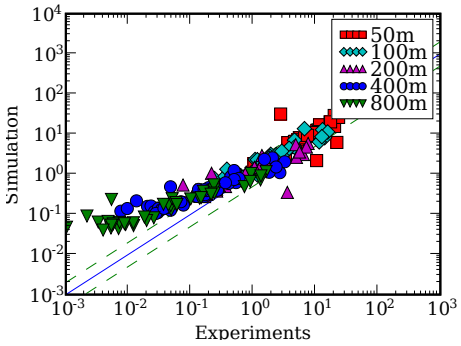

Figure 1: Scatter plot of maximum arc concentrations for observations and simulations with similarity theory parameterization. Concentrations are normalized by source rate Q and the unit is $\mathrm{mg{\cdot}s^{-1}/g{\cdot}s^{-1}}$. Prairie Grass experiment, 43 trials.

Those results provide a first validation of Polyphemus Gaussian models. One should note that the same results were obtained both with the plume model and with the puff model, where the continuous source has been discretized into a series of puffs and the simulation has been made on a period long enough to reach the stationary state. Hence, these models can be taken as a basis for further modeling, such as the plume-in-grid model development.

3 The Plume in Grid model

The principle of a plume-in-grid model is to couple a Gaussian Puff model with an Eulerian model in order to describe the dispersion of a plume emitted by a point source in a more accurate way than the sole Eulerian model. These models are generally used to deal with chemically reactive plumes, and have been proved useful to model ozone chemistry in particular (see Viyaraghavan et al. [2006] for example). However, there is hardly any example of study for this kind of models in passive cases. The plume-in-grid model developed in Polyphemus is currently used to deal with passive tracers, and has been tested on the ETEX experimental data. Hence, the aim of the present study is twofold:

1. To investigate whether or not the use of a plume-in-grid model is relevant in passive cases, and if possible, to issue recommandations concerning its use (which parameterizations to choose, and which criteria for puff feedback) and applications,
2. To validate the method used in coupling the Gaussian and Eulerian models before extending it to the reactive case.

3.1 Model description

The plume-in-grid model developed in Polyphemus is able to couple an Eulerian and a Gaussian puff model, provided that those models have a minimal C++ interface. It is currently tested with Polyphemus Gaussian puff model and with the Eulerian model Polair3D.

The two models run independantly from one another. They only need to exchange some information with the plume-in-grid model:

Meteorological data. They have been computed on the Eulerian grid and can be either interpolated at the puff center or taken as the value of the cell where puff is located. They are then used by the Gaussian model.

Puff data. At each time step, the puff center cell is determined from the puff center coordinates (see section 3.2). A test is made to see whether the puff has to be injected. If it is the case, the puff is erased, and is transfered into the Eulerian model (see section 3.4).

Concentrations are computed as the sum of the Eulerian and Gaussian contributions. Hence, there are three different parts in a simulation that takes into account one point source:

1. When the Eulerian contribution is equal to zero, and concentrations are computed with the Gaussian formula,
2. A period, between the first and last puff injection into the Eulerian model when both Eulerian and Gaussian concentrations are added,
3. After the last puff feedback, there is only the Eulerian contribution.

3.2 Coordinates

Since Polair3D uses longitude and latitude coordinates, and a Gaussian model uses Cartesian coordinates, it is necessary to be able to do the transformation. The Cartesian coordinates are the coordinates in the tangent plane of the point source. If the distance between the source and the puff center becomes too great, the error in assimilating the puff trajectory to that in the plane cannot be neglected anymore. The transformation formulae are:

$$\begin{pmatrix} dx \\ dy \end{pmatrix} = \begin{pmatrix} R\, cos\phi\, d\lambda \\ R\, d\phi \end{pmatrix} \quad (5)$$

Where x, y, z are the point Cartesian coordinates, λ is the longitude and ϕ is the latitude, in radians, and R is the Earth radius in meters.

3.3 The "increasing sigma" method

The parameterizations to compute standard deviations assume that the meteorological data is stationary and homogeneous, which is not the case in the plume-in-grid model. Hence, if at time t_1 the puff has a size σ_1 which has been computed with formulae for unstable cases, and at time $t_2 = t_1 + \Delta t$ meteorological conditions become stable (for example if night has fallen), the new puff size σ_2 will be computed with meteorological data at time t_2, which can lead to the unrealistic situation where $\sigma_2 < \sigma_1$. This is illustrated by Figure 2.

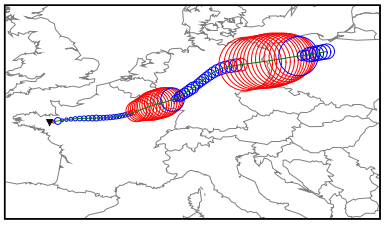

Figure 2: Size evolution of one puff. The puff is represented at each time step at its present location (in latitude/longitude), and the circle radius is proportional to σ_y. Puffs are drawn in red when it is daytime and in blue during nighttime. The green line is the puff center. The black triangle is the ETEX source location.

To deal with this problem, at time t_2, we compute the virtual time t'_1 corresponding to the time when the puff would have reached the size σ_1 if the meteorological conditions had been stationary and equal to those at time t_2. The new puff size σ_2 is then computed at time $t'_2 = t'_1 + \Delta t$ and corresponds to a realistic puff growth during Δt.

This applies to horizontal standard deviations. For vertical standard deviations, we only insure that the puff size cannot decrease.

3.4 Puff feedback criteria and method

3.4.1 Criteria

There are two possible criteria to feed the puff back to the Eulerian model:

- If the puff horizontal size has reached the cell size
- If the time after emission exceeds a chosen value

The puff size is $C_y \times \sigma_y$, where C_y is a coefficient usually taken equal to 4.

3.4.2 Feedback methods

Since the puff horizontal size is supposed to span at most one cell horizontally at the moment of injection, it is fully injected in the cell where its center is located. However, the puff covers vertically several cells. The puff vertical extent is computed in a similar way than the horizontal size, that is, $C_z \times \sigma_z$ (C_z usually equal to 4). The puff quantity has then to be divided into the number of cells vertically covered, and injected into them, supposing that the concentration is uniform in the puff. Note that the puff will not be reinjected into cells above the boundary layer height.

4 Evaluation with ETEX experiment

4.1 The ETEX case

This experiment has taken place at the European scale on October 1994. A passive tracer, SF_6, was released continuously during twelve hours at a given location in the west of France (location is shown Figure 2). There were about 3000 measurement stations all over Europe. Measurement were made during one week after release.

The simulation was made during seven days with a time step equal to ten minutes. The simulation grid covers all Europe and its cell width is $0.5625°$ in longitude and latitude.

4.2 Model results

Results for several plume-in-grid simulations are presented. Sections 4.2.1 and 4.2.2 are meant to compare the injection criteria. Section 4.2.3 analyses the effect of the plume-in-grid model on results.

4.2.1 Reinjection based on puff size

Table 2 shows the statistical results on all stations for the whole simulation with puff size criterion. The results have been compared for all available parameterizations to compute standard deviations, as well as for Polair3D without plume-in-grid.

Although the use of plume-in-grid seems to better the bias, the correlations are all rather lower than with the Eulerian model alone, except for Doury parameterization. This comes from the fact that puff size meets reinjection criterion very late or never for all parameterizations except Doury. This is illustrated by Figure 3: after a while σ_y becomes constant with Doury parameterization since puff has been injected into the Elerian model, whereas it

keeps growing in the other cases.

Table 2: ETEX experiment statistics on 168 stations for five plume-in-grid configurations: (1) similarity theory with Weil parameterization, (2) similarity theory with Hanna parameterization, (3) Doury, (4) Briggs with rural formulae, (5) Briggs with urban formulae.

Model	Mean	FB	NMSE	Corr	FAC2
Obs	0.21	0.00	0.00	1.00	1.00
Polair3D	0.44	0.72	24.87	0.61	0.19
1	0.18	-0.15	64	0.31	0.02
2	0.18	-0.13	61.7	0.35	0.02
3	0.20	-0.05	6.86	0.66	0.19
4	0.11	-0.57	20.14	0.51	0.02
5	0.08	-0.81	26.3	0.37	0.02

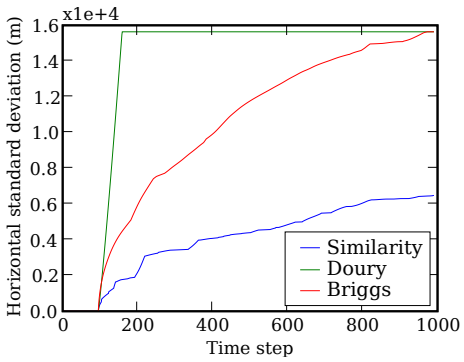

Figure 3: Evolution of σ_y in time for one puff for the different parameterizations. It is computed using the "increasing sigma" method. Time step is 600 s. When the puff has been injected into the Eulerian model, σ_y becomes constant.

4.2.2 Reinjection based on time

In Table 3, the same parameterizations are used but the reinjection time is now always set to twelve hours after puff release. When injection time tends toward 0, plume-in-grid results tend toward Polair3D results, so setting a lower injection time should mechanically improve the results for several parameterizations. The results presented here are better than the previous ones, except for Doury parameterization where they do not change. Results for Briggs parameterization with rural formulae are now better than without plume-in-grid. However, the similarity theory parameterizations still give substantially lower correlations. The only difference between parameterizations in that case is the number of vertical levels covered by the puff at reinjection time. As shown Figure 4, the puff vertical extent with similarity theory is about 1.5 times the extent with Doury parameterization at time step 168, which corresponds to the reinjection time. This might be improved by extending the increasing sigma method to vertical standard deviations, which has not been attempted yet.

Table 3: ETEX experiment statistics on 168 stations for five plume-in-grid configurations. Reinjection time is 12 hours after puff release.

Model	Mean	FB	NMSE	Corr	FAC2
Obs	0.21	0.00	0.00	1.00	1.00
Polair3D	0.44	0.72	24.87	0.61	0.19
1	0.42	0.67	48.38	0.36	0.15
2	0.42	0.67	48.38	0.36	0.15
3	0.20	-0.05	6.86	0.66	0.19
4	0.21	-0.001	7.32	0.63	0.18
5	0.17	-0.22	8.917	0.51	0.17

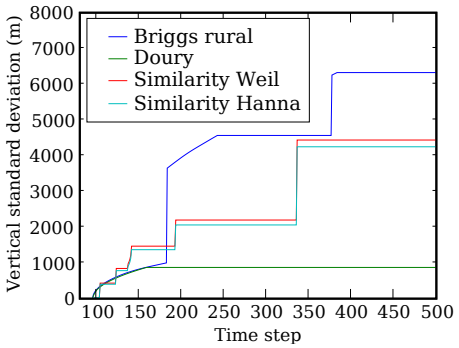

Figure 4: Evolution of σ_z in time for the different parameterizations, for one puff. The evolution has been plotted without imposing the injection time. An injection time of 12 hours after emission corresponds to time step 168.

4.2.3 Analysis of the plume-in-grid results

We present an analysis for different stages of the simulation, and several stations, since local improvements can be overlooked in global statistical results. Figure 5 shows that three days after emission, the plume is split in two parts. Plume-in-grid gives substantially lower concentrations than Polair3D in the smaller part of the plume (eastern Europe).

We can distinguish three different zones in the domain:

1. Near the source: north of France. The puffs have not been injected yet (nearest injection occurs in north-east of France). The splitting occurs shortly after injection.
2. North-west of Europe, where the greater concentrations are observed. Plume-in-grid models improve results at stations in this zone.
3. East of Europe. Concentrations are smaller. Polair3D tends to underestimate concentrations, and plume-in-grid model gives even lower

concentrations. When puff injection is late in the simulation (with size criterion), there are no concentrations modeled in this part.

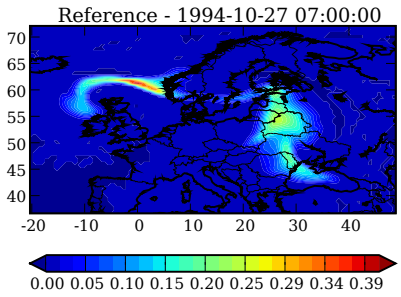

(a) Polair3D (no plume-in-grid)

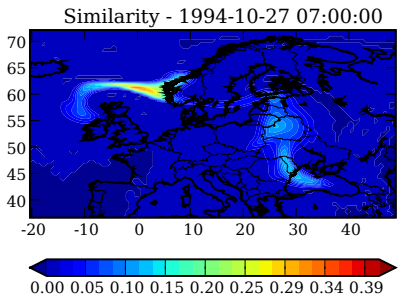

(b) Plume-in-grid with similarity theory

Figure 5: ETEX simulation: concentration on the domain, three days and a half after beginning, with and without plume-in-grid. Plume-in-grid simulation was performed with similarity theory. Injection time was set to 12 hours after emission. Unit is $\mathrm{ng \cdot m^{-3}}$.

Figure 6 shows the difference of Figure of Merit in Time (FMT) between plume-in-grid and Polair3D. The FMT corresponds to the overlap area at a given station between simulated and observed time series. This figure shows clearly that plume-in-grid is better at stations in the main plume trajectory (north-west of Europe) but is worse than Polair3D alone in the other parts of the plume. The Eulerian model also tends to overestimate concentrations near the source, since diffusion is too important. For these stations, plume-in-grid results are generally better for all parameterizations.

4.3 Conclusion

The results presented tend to show that plume-in-grid models should be used very carefully since they can provide a wide range of results, depending on the chosen parameterization and feedback method. However, when computing concentrations on the whole domain and imposing a maximum time for puff feedback, results are promising and can be better than the Eulerian model alone. Also, a finer analysis on stations shows that even if global performances can be lower, the use of plume-in-grid tends to improve the results near the source and in the main plume trajectory.

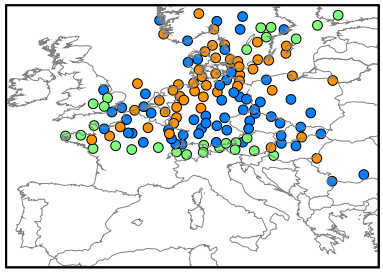

Figure 6: Difference of FMT for all stations between plume-in-grid model (with similarity theory) and Polair3D alone. Red: fmt for plume-in-grid is greater. Blue: fmt for plume-in-grid is lower. Green: no difference (stations where no significant concentrations are modeled).

REFERENCES

Arya, S. (1999). *Air pollution meteorology and dispersion*. Oxford University press.

Doury, A. (1976). Une méthode de calcul pratique et générale pour la prévision numérique des pollutions véhiculées par l'atmosphère. Technical Report 4280, CEA, France.

Hanna, S. (1984). Applications in air pollution modeling. In Niewstadt, F. and van Dop, H., editors, *Atmospheric turbulence and Air Pollution modeling*. D. Reidel Publishing Co.

Irwin, J. (1979). Scheme for estimating dispersion parameters as a function of release height. Technical Report 600:4-79-062, EPA.

Mallet, V., Quélo, D., Sportisse, B., Ahmed de Biasi, M., Debry, É., Korsakissok, I., Wu, L., Roustan, Y., Sartelet, K., Tombette, M., and Foudhil, H. (2007). Technical Note: The air quality modeling system Polyphemus. *Atmos. Chem. Phys. Discuss.*, 7(3):6,459–6,486.

McHugh, C., Carruthers, D., Higson, H., and Dyster, S. (2001). Comparison of model evaluation methodologies with application to ADMS 3 and US models. *Int. J. Env. and Pollution*, 16(1-6).

Viyaraghavan, K., Karamchandani, P., and Seigneur, C. (2006). Plume-in-grid modeling of summer air pollution in central california. *Atmos. Env.*, 40.

Weil, J. (1988). Dispersion in the convective boundary layer. In Venkatram, A. and Wyngaard, J., editors, *Lectures on Air Pollution modeling*. American Meteorological Society.

DEVELOPMENT AND APPLICATION OF A COMPUTATIONALLY-EFFICIENT MADRID 2 FOR SIMULATING SECONDARY ORGANIC AEROSOL

Ping Liu and Yang Zhang*
Department of Marine, Earth, and Atmospheric Sciences,
North Carolina State University, Raleigh, NC, USA

Betty Pun
Atmospheric & Environmental Research, Inc., San Ramon, CA, USA

1. INTRODUCTION

Simulating organic aerosols posts a challenge in aerosol and climate modeling due to the complicated physical and chemical processes associated with their formation and fate. The Model of Aerosol Dynamics, Reaction, Ionization, and Dissolution 2 (MADRID 2) that has been incorporated into the U.S. EPA Models-3/Community Multiscale Air Quality (CMAQ) (referred to as CMAQ-MADRID 2) uses a mechanistic representation for secondary organic aerosol (SOA) formation that simulates an external mixture of hydrophilic and hydrophobic aerosols. However, MADRID 2 is computationally expensive in its original formulation, limiting its 3-D applications.

2. SUMMARY

A box model version of MADRID2 that is computationally efficient (reducing the total CPU cost by 60 to 97% with less than 20% deviation from benchmark results) (referred to as MADRID 2-FAST) has been recently developed for long-term 3-D model simulations and real-time air quality forecasting. In this study, MADRID2-FAST is being implemented into CMAQ (referred to as CMAQ-MADRID 2-FAST). Both CMAQ-MADRID 2 and CMAQ-MADRID 2-FAST are being applied to the 1999 Southern Oxidants Study episode for the period of 12-28 June 1999 with a 32-km horizontal resolution. The simulated concentrations of chemical species (e.g., ozone (O_3), fine particles ($PM_{2.5}$), and PM chemical composition) will be compared with the observations from several routine monitoring networks and special field studies. The accuracy and computational efficiency of CMAQ-MADRID 2-FAST will be evaluated against CMAQ-MADRID 2.

ACKNOWLEDGEMENTS AND DISCLAIMER

This work is performed under the National Science Foundation Award No. Atm-0348819, and the Memorandum of Understanding between the U.S. Environmental Protection Agency (EPA) and the U.S. Department of Commerce's National Oceanic and Atmospheric Administration (NOAA) and under agreement number DW13921548.

This work constitutes a contribution to the NOAA Air Quality Program.

**Corresponding author:* Yang Zhang, Department of Marine, Earth and Atmospheric Sciences, Campus Box 8208, NCSU, Raleigh, NC 27695; phone number: (919) 515-9688; fax number: (919) 515-7802; e-mail: yang_zhang@ncsu.edu

THE AIR QUALITY MODELING SYSTEM POLYPHEMUS

Vivien Mallet[1,*], Denis Quélo[2], Bruno Sportisse[3], Meryem Ahmed de Biasi[1], Édouard Debry[4], Irène Korsakissok[4], Lin Wu[1], Yelva Roustan[4], Karine Sartelet[4], Marilyne Tombette[4] and Hadjira Foudhil[4]

[1] INRIA, CLIME project (common project ENPC - INRIA) [France]

[2] IRSN [France]

[3] ENPC, laboratory CEREA (joint research laboratory ENPC - EDF R&D), CLIME project [France]

[4] ENPC, laboratory CEREA (joint research laboratory ENPC - EDF R&D) [France]

INTRODUCTION

Polyphemus [Mallet et al., 2007] is an air quality modeling platform which aims at covering the scope and the abilities of modern air quality systems. With two Gaussian models and two Eulerian models, it handles applications from local scale to continental scale for multiple pollutants: passive tracers, radionuclides, photochemical pollutants, aerosols, and (in development) heavy metals and persistent organic pollutants.

The system is designed to deal with model coupling, ensemble forecast, data assimilation and other advanced simulation methods. The platform-oriented design (with multiple models) and the availability of alternative parameterizations enable to generate ensemble forecasts. On top of the model (and independently of the models), the advanced simulation methods are implemented as drivers in which a model is a black box.

The system is developed at École Nationale des Ponts et Chaussées (one of the top French engineering schools, member of the Paris Institute of Technology), INRIA (French National Institute for Research in Computer Science and Control) and Électricité de France R&D. It is supported by IRSN (Institut de Radioprotection et de Sûreté Nucléaire) and INERIS (French National Institute for Industrial Environment and Risks) which are the main French governmental institutes for atmospheric risk management. It is an open source system distributed at `http://cerea.enpc.fr/polyphemus/`.

1 DESIGN: TECHNICAL DESCRIPTION

1.1 Structure

Polyphemus is built around four bases:

1. data management, data processing facilities (input/output operations, coordinate transformations, interpolations, ...);
2. physical parameterizations (cloud attenuation, turbulence closure, parameterizations for aerosols dynamics, ...);
3. numerical solvers for advection, diffusion and chemistry (including multiphase chemistry);
4. high-level methods (chiefly data assimilation, ensemble forecast and model coupling), in which a chemistry-transport model is simply viewed as a function.

The data management and the physical parameterizations are gathered in dedicated libraries, called SeldonData and AtmoData (the latter being dedicated to atmospheric-related operations). They are the prominent components in the preprocessing steps. In fact, a set of programs process the raw input data (meteorological data, land use data, chemical data, ...), primarily through interpolation, and make calls to physical parameterizations. As far as possible, all fields are computed in this preprocessing stage. This means that the physical formulation in use for a simulation is mostly defined in preprocessing steps.

After preprocessing, the numerical model only performs the time integration of the advection-diffusion-reaction equation. Hence the numerical model includes very few physical calculations.

The numerical model is embedded in a driver. A driver controls the model and interacts with it. The model is seen as a black box with an interface to manage it. For instance, the most simple driver performs a forward simulation with basic calls to the model (initialization and time integration over one time step). Complex drivers are implemented for data assimilation (where, for instance, the driver computes the analysis), for model coupling (the driver then manages two models) and other advanced simulation methods.

The last stage is postprocessing, with visualization, statistical analysis, comparison with measurements, ... It is mostly handled by the Polyphemus library AtmoPy.

The overall structure is shown in Figure 1.

1.2 Technical Choices

Polyphemus relies on three computer languages: C++, Python and Fortran 77.

C++ is the main language. It brings advanced object-oriented abilities. These abilities are needed in order to implement convenient data management

[*] *Corresponding author:* Vivien.Mallet@inria.fr

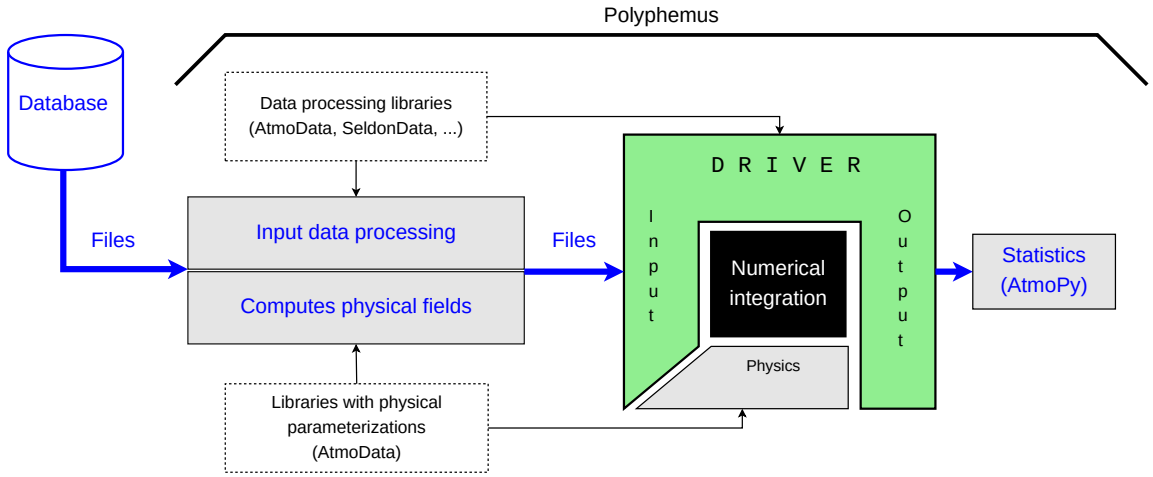

Figure 1: Polyphemus overall work flow. Data is first processed with dedicated C++ libraries (mainly SeldonData and AtmoData). The library AtmoData [Mallet and Sportisse, 2005b; Njomgang et al., 2005] provides in addition most physical parameterizations needed in the preprocessing step. The preprocessing steps output most coefficients of the reactive-transport equation. The numerical model (e.g., an Eulerian chemistry-transport model) integrates in time this equation, and a driver manages the numerical model (e.g., to perform data assimilation). For postprocessing (statistics, visualization, ...), Python scripts and the Python library AtmoPy are used.

and to deal with complex models. The models are C++ objects, that is, black boxes with a clear interface to interact with them and to control them. The drivers therefore manage C++ objects. They are implemented independently of the models; they only require that a model has the right interface, whatever the underlying processes and numerical schemes may be.

Fortran 77 is used for historical reasons and for automatic differentiation (generation of tangent linear model and adjoint model). Python, which is another powerful object-oriented language, covers the other needs, that is, process management and postprocessing (statistics, visualization).

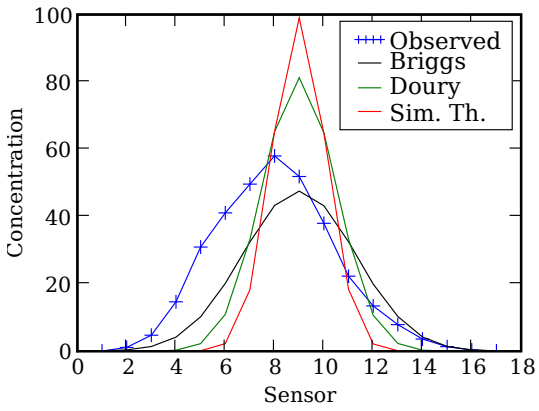

Figure 2: Simulated concentrations and measurements at 100 m from the source and during one Prairie Grass experiment. The simulated concentrations are computed using Briggs formulae (based on Pasquill classes diagnosed with Turner [1969]), Doury formula [Doury, 1976] and a parameterization derived from similarity theory.

2 Contents and Illustrations

2.1 The Models

Polyphemus includes several models:

- a Gaussian plume model;
- a Gaussian puff model;
- an Eulerian chemistry-transport model called Polair3D [Boutahar et al., 2004], relevant up to continental scale;
- an Eulerian chemistry-transport model called Castor, also relevant up to continental scale, clone written in C++ of the gaseous version of Chimere [Schmidt et al., 2001].

The first two models are applied to dispersion at local scale, possibly with radioactive or biological decay. Both models have a gaseous and an aerosol version. They include several alternative physical parameterizations for dispersion coefficients (Figure 2), dry deposition and wet deposition. The Gaussian puff model is also used in a plume-in-grid model (with any of the two Eulerian models).

The Eulerian model Polair3D is derived in three versions: a passive version, a version with gas-phase chemistry (most of the time, radionuclides or

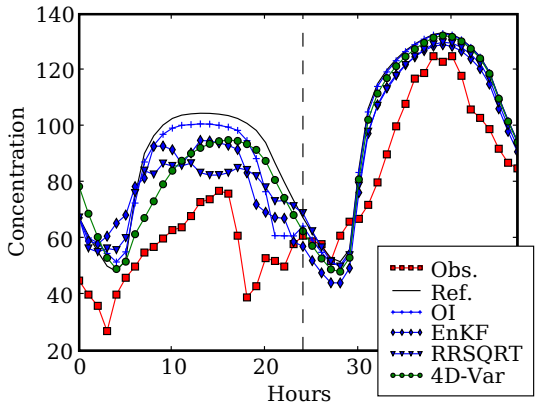

Figure 3: Time evolution of ozone concentrations at EMEP station Montandon, for the reference simulation (without assimilation), the simulation with assimilation (optimal interpolation, OI; ensemble Kalman filter, EnKF; reduced-rank square root Kalman filter, RRSQRT; 4D-Var). The dotted vertical lines delimits the assimilation period.

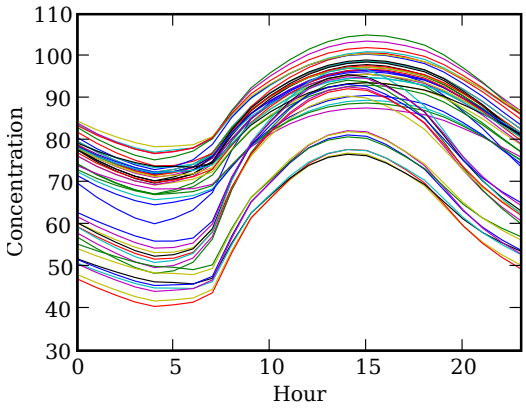

Figure 4: Ozone daily profiles of 48 models built in Polyphemus. The concentrations are in $\mu g\,m^{-3}$ and are averaged over Europe (at ground level) and over summer 2001.

photochemistry) and a version with aerosol dynamics. It may be used with RACM [Stockwell et al., 1997] or RADM 2 [Stockwell et al., 1990] for photochemistry. The aerosol module SIREAM [Debry et al., 2007] is plugged into the aerosol version. Polair3D was evaluated in several studies [e.g., Quélo et al., 2007; Mallet and Sportisse, 2004; Sartelet et al., 2007]. It may be differentiated, essentially with automatic differentiation, to generate a tangent linear model and an adjoint model [Mallet and Sportisse, 2004, 2005a].

2.2 Data Assimilation

Four data assimilation algorithms are available in Polyphemus: optimal interpolation, ensemble Kalman filter [Evensen, 1994], reduced-rank square root Kalman filter [Heemink et al., 2001] and 4D-Var [Le Dimet and Talagrand, 1986]. The Eulerian models Castor and Polair3D have a sufficient interface for sequential algorithms (optimal interpolation and Kalman filters). Only Polair3D may be used in combination with the 4D-Var driver since the latter requires an adjoint model.

A comparison of the four assimilation methods is under progress (Figure 3).

2.3 Ensemble Forecast

At preprocessing stage, most physical fields are computed and they essentially define the physics of a simulation. The model itself only performs the time integration. Polyphemus enables to use alternative parameterizations and alternative data sources in the preprocessing steps. Hence an ensemble of simulations with many different physical choices may be built. This generates a multimodel ensemble [Mallet and Sportisse, 2006b] (Figure 4).

Other ensemble capabilities are available, chiefly Monte Carlo simulations (with a dedicated driver) and model aggregation (“superensembles”, machine learning, . . .) [Mallet and Sportisse, 2006a].

Conclusion

The air quality modeling system Polyphemus is a platform with several chemistry-transport models, with the ability to manage data from several sources, with alternative physical parameterizations for many fields, with several advanced simulation methods (data assimilation, ensemble forecast, model coupling). The multiple choices and methods in the system justify its name: the roots of Polyphemus, in Ancient Greek, mean “multiple speeches”.

Polyphemus structure is open, with the ability to host new models, new physical parameterizations, new advanced simulation methods, . . . Its technical bases enable a strong flexiblity, especially in the management of models. Polyphemus is used in research, but also for in operational forecasts. It is an open source system distributed at `http://cerea.enpc.fr/polyphemus/`. Further details may be found in Mallet et al. [2007] and on Polyphemus website.

References

Boutahar, J., Lacour, S., Mallet, V., Quélo, D., Roustan, Y., and Sportisse, B. (2004). Development and validation of a fully modular platform for numerical modelling of air pollution: POLAIR. *Int. J. Env. and Pollution*, 22(1/2):17–28.

Debry, E., Fahey, K., Sartelet, K., Sportisse, B.,

and Tombette, M. (2007). Technical Note: A new SIze REsolved Aerosol Model (SIREAM). *Atmos. Chem. Phys.*, 7:1,537–1,547.

Doury, A. (1976). Une méthode de calcul pratique et générale pour la prévision numérique des pollutions véhiculées par l'atmosphère. Technical Report 4280, CEA, France.

Evensen, G. (1994). Sequential data assimilation with a nonlinear quasi-geostrophic model using Monte Carlo methods to forecast error statistics. *J. Geophys. Res.*, 99(C5):10,143–10,162.

Heemink, A. W., Verlaan, M., and Segers, A. J. (2001). Variance reduced ensemble Kalman filtering. *Mon. Wea. Rev.*, 129:1,718–1,728.

Le Dimet, F.-X. and Talagrand, O. (1986). Variational algorithms for analysis and assimilation of meteorological observations: theoretical aspects. *Tellus*, 38A:97–110.

Mallet, V., Quélo, D., Sportisse, B., Ahmed de Biasi, M., Debry, É., Korsakissok, I., Wu, L., Roustan, Y., Sartelet, K., Tombette, M., and Foudhil, H. (2007). Technical Note: The air quality modeling system Polyphemus. *Atmos. Chem. Phys. Discuss.*, 7(3):6,459–6,486.

Mallet, V. and Sportisse, B. (2004). 3-D chemistry-transport model Polair: numerical issues, validation and automatic-differentiation strategy. *Atmos. Chem. Phys. Discuss.*, 4:1,371–1,392.

Mallet, V. and Sportisse, B. (2005a). A comprehensive study of ozone sensitivity with respect to emissions over Europe with a chemistry-transport model. *J. Geophys. Res.*, 110(D22).

Mallet, V. and Sportisse, B. (2005b). Data processing and parameterizations in atmospheric chemistry and physics: the AtmoData library. Technical Report 2005-12, CEREA.

Mallet, V. and Sportisse, B. (2006a). Ensemble-based air quality forecasts: A multimodel approach applied to ozone. *J. Geophys. Res.*, 111.

Mallet, V. and Sportisse, B. (2006b). Uncertainty in a chemistry-transport model due to physical parameterizations and numerical approximations: An ensemble approach applied to ozone modeling. *J. Geophys. Res.*, 111(D1).

Njomgang, H., Mallet, V., and Musson-Genon, L. (2005). AtmoData scientific documentation. Technical Report 2005-10, CEREA.

Quélo, D., Krysta, M., Bocquet, M., Isnard, O., Minier, Y., and Sportisse, B. (2007). Validation of the Polyphemus platform: the ETEX, Chernobyl and Algeciras cases. *Atmos. Env.* In press.

Sartelet, K. N., Debry, E., Fahey, K., Roustan, Y., Tombette, M., and Sportisse, B. (2007). Simulation of aerosols and related species over Europe with the Polyphemus system. Part I: model-to-data comparison for 2001. *Atmos. Env.* Accepted for publication.

Schmidt, H., Derognat, C., Vautard, R., and Beekmann, M. (2001). A comparison of simulated and observed ozone mixing ratios for the summer of 1998 in Western Europe. *Atmos. Env.*, 35:6,277–6,297.

Stockwell, W. R., Kirchner, F., Kuhn, M., and Seefeld, S. (1997). A new mechanism for regional atmospheric chemistry modeling. *J. Geophys. Res.*, 102(D22):25,847–25,879.

Stockwell, W. R., Middleton, P., Chang, J. S., and Tang, X. (1990). The second generation regional acid deposition model chemical mechanism for regional air quality modeling. *J. Geophys. Res.*, 95(D10):16,343–16,367.

Turner, D. B. (1969). Workbook of atmospheric diffusion estimates. Technical Report 999-AP-26, US EPA, Washington, DC.

Presented at the 6th Annual CMAS Conference, Chapel Hill, NC, October 1-3, 2007

PREDICTION OF AIR QUALITY OVER TOKYO METROPOLITAN AREA BY USING THE JCAP II AIR QUALITY SIMULATION SYSTEM

Satoru Chatani*, Tazuko Morikawa, Midori Ashizaki, Hideki Tashiro and Hitoshi Kunimi
Japan Petroleum Energy Center, Minato-ku, Tokyo, Japan

Hiroshi Hirai
Japan Automobile Research Institute, Tsukuba, Ibaraki, Japan

Satoshi Yamazaki
Toyota Central R&D Labs., Inc., Nagakute, Aichi, Japan

1. INTRODUCTION

Air quality in Japan is getting improved, but some observational stations cannot meet the Japanese national air quality standard for some pollutants such as NO_2 and PM. Additional strategies may be necessary to improve air quality further. In order to consider new regulations on emission sources, it is desirable to evaluate future potential effectiveness of them by conducting air quality simulations. However, currently no official procedure and modeling system for the evaluation of new regulations are available in Japan. Japan Clean Air Program (JCAP) II developed the air quality simulation system to satisfy such kind of needs. In this paper, outlines and results of the prediction of effectiveness of the new regulation on vehicle emissions by using the JCAP II air quality simulation system are presented.

2. METHOD

The JCAP II air quality modeling system consists of the air quality model, the meteorological model and the emission inventory database. Details of each component and simulation cases conducted in this study are described in the following subsections.

2.1 Air Quality Model

CMAQ (Community Multi-scale Air Quality modeling system) (Byun and Ching, 1999) ver. 4.6 was used to simulate pollutant concentrations. Target domains in this study are shown in Fig. 1. Three nested domain, Asian, Japan G1 and Japan G2, were used. Asian domain covers eastern and southeastern Asian countries to take the transboundary transport of pollutants to Japan into account. Japan G1 domain covers the most part of Japan, and Japan G2 domain focuses on Kanto region including Tokyo metropolitan area where is facing the severest air pollution in Japan. Number of meshes is 114 x 114 x 24 in Asian domain, 68 x 64 x 27 in Japan G1 domain, and 40 x 44 x 33 in Japan G2 domain. Size of meshes is 64 x 64km in Asian domain, 16 x 16km in Japan G1 domain, and 4 x 4km in Japan G2 domain. The horizontal coordinate is based on the polar stereographic coordinate and the vertical coordinate is based on the sigma-z coordinate. Capabilities dealing with both coordinates in CMAQ were added by modifying source codes.

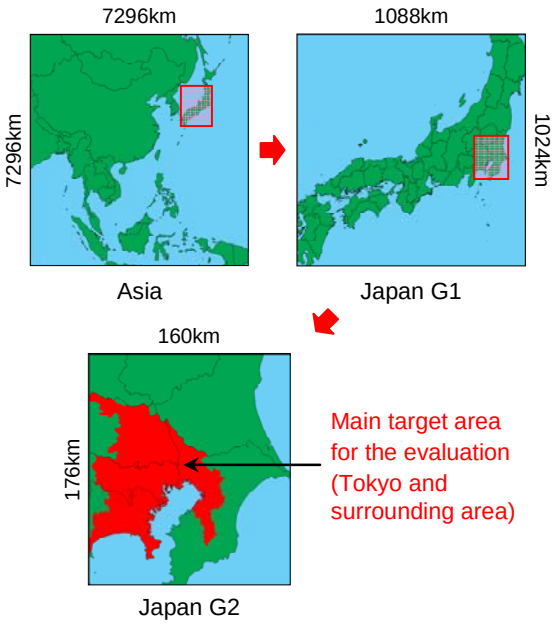

Fig. 1. Target domains of the simulation.

*Corresponding author: Satoru Chatani, Japan Petroleum Energy Center, Sumitomo Shin-Toranomon bldg., 3-9 Toranomon 4-choume, Minato-ku, Tokyo 105-0001; e-mail: schatani@mosk.tytlabs.co.jp, URL: http://www.pecj.or.jp/english/jcap/index_e.html.

2.2 Meteorological Model

RAMS (Regional Atmospheric Modeling System) (Pielke et al., 1992) ver. 4.4 was used to simulate meteorological field. Target domains are one-mesh larger than those of CMAQ shown in Fig. 1. ECWMF (European Centre for Medium-Range Weather Forecast) operational analysis data was utilized for the initial and boundary condition. MCIP developed by Sugata et al. (2001) was used to convert RAMS output to CMAQ meteorological input data.

2.3 Domestic Vehicle Emission data

We developed the JCAP II vehicle emission estimation model. Running emissions, cold-start emissions, evaporative emissions (running loss, hot soak loss, diurnal breathing loss), road dust and tire wear are estimated. This model follows methodologies similar to EMFAC and MOBILE. The estimation of running emissions is briefly described below as an example.

Running emissions are calculated by multiplying emission factors by traffic amounts. Basic emission factors have been prepared for each vehicle category and model year. They are corrected by considering influences of deterioration, speed, temperature and humidity on emissions. Traffic amounts were based on the census data developed by the government. They were allocated to each link on the digital road map, and were divided into meshes by GIS. In this study, resolution of meshes was about 10 x 10 km for whole Japan, and 1 x 1km within the Japan G2 domain including Tokyo metropolitan area.

Nowadays, vehicle exhaust emitted from new vehicles is getting cleaner, and high emissions from “high-emitters” (e.g. malfunctioned or tampered vehicles) have been concerned. In order to examine the status of high-emitters in the real world, the measurement at the roadside was conducted in which emissions from each vehicle were measured by Remote Sensing Devices (RSD). As an example, Fig. 2 shows average values and distributions of NO emissions measured by RSD. Vehicles with high emissions were found as the age is getting old. The ratio of high-emitters was derived by counting vehicles with emissions exceeding the threshold given for each pollutant. This ratio and the emission factors of high-emitters were used to estimate emissions from high-emitters.

Target years of estimating vehicle emissions were 1999 and 2015. For year 1999, data already available were utilized. For year 2015, emission

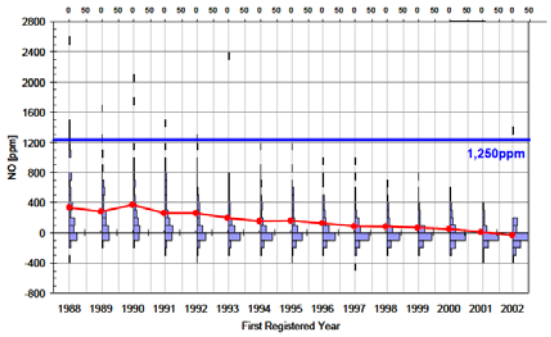

Fig. 2. Average values and distributions of NO emissions measured by RSD.

factors and the distribution of model years were changed. Changes in other factors related to emissions (e.g. vehicle mileages traveled or new road constructions) were not considered.

2.4 Other Emission Data

The emission inventory developed by Kannari et al. (2007) was used for Japanese domestic sources except for vehicles. Emissions from large stationary combustion sources, small combustion sources, ships, airplanes, machineries, stationary evaporative NMVOC sources, ammonia emission sources, incinerators, open burnings, and biogenic NMVOC are included in this inventory. Resolution of the data is 1km x 1km.

REAS (Regional Emission inventory in ASia, Ohara et al., 2007) ver. 1.1 was used for anthropogenic sources in Asian countries. GEIA emission data (Granier et al., 2005) was used for biogenic NMVOC and biomass burning in Asian countries.

Target year of all emission data except for domestic vehicles is 2000 and they were used in all of simulation cases in this study. Therefore, influences of future changes in emissions except for domestic vehicles and in the transboundary transport are not evaluated in this study.

2.5 Simulation Cases

Six simulation cases shown in Table 1 were conducted in this study. Case 1 is the case for reproducing the current status of air quality using vehicle emission data for year 1999. Estimated vehicle emission data for year 2015 was used in Case 2-4. Replacement with newer vehicles and regulations which have been already determined were considered in Case 2. A more stringent emission regulation was assumed in Case 3, and

NOx and PM emission factors of diesel vehicles in year 2008 and subsequent years were reduced by 50% and 25%, respectively. A regulation on high-emitters was assumed in Case 4, and the ratio of high-emitters was set to be zero. Vehicle emission data for year 1999 was used in Case 5 and 6, but the boundary concentration of the Japan G1 domain was changed to -50% and +50%, respectively, in order to examine influences of the transboundary transport.

Table 1. Simulation cases.

	Vehicle emission	Boundary conc.
Case 1	Year 1999	
Case 2	Year 2015	
Case 3	Year 2015 + New regulation from year 2008 [1]	
Case 4	Year 2015 + Excluding HE [2]	
Case 5	Year 1999	-50% in Japan G1
Case 6	Year 1999	+50% in Japan G1

1 : -50% and -25% of diesel NOx and PM EF from year 2008

2 : HE : High-emitters

The target period of the simulations is from Nov. 1st to Dec. 10th, 1999. Daily average concentrations on Dec. 10th in the target area shown in Fig. 1 were mainly used for the evaluation in this study.

3. RESULTS

3.1 Estimated Emission

Estimated weekday vehicle NOx and SPM (equivalent to PM_7) emissions summed over the target area for Case 1-4 are shown in Fig. 3. In year 2015, vehicle NOx and SPM emissions were estimated to be reduced from year 1999 by 44% and 45%, respectively, only by the replacement with newer vehicles and current regulations. An additional regulation would reduce NOx emission further by 8%, but excluding high-emitters may be more effective than new regulations. Fraction of road dust and tire wear became larger in SPM emission, and influences of a new regulation on vehicle exhaust were negligible.

NOx and SPM emissions from all sources summed over the target area for Case 1-4 are shown in Fig. 4. 53% of NOx and 67% of SPM (40% from vehicle exhaust only) were estimated to be emitted from vehicles. Fraction of vehicles would be significantly reduced unless emissions from sources except for vehicles are reduced as well.

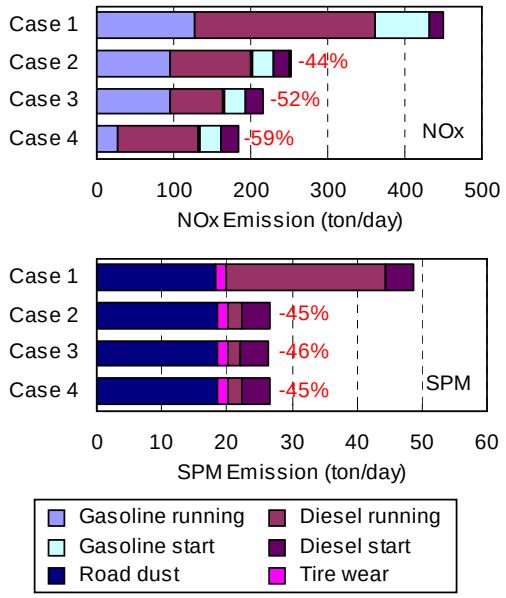

Fig. 3. Estimated weekday vehicle NOx and SPM emissions summed over the target area.

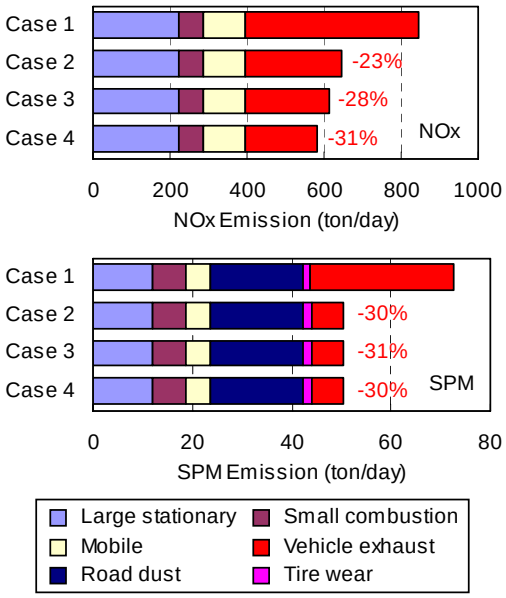

Fig. 4. Estimated NOx and SPM emissions from all sources summed over the target area.

3.2 Performance of the Air Quality Simulation

Time series of observed and simulated NO_2 and SPM concentrations in Case 1 at Kanda and Shirokane observational stations are shown in Fig. 5. Both stations are located in the center of Tokyo metropolitan area. Hourly variation of NO_2 was reproduced well but slightly underestimated especially in the evening of Dec. 10th, 1999. SPM was underestimated for most hours and peaks were not reproduced well.

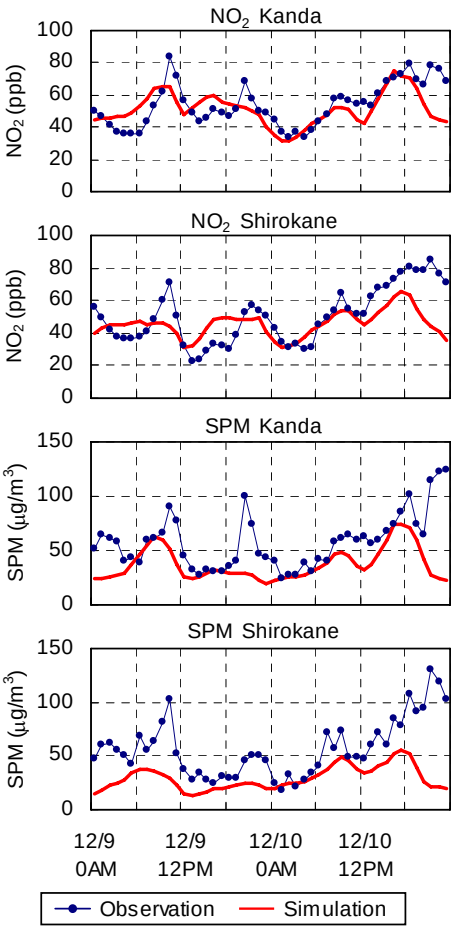

Fig. 5 Time series of observed and simulated NO_2 and SPM concentration.

Mean normalized bias (MNB) and mean normalized error (MNE) of daily NO_2 and SPM concentration on Dec. 10th, 1999 were calculated using observation data at about 200 stations located in the target area. Table 2 shows calculated MNB and MNE. MNB and MNE of NO_2 are reasonable, although the performance for SPM should be improved.

Table 2. MNB and MNE of daily NO_2 and SPM concentration on Dec. 10th, 1999 in the target area.

	MNB	MNE
NO_2	-17.9%	21.1%
SPM	-51.4%	53.3%

3.3 Predicted Pollutant Concentrations

Predicted daily NO_2 and SPM concentration on Dec. 10th, 1999 averaged over the target area in Case 1-4 are shown in Fig. 6. NO_2 and SPM concentrations were reduced in a similar way as NOx and SPM emissions. However, reduction ratios of concentrations were smaller than emissions. The reasons were examined in the following subsections.

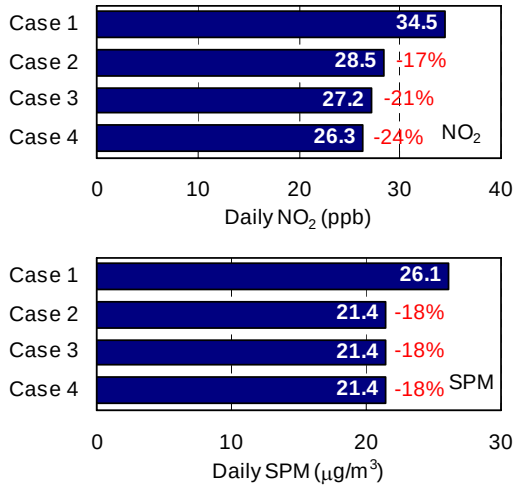

Fig. 6. Predicted NO_2 and SPM concentrations on Dec. 10th, 1999 averaged over the target area.

3.4 Predicted Concentrations of PM Components

Predicted daily concentration of PM components on Dec. 10th, 1999 averaged over the target area in Case 1-4 are shown in Fig. 7. EC, OC and other PM2.5, which are mainly primary emitted components, were reduced in Case 2-4. However, SO_4^{2-}, NO_3^-, NH_4^+, which are mainly

secondary components, were not reduced so much. On the other hand, secondary components varied greatly in Case 5 and 6 in which the boundary concentration of the Japan G1 domain was changed. Therefore, secondary components may be much influenced by the transboundary transport. In future, fraction of secondary components is expected to increase, and strategies over wide area including several countries would be necessary to reduce them.

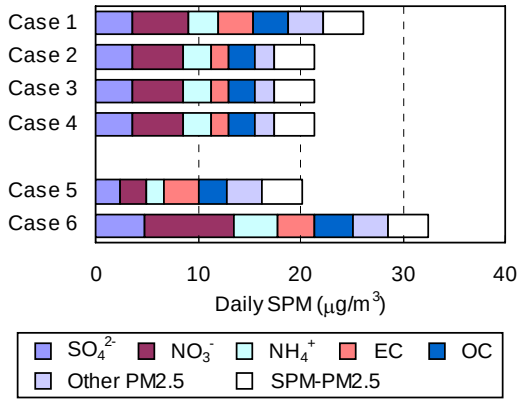

Fig. 7. Predicted concentrations of PM components on Dec. 10th, 1999 averaged over the target area.

3.5 Relation between NOx Emissions and Pollutant Concentrations

Predicted NOx, NO_2 and O_3 concentration in Case 1-6 were plotted against total NOx emissions in the target area in Fig. 8. NOx concentration was headed toward zero as NOx emission decreases. Similar trend was found in NO_2 concentration, but reduction was not as much as NOx. O_3 increased as NOx emission decreases. Most of NOx is emitted as NO, and titrated by O_3 and converted to NO_2 in the atmosphere. Therefore, NO_2 and O_3 concentrations are inversely correlated against NOx emission. In addition, NO concentration in the metropolitan area is so high that a part of NO is not oxidized by O_3 and remains in the atmosphere. NO_2 in the metropolitan area is what is called "O_3 sensitive". That is why reduction of NO_2 concentration was smaller than NOx. Moreover, NO_2 and O_3 concentration in Case 5 and 6 varied even though the same emission data as Case 1 was used. O_3 may be greatly influenced by the transboundary and hemispheric transport (Akimoto, 2003), and that may affect on the NO - O_3 titration. Strategies on the hemispheric transport of O_3 are important from the viewpoint of NO_2 in the metropolitan area.

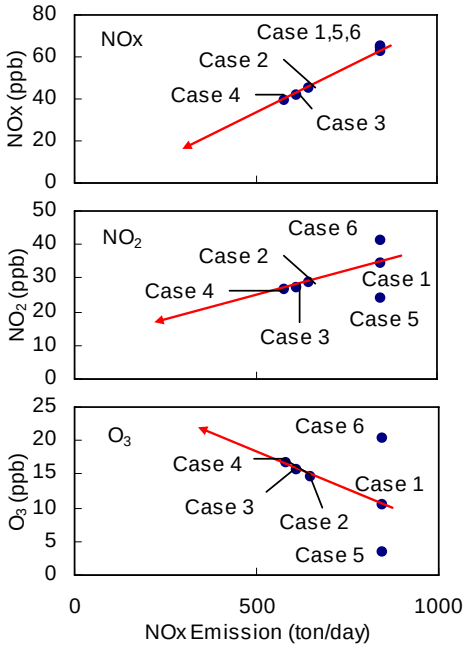

Fig. 8. Predicted NOx, NO_2 and O_3 concentration plotted against total NOx emission in the target area.

4. SUMMARY

By using the JCAP II air quality simulation system, current and future vehicle emissions were estimated by considering the replacement with newer vehicles and regulations, and pollutant concentrations were simulated. As a result, following future directions toward improving air quality in Tokyo metropolitan area were implied.

- Additional regulations on new vehicles may not be effective. High-emitters running in the real-world should be eliminated.
- Reduction of NOx emissions may cause increase of O_3. Overall strategies including NMVOC are important to reduce multiple pollutant concentrations.
- Most of SPM emission would be consisted of road dust and sources except for vehicles.
- Fraction of secondary components in SPM may become larger. The transboundary transport

influences on secondary components of particles and O_3, and even NO_2 in the metropolitan area. Strategies on the transboundary transport are necessary.

It was found that the JCAP II air quality simulation system is a powerful tool for seeking strategies for improving air quality as shown in this paper.

5. ACKNOWLEDGEMENT

This study was done in the Japan Clean Air Program (JCAP) II conducted by Japan Petroleum Energy Center and supported by the Ministry of Economy, Trade and Industry, Japan.

6. REFERENCES

Akimoto, H., 2003: Global air quality and pollution. *Science*, **302**, 1716-1719.

Byun, D. W., and J. K. S. Ching, Eds., 1999: Science algorithms of the EPA Models-3 Community Multiscale Air Quality (CMAQ) Modeling System. EPA-600/R-99/30.

Granier, C., J. F. Lamarque, A. Mieville, J. F. Muller, J. Olivier, J. Orlando, J. Peters, G. Petron, G. Tyndall, and S. Wallens, 2005: POET, a database of surface emissions of ozone precursors. Available on internet at http://www.aero.jussieu.fr/projet/ACCENT/POET.php.

Kannari, A., Y. Tonooka, T. Baba, and K. Murano, 2007: Development of multiple-species 1km x 1km resolution hourly basis emissions inventory for Japan. *Atmos. Environ.*, **41**, 3428-3439.

Ohara, T., H. Akimoto, J. Kurokawa, N. Horii, K. Yamaji, X. Yan, and T. Hayasaka, 2007: An Asian emission inventory of anthropogenic emission sources for the period 1980-2020. *Atmos. Chem. Phys. Discuss.*, **7**, 6843-6902.

Pielke, R. A., W. R. Cotton, R. L. Walko, C. J. Tremback, W. A. Lyons, L. D. Grasso, M. E. Nicholls, M. D. Moran, D. A. Wesley, T. J. Lee, and J. H. Copeland, 1992: A comprehensive meteorological modeling system—RAMS. *Meteorol. Atmos. Phys.*, **49**, 69-91.

Sugata, S., D. W. Byun, and I. Uno, 2001: Simulation of sulfate aerosol in East Asia using Models- 3/CMAQ with RAMS meteorological data, *Air Pollution Modeling and Its Application XIV*, Gryning and Schiermeier eds., 267-275.

Evolution of $PM_{2.5}$ Components in the Long-range Transport Plume accompanied with the Southward Asian Continental Outflow

Ming-Tung Chuang[1] , S-Yuan Joshua Fu[2], Ji-Cheng Carey Jang[3], Pei-Cheng Ni[4], Chang-Chuan Chan[5], Chung-Te. Lee[1]

[1]*Graduate Institute of Environmental Engineering, National Central University Jhongli, Taoyuan, Taiwan*

[2]*Department of Civil and Environmental Engineering, University of Tennessee, Knoxville, Tennessee, U.S.*

[3]*Office of Air Quality Planning and Standards United States Environmental Protection Agency*

[4]*CTCI Corporation, Taipei, Taiwan*

[5] *Institute of Occupational Medicine and Industrial Hygiene, National Taiwan University, Taipei, Taiwan*

1. Introduction

The main media of long-range transport originating from Asia continent is that Asia high pressure system moves eastward or southward. Dignon and Hameed (1998) has pointed out that Asia had become the area that emitted most sulfur globally. The main cause was the sustained increasing consumption of sulfur in China. In the last few years, there have been several publications that observed and estimated the contribution of acid deposition from China on a level from 20% to 50% (Kitada et al., 1992; Ichikawa and Fujita, 1995; Chung et al., 1996; Chang et al., 2000; Holloway et al., 2002).

In this study, the events occur in Taipei by long-range transport from Asian continent have been defined as HPP (Chuang et al., 2007). 53 events were observed in Taipei from March 2002 to February 2005. For HPP and non-HPP days observed air quality at TAS (in Fig. 1) is in Table 1. Especially, $PM_{2.5}$, $PM_{2.5}$ sulfate hourly average concentrations are 54.1 and 12.0 μ g m^{-3} respectively, which are much higher than 22.6 and 4.7 μ g m^{-3} that are observed on non-HPP days. It appears that the influence of pollutants originating from Asian continental outflow to downwind area is very significant.

Table 1. Basic statistics of aerosol characteristics and weather parameters for high pressure pushing (HPP) weather pattern and non-HPP time period from March 2002 to February 2005.

	Monitoring item	Effective hours	Avg.	s.d.	Max.	Min.
HPP	$PM_{2.5}$ (μg m^{-3})	937	54.1	23.8	148.3	6.5
	$PM_{2.5}$ sulfate (μg m^{-3})	819	12.0	7.2	55.1	1.3
	$PM_{2.5}$ nitrate (μg m^{-3})	806	2.6	2.0	14.9	0.4
	$PM_{2.5}$ OC (μg m^{-3})	803	4.5	1.0	13.9	1.0
	$PM_{2.5}$ EC (μg m^{-3})	524	1.7	0.8	8.6	1.0
non-HPP*	$PM_{2.5}$ (μg m^{-3})	8250	22.6	11.4	64.5	5.0
	$PM_{2.5}$ sulfate (μg m^{-3})	7662	4.7	3.5	28.5	0.4
	$PM_{2.5}$ nitrate (μg m^{-3})	6717	1.4	1.1	20.2	0.4
	$PM_{2.5}$ OC (μg m^{-3})	6747	3.5	1.7	18.0	1.0
	$PM_{2.5}$ EC (μg m^{-3})	2142	1.7	1.2	13.9	1.0

*Non-HPP time period is for days excluding June, July, August, and events time defined in Chuang et al. (2007).

2. Study area and monitoring data and model setup

From Figure 1, it is seen that Taiwan is located at the West Pacific, with 200 km wide Taiwan Strait, opposite to southeast of China mainland.

The greater Taipei area is located in the northern Taiwan which is the firstly influenced by long-range transport originating from the north.

In this study, the fifth-generation Pennsylvania State University-National Center for Atmospheric Research Mesoscale Model (MM5, Grell et al., 1994) is utilized to generate meteorological data as input for chemical model. For chemical model, the Models-3 Community Multiscale Air Quality (CMAQ, version 4.4, Byun and Ching, 1999; U.S.EPA, 1999) modeling system is utilized. In order to save computation time and reduce the size of output files, 25-layer output of meteorological model is transformed into 14 layers as inputs for CMAQ.

Basic emission data of domain 1 and domain 2 is from Asian emission database estimated by Streets et al. (2003). In order to reflect rapid economic development in China in the last few years, we refer to Hao and Wang (2005) and Heo and Feng (2005)'s statistics to estimate the anthropogenic growth factor from 2001 to 2004. Yearly growth factors of 1.13 and 1.19 is used for 2001 to 2003 and 2003 to 2004 respectively. Biogenic source is assumed to remain constant. Emissions of domain 3 and domain 4 are from TEDS6.1 (Taiwan Emission Database System for 2003, Fu et al., 2007) which is then spatially and temporally distributed by SMOKE (Houyoux and Vukovich, 1999) to estimates grid/hourly emission rate. It is expected that emission was not fluctuant too much from 2003 to 2004. Besides, it is noted that TEDS is the only emission database available in Taiwan.

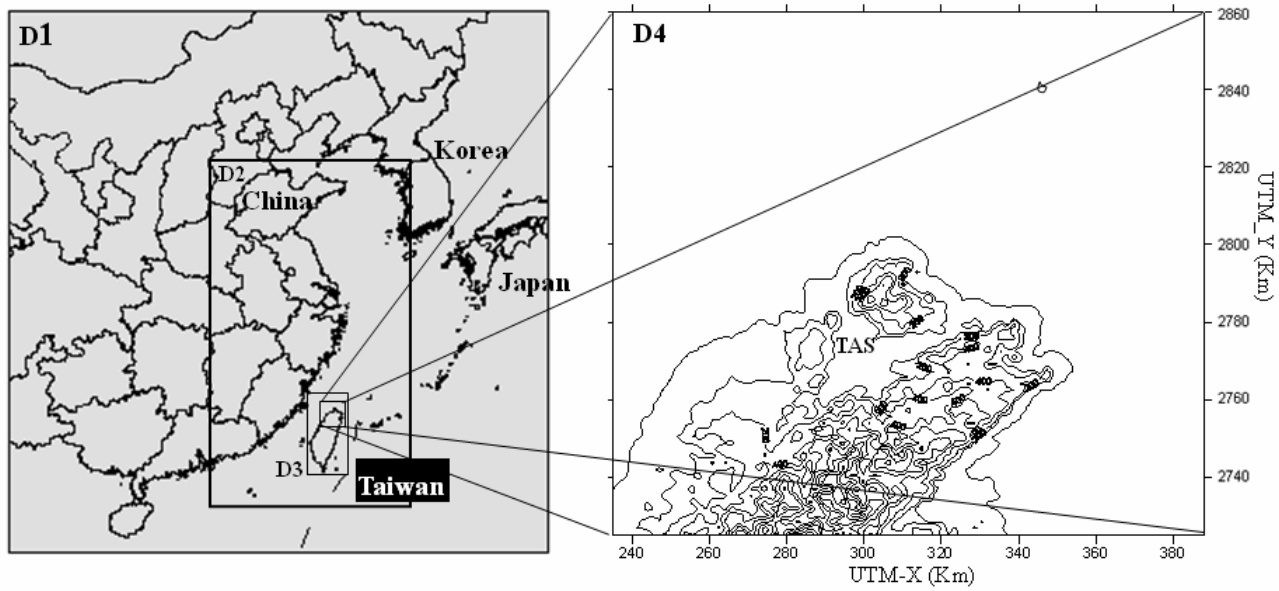

Fig. 1. Model simulation domains (D1 to D4) and geographical locations of the Taipei aerosol supersite (TAS).

3. Results and discussion

We select backward trajectory from 16:00 (at TAS, number 31 in Figure 2) on 20 December 2004. On that day, a high pressure system and $PM_{2.5}$ plume moved southward simultaneoutly as shown in Figure 3. Figure 4 characterizes the variation of percentile of $PM_{2.5}$ components along the path of moving plume shown in Figure 2.

4.1 $PM_{2.5}$ nitrate

As $PM_{2.5}$ plume moves southward, $PM_{2.5}$ nitrate concentration decreases. The ratio of $PM_{2.5}$ nitrate to $PM_{2.5}$ decreases during long-range transport from 25% in Shanghai to 1% on the waters of north Taiwan. In the morning on 20 December, $PM_{2.5}$ nitrate is only about 1 μ g m^{-3}. Kin and Park (2001) found that NO_3^- was quite low in fine mode particles transported from Asia continent. This explains that the lifetime of NO_3^- in fine mode particles is very short. It is known that NO_2 can react with NO_3 radical and form N_2O_5 at night and then N_2O_5 may react with H_2O and form HNO_3 (Waston et al., 1994). However, N_2O_5 and NO_3 radical are only a few pptv at night on 19 December (unshown). When $PM_{2.5}$ nitrate decreases, HNO_3 apparently increases. It is concluded that HNO_3 is mainly evaporated from $PM_{2.5}$ nitrate. The high volatility of NH_4NO_3 makes itself dissociate into HNO_3 and NH_3 at higher temperature (Stelson and Seinfeld, 1982). NH_3 reacted with H_2SO_4 transformed from SO_2 would form NH_4HSO_4 or $(NH_4)_2SO_4$. It can be related to raise of $PM_{2.5}$ sulfate along the transport of $PM_{2.5}$ plume.

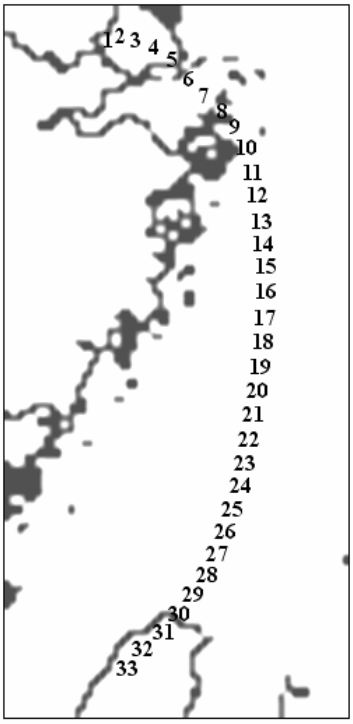

Fig.2. Hourly backward trajectory path of southward $PM_{2.5}$ plume

4.2 $PM_{2.5}$ sulfate

SO_2 can either react with HO_2 and form HSO_3- or oxidize to SO_3. HSO_3^- and SO_3 can react with H_2O_2 and H_2O (unshown, relative humidity was around 80% in the plume) respectively and form H_2SO_4, which reacts with NH_3 (evaporated from $PM_{2.5}$ nitrate) and forms $(NH_4)_2SO_4$ or NH_4HSO_4 through heterogeneous reaction. Thus $PM_{2.5}$ sulfate gradually increases in the early morning on 20 December. On the daytime on 20 December, less $PM_{2.5}$ sulfate is formed since $PM_{2.5}$ nitrate is low and less NH_3 is evaporated. Therefore, $PM_{2.5}$ sulfate slightly decreases due to dilution after 08:00 on 20 December. Relative to ammonium nitrate, ammonium sulphate is more stable. From Figure 4, it is seen that percentile of $PM_{2.5}$ sulfate increases from 10% in Shanghai at 10:00 19 December to 35% while the plume is near Taipei at 15:00 on 20 December.

4.3 $PM_{2.5}$ ammonium

Jordan et al. (2003) think that in the long-range transport plume there should be enough nss-SO_4^{2-} to react with NH_4^+. This implies that NH_3 evaporated from ammonium nitrate would transfer into sulfate ammonium. In Figure 4, the percentile of $PM_{2.5}$ ammonium remains around 13%. $PM_{2.5}$ ammonium may in the form of NH_4NO_3 or $(NH_4)_2SO_4$ or NH_4HSO_4 in source area. Since NH_3 can evaporate from NH_4NO_3 during long-range transport where SO_4^{2-} or HSO_4^- is present, it can be derived that $PM_{2.5}$ ammonium can be in the form of $(NH_4)_2SO_4$ or NH_4HSO_4 mostly when the plume is near Taiwan. Further, it is expected that the percentile of $PM_{2.5}$ ammonium remains nearly constant.

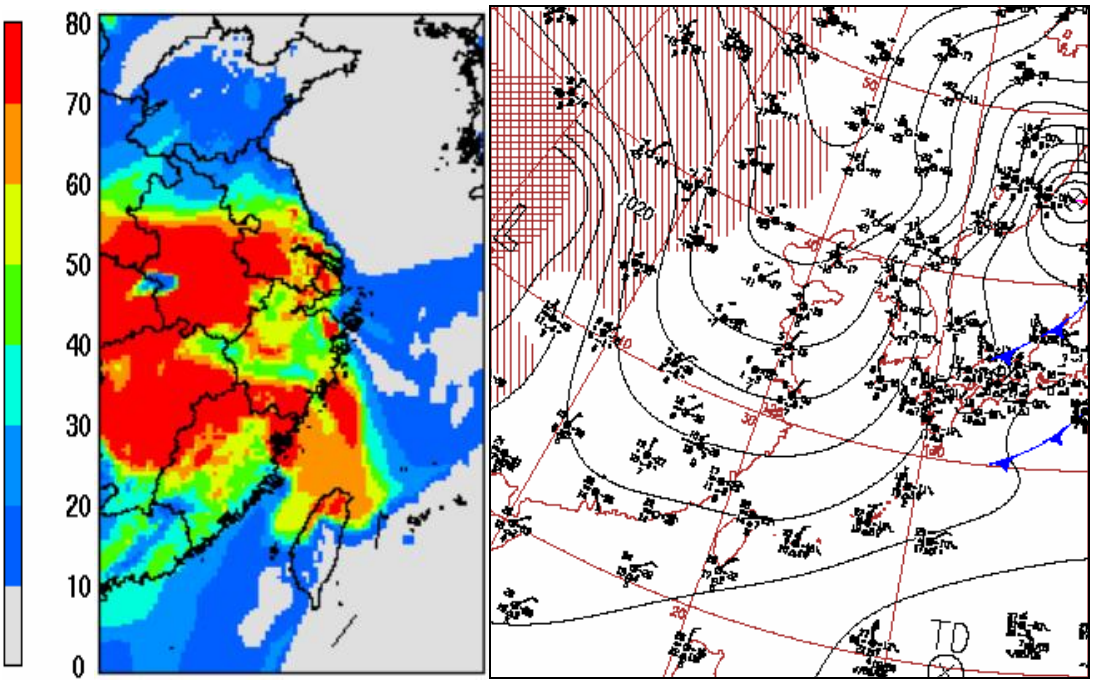

Fig. 3. Simulated near-surface $PM_{2.5}$ concentration of domain 2 and surface weather map (announced by JMA, Japan Meteorology Agency, http://www.jma.go.jp/jp/g3/) at 14:00 on 20 in December 2004.

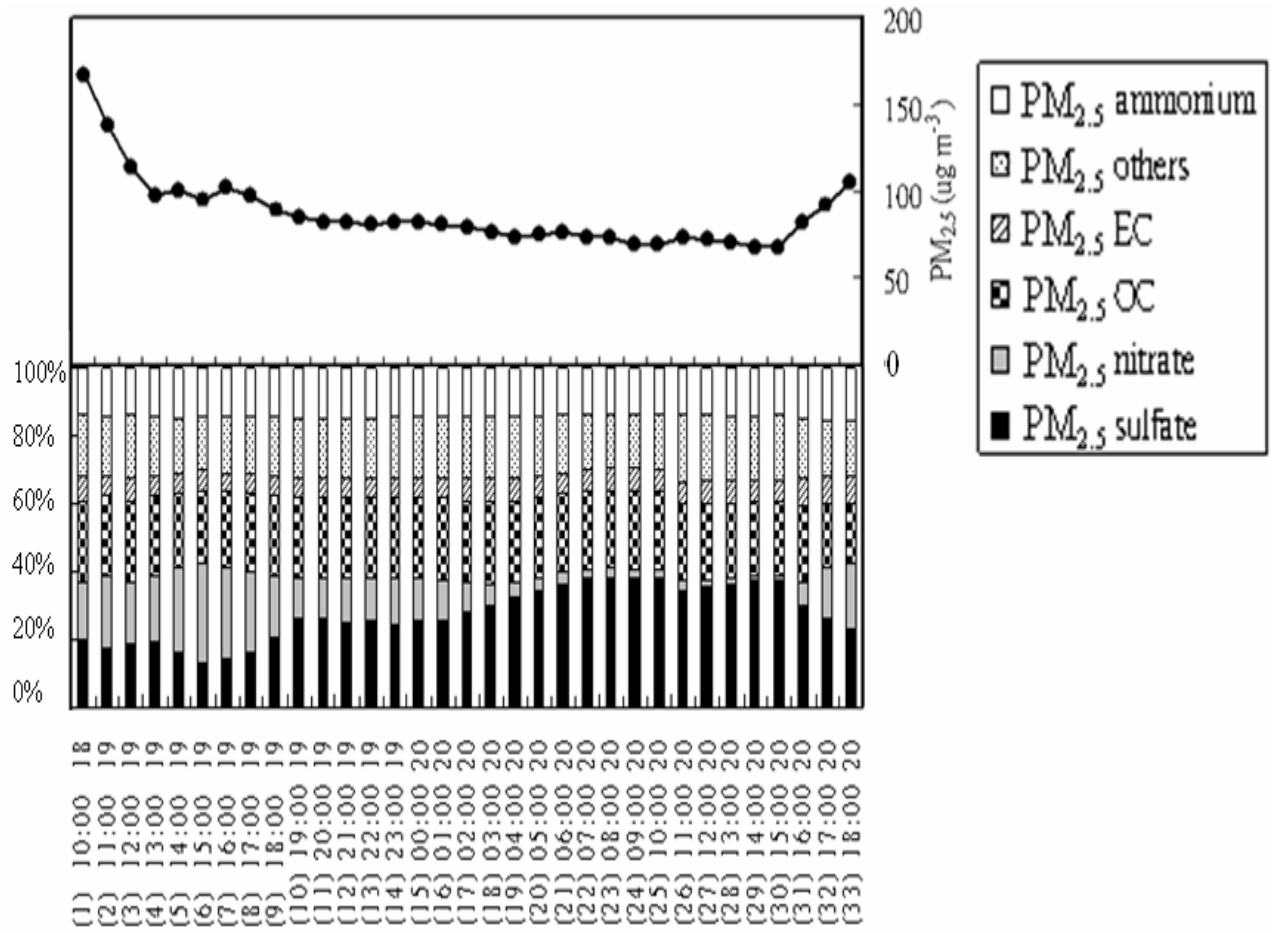

Fig. 4. The $PM_{2.5}$ mass concentration and the percentage of $PM_{2.5}$ chemical components in $PM_{2.5}$ during the path of Fig. 2

4.4 $PM_{2.5}$ carbonaceous content

$PM_{2.5}$ OC and $PM_{2.5}$ EC slowly decrease in the moving plume. Notably, $PM_{2.5}$ OC decreased faster than $PM_{2.5}$ EC. Therefore OC/EC ratio decreased from 4.1 near the outlet of Changjiang River to 2.7 in Taipei. From Shanghai to Taipei, the ratio of $PM_{2.5}$ OC to $PM_{2.5}$ just slightly decreases from 24% to 21%. In contrast, percentile of $PM_{2.5}$ EC remains nearly the same, 6%.

4. Summary

Pollutants from Asia continent would influence air quality in Taipei countries by means of southward long-range transport. Especially $PM_{2.5}$ sulfate is the major chemical components. A classical long-range transport case from Asia continent to Taiwan occurred on 20 December 2004 is simulated in this study. Simulation results show that the percentage of OC in $PM_{2.5}$ only slightly decreases from 24% to 21%. However, percentage of nitrate $PM_{2.5}$ decreases from 25% to a very lower value 1%. Relatively, the percentage of $PM_{2.5}$ sulfate increased from 10% to 35%.

5.Acknowledgements

We would like to express our deep gratitude to the Taiwan National Science Council, Taiwan Environmental Protection Administration (TWEPA) and U.S EPA for providing financial support to this study. We would also like to thank Dr. Streets for providing Asian emission database. In addition, we acknowledge NCEP (National Centers for Environmental Prediction) and DBAR (Data Bank of Atmospheric Research, managed by the Department of Atmospheric Sciences, National Taiwan University) for sharing the atmospheric monitoring data used in this study.

6. References

Byun, D.W., Ching J. K.S., Science Algorithm of the EPA Models-3 Community Multiscale Air Quality(CMAQ) Modeling System", EPA/600/R-99/030, USEPA/ORD, March 1999.doi:10.1029/2002JD003116.

Chang, K.H., Jeng, F.-T., Tsai, Y.L., Lin, P.L., 2000. Modeling of long-range transport on Taiwan' s acid deposition under different weather conditions. Atmospheric Environment 34, 3281–3295.

Chuang, M.T., Lee, C.T., Chiang, P.C., Wang, C.F., Chang, Y.Y., 2007. The effects of synoptical weather pattern and complex terrain on the formation of aerosol events in the greater Taipei area, submitted to Science of the Total Environment.

Chung, Y.S., Kim, T.K., Kim, K.H., 1996. Temporal variation and cause of acidic precipitation from a monitoring network in Korea, Atmospheric Environment 30, 2429-2435.

Dignon, J., Hameed, S., 1989. Global emissions of nitrogen and sulfur oxides from 1860 to 1980. Journal of Air Pollution Control Association 39, 180-186.

Fu, J.S., Yeh, F.L., Chien, H.C., Carey, R.J. C., Chuang, M.T., 2007. Environmental Technology Implementation: Modeling air quality impacts on Taiwan island. International Journal of Environmental Technology Management. (accepted)

Grell, G. A., J. Dudhia and D. R. Stauffer, 1994: A description of the fifth-generation Penn State/NCAR mesoscale model (MM5). NCAR Technical Note, NCAR/TN-398+STR, 117 pp.

Hao, J., Wang, L., 2005. Improving urban air quality in China: Beijing case study. J. Air & Waste Manage. Assoc. 55, 1298-1305.

Heo, E., Feng, Y., 2005. Recent development of energy use in China at the industrial sector level. http://www.cenet.org.cn/cn/CEAC/2005 in /zyhj011.doc

Holloway, T., Levy II, H., Carmichael, G., 2002. Transfer of reactive nitrogen in Asia: development and evaluation of a source – receptor model. Atmospheric Environment 36, 4251 – 4264.

Houyoux, M., Vukovich, J., 1999. Updates to the Sparse Matrix Operator Kernel Emissions (SMOKE) modeling system and integration with Models-3, Presented at The Emissions Inventory : Regional Strategies for the Future Conference, Air & Waste Management Association, Raleigh, NC.

Ichikawa, Y., and S. Fujita, 1995: An analysis of wet deposition of sulfate using a trajectory model for east Asia. Water, Air, Soil Pollut., 85, 1927–1932.

Jordan, C.E., Dibb, J.E., Anderson, B.E., Fuelberg, H.E., 2003. Uptake of nitrate and sulfate on dust aerosols during TRACE-P. Journal of Geophysical Research 108(D21), 8817, doi:10.1029/2022JD003101.

Kitada, T., and Tanaka, K., 1992. Simulated semi-global scale transport of SO_2 and $SO^{=}_4$ from East Asia to the Northern Pacific in spring season: The role of low and high pressure systems. Air Pollution Modeling and Its Application IX, H. van Dop and G. Kallos, Eds., Plenum Press, 445–454.

Kleinman, L.I., 1991. Seasonal dependence of boundary layer peroxide concentration: the low and high NOx regimes J. Geophys. Res. 96, 20721-20733.

Stelson, A.W., Seinfeld, J.H., 1982. Relative humidity and temperature dependence of the ammonium nitrate dissociation constant. Atmos. Environ. 16, 983-992.

Streets, D.G., Bond, T.C., Carmichael, G.R., Fernandes, S., Fu, Q., He, D., Klimont, Z., Nelson, S.M., Tsai, N.Y., Wang, M. Qm., Woo, J.-H., Yarber, K.F., 2003. An inventory of gaseous and primary aerosol emissions in Asia in the year 2000. Journal of Geophysical Research 108 (D21), 8809.

Waston, J.G., Chow, J.C., Lurmann, F.W., Musarra, S.P., 1994. Ammonium nitrate, nitric acid, and ammonia equilibrium in wintertime Phoenix, Arizona. J. Air & Waster Manage. Assoc. 44, 405-412.

Urban Effects of Hong Kong and Pearl River Delta Region on Sulfur Cycle

Roger H.F. Kwok*, Jimmy C.H. Fung, Alexis K.H. Lau
Institute for the Environment, Hong Kong University of Science & Technology, HK

Joshua S. Fu
Department of Civil Engineering, University of Tennessee, Knoxville, TN, USA

1. INTRODUCTION

Rapid development in Hong Kong (HK) and neighboring Pearl River Delta (PRD) region of China induces air pollution problems in both places. In the year 2004 alone, the most dominating pollutants contributing to the air pollution index (API) in HK are respirable suspend particulates (RSP) (Table 1). Within the RSP, 30-40% of fine particulate mass is contributed by sulfate. The high SO4 concentration level often occurs in HK, despite the implementation of local low sulfur control by HK government since 1997 (LEGCO 1997).

Pollutant	RSP	O3	NO2	SO2	Total
Station	Pcent	Pcent	Pcent	Pcent	Hrs
YuenLong	76%	2%	22%	1%	8076
TsuenWan	64%	1%	34%	1%	8586
TungChung	79%	8%	11%	2%	8517
TaiPo	87%	2%	11%	0%	2942
KwaiChung	63%	0%	32%	5%	8585
Central/West	70%	3%	22%	5%	8561
ShamShuiPo	61%	1%	34%	4%	6946
ShaTin	82%	6%	11%	1%	8559
KwunTong	66%	1%	33%	1%	8522
TapMun	84%	15%	0%	0%	8272
Eastern	63%	1%	34%	2%	8459

Table 1. Percentage of hours in 2004 contributed to HK API by criteria pollutants

*Corresponding author: Roger H.F. Kwok, Institute for the Environment, Hong Kong University of Science & Technology, Clear Water Bay, Kowloon, Hong Kong, China; e-mail: maroger@ust.hk
Fax: 852 2358 8400

As a coastal city with major power plants and numerous industrial sites scattering across the neighboring PRD regions, HK becomes an interesting location combining maritime/continental meteorology and vivid anthropogenic activities into air pollution events, especially particulate matters (PM). With sufficient provision of meteorological and emission data, an air quality model is devised to study the problem.

Fig 1. China, Pearl River Delta, HK. In HK, reds indicate availability of SO4 observations.

2. DATASET AND METHODOLOGY

For all meteorological and air quality modelings, four nesting domains are constructed covering China, Guangdong province (GD), PRD, and HK, respectively (Figure 1). Grid resolutions range from the coarsest 40.5 km, through intermediate 13.5 km and 4.5 km, to the finest 1.5 km. Meteorological fields are simulated using MM5

v3.6, nudged with NCEP analysis data in MM5's 40.5 km grid, as well as observed winds and temperature provided by Hong Kong Observatory in MM5's 1.5 km. Emissions data are constructed as follow. For domains at 4.5 km and 1.5 km resolutions, emission inventories provided by Hong Kong Environmental Protection Department (HKEPD), together with MM5 outputs, are processed via SMOKE 2.1 to generate time-varying, gridded emission files. For domains outside GD; ie, at 40.5 km and 13.5 km, TRACE-P emissions at true lat-lon intervals are regridded before being inserted with the PRD and HK SMOKE emissions. CMAQ 4.5 with CBIV and AE4 modules is applied to study the problem in first half of September 2004. The climate of the month is a period of intertwining patterns of summer monsoon winds, high pressure-induced easterly winds, and subsidence due to the outflow of remote tropical cyclones. So that pollutant concentrations are greatly affected by these meteorological patterns.

3. MODEL RESULTS

Figure 2 displays modeled and observed particulate sulfate time series at Yuen Long, northwestern part of HK, showing the capability of capturing the overall observed trends by the model simulation, though the latter underpredicts the observed peak around Sep 15. While there is room for improvement of model performance, it is more interesting to experiment possible effects on the sulfate concentration level by factors that characterize PRD and HK regions. Firstly, fast developing regions generally demand more energy supply, it is expected that more pollutants might have been emitted to the atmosphere. Secondly, the rapid development is almost certainly characterized by the expansion of urban areas. And it has been shown that urban areas alter thermal properties of land use and therefore change the local atmospheric circulation patterns (Lo 2006). The change is more significant when the areas are in the proximity of vast water bodies such as rivers and seas. Therefore we devise three sensitivity studies to examine the extent of SO4 level change by these factors: doubling SO2 emissions, 50% increase in cloud and rain water content, and 83% reduction in wind speeds in the urban areas of PRD and HK up to around 1 km above ground. The dramatic wind reduction merely explores the extreme situation. The choice of the altitude reflects an average PBL height in these regions.

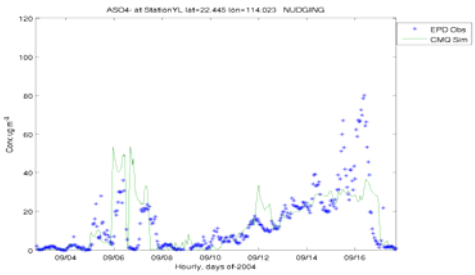

Fig 2. Time series of observed (blue) and simulated (green) particulate SO4 at Yuen Long during 3-16 September 2004.

The results are shown in Figure 3. Doubled SO2 emissions increase SO4 concentrations mainly in areas of emission sources. Increase in cloud/rain water content, on the other hand, does not result in significant rise in SO4 concentrations. However, the supply of additional clouds may have converted more SO2 into SO4 at all times, so that the minimum SO4 level is way beyond that in the base case. The wind speed reduction results in two-fold increase in SO4 concentrations in regions west of Pearl River estuary, but it also inhibits efficient transport of the pollutant into HK. The low SO4 concentrations in HK in this case is probably also due to low local SO2 emissions. In other words, the majority of the observed SO4 in HK appears to come from its neighboring regions.

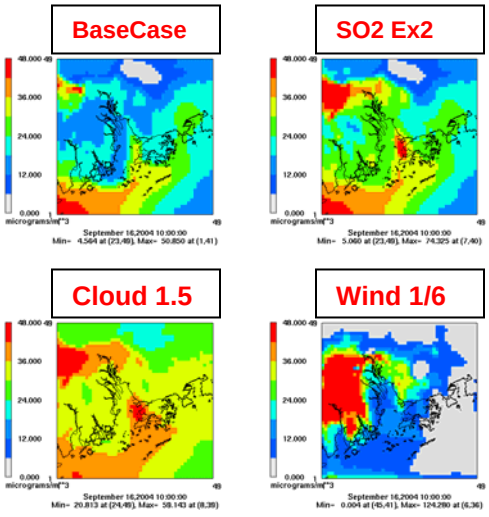

Fig 3. Spatial distributions of PRD particulate sulfate at 10UTC (18 local time),16 September 2004. (Top left) Base case, (Top right) SO2 emissions doubled, (Bottom left) Cloud and rain water content 50% increase, (Bottom right) urban wind speed reduced to one-sixth.

To further understand what processes the sulfur has gone through in the region of high sulfate concentrations, process analysis of total sulfur is applied to west PRD, as shown in Fig 4. That is, we only "strip" the model sulfur from SO2, SO4 and gaseous sulfuric acid and calculate the budget of it during the whole process.

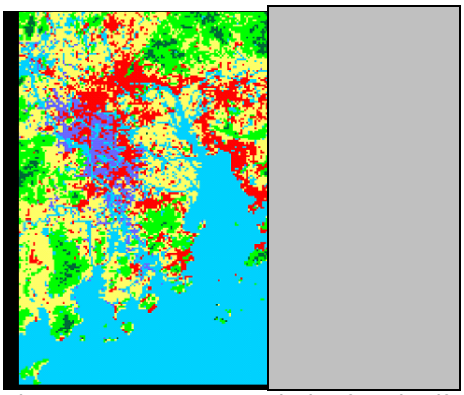

Fig 4. PRD – process analysis of total sulfur will be done on the *unshaded* area (i.e. west)

We wish to choose 04-09 Local Time September 16 as the study period, during which PM pollution becomes episodic (Fig 2). Process analysis is performed on base case and the one with urbanization treatment. Comparison of the process terms may help identify major qualitative changes.

Fig 5 shows such results that may discern the urban treatment case (URB case) from the base case. Generally, the net increase in sulfur concentration is bigger in the former than in the latter at low altitude (40 m). Similarly, the net decrease is also bigger in the URB case. It seems that reduction in horizontal wind speed near surface levels enhances vertical transport which is big enough to compensate the reduction of horizontal transport. Therefore the net increase in surface sulfur becomes bigger. On the other hand, the more profound negative vertical transport terms in the URB case suggest a likelihood of downward motion bringing the sulfur to lower altitudes. In addition, the negative horizontal transport terms at this PBL level suggests spreading of the sulfur from around sources. The chemical terms, on the other hand, change little across the two cases. Nor do they vary over different vertical layers. These suggest that concentration change can be enhanced by wind speed perturbation without changing the quality of gaseous chemical reactions.

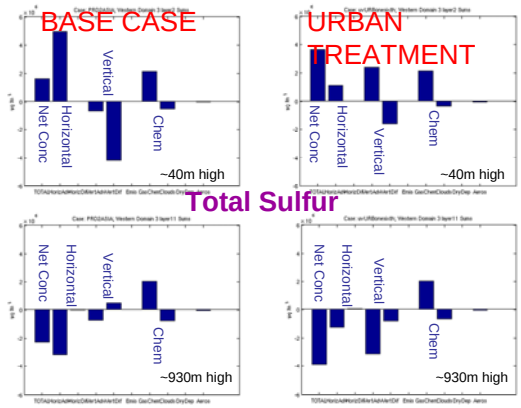

Fig 5. Net sulfur concentration and total process terms between 04-09 local time on Sep 16, 2004. Left column: base case; right column: urban treatment by wind speed reduction; top row: 40 m above ground; bottom row: 930 m above ground.

4. SUMMARY

The CMAQ modeling system is capable of capturing the trends of the observed SO4. As expected, changes in SO2 emissions, cloud/rain water content have impacts on PM SO4. Mimicked by PBL-layer horizontal wind speed reduction, urbanization treatment alone results in sulfur concentration increase due to enhanced vertical transport, without altering the gaseous chemistry.

5. ACKNOWLEDGMENT

The authors wish to thank Hong Kong Environmental Protection Department for the provision of air quality data, and TRACE-P for China emissions

6. REFERENCE

LEGCO, 1997: Air Pollution Control (Fuel Restriction) Regulations, Chapter 311I, **4**, Legislative Council, Hong Kong.

Lo, J.C.F, Lau, A.K.H., Fung, J.C.H., and Chen, F., 2006: Investigation of enhanced cross-city transport and trapping of air pollutants by coastal and urban land-sea breeze curculations. *J.Geophys. Res*, **111**, D14104, doi:10.1029/2005JD006837.

Presented at the 6th Annual CMAS Conference, Chapel Hill, NC, October 1-3, 2007

Overview of JCAP II Air Quality Model Integration System (Japanese version of Models-3)

Hideki Tashiro*and Hitoshi Kunimi
Japan Petroleum Energy Center, Minato-ku, Tokyo, Janpan

Seiji Nakatsuka and Midori Ashizaki
Central Computer Service Co., Ltd., Koto-ku, Tokyo, Japan

Hiroshi Hirai, Tazuko Morikawa, Seiji Hayashi and Akiyoshi Ito
Japan Automobile Research Institute, Tsukuba, Ibaraki, Japan

Satoru Chatani
Toyota Central R&D Labs., Inc. ,Aichi, Japan

Yasuo Yoshikawa
Nissan Motor Co., Ltd., Atsugi-sh, Kanagawa, Japan

1. INTRODUCTION

No integrated systems for air quality simulation including vehicle emissions calculation were established in Japan. Under a joint research program between auto and oil industries organized by Japan Petroleum Energy Center called “Japan Clean Air Program (JCAP)”, we developed traffic flow model, emission inventory model and air quality simulation model, which enables a detailed analysis of the impact of vehicle emissions, and provided data that could contribute to environmental policy making to policy makers.

And under JCAP II (second phase of the joint research program), we developed “JCAP II Air Quality Model Integration System”, so-called a Japanese versions MODELS-3. The air quality models developed under JCAP are integrated, so that the integration system enables a consequent simulation that ranges from emissions estimation to air quality simulation, and disclosure of the system has been done in June 2007.

Purpose of the disclosure is to promote the use of the system by people involved in air quality research in industry, government and academia, and to become a common tool that might be useful for discussion for air quality improvement in Japan.

2. JCAPII Air Quality Model Outline

JCAP II Model is roughly divided into two parts: urban and roadside air quality simulation models, each of which consists of traffic flow model, emission inventory model and air quality model. (Fig.1)

	Urban area	Roadside
Traffic flow	•Macro-scale Allocation calculation method	•Micro-scale Measured per vehicle, Chasing method
Emission Inventory	•Motor vehicles •Non-auto sources	•Motor vehicles
Air Quality Model	•Meteorology •Air Qualitv prodiction Advection/diffusion, Photochemical reaction	•Airflow/ diffusion calculation Computational fluid Dynamics (CFD)

Fig.1 JCAP Ⅱ Air Quality Model Configuration

JCAP II Air Quality Model Integration System consists of five submodels and a sever system, as shown in Fig.2: 1) Urban motor vehicle emission inventory model, 2) Urban non-auto source emission inventory model, 3) Urban Air Quality Model (airflow + air quality), 4) Roadside motor vehicle emission inventory model and 5)Roadside Air Quality Model.

3. JCAPII Air Quality Model Integration System Features

3.1. Urban Motor Vehicle Emission Inventory Model

Urban motor vehicle emission inventory model is a computational system. Use traffic volume and vehicle speed from Road Traffic Census data, vehicle population and other information that are allocated to grid cells as input data, and calculate emissions of each species by vehicle type and emission process as grid cell data.

*Hideki Tashiro, Japan Petroleum Energy Center, Sumitomo shin-Toranomon Bldg., 4-3-9 Toranomon Minato-ku, Tokyo 101-0001, Japan; +81-3-5402-8505, e-mail: h-tashiro@jcap.pecj.or.jp

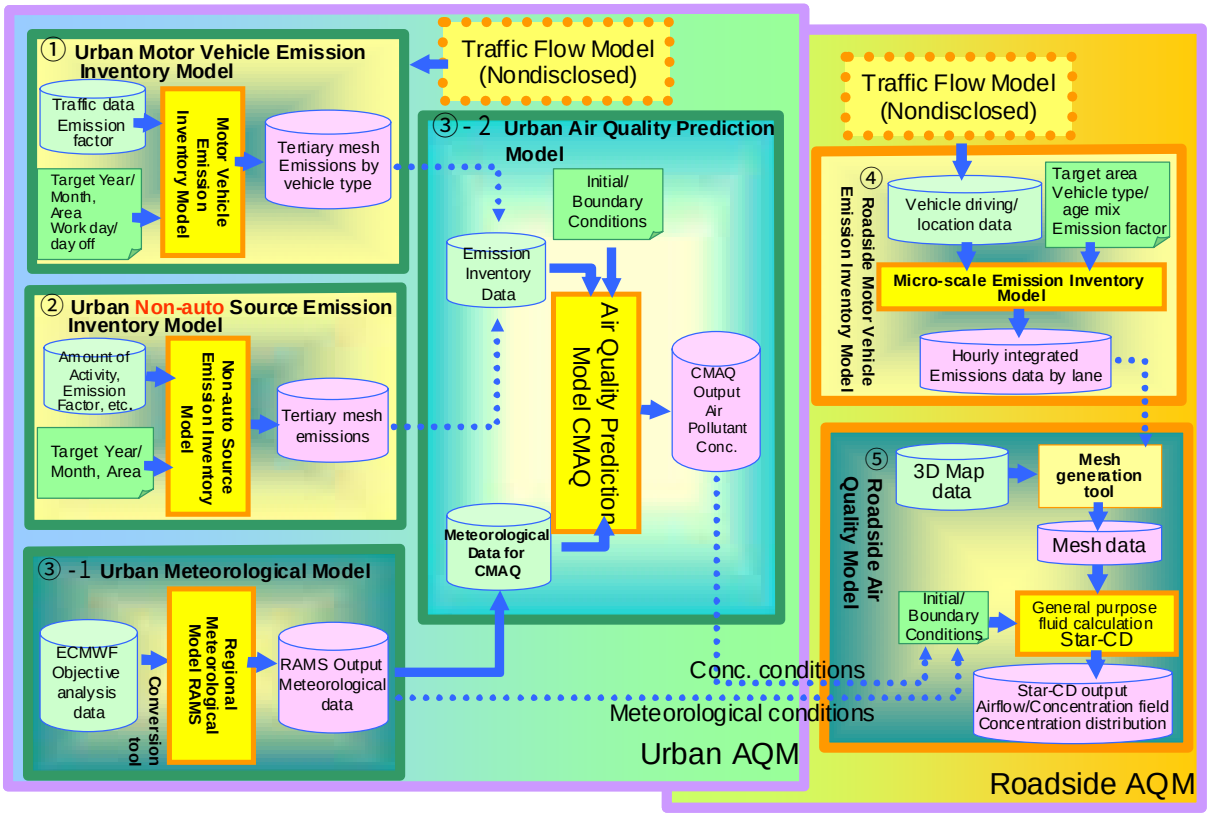

Fig.2 JCAPII AQM Integration System Association Chart

In this model, consideration is taken of not only tailpipe emissions but PM including tire wear and road dust, evaporation loss, and emissions during parking (Fig.3).

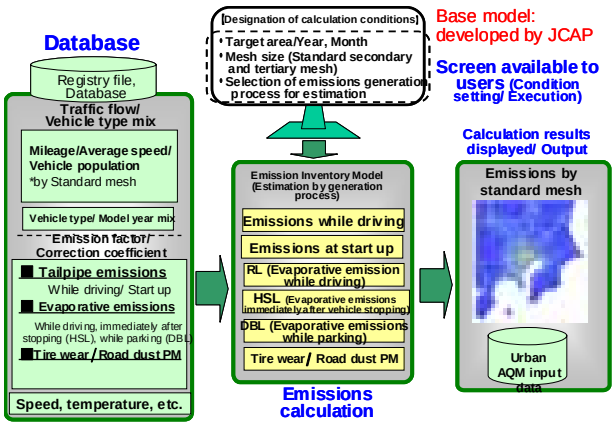

Fig.3 Motor Vehicle Emission Inventory Model Schematic Diagram

Traffic volume grid data by vehicle type and time are developed from traffic flow data on major roads in FY 1999 Road Traffic Census data (cross-sectional traffic volume and average vehicle speed during congestion by link (a road divided by several km for survey) (at a point/day)). Grid data are generated by apportioning link length (L), cross-sectional traffic volume by vehicle type (Si), and average speed during congestion (V) within a grid cell by time period. Emissions from vehicles traveling within a grid cell are calculated by vehicle type, species and time period, using correction

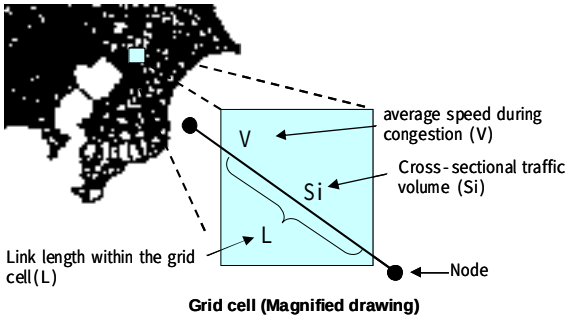

Fig.4 Traffic flow grid cell data

coefficients including mileage (calculated from Si x L), emission factor, vehicle speed and etc. (Fig.4) .

Roads other than major roads are defined as minor streets, average traffic volume on minor streets within the grid is calculated separately to calculate emissions on major roads.

3.2. Urban Non-Auto Source Emission Inventory Model

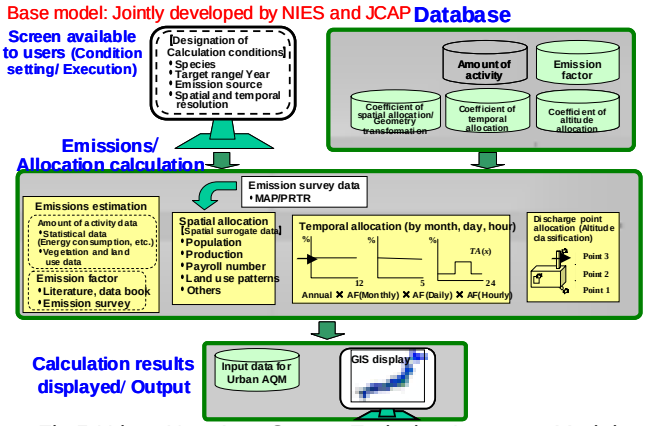

Fig.5 Urban Non-Auto Source Emission Inventory Model Outline

This is a system that performs spatial allocation of emissions from non-auto sources. First of all, multiply the amount of activity data (including fuel consumption and etc.) by emission factor to calculate total emissions in Japan, and using appropriate substitute apportionment data including factory shipment value, etc., perform spatial allocation of the total emissions, such as prefectural allocation, grid cell allocation or other allocation (Fig.6). This system can also perform monthly and hourly allocation, or allocation considering emission height.

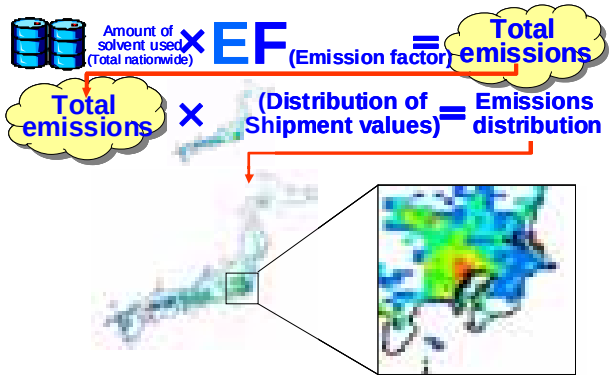

Fig.6 Urban Non-auto Source Emission Inventory Estimation Method

3.3 Urban Air Quality Simulation Model

This system consists of two sections: A section covers meteorological simulation using ECMWF data as input data, and another section covers calculation of pollutant concentrations in the air using meteorological and emission inventory data as input data.

ATMET RAMS4.4 is used as base model for meteorological simulation, and CMAQ4.4 for air quality simulation (Fig.7).

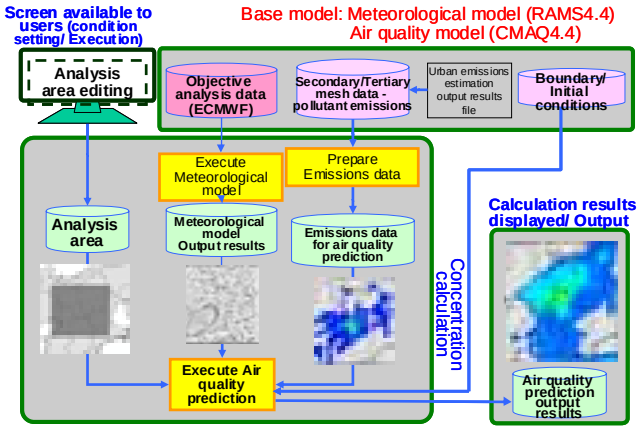

Fig.7 Urban Air Quality Simulation Model Outline

In both systems integrated interface is provided in each system, which manages up to triple nesting (Fig.8)

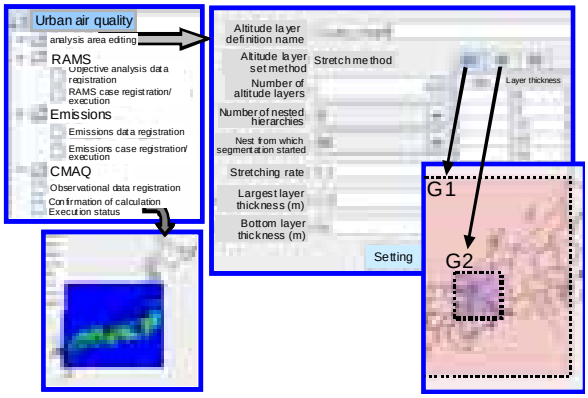

Fig.8 Graphical User Interface for Urban Air Quality Simulation Model

3.4. Roadside Motor Vehicle Emission Inventory Model

This system calculates emissions from individual vehicles corresponding to vehicle speed and acceleration, using output results from Micro-scale traffic flow model as input data that enable to express actual vehicle behavior (including starting, stopping, accelerating and etc.), and based on emission maps under transient conditions developed under JCAP. This system can calculate target species including NOx and etc. with resolution of 1m, and their hourly integrated values. Therefore, target area ranges from 1 to 5 km square at the largest, so that this model is applicable to estimation of emissions surrounding

an intersection on a highway with frequent starting/stopping in traffic.

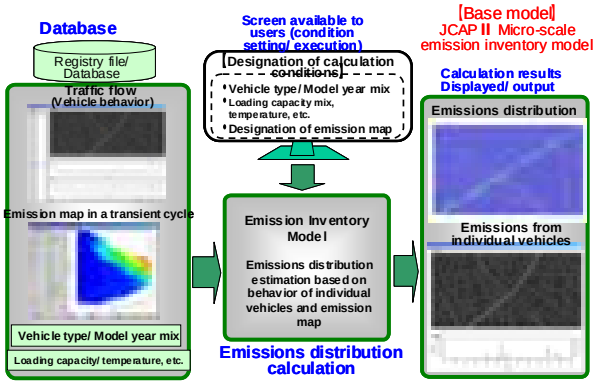

Fig.9 Roadside Motor Vehicle Emission Inventory Model Outline

Prior to estimation of transient emissions, chassis dynamometer testing should be conducted to measure transient emissions in JMEC mode test cycle, and emission map of vehicle speed and driving force should be prepared using the data. Transient emission map was prepared using data from about 100 vehicles under JCAP. And vehicle speed and acceleration data from traffic flow model are converted into driving force taking into consideration load, road grade and so on, so that transient emissions are calculated with the emission map (Fig.10).

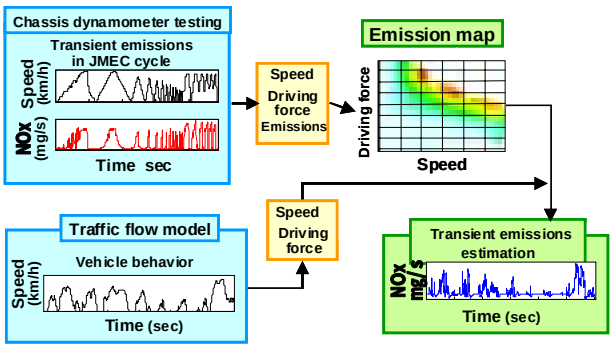

JMEC: A test cycle based on MEC 01-03 cycle of Comprehensive modal emission model (CMEM) and modified to suit with vehicle driving conditions in Japan

Fig.10 Transient emissions estimation method

3.5 Roadside Air Quality Simulation Model

CD Adapco Star-CD is used as base software in this model. First of all, incorporate building shape information into the model using 3D digital map, generate spatial grid cells, and do air flow field calculation. Motor vehicle emissions in the target area, which are calculated using Roadside Motor Vehicle Emission Inventory Model, are inputted into the model, and advection/diffusion calculation is done to calculate concentrations of vehicle-derived pollutants.

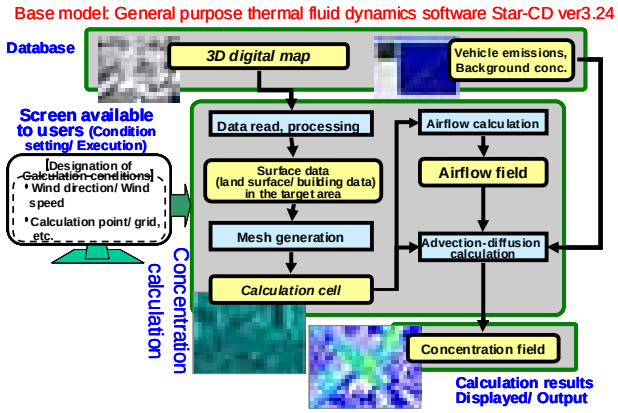

Fig.11 Roadside Air Quality Simulation Model Outline

3.6 Data Sever System

We developed a data server system that unifies management of data from individual subsystems. This system is characterized in that system manipulation is available on Web browser, and data exchange between researchers is performed easily.

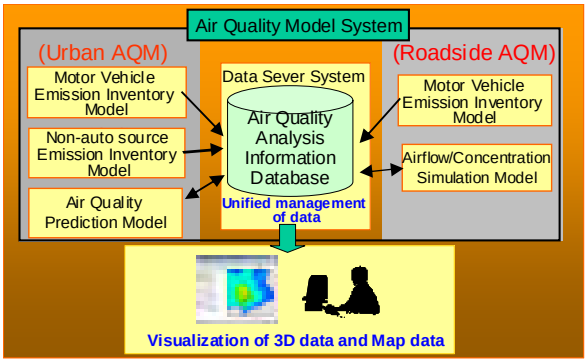

Fig.12 Data Sever System Outline

4. Summary

Under JCAP, a comprehensive air quality simulation model was developed that covers from vehicle emissions estimation to multi-scale simulation of air quality ranging from urban area to roadside, and graphic user interface (GUI) was provided to improve in operability. And then, a function of unified data management was added to the model, so that “Air Quality Model Integration System” has been developed and disclosed.
In the future, we intend to promote widespread use of the Air Quality Model Integration System”

by people involved in air quality research in academia, industry and government in Japan, and expect the system to become a tool served as common basis of discussion for air quality improvement in Japan.

5. References

Kunimi, H, 2007; 5th JCAP Conference, Air Quality Study Group Report at http://http://www.pecj.or.jp/english/jcap/pdf/jcap5thE/1-8_kunimi.pdf

Regional Climate Change Induced by Land-Use Change and Impact on O_3 in the Pearl River Delta, China

Xuemei Wang*
School of Environmental Science and Engineering, Sun Yat-sen University, Guangzhou, China

Fei Chen, Christine Wiedinmyer, Alex Guenther, Mukul Tewari
National Center for Atmospheric Research, Boulder, CO, USA

Wenshi Lin
School of Environmental Science and Engineering, Sun Yat-sen University, Guangzhou, China

Ziwei Chai
School of Geographical Science and Planning, Sun Yat-sen University, Guangzhou, China

1. INTRODUCTION

Changes in land use and land cover (LULC) alter the exchange of energy, momentum, moisture and other trace gases within vegetation-soil atmosphere continuum, subsequently affecting the global and regional climate and terrestrial carbon cycle process. As a result, the LULC change has been recognized as one of the largest and most convincing mechanisms for the earth climate change. Recently, availability of higher spatial resolution land cover data, along with improved parameterization of the planetary boundary layer (PBL) and urban processes, has been used to improve mesoscale numerical simulations over urban areas. Numerical modeling is a powerful tool to investigate consequences of urbanization on regional climate, particularly for the Chinese Pearl River Delta (PRD) region, which experienced rapid urban development in the last ten years. The primary objective of this research is to quantify major impacts of LULC change on regional climate and potential impacts on O_3 concentration over the PRD.

2. MODELING SYSTEMS AND NUMERICAL EXPERIMENTS

The coupled fifth-generation Pennsylvania State University–National Center for Atmospheric Research nonhydrostatic Mesoscale Model (MM5)–land surface modeling system is used in this study. MM5 is configured for the current study with three two-way interactive grids having horizontal grid spacings of 27, 9, and 3 km and grid point dimensions of 127×118, 97×97, and 79×79 respectively[Lin et al. 2007, Wang et al., 2007]. To better capture influences of urban heat islands (UHIs) and urbanization on the PRD, a 3-km grid, in conjunction with high-resolution land-use maps, is used for the MM5 inner domain. The same 22 sigma levels are specified for all simulations. Pressure at the top of the model, where a radiative boundary condition is used, is 100 hPa. The lowest half-sigma level is located at 38 m above ground level. Since a major goal of the current study is to examine the effect of urbanization on PBL structures, vertical resolution is significantly enhanced in the lowest 1-km atmosphere. The Noah land surface model (LSM) with a simple urban parameterization is used in this study (Chen 2005). More details about the model parameterizations and initial and boundary conditions are described in Wang et al. [2007].

Two land cover data sets are used in the PRD within the domain D3 (Figure 1) in this case study. One land cover (namely NU) employs the original United States Geological Survey (USGS) land cover data with 24-category, corresponding to the 1990s land-use condition with less human disturbance, while the other land cover data (namely HU) is based on the urban data of 2004 (after urban expansion took place) derived from 2004 MODIS satellite images at 500m spatial resolution. October 2004 is chosen for this study bees of relatively high pollution index in autumn over the PRD.

In this study, STEM (Sulfur Transport and dEposition Model)-2K1 (Carmichael et al., 2003a) is executed on the same grids as MM5

*Corresponding author: Xuemei Wang, School of Environmental Science and Engineering, Sun Yat-sen University, Guangzhou 510275, China; Tel. 020-84112293; Fax. 020-84113616; e-mail: eeswxm@mail.sysu.edu.cn

(i.e., 27-, 9-, and 3-km grid) using the PRE-URBAN (NU) and URBAN (HU) land use maps to investigate the influence of land use change on ozone over the PRD. This model was used in the TRACE-P (Transport and Chemical Evolution over the Pacific) experiment and compared with observed data in the PRD region by Wang et al. (2005). STEM-2K1 is driven by MM5 meteorological output in the three domains, which have the same vertical and horizontal resolution as MM5. For chemical species initial and boundary conditions, the profiles obtained from the TRACE-P aircraft observations are used for the coarse domain. The initial and boundary conditions for the inner two domains are interpolated from corresponding mother domain. Emissions are interpolated into each domain from 6 min resolution emission inventory. The simulation length is different from MM5. Because running the nested chemical model is expensive, we start, for this preliminary runs, with a 3-day simulation to assess impacts of land-use change on O3. The simulation started from 0000UTC 28 October and ended at 2300 UTC 30 October 2004. The whole month simulation by chemical model will be done in the near future. As our main objective is to explore the influences of urban-induced changes in meteorological conditions on air quality, we use the same surface biogenic and industrial emission rates (reflecting today's situation) in both simulations with different land use maps. The impacts of emission rate changes will be investigated in the future.

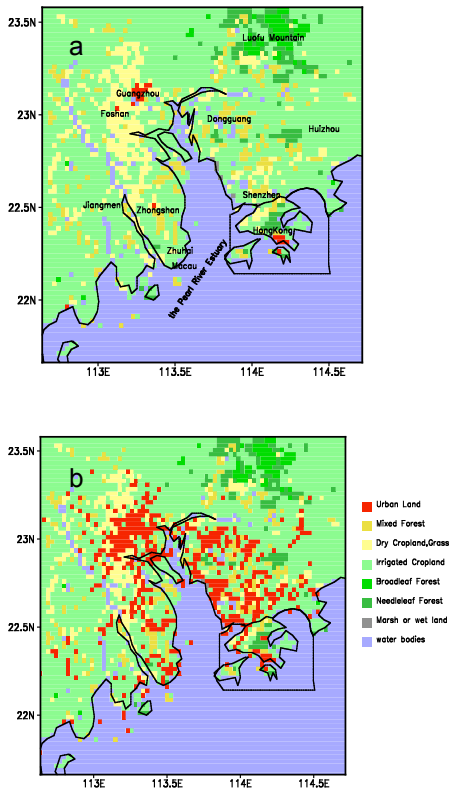

Fig. 1. Land-use data sets used for MM5 simulations. (a) USGS data, (b) Land-use data based on 2004 0.5-km MODIS products. The only change between (a) and (b) is the urban areas marked in red color.

3. RESULTS AND ANALYSES

3.1 Regional Climate Change Induced by Land-Use Change

The observed monthly mean temperature (from six-hourly observations) and the simulated monthly mean 2-m temperature are shown in Figure 2. The magnitude of simulated results is close to the observed in the northern part of Guangdong province but lower than the observed near the coast. Different thermal properties (heat capacity and conductivity) for urban and rural resulted in faster daytime (nighttime) temperature increase (decrease) in urban areas than that in rural areas.

The 2-m mixing ratio, 2-m temperature (℃) , sensible heat flux, and PBL depth difference between HU and NU are shown in figure 2. The spatial distribution of the urban expansion effect on humidity in the figure indicates that the maximum decrease of mixing ratio is about 0.4 g kg^{-1} in Guangzhou and Dongguan. Further calculations show that the mixing ratio decreases from NU to HU by 0.02, 0.02, and 0.01 g kg^{-1} for the domain-averaged value, land-averaged value and urban area averaged value, respectively. The maximum difference of monthly mean 2-m temperature is about 0.9℃ over urban areas in Guangzhou, Dongguan, Zhongshan and Shenzhen. Although warm centers dominate in the whole domain, there are some cool centers (minimum temperature difference <-1.2℃) in the Pearl River estuary with urban expansion.

The differences of monthly mean sensible heat fluxes between HU and NU indicate that there is an increase of sensible heat flux in the eastern, northeastern part of the PRD and all

urbanized areas where maximum increase is about 90 W m^{-2}. The monthly mean surface sensible heat fluxes averaged for the whole domain, land area and urban area increase, respectively, from 24.8 W m^{-2} to 28.9 W m^{-2}, 16.6 W m^{-2} to 21.5, and 28.5 W m^{-2} to 86.0 W m^{-2} from NU to HU.

The spatial distribution of monthly mean PBL height difference between NU and HU shows that the PBL height over the urban areas increases significantly. The average increase is about 20-80 m near urban areas, and the maximum increase is about 180 m in Guangzhou. The monthly mean PBL height averaged for the domain D03, land, and urban areas increases, respectively, from 827 m to 839 m (12 m deeper), 765 m to 783 m (18 m deeper), 780 m to 855 m (76 m deeper) from NU to HU. This difference is a result of urban-expansion induced increase of daily mean PBL height which exhibits a diurnal variability of daytime increases but nighttime decreases in PBL height. But the magnitude of daytime increase is larger than that of nighttime decrease.

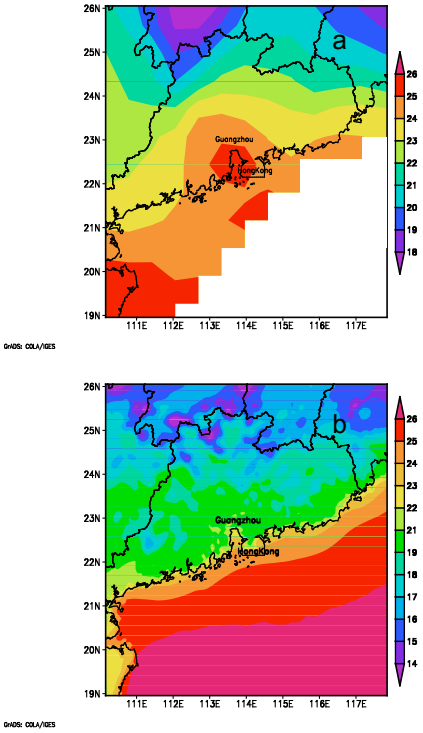

Fig. 2. Monthly mean 2-m temperature (℃) (a) Observation and (b) Simulation.

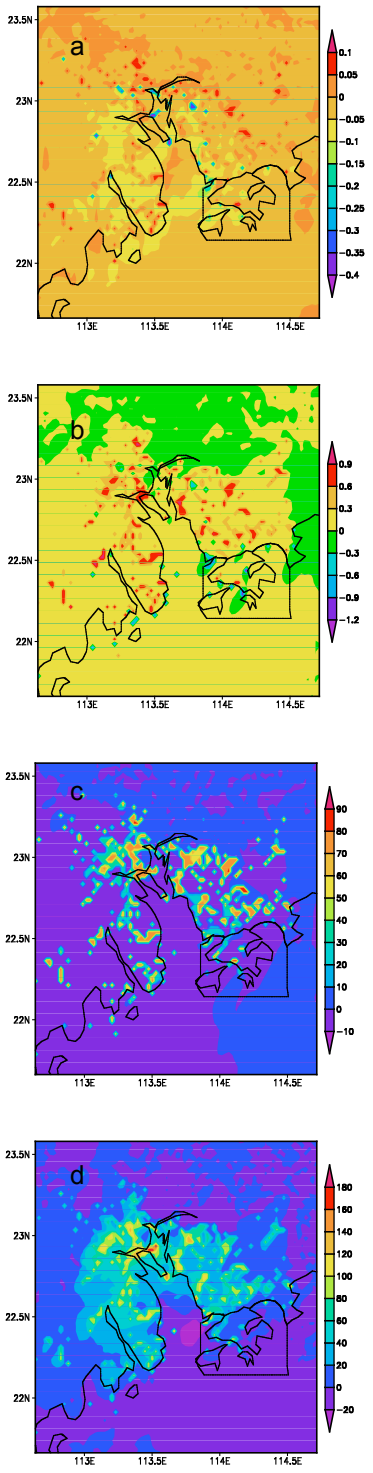

Fig. 3. Monthly mean difference between HU and NU. (a) 2-m mixing ratio (g kg-1), (b) 2-m temperature (℃) ,(c) Sensible heat flux, (d) PBL depth

3.2 Impact on O_3 concentration due Land-Use Change

We have seen so far that urbanization can modify temperature, humidity, sensible heat flux and the PBL mixing-layer depth and stability. In this section, we focus on impacts of those modified meteorological conditions on spatial and temporal distributions of ozone ($O_{3)}$ concentration , because it is the traditional indicator of photochemical smog in the PRD. Figure 4 shows influences of urban expansion on daytime and nighttime averaged surface O_3 concentrations. While surface O_3 concentrations over major cities increase both during daytime and during nighttime, the nighttime enhancements in O_3 concentrations outpace those during daytime in the urban expansion regions. For instance, during daytime, the maximum O_3 concentrations augmentation occurs over the Hongkong area (~ 10 ppbv) with a second maximum over the Guangzhou area (~ 4 ppbv). The nighttime maximum O_3 increase has larger amount (> 15 ppbv) and is located over major urban expansion areas such as Guangzhou and Dongguan. Areas with main O_3 concentrations increase generally coincide with the areas of temperature increase, humidity reduction, sensible heat flux increase. These results are consistent with previous studies showing the direct link between increased ozone concentrations and higher temperatures. Nevertheless, it should be noted that, in the daytime, some urban regions such as Foshan and suburb of Guanghou experience slight reduction in surface ozone concentration even with higher temperature and lighter wind in those areas. This implies that the temperature enhancement alone is not sufficient to explain changes in surface O_3 concentrations. Because in the real world, temperature change will likely be coupled to changes in other meteorological variables such as the PBL depth that will in turn affect O_3 concentrations. In fact, deeper daytime, convective boundary layer over major urbanized areas can lead to stronger vertical mixing that dilutes surface O_3 concentrations. For example, over the Guangzhou district, the daytime increase in the PBL depth (> 400 m) is greater than the nighttime increase (~ 100 m). Hence, the surface O_3 is transported to upper mixing layer and the O_3 concentration increases throughout the entire mixing layer up to 1700 m (not shown). By contrast, despite the slightly unstable, nocturnal surface layer caused by more pronounced nighttime UHI, the increase of O_3 is mainly confined within the lowest 150 m above the ground, leading to higher surface O_3 concentration. Therefore, the more enhanced nighttime surface O_3 is a consequence of slightly higher surface temperature and, more importantly, of shallower mixing layer. The other reason for large nocturnal increase in surface O_3 concentration is weaker wind speed, which reduces horizontal transport of pollutants and results in local O_3 accumulation.

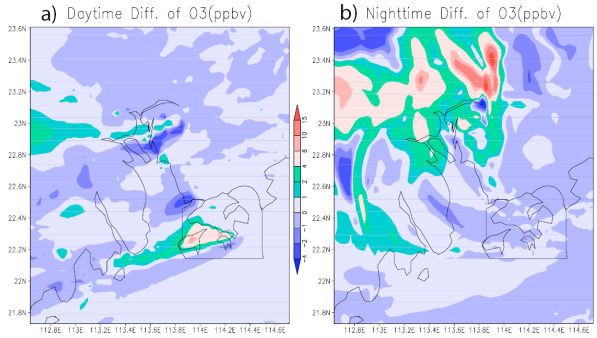

Fig. 4. Differences of surface ozone concentration (ppbv) between URBAN and PRE-URBAN simulations (URBAN minus PRE-URBAN). (a) averaged for the daytime and (b) averaged for nighttime simulation.

4. SUMMARY

Preliminary results show that urbanization can increase 2-m temperature, decrease water mixing ratio and sensible heat flux, increase the PBL mixing-layer depth over urban area in Autumn. These meteorological change can induce feasible surface ozone concentration through three days simulation. During daytime, the maximum O_3 concentrations augmentation occurs over the Hongkong area (~ 10 ppbv) with a second maximum over the Guangzhou area (~ 4 ppbv). The nighttime maximum O_3 increase has larger amount (> 15 ppbv) and is located over major urban expansion areas such as Guangzhou and Dongguan.

Nevertheless, our results may be limited due to the one season and three days simulation for ozone in this study. The seasonal simulations should be further investigated.

Acknowledgements

The study is supported by the Chinese academy joint creative young scholar plan in IAP, the Natural Science Foundation of China (40645024) and State Key Laboratory of Atmospheric Boundary Layer Physics and

Atmospheric Chemistry (LAPC) of Institute of Atmospheric Physics (IAP) (LAPC-KF-2006-12).

References

Carmichael, G.R., Y. Tang, G. Kurata, I. Uno, and co-authors(2003a). Evaluating regional emission estimates using the TRACE-P observations. J. Geophys. Res., 108, (D21), 8810, doi:10.1029/2002JD003116.

Chen, F. (2005). Variability in global land surface energy budgets during 1987-1988 simulated by an offline land surface model. Climate Dynamics, doi: 10.1007/s00382-004-0439-4.

Dudhia, J. (1996). A multi-layer soil temperature model for MM5. Preprint from the Sixth PSU/NCAR Mesoscale Model Users' Workshop, Boulder CO (http://www.mmm.ucar.edu/mm5/lsm/lsm-docs.html)

Lin, W. S., C.-H. Sui, L. M. Yang, X. M. Wang and co-authors (2007). A numerical study of the influence of urban expansion on monthly climate in dry autumn over Pearl River Dealta,China. Theoretical and Applied Climatology, 89(1-2), 63-72.

Wang, X. M., G. R. Carmichael, D. L. Chen, Y. H. Tang, T.J. Wang (2005). Impacts of different emission sources on air quality during March 2001 in the Pearl River Delta (PRD) region. Atmospheric Environment, 39, 5227–5241.

Wang, X. M., W. S. Lin, L. M. Yang, R. R. Deng and H. Lin (2007). A Numerical Study of Influences of Urban Land-use Change on Ozone Distribution over the Pearl River Delta Region, China. Tellus B, 59B, 633-641.

FUTURE PREDICTION OF SURFACE OZONE OVER EAST ASIA UP TO 2020

Kazuyo Yamaji* and Hajime Akimoto
Frontier Research Center for Global Change, Japan Agency for Marine Science and Technology, Yokohama, Japan

Toshimasa Ohara and Jun-ichi Kurokawa
National Institute for Environmental Studies, Tsukuba, Ibaraki, Japan

Itsushi Uno
Research Institute for Applied Mechanics, Kyushu University, Kasuga, Fukuoka, Japan

1. INTRODUCTION

Tropospheric ozone (O_3) produced through photochemical reactions involving primary pollutants such as nitrogen oxides (NOx) and non-methane volatile organic compounds (NMVOC) is a major secondary pollutant. These O_3 precursors, which are mainly emitted due to fossil fuel uses, have rapidly increased over Asia during the last decade. Ohara et al. (2007) reported a NOx emission increase from 10.7 Tg in 1980 to 25.1 Tg in 2000 over Asia as shown in Figure1. Enhanced NOx emissions in Asia have a great potential for increasing the amount of tropospheric O_3 not only in the emission source region but also on a hemispheric scale (Wild and Akimoto, 2001).

Over East Asia, O_3 concentration was enhanced from spring to autumn by chemically-produced O_3 by regional emissions (Yamaji et al., 2006). This means that the future O_3 over East Asia would be significantly affected by changes of O_3 precursor emissions depending on future economic growth and environmental policies in this area. In particular, China with its large population and extensive land mass that sustains high economic development is of great importance. Therefore we tried to predict the future surface O_3 using a regional chemical transport model and a regional emission inventory for Asia.

A regional emission inventory in Asia for anthropogenic air pollutants with a 0.5°×0.5° spatial resolution that employs specific information of regional, country, and province levels has been completed by the Frontier Research Center for Global Change (FRCGC) in Japan (Yan et al., 2003a,b; Yamaji et al., 2003,2004; Ohara et al., 2007). This emission inventory, named Regional Emission inventory in ASia (REAS), is available at http://www.jamstec.go.jp/frcgc/research/p3/emission.htm and provides a sequence of gridded emission data from the past to the future, which has been built under a consistent concept. Especially for future emissions, REAS employed three emission scenarios (the reference (REF), the policy succeed case (PSC), and the policy failure case (PFC) scenarios) for China, and the moderate scenario (the REF) for other countries.

This study used a regional chemical transport model, the Models-3 Community Multi-scale Air Quality Modeling System (CMAQ) (Byun and Ching, 1999) and REAS to prediction the future O_3 change caused by anthropogenic emission changes over East Asia.

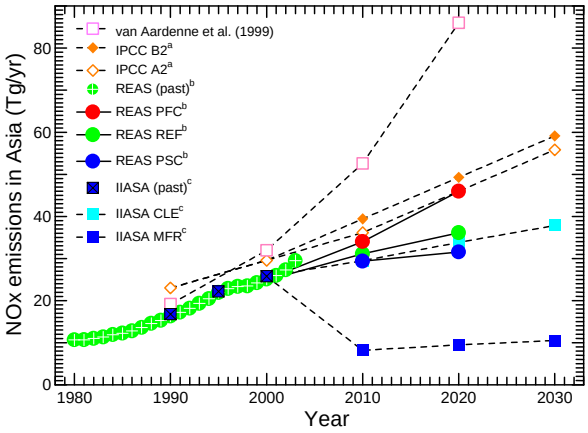

Figure 1. NOx emission trends in Asia including South, Southeast, and East Asia. [a]IPCC, http://sres.ciesin.columbia.edu/ [b]Ohara et al. (2007) [c]Amann (2006)

*Corresponding author: Kazuyo Yamaji, Frontier Research Center for Global Change, Japan Agency for Marine Science and Technology, 3173-25 Showa-machi, Kanazawa-ku, Yokohama 236-0001 Japan; e-mail: kazuyo@jamstec.go.jp; Web address: http://www.jamstec.go.jp/frcgc

2. DESCRIPTION FOR MODEL EXPERIMENTS

2.1 Model Descriptions

We used CMAQ version 4.4 driven by meteorological fields calculated by the Regional Atmospheric Modeling System (RAMS) Version 4.3 (Pielke et al., 1992; Cotton et al., 2003). The RAMS simulation used three-dimensional meteorological fields from NCEP/NCAR reanalysis data sets (2.5°×2.5°) with 6-hour intervals in 2000. Spatial domains for CMAQ and RAMS (shown in Figure 2) are 6240 × 5440 km^2 (inside domain) and 8000 × 5600 km^2 (outside domain) centered at 25˚N and 115˚E, respectively, with 80 × 80 km^2 grid resolutions. For vertical resolution, both model systems have the same model height of 23 km and employ a hybrid sigma-pressure coordinate. CMAQ and RAMS have 14 and 23 vertical layers, respectively.

The CMAQ chemical-transport model (CCTM) requires information for initial and boundary chemical concentrations. In this study, the initial conditions were chosen to reflect the East Asian situation and the validity of these was examined in a previous study by Zhang et al. (2002). The boundary conditions of O_3 and its precursors, NO_2, HNO_3, CO, PAN, PAN2 Ethene, Isoprene, Formaldehyde, Alkanes, and Alkenes were obtained from monthly-averaged outputs from the CHemical AGCM for Study of Atmospheric Environment and Radiative forcing, CHASER (Sudo et al., 2002), which used Emission Database for Global Atmospheric Research (EDGAR) version 3.2. As for the gas-phase atmospheric chemical mechanism and the aerosol module, we used SAPRC–99 and AERO3, respectively. Chemical concentrations used in this study are instant CCTM outputs every three hours starting at 0 UTC for each day.

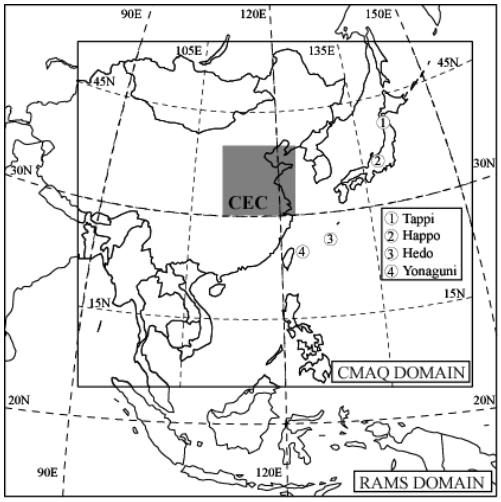

Figure 2 Model domains for CMAQ (inside) and RAMS (outside) simulations. The numerical characters indicate the locations of Japanese remote monitoring sites of EANET (Tappi, Happo, Oki and Hedo)

Table 1 Annual emissions of major O_3 precursors (NOx, $Tgyr^{-1}$ and NMVOC, $Tgyr^{-1}$) from anthropogenic sources for the years 2000, 2010, and 2020 (PSC, REF, and PFC for China and REF for the other regions)[a].

	NOx							NMVOC						
	2000	2010			2020			2000	2010			2020		
		PSC	REF	PFC	PSC	REF	PFC		PSC	REF	PFC	PSC	REF	PFC
China	11.2	12.2(9)	14.0(25)	16.9(51)	11.0(-2)	15.6(39)	25.5(128)	14.7	20.8(41)	22.5(53)	23.6(61)	29.0(97)	35.2(139)	38.7(163)
BB[b]	0.8							2.7						
Japan	2.0		1.8(-10)			1.8(-10)		1.9		2.2(16)			2.5(32)	
BB[b]	< 0.1							< 0.1						
Other East Asia[c]	2.5		3.1(24)			3.7(48)		1.9		2.7(42)			3.8(100)	
BB[b]	0.2							0.5						
Southeast Asia[d]	3.8		4.8(26)			5.8(53)		11.1		14.7(32)			19.1(72)	
BB[b]	1.1							5.7						
China[e] (IIASA CLE)	11.7					13.8								

[a]Values were obtained from REAS v1.1 (http://www.jamstec.go.jp/frcgc/research/p3/emission.htm; Ohara et al., 2006). [b]BB means emissions from biomass burning obtained from ACESS final version (http://www.cgrer.uiowa.edu/ACESS/acess_index.htm; Streets et al., 2003). [c]Other East Asia is Mongolia, North Korea, South Korea, and Taiwan. [d]Southast Asia is Brunei, Cambodia, Indonesia, Indonesia, Laos, Malaysia, Myanmar, Philippines, Singapore, Thailand, and Viet Nam. [e]Amann (2006).

2.2 Emission Inventories

Past (2000) and future (2010 and 2020) emissions from anthropogenic sectors except biomass burning were obtained from REAS (Ohara et al., 2007). Future projection for the Asian emissions was performed on the basis of emission scenarios and emissions for the year 2000. Three emission scenarios, REF, PSC, and PFC for China, were developed by Zhou et al. (2003). For the other countries, the future emissions were on the basis of reference scenario projections in the World energy outlook (IEA, 2002). The REF is a sustainable scenario with moderate emission increases caused by suppression of energy consumption through energy conservation, clean energy strategy, and moderate deployment of new energy technologies and new emission control technologies. The PSC is an optimistic scenario with low emission increase due to the implementation of strong energy and environmental policies and fast deployment of new energy technologies and new emission control technologies. As shown in Figure 1, NOx emission changes based on the REF and PSC are similar to IIASA CLE (Amann, 2006). The PFC is a pessimistic scenario with high emission increases caused by continuation of current energy supply structure, increased energy consumption, and slow deployments of new energy and emission control technologies. NOx emission changes based on the PFC is close to IPCC A2.

Emissions from biomass burning and volcanoes were obtained from ACE-Asia and TRACE-P Modeling and Emission Support System (ACESS) final version and Streets et al. (2003). Biogenic NMVOC, isoprene and terpene, emissions were obtained from the Global Emission Inventory Activity (GEIA) monthly global inventory (Guenther et al., 1995). Emissions from natural sources, e.g., soil and lightning NOx are not considered in our model simulations.

Table 1 shows major O_3 precursors, annual NOx ($TgNO_2$ yr^{-1}, hereafter Tg yr^{-1} is used) and NMVOC (Tg yr^{-1}), emissions from anthropogenic sources including biomass burning (described as 'BB' in Table 1). Under the REF in 2020 (2020REF), NOx emission increases from 11.2 Tg yr^{-1} in 2000 to 14.0 Tg yr^{-1} in 2010 and 15.6 Tg yr^{-1} in 2020 over China. The 2020REF causes a little NOx decrease (10%) over Japan in 2000–2020. An increase in NOx emissions in other East Asia is predicted as 48 % during 2000–2020. As for NMVOC emissions, the 2020REF brings about large increases. For example, NMVOC emission in China increases by 139% from 14.7 Tg yr^{-1} in 2000 to 35.2 Tg yr^{-1} in 2020, and that is much higher than the NOx case. The PSC brings about a little NOx decrease (-2%) but a large NMVOC increase (139%) during 2000-2020 over China. Meanwhile, the PFC brings about large increases in both NOx (128%) and NMVOC (163%) during 2000-2020 over China. Full details, emission spatial distributions, and comparisons with the other inventories were reported by Ohara et al. (2007).

We have to mention here that all input parameters (boundary conditions, meteorological conditions, and biomass burning, volcanic, and natural emissions) except REAS emissions were held constant in these model experiments, because this work focuses on surface O_3 change caused by future anthropogenic emission changes on the basis of REAS.

3. RESULTS AND DISCUSSIONS

3.1 Validation of Modeled O_3 Concentrations by Observations

O_3 concentrations by CMAQ reproduce observed annual O_3 variations at 4 Japan remote monitoring sites, Tappi (42°N, 139°E), Happo (38°N, 136°E, 1840 m asl), Oki (37°N, 132°E), and Hedo (28°N, 127°E) of the Acid Deposition Monitoring Network in East Asia (EANET) as shown in Figure 2. Figure 3 compares daily-averaged simulated O_3 concentrations with daily-averaged observed O_3 concentrations at the four monitoring sites. These daily-averaged concentrations were obtained from data taken every three hours. This model system can capture

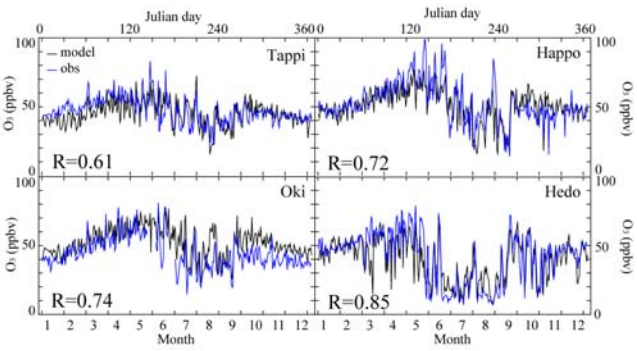

Figure 3 Observed (blue lines) and simulated (black lines) daily-averaged O_3 concentrations at the Japanese monitoring sites of EANET (Tappi, Happo, Oki, and Hedo) for the year 2000. The correlation coefficients between observed and simulated concentrations are shown in the graphs.

the observed O_3 concentration levels with correlation coefficients ranging between 0.61 and 0.85 based on daily-averaged O_3. More detailed comprehensive and systematic validations have been conducted in Yamaji et al. (2006 and 2007).

3.2 Future Surface O_3 Changes over East Asia under Three Different Emission Scenarios

This section compares surface O_3 concentration changes (below 2 km) over East Asia from the year 2000 to the years 2010 and 2020 under the REF, PSC, and PFC. Figure 4 shows the yearly-averaged increases from 2000 to 2010 and 2020 for the three future emission scenarios, respectively.

Under the REF scenario, yearly-averaged O_3 increases in 2-4 ppbv up to 2010 (see 10REF-2000) and 3-7 ppbv up to 2020 (see 20REF-2000) from central China to the Korean peninsula. Even over south Japan (Kyushu area), yearly-averaged O_3 increases in approximately 3 ppbv during 2000-2020 though NOx emission is projected to decrease there. The PSC causes a little O_3 changes during 2000-2010 (see 10PSC-2000) and 2000-2020 (see 20PSC-2000). It is noted that yearly-averaged O_3 over northeast China (but excluding central and east China plane) shows a little decrease (-2ppbv) from 2000 to 2020 under the PSC with a little NOx reduction and a large NMVOC emission increase from 2000 to 2020. As shown in 10PFC-2000 and 20PFC-2000 in Figure 4, the PFC leads to much higher O_3 increases compared to the PSC and the REF cases. Especially for central and east China, yearly-averaged O_3 increases reach 3-7 ppbv in 2000-2010 and more than 10 ppbv in 2000-2020. During 2000-2020, moreover, the predicted yearly O_3 increases, which are only 0-2 ppbv over most of Northeast Asia under the PSC, are enhanced by 6-8 ppbv over the Korean peninsula and by 2-6 ppbv in Japan under the PFC scenario, though there are no differences between scenarios over Japan and the Korean peninsula. These results suggest that the PSC scenario can help lower the potential increase in O_3 concentration and that the PFC scenario promotes a substantial increase in O_3 concentration, not only over China but also over the Korean peninsula and Japan.

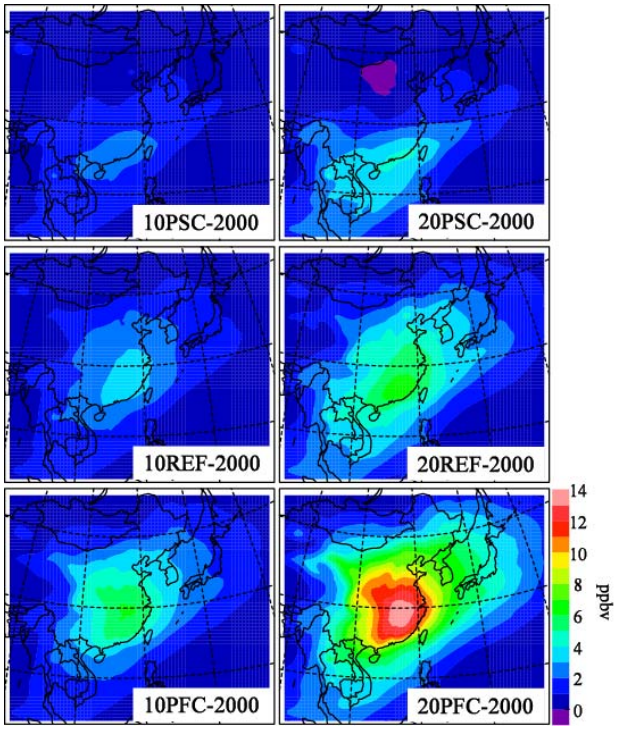

Figure 5 Yearly-averaged O_3 changes (below 2 km) from the year 2000 to the years 2010 and 2020 under three scenarios (PSC, REF, PFC).

3.2 Surface O_3 in Early Summer

Early summer, especially June is the highest O_3 month over Northeast Asia (Yamaji 2006 and 2007), thus this section focus on surface O_3 concentrations in June. Figure 5 shows the monthly-averaged surface O_3 concentrations (below 2 km) in 2000 and 2020 (20REF, 20PSC, 20PFC).

The highest O_3 area, from the North China Plain to the Korean peninsula is covered with 70-80 ppbv of O_3 in the year 2000. The projected 2020REF emissions increase the O_3 concentrations to 80-90 ppbv in the central North China Plain and north the Korean peninsula. Over Northeast Asia, from central eastern China to Japan, the predicted monthly-averaged O_3 concentrations are increased by around 5-10 ppbv during 2000-2020 by anthropogenic emission increases. Meanwhile, the PSC is helpful to moderate the O_3 increase in June. In large parts of northeastern and central China, the monthly–averaged O_3 decreases up to 2 ppbv. On the other hand, a little O_3 increase (2–4 ppbv) is confirmed at a few points near mega–cities at northeastern and central China where NOx emission increase are projected under the PSC (Ohara et al., 2007; Yamaji et al., 2007). The 2020PFC leads to much higher O_3 increases compared to the 2020REF case. Especially, monthly-averaged O_3 concentrations increase to

90-105 ppbv over the North China Plain and a part of the Korean Peninsula.

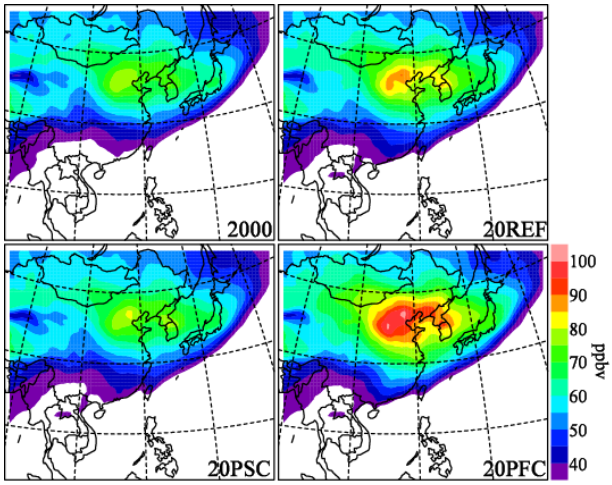

Figure 6 Monthly-averaged O_3 concentration (below 2 km) in June for the year 2000 and the years 2020 under three scenarios (PSC, REF, PFC).

4. SUMMARY

Tropospheric O_3 over East Asia in the future has been simulated by CMAQ coupled REAS emission inventory to predict the surface O_3 changes caused by future anthropogenic emission changes. For future predictions, REAS provides three emission scenarios for China, the REF, PSC, and PFC and one emission scenario, the REF for the other countries. Yearly-averaged O_3 increases in 3-7 ppbv up to 2020 under the REF. The PSC brings about a little O_3 changes in 2000-2020. Yearly-averaged O_3 over the North China Plain increases in more than 10 ppbv in 2000-2020. Especially in June, monthly-averaged O_3 concentrations increase to 90-105 ppbv over the North China Plain and a part of the Korean Peninsula. These model results suggest that the PSC scenario can help lower the potential increase in O_3 concentration and that the PFC scenario promotes a substantial increase in O_3 concentration, not only in China but also over northeast Asia.

5. ACKNOWLEDGMENTS

We would like to thank EANET for providing ozone measurement data. This study has been supported by Global Environment Research Fund of the Ministry of the Environment, Japan (B-051).

6. REFERENCES

Amann, M., 2006: Scenarios of world anthropogenic emissions of air pollutants and methane up to 2030, IIASA report (IR-06-023).

Byun, D.W. and J.K.S. Ching (Eds.), 1999: Science algorithms of the EPA Models-3 community multi-scale air quality (CMAQ) modeling system. *NERL*, Research Triangle Park, NC. EPA/600/R-99/030.

Cotton, W.R., R.A. Pielke, and R.L. Walko, 2003: RAMS 2001: Current status and future directionds. *Meteorol. Atmos. Phys.* **82**, 5-29

Guenther, A., C.N. Hewitt, D. Erickson, R. Fall, C. Geron, T. Graedel, P. Harley, L. Klinger, M. Lerdau, W.A. Mckay, T. Pierce, B. Scholes, R. Steinbrecher, R. Tallamraju, J. Taylor, and P. Zimmerman, 1995: A global model of natural volatile organic compound emissions. *J. Geophys. Res.* **100**, 8873–8892.

IEA, 2002: World Energy Investment Outlook 2002 [CD-ROM].
IPCC, http://sres.ciesin.columbia.edu/

Ohara, T., H. Akimoto, J. Kurokawa, N. Horii, K. Yamaji, X. Yan, and T. Hayasaka, 2007: An Asian emission inventory of anthropogenic emission sources for the period 1980–2020. *Atmos. Chem. Phys.* **7**, 4419-4444.

Pielke, R.A., W. R. Cotton, R.L. Walko, C.J. Tremback, W.A. Lyons, L.D. Grasso, M.E. Nicholls, M.D. Moran, D.A. Wesley, T.J. Lee, and J.H. Copeland, 1992: A comprehensive meteorological modeling system–RAMS. *Meteorol. Atmos. Phys.* **49**, 69–91.

Streets, D.G., K.F. Yarber, J.-H. Woo, and G.R. Carmichael, 2003: Biomass burning in Asia: Annual and seasonal estimates and atmospheric emissions. *Global Biogeochem. Cycles.* **17**, Art. No. 1099, doi:10.1029/2003GB002040.

Sudo, K., M. Takahashi, J. Kurokawa, and H. Akimoto, 2002: CHASER: A global chemical model of the troposphere-1. Model description. *J. Geophys. Res.* **107**, Art. No. 4339, doi:10.1029/2001JD001113.

van Aardenne, JA., GR. Carmichael, H. LevyII, D. Streets, and L. Hordijk, Anthropogenic NOx emissions in Asia in the period 1990–2020, Atmospheric Environment, 33(4), 633-646, 1999

Wild, O. and H. Akimoto, 2001: Intercontinental transport of ozone and its precursors in a three-dimensional global CTM. *J. Geophys. Res.* **106**, 27729-27744

Yamaji, K., T. Ohara, I. Uno, H. Tanimoto, J. Kurokawa, and H. Akimoto, 2006: Analysis of the seasonal variation of ozone in the boundary

layer in East Asia using the Community Multi-scale Air Quality model: What controls surface ozone levels over Japan? *Atmos. Environ.* **40**, 1856-1868.

Yamaji, K., T. Ohara, I. Uno, J. Kurokawa, and H. Akimoto, 2007: Future Prediction of Surface Ozone over East Asia using the Models-3 Community Multi-scale Air Quality Modeling System (CMAQ) and the Regional Emission Inventory in Asia (REAS), *submitted to J. Geophys. Res.*

Yamaji, K., T. Ohara, and H. Akimoto, 2003: A country-specific, high-resolution emission inventory for methane from livestock in Asia in 2000. *Atmos. Environ.* **37**, 4393-4406.

Yamaji, K., T. Ohara, and H. Akimoto, 2004: Regional-specific emission inventory for NH_3, N_2O, and CH_4 via animal farming in South, Southeast, and East Asia. *Atmos. Environ.* **38**, 7111-7121.

Yan, X., Z.C. Cai, T. Ohara, and H. Akimoto, 2003a: Methane emission from rice fields in mainland China: Amount and seasonal and spatial distribution. J. Geophys. Res. **108**, Art. No. 4505, doi:10.1029/2002JD003182.

Yan, X., H. Akimoto, and T. Ohara, 2003b: Estimation of nitrous oxide, nitric oxide, and ammonia emissions from croplands in East, Southeast, and South Asia. *Global Change Biology* **9**, 1080-1096.

Zhang, M.G., I. Uno, S. Sugata, Z.F. Wang, D. Byun, and H. Akimoto, 2002: Numerical study of boundary layer ozone transport and photochemical production in east Asia in the wintertime. *Geophys. Res. Lett.* **29**, Art. No. 1545, doi:10.1029/2001GL014368.

Zhao D., Y. Dai, C. Yu, Y. Guo, Y. Zhu, 2003: China's Sustainable Energy Scenarios in 2020. China Environment Science Press, Beijing, China.

NUMERICAL EXPERIMENTS ON THE SENSITIVITY OF WRF-CMAQ SIMULATIONS OF AIR QUALITY IN THE MISSISSIPPI GULF COASTAL REGION TO PBL AND LAND SURFACE MODELS

Venkata Srinivas Challa, Jayakumar Indracanti, Monika K.Rabarison, John Young, Chuck Patrick, Julius M.Baham, Robert Hughes and Anjaneyulu Yerramilli *
Trent Lott Geospatial and Visualization Research Centre @Mississippi e-Centre, Jackson State University, MS USA

1. INTRODUCTION

Atmospheric Dispersion Studies are carried out in the Mississippi Gulf coastal zone to develop predictive modeling capability for air pollution dispersion and air quality assessment. The ARW Weather Research and Forecasting model (ARW-WRF) (Skamarock et al., 2005) has recently been used to provide meteorological inputs to Community Multiscale Air Quality Model (CMAQ) (Byun and Ching, 1999) for air quality research applications due to WRF's accurate numerics and high quality mass conservation characteristics (Byun and Kim, 2003). Several physical schemes are available in WRF for boundary layer turbulence and surface processes which play important role in the simulation of lower atmospheric winds, temperature and mixing layer depth which in turn effect the simulations of dispersion / air quality. It is important to ensure accurate meteorological inputs from weather model to obtain precise estimations from air quality models since errors in the meteorological fields are passed on to the air quality model (Gilliam et al., 2006). Present study attempts to explore the sensitivity of CMAQ predicted air quality estimations to two PBL and two land surface schemes in the WRF model. The goal of the work is to study the relative performance of the above schemes and model sensitivity to minimize the uncertainty in air quality simulations.

2. NUMERICAL EXPERIMENTS

Meteorological conditions of Mississippi Gulf coastal region are simulated using ARW-WRF version 2.2 for a 3-day period in June 8-11, 2006 and for a 2-day period in June 28-30, 2007 in typical summer synoptic condition. Three nested grids with 60x50 grid points (36 km grid spacing), 124x82 grid points (12 km grid spacing) and 202x136 grid points (4 km grid spacing) and with 34 vertical layers are used in the model (Fig 1). The area of interest is the inner fine grid (4km) covering the MS Gulf coast. The NCEP Eta analysis data at 40 km resolution is used for initial and boundary conditions. FDDA observation nudging is performed to temperature, mixing ratio, and wind fields using NCEP ADP surface and upper air observations up to 720 min. The model physics options are selected as WSM3 class simple ice scheme for microphysics, Kain-Fritisch scheme for convection, RRTM for long wave radiation and Dudhia scheme for shortwave radiation processes. Two PBL schemes (Yonsei University scheme (YSU); Mellor-Yamada-Janjic (MYJ)) and two surface schemes (5-layer soil diffusion model ; Noah land surface model (Noah LSM)) are considered alternatively for the study.

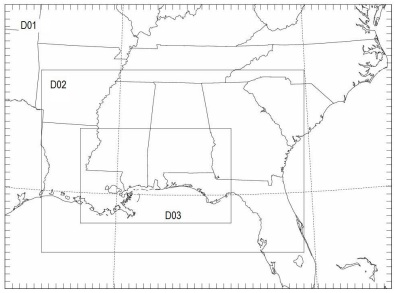

Fig. 1. Model domains in WRF model

The four numerical experiments are i)YSU PBL with Soil model ii)YSU PBL with Noah LSM iii) MYJ PBL with soil model and iv) MYJ PBL with Noah LSM. Air quality simulations are made using CMAQ v4.6 over the MS Gulf coastal region covered by WRF inner fine domain. Same emissions data, initial and boundary conditions are used in CMAQ in the four experiments except the meteorological data which is taken separately from the above runs in each case. Same grid dimensions as in WRF 3rd domain are used in CMAQ while creating meteorological inputs through Meteorology-Chemistry Interface Processor (MCIP).

**Corresponding author:* Yerramilli Anjaneyulu, e-mail: yerramilli.anjaneyulu@jsums.edu, Phone: 601-979-3654

3. RESULTS

Simulation results are evaluated with observations of surface air temperature, surface wind from meso-net stations, and pollutant concentrations from continuous ambient monitoring stations. About 8 upper air stations and 12 meso-net station data is used for evaluating model performance. Diurnal trends of the surface wind and air temperature from the model experiments are compared with observations at an inland station Newton and the coastal site Pascagoula (Figs. 2,3 and 4). After the initial spin up time the model values followed the observed trends. Surface wind speed and wind direction are better simulated in the experiment with YSU PBL and Noah LSM. Strengthening surface winds, and shift in direction associated with sea breeze observed at Pascagoula coastal place is better noticed in the second experiment.

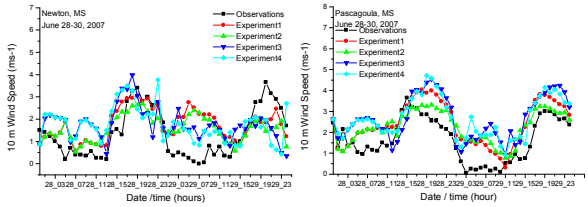

Figure 2. Time series of 10 m wind-speed at Newton (left) and Pascagoula (right).

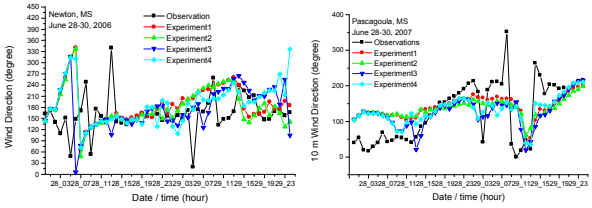

Figure 3. Time series of 10 m wind-direction at Newton (left) and Pascagoula (right)

While the diurnal trend in surface air temperature is similarly predicted in all the experiments, the values obtained in the second experiment are more closer to the observations both during day time and in the night conditions. Temperatures are generally predicted more during the night time and are close to observations during day time in all the cases.

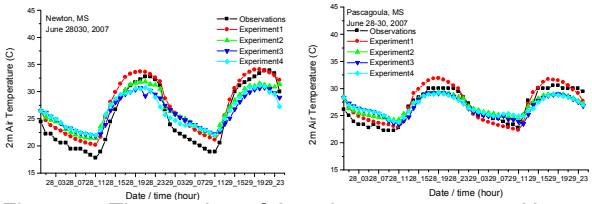

Figure 4. Time series of 2m air temperature at Newton (left) and Pascagoula (right)

Boundary layer height is an important parameter in air quality studies as it determines the effective depth of turbulent mixing of pollutants and their dilution. Model potential temperature at Harrison location near Gulfport is qualiltatively compared with GP Sonde observations taken in a boundary layer experiment at the site for June 28th (Fig. 5). Among the different physics used the YSU PBL with Noah LSM produces the observed stable boundary layer in the morning and the well mixed convective boundary layer in the day time.

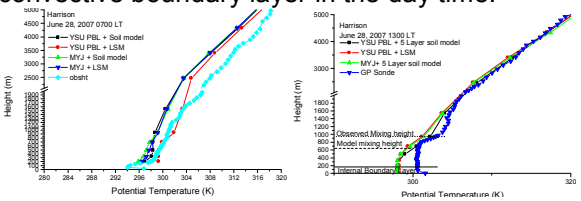

Figure 5. Model and observed potential temperature profiles at Harrison coastal site near MS Gulf coast.

PBL height is expected to be low at the coastal site Pascagoula and relatively high at the inland location Newton. Time series of PBL height in all the model experiments shows this pattern, however experiments with the MYJ scheme shows fluctuations and the daytime PBL height given by it are relatively very high (Fig 6). Experiment with YSU PBL and Noah LSM gives a smooth variation and realistic values at both the sites, however this needs comparison with observations.

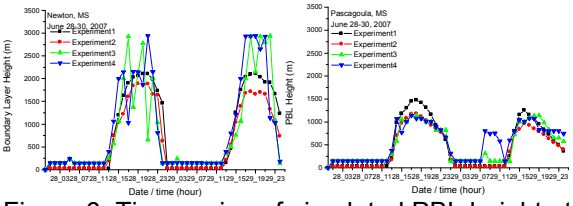

Figure 6. Time series of simulated PBL height at Newton (left) and Pascagoula (right).

Spatial plots of horizontal wind in the 3rd domain show almost similar trends in all the experiments (Fig 7). All the experiments indicate strong southeasterly winds associated with sea breeze and its considerable inland extent. Spatial plots of boundary layer height (Fig 8) indicate coastal belts in Mississippi, Louisiana and Alabama have relatively lower mixing height in the experiments with YSU PBL scheme. GP Sonde observations of potential temperature (Fig 5) confirmed this shallow mixing height forming in the day time due to internal boundary layer development after sea breeze setting at the coast.

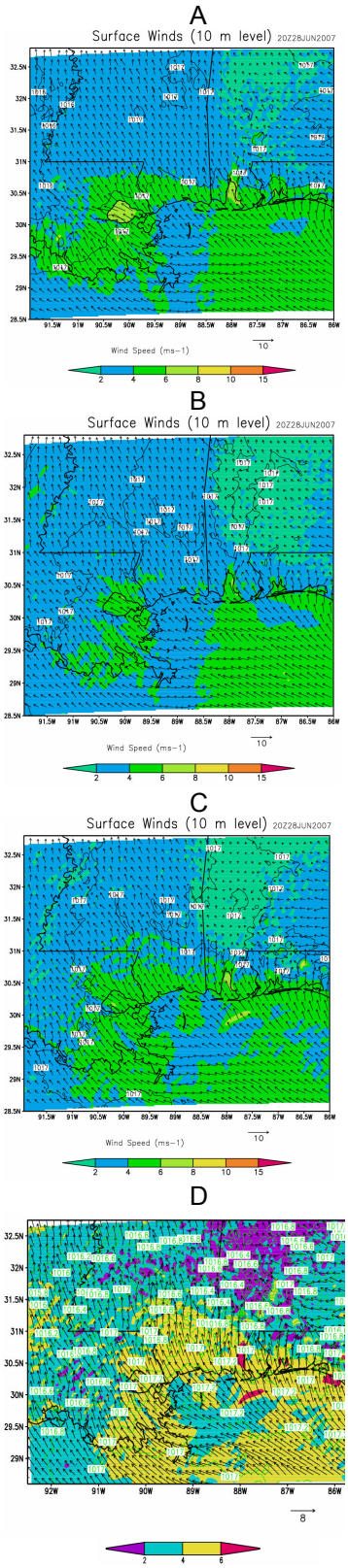

Figure 7. Spatial plots of horizontal wind and sea level pressure at 20 UTC (14 LTC), 28th June, 2007, a) YSU PBL, Soil model b) YSU PBL, Noah LSM c) MYJ PBL, Soil model and d) MYJ PBL, Noah LSM.

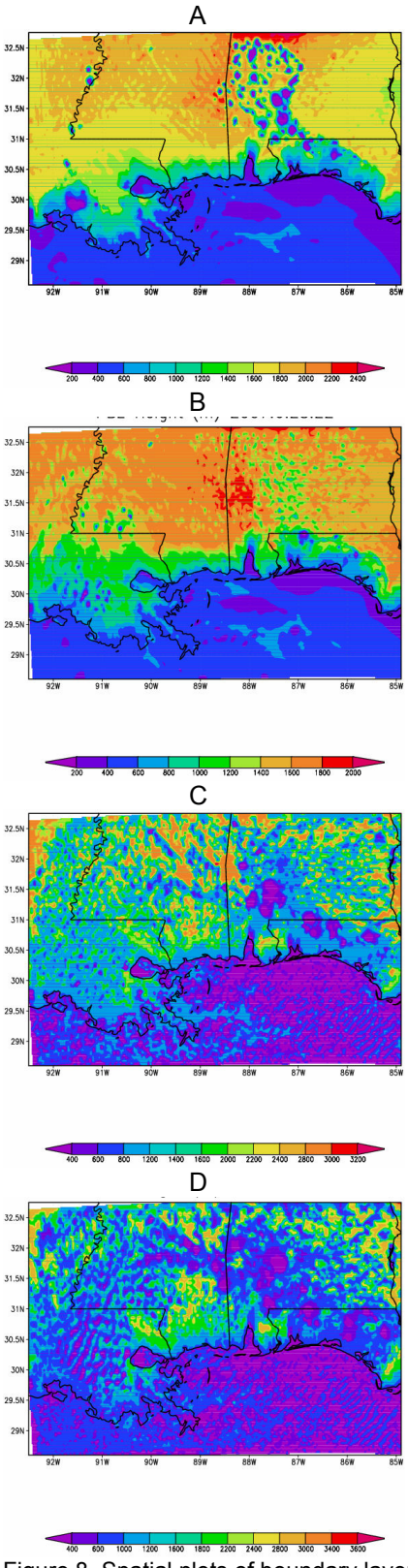

Figure 8. Spatial plots of boundary layer height at 20 UTC (14 LTC), 28th June, 2007, a) YSU PBL, Soil model b) YSU PBL, Noah LSM c) MYJ PBL, Soil model and d) MYJ PBL, Noah LSM

Additional analysis with detailed statistics (correlation, bias and root mean square error) of the predicted and observed mean meteorological parameters both at surface and 850 hpa levels are being made to study the relative performance of the experiments with different options for PBL and surface processes. Analysis of CMAQ model predicted ozone and other pollutant concentrations in each case of the meteorological inputs from the above experiments are being conducted to study the sensitivity of the predicted air concentrations.

4. CONCLUSION

WRF ARW model (version 2.2) is used to simulate the meteorological conditions in the Mississippi Gulf coastal region to simulate a high ozone episode during June 28-30, 2007 and June 8-11, 2006 using CMAQ. Numerical experiments with several physics options for PBL and surface processes indicate YSU PBL along with Noah LSM give realistic meteorological predictions in the lower atmospheric region. Winds, temperature and mixing height near the coast are better simulated with the above combination. Further work for inferring the relative performance of the model with the PBL and surface process schemes is being performed basing on detailed statistical indices of correlation, root mean square error and bias. Also the skill of each experiment and its sensitivity on the CMAQ simulated concentrations is to be studied.

ACKNOWLEDGEMENT

Authors thank for the support of the Atmospheric Dispersion Project (ADP) funded by the National Oceanic and Atmospheric Administration through the U.S. Department of Commerce (Silver Springs, MD); Contract #NA06OAR4600192.

REFERENCES

Byun, D.W., Ching, J.K.S. (Eds.), 1999. Science algorithms of the EPA Models-3 Community Multiscale Air Quality Model (CMAQ) modeling system. EPA/600/R-99/030, US Environmental Protection Agency, Office of Research and Development , Washington, DC 20460.

Gilliam, R.C., Hogrefe, and Rao, S.T. 2006. New methods for evaluating meteorological models used in air quality applications. Atmos Envi. 40, 5073-5086.

Skamarock, W.C., Klemp, J., Dudhia, J., Gill, D.O., Barker., D.M., Wang, W., and Powers, J.G. 2005. A Description of the Advanced Research WRF Version 2. NCAR Technical Note, NCAR/TN-468+STR. Mesoscale and Microscale Meteorology Division, National Center for Atmospheric Research, Boulder, Colorado, USA

Byun, D.W. and S.B.Kim, 2003. On-line and off-line paradigms of linking WRF with an air quality modeling system, The fourth WRF User's Workshop, Boulder, CO, USA.

DATA ASSIMILATION AND PERFORMANCE EVALUATION OF WRF FOR AIR QULAITY MODELING IN MISSISSIPPI GULF COASTAL REGION

Venkata Srinivas Challa, Jayakumar Indracanti, Sugam Sharma, Julius M.Baham, Chuck Patrick, Monika K.Rabarison, John Young, Robert Hughes and Anjaneyulu Yerramilli *
Trent Lott Geospatial and Visualization Research Centre @Mississippi e-Centre, Jackson State University, MS USA

1. INTRODUCTION

Atmospheric Dispersion Studies are carried out in the Mississippi Gulf coastal zone to develop predictive modeling capability for air pollution dispersion and air quality assessment. The ARW Weather Research and Forecasting model (ARW-WRF) (Skamarock et al., 2005) along with Community Multiscale Air Quality Model (CMAQ) (Byun and Ching, 1999) is widely used for air quality research applications. It is important to ensure accurate meteorological inputs from weather model to obtain precise estimations from air quality models since errors in the meteorological fields are passed on to the air quality model (Gilliam et al., 2006). Interaction of the synoptic flow and the local meso-scale circulations such as sea-breeze at the Mississippi coastal region attain importance in meso-scale simulations and consequently on the predicted air quality. Data assimilation has been shown to improve the initial conditions to the meteorological models and their performance (Seaman, 1992; Stauffer and Seaman, 1994). In this work an attempt is made to examine the impact of data assimilation on the WRF produced meteorological fields using the conventional observations and analysis fields and their sensitivity to air quality estimations in the Mississippi Gulf coastal region for the summer 2006.

2. NUMERICAL EXPERIMENTS

Meteorological conditions of Mississippi Gulf coastal region are simulated using ARW-WRF version 2.2 for the period June 8-11,2006 associated with a high ozone occurrence event in the region. Three nested grids with 60x50 grid points (36 km grid spacing), 124x82 grid points (12 km grid spacing) and 202x136 grid points (4 km grid spacing) and with 34 vertical layers are used in the model (Fig 1). The area of interest is the inner fine grid (4km) covering the MS Gulf coast. The NCEP Eta analysis data at 40 km resolution is used for initial and boundary conditions. Model physics options selected are WSM3 class simple ice scheme for microphysics, MRF scheme for PBL turbulence parameterization, Noah LSM for ground temperature and moisture prediction, Kain-Fritisch scheme for convection, RRTM for long wave radiation and Dudhia scheme for shorwave radiation processes.

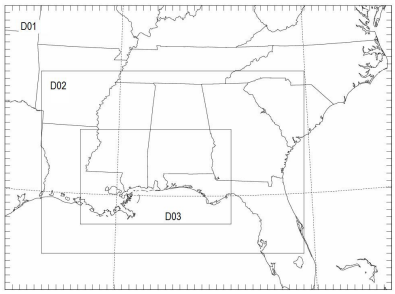

Fig. 1. Model domains in WRF model

Three numerical experiments are conducted: the first is a control run with no data assimilation, the second one with FDDA observation nudging using NCEP ADP surface and upper air observations upto 720 min and the third with grid nudging up to 12 hours.

Air quality simulations are made using CMAQ v4.6 over the MS Gulf coastal region covered by WRF inner fine domain. Same emissions data, initial and boundary conditions are used in CMAQ in the three experiments except the meteorological data which is taken separately from the above runs in each case. Same grid dimensions as in WRF 3rd domain are used in CMAQ while creating meteorological inputs through Meteorology-Chemistry Interface Processor (MCIP).

3. RESULTS

Model simulation results are evaluated with observations of air temperature, surface wind, from meso-net stations , and pollutant concentrations from continuous ambient monitoring stations. Diurnal trends of the surface

*Corresponding author: Yerramilli Anjaneyulu, e-mail: yerramilli.anjaneyulu@jsums.edu, Phone:601-979-3654

wind speed and wind direction from the three individual runs are compared with observations at an inland station Newton and the coastal site Pascagoula (Figs.2 and 3). Both the experiments with data assimilation show improvement in day time wind over the control run which is significantly noticed at Pascagoula coastal place. Wind shift at the coastal site due to sea breeze, timing of its onset and associated strong winds are better predicted in the experiment with data assimilation. Also results from grid nudging appear to be better predicted than those from observation nudging.

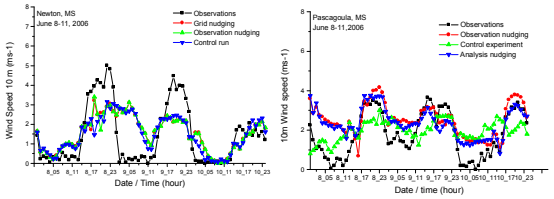

Figure 2. Time series of 10 wind-speed at Newton (left) and Pascagoula (right).

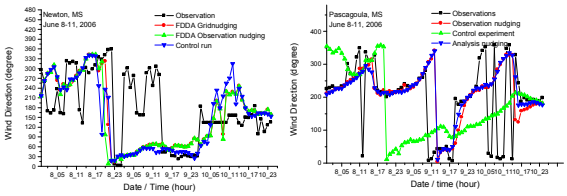

Figure 3. Time series of 10 wind-direction at Newton (left) and Pascagoula (right)

Surface air temperature at 2 m height is predicted similarly in all the three experiments (Fig.3). Temperatures are over predicted during the night time and are close to observations during day time.

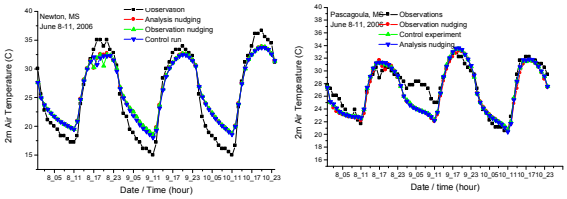

Figure 3. Time series of 2m air temperature at Newton (left) and Pascagoula (right)

Boundary layer height is an important parameter in air quality studies as it determines the effective depth of turbulent mixing. PBL height from the three experiments (Fig 4) indicates smooth diurnal variation in the case with analysis nudging and seems to be more realistic, however this needs comparison with observations.

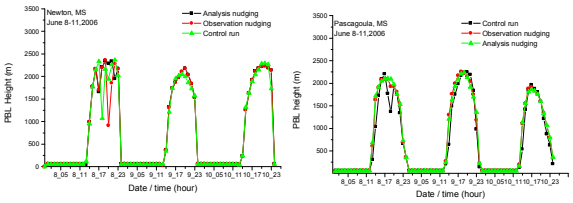

Figure 4. Time series of simulated PBL height at Newton (left) and Pascagoula (right).

Plots of horizontal wind in the 3rd domain show almost similar spatial trends in the experiments with data assimilation (Fig 5). Winds associated with sea breeze, its spatial extent are better simulated in both the experiments with data assimilation.

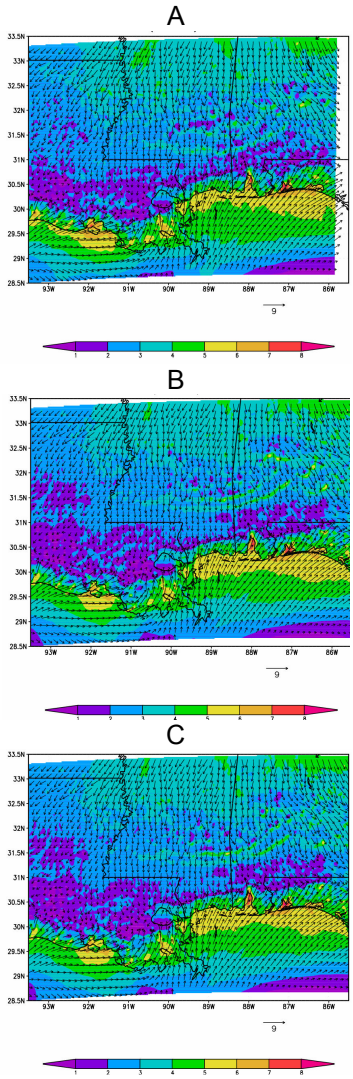

Figure 5. Spatial plots of horizontal wind at 22 UTC (16 LTC), 8th June,2006, a) control run b) observation nudging c) analysis nudging.

Spatial plots of boundary layer height (Fig 6) indicate coastal belts in Mississippi and Alabama have relatively lower mixing height in the experiment with observation nudging than the control run and the analysis nudging. This needs verification with profiler observations in the region. However lower mixing heights are anticipated adjacent to the coast especially in the day time when sea breeze penetrates inland and forms an internal boundary layer.

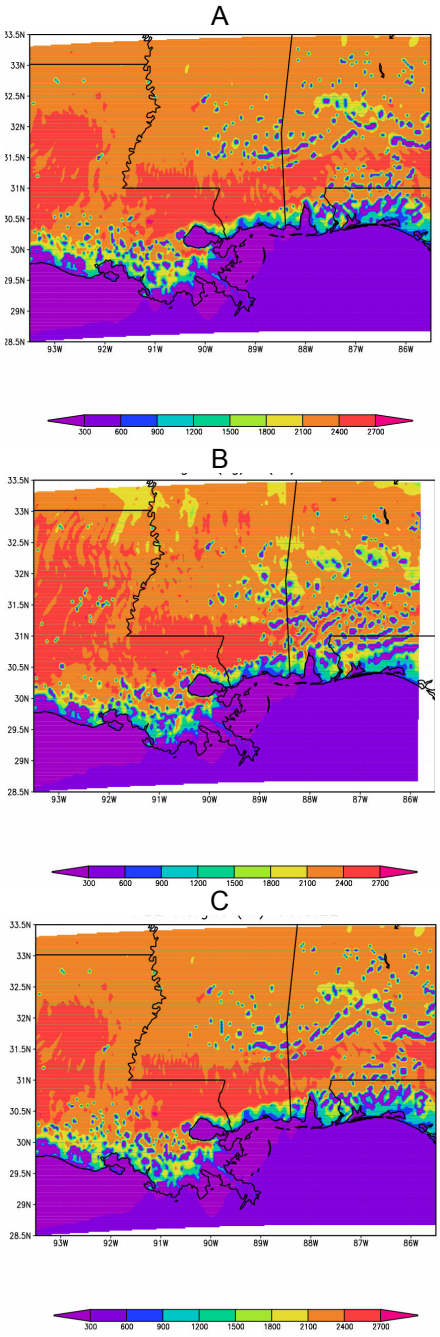

Figure 6. Spatial plots of boundary layer height at 22 UTC (16 LTC), 8th June,2006, a) control run b) observation nudging c) analysis nudging

Additional analysis with detailed statistics (correlation, bias and root mean square error) of the predicted and observed meteorological parameters both at surface and 850 hpa levels are being carried out to study the relative performance of the experiments with nudging. Analysis of CMAQ model predicted ozone and other pollutant concentrations in each case of the meteorological inputs from the above experiments are being conducted to study the impact of data assimilation and their relative skills on the predicted concentrations.

4. CONCLUSION

WRF ARW model version 2.2 is used to simulate the meteorological conditions in the Mississippi Gulf coastal region to simulate a high ozone episode during June 8-11, 2006 using CMAQ. WRF simulations with data assimilation have shown improvement over the control run in the prediction of near surface winds, temperature and the spatial trends of mixing height. Model parameters near the coast are better simulated with data assimilation, such as wind direction and mixing height. Further work for determining the relative performance of data assimilation techniques has to be done basing on the detailed statistical indices of correlation, root mean square error and bias. Also the skill of each experiment on the CMAQ simulated concentrations is to be studied.

ACKNOWLEDGEMENT

Authors thank for the support of the Atmospheric Dispersion Project (ADP) funded by the National Oceanic and Atmospheric Administration through the U.S. Department of Commerce (Silver Springs, MD); Contract #NA06OAR4600192.

REFERENCES

Byun, D.W., Ching, J.K.S. (Eds.), 1999. Science algorithms of the EPA Models-3 Community Multiscale Air Quality Model (CMAQ) modeling system. EPA/600/R-99/030, US Environmental Protection Agency, Office of Research and Development , Washington, DC 20460.

Gilliam, R.C., Hogrefe, and Rao, S.T. 2006. New methods for evaluating meteorological models used in air quality applications. Atmos Envi. 40, 5073-5086.

Seaman, N.L., 1992. Meteorological modeling applied to regional-air quality studies using four-dimensional data assimilation. Environmental modeling. P.Melli and P.Annetti, Eds., Computational Mechanics Publications, 65-88.

Skamarock, W.C., Klemp, J., Dudhia, J., Gill, D.O., Barker., D.M., Wang, W., and Powers, J.G. 2005. A Description of the Advanced Research WRF Version 2. NCAR Technical Note, NCAR/TN-468+STR. Mesoscale and Microscale Meteorology Division, National Center for Atmospheric Research, Boulder, Colorado, USA

Stauffer, D.R., and Seaman, N.L., 1994. Multiscale Four-Dimensional Data Assimilation. J.Appl.Meteor. Vol.33, 416-434.

High Time-Resolution Winds and Effects upon Air Quality Modeling A 4KM California August 2006 Case Study

Carlie J. Coats, Jr.* [*1,]
M. Talat Odman[2]
and Saswatti Datta[1]

[1]Baron Advanced Meteorological Systems, LLC.
[2]Department of Environmental Engineering, Georgia Institute of Technology

Statement of the Problem

Both temporal and spatial resolution are closely tied to the scale of phenomena that may be simulated, as indicated by the *Nyquist–Shannon Sampling Theorem*: a model with spatial scale *dx* or temporal scale *dt* cannot resolve phenomena smaller than *2 dx* or *2 dt*, respectively. One may further add a principle that speed is the transformation factor between spatial and temporal resolution, and arrive at criteria for determining the desired temporal resolution for driving an air quality model with 4 KM resolution. This is somewhat limited by the *actual* spatial and temporal resolution achieved by the driving meteorology model, due to internal smoothing and other effects within the model.

Spectral analysis of spatial variability various mesoscale meteorology models shows that they do not achieve the theoretical *2dx* limit of resolution: MM5 and RAMS do not resolve features smaller than *7 dx* well; WRF achieves *5 dx*, whereas Eta is limited to about *10 dx*. Given MM5 as a driver and a 4 KM model resolution, we will see features of size 28 KM, requiring *dx*=14 KM to resolve. Assuming a "reasonable" top-of-PBL wind speed of 10 m/sec, this corresponds to a temporal resolution *dt*=1400 sec, a little over 20 minutes. Larger time steps for the input meteorology will not resolve atmospheric features actually simulated by the meteorology model. Another issue is *temporal features* in the meteorology, one of the most prominent of which is *gravity waves,* which have observed periods on the order of 10-30 minutes in MM5 simulations and a theoretical limit of the *Brunt-Vaisala Period*, which is about 10 minutes. When these are not resolved correctly, there will be anomalies in the vertical wind components leading to transport and/or conservation errors, when the sampled upward or downward component of the gravity waves are applied for much too long a modeling period.

This failure to resolve meteorology features will result in (among other things) conservation and/or transport failures that can only partially be alleviated by after-the-fact "conservative" advection algorithms in the air quality model.

We selected an August 2006 air quality episode, constructed a nested 36/12/4 KM MM5 domain consistent with the CCOS CAMx domain, and ran MCPL-augmented MM5 for this domain and episode, generating 10-minute time step output compatible with CMAQ and MAQSIP. We constructed a tracer emissions data set with ten time-invariant stack-plumes located at the ten largest NOx emissions sites in the CCOS domain (as determined by the analysis of the CCOS year-2000 episode emissions files), and ran the tracer version of MAQSIP-RT on these data sets

MM5 Set-Up

We constructed a nested 36/12/4 KM MM5 domain using the same 51-level layer definitions as the CCOS MM5, and with at least 5-cell borders around the CCOS atmospheric chemistry domain and around each nest within its parent. Grid dimensions were 42x42 at 36 KM, 78x78 at 12 KM, and 195x195 at 4 KM. This last is shown in Figure 1, below. The

Corresponding author: Carlie J. Coats, Jr., Baron Advanced Meteorological Systems LLC., 920 Main Campus Drive, Suite 101, Raleigh NC 27606

TERRAIN program was run in *Mode 6,* i.e., using 30-arcsecond terrain and land use data for all grids. Input meteorology data were from the GFS model.

MM5 is run with the MCPL output module, giving very flexible windowing on-the-fly to the air quality domain, and directly producing Models-3 I/O API files for input to MAQSIP and CMAQ. The same physics options used in the BAMS operational forecast modeling were used for this run, including particularly:

ICUPA=8,8,1 Kain-Fritsch-2 convection at 36,12 KM
IMPHYS=5,5,5 Reisner-1 microphysics
IBLTYP=5,5,5 MRF PBL

The 36 KM coarse MM5 grid was run from 00 Z on August 1, 2006, through 12 Z on August 4, 2006. The 12KM intermediate MM5 grid started at 06 Z. and the 4 KM fine grid (containing the CCOS grid) started at 12 Z. Note that grid start-up tends to cause "shocks" to the system which take 2-3 hours to settle down, so the MAQSIP-RT runs were started 3 hours later yet, at 15 Z.

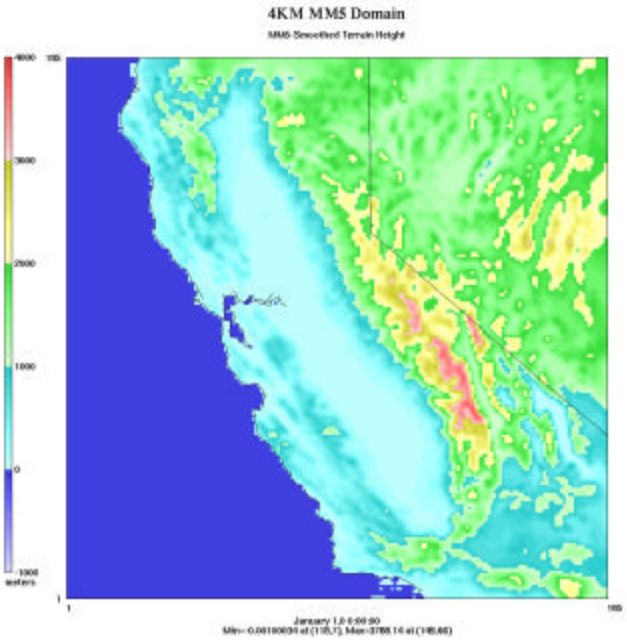

Figure 1 Terrain Elevation for 4KM domain

Output time step for the 4 KM grid was set at 10 minutes, adequate to resolve features reproduced by MM5, while at the same time keeping data volumes from exceeding available resources. (The three-day 4 KM MAQSIP-input file sets amounted to about 90 GB; 5-minute time step output that would have resolved the theoretical 10-minute *Brunt-Vaisala period* for gravity waves would have exceeded available resources. Features that short are not captured by a 4 KM MM5, in any case.). For the same reason, 4 KM run length was limited to three days rather than the hoped-for five days.

We used standard off-the-shelf Models-3 tools **`M3CPLE`** and **`M3INTERP`** to sample the output (the *HTR case*) meteorology files to files with a 1–hour time step and then **`M3TINTERP`** to interpolate the one-hour data back to files with a 10-minute time step for analysis of time-interpolation errors and for input to MAQSIP-RT (the *INTERP* case). These latter files provide a visualizable/analyzable counterpart to the time interpolation that occurs internally within the air quality models.

MAQSIP-RT Set-Up

MAQSIP-RT is an air quality model from the same original code base as CMAQ, but has been substantially restructured, optimized, and parallelized using OpenMP. It has been used for twice-daily air quality forecasts (as well as for regulatory applications) at MCNC and then at BAMS since 1998. Current versions use the Bott version of the Odman-Russel conservative advection scheme; unlike vanilla CAMx it maintains mass consistency between the concentration and dry deposition fields (a discrepancy we found in another phase of this project). A nice feature of MAQSIP-RT for this study is that it uses Models-3 I/O API *INTERP3()* functionality to support virtually any regular time step structure on any of its input files (including time-independent data files; the time step granularity is one second) ; moreover, these are independent on a file-by-file basis.

Emissions were constructed with 10 tracer species, each with its own unique source, with locations selected from the top-10 NO_X emissions cells. Each source was an idealized point source with uniform unit emissions for 10 layers in the vertical, with time independent emissions fluxes. MAQSIP-RT was configured tracer-only, on a 185x185 window into the MM5 4 KM grid, with the same vertical structure as the MM5. Dry deposition velocities for ozone were used for all tracers; wet deposition was set to zero, and the full model dynamics (advection and diffusion) and cloud physics were used.

The tracer-MAQSIP-RT was run with both HTR-case and INTERP-case meteorology, started at 15 Z (three hours after nest initialization in MM5), and ran for 66 hours with a 30-minute output time step. **PAVE** and **M3STAT** analyses were made of both cases and of the differences.

MM5 Analysis

Analysis was performed on the wind fields, that being a primary driver of transport in the air quality models. Qualitatively, this analysis indicates that the interpolation error is concentrated mostly in the mountains, and is mostly weak and disorganized in the San Joaquin Valley. Exceptions to this pattern occur in the 07:00-09:00 AM and PM hours (local daylight time), when there are larger and more organized wind-error patterns there. We conjecture that this is due to the failure of the hourly data to capture transport effects associated with the morning and evening stability transitions. These effects seem to be a major driver to the differences in tracer-species plume trajectories, as well. An example morning vector/tile wind error plot is found in Figure 2 below. Note that error in interpolating from hourly data is zero on the hour, and typically increases to a maximum on the half-hour. Note also that the error is *much* larger at the 12Z start of the MM5 runs, dying off to its "normal" levels by the 15Z time used to start MAQSIP-RT.

Grid-wide statistical and error analysis was performed on selected layers (1, 5, 10, 20) of the wind fields. For each wind component, selected layer, and (10-minute) time step, the grid-maximum and grid-mean of the INTERP-case field and of the interpolated-field vector error were computed. Likewise, the grid-maximum and grid-mean of the magnitude (wind-speed) for the INTERP-case field and for the magnitude of the error-field (which has units M/S) was computed. The time series plot for Layer 1 wind speed and error-magnitude is shown in Figure 3 below. Note that there is a strong diurnal pattern in the magnitude of the interpolation errors. This pattern has a minimum around 3:00 PM local time. Note also that on occasion the maximum error magnitude exceeds the grid mean wind speed (an effect that is even stronger in Layer 5 than in Layers 1, 10, or 20). The magnitude of grid-mean interpolation error typically ranges from 0.2-0.5 M/S at the half-hours for all layers; the magnitude of grid-maximum interpolation error ranges from 1-5 M/S in Layer 1, 2-10 M/S in Layer 5, 2-7 M/S in Layer 10, and 1–5 M/S in Layer 20.

MAQSIP-RT Analysis

We made statistical and graphical analyses of Layer 1 and Layer 5 *HTR Case* and *INTERP Case* and outputs and of their differences, for all ten MAQSIP-RT tracer variables. Treating the 10-minute meteorology time-step HTR Case runs as "reality", and the 1-hour met-step INTERP Case runs as differing from it by errors due to the interpolation of meteorology data, the largest error found in the study was for *TRAC04* at 14:30Z on Aug. 3, 2006 (Figures 4, and 5, below), where a substantial difference in plume placement and down-wind transport caused an error range [–1.68256 to 0.315026]. For comparison, at this time the HTR case and the INTERP case *TRAC04* had ranges [0,1.09999] and [0,2.24491], respectively (comparable in magnitude to the error-range). Generally, the largest plume-errors were found at 02:30-03:30 and 14:30-15:30Z, following the largest met-interpolation errors.

Of the grid-aggregate error statistics, we found the grid-mean statistics least useful, since the grid was dominated by the near-zero tracer concentrations distant from the sources. Time series plots for *TRAC04* concentration maximum and maximum absolute error were most useful. Layer 1 time series are given in Figure 6, below. Typically, maximum absolute error is about one order of magnitude smaller than maximum concentration for all the layers (1-20) studied.

Acknowledgements

This work was funded under the Central California Ozone Study's request for proposals, "Improve Conservation of Mass Module in Air Quality Models". The statements and conclusions of this report are those of tine Investigator, and not necessarily those of the California Air Resources Board, the San Joaquin Valleywide Air Pollution Study Agency, or its Policy Committee, their employees or their members. The mention of commercial products, their source, or their use in connection with material reported herein is not to be construed as actual or implied endorsement of such products.

References

Grell, G., J. Dudhia and D. Stauffer, 1994.A description of the Fifth-Generation Penn State/NCAR Mesoscale Model (MM5), *NCAR Technical Note: NCAR/TN-398+STR*

Odman, M.T. and A.G. Russell, 2000. Mass conservative coupling of non-hydrostatic meteorological models with air quality models, in *Air Pollution Modeling and its Application XIII*, (S.-E. Gryning and E. Batchvarova, Eds.), New York, Kluwer Academic/Plenum Publishers, pp. 651-660.

Figures

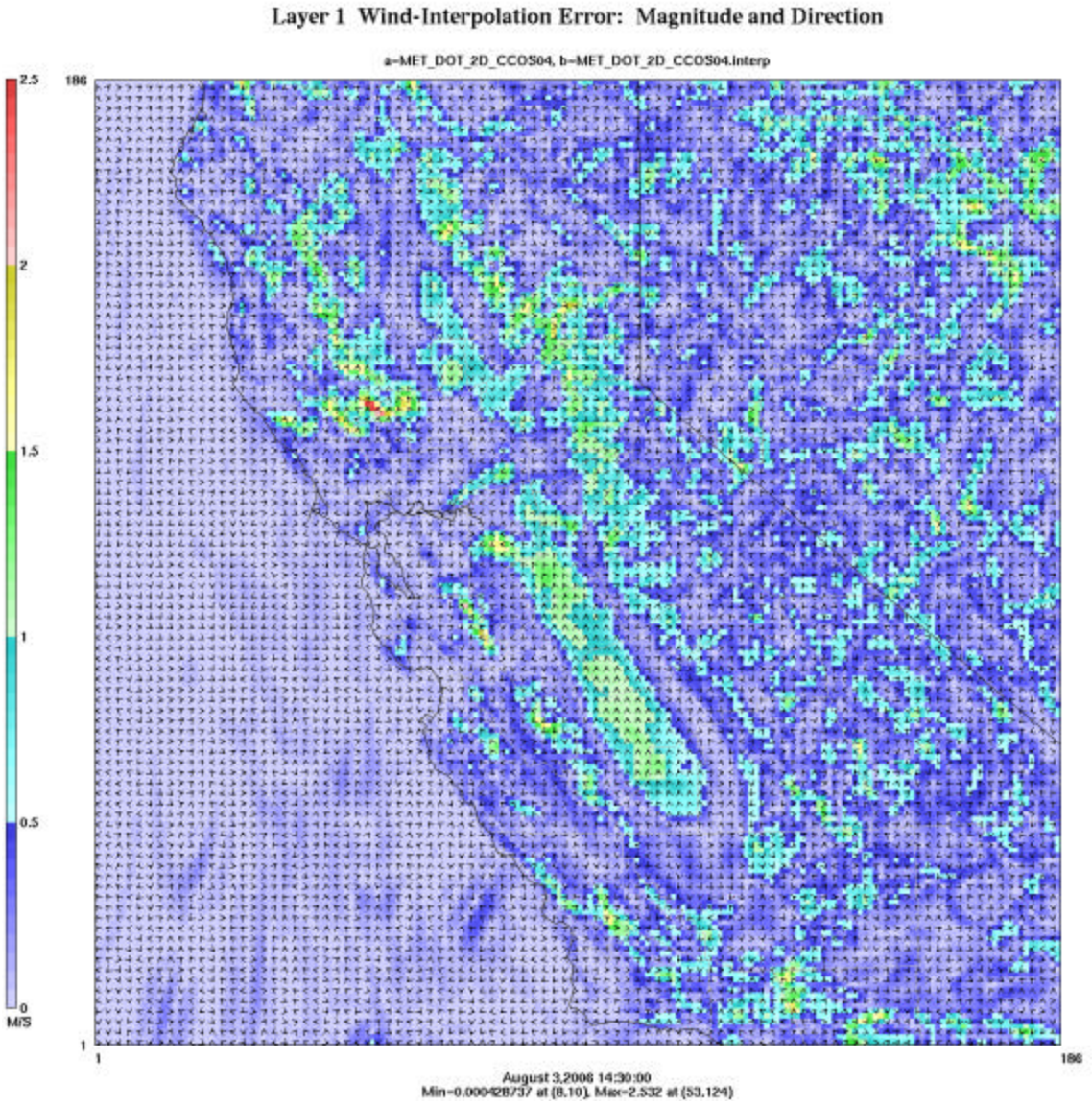

Figure 2: Morning-transition wind interpolation error for Layer 1 at 14:30 Z on August 3, 2006, (local time 7:30 AM PDT). Wind arrows denote the direction, and color denotes magnitude of the error (M/S). Note the organized flow in the south/central San Joaquin Valley. The spatial pattern is typical of 14:30Z, but this may be the most prominent case in the 69-hour run. For related tracer-plumes and their errors at this time, see Figures 4, and 5 below.

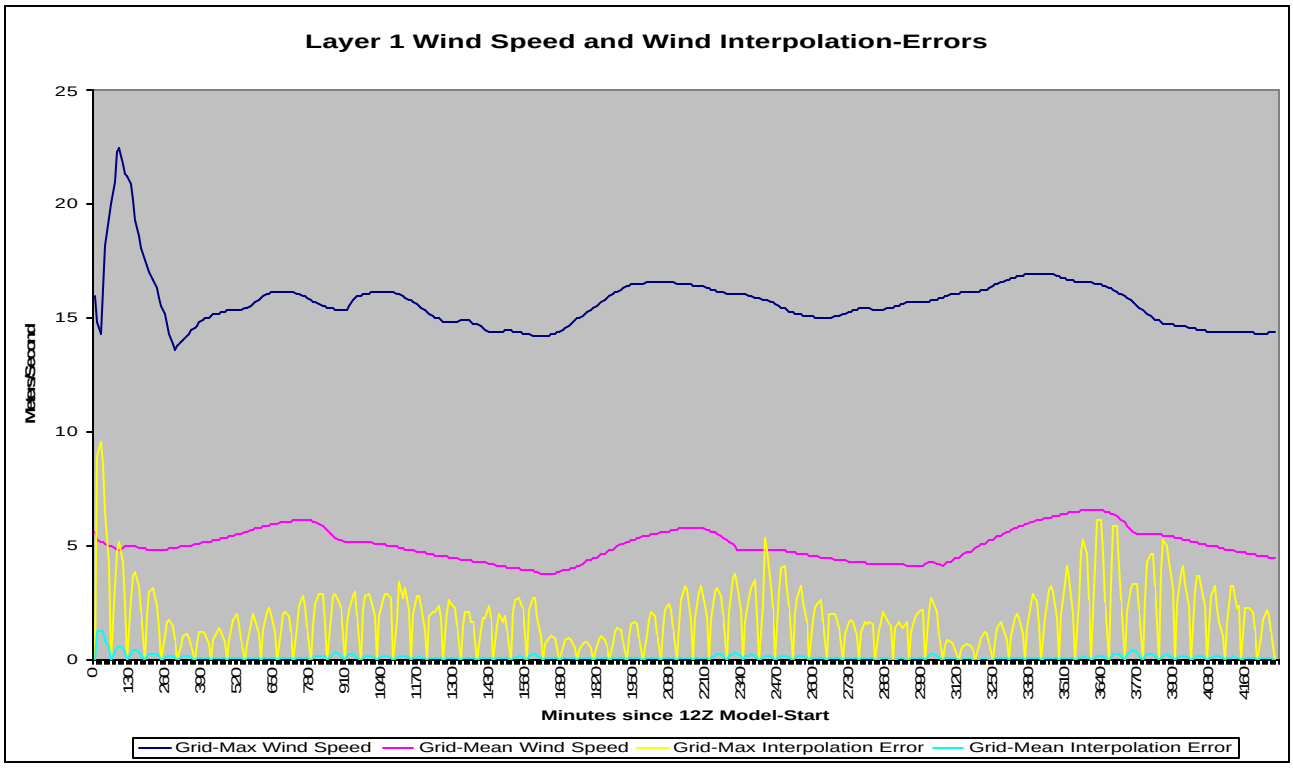

Figure 3: .Grid-mean and grid-maximum wind speed and magnitude of wind error for Layer 1. Note that error is zero on the hour, and is greatest at the half-hour.

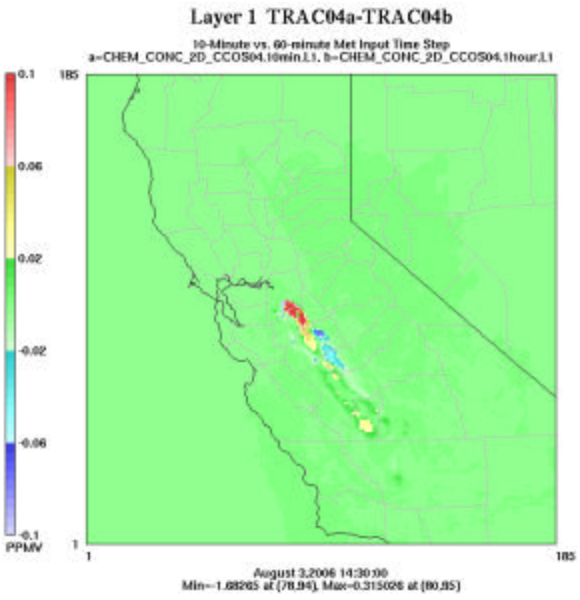

Figure 4: Error in early-morning INTERP-Case tracer plume for *TRAC04* at 14:30Z (07:30 AM PDT, simulation hour 47.5) August 3, 2007. See Figure 2 for the wind-error plots for the same date and time.

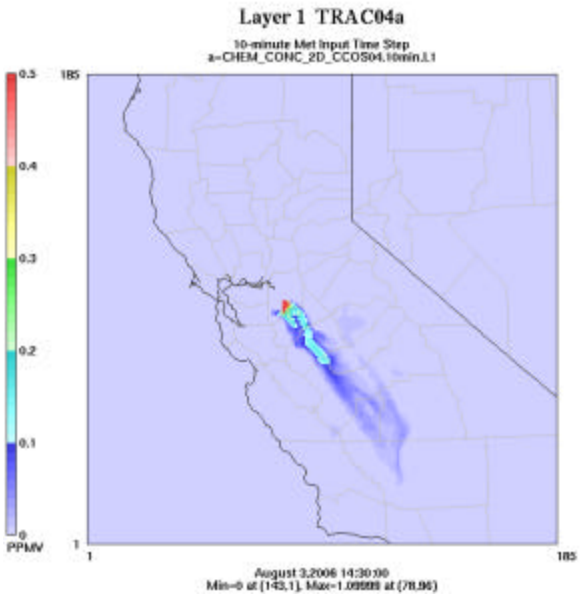

Figure 5: HTR-Case tracer plume for *TRAC04* at 14:30Z August 3, 2007

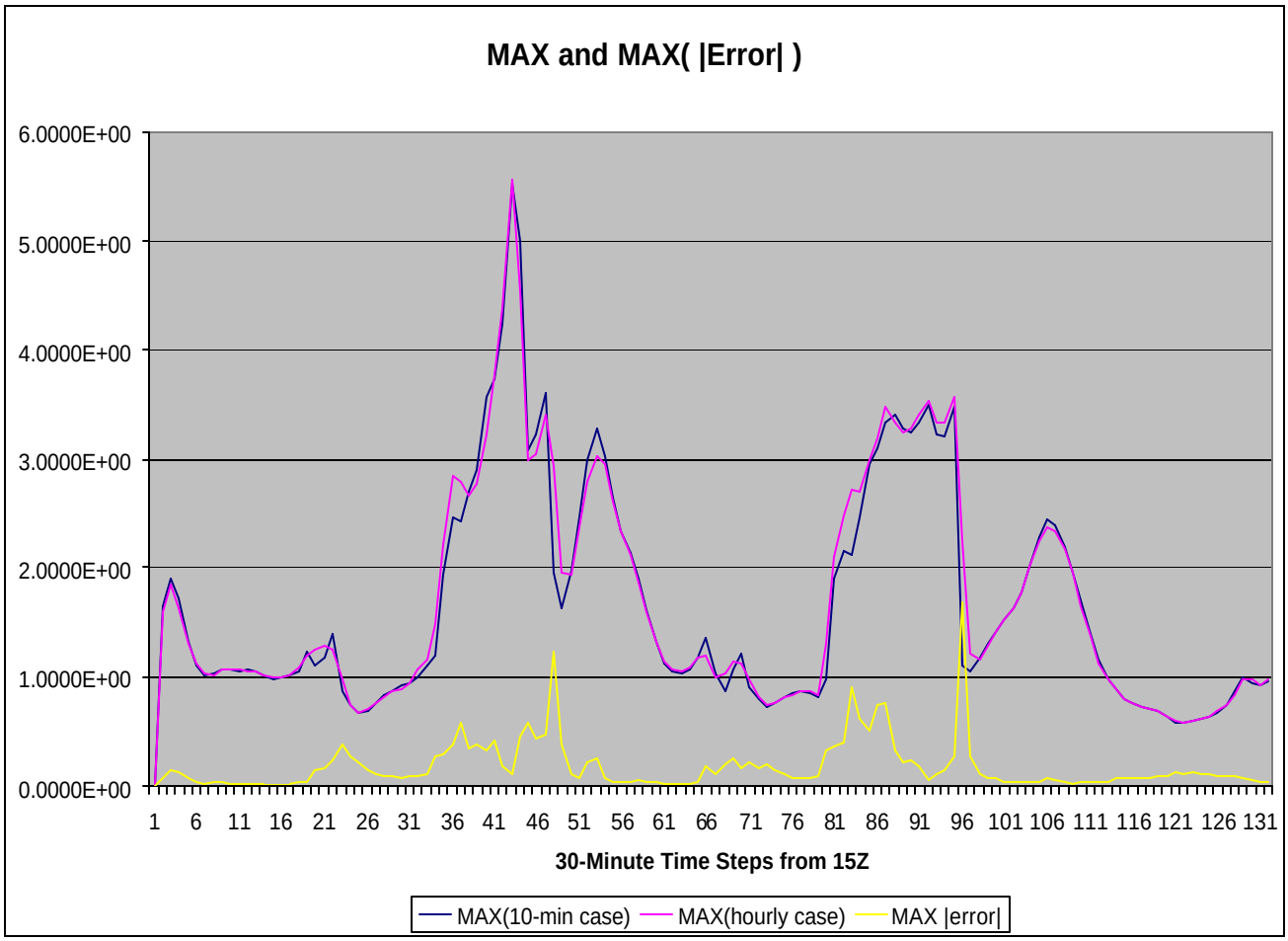

Figure 6: Time series for *TRAC04* maximum HTR Case concentration, maximum INTERP Case concentration, and maximum absolute error.

REGIONAL AND LOCAL-SCALE EVALUATION OF 2002 MM5 METEOROLOGICAL FIELDS FOR VARIOUS AIR QUALITY MODELING APPLICATIONS

Pat Dolwick*
U.S. Environmental Protection Agency, Research Triangle Park, NC, USA

Rob Gilliam
National Oceanic and Atmospheric Administration, Research Triangle Park, NC, USA

Lara Reynolds and Allan Huffman
Computer Sciences Corporation, Research Triangle Park, NC, USA

1. INTRODUCTION

Prognostic meteorological models are often used in a retrospective mode to provide inputs to air quality models. In turn, these air quality models are used for environmental planning. The meteorological inputs govern the advection, diffusion, chemical transformation, and eventual deposition of pollutants within regional air quality models such as the Community Multi-scale Air Quality (CMAQ) modeling system (Byun and Schere, 2006). The air quality models have traditionally been subjected to a rigorous performance assessment, but in many cases the meteorological inputs to these models are accepted as is, even though this component of the modeling arguably contains equal uncertainty.

Before initiating the air quality simulations, it is important to identify the biases and errors associated with the meteorological modeling inputs. The goal of the meteorological evaluation should be to move toward an understanding of how the bias and error of the meteorological input data may impact the resultant AQ modeling. Typically, there are two specific objectives. First, determine if the meteorological model output fields represent a reasonable approximation of the actual meteorology that occurred during the modeling period (i.e., the "operational" evaluation). The second goal should be to identify how the existing biases and errors in the meteorological predictions may affect the air quality modeling results (i.e., the "phenomenological" evaluation). Once these two sets of information are generated, it is important to highlight the parts of the analysis expected to most influence the air quality model.

**Corresponding author:* Pat Dolwick, U.S. Environmental Protection Agency, MD C439-03, RTP, NC 27711; e-mail: dolwick.pat@epa.gov

This analysis looks at the performance of the Penn State University / National Center for Atmospheric Research mesoscale model known as MM5 (Grell et al, 1994) for a specific year (2002) at two separate model resolutions. The model evaluation is summarized for the entire domain, individual subregions within the domain, and certain individual sites. The goal is to provide a snapshot of the types of analyses that can be completed to assess the utility of using this data to drive regional-scale, photochemical models (e.g., CMAQ) as well as local-scale dispersion models (e.g., AERMOD[1]).

2. MM5 MODEL CONFIGURATION

Meteorological model input fields were prepared for two separate grids as shown in Figure 1. A 36 km grid covering the contiguous portion of the U.S. was modeled using MM5 v.3.6.0 using land-surface modifications that were added in v3.6.3. Additionally, a 12 km grid that covered the eastern two-thirds of the U.S. was modeled with MM5 v3.7.2. Both domains contained 34 vertical layers with a ~38 m surface layer and a 100 mb top. Both sets of model runs were conducted in 5.5 day segments with 12 hours of overlap for spin-up purposes.

Table 1 lists the physics options used in the two sets of MM5 simulations. The initial state analyses were derived from the 3-hourly, Eta Data Assimilation System (EDAS) data. Analysis nudging was utilized outside of the boundary layer for temperatures and water vapor mixing ratios, and in all locations for wind components, using relatively weak nudging coefficients.

[1] AERMOD is a Gaussian dispersion model used to predict air quality in the vicinity of a single source, or group of sources. For more information on AERMOD:

http://www.epa.gov/ttn/scram/dispersion_prefrec.htm#aermod

Figure 1. Plot of 36 and 12 km MM5 modeling domains in the 2002 modeling.

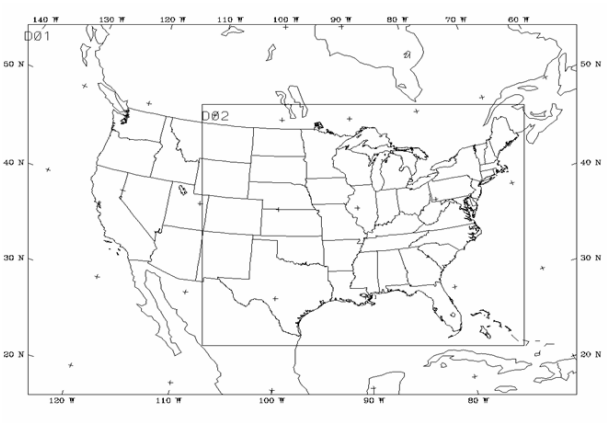

Table 1. List of MM5 model physics options used in the 2002 MM5 simulations.

Physics Option	2002 MM5 Modeling
Planetary boundary layer model	Pleim-Chang / ACM1
Sub-grid convection scheme	Kain-Fritsch 2
Explicit microphysics scheme	Reisner 1
Land-surface model	Pleim-Xiu
Longwave radiation scheme	RRTM

3. OPERATIONAL EVALUATION

The operational evaluation includes statistical comparisons of model/observed pairs (e.g., mean normalized bias, mean normalized error, index of agreement, root mean square errors, etc.) for multiple meteorological parameters. For this portion of the evaluation, four meteorological parameters were investigated: temperature, humidity, wind speed, and wind direction. The operational piece of the analyses focuses on surface parameters. The Atmospheric Model Evaluation Tool (AMET) was used to conduct the analyses as described in by Gilliam et al (2005).

3.1 Eastern U.S. results (12 km grid)

Tables 2a and 2b show the monthly results of the 12 km evaluation. One of the key findings of the operational evaluation is that MM5 surface temperatures have a cold bias. This bias is especially notable in the winter and early spring (e.g., Jan - Apr). This artifact in the meteorological modeling is expected to have a major impact on the eventual air quality modeling results for those pollutants that are temperature-dependent (e.g., nitrates).

Otherwise, the model reproduces observed water vapor mixing ratios with considerable accuracy, though there is a seasonal pattern with highest error in the summer, due to overall higher moisture content. Wind speeds are generally underestimated across the year, but typically the underestimation bias is less than 0.5 m/s. The average error in wind direction ranges from 24-31 degrees. Generally speaking, the operational statistics from the 36 km grid closely approximated the 12 km results.

Table 2a. Mean absolute error by month in the 2002 12 km MM5 simulation.

Month	Temp. (K)	Mix Ratio (g/kg)	W Spd (m/s)	W Dir (deg)
Jan	3.0	0.6	1.3	24.1
Feb	2.5	0.6	1.3	23.6
Mar	2.7	0.7	1.4	24.9
Apr	2.3	0.9	1.3	24.9
May	1.8	1.0	1.3	25.8
Jun	1.5	1.2	1.2	29.2
Jul	1.5	1.4	1.1	31.4
Aug	1.5	1.3	1.1	30.5
Sep	1.5	1.1	1.1	28.1
Oct	1.6	0.8	1.1	26.7
Nov	2.0	0.7	1.2	24.3
Dev	2.5	0.6	1.3	24.5

Table 2b. Mean bias by month in the 2002 12 km MM5 simulation.

Month	Temp. (K)	Mix Ratio (g/kg)	W Spd (m/s)	W Dir (deg)
Jan	-2.4	-0.2	-0.3	7.4
Feb	-1.3	-0.2	-0.4	7.8
Mar	-1.5	-0.1	-0.7	7.5
Apr	-1.5	-0.1	-0.4	6.2
May	-0.5	-0.1	-0.3	6.8
Jun	-0.5	-0.2	-0.4	6.8
Jul	-0.1	-0.1	-0.4	7.8
Aug	-0.1	-0.1	-0.4	7.1
Sep	0.0	-0.3	-0.3	7.8
Oct	0.4	-0.2	-0.2	8.3
Nov	-0.2	0.0	-0.2	8.4
Dev	-0.6	0.1	-0.5	8.1

Model performance was also considered by region, by underlying land use type, and by proximity to coastline or mountainous regions. The tabular results are not shown here for space

considerations, however, there was a clear spatial gradient in model performance. Model performance was more accurate in the eastern portions of the domain, than the more topographically-influenced western portion of the 12 km EUS grid. For instance, mean annual temperature errors ranged from 1.4 to 1.6 degrees over subregions in the eastern U.S., while the errors ranged from 2.0 to 2.2 degrees over the western portion of the domain. Additionally, errors in wind direction were almost 20 degrees greater over the Rocky Mountain portions of the 12 km MM5 grid. Conversely, model performance at locations determined to be coastal tended to be similar to the performance at inland locations. There was no significant error tendencies that were a function of land use type.

3.2 Local-scale results (12 km grid)

Beyond the domainwide results, which are aggregations of numerous model - observed pairs, there was also a limited evaluation of meteorological model performance at a handful of specified sites. This was done to assess the utility of using gridded MM5 data to drive dispersion models such as AERMOD. For the 12 km grid, an local scale analysis was completed for two locations: Birmingham and Detroit. Figures 2a-2d show the bias and error of the four meteorological parameters, for each quarter, and at each site. The statistical output are compared against target values of bias and error in the "soccer plot" mode. Points within the brown boxes are thought to be representative of exceptional model performance. Points that are outside the green box indicate areas in which model performance may be in need of improvement. This analysis confirms the expected, that is, local performance can differ greatly from the national means.

Figure 2a. Quarterly values of temperature bias and error for Birmingham (triangles) and Detroit (squares) within the 2002 12 km MM5 simulation.

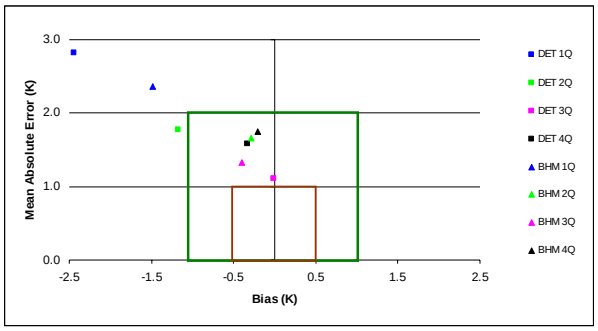

Figure 2b. Quarterly values of water vapor mixing ratio bias and error for Birmingham (triangles) and Detroit (squares) within the 2002 12 km MM5 simulation.

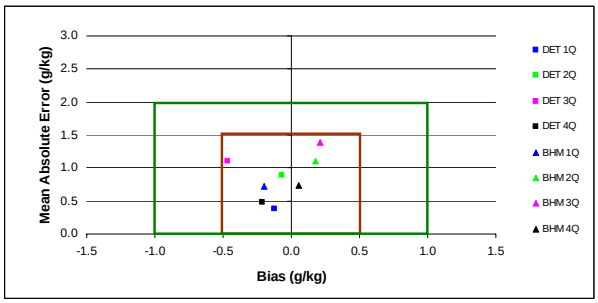

Figure 2c. Quarterly values of wind speed bias and error for Birmingham (triangles) and Detroit (squares) within the 2002 12 km MM5 simulation.

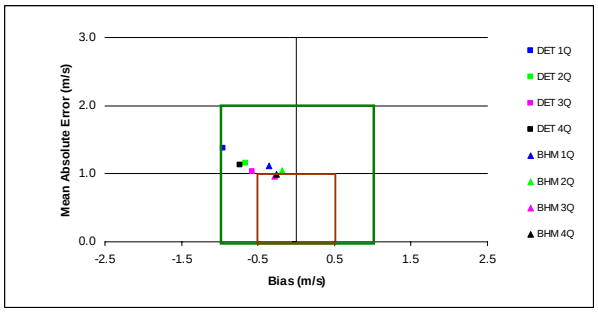

Figure 2d. Quarterly values of wind direction bias and error for Birmingham (triangles) and Detroit (squares) within the 2002 12 km MM5 simulation.

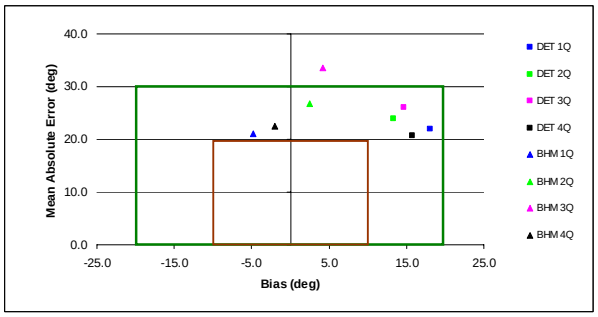

4. PHENOMENOLOGICAL EVALUATION

The phenomenological evaluation ideally would be based on existing air quality conceptual models (i.e., how is air pollution generated, transported, and removed over the area of interest). At a local level, this type of evaluation would assess performance for varied phenomena

such as trajectories, low-level jets, fronts, and air mass residence time. In these instances, a different universe of statistics such as false alarm rates and probabilities of detection are applicable.

For an evaluation of any set of meteorological input data, it is necessary to expand the phenomenological evaluation to include all effects not captured in the operational evaluation. As such, for the 2002 MM5 evaluation additional parameters were considered, beyond the four discussed in Section 3 (e.g., precipitation, upper air analyses). Additionally, a more detailed examination of the cold bias identified earlier was undertaken. Lastly, a more detailed evaluation of an ozone episode was undertaken.

4.1 Precipitation (12 km grid)

There was a general tendency in the 2002 MM5 12 km modeling to underestimate the monthly observed precipitation, when compared to the National Precipitation Analysis. The model under prediction was greatest in the fall and least in the spring months. Figures 3a and 3b show the comparison between observed and predicted precipitation for the months with the best and poorest performance. Qualitatively, the model appears to locate the precipitation in the proper location.

Figure 3a. Comparison of observed (left) and MM5 simulated (right) precipitation for May 2002.

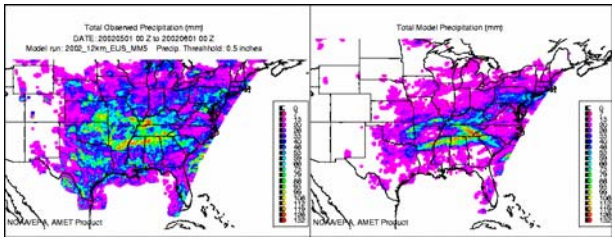

Figure 3b. Comparison of observed (left) and MM5 simulated (right) precipitation for October 2002.

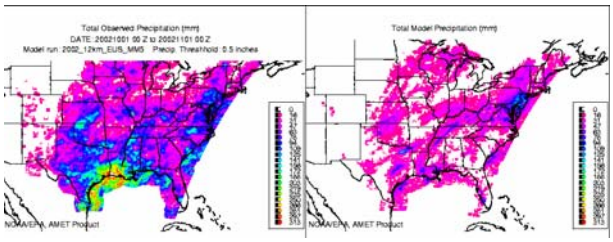

4.2 Model performance aloft

Because of the importance of transport in many air pollution events, it is necessary to examine model performance above the surface layer. Figures 4a (spring) and 4b (fall) show the seasonally-averaged model and observational profiles of potential temperature, relative humidity, wind speed, and wind vectors over the lowest five km of the atmosphere at Greensboro NC (GSO). These analyses have been done for all available upper air sites. The GSO comparisons show a pattern seen elsewhere which is that lower-tropospheric wind speeds appear to be too low in the MM5 simulations (~ 1 m/s). The profiles of potential temperatures and relative humidity are consistent between the model and the actual data.

Figure 4a. Seasonally-averaged model (blue) and observed (red) values of four meteorological parameters at Greensboro NC for Apr - Jun 2002.

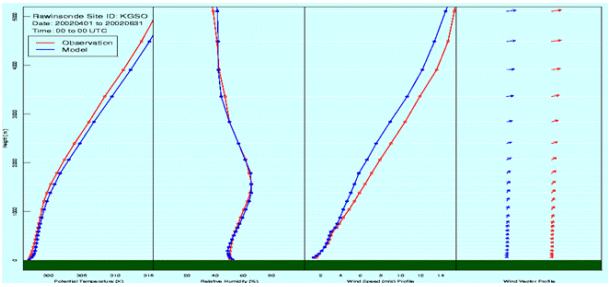

Figure 4b. Seasonally-averaged model (blue) and observed (red) values of four meteorological parameters at Greensboro NC for Oct - Dec 2002.

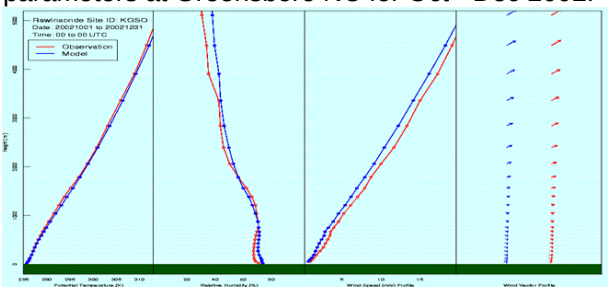

4.3 Assessment of the cold bias by time of day

When the operational statistics are binned into hours of day and then aggregated nationally over the diurnal cycle, it becomes evident (see Figure 5) that the overall cold bias is greatest during the nighttime period. During the daytime the cold bias still exists but averages only ~ 1 deg K as opposed

to the ~2 deg K that is calculated near 0000 UTC. Thus, any impacts from the cold bias on the CMAQ simulations will be greatest at night.

Figure 5. Plot of winter temperature bias (green), error (blue), and standard deviation (red) as a function of the hour of day in the 2002 12 km MM5 simulation. The dark shading on the plot is intended to approximately represent nighttime conditions.

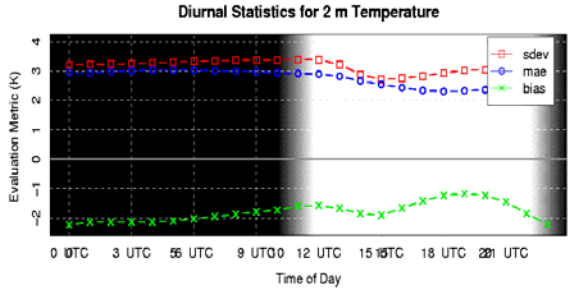

4.4 Early-August Ozone Episode

As discussed earlier, one of the most important meteorological evaluation steps is to incorporate the results into the air quality model evaluation. This can involve identifying regions/periods where the meteorological model predictions are most uncertain, and it can also involve reviewing the meteorology in regions/periods in which there are questions about the air quality model performance. A high ozone episode in early-August 2002 has been investigated in more detail because of questions about ozone performance in the CMAQ model.

Figure 6 shows that there was an area of high ozone (e.g., maximum 8-hour ozone > 80 ppb) over the Ohio and Tennessee valleys and extending into the northeastern U.S. There is a sharp gradient between ozone values in this area and much lower values just to the north of this region. A stationary front marked the boundary between the relatively cleaner and more polluted airmasses.

Fortunately, there happened to be a radar wind profiler in the vicinity of the front. Figure 7 shows a comparison between the model and observed wind vectors on August 3rd at that site. Note that the model does not capture the strong NNE flow behind the front. Thus, in MM5, the front is likely weaker than observed, or possibly misplaced. Generally, the MM5 simulations were found to replicate synoptic patterns quite well, but for individual cases any differences in timing of frontal passages can be significant.

Figure 6. Plot of observed 8-Hour ozone maxima over the eastern U.S. on August 3, 2002.

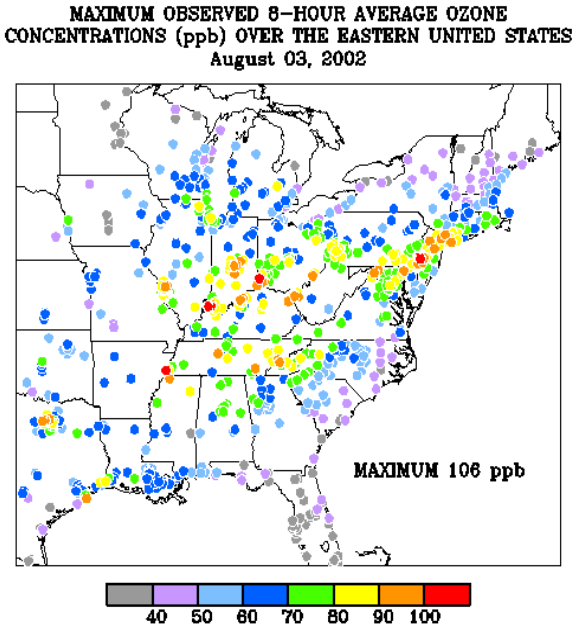

Figure 7. Comparison of model wind vectors (red) and profiler-observed wind vectors (black) at a northern Indiana site on August 3, 2002.

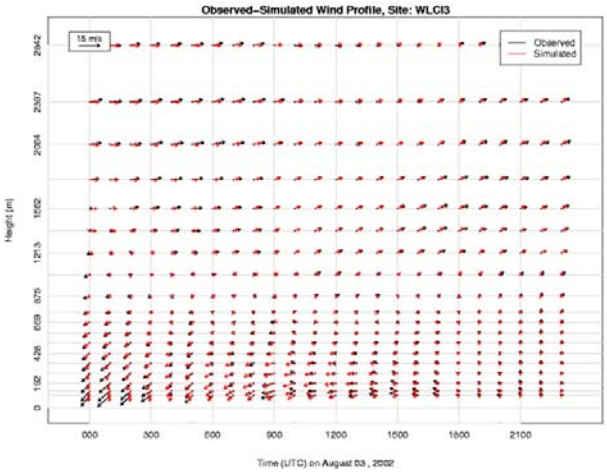

5. SUMMARY OF EVALUATION RESULTS

Both sets of 2002 MM5 meteorological model output fields represent a reasonable approximation of the actual meteorology that occurred during the modeling period at a national level. It is expected that these sets of input meteorological data are appropriate for use in regional and national air quality modeling simulations. For local scale analyses, it is recommended that a detailed, area-specific evaluation be completed before using in those applications.

The most troublesome aspect of meteorological model performance is the cold bias in surface temperatures during the winter of 2002, especially in January. Across the two MM5 simulations, the January cold bias typically averaged around 2-3 deg C. The effect is largest overnight which results in a tendency to overestimate stability in the lowest layers. These artifacts from the meteorological modeling could have a significant impact on the air quality results. The underestimation of precipitation is almost certainly going to have an impact on model deposition calculations.

Generally, the MM5 model bias and error do not appear to be a function of region. However, individual model / observation comparisons in space/time can show large deviations. Caution should be exercised when using these meteorological data west of 100-105 degrees longitude. Model errors/biases are much larger in this mountainous region than any other part of the domain.

Caution will also have to be exercised when using these MM5 results on the local scale. When averaged regionally, there is little to no bias in wind directions, but as shown in section 3.2, local variances can be considerably higher. Additionally, the "key site" analyses shown in section 4.2 looked at MM5 performance over a specific ozone event in the Ohio Valley. These evaluations can be time-consuming but are important for identifying possible causes of air quality modeling biases in important periods.

The 2002 MM5 model evaluation is not entirely complete. We would like to do more analysis on cloud coverage, planetary boundary layer heights, as well as try to assess model performance as a function of meteorological regime (clusters). This extended abstract represents only a small subset of the actual evaluation analyses completed. The figures and tables selected for inclusion were intended to provide a "snapshot" of the potential air quality modeling concerns expected to result from application of the 2002 MM5 input meteorological data.

6. ACKNOWLEDGEMENTS

The authors would like to acknowledge the contributions to this analysis from Jason Brewer who served as a 2006 summer EPA intern from North Carolina State University. Norm Possiel provided helpful comments on an initial draft of this extended abstract. Additionally, we would like to thank Gopal Sistla and the New York Department of Environmental Conservation for the use of Figure 6.

7. REFERENCES

Byun, D.W., and K. L. Schere, 2006: Review of the Governing Equations, Computational Algorithms, and Other Components of the Models-3 Community Multiscale Air Quality (CMAQ) Modeling System. Applied Mechanics Reviews, Volume 59, Number 2 March 2006, pp. 51-77.

Gilliam, R. C., W. Appel, and S. Phillips. The Atmospheric Model Evaluation Tool (AMET): Meteorology Module. Presented at 4th Annual CMAS Models-3 Users Conference, Chapel Hill, NC, September 26 - 28, 2005.

Grell, G., J. Dudhia, and D. Stauffer, 1994: A Description of the Fifth-Generation Penn State / NCAR Mesoscale Model (MM5), NCAR/TN-398 +STR., 138 pp, National Center for Atmospheric Research, Boulder CO.

SENSITIVITY OF AIR QUALITY MODEL PREDICTIONS TO VARIOUS PARAMETERIZATIONS OF VERTICAL EDDY DIFFUSIVITY

Zhiwei Han* and Meigen Zhang

Institute of Atmospheric Physics,Chinese Academy of Sciences, Beijing 100029, China

1.INTRODUCTION

This paper investigates the effect of predicted different vertical diffusivity from 3 commonly used PBL schemes on chemical components in the troposphere of East Asia. The 3 schemes are Gayno-Seaman (Shafran et al.,1998), Medium-Range Forecasts (Hong and Pan, 1996), Byun and Dennis (1995)(approach in MCIP/CMAQ), namely GSE, MRF and B&D hereinafter and were incorporated into a regional air quality model (RAQM) to represent vertical mixing process. RAQM is a three-dimensional Eulerian model, which is built on a spherical and terrain-following coordinate system. It represents a series of major processes of chemical components in the troposphere, such as advection, diffusion, dry deposition, cloud and scavenging, gas and aqueous chemistry etc and has been applied to study a number of environmental problems regarding ozone, acid deposition and soil dust transport (Han et al.,2004; Han et al.,2007).

The study domain covers most of East Asia (100ºE-145ºE, 20º-50ºN), with a horizontal grid resolution of 0.5º, and 12 layers extending vertically from surface to 10 km. About 6 layers lie in the planetary boundary layer (PBL). Anthropogenic and biomass emissions are from Streets et al (2003), which is monthly based and on a horizontal grid of 0.5º×0.5º. March 2001 was selected as study period due to the occurrence of significant vertical mixing and availability of high quality observation of TRACE-P aircraft experiment and ground-level observation from Japan site. 3 days prior to March 2001 were taken as spin-up period. Boundary conditions were derived from a global model Mozart II, which provides monthly mean concentrations of several key species including O_3. Model results were evaluated by comparison against the above observations to find out the relative skill of the 3 schemes. Model results using the 3 schemes were also intercompared in terms of vertical diffusivity coefficients and species concentrations to help understand the similarity and discrepancy among them.

TRACE-P aircraft observation comprises a number of important gases and aerosols, with sampling frequency from several seconds to minutes. This study chooses 5 flights which encounter prevailing continental outflow at wide altitudes. For comparison, model results were extracted every 5 minutes and interpolated trilinearly to flight tracks. Statistics measures of correlation coefficient(R), mean bias error

**Corresponding author*: Zhiwei Han, Institute of Atmospheric Physics, Chinese Academy of Science, Beijing 100029, China;
Tel: 86 10 82995158, Fax: 86 10 82995135
E-mail: hzw@mail.iap.ac.cn

(MBE), root mean square error (RMSE), normalized mean bias (NMB) and normalized mean error (NME) are calculated for pairs of data to help evaluate model performance.

2. RESULTS

2.1 Statistical analysis

Table 1 shows the statistics for the predicted near surface hourly species concentrations with the 3 schemes at Hedo site of Japan. It is interesting to find that the 3 schemes consistently produce similar correlations for SO_2 (0.59~0.61) and O_3 (0.63~0.65), but more varied correlation for NO_x (0.14~0.25). MRF appears to predict lower SO_2 concentration (with MBE of -0.18 and NMB of -0.26), whereas B&D predicts higher NO_x concentration (MBE 0.53, NMB 0.86). The 3 schemes are very consistent to predict O_3 magnitude, with NMB being 0.27~0.28.

Table 1 Statistics for the predicted hourly species concentrations (ppbv) with the 3 schemes at Hedo site

Scheme	Species	R	MBE	RMSE	NMB	NME
B&D	SO_2	0.61	-0.07	0.55	-0.12	0.68
	NO_x	0.25	0.53	0.75	0.86	0.94
	O_3	0.65	12.35	15.0	0.28	0.30
MRF	SO_2	0.59	-0.18	0.60	-0.26	0.63
	NO_x	0.19	0.46	0.73	0.67	0.79
	O_3	0.64	11.98	14.75	0.27	0.29
GSE	SO_2	0.59	-0.07	0.57	-0.12	0.68
	NO_x	0.14	0.39	0.74	0.52	0.74
	O_3	0.63	12.36	15.1	0.28	0.30

Table 2 shows the statistics for model results in the region of < 2 km by comparison with the TRACE-P aircraft observational data. It is noted that all schemes show a similar skill for SO_2, with R ranging 0.65~0.67, and NMB being 0.14~0.18, but yield relatively large difference in NO_x concentration, with R in a range of 0.29~0.36 and NMB being -0.26~0.04. The consistency for O_3 among the 3 schemes appears to lie between that for SO_2 and NO_x. For <2km region, there is a tendency to overpredict SO_2 and underpredict O_3 concentrations for all schemes, but for NO_x, GSE scheme shows a little overprediction, in contrast to others.

Correspondingly, Table 3 shows the statistics for the region of 2~5 km. The difference in correlation among schemes increases for NO_x, whereas for SO_2 and O_3, the consistency among schemes is similar to that in Table 2. The model skill apparently degrades in the region of 2-5 km compared with that in <2 km region. The significant overprediction for SO_2 is due to the inappropriate treatment of volcano emissions. The predicted higher O_3 concentration is associated with the prescribed O_3 boundary conditions. For NO_x, all schemes show an opposite aspect to that in the < 2km region, with GSE showing underprediction and other 2 schemes exhibiting overprediction.

Table 2 Statistics for the predicted species concentrations with the 3 schemes at

altitudes <2 km in the TRACE-P region (ppbv for O_3, pptv for others)

Scheme	Species	R	MBE	RMSE	NMB	NME
B&D	SO_2	0.67	231.6	2526.6	0.15	0.90
	NO_x	0.29	-132.8	690.5	-0.26	0.79
	O_3	0.65	-8.01	15.91	-0.16	0.25
MRF	SO_2	0.65	265.1	2572.6	0.18	0.92
	NO_x	0.30	-81.4	676.3	-0.16	0.81
	O_3	0.62	-8.68	16.80	-0.17	0.26
GSE	SO_2	0.66	217.2	2540.5	0.14	0.88
	NO_x	0.36	21.5	719.8	0.04	0.84
	O_3	0.61	-7.61	16.68	-0.15	0.25

Table 3. Same as Table 2 but for 2-5 km region

Scheme	Species	R	MBE	RMSE	NMB	NME
B&D	SO_2	0.16	491.4	820.4	3.87	4.27
	NO_x	0.21	34.2	234.7	0.32	1.33
	O_3	0.44	13.5	21.5	0.26	0.32
MRF	SO_2	0.18	491.6	798.7	3.88	4.25
	NO_x	0.02	6.1	245.8	0.06	1.22
	O_3	0.43	14.1	22.1	0.27	0.33
GSE	SO_2	0.11	364.8	708.6	2.88	3.48
	NO_x	0.01	-20.6	250.2	-0.2	1.13
	O_3	0.44	13.3	21.3	0.25	0.32

2.2 Spatial distribution

Figure 1 shows the monthly averaged near surface Kz (150m) at 14:00 LST. It is found that MRF scheme produces the largest Kz in the entire domain among all, followed by B&D scheme, and GSE produces the smallest Kz. It appears that the small Kz of GSE near surface inhibit ventilation of SO_2 emission (Figure 2), leading to apparently higher SO_2 concentration than that from the other 2 schemes. The difference in SO_2 concentration between B&D and MRF looks small, although the difference in Kz is apparent between them. Figure 3 shows the monthly mean near surface O_3 concentration predicted with the 3 schemes. The distinctly higher O_3 concentrations in the western parts of domain are due to the influence of constant boundary conditions from the global model. B&D and MRF produce quite similar pattern, with main differences in the southwestern areas of the domain. GSE yields apparently lower O_3 concentration in northeast China and over Tibet than others. However, the 3 schemes appear to be more consistent in the western Pacific Ocean (TRACE-P region). Further analysis of vertical structure of eddy coefficients and associated distribution of species concentrations are undergoing.

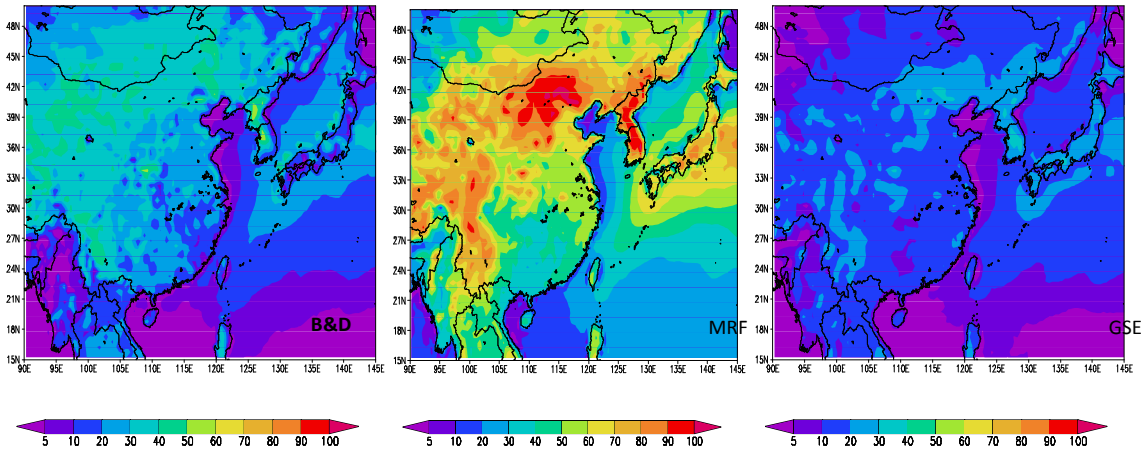

Figure 1 Monthly mean near surface vertical eddy coefficients (150m) at 14:00 LST for the 3 PBL schemes (m^2s^{-1})

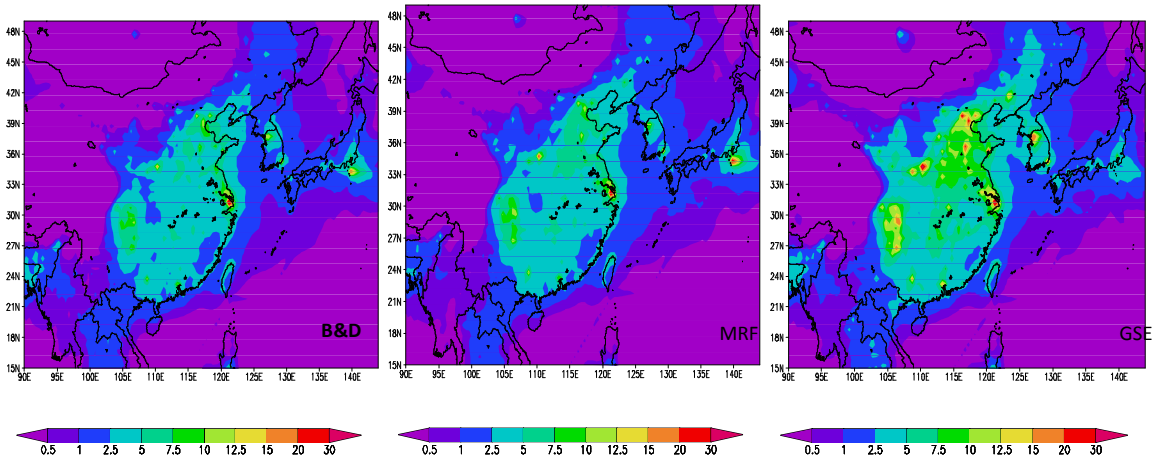

Figure 2 Same as Figure 1 but for SO_2 (ppbv)

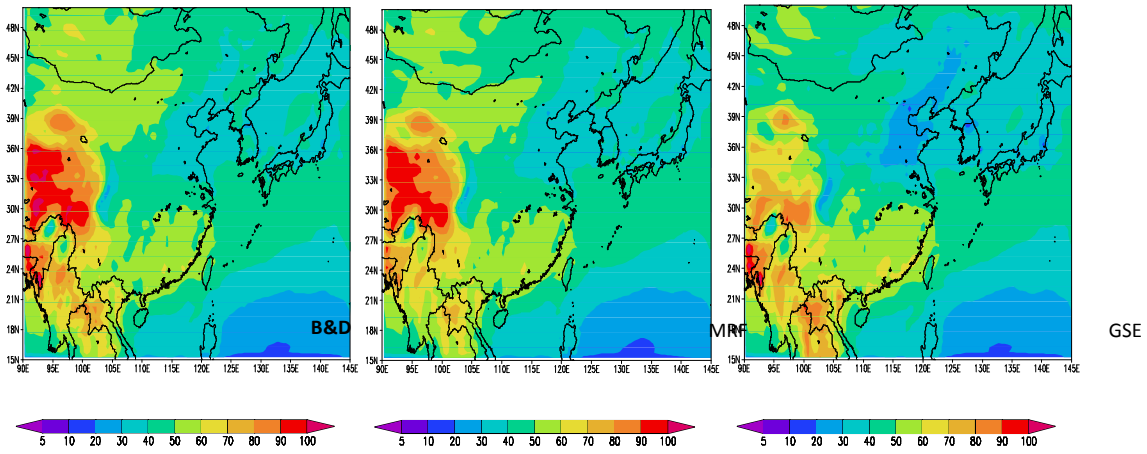

Figure 3 Same as Figure 1 but for O_3 (ppbv)

Reference

Byun, D.W., Dennis, R., 1995. Design artifacts in Eulerian air quality models: evaluation of the effects of layer thickness and vertical profile correction on surface ozone concentrations. *Atmospheric Environment* 29, 105-126.

Han, Z., Ueda H., Matsuda K., Zhang, R., Arao K., Kanai Y., Hasome H., 2004. Model study on particle size segregation and deposition during Asian dust events in March 2002, *Journal of Geophysical Research*, 109, D19205, doi: 10.1029/2004jd004920.

Han Z. W. 2007. A regional air quality model: Evaluation and simulation of O_3 and relevant gaseous species in East Asia during spring 2001. *Environmental Modelling & Software* 22(9), 1328-1336.

Hong, S. H., Pan, H. L., 1996. Monlocal boundary layer vertical diffusion in a medium-range forecast model. *Mon. Wea. Rev*. 124, 2322-2339.

Shafran, P. C., Seaman, N. L., Gayno, G. A. 1998. Evaluation of numerical predictions of boundary layer structure during the Lake Michigan Ozone Study. *Journal of Applied Meteorology*, 39, 412-426.

WRF/NMM-CMAQ derived planetary boundary layer heights and vertical diffusivity for transport of trace species

Pius Lee*, Marina Tsidulko, You-Hua Tang, and Ho-Chun Huang
Scientific Applications International Corporation, Beltsville, MD.

Hsin-Mu Lin, Daiwen Kang, Daniel Tong, and Shaocai Yu
Science and Technology Corporation, Hampton, VA

Jeff McQueen, and Geoff DiMego
Mesoscale Modeling Branch
NOAA/NWS/NCEP/Environmental Modeling Center, Camp Springs, MD

Paula Davidson
NOAA/NWS/Office of Science and Technology, Silver Spring, MD

1. INTRODUCTION

During 2003, NOAA and the U.S. EPA signed a Memorandum of Agreement to work together to develop a National air quality forecasting capability. To meet this goal, NOAA's National Weather Service (NWS), the Office of Atmospheric Research (OAR) and the U.S. EPA developed and evaluated a prototype ozone forecast capability for the North Eastern U.S. (Davidson et al. 2004). Subsequently, a national Air Quality Forecast System (AQFS) was constructed comprising the NWS/National Centers for Environmental Prediction (NCEP) North American Model (NAM) model at 12 km (Janic 2003) to provide meteorological predictions for the EPA Community Multi-scale Air Quality (CMAQ) model (Byun and Schere 2007). The capability of AQFS has been expanded to cover the eastern half of U.S. and the 48 contiguous states (CONUS) in September of 2005, and 2007, respectively (McQueen et al. 2007).

It is advantageous to have a common dynamical package to drive both the meteorological and the air quality models. Among other advantages of such an ideal coupling between the models is a good confidence in mass consistency of the atmospheric constituents (e.g. Lee et al. 2004).

In the interim of the 2007 upgrade of AQFS and the end of the 2006 ozone season, a thorough investigation on the commonality of the vertical mixing schemes within the Planetary Boundary Height (PBL), *h*, between the models has been conducted. Two alternative schemes have been tested besides the default scheme of using NAM-forecasted PBL to derive CMAQ's vertical eddy diffusivity for tracer species, *Kz*, for vertical mixing parameterization for both stable and unstable atmospheric conditions. The alternative vertical mixing schemes have been incorporated into the air quality modeling part of the AQFS aiming to strengthen the commonality between the vertical mixing processes of the meteorological and air quality models below the free troposphere.

Sensitivity studies of these schemes basing on a selected period of elevated surface O_3 concentration of last August have been carried out. The following sections describe the parameterization, characteristic, and rankings of these schemes in the context of an AQFS-like air quality forecast of this period, respectively.

2. VECTICAL MIXING SCHEMES IN AQFS

In 2006, AQFS uses a version of CMAQ closely abided to CMAQ-4.5. It is configured with Asymmetric Convective Model for in-cloud convective mixing (Pleim 2007), NAM derived radiative field for photolysis attenuation calculation, and static boundary conditions for all chemical constituents.

a. RADM scheme with TKE-based PBL height

The vertical mixing scheme used was the default parameterization methodology applied to RADM and CMAQ (Pleim and Chang, 1992; Byun and Dennis, 1995). It is a similarity parameterization of the mixing in the surface and convective boundary layer. For the sake of completeness, the equations for *Kz* for the two stability regimes for the surface layer and layers

above that and below PBL are repeated below (Byun and Ching, 1999):

$$K_Z = \begin{cases} \dfrac{ku_* z}{\phi_H(z/h)} & \text{for surface layer} \quad (1a) \\ \dfrac{ku_* z(1-z/h)^{3/2}}{\phi_H(z/L)} & \text{for stable PBL above surface layer when } z/L > 0 \quad (1b) \\ kw_* z(1-\dfrac{z}{h}) & \text{for unstable PBL above surface layer when } z/L < 0 \quad (1c) \end{cases}$$

where k is the von Karman constant, u_*, friction velocity, z is height, w_* is convective velocity, and L is the Monin-Obukhov length. The non-dimensional profile functions of the vertical gradient of potential temperature, Φ_H, were also given (Byun and Ching, 1999):

$$\phi_H = \begin{cases} \mathrm{Pr}_0\left(\beta_H + \dfrac{z}{L}\right) & \text{for very stable conditions } (z/L \geq 1) \quad (2a) \\ \mathrm{Pr}_0\left(1+\beta_H \dfrac{z}{L}\right) & \text{for moderately stable conditions } (1 \geq z/L \geq 0) \quad (2b) \\ \left(1-\gamma_H \dfrac{z}{L}\right)^{-1/2} & \text{for unstable conditions } (z/L < 1) \quad (2c) \end{cases}$$

where Pr_o is the Prandle number for neutral stability, and β_h and γ_h are coefficients of the profile functions determined through field experiments.

The determination of h is defined in NAM as the first vertical height at which the Turbulent Kinetic Energy (TKE) value drops below 0.1 J Kg^{-1} during an upward search from the surface along an atmospheric column.

b. RADM scheme but MIXHT as PBL height

There is an opinion that the TKE-based PBL height overshoots the height within which atmospheric mixing of the tracer species actually take place. There are weak shallow convection and horizontal advection processes that entrain TKE into layers above the actual mixing depth of the atmospheric column. Therefore it is observed that NAM often predicts the TKE-based PBL height more than one to two layers above that of mixed layer depth.

In light of this, it has been proposed that the mixed layer height (MIXHT), which in essence represents the capping of turbulence production due to the diminishing buoyancy of a convective plume at that height, should be used as h in Equations 1 and 2. In NAM, MIXHT has been quantified by a cut-off value 0.505 of the local bulk Richardson number, Ri_{bk}, when exercising an upward search from the surface along an atmospheric column.

$$Ri_{bk} = \frac{gz[\theta_v(z) - \theta_v(1)]}{\theta_v(1)[(u(z)-u(1))^2 + (v(z)-v(1))^2 + \beta u_*^2]} \quad (3)$$

where g is gravitational acceleration, θ_v is virtual potential temperature, u and v are the latitudinal and longitudinal components of wind, respectively; and β is a field experiment determined coefficient.

c. Use NAM predicted Kz for vertical mixing

Due to the geometrical and package differences between NAM and CMAQ (Otte el al. 2005) of the AQFS, it can be a challenge to maintain high precision of mass consistency as discussion in the introductive section. However, there has been an important vertical grid alignment improvement between NAM and CMAQ since 2005 (Lin et al. 2006). Both models are now using a hybrid sigma-P vertical coordinate; namely, NAM uses 61 interface levels, and CMAQ in AQFS selects from them a 23 interface levels with finer spacing near the surface. In NAM, Kz is defined at these interface surfaces basing on the Mellor-Yamada Level 2.5 turbulence closure scheme (Janjic 1996).

3. SENSITIVITY CASES: AUGUST 2-3, 2006

There were a few elevated surface O_3 concentration scenarios in many cities in continental U.S. between August 2 and 4, 2006. Figure 1 shows the 1 h daily maximum surface O3 concentration on August 3: Fig. 1a shows that compiled by the AIRNOW observation network (EPA 2006), and Fig. 1b shows that forecasted by AQFS and overlaid by the AIRNOW data. It can be noted that there were areas with 1 h daily max value in excess of 100 ppb.

This study aims to investigate the spatial and temporal characteristics of the various vertical mixing schemes discussed in section 2. Pertinent to the context of maximum surface level O_3 concentration prediction, the distributions of O_3 and its precursors, the temporal evolutions of PBL height, and the vertical profiles of Kz will be examined where

and when the surface O_3 concentration is at its peaks.

Table 1 Run cases included in the sensitivity study

Case	Vertical mixing scheme
Base	Use *Kz* derived in Eq. 1 & 2 basing on NAM TKE-based *h*
MIXHT	Use *Kz* derived in Eq. 1 & 2 using NAM Predicted MIXHT as *h*
NAM-Kz	Use NAM predicted *Kz*

Three sites of interest has been selected in accordance with the aforementioned rationales, and restrained by the availability of ozone-sonde and RAOBS data for verification purposes for chemistry and meteorological fields, respectively. They are the Beltsville, MD; Huntsville, AL, and Table-mount, CA sites. The Table-mount site represents an interesting location down wind of the LA basin often subjected to polluted outflow from the city. It is an elevated site at 2250 m, its reading in late afternoon and at night can reveal the lofted O_3 and precursor plumes transported from LA.

Investigations focused on the afternoon hours on August 2 and 3, 2006. However regional verification is based on runs of the three cases between July 21 and August 4, 2006.

4. DISTRIBUTION OF O_3

Figure 1b depicted the Base-case forecasted daily maximum hourly surface O_3 over continental U.S. on August 3, 2006, overlaid with that compiled by AIRNOW. The state of California represents a challenging area for AQFS. Patterns of low and high biases closely co-located in relative small regions in around central San Joaquin Valley and immediately downwind of LA are often registered by verification records. Figure 2a shows the mean bias of daily maximum 8 h averaged surface O_3 forecasted by the Base-case verified with AIRNOW. This reinforces the impression that this intricate pattern occurs rather often. Figure 2b shows the topology of the state. Figure 3 shows a verification diagram for NAM predicted 10 m wind from 15Z August 1st to 12Z August 3rd, 2006 for the western half of continental U.S. Figure 4 shows the definition of regions for the meteorological and chemical concentration verification statistics.

Figures 5a and b show the temporal evolution of *h* in both the Base and MIXHT cases over LA, CA; and Table-mount, CA, respectively. It also shows evolution of the vertical structures of the O_3 concentration predicted by the Base-case, and wind and temperature fields given by the NAM model at the locations.

It is evident from Fig. 5a and b that the lower level O_3 concentration over the city of LA is considerably lower than that over the outskirt site at Table-mount. It is particularly truth for the lowest level, where emitted NO_2 titrates out O_3 at a rapid rate during both day and night hours. The predicted low level wind below 4000 m is largely south-south-westerly. Therefore it can be postulated that Table-mount can be subjected to the downwind transport of pollution plumes from LA.

Figure 5c shows the profiles of predicted and observed O_3 taken at 20:45Z on 2 August (Thompson et al. 2006). The large spike of O_3 concentration between 2000 and 4000 m registered by the ozone-sonde was not reconstructed by the model.

Figures 6a and b show a difference map by subtracting from Fig. 4b by the predicted O_3 concentration by case MIXHT and NAM-Kz, respectively. The two difference maps looked similar with the ground level difference stronger in the former than the latter. This becomes the most obvious at around 21 to 22Z August 3, 2006, when the difference between the NAM TKE-based *h* and MIXHT is large when predicted surface O_3 concentration was at its temporal peak.

Figures 7a and b are similar to those of Fig. 5b and c but for Huntsville, AL; and Beltsville, MD, respectively. The two sites are in relatively flat terrains at elevations of 24 m and 196 m, respectively. The daily hourly maximum surface O_3 concentration prediction of these sites verified quite well basing on the AIRNOW data. In contrary with the gradual collapsing of PBL in LA and Table-mount, CA, as shown in Figs. 5a and b, respectively; it collapsed rather abruptly in Huntsville, AL; and Beltsville, MD on 2 August, 2006, as shown in Figs. 7a and b. However, this timing behavior is different between the two different schemes at these two sites: namely; at Huntsville, PBL collapsed at 22Z and 23Z basing on the MIXHT and NAM TKE-based scheme, respectively. On the other hand, the collapses of PBL at Beltsville in accordance with the two schemes were both at 23Z. In Beltsville, AQFS predicts that a significant amount of O_3 has been lofted above the mixing layer just after sun set.

5. *KZ* PROFILES ON 2 AUGUST, 2006

Figures 8a-d shows the *Kz* profile over Table-mount, CA, with respect to the three runs stipulated in Table 1 at 18Z, and 21Z, August 2, and 00Z, and 02Z, August 3, 2006, respectively. The NAM TKE-based *Kz* and MIXHT-based *Kz* are both parabolic in shape as governed by Eq. 1c. However, as explained in Section 2c, the peak value and extent of the latter is smaller than those of the former. The NAM predicted *Kz* profile is usually non-parabolic in shape, and has maximum values in lower in attitude than those of the first two schemes. As the figures show, PBL Height rose gradually between noon and 6 pm local time, and collapsed completely by 8 pm, as depicted in Fig. 8a,b,c, and d, respectively.

Figures 9 and 10 are similar to Fig. 8 but for Huntsville, AL, and Beltsville, MD, respectively. Another difference is the timing of the sub-figures a-d. They are for 15Z, 18Z, 21Z, August 2, and 00Z, August 3, 2006, respectively. The observations in the above paragraph also apply to Fig. 9 and 10, for in these two eastern sites. The NAM predicted *Kz* has rather large values over Huntsville, AL.

6. REGIONAL MEAN BIAS

Figure 11 shows the regionalized mean bias of the 2 week forecast by the three runs described in Table 1. The definitions of the regions are illustrated in Fig. 4.

The NAM-predicted *Kz* case has the tendency to have the largest high biases among all regions except for the Pacific Coast (PC). On 2 August, this high bias dominance is the most noticeable in the Northeastern U.S. (NE). The Base-case and the MIXHT-case usually track one another closely over all the regions.

There is no episode specific trend of bias increase in the western regions of Rocky Mountain (RM) and PC. For instance there were 14, 17, and 13, O_3 officially declared exceedance episodes in Western U.S. on July 24, 25 and 26, respectively. On record, these three days stood out from the rest of the two week period between 21 July and 4 August, where there were at most 4 declared exceedances per day, except for the 9-exceedance day of 3 August, 2006. However, Fig. 11a and b do not show any characteristic bias change for those high exceedance days for any of the Kz scheme.

For the eastern regions of Upper Midwest (UM), Northeastern (NE), Lower Midwest (LM), and Southeastern (SE) U.S., there is no clear episode specific bias change characteristics either, especially for LM and SE. During the aforementioned two week period there was a cluster of consecutive high O_3 declared exceedance days with 8, 24, 14, and 9 exceedances on 31 July, and 1, 2, and 3 August, 2006, respectively. The NE and UM regions do have their high biases increased for those high exceedance days for all three Kz schemes tested.

The sample sizes for the various regions are: LM has 135, NE has 161, PC has 156, RM has 108, SE has 216, and UM has 231 observation stations, respectively.

All the three Kz schemes tested have high biases for most of the days of the two week period considered. The NAM-predicted Kz scheme did best for PC, but it has the largest high bias for all the other regions. The MIXHT and Base schemes are similar in their performance for the period, having a slight edge over that forecasted by the NAM-predicted Kz scheme overall, when all the regions were taken into consideration.

7. SUMMARY

Three vertical mixing schemes have been tested in a recent version of the national Air Quality Forecast System (AQFS). They are namely: (1) the Base-case of using the default AQFS scheme of supplying NCEP's NAM predicted Planetary Boundary Layer Height, *h*, to CMAQ-4.5's default RADM mixing scheme (Chang et al, 1987), (2) same as the previous configuration but uses NAM predicted Mixed Layer Height (MIXHT) as *h*, and (3) directly use NAM predicted vertical eddy diffusivity, *Kz*, to parameterize the mixing process. The schemes are tested for a 2 week period with high O_3 exceedance episodes between 21 July and 4 August, 2006.

The *Kz* profiles derived in the schemes have characteristics pertinent to geographical and temporal variations. The first two schemes show profiles of parabolic distribution. During full blown PBL growths in late afternoons, *Kz* peaks are often hundreds of J Kg^{-1}. They collapsed rather abruptly around sunset.

The MIXHT and NAM-predicted *Kz* approaches may be aligning the vertical mixing processes better between the methodologies

used in NAM and CMAQ. However, they are not doing convincingly better as shown in the runs done in the test period. It may be said that the MIXHT approach is showing promise as it is as good as the Base case approach and it does best in the challenging region of the Pacific Coast.

ACKNOWLEDGEMENTS

The authors are indebted to Mr. Jerry Gorline of Meteorological Development Laboratory of NOAA for providing Figure 1 of the paper.
The views expressed are those of the authors and do not necessarily represent those of the National Weather Service, NOAA or the EPA. EPA AIRNOW program staff provided the observations necessary for quantitative model evaluation.

REFERENCES

Byun, D. W., and K. L. Schere, 2007: Description of the Models-3 Community Multiscale Air Quality (CMAQ) Model: System overview, governing equations, and science algorithms. *Appl. Mech. Rev*., in press.

Byun, D. W., and J. K. S. Ching (Eds.), 1999: Science algorithms of the EPA Models-3 Community Multiscale Air Quality (CMAQ) Modeling System. EPA-600/R-99/030, Office of Research and Development, U.S. Environmental Protection Agency, Washington, D.C. [Available from U.S. EPA, ORD, Washington, D.C. 20460.]

Byun, D. W., and R. L. Dennis, 1995: Design artifacts in Eulerian air quality models: Evaluation of the effects of layer thickness and vertical profile correction on surface ozone concentrations. *Atmos. Envi.*, **29**, 105-126.

Davidson, P.M., N. Seaman, K. Schere, R.A. Wayland, J.L. Hayes and K.F. Carey, 2004: National Air Quality Forecasting Capability: First Steps toward Implementation. Preprints, 6th Conference on Atmospheric Chemistry: Air Quality in Megacities. Seattle, WA, January 11-15, 2004.

EPA, cited 2006: 2006 summer ozone season – Archive. [Available online at http://www.airnow.gov/index.cfm?action=airnow.archivescalendar

Janjic, Z.I., 1996: The Mellor-Yamada level 2.5 scheme in the NCEP Eta model. Preprints, *11th Conference on Numerical Weather Prediction.* Norfolk, VA, Amer. Meteor, Soc., 333-334.

Janjic, Z.I., 2003: A nonhydrostatic model based on a new approach, *Meteorol. Atmos. Phys.*, **82**, 271-285.

Lee, S. M., S.-C. Yoon, and D. W. Byun, 2004: The effect of mass inconsistency of meteorological field generated by a meteorological model on air quality modeling, *Atmos. Envi.*, **38**, 2917-2926.

Lin H. M., P. Lee, and H.Y. Chuang, 2006: Direct linkage of meteorological data for WRF-NMM/CMAQ Coupling. Preprints, *8th Conference on Atmospheric Chemistry*: Atlanta, GA, Jan 2006.

McQueen, J., P. Lee, M. Tsidulko, Y. Tang, H. Huang, S. Lu, R. Mathur, D. Kang, H. Lin, S. Yu, G. DiMego and P. Davidson, 2007: An overview of the NAM-WRF CMAQ Air Quality Forecasting System run operationally during the Summer 2007. Session 6, This Conference

Otte, T. L., G. Pouliot, J. E. Pleim, J. O. Young, K. L. Schere, D. C. Wong, P.C. Lee, M. Tsidulko, J. T. McQueen, P. Davidson, R. Mathur, H. Y. Chuang, G. DiMego, and N. Seaman, 2005: Linking the Eta Model with the Community Multiscale Air Quality (CMAQ) modeling system to build a national air quality forecasting system. *Wea. Forecasting*, **20**, 367-384.

Pleim, J.E., and J. Chang, 1992: A non-local closure model for vertical mixing in the convective boundary layer. *Atmos. Envi.*, **26A**, 965-981.

Pleim, J.E., 2007: A combined local and non-local closure model for the atmospheric boundary layer. PBL model for meteorological and air quality modeling: Part 1: Model description and testing. *J. Appli Meteor. and Climatology*. (in press).

Thompson, A., and J. Witte, 2006: INTEX ozonesonde network study August/September 2006 , [Available online at http://croc.gsfc.nasa.gov/intexb/SONDES/ions06_augsept.html]

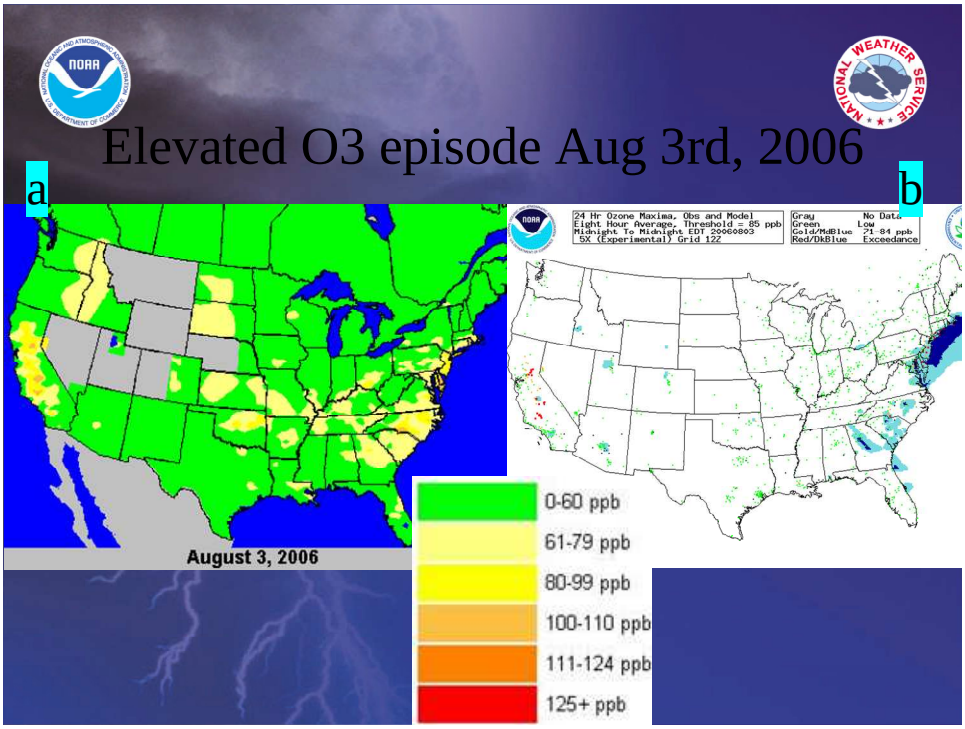

Fig. 1 Daily maximum hourly surface O_3 concentration on August 3, 2006 (a) Compiled by AIRNOW, and (b) Forecasted by AQFS (Base case) verified with the AIRNOW data.

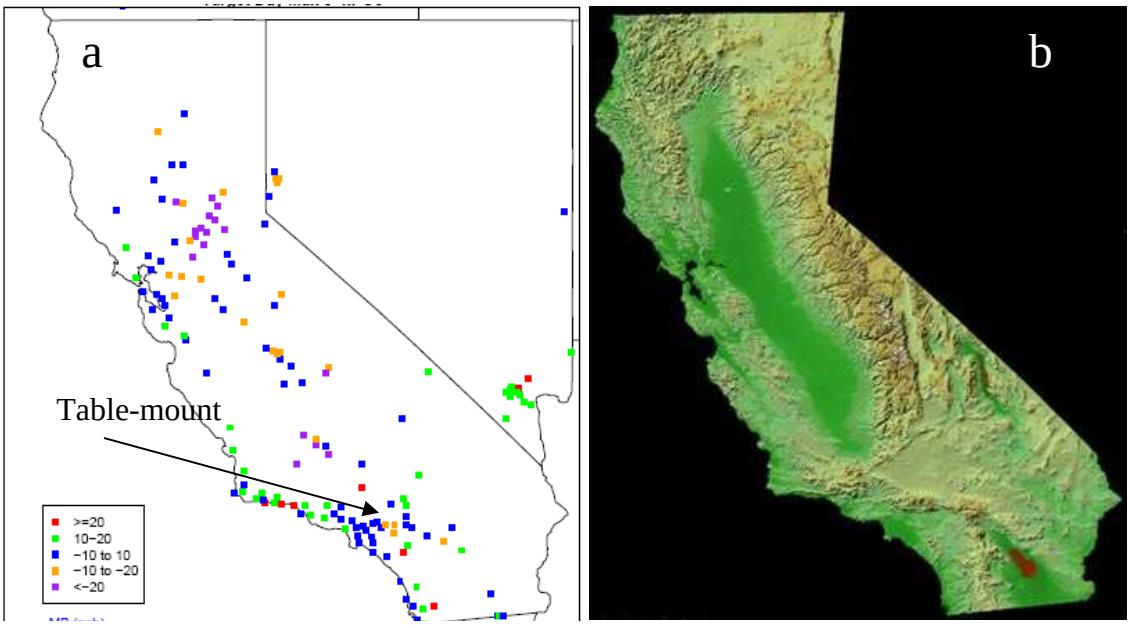

Fig. 2 Features of State of California: (a) Second day forecast of daily maximum 8 h averaged surface O_3 predicted by Base-case verified with AIRNOW for 2 August, 2006, and (b) Topology.

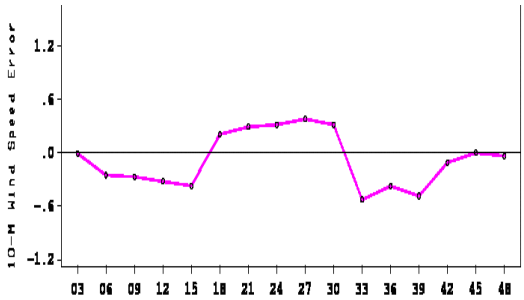

Fig. 3 10 m wind bias (m/s) over forecast hour 03 to 48 for NAM run starting at 12Z 1 August, 2006. over regions PC+RM as shown in Fig. 4.

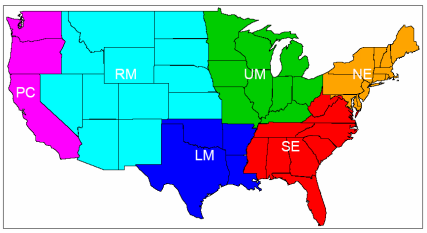

Fig. 4 Definition of regions for verification purposes.

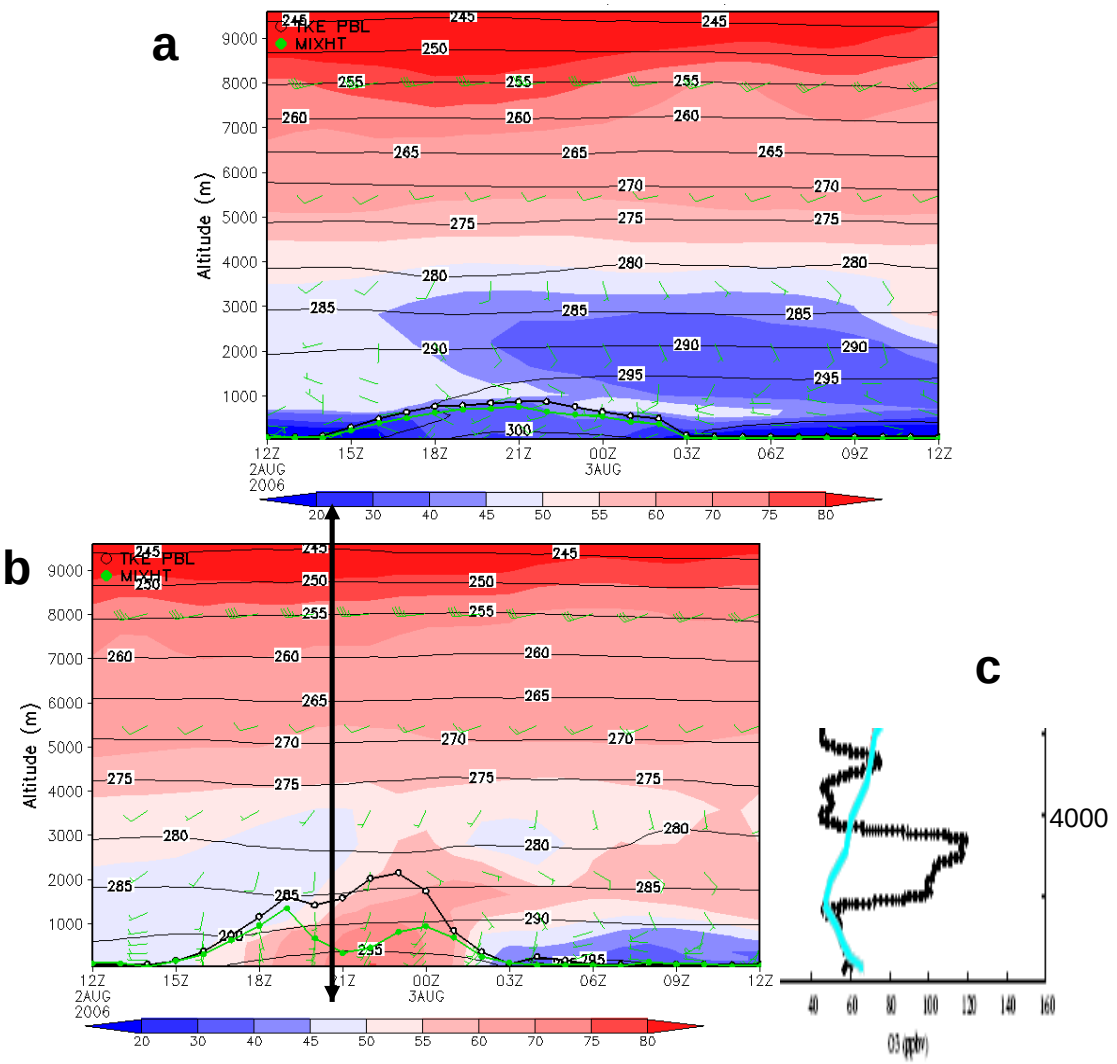

Fig. 5 Time evolution of predicted O_3 (shaded), temperature (contoured), wind (barbs), and planetary boundary height, *h*: (TKE) for Base, and (MIXHT) for MIXHT schemes over (a) LA, CA, at (118W, 34N), and (b) Table-mount, CA, at (117.7W, 34.4N) by the Base-case second day forecast valid between 12Z 2 August to 12Z 3 August, 2006. The black arrow at 20:45Z indicates the lauching time of an ozonesonde at the site whose readings (black) and modeled predicted value (blue) is depicted in (c).

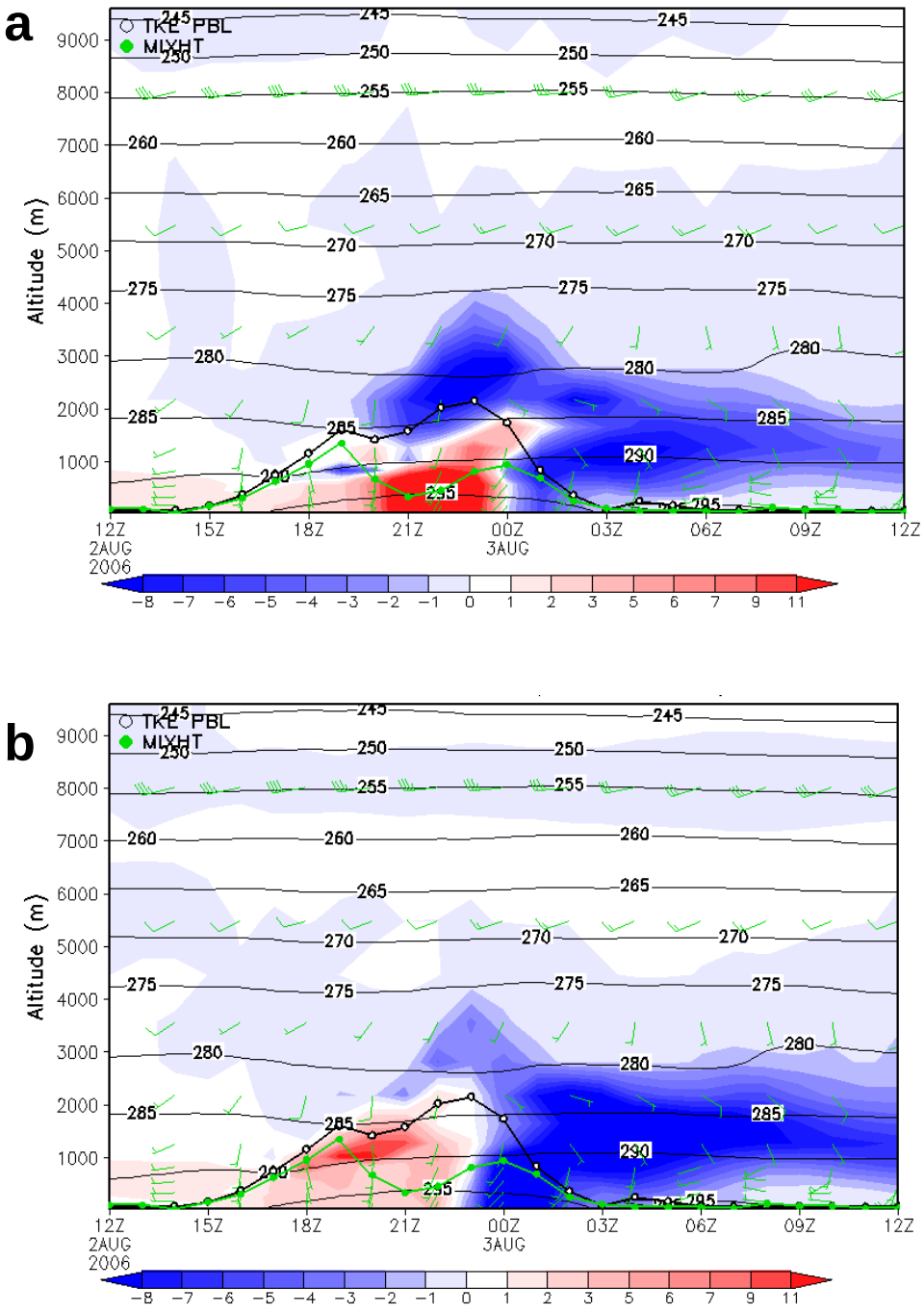

Fig. 6 Difference maps of predicted O_3 concentrations with respect to Fig. 5b by subtracting it from results based on (a) MIXHT, and (b) NAM-Kz schemes.

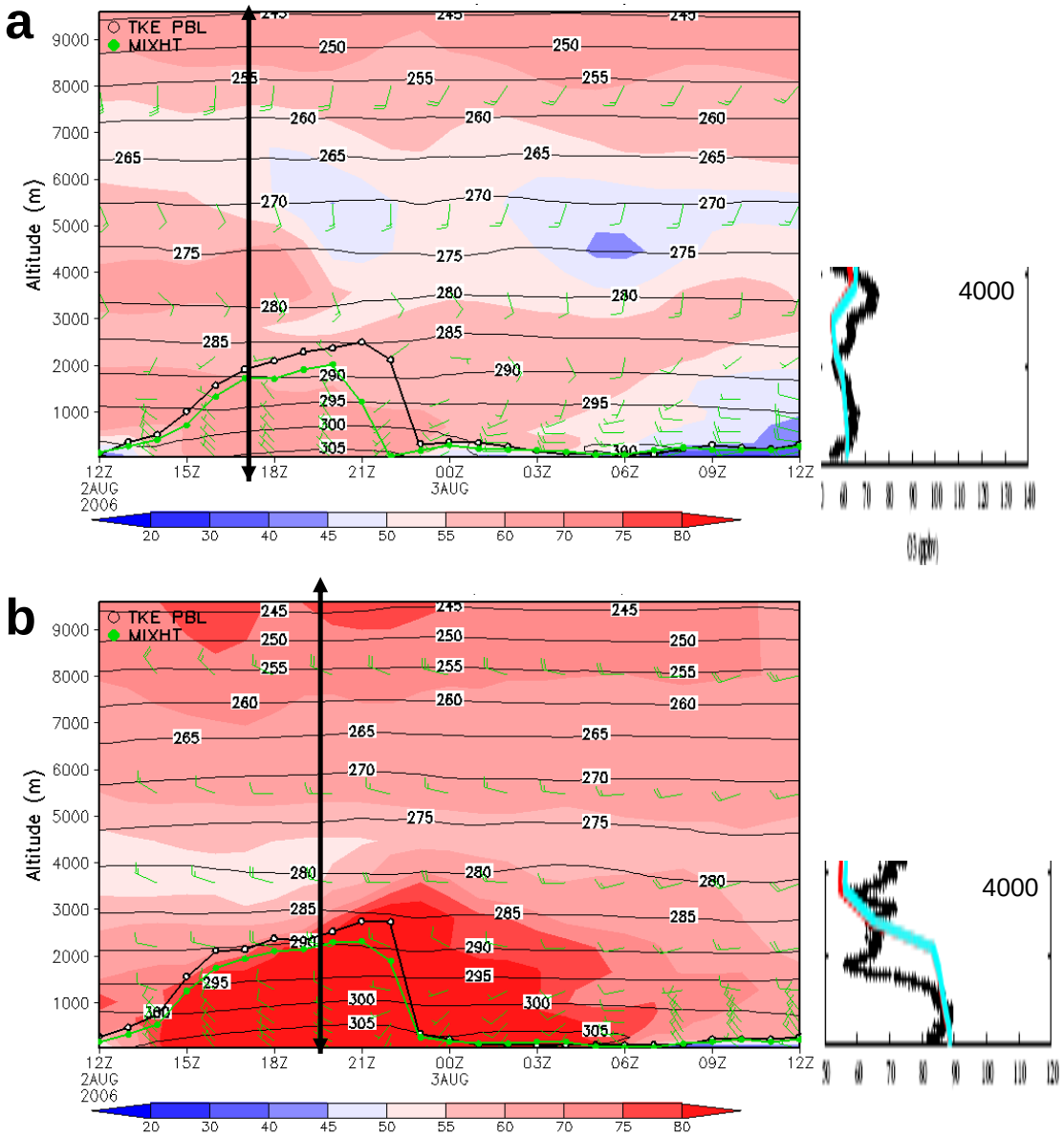

Fig. 7 Same as Figs. 5b and c but for over (a) Huntsville, AL, at (86.5W, 34.7N) with ozonesonde launched at 17:36Z 2 August, 2006, and (b) Beltsville, MD, at (76.5W, 39.0N) with ozonsonde launched at 19:18Z 2 August, 2006, respectively.

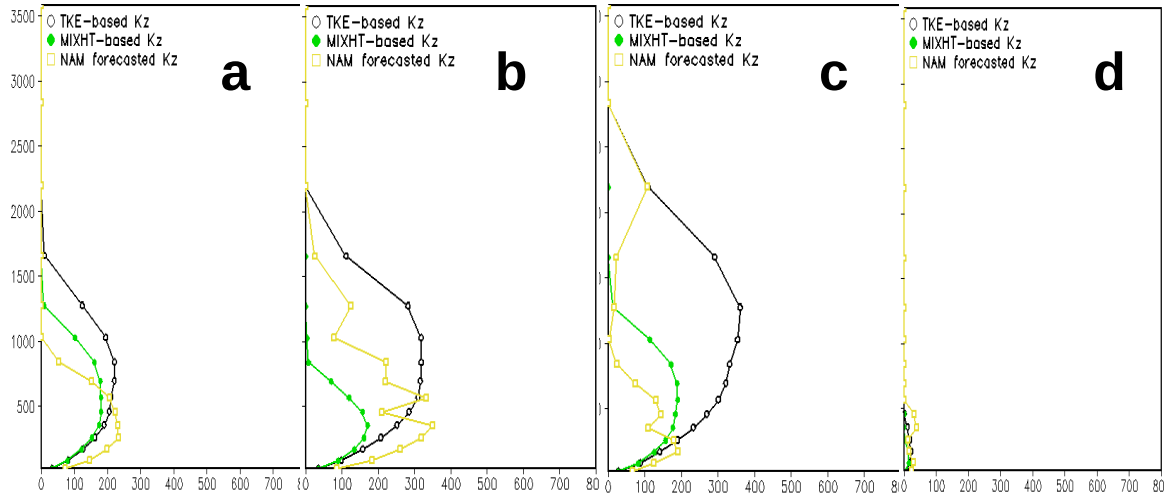

Fig. 8 Modeled vertical profiles of *Kz* (J Kg^{-1}) over attitude (m) above ground at Table-mount: TKE-based (open circle), MIXHT-based (filled circle), and NAM-forecasted (open square), at (a) 18Z, 2nd, (b) 21Z, 2nd, (c) 00Z, 3rd, and 02Z, 3rd of August, 2006.

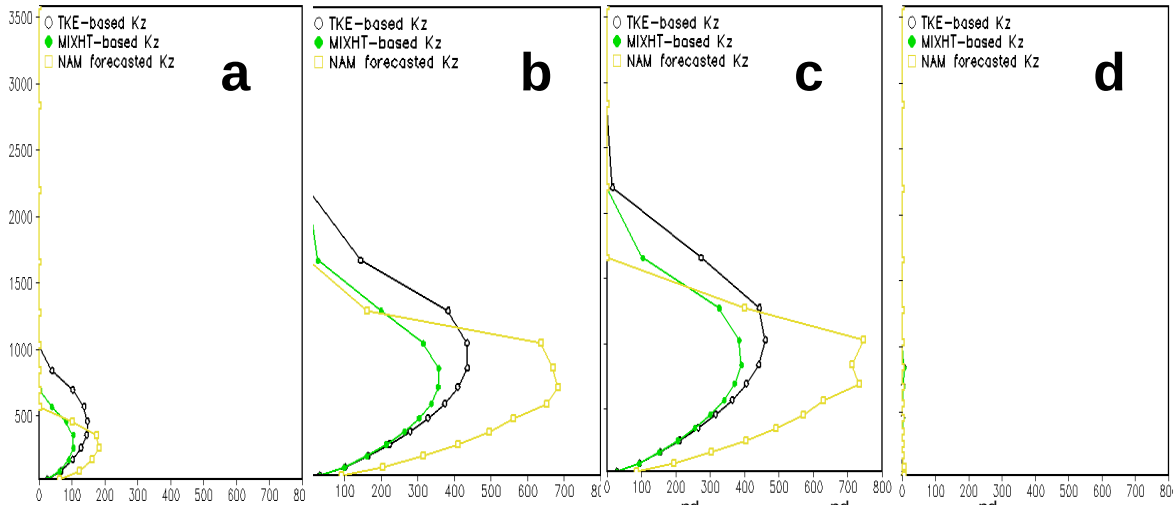

Fig. 9 Same as Fig. 8 but for over Huntsville, at (a) 15Z, 2nd, (b) 18Z, 2nd, (c) 21Z, 2nd, and (d) 00Z, 3rd of August, 2006.

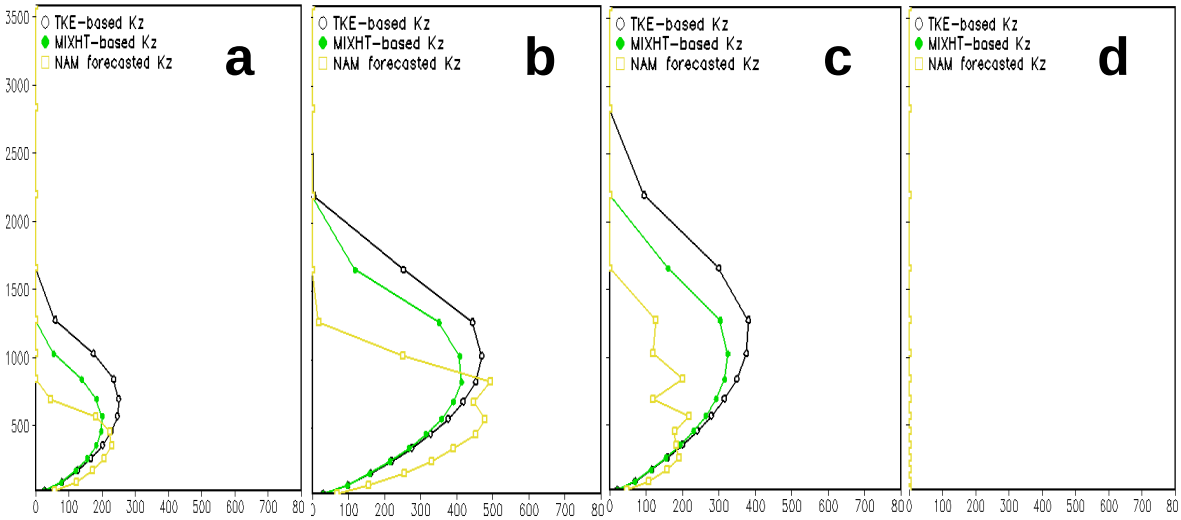

Fig. 10 Same as Fig. 9 but for over Beltsville.

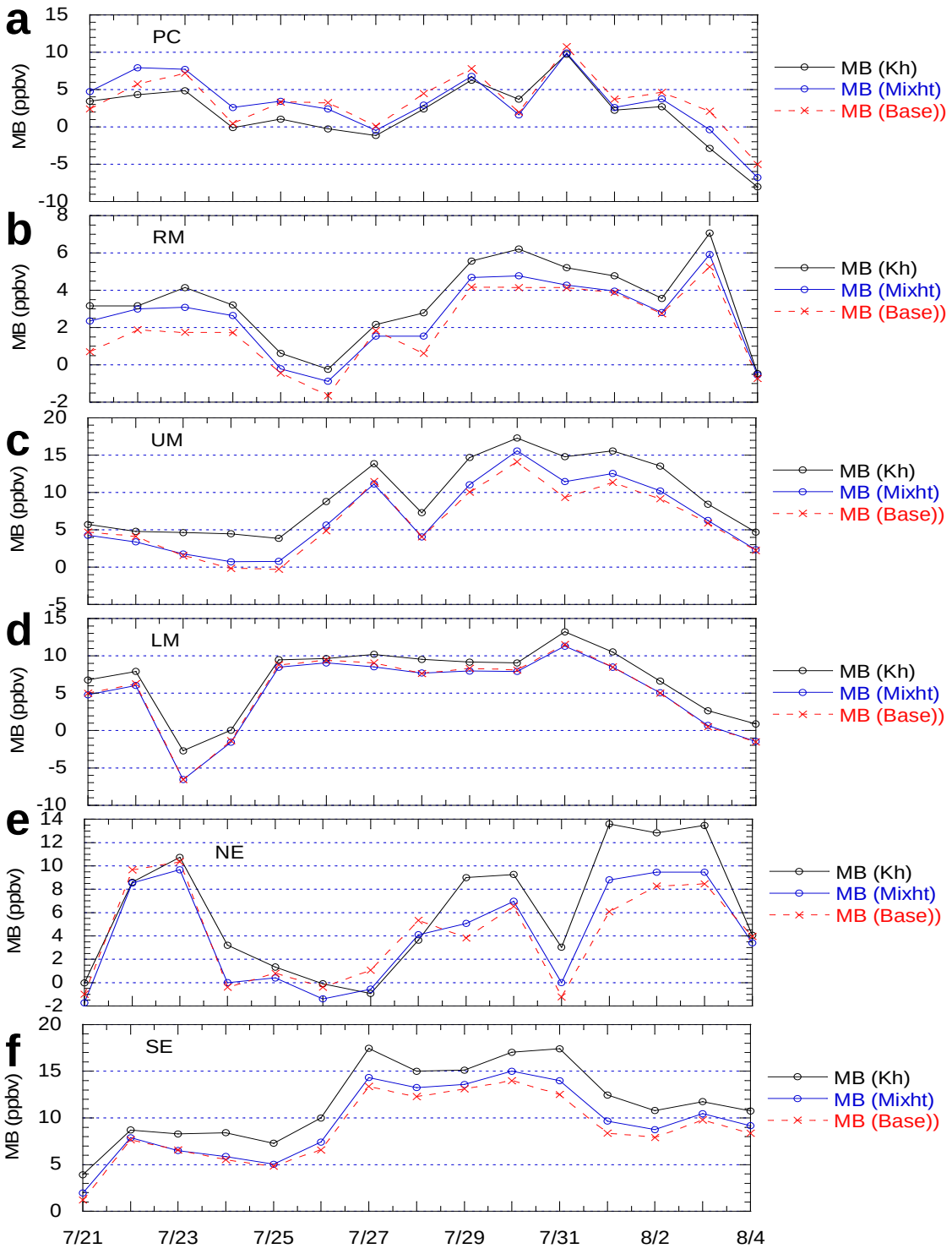

Fig. 11 Regional verification plot on mean bias based on AIRNOW data for daily maximum 8 h averaged surface O_3 for the periods between 21 July and 4 August 2006, using vertical mixing schemes described in Table 1 as: Base-case (red), MIXHT-case (Blue), and NAM-Kz case (Black) over: (a) Pacific Coast (PC) with 156, (b) Rocky Mountain (RM) with 108, (c) Upper Midwest (UM) with 231, (d) Lower Midwest (LM) with 135, (e) Northeastern (NE) with 161, and (f) Southeastern (SE) with 216 stations, respectively.

FORECASTING OZONE AT EUROPEAN SCALE WITH ENSEMBLES

Vivien Mallet[1,*], Bruno Sportisse[2]

[1] INRIA, CLIME project (common project ENPC - INRIA) [France]

[2] ENPC, laboratory CEREA (joint research laboratory ENPC - EDF R&D), CLIME project [France]

INTRODUCTION

A major limitation of air quality forecasts is the numerous uncertainties in the chemistry-transport models (CTMs) and their input data. The physical formulation of a CTM is uncertain. The numerical discretization introduces further uncertainties in the computed concentrations. The large set of input data to the models (emissions, meteorological fields, ...) shows high uncertainties, often ranging from 30% to 50%, sometimes reaching 100% or more. Considering practical issues, one may mention the uncertainties lying in the computer code (approximations, bugs) and in the use of the code (choices left to the user, mistakes). All these uncertainties result in uncertain output concentrations of observed and unobserved pollutants.

The state (i.e., the concentrations vector) of a CTM is of high dimension: its size is usually 10^6 or 10^7. Meanwhile about a few hundreds of components are observed with monitoring stations or with dedicated instrument during intensive observation periods. Consequently, the models are slightly constrained by the observations and the uncertainties in the forecasts remain, especially for unobserved components.

In order to improve the forecasts, the current developments mainly rely on advances in physics and chemistry. Meanwhile the model performances slightly increase, probably because the uncertainties shadow the modeling efforts and because the models abilities are based on tuned configurations.

As a consequence, the models should be considered as stochastic models. In this context, ensemble approaches, based on a set of simulations instead of a single simulation, are suited to estimate the uncertainties (Section 2) and to improve the forecasts (Section 3). Multimodel ensembles are generated within the framework of the Polyphemus air quality modeling system (Section 1).

1 THE AIR QUALITY MODELING SYSTEM POLYPHEMUS

1.1 Purpose

Polyphemus [Mallet et al., 2007] is a rather new air quality modeling system, developed by the École Nationale des Ponts et Chaussées (ENPC), the French National Institute for Research in Computer Science and Control (INRIA) and Électricité de France (EDF R&D), with support from Institut de Radioprotection et de Sûreté Nucléaire (IRSN) and the French National Institute for Industrial Environment and Risks (INERIS).

It was built to cover the scope and the abilities of modern air quality systems, notably ensemble forecasting and data assimilation. It was designed to share developments inside and outside the system, and to host several models. A strong flexibility at preprocessing stages and simulation stage enables to deal with multiple model configurations. High-level methods that embed one or more CTMs, such as data assimilation, are implemented independently of the models, so that they may be applied to several models available on the platform.

Polyphemus deals with applications at different scales (from local to continental scale) with two Gaussian models and two Eulerian models (Castor and Polair3D). Its target pollutants are currently passive tracers, radionuclides, photochemical species and aerosols.

1.2 Structure

The system is made of four independent levels: data management, physical parameterizations, numerical solvers and high-level methods such as data assimilation, ensemble forecast or model coupling.

At preprocessing stage, data from several sources are managed, and several alternative parameterizations are available to compute the main fields (deposition velocities, vertical diffusion coefficients, ...). At simulation stage, the model is essentially a numerical solver: most physical calculations have been performed in preprocessing steps. Within a model, the numerical schemes for advection, diffusion and chemistry may be changed.

On top of the model(s), a driver implements a method like data assimilation or Monte Carlo simulations. In a driver, the model (or the models) is seen as a black box with a light interface. The drivers are implemented independently of the models so that any driver may be used in combination with any model (that has the light interface required by the driver).

The development of such a system requires advanced technical features. Hence Polyphemus is mostly written in C++.

[*] *Corresponding author:* Vivien.Mallet@inria.fr

1.3 Uncertainty Estimation and Ensemble Forecasts in Polyphemus

In Polyphemus, estimation of uncertainties due to input data may be carried out with drivers: a driver for Monte Carlo simulations (perturbation of input data fields), a driver to perform adjoint simulations (sensitivity analysis). Note that the adjoint of one CTM (Polair3D, gas phase version) is mainly obtained through automatic differentiation.

In order to estimate the uncertainties coming from the physical formulation (physical parameterizations) and the numerical schemes, the flexibility of Polyphemus is used to build multimodel ensembles. Each model of the ensemble is built with a different set of physical parameterizations and numerical schemes. The raw data sources can also be changed from one model to another (e.g., land use data, or meteorological data).

2 Uncertainty Estimation

2.1 Experimental Setup

In this abstract, all base simulations have essentially the same configuration. They are primarily set up to estimate ozone concentrations over Europe in summer 2001. In short, the reference configuration is

1. domain: $[40.25°\mathrm{N}, 10.25°\mathrm{W}] \times [56.75°\mathrm{N}, 22.25°\mathrm{E}]$ with $0.5°$ resolution on the horizontal and five vertical levels;

2. meteorological data: ECMWF[1] fields (resolution of $0.36° \times 0.36°$, TL511 spectral resolution in the horizontal, 60 levels, time step of 3 hours, 12 hours forecast-cycles starting from analyzed fields);

3. chemical mechanism: RACM [Stockwell et al., 1997];

4. emissions: the EMEP[2] inventory, converted according to Middleton et al. [1990];

5. biogenic emissions: computed as proposed in Simpson et al. [1999];

6. deposition velocities: the revised parameterization from Zhang et al. [2003];

7. vertical diffusion: within the boundary layer, the Troen and Mahrt parameterization described in Troen and Mahrt [1986]; above the boundary layer, the Louis parameterization found in Louis [1979];

8. boundary conditions: output of the global chemistry-transport model Mozart 2 [Horowitz et al., 2003];

9. numerical schemes: a first-order operator splitting; a direct space-time third-order advection scheme with a Koren flux limiter; a second-order order Rosenbrock method for diffusion and chemistry [Verwer et al., 2002].

[1] European Centre for Medium-Range Weather Forecasts

[2] Co-operative Programme for Monitoring and Evaluation of the Long-range Transmission of Air Pollutants in Europe

Input data	Uncertainty
Cloud attenuation	$\pm 30\%$
Deposition velocities (O_3 et NO_2)	$\pm 30\%$
Boundary conditions (O_3)	$\pm 20\%$
Anthropogenic emissions	$\pm 50\%$
Biogenic emissions	$\pm 100\%$
Photolysis rates	$\pm 30\%$

Table 1: Assumed uncertainties in input data.

The simulated concentrations are compared to observations from a set of monitoring stations in Europe (mainly in France and Germany) in summer 2001. On ozone peaks, the root mean square error is 22.4 $\mu g\, m^{-3}$ and the correlation is 0.78.

2.2 Uncertainties Due to Input Data

In order to assess the uncertainties due to input data (except base meteorological fields), we carried out Monte Carlo simulations. We used the full configuration introduced in Section 2.1 over 7 days (plus 4 days of spin-up). The perturbations in the input data were devised from several sources – mainly Hanna et al. [1998, 2001]. See Table 1.

800 Monte Carlo simulations were performed. About 200 to 400 simulations were needed for convergence of highly averaged outputs such as the spatio-temporal average of hourly ozone concentrations (Figure 1). To summarize, the uncertainty (relative standard deviation) on mean ozone peaks was about 8%. Details may be found in Mallet [2005].

2.3 Uncertainties Due to the Model Formulation

The numerical model formulation is defined by a set of physical parameterization and a set of numerical schemes. In order to account for uncertainties in the model formulation, a multimodel ensemble was derived from the reference configuration with changes in the parameterizations and in the model discretization (resolution, numerical schemes). For instance, two chemical mechanisms (RACM and RADM [Stockwell et al., 1990]) were used and three vertical diffusion estimates were considered. Changes in the input-data sources were also included (e.g., land use categories). About 20

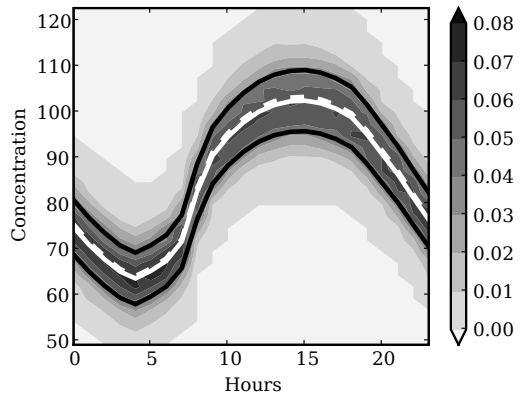

Figure 1: Mean daily profiles for ozone (concentrations in $\mu g\,m^{-3}$). The probability density (shaded) is shown in (b), together with the expectation (continuous white line), the expectation plus ou minus the standard deviation (black lines) and the profile of the reference simulation (discontinuous white line).

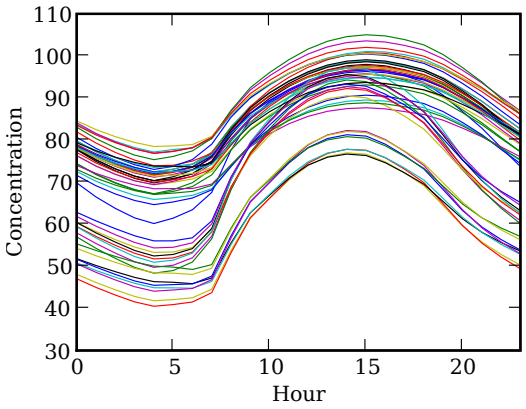

Figure 2: Ozone daily profiles of 48 models built in Polyphemus. The concentrations are in $\mu g\,m^{-3}$ and are averaged over Europe (at ground level) and over four months (mostly summer 2001).

changes were available, which enabled to build an ensemble with 48 members.

The ensemble shows a wide spread – see Figure 2. The estimated uncertainty (relative standard deviation) is over 15%. Details may be found in Mallet and Sportisse [2006b].

3 Ensemble Methods: Combining Models

3.1 Introduction

Ensemble simulations bring more information than a single simulation, which may be used to improve the forecasts. As an illustration of the information brought by the ensemble of 48 members, Figure 3 shows the index of the best model over Europe for

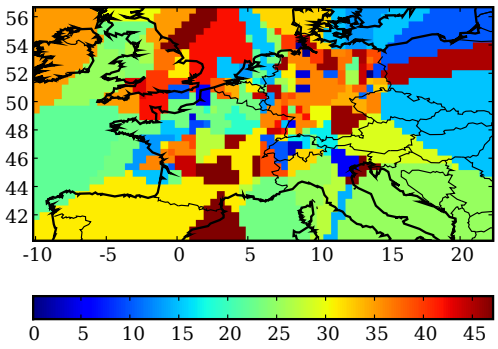

Figure 3: Map of best model indices. In each cell of the domain, the color shows which model (marked with its index, in $[\![0, 47]\!]$) gives the best ozone peak forecast on 7 May 2001 at the closest station to the cell center. It shows that many models can deliver the best forecast at some point.

ozone peaks on 7 May 2001.

In order to overtake the limitations of uncertainties in forecasts, we tried to linearly combine the models of our multimodel ensemble (Section 2.3). At a given forecast date, the weight associated with a member of the ensemble may depend on past concentrations (of all ensemble members) and on past observations. The methods are applied to ozone peaks in the sequel.

The output of model m at time t (or day t as we focus on ozone peaks) and position x (or station x) is denoted $M_{m,t,x}$. The ensemble method computes a linear combination with weights $\alpha_{m,t}$: $E_{t,x} = \sum_m \alpha_{m,t} M_{m,t,x}$. Note that the weights do not depend on the position. This way, it is still possible to compute 2D fields of concentrations as output of the modeling effort – although this point needs further investigation. Moreover, if the weights were dependent of the position, the ensemble method would compete with purely statistical methods which are highly efficient and less computationally expensive. The available observations are $O_{t,x}$. The performance of a combination E is measured by the root mean square error $\mathrm{RMSE}(E,O) = \sqrt{\frac{1}{N_o}\sum_{t,x}(E_{t,x}-O_{t,x})^2}$, where N_o is the total number of observations.

The reference to be improved is the best model EB in the ensemble, which satisfies $EB_{t,x} = M_{\widehat{m},t,x}$ where $\widehat{m}$ minimizes $\mathrm{RMSE}(M_m, O)$. The reference performance for ozone peaks is $\mathrm{RMSE}(EB,O) = 22.4\ \mu g\,m^{-3}$.

The ensemble mean is defined as $EM_{t,x} = \overline{M_{m,t,x}}^m$, that is, with $\alpha_{m,t} = \frac{1}{48}$ since there are 48 models in the ensemble. It shows poor performances $\mathrm{RMSE}(EM,O) = 23.9\ \mu g\,m^{-3}$. Hence methods that take into account past observations

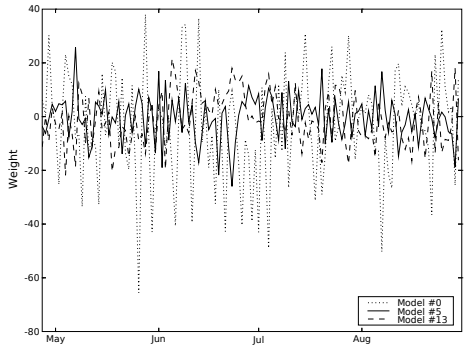

Figure 4: Optimal weights in the least-squares sense (ELS) against time, for three models.

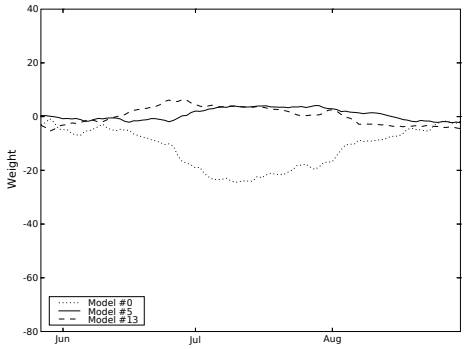

Figure 5: Weights associated with ELS^{30} against time, for three models (same models and same ordinate range as in Figure 4).

are required.

3.2 Least-Squares Methods

Least-squares methods, called "superensembles" in [Krishnamurti et al., 2000], minimize a squared error: $ELS_{t,x} = \sum_m \alpha_{m,t} M_{m,t,x}$ where $\forall t \quad \alpha_{\cdot,t} = \operatorname{argmin} \sum_x \left(O_{t,x} - \sum_m \alpha_{m,t} M_{m,t,x}\right)^2$. In this case, all observations are taken into account (in the past and in the future). Hence ELS shows the potential of least-squares methods: $\mathrm{RMSE}(ELS, O) = 12.0\ \mu\mathrm{g\,m}^{-3}$. Unfortunately, the optimal weights show rapid variations in time, which makes them hard to forecast (Figure 4).

Hence forecasting weights in this framework requires some smoothing. Then the optimal weights are computed over a learning period. This learning period is a moving window of 30 days preceding the day to be forecast. The combination is $ELS^{30}_{t,x} = \sum_m \alpha^{30}_{m,t} M_{m,t,x}$ where $\forall t \quad \alpha^{30}_{\cdot,t} = \operatorname{argmin} \sum_{t-30 \leq T < t,x} \left(O_{T,x} - \sum_m \alpha_{m,T} M_{m,T,x}\right)^2$. This method successfully computes improved forecasts: $\mathrm{RMSE}(ELS^{30}, O) = 20.2\ \mu\mathrm{g\,m}^{-3}$ (against $22.4\ \mu\mathrm{g\,m}^{-3}$ for the best model). This time, the weights are much smoother, which explains the good performances – see Figure 5

For further details, refer to Mallet and Sportisse [2006a].

3.3 Machine Learning Algorithms

Least-squares methods can be efficient, but – as far as we know – there is no theoretical background to support them. Other algorithms have been developed in the machine learning community. These algorithms come with theoretical bounds on the discrepancy between the performances of the forecast combination and the performance of the best combination (with constant weights). Preliminary tests in Mallet and Sportisse [2006a] and undergoing work (in collaboration with Gilles Stoltz, École Normale Supérieure de Paris) show that good performances may be reached with these algorithms: the root mean square error may decrease down to $19.5\ \mu\mathrm{g\,m}^{-3}$.

Conclusion

The air quality modeling system Polyphemus enables ensemble forecasting thanks to its flexible structure. Monte Carlo simulations were carried to assess the uncertainties due to input data (except base meteorological fields). The uncertainties due to the model formulation were also studied through a multimode ensemble, and a strong impact on the output uncertainties was found. The multimodel ensemble brings useful information. Its members can be efficiently combined to improve the forecasts.

Among the next steps, one may find the use of ensembles in daily operational forecasts. Polyphemus has already run for several months in ensemble mode (with 43 models and daily forecasts) for a test on the operational platform Prév'air (operated by INERIS), but no online combination of the members was performed.

References

Hanna, S. R., Chang, J. C., and Fernau, M. E. (1998). Monte Carlo estimates of uncertainties in predictions by a photochemical grid model (UAM-IV) due to uncertainties in input variables. *Atmos. Env.*, 32(21):3,619–3,628.

Hanna, S. R., Lu, Z., Frey, H. C., Wheeler, N., Vukovich, J., Arunachalam, S., Fernau, M., and Hansen, D. A. (2001). Uncertainties in predicted ozone concentrations due to input uncertainties for the UAM-V photochemical grid model applied

to the July 1995 OTAG domain. *Atmos. Env.*, 35(5):891–903.

Horowitz, L. W., Walters, S., Mauzerall, D. L., Emmons, L. K., Rasch, P. J., Granier, C., Tie, X., Lamarque, J.-F., Schultz, M. G., Tyndall, G. S., Orlando, J. J., and Brasseur, G. P. (2003). A global simulation of tropospheric ozone and related tracers: description and evaluation of MOZART, version 2. *J. Geophys. Res.*, 108(D24).

Krishnamurti, T. N., Kishtawal, C. M., Zhang, Z., T. LaRow, D. B., and Williford, E. (2000). Multimodel ensemble forecasts for weather and seasonal climate. *J. Climate*, 13:4,196–4,216.

Louis, J.-F. (1979). A parametric model of vertical eddy fluxes in the atmosphere. *Boundary-Layer Meteor.*, 17:187–202.

Mallet, V. (2005). *Estimation de l'incertitude et prévision d'ensemble avec un modèle de chimie-transport – Application à la simulation numérique de la qualité de l'air*. PhD thesis, École nationale des ponts et chaussées.

Mallet, V., Quélo, D., Sportisse, B., Ahmed de Biasi, M., Debry, É., Korsakissok, I., Wu, L., Roustan, Y., Sartelet, K., Tombette, M., and Foudhil, H. (2007). Technical Note: The air quality modeling system Polyphemus. *Atmos. Chem. Phys. Discuss.*, 7(3):6,459–6,486.

Mallet, V. and Sportisse, B. (2006a). Ensemble-based air quality forecasts: A multimodel approach applied to ozone. *J. Geophys. Res.*, 111.

Mallet, V. and Sportisse, B. (2006b). Uncertainty in a chemistry-transport model due to physical parameterizations and numerical approximations: An ensemble approach applied to ozone modeling. *J. Geophys. Res.*, 111(D1).

Middleton, P., Stockwell, W. R., and Carter, W. P. L. (1990). Aggregation and analysis of volatile organic compound emissions for regional modeling. *Atmos. Env.*, 24A(5):1,107–1,133.

Simpson, D., Winiwarter, W., Börjesson, G., Cinderby, S., Ferreiro, A., Guenther, A., Hewitt, C. N., Janson, R., Khalil, M. A. K., Owen, S., Pierce, T. E., Puxbaum, H., Shearer, M., Skiba, U., Steinbrecher, R., Tarrasón, L., and Öquist, M. G. (1999). Inventorying emissions from nature in Europe. *J. Geophys. Res.*, 104(D7):8,113–8,152.

Stockwell, W. R., Kirchner, F., Kuhn, M., and Seefeld, S. (1997). A new mechanism for regional atmospheric chemistry modeling. *J. Geophys. Res.*, 102(D22):25,847–25,879.

Stockwell, W. R., Middleton, P., Chang, J. S., and Tang, X. (1990). The second generation regional acid deposition model chemical mechanism for regional air quality modeling. *J. Geophys. Res.*, 95(D10):16,343–16,367.

Troen, I. and Mahrt, L. (1986). A simple model of the atmospheric boundary layer; sensitivity to surface evaporation. *Boundary-Layer Meteor.*, 37:129–148.

Verwer, J. G., Hundsdorfer, W., and Blom, J. G. (2002). Numerical time integration for air pollution models. *Surveys on Math. for Indus.*, 10:107–174.

Zhang, L., Brook, J. R., and Vet, R. (2003). A revised parameterization for gaseous dry deposition in air-quality models. *Atmos. Chem. Phys.*, 3:2,067–2,082.

Presented at the 6th Annual CMAS Conference, Chapel Hill, NC, October 1-3, 2007

THE INFLUENCE OF MM5 NUDGING SCHEMES ON CMAQ SIMULATIONS OF BENZO(A)PYRENE CONCENTRATIONS AND DEPOSITIONS IN EUROPE

Volker Matthias*, Markus Quante and Armin Aulinger
GKSS Research Center, Institute for Coastal Research, Geesthacht, Germany

1. INTRODUCTION

Three dimensional Eulerian chemistry transport models (CTMs) like CMAQ need highly resolved meteorological fields as input data. These fields can be a source of significant errors which contribute to uncertainties in simulations of the atmospheric distribution of chemical species and aerosols. Therefore, the evaluation of the quality of meteorological simulations used for chemistry transport studies is indispensable.

At GKSS, the 5th generation NCAR/Penn State University mesoscale meteorological model (MM5) is used as meteorological preprocessor for CMAQ. MM5 can be used with different nudging options to assure a close connection between the simulated fields and the driving global reanalysis data. In this paper we investigate the influence of different nudging options on the results of a long term CMAQ model run for persistent pollutants, in this case benzo(a)pyrene.

2. MODEL

CMAQ has been expanded at GKSS to study the trans-boundary transport of polycyclic aromatic hydrocarbons (PAHs; i.e. benzo(a)pyrene) and their deposition within coastal regions of Europe (Aulinger et al., 2007). The goal of our studies are multi-year runs of MM5-CMAQ for the assessment of past trends in PAHs concentrations and deposition. The model is set up on a 54 x 54 km² grid for Europe and on a nested smaller domain with a 18 x 18 km² grid for the North Sea region.

MM5 is operated with the more sophisticated parameterizations for cloud micro physics (Reisner2, Reisner et al., 1998), the planetary boundary layer (MRF, Hong and Pan, 1996), and the subscale cumulus convection (Kain Fritsch 2, Kain, 2004). The Noah land surface module (LSM, Chen and Dudhia, 2001) is used and the model is driven by ERA40 reanalysis data (1 x 1 degree, 6 hourly atmospheric fields, surface and soil data). Four dimensional data assimilation (FDDA) is used in different configurations to nudge the model results with the ERA40 gridded data.

**Corresponding author:* Volker Matthias, GKSS Research Center, Institute for Coastal Research, Environmental Chemistry Department, Max-Planck-Strasse 1, 21502 Geesthacht, Germany; e-mail: volker.matthias@gkss.de

3. MEASUREMENT DATA

Our modeling of persistent pollutants, that are only present in very low concentrations in the atmosphere, aims at long times series of several years. Therefore the meteorological fields were tested for systematic deviations from long term observations. Because the long range transport of atmospheric pollutants is closely connected to its vertical transport, it is important to compare the model results to data that contains also vertical information and not only ground data.

Radiosoundings that are routinely performed by the European Weather Services and that can be publicly accessed are well suited for this purpose. The data comprises regular observations (usually twice a day) of temperature, wind, and humidity up to the tropopause. One disadvantage is of course that the data is already assimilated in the driving reanalysis fields. However there is no real alternative to the data if a homogeneous data set covering whole Europe is needed. Nevertheless, we used also wind profiler data to check wind speed and wind direction at three stations in Central Europe.

All radiosoundings used in this study were extracted from the IGRA data set (Durre et al., 2006), that contains data from more than 1000 stations world wide in a common format. Figure 1 shows the locations of 88 stations in Europe that were selected for our tests.

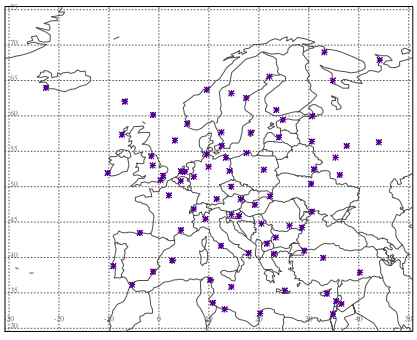

Fig.1 : Map of the selected radiosonde stations

4. RESULTS

4.1 Nudging schemes

To test the different nudging schemes, several runs with different options were performed for April 2000 and the results were compared to the measurements at 19 selected stations. Afterwards the whole year 2000 was modeled with the optimal nudging options and these results were compared to the radiosonde data from 88 stations and to the wind profilers.

Nine different model setups were chosen for the initial tests:

1. No nudging
2. Periodic restart every 96 hours
3. Wind (U,V) nudging
4. U,V and temp. (T) nudging
5. U,V,T and rel. hum.(RH) nudging
6. U,V,T,RH nudging, no LSM
7. U,V,T,RH nudging, daily var. SST
8. U,V,T,RH nudging, only 9 vert. lay.
9. U,V,T,RH nudging, only 12 vert. lay.

All runs except case 2 were performed for 34 days (from 28 March 2000 to 30 April 2000) without restart. The results from 1 April to 30 April were then used for the comparisons (resulting in a spin up time of 4 days). Only for the periodic restart, the model was run for 11 periods of 4 days each, using only the last 3 days for the comparisons. Temperature and Humidity were only nudged above the PBL. The sea surface temperature is usually initialized at the beginning of a MM5 run and then kept constant over the whole run. In one setup, the SST was daily adapted to the SST given in the reanalysis data.

At each station, the mean difference and the root mean square (rms-)error were calculated for each profile and then averaged for the whole month. The results for temperature and relative humidity are displayed in Figures 2 and 3.

It can be clearly seen that nudging of the temperature leads to a significantly lower rms-error and to a very small mean difference between model and observations. This is also connected to the number of vertical layers that was used in MM5. The simulations with 9 and 12 vertical layers showed the largest rms-errors and on average 1 K too high temperatures. If no nudging was applied, temperatures were underestimated by the model. The effect was less severe when the model was restarted every 4 days, but the results were still significantly worse than for the nudging cases.

The picture is slightly different for the relative humidity. Again, highest deviations from the observations were detected for the cases without

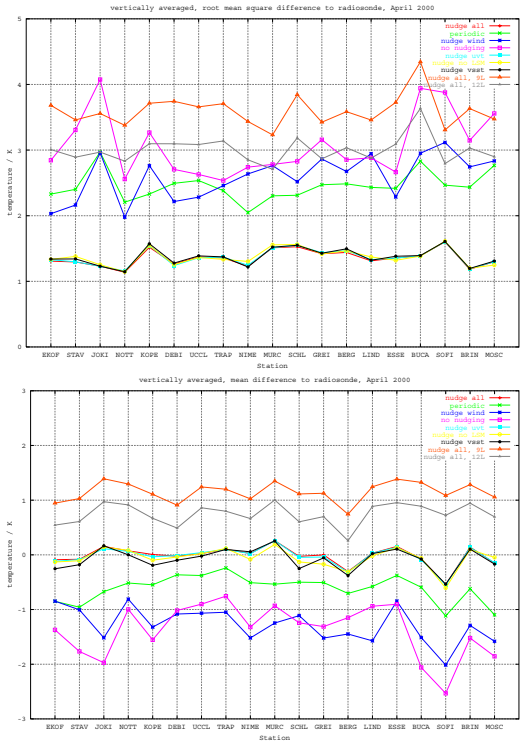

Fig. 2: Mean rms error (top) and mean deviation (bottom) of the modeled temperature compared to radiosoundings at 19 selected stations in Europe in April 2000.

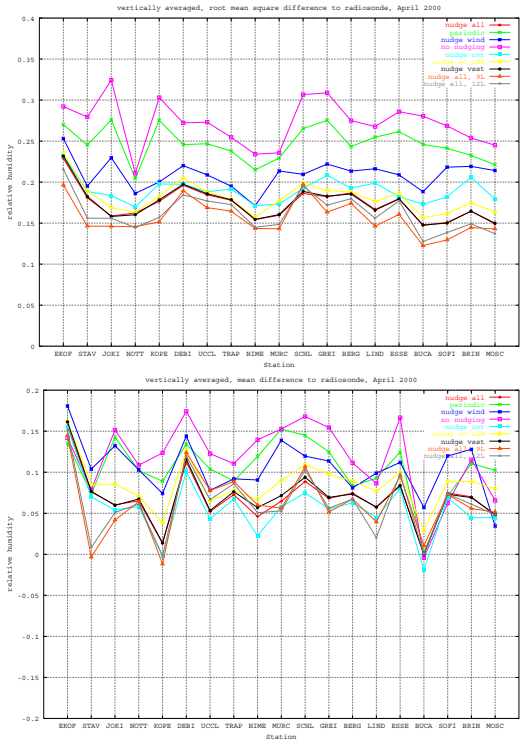

Fig.3: Same as Fig. 2 but for relative humidity

nudging. All other results were quite close together and even if only the wind components u and v were nudged, the rms-error and the mean deviation were much lower than for the cases without nudging. The use of a land surface model slightly improved the results. However, at all stations the modeled values of the relative humidity were higher than the observations.

For wind direction and wind speed, the two runs without nudging also showed much higher rms-errors than all other runs. In contrast, the mean deviations of wind speed and wind direction were similar for all runs.

4.2 Seasonal and regional dependence

Additional to the dependence on the nudging scheme, which was tested only for April 2000, the model results might also depend on season and on location. Therefore annual runs were performed with complete nudging of u, v, T and RH, the use of the Noah LSM and monthly varying SST. Each month was modeled separately with a spin up time of 4 days. It was tested before that this time is sufficient to achieve results that are independent from the initial conditions.

The results are displayed in color code in Figures 4 – 7.The x-axis shows the temporal variation and the y-axis shows the stations which were sorted from west (No.1) to east (No.88). Here, only the bias in temperature, rel. humidity, u-wind and v-wind are given. Black colors denote not enough data.

Some scatter in the results for the temperature can be seen in Fig. 4, but no systematic effects were present. Some stations (in particular Reykjavik, the most westerly station in the model domain) show large discrepancies between model and observations but mostly the bias is below 0.5 K.

Some seasonal and regional effects were found for the relative humidity. While in winter and spring, RH is mostly overestimated (as it has already been seen for the April results), some underestimations are also observed in summer and fall at the more easterly stations. Nevertheless, the results give a quite uniform picture.

The wind components are more variable and they show some systematic effects. The u-wind component is mostly underestimated, in particular in winter when the average wind speed is higher than in summer. The v-wind component shows a clear geographical dependence with too low values in the western part of Europe and too high

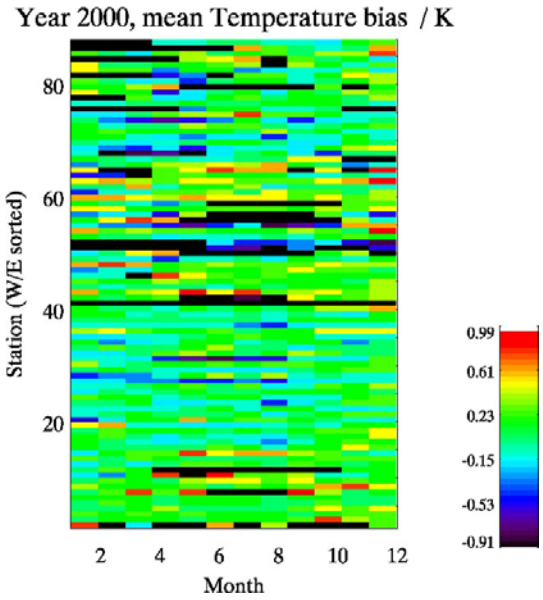

Fig. 4: Monthly comparison of the mean deviation of temperature from radiosonde profiles at 88 European stations and MM5 model results calculated with complete nudging.

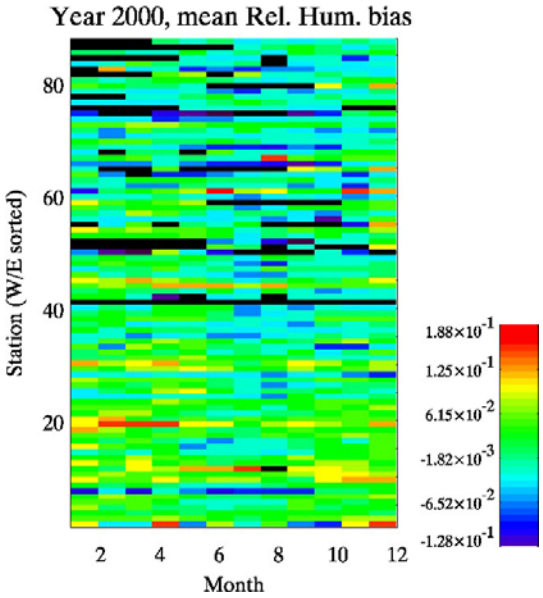

Fig. 5: Same as Fig. 4 but for RH.

values in the eastern part. Again, the situation is more pronounced in winter than in summer.

To investigate the effect further, the modeled wind data was also compared to hourly wind profiler data at three European stations: Pendine/UK, Cabauw, The Netherlands and Lindenberg/Germany. In this case, the annual time series at all model levels where profiler data was

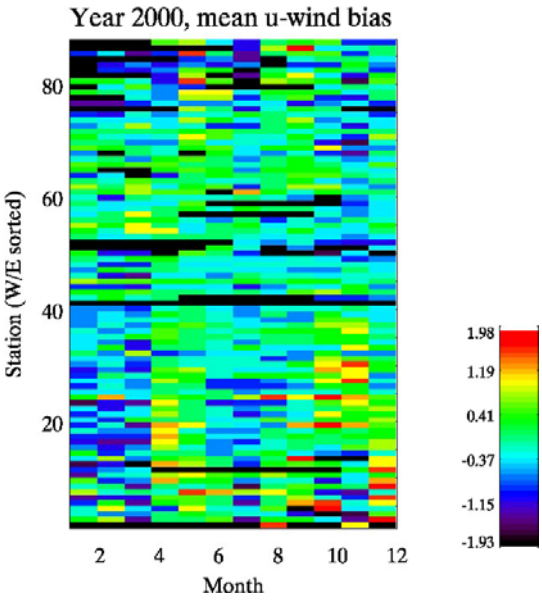

Fig.6: Same as Fig. 4 but for the u-wind (in m/s).

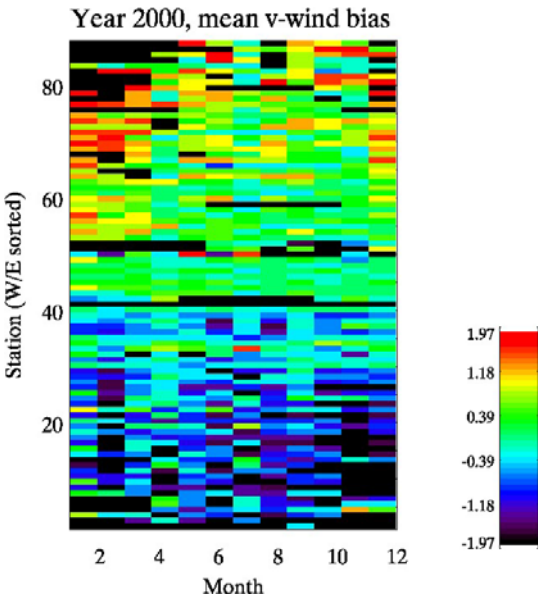

Fig. 7: Same as Fig. 4 but for the v-wind (in m/s).

available were investigated. At Pendine, the negative v-wind bias was also observed, the u-wind bias was slightly positive over the whole year. The absolute deviations increase with wind speed and therefore with altitude. The temporal correlation of the time series is larger than 0.9 in all heights. The bias is smaller at Cabauw, but here v is also underestimated while u is overestimated. The temporal correlations are not as high as at Pendine, they vary between 0.8 and 0.9. Closest agreement was achieved at

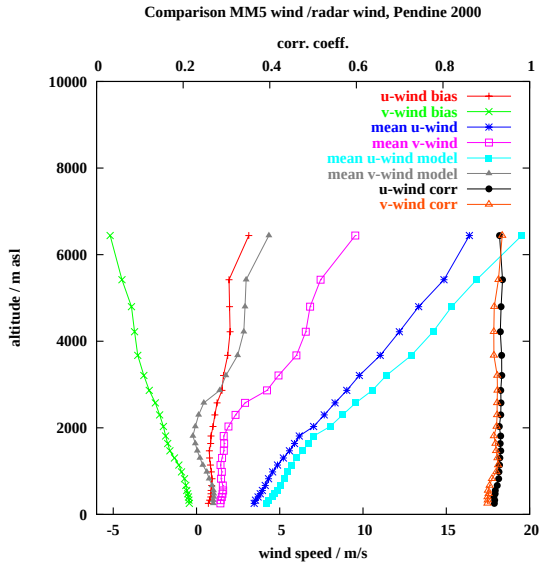

Fig. 8: Comparison of u- und v-wind components calculated with MM5 for 2000 with hourly wind profiler data at Pendine/UK.

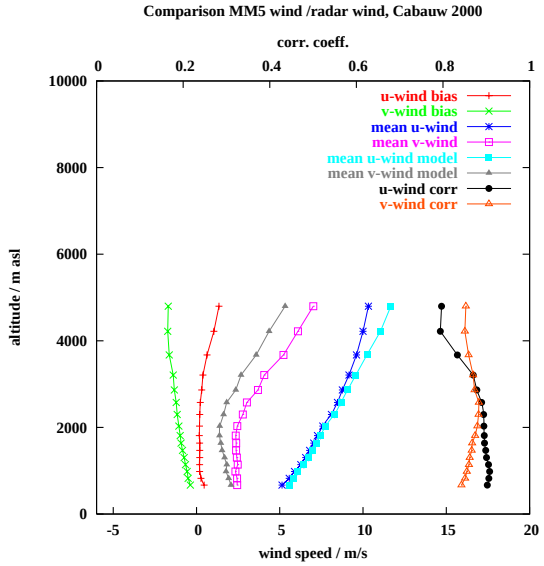

Fig. 9: Same as Fig.8, but at Cabauw, The Netherlands.

Lindenberg, where the bias is almost zero and the correlations are around 0.95.
Although wind profiler data was available only at a few stations, the results of the comparisons between model simulations and radiosondes could be confirmed. Up to now an explanation for this effect could not be found.

4.2 Influence on B(a)P distributions

The influence of the different model setups on the B(a)P concentrations was investigated for two of the nine different cases described in section 4.1.

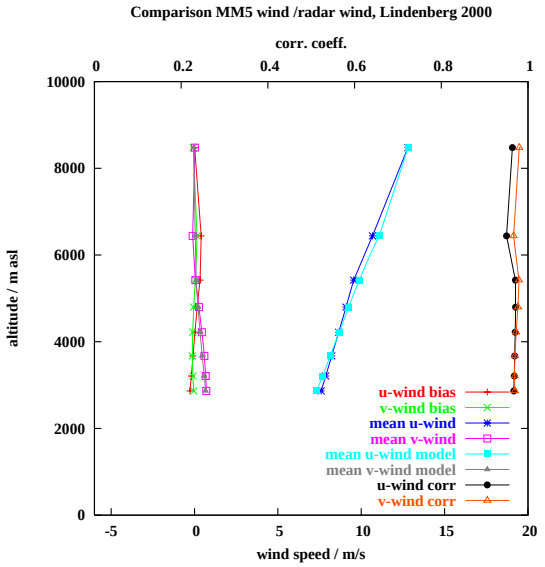

Fig. 10: Same as Fig.8, but at Lindenberg, Germany.

The reference run was performed with complete nudging and it was compared to the case when the model was periodically restarted but none of the variables was nudged. The results are shown in Fig. 11 for the mean concentration at ground level in April 2000 and in Figure 12 for the mean wet deposition.

In the simulation with periodic restart, lower concentrations were modeled in some regions (like the Po basin in north Italy and around Moscow). Here, higher wet depositions occur which leads to the conclusion that changes in the hydrological cycle might cause the differences in the concentrations.

6. CONCLUSIONS

The influence of different nudging options in the mesoscale meteorological model MM5 on the B(a)P concentrations and depositions in April 2000 was investigated. Significant differences, particularly in regions with high B(a)P concentrations were observed. Because in regions with lower B(a)P concentrations, enhanced wet deposition was modeled, it is likely that the hydrological cycle is significantly different in the two simulations.

Out of the nine investigated cases, the meteorological fields calculated with complete nudging of T, RH, u and v showed the lowest deviations from regular radiosonde observations. Nevertheless, some systematic deviations from the measured wind components, particularly the v-wind component exist. The v-wind component is

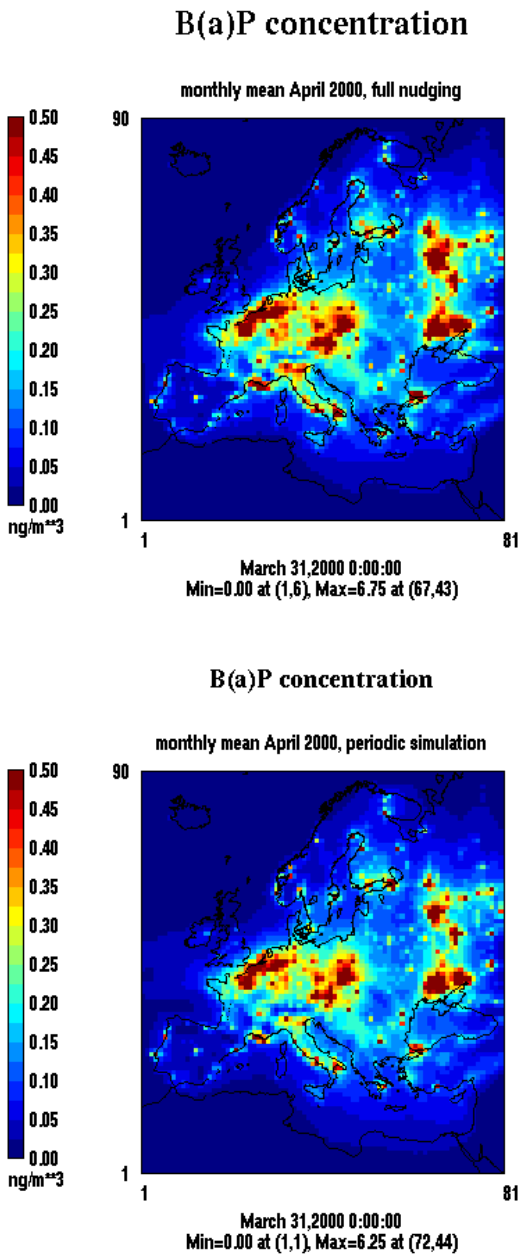

Fig. 11: Modeled B(a)P concentrations in Europe in April 2000 calculated with different meteorological input fields. Top: with full nudging of T,RH, u and v. Bottom: without nudging but with a periodic restart of the model every 4 days.

underestimated in western Europe while it is overestimated in eastern Europe. This result was confirmed when selected wind profiler time series were compared to the modeled wind field. However, an explanation could not be found up to now.

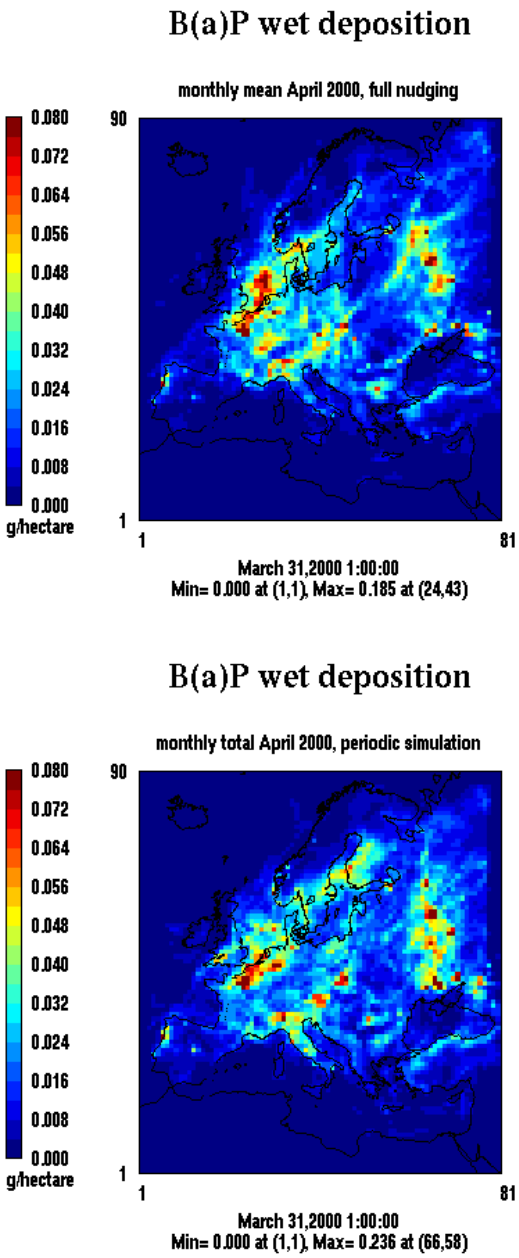

Fig. 12: Same as Fig. 11 but for wet deposition.

Acknowledgements

The authors are grateful to NCAR and Penn State University for the use of MM5 and to US EPA for the use of CMAQ. We thank Myles Turp (UK Met office) for providing wind profiler data from the CWINDE project.

References

Aulinger, A., Matthias, V., Quante, M., 2007: Introducing a partitioning mechanism for PAHs into the Community Multiscale Air Quality modelling system and its application to simulating the transport of benzo(a)pyrene over Europe. *Journal of Applied Meteorology*, accepted

Byun, D.W., Ching, J.K.S., 1999: *Science Algorithms of the EPA Models-3 Community Multiscale Air Quality Modeling System. EPA/600/R-99/030*, US Environmental Protection Agency, Office of Research and Development, Washington DC.

Chen, F. and Dudhia, J., 2001: Coupling an advanced land-surface/hydrology model with the Penn State/NCAR MM5 modeling system. Part I: Model implementation and sensitivity. *Monthly Weather Review,* **129**, 569-585.

Durre, I., Vose, R.S., and Wurtz, D.B., 2006: Overview of the Integrated Global Radiosonde Archive. *Journal of Climate,* **19**, 53-68.

Grell, G., Dudhia, J., and Stauffer, D.R., 1995: *A Description of the Fifth-Generation Penn State/NCAR Mesoscale Model (MM5).* NCAR Technical Note 398, NCAR, Boulder, Colorado, USA.

Hong, S.Y., Pan, H.L., 1996: Nonlocal boundary layer vertical diffusion in a Medium-Range Forecast Model. *Monthly Weather Review,* **124**, 2322.

Kain, J., 2004: The Kain Fritsch Convective Parameterization: An Update. *Journal of Applied Meteorology*, **43**, 170-181.

Reisner, J., Rasmussen, R. J., Bruintjes, R. T., 1998: Explicit forecasting of supercooled liquid water in winter storms using the MM5 mesoscale model, *QJRMS*, **124B**, 1071.

AN EXAMINATION OF WRF/CHEM: PHYSICAL SCHEMES, NESTING OPTIONS, AND GRID RESOLUTIONS

Chris Misenis, Xiaoming Hu, and Yang Zhang*
Department of Marine, Earth, and Atmospheric Sciences,
North Carolina State University, Raleigh, NC, USA

Jerome Fast
Pacific Northwest National Laboratory, Richland, WA, USA

Georg Grell and Steven Peckham
National Oceanic Atmospheric Administration, Earth Systems Research Laboratory, Boulder, CO, USA

SUMMARY

The Weather Research and Forecast/Chemistry Model (WRF/Chem) offers several options for planetary boundary layer (PBL) schemes (i.e., the YSU and MYJ schemes), land-surface models (LSM) (i.e., the slab, NOAH, and RUC schemes), and nesting (i.e., one- and two-way). In this work, we examine the sensitivity of WRF/Chem predictions to various PBL schemes and LSMs, nesting options, and grid resolutions. WRF/Chem is applied for the 28 Aug. – 2 Sept. 2000 Texas Air Quality Study (TexAQS-2000) episode over a domain that covers primarily Louisiana and eastern Texas. Simulations at a 12-km grid spacing with various combinations of LSM and PBL schemes (e.g., slab/YSU, RUC/YSU, and NOAH/MYJ) are conducted and compared with those from the baseline simulation with NOAH/YSU. In addition, one- and two-way nested simulations with 12- and 4-km grid spacings have been conducted with NOAH/YSU. For this episode, results show that for meteorological predictions, the NOAH/YSU and RUC/YSU pairs perform similarly in terms of normalized mean bias (NMB) for temperature (-0.3%), while slab/YSU performs more accurately for wind speed, wind direction and relative humidity (RH) (NMBs of 1.7%, 5.7%, and 2.5%, respectively). The NOAH/MYJ pair simulates PBL height more accurately than others, with an NMB of 22.7%. For chemical species, the slab/YSU pair performs best for O_3 and CO (NMBs of 9.7% and -14.9%, respectively), while the RUC/YSU pair performs slightly better for $PM_{2.5}$ (NMB of 0.5%). All simulations perform poorly for NO_x with NMBs < -50% for NO and > 50% for NO_2. The model predictions are also sensitive to nesting options and grid spacing, particularly at 4-km. The relative accuracy and computational efficiency for various physical parameterizations and configurations will be evaluated. These simulations and analyses will provide insights into WRF/Chem's capability of capturing the variability of meteorological variables and chemical species at various grid resolutions.

*Corresponding author: Yang Zhang, Department of Marine, Earth and Atmospheric Sciences, Campus Box 8208, NCSU, Raleigh, NC 27695; phone number: (919) 515-9688; fax number: (919) 515-7802; e-mail: yang_zhang@ncsu.edu

ACKNOWLEDGEMENTS AND DISCLAIMER

This work is performed under the National Science Foundation Award No. Atm-0348819, and the Memorandum of Understanding between the U.S. Environmental Protection Agency (EPA) and the U.S. Department of Commerce's National Oceanic and Atmospheric Administration (NOAA) and under agreement number DW13921548.

This work constitutes a contribution to the NOAA Air Quality Program.

Presented at the 6th Annual CMAS Conference, Chapel Hill, NC, October 1-3, 2007

Evaluation of the Regional Atmospheric Modeling System (RAMS) with aircraft observations over East Asia during the spring of 2001

Meigen Zhang*
State Key Laboratory of Atmospheric Boundary Layer Physics and Atmospheric Chemistry, Institute of Atmospheric Physics, Chinese Academy of Sciences, Beijing 100029, China

Zhiwei Han
Key Laboratory of Regional Climate-Environment Research for Temperate East Asia, Institute of Atmospheric Physics, Chinese Academy of Sciences, Beijing 100029, China

1. INTRODUCTION

Three-dimensional photochemical modeling systems are the primary tools being applied by regulatory agencies for the development of emission strategies to improve air quality. Meteorological information is one of the most critical inputs to the photochemical models because meteorology encompasses many atmospheric processes that control and strongly influence the evolution of emissions, chemical species, aerosols and particulate matter, and is typically provided by prognostic regional/mesoscale models (Seaman, 2000; Chandrasekar et al., 2003). Due to the critical role played by the meteorological inputs in the photochemical modeling systems, there is a need to performance extensive evaluations of mesoscale meteorological models with observations in order to understand their limitations and strengths (Pielke and Uliasz, 1998).

The Regional Atmospheric Modeling System (RAMS) is a highly versatile numerical code developed by scientists at Colorado State University and the ASTER division of Mission Research Corporation for simulating and forecasting meteorological phenomena (Pielke et al., 1992; Walko and Tremback, 2001). Presently it is widely used to drive air quality models (e.g., Lyons et al., 1995; Sistla et al., 2001; Fast, 2002; Zhang et al., 2003, 2004) and has been evaluated using traditional statistical measures as well as qualitative assessments such as graphical comparisons of observed and simulated meteorological fields (Lyons et al., 1995; McQueen et al., 1997; Cox et al., 1998; Hogrefe et al., 2001; Oh and Ghim, 2001; Chandrasekar et al., 2003), but extensive evaluations are found nearly exclusively for applications to North American (e.g., Cox et al., 1998; Chandrasekar et al., 2003).

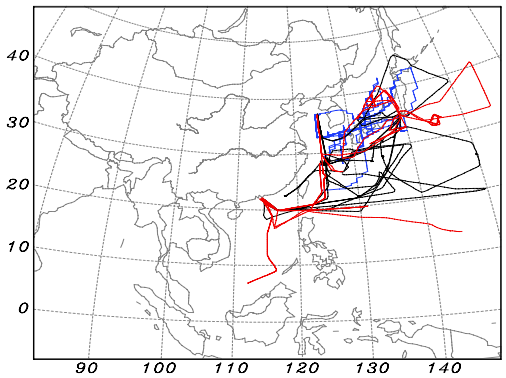

Fig. 1. Model domain for RAMS used in this study. Also shown are horizontal flight tracks of the aircrafts DC-8 (black lines), P-3B (red lines) and C-130 (blue lines) during the period.

In the spring of 2001 two large field campaigns, the transport and chemical evolution over the Pacific (TRACE-P; Jacob et al., 2003) and the Asian Pacific regional aerosol characterization experiment (ACE-Asia; Huebert et al., 2003), were consecutively conducted over the western Pacific and the islands of Japan. In the TRACE-P period from 4 March to 2 April 2001 two NASA aircrafts DC-8 and P-3B performed 11 (flight numbers DC-8 07~17) and 12 (flight numbers P-3B 08~19) observations, respectively, over the western Pacific with bases near Hong Kong, Okinawa and Tokyo, and each flight lasted more than 8 hours. During the ACE-Asia missions from 30 March to 3 May 2001, instrumented NCAR aircraft C-130 conducted 19 flights over the Yellow Sea, the Sea of Japan and south of Japan. Three aircrafts obtained an extensive suite of meteorological parameters, and this dataset provides a strong basis for extensive evaluations of mesoscale meteorological models. This study is to take advantage of the dataset to extensively examine

**Corresponding author:* Meigen Zhang; e-mail: mgzhang@mail.iap.ac.cn

regional-scale performances of RAMS when applied to Asia.

This paper is divided into four sections. We describe the RAMS application in Section 2. In Section 3 we first compare model results with observations from a mission-wide perspective, and then evaluate the model's ability to predict about absolute values of wind speed, wind direction, temperature and water vapor mixing ratio along flight tracks. Conclusion is presented in Section 4.

2. Model description

RAMS version 4.3 (RAMS 4.3) is evaluated in this study. Its code is based on an implementation of the full set of primitive equations, supplemented by optional parameterizations of several physical phenomena. In the study the Kuo-type approach (Molinari, 1985) was employed to represent the subgrid scale convective cumulus, and a scheme which employs prognostic turbulent kinetic energy approach (Mellor and Yamada, 1982) was chosen to parameterize the vertical diffusion. The radiation parameterization used the Chen and Cotton scheme (Chen and Cotton, 1983) and the bulk microphysics parameterization was activated. A soil-vegetation model was also activated. A general description of the model physics and application fields are given in Pielke et al. (1992).

During the simulations RAMS 4.3 was exercised in a four-dimensional data assimilation mode using analysis nudging with re-initialization every 4 days, leaving the first 24 hours as the initialization period. The three-dimensional meteorological fields for input were obtained from the European Center for Medium-Range Weather Forecasts (ECMWF) analyzed datasets, and were available every 6 hours with $1^o \times 1^o$ resolution. Observed monthly snow cover information and sea surface temperatures (SST) based on weekly mean values were used to set the boundary conditions for the RAMS calculation.

3. MODEL RESULTS AND DISCUSSION

Three-dimensional meteorological fields were simulated in the period from 22 February to 5 May 2001 by use of RAMS 4.3. To characterize the model's abilities and limitations, modeled meteorological parameters such as wind speed, wind direction, temperature and water vapor content are compared with observations obtained on board of three aircrafts DC-8, P-3B and C-130 during the TRACE-P and ACE-Asia field experiments. These aircrafts made totally 52 extensive observations over the western Pacific, the Yellow Sea and the Sea of Japan during the simulation period, and each flight lasted at least 8 hours. Their horizontal flight coverages are presented in Figure 1. The DC-8 flights had an altitude variation from 150 m to 12 km, the P-3B flight altitudes ranged from 150 m to 7 km, and the ceiling height of C-130 was ~ 8 km. For these comparisons the model was sampling along 11 DC-8, 12 P-3B and 19 C-130 flight paths at 5-min intervals and compared with the measured values in the merged data set. The merged data set consists of all measurements taken on the aircraft combined together in a single data set with common and uniform time intervals and consistent format. These data are available for download on the website http://www-gte.larc.nasa.gov and http://www.joss.ucar.edu/ace-asia. Model results are interpolated to the exact times and locations of the aircraft measurements.

Table 1 presents statistical summaries of the comparison of modeled and observed values of wind speed, wind direction, temperature and water vapor mixing ratio during the flights of DC-8 07~17, P-3B 08~19 and C-130 01~19 in the period from 4 March to 3 May 2001, respectively. In the table N is the number of paired samples, C_M and C_O are average values of modeled and observed meteorological parameters, R stands for the correlation coefficient, E_{MAGE} and E_{RMSE} stand for the mean absolute gross error and the root mean squared error, and B_{NMBF} and E_{NMEF} are the normalized mean bias factor and the normalized mean error factor.

Table 1. Observed and modeled values of wind speed, wind direction, temperature and water vapor mixing ratio for the flights of DC-8 07~17

	DC-8			
	WS[a]	WD[a]	TA[a]	QV[a]
N[b]	1189	1189	1198	1192
C_O[c]	24.2	248.2	260.5	2.64
C_M[c]	24.8	239.8	260.9	2.90
R[d]	0.96	0.76	0.99	0.98
E_{MAGE}[e]	3.47	18.2	1.71	0.55
E_{RMSE}[f]	4.92	30.4	2.22	0.86
B_{NMBF}[g]	0.03	-0.03	0.002	0.10
E_{NMEF}[h]	0.14	0.08	0.007	0.21

[a]WS, WD, TA and QV represent for wind speed (m/s), wind direction (deg), temperature (^{o}K) and water vapor mixing ratio (g/kg)
[b]N is the number of paired samples
[c]C_O and C_M are averaged values of observed and modeled meteorological parameters
[d]R stands for the correlation coefficient between observed and modeled meteorological parameters

[e] E_{MAGE} means the mean absolute gross error
[f] E_{RMSE} stands for the root mean squared error
[g] B_{NMBF} is the normalized mean bias factor
[h] E_{NMEF} represents the normalized mean error factor

Comparison of modeled and aircraft-based observed vertical distributions provides an assessment for the ability of the model to simulate the vertical structure of meteorological parameters. We plot the paired data points used in the previous statistics against height in Figures 2~4 to show their vertical variations. The figures show that observed maximum wind speeds increase with height and reached 70 m/s above 8 km (cf. Figure 2a), and in the layers above ~3 km prevailing wind directions are westerly, while temperatures and water vapor mixing ratios generally decrease with height. The figures also show that the observed meteorological parameters exhibit strong variations even at a fixed height. Comparing model results with the observations, we see that the model reproduced these major observed features quite well, and the simulated vertical distribution patterns are generally similar to their observed ones, even the model overestimated temperatures in the layers above 6 km and water vapor mixing ratios show a high model bias at low altitudes. Reasonable agreement of vertical distributions between observed and simulated meteorological parameters indicates that the model captured the tempo-spatial distributions reasonably well, as the aircraft observations covered a wide area over the western Pacific (cf. Figure 1) and lasted nearly two months.

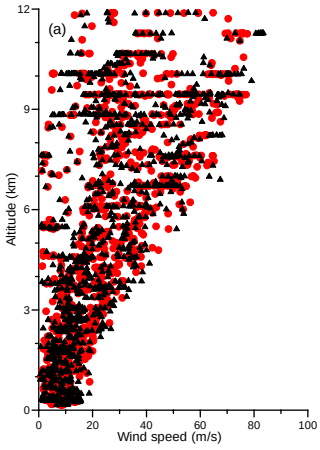

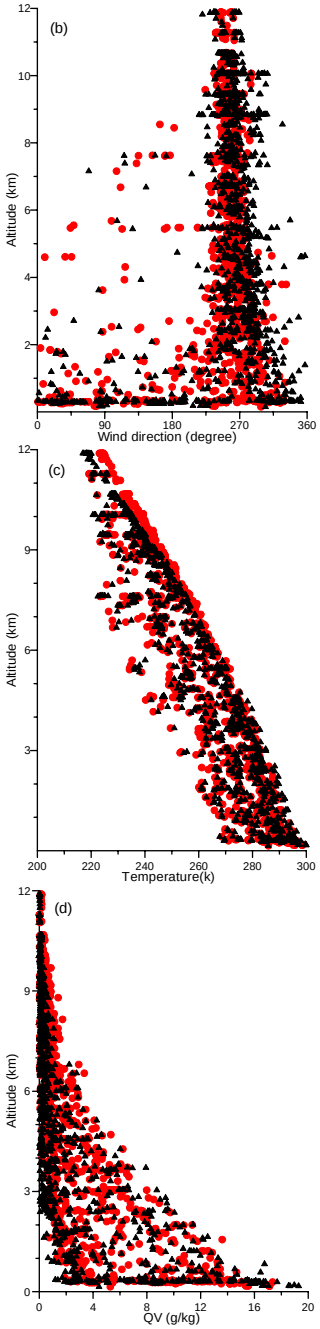

Fig. 2. Observed (triangles) and simulated (dots) vertical variations in (a) wind speed, (b) wind direction, (c) temperature, and (d) water vapor mixing ratio for the DC-8 flights 07~17 in the period from 4 March to 2 April 2001. Shown are values for each 5-min flight segments from the merged data set.

4. CONCLUSION

RAMS 4.3 was applied to East Asia to simulate three dimensional meteorological fields from 22 February to 5 May 2001, and modeled wind directions, wind speeds, temperatures and water vapor mixing ratios were compared with observations obtained on board of 3 aircrafts during the TRACE-P and ACE-Asia field campaigns to evaluate the model's performances. Comparison of the modeled and observed values on mission-wide perspective showed that 1) average values of the four simulated meteorological parameters are all in good agreement with their observations; 2) RAMS reproduces the mean observed wind speed to within about 0.7 m/s with rather mean absolute gross error and high correlation coefficients, and the percentages of simulated wind directions within the desired accuracy (Cox et al., 1998) are all over 67%; 3) modeled and simulated temperatures are high correlated, their correlation coefficients are all larger than 0.95, but model results have a positive bias of 0.6 ^{o}C for the flights of DC-8 and a negative bias of 0.5 and 0.6 ^{o}C for the flights of P-3B and C-130; 4) modeled water vapor mixing ratios have a good correlation with their observed ones, but RAMS generally overestimates them by 10%; 5) modeled vertical distribution patterns of the four parameters are quite similar to their observed ones, but the model tends to overestimate temperatures in the layers above 6 km.

Peak 8-hr Ozone Model Performance when using Biogenic VOC estimated by MEGAN and BIOME (BEIS)

Kirk Baker
Lake Michigan Air Directors Consortium, Rosemont, IL, USA

1. INTRODUCTION

Biogenic emissions are a large contributor of regional VOC in the central and eastern United States that participate in photochemical reactions which form ozone (Wiedinmyer et al, 2005). It is important to capture the magnitude and spatial scale of VOC emissions, especially isoprene, to appropriately model high ozone episodes in the Midwest United States. The Model of Emissions of Gases and Aerosols from Nature (MEGAN) was recently developed as the next generation emission model for biogenic emissions of gases and aerosols (Guenther and Wiedinmyer, 2006). MEGAN has been implemented into the CONsolidated Community Emissions Processing Tool (CONCEPT) emissions modeling framework (Wilkinson, 2006). The CONCEPT emissions framework (CONCEPT, 2007) also includes the biogenic emissions model BIOME, which is a combination of BEIS3 (Geron et al, 1994) and GloBEIS (Guenther et al 1999, 2000) methodologies. A slightly different version of BIOME was implemented in the EMS-2003 emissions model (Janssen and Hua, 2007; Wilkinson et al, 1994).

The biggest difference in BIOME implementations is in the canopy parameterization scheme. EMS/BIOME has a simple canopy formulation and CONCEPT/BIOME uses canopy and environmental adjustment factors from GloBEIS. MEGAN uses a canopy environmental correction factor based on photosynthetically activated radiation (PAR) and temperature for isoprene emissions, which is similar to the GloBEIS approach (Guenther and Wiedinmyer, 2006). The emissions estimation equation in MEGAN is augmented to include a factor to account for the natural cycle of the changing structure of leaves and a factor to account for plant stress due to the lack of soil moisture. Leaf area index and average temperature across the current and previous time period is used to estimate the factor that adjusts for leave structure. Soil moisture and wilting point data are used to estimate the factor that adjusts emissions based on moisture availability (Wilkinson, 2006).

MEGAN groups plants and area coverages by plant functional type (PFT) rather than treating plant species explicitly as in the BIOME (and BEIS) models. Total emissions are the sum of emissions estimated for each PFT in a given grid cell. PFTs include broadleaf trees, fine leaf evergreen trees, fine leaf deciduous trees, shrubs, grass, and crops. Plant functional type data has been gridded to a scale of 30 seconds by 30 seconds and made available with the MEGAN model (Guenther et al, 2006). Soil wilting point data and leaf area index are also gridded to the same scale and used as input to MEGAN.

MEGAN, CONCEPT/BIOME, and EMS/BIOME are used to generate emissions estimates for each day of the summer of 2002. Each of the 3 biogenic emissions estimates are modeled with a state of the science photochemical transport model, the Comprehensive Air Quality Model with Extensions (CAMx4), to determine how well model estimates of ozone compare with observations.

2. METHODS

The Comprehensive Air Quality Model with Extensions (CAMx) version 4.50 uses state of the science routines to model ozone formation and removal processes over regional and urban scales (Nobel et al, 2002; Chen et al, 2003; Morris et al, 2005). The model is applied with an updated carbon-bond 05 (CB05) gas phase chemistry module (ENVIRON, 2006). CAMx is applied using the PPM horizontal transport scheme and an implicit vertical transport scheme with the fast CMC chemistry solver (ENVIRON, 2006). The photochemical model is initiated at midnight Eastern Standard Time and run for 24 hours for each episode day. The summer

simulations are initiated on June 2 and run through August 31. The first 11 days of the simulation are not used in any analysis to minimize the influence of initial concentrations (Baker, 2007).

The meteorological, emissions, and photochemical models are applied with a Lambert projection centered at (-97, 40) and true latitudes at 33 and 45. The 36 km photochemical modeling domain consists of 97 cells in the X direction and 90 cells in the Y direction covering the central and eastern United States (Figure 1). The 2-way nested 12 km domain covers most of the upper Midwest region with 131 cells in the X and Y directions. CAMx is applied with the vertical atmosphere resolved with 16 layers up to approximately 15 kilometers above ground level.

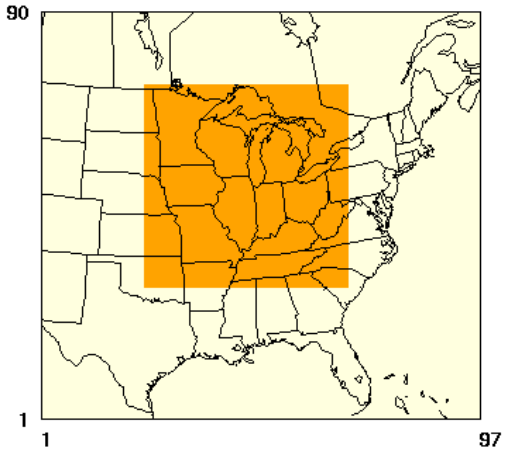

Fig. 1. 36 km (large box) and 12 km (small dark box) modeling domain.

Meteorological input data for the photochemical modeling runs are processed using the National Center for Atmospheric Research (NCAR) 5th generation Mesoscale Model (MM5) version 3.6.1 (Dudhia, 1993; Grell et al, 1994). Important MM5 parameterizations and physics options include mixed phase (Reisner 1) microphysics, Kain-Fritsch 2 cumulus scheme, Rapid Radiative Transfer Model, Pleim-Chang planetary boundary layer (PBL), and the Pleim-Xiu land surface module. Analysis nudging for temperature and moisture is only applied above the boundary layer. Analysis nudging of the wind field is applied above and below the boundary layer. These parameters and options are selected as an optimal configuration for the central United States based on multiple MM5 simulations using a variety of physics and configuration options (Johnson, 2003; Baker, 2004).

Anthropogenic emission estimates are made for a weekday, Saturday, and Sunday for each month. The biogenic emissions are day-specific. Daily emissions estimates for June through August 2002 from each biogenic model are merged with the same 2002 anthropogenic emissions. Volatile organic compounds are speciated to the Carbon Bond 05 chemical speciation profile. The BELD3 land use dataset is input to the BIOME biogenic models for fractional land-use and vegetative speciation information (US EPA, 2006; Kinnee et al, 1997). Inputs to all 3 biogenic models include hourly satellite photosynthetically activated radiation (PAR) and 15 m (above ground level) temperature data output from MM5 (Pinker and Laszlo, 1992).

Other inputs to MEGAN include plant functional type emission factors, PFT area coverage, soil wilting point data, leaf area index, and additional meteorological variables including soil moisture. Soil moisture estimated by MM5 for the 1 m soil depth is used as input to MEGAN because it represents the plant root layer.

3. RESULTS & DISCUSSION

3.1 Biogenic Emissions Modeling

MEGAN estimated VOC is compared to estimates from alternative biogenic emissions models including the CONCEPT and EMS-2003 implementations of the BIOME model. Total isoprene emissions over the entire summer for the entire modeling domain are 3.6 Mt from MEGAN, 3.1 Mt from EMS/BIOME, and 2.9 Mt from CONCEPT/BIOME. Daily total isoprene emissions estimated by MEGAN, EMS/BIOME, and CONCEPT/BIOME over the entire modeling domain are shown in Figure 2.

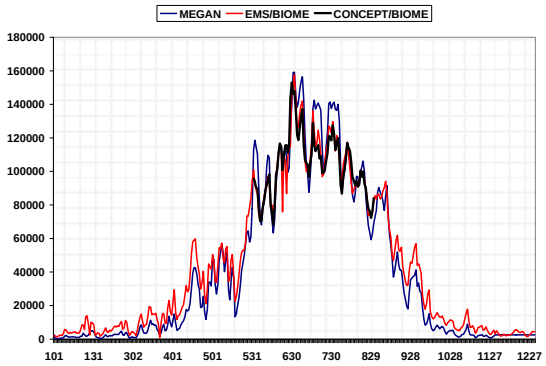

Fig. 2. Daily total isoprene emissions (tpd) for 2002.

Emissions estimates for each of the BIOME implementations are very similar, which is expected given the similarities in formulation. The CONCEPT implementation estimates slightly less isoprene on high emission days than the EMS version. Typically in the summer MEGAN estimates more total isoprene than BIOME. MEGAN tends to estimate less daily isoprene emissions in the early fall and late spring than BIOME. Total daily emissions for all species are shown in Table 1 for July 1, 2002.

Table 1. Total daily emissions (tpd) by model.

	Model		
Species	megan	concept/biome	ems/biome
ALD2	8,633	14,294	16,149
ALDX	1,732		
CO	25,343		
ETH	4,956		
ETHA	770		
ETOH	6,233		
FORM	1,442		
IOLE	2,549		
ISOP	158,793	146,376	149,575
MEOH	46,651		
NO	4,970	4,684	3,921
NR	22,591	2,561	2,424
OLE	4,683	9,887	10,230
PAR	14,333	72,129	73,498
SQT	8,918		
TERP	37,210	40,499	22,877
TOL	322		
XYL	170		

MEGAN outputs more explicit species than BIOME: carbon monoxide, ethane (ETHA), ethene (ETH), ethanol (ETOH), methanol (MEOH), formaldehyde, toluene, xylene, and sesquiterpenes. BIOME estimates much more mass in the more reactive VOC groupings of paraffins, olefins, and aldehydes as opposed to MEGAN which estimates much more mass as non-reactive (NR) VOC. This decrease in reactive VOC groups may offset some of the increases in ozone formation expected from the higher isoprene emissions estimated by MEGAN.

The spatial pattern of isoprene emissions varies between models. Figure 3 shows daily total emissions of isoprene in each grid cell for July 1, 2002.

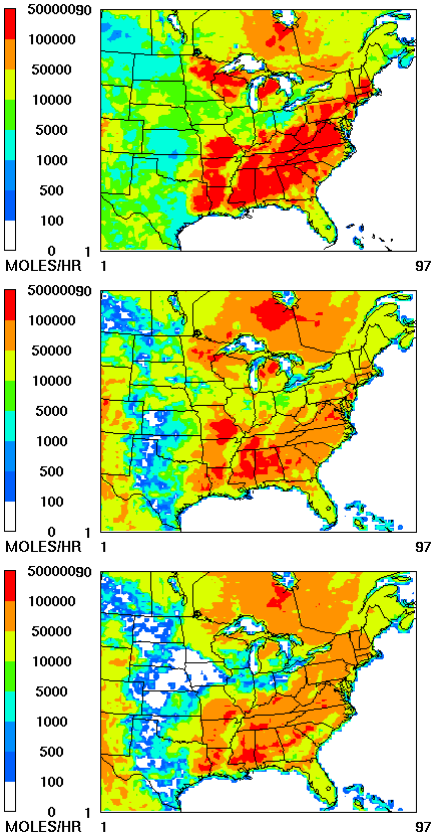

Fig. 3. Total emissions for July 1, 2002 estimated by MEGAN (top), EMS/BIOME (middle) and CONCEPT/BIOME (bottom).

The spatial plots in Figure 3 show higher regional isoprene emissions in the southeast United States, mid-Appalachian region, and mid-Great Lakes region estimated by MEGAN. There are less isoprene emissions estimated with MEGAN in Canada and Mexico. The implications about the change in spatial pattern of isoprene emissions are that more regional isoprene is available for ozone formation in the central and eastern United States when using MEGAN estimates.

3.2 Photochemical Modeling

When modeled with a photochemical transport model, each set of biogenic emissions result in a similar spatial pattern of peak ozone formation. The MEGAN emissions have the highest ozone peaks of the 3 sets of biogenic emissions. The 99th percentile daily maximum 8-hourly average ozone observation for each monitor is paired with model estimates. The mean bias of 99th percentile 8-hourly average maximum ozone over all stations (N=303) in the 12 km domain is -16.5 ppb with MEGAN biogenics, -18.0 with CONCEPT/BIOME biogenics, and -19.4 with EMS/BIOME biogenics. The isoprene estimated by MEGAN resulted in ozone estimates closest to peak observations over the entire 12 km modeling domain.

Figure 4 shows daily average mean gross error over all stations in the 12km modeling domain estimated for 8-hr ozone greater than 80 ppb. This high minimum threshold is selected to assess model performance for high ozone that is used as part of ozone attainment model demonstrations (US EPA, 2007). The ozone predictions using MEGAN biogenic emissions tend to be closest to high observed ozone values in the upper Midwest United States, but all three are fairly close on most days.

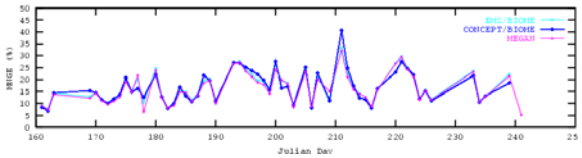

Fig. 4. Daily average mean gross error for all 3 simulations for 8-hr ozone > 80 ppb.

The day to day model performance features in daily average mean gross error change little when using different biogenic emissions. This suggests the day to day performance for ozone is more closely related to anthropogenic emissions and meteorology. The difference in mean normalized gross error for 8-hr ozone greater than 80 ppb between MEGAN and EMS/BIOME simulations is shown for each monitor in Figure 5. The blue shades (cool colors) represent monitor locations where the error is lower using MEGAN biogenics and red shades (hot colors) represent monitor locations where the error is lower using EMS/BIOME biogenics.

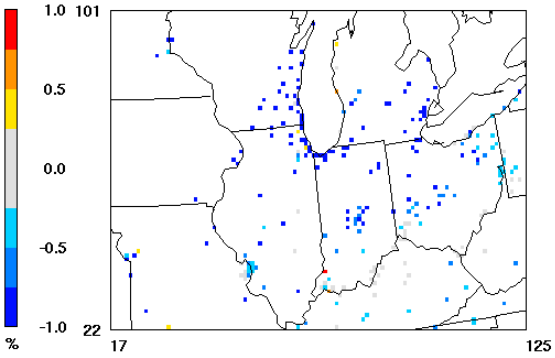

Fig. 5. MNGE (%) difference between simulations (megan – ems/biome).

Most stations in the region have better performance when the MEGAN biogenic emissions are used. This is seen in particular in urban areas like Indianapolis, St. Louis, Chicago, Milwaukee, Detroit, Columbus, and Cleveland.

4. CONCLUSIONS

The MEGAN isoprene emissions improve model estimates of high ozone in the upper Midwest compared to 2 implementations of the BIOME model. In general, each of the 3 biogenic emissions estimates resulted in similar spatial patterns of ozone formation in the region which suggests that ozone performance is more closely related to anthropogenic emissions and meteorology. Future work will include a comparison of photochemical model estimated secondary organic aerosol using emissions from MEGAN and BIOME.

5. REFERENCES

Baker, K. Ozone Source Apportionment Results for Receptors in Non-Attainment Counties in the Great Lakes Region. 2007. AWMA Annual Conference. Pittsburgh, PA.

Baker, K. Meteorological Modeling Protocol For Application to PM2.5/Haze/Ozone Modeling Projects, 2004. http://www.ladco.org/tech/photo/photochemical.html

Chen, K. S.; Ho Y.T.; Lai C.H.; Photochemical modeling and analysis of meteorological parameters during ozone episodes in Kaohsiung, Taiwan, *Atmospheric Environment*, **2003**, *37(13),* 1811-1823.

CONCEPT. Accessed July 29, 2007. www.conceptmodel.org

Dudhia, J. A nonhydrostatic version of the Penn State/NCAR mesoscale model: Validation tests and simulation of an Atlantic cyclone and cold front, *Mon. Wea. Rev.*, **1993**, *121*, 1493-1513.

ENVIRON International Corporation. User's Guide Comprehensive Air Quality Model with Extensions (CAMx) Version 4.30; ENVIRON International Corporation: Novato, CA, 2006. www.camx.com

Grell, G. A.; Dudhia, J.; Stauffer, D. A description of the Fifth Generation Penn State/NCAR Mesoscale Model (MM5), NCAR Tech. Note, 1994; NCAR TN-398-STR.

Geron, C.D., Guenther, A.B. and Pierce, T.E. (1994) An improved model for estimating emissions of volatile organic compounds from forests in the eastern United States. *J. Geophys. Res.* **99**, 12773-12791.

Guenther, A and C. Wiedinmyer (2006). MEGAN User's Guide. acd.ucar.edu/~guenther/MEGAN/MEGANusersguide.pdf

Guenther, A., T. Karl, P. Harley, C. Wiedinmyer, P. Palmer and C. Geron (2006). Model of Emissions of Gases and Aerosols from Nature (MEGAN). bai.acd.ucar.edu/Megan/index.shtml

Guenther A.; Geron C.; Pierce T.; Lamb; Harley P.; Fall R. Natural emissions of non-methane volatile organic compounds; carbon monoxide, and oxides of nitrogen from North America, *Atmos. Environ*., **2000**, *34*, 2205-2230.

Guenther, A., B. Baugh, G. Brasseur, J. Greenberg, P. Harley, L. Klinger, D. Serca, L. Vierling. 1999. Isoprene emission estimates and uncertainties for the Central African EXPRESSO study domain. *Journal of Geophysical Research- Atmospheres,* 104 (D23):30625-30639.

Janssen, M.; Hua., C. Emissions Modeling System-95 User's Guide. Lake Michigan Air Directors Consortium: Rosemont, IL. See http://www.ladco.org/emis/guide/ems95.html

Johnson, M. Meteorological Modeling Protocol: IDNR 2002 Annual MM5 Application, 2003.

Kinnee, E.; Geron C.; Pierce T. United States land use inventory for estimating biogenic ozone precursor emissions. *Ecological Applications*, **1997**, *7(1)*, 46-58.

Morris, R.E.; Mansell G.; Tai. E. Air Quality Modeling Analysis for the Denver Early Action Ozone Compact. Prepared for Denver Regional Air Quality Council, Denver, CO. ENVIRON International Corporation, Novato, California, 2005.

Nobel, C. E.; McDonald-Buller E.C.; Kimura, Y.; Lumbley, K.E.; Allen, D.T. Influence of population density and temporal variations in emissions on the air quality benefits of NOx emission trading, *Environmental Science & Technology*, **2002**, *36*, 3465-3473.

Pinker, R.T.; Laszlo I. Modeling surface solar irradiance for satellite applications on a global scale. *J. Appl. Meteor*., **1992**, *31*, 194-211.

U. S. Environmental Protection Agency, *Guidance on the Use of Models and Other Analyses for Demonstrating Attainment of Air Quality Goals for Ozone, PM2.5, and Regional Haze*. April 2007.

U. S. Environmental Protection Agency. See http://www.epa.gov/ttn/chief/emch/biogenic/ (accessed August 9, 2006).

Wiedinmyer, C., Greenberg, J., Guenther, A., Hopkins, B., Baker, K., Geron, C., Palmer, P. I., Long, B. P., Turner, J. R., Petron, G., Harley, P., Pierce, T., Lamb, B., Westberg, H., Baugh, W., Koerber, M., Janssen, M. (2005), Ozarks Isoprene Experiment (OZIE): Measurements and modeling of the ''isoprene volcano,'' J.

Geophys. Res., 110, D18307, doi:10.1029/2005JD005800.

Wilkinson, J. Implementation of the model of emissions of gases and aerosols from nature (MEGAN) into the concept modeling framework. June 16, 2006.AG-TS-90/236

Wilkinson, J.; Loomis, C.; Emigh, R.; McNalley, D.; Tesche, T., Technical Formulation Document: SARMAP/LMOS Emissions Modeling System (EMS-95). Final Report prepared for Lake Michigan Air Directors Consortium (Rosemont, IL) and Valley Air Pollution Study Agency (Sacramento, CA), 1994.

SPECIATE - EPA's Database of Speciated Emission Profiles

J. David Mobley, Lee L. Beck, Golam Sarwar, Adam Reff, and Marc Houyoux
U.S. Environmental Protection Agency, Research Triangle Park, NC

Abstract
SPECIATE is the U.S. Environmental Protection Agency's (EPA) repository of total organic compound (TOC) and particulate matter (PM) speciation profiles for emissions from air pollution sources. The profiles are key inputs to air quality modeling and source-receptor modeling applications. This paper addresses Version 4.0 of the SPECIATE Database.

INTRODUCTION

The SPECIATE Database is an important EPA product which serves as the repository for source category-specific emission speciation profiles. The profiles contain weight fractions of species of both volatile organic compounds (VOC) and Particulate Matter (PM). The weight fractions of VOC species are grouped into reactivity classes to support air quality modeling for ozone. The profiles of PM species weight fractions are specific to particle size ranges and are being used to support air quality modeling for PM and visibility. The Database has also supported air toxic assessments and is essential for source-receptor modeling applications.

The Database was first computerized in 1988. Although accessibility to the Database has been sustained through the Clearing House for Inventories and Emission Factors (CHIEF) website, updates to SPECIATE have languished since the mid-1990s due to decreasing budgets. The US National Research Council in its report on Research Priorities for Airborne Particulate Matter (2004), the Clean Air Act Advisory Committee in its report of the Air Quality Management Working Group (December 2004), NARSTO in its Emission Inventory Assessment (September 2005), and other groups have recommended that the Database be extensively updated and maintained in a dynamic manner.

Given the importance of SPECIATE to the process of air quality management, a team was organized to undertake an update of the Database. The scope of the team's project was to: (1) Update the Database with profiles from the literature and EPA source test data sets; (2) Link the new profiles to Source Classification Codes (SCCs) in the National Emissions Inventory (NEI); (3) Assign any new species to reactivity classes; and (4) Update the air quality models to use the new information.

SPECIATE VERSION 4.0

The final report, "SPECIATE 4.0—Speciation Database Development Documentation (EPA/600/R-06/161, November 2006)" summarizes the development and provides guidance on use of the Database. The Database is posted on the CHIEF Website, (http://www.epa.gov/ttn/chief/software/speciate/index.html). The final version of the Database has been integrated into the Emissions Modeling Platform for subsequent research and regulatory modeling applications. The ability to speciate the emissions inventory with the new SPECIATE composite profiles will bring substantial benefits to the fields of air quality modeling and source apportionment, including:

- Support the creation of speciated emissions inventories for air quality modeling applications for fine particulate matter ($PM_{2.5}$), ozone (O_3), and regional haze;
- Estimate hazardous and toxic air pollutant emissions from total PM and VOC primary emissions;
- Support source-receptor modeling with chemical-mass balance models, positive matrix factorization, and factor analysis models;
- Verify profiles derived from receptor modeling using ambient measurements
- Facilitate source apportionment using air quality models by using source tagging of the trace elements and indicator species.

Results from these improved analyses will enable the development of more effective control strategies for sources of these species. Further, estimates of uncertainty in the results of air quality and receptor models will be improved by providing the most representative and up-to-date information to characterize emissions from the myriad point, area, mobile, and biogenic sources that contribute to ambient pollutant concentrations.

The initiative to update SPECIATE has produced:

- 2,856 PM profiles (1,503 legacy profiles, plus 1,258 new profiles including 95 simplified profiles);
- 1,215 gas profiles, 648 of which are new profiles;
- 1902 unique species, 1012 of which are new species;
- 58 Composite profiles for source categories (47 PM and 11 VOC);
- An updated cross-reference table linking profiles to source classification codes;
- VOC-to-TOG conversion factors for applicable gas profiles;
- A protocol for expansion of the Database;
- A mapping of the new VOC compounds into model species categories; and
- Review and prioritization of 49 studies entailing 614 PM and 822 VOC profiles for potential future inclusion in the SPECIATE Database.

APPLICATIONS

The SPECIATE 4.0 Database has been integrated into the Sparse Matrix Operator Kernel Emissions (SMOKE) modeling system, and its impact on predictions of ambient O_3 and PM concentrations has been evaluated by using the Community Multiscale Air Quality (CMAQ) modeling system. The results indicate that the new species profiles change the levels of predictions but do not change the levels significantly such that previous regulatory applications will be adversely impacted. In addition, the Database has been used to speciate $PM_{2.5}$ emissions for investigations into source-receptor modeling evaluations. The latter application of the improved database resulted in a national inventory of $PM_{2.5}$ emissions that is more resolved at both the chemical and source-category levels than any known before.

SUMMARY

SPECIATE 4.0 represents a significant enhancement of the data available to characterize emissions by species and source category. Air quality modeling and source-receptor modeling applications have benefited from using these enhanced speciation profiles. Additional efforts are needed to capture new data from current testing based on data submitted via the protocol for database expansion. The user community can support the Database development by supplying electronic data with full references.

ACKNOWLEDGEMENTS

The authors acknowledge Ying Hsu, Randy Strait, and Frank Divita of E.H. Pechan & Associates, Inc. for their support to the SPECIATE project.

REFERENCES

NRC. 2004. Research Priorities for Airborne Particulate Matter: IV. Continuing Research Progress, National Research Council, National Academies Press, Washington, DC.

CAAAC. 2004. Recommendations to the Clean Air Act Advisory Committee, Air Quality Management Working Group, December 2005.

NARSTO. 2005. Improving Emission Inventories for Effective Air Quality Management Across North America—A NARSTO Assessment. NARSTO-05-001, September 2005.

US EPA. 2006. SPECIATE 4.0—Speciation Database Development Documentation. EPA/600/R-06/161, (http://www.epa.gov/ttn/chief/software/speciate/index.html), US Environmental Protection Agency, Research Triangle Park, NC, November 2006.

Estimate of Mercury Emission from Natural Sources in East Asia

Suraj K. Shetty[1], Che-Jen Lin[1*], David G. Streets[2], Carey Jang[3], Thomas C. Ho[1] and Hsing-wei Chu[1]

[1]College of Engineering, Lamar University, Beaumont, TX 77710, USA
[2]Decision and Information Sciences Division, Argonne National Laboratory, Argonne, IL 60439, USA
[3]Office of Air Quality Planning and Standards, USEPA, Research Triangle Park, NC 27711, USA

1. INTRODUCTION

Mercury is emitted from anthropogenic and natural sources (or "re-emission" from previously deposited mercury from both natural and anthropogenic emissions). While anthropogenic emission has been relatively well documented and used in various global chemical transport models of mercury, natural emission were previously either neglected or estimated to be a certain fraction (35-40%) of previously deposited mercury. This is one of the model uncertainties and it is important to estimate mercury emission from natural sources for atmospheric mercury simulation (Lin et al., 2006a; 2007).

Many recent studies have developed natural emission models of mercury for emission estimate from vegetation, soil, soil under canopy, and water surfaces (Xu et al., 1999; Bash et al, 2004; Lin et al., 2005; Gbor et al., 2006). These estimates have also indicated natural emission to be about 1 to 2 times that of anthropogenic emission. The emission patterns exhibit strong diurnal and seasonal variations, a phenomenon that has also been observed from measurement. However, these studies were mainly focused on the North American region. Asia amounts to about 54 % of the total global anthropogenic mercury emissions (Seigneur et al., 2004; Pacyna and Pacyna, 2006), among those the emission from China constitutes a significant fraction (Streets et al., 2005). This leads to concerns of regional and global deposition due to its long-range transport and global dispersion (Seigneur et al., 2004; Jaffe et al., 2005; 2007).

The objective of this study is to estimate mercury emission from the East Asia domain by using a natural emission model to estimate emission from vegetation, soil and water surfaces. Inclusion of a natural emission model for the region would reduce mercury emission input uncertainty in emission inventories. The simulation was carried out for the months of January, April, July, and October, 2001 to observe the seasonal trend and to project annual emissions for an East Asia domain.

**Corresponding author:* Che-Jen Lin, Department of Civil Engineering, Lamar University, Beaumont, TX 77710-0024; e-mail: Jerry.Lin@lamar.edu.

2. METHOD

2.1 Meteorological and LAI data

The East Asia domain, which covers the entire China region and some parts of its neighboring countries, is a 36-km one-layer Lambert Conformal projection having 164x97 grids. The hourly meteorological data from the Mesoscale Model 5 (MM5) for the East Asia domain was processed by the University of Tennessee using the Meteorological Chemistry Interface Processor version 2.1 (MCIP2). These four months are representative of the seasonal meteorological variation in the domain. The 8-day average Leaf Area Index (LAI) data was obtained from MODIS satellite products: (ftp://primavera.bu.edu/pub/datasets/MODIS). The downloaded binary formats were converted into the model ready format using ENVI® (Environment for Visualizing Images), an image processing software.

2.2 Hg Concentrations

Spatially distributed soil mercury concentrations were created by digitizing the graphical data obtained from Chinese Environmental Monitoring Center and regridded for the 36 km East China domain. A mean aqueous concentration of 0.04 ng l^{-1} was used for dissolved Hg° in sea-water (Xu et al., 1999). Monthly-averaged ambient Hg° concentration was obtained from the output of a simulation performed using CMAQ-Hg for the ICAP trans-Pacific domain for the year 2001 (Lin et al, 2006b).

2.3 Model Implementation

Elemental mercury emission from vegetation was calculated as a product of evapotranspiration rate and the concentration of elemental mercury in soil water.

$$F_e = E_t \times C_s \quad (1)$$

Where, F_e is the emission flux of elemental mercury (ng m^{-2} h^{-1}), E_t is the rate of evapotranspiration rate (kg m^{-2} h^{-1}), and C_s is the Hg concentration in soil water (ng kg^{-1}). Penman-Monteith equation (Monteith and Unsworth, 1990) is used for the calculation of evapotranspiration rate.

Mercury soil emission was based on the empirical correlations obtained from the literature (Gbor et al., 2006), which is an extended form of the correlation developed following Xu et al. (1999).

$$\ln F_s = n \ln[Hg_s] - \frac{\beta}{T_s} + m \quad (2)$$

Where, F_S is the net exchange rate (ng m^2 hr^{-1}), Hg_s is the mercury soil concentration, T_s is the soil temperature (K), β is a function of activation energy 1.26×10^4 (K), *n* and *m* are constants with values of 1.0 and 38.67 respectively. Mercury emission from soil under the canopy was estimated based on the correlation obtained in Gbor et al, (2006).

$$\ln F_{sc} = b \ln[Hg_s] + aR_{gc} + c \quad (3)$$

Where, *a* is 3.5×10^{-3}, *b* is 0.28 and *c* is –1.24. R_{gc} is the solar radiation reaching the soil under the canopy.

Mercury emission from water was calculated by considering an overall mass transfer coefficient (parameterized as a function of wind speed) and Hg concentration in water (Bash et al., 2004).

$$F_w = k_l \left[C_w - \frac{C_a}{H} \right] \quad (4)$$

Where, F_w is the emission rate of elemental Hg from water (ng m^{-2} h^{-1}), k_l is the overall mass transfer coefficient (m s^{-1}), H is the Henry's law constant, C_w is the mercury concentration in water (ng m^{-3}) and C_a is the mercury concentration in air ng m^{-3}). The overall mass transfer coefficient (k_l) was estimated according to Wanninkhof (1992).

$$k_l = 0.45 U^{1.6} \left[\frac{Sc_{hg}}{Sc_{co2}} \right]^{-1/2} \quad (5)$$

Where, k_l is the overall mass transfer coefficient (cm h^{-1}), *U* is the wind speed at 10 m (m s^{-1}), and Sc_{hg} and Sc_{co2} are the Schmidt numbers for mercury and carbon dioxide respectively.

2.4 Model Simulations

This model run was performed using MATLAB 7.0 to simulate hourly Hg° emissions for the month of January, April, July, and October for the year 2001. The outputs were processed as netCDF files and visualized in PAVE v2.2 (Package for Analysis and Visualization of Environmental data) for analysis.

3. RESULTS AND DISCUSSION

The Hg° model simulation was performed for the month of January, April, July, and October 2001. The Hg flux from vegetation ranged between 0 and 66 ng m^{-2} h^{-1}, while Hg flux from soil and water surfaces were generally less than 12 ng m^{-2} h^{-1} and 5 ng m^{-2} h^{-1} respectively. The result depicts both diurnal (Fig.1) and seasonal variation (Fig. 2), which is the characteristic of natural Hg° emissions as shown in several recent studies. Fig. 1 shows a typical (July) summer time diurnal variation simulated from the natural emission model. As the day begins, the emission flux starts from the east and gradually moves to the west side of the domain according to the diurnal cycle of solar irradiation. Similar diurnal variation is also observed during the other months, with the intensity decreasing from summer to winter season.

Fig. 2 shows the seasonal variation of the estimated natural emission. It can be clearly seen that the natural Hg° emission peaks during the summer season, with highest emission occu-

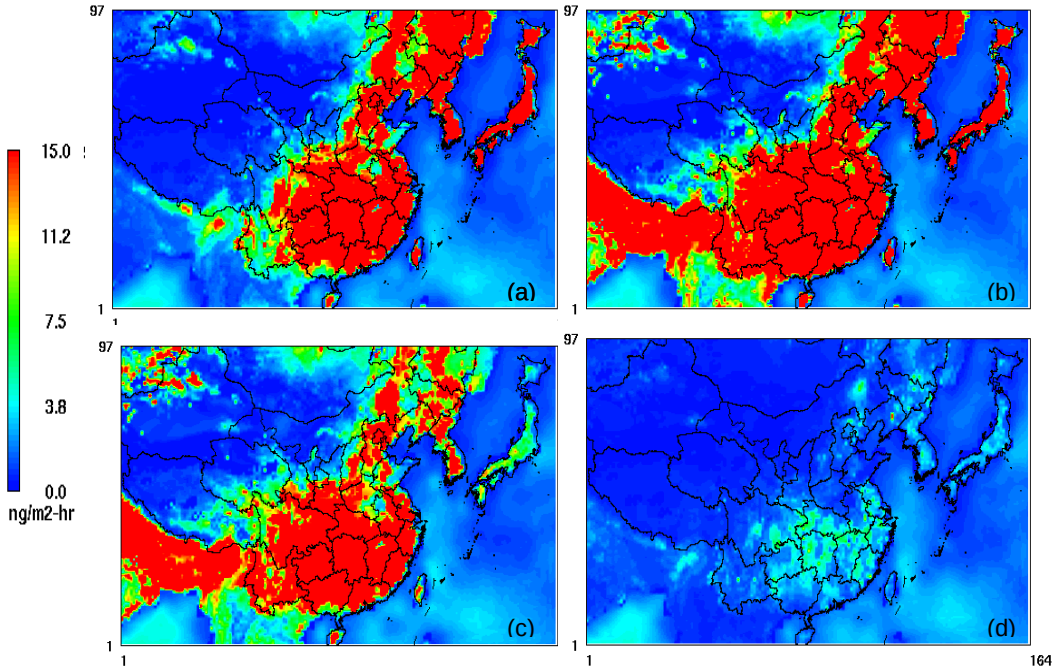

Fig. 1. Simulated averaged natural mercury emission flux showing diurnal variation for the month of July 2001 at (a) 8.00 am, (b) 1.00 pm, (c) 6.00 pm and (d) 11.00 pm using the natural emission model. It represents the flux averaged over 31days of July at that time period.

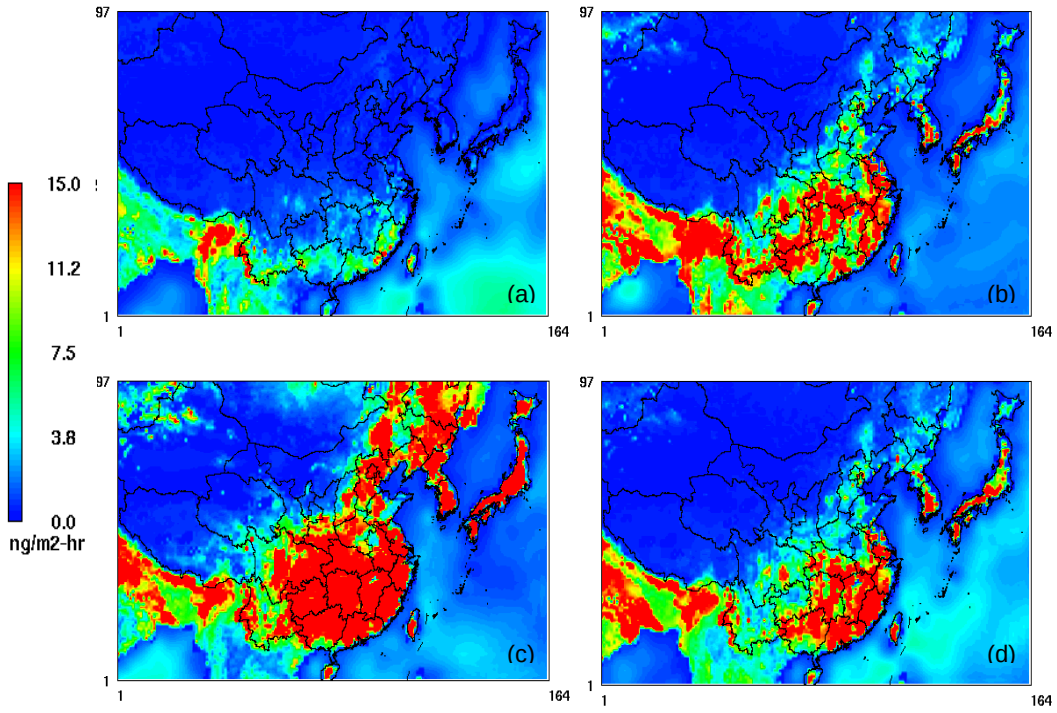

Fig. 2. Simulated averaged natural mercury emission flux showing the seasonal variation and trend during the months of (a) January, (b) April, (c) July, and (d) October. It represents the monthly flux averaged over 24 hour period.

Table 1. Estimated monthly natural emission from vegetation, soil and water (Mg)

	Vegetation	Soil (1)	Water	Total Emission from East Asia	Total Emission from China region
January	13	6	11	30	8
April	46	7	8	61	29
July	108	9	9	126	88
October	42	7	12	61	29
Total Annual Emission				834	462

(1) Includes emission from soil and emission from soil under canopy

-rring in the southeast China region. In winter season (Fig. 2a), natural mercury emission decreases drastically due to the lower temperature and weaker solar intensity. Only the southern part of the domain has significant emission as the region is well forested and does not have much decrease in surface temperature as compared to the northern side of the domain.

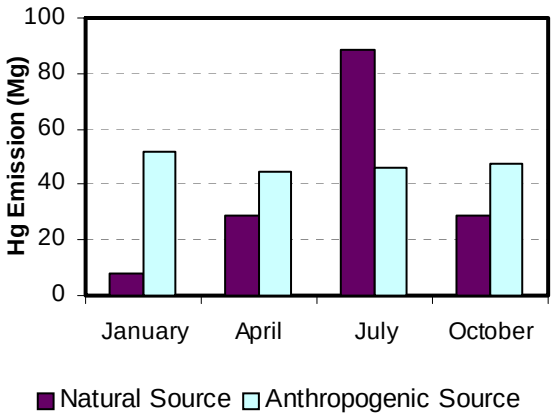

Fig.3. Comparison of natural mercury emission to anthropogenic emission from China region.

Table.1 shows the estimated seasonal mercury emission quantity in Mg mo^{-1}. It clearly indicates that emission due to vegetation is the most important contributing source of natural mercury emission. Vegetative emission also exhibit strong seasonal variations. It is due to the increase in the vegetation coverage, the higher temperature and solar irradiation during summer as compared to winter. This enables greater evapotranspiration rates during summer. Emissions from soil and water do not show much seasonal variation. The summer emission is slightly higher than the winter emission because of the higher summer temperatures.

Emissions from water surface show a slightly different trend that increases from July through October and thereafter begins to decrease from January through April. This is largely caused by the higher wind speeds in the months of October and January as compared to April and July, resulting in respective variation in the overall mass transfer between the water and the air surfaces.

The simulation result estimated that the annual natural mercury emission in the East Asia domain was about 834 Mg for the year 2001, with China contributing 462 Mg to the total natural emissions. The anthropogenic mercury emissions from China are estimated to be 575 Mg for the year 2001 (Streets et al., 2005, Wu et al., 2006). As anthropogenic mercury emission does not show much seasonal variation, natural mercury emission can be compared to an average anthropogenic emission of 48 Mg mo^{-1}.

It can be clearly seen in Fig. 3 that natural mercury emission quantity is almost twice as large as that of anthropogenic emission in the month of July. However, in April and October, it is almost 3/4th of that of anthropogenic emission. In January, anthropogenic mercury emissions amount to almost six times that of natural mercury emission.

The total annual mercury emission from China i.e. combining natural and anthropogenic mercury emission is estimated to be about 1040 Mg. This value is similar to a recent estimate of total mercury emission (1100 Mg/yr) using an inverse modeling approach (Pan et al., 2007). As the natural mercury emission is comparable to anthropogenic emissions, it should also be considered as an important parameter along with other emission inventories in the modeling of atmospheric mercury.

4. ACKNOWLEDGEMENT

The authors would like to acknowledge the funding support from Texas Commission on Environmental Quality (TCEQ Work Order Number: 64582-06-15), the USEPA Office of Air Quality Planning & Standards (RTI Subcontract Number: 6-321-0210288) and Texas Air Research Center (TARC Project Number: 077LUB0976).

5. REFERENCES

Bash, J.O., Miller, D., Meyer, T., Bresnahan, P., 2004. Northeast United States and Southeast Canada natural mercury emissions estimated with a surface emission model. *Atmospheric Environment* 38, 5683–5692.

Gbor, P.K., Wen, D., Meng, F., Yang, F., Zhang, B., Sloan, J.J., 2006. Improved model for mercury emission, transport and deposition. *Atmospheric Environment* 40, 973-983.

Lin, C.-J., Lindberg, S.E., Ho, T.C., Jang, C., 2005. Development of a processor in BEIS3 for estimating vegetative mercury emission in the continental United States. *Atmospheric Environment* 39, 7529-7540.

Lin, C.-J., Pongprueksa, P., Lindberg, S.E., Pehkonen S.O., Byun, D., Jang C., 2006a. Scientific uncertainties in atmospheric mercury models I: Model science evaluation. *Atmospheric Environment* 40, 2911-2928.

Lin, C.-J., Pongprueksa, P., Vanjani, T., Ho, T. C., Chu, H.W., Jang, C., Braverman, T., Streets, D.G., Fu, J.S., 2006b. Trans-Pacific chemical transport of mercury: Sensitivity analysis on potential Asian emission contribution to mercury deposition in North America using CMAQ-Hg. In: The 5th CMAS Conference, Research Triangle Park, NC, 16-18 October 2006.

Lin, C.-J., Pongprueksa, P., Bullock, O.R., Lindberg, S.E., Pehkonen, S.O., Jang, C., Braverman, T., Ho, T.C., 2007. Scientific uncertainties in atmospheric mercury models II: Sensitivity analysis in the CONUS Domain. *Atmospheric Environment* 41, 6544-6560.

Lin, X., and Tao, Y., 2003. A numerical modelling study on regional mercury budget for eastern North America. *Atmospheric Chemistry and Physics* 3, 535–548.

Li, Pan, Chai, T., Carmichael, G.R., Tang, Y., Streets, G.G., Woo, J.-H. Friedli, H.R., Radke, L.F., 2007, Top-down estimate of mercury emissions in China using four-dimensional variational data assimilation. *Atmospheric Environment* 41, 2804-2819.

Monteith, J.L., Unsworth, M.H., 1990. *Principles of environmental physics*. London: Edward Arnold Publication.

Pacyna, J.M., Pacyna, E., Steenhuisen, F., Wilson, S., 2006. Global anthropogenic mercury emission inventory for 2000. *Atmospheric Environment* 40, 4048-4063.

Seigneur, C., Vijayaraghavan, K., Lohman, K., Karamchandani, P., Scott, C., 2004. Global attribution for mercury deposition in the United States. *Environmental Science & Technology* 38, 555–569.

Streets, D.G., Hao, J., Wu, Y., Jiang, J., Chan, M., Tian, H., Feng, X., 2005, Anthropogenic mercury emissions in China. *Atmospheric Environment* 39, 7789-7806.

Wanninkhof, R., 1992. Relationship between wind speed and gas exchange over the ocean. *Journal of Geophysical Research* 97, 7373-7382.

Wu, Y., Wang, S., Streets, D.G., Hao, J., Chan, M., Jiang, J., 2006. Trends in Anthropogenic Mercury Emissions in China from 1995 to 2003. *Environmental Science & Technology* 40, 5312-5318.

Xu, X., Yang, X., Miller, D., Helble, J., Carley. R., 1999. Formulation of bi-directional atmosphere-surface exchanges of elemental mercury. *Atmospheric Environment* 33(27), 4345–4355.

Presented at the 6th Annual CMAS Conference, Chapel Hill, NC, October 1-3, 2007

INTEGRATION AND RECONCILIATION OF SATELLITE-DETECTED AND INCIDENT COMMAND-REPORTED WILDFIRE INFORMATION IN THE BLUESKY SMOKE MODELING FRAMEWORK

Sean Raffuse*, Dana Sullivan, Lyle Chinkin, Daniel Pryden, and Neil J. M. Wheeler
Sonoma Technology, Inc., Petaluma, CA

Sim Larkin and Robert Solomon
U.S. Forest Service AirFire Team, Seattle, WA

Amber Soja
National Institute of Aerospace, Hampton, VA

1. INTRODUCTION

The BlueSky smoke modeling framework is a tool for modeling the cumulative impacts from multiple fires (Larkin et al., 2007). Developed by the U.S. Department of Agriculture-Forest Service (USFS), it combines existing models in a unified structure to predict ground-level concentrations of particulate matter less than 2.5 microns in diameter ($PM_{2.5}$). BlueSky was originally designed to assist prescribed burn and smoke managers in making burn decisions based on expected smoke impacts, but it has been expanded to predict and track smoke from wildfires and wildland fire use (WFU) fires.

Currently, BlueSky ingests wildfire incident data from Incident Status Summary (ICS-209) reports. The ICS-209 is a two-page form, the main purpose of which is to provide incident information for operational decision support and firefighting resource allocation at a regional level. ICS-209 reports are typically created daily for large (>100 acre) wildfires and WFU fires. Because ICS-209 reports were not created to provide information for smoke modeling, their use is limited in this context. Each ICS-209 report contains a latitude and longitude pair that represents the point of origin of the incident. This location does not change, even as the fire propagates several kilometers away from the point of origin after weeks of burning. Daily ICS-209 reports contain a size value expressed as acreage. This value is cumulative and represents an estimate of the total acreage burned by the fire since the beginning of the incident. For BlueSky, day-specific information on location and area burned are required to estimate daily smoke emissions.

* *Corresponding author:* Sean Raffuse, Sonoma Technology, Inc., 1360 Redwood Way, Suite C, Petaluma, CA 94954-1169; e-mail: sraffuse@sonomatech.com

Satellites with infrared channels have long been used to detect actively burning fires (Dozier, 1981). There are currently several satellite-borne instruments delivering operational fire-detection products. Instruments onboard polar-orbiting satellites, such as Moderate Resolution Imaging Spectroradiometer (MODIS) on NASA's Terra and Aqua satellites, are able to detect active burning as small 0.25 acre (Giglio, 2005). The MODIS active fire product (MOD14) has a 1-km nadir resolution. Large fires are detected as several pixel "hot spots". The spatial resolution of these data is significantly better than that of ICS-209-reported fires and can provide daily snapshots of the burning areas to the BlueSky framework. In addition, many fires detected by satellite do not have associated ICS-209 reports.

Unfortunately, satellite-detected fire data also have limitations. Clouds preclude fire detection. Though MODIS, for example, can detect instantaneous burning as small as 0.25 acre, this translates to a much larger area burned over 24 hours; an examination of wildfires in the western United States showed that fires less than 300 acres in size are not reliably detected. Also, because current operational algorithms only detect actively burning fires, they may miss short-duration fires.

A new system was developed to integrate and reconcile human-recorded ICS-209 data with satellite-detected fire data and provide burn area predictions to the BlueSky framework. This system is called the Satellite Mapping Automatic Reanalysis Tool for Fire Incident Reconciliation (SMARTFIRE). By reconciling both satellite-detected and human-observed fires, SMARTFIRE harnesses the advantages of both data sets. Satellite-detected fire data come from the National Oceanic and Atmospheric Administration (NOAA) Hazard Mapping System (HMS; http://www.ssd.noaa.gov/PS/FIRE/hms.html). HMS

fire data are created by combining hot-spot detections from three instrument types onboard several satellite platforms and applying manual quality control by a trained satellite-data analyst.

The SMARTFIRE system was tested on data from the 2005 fire season. A handful of preliminary test cases were studied in to examine SMARTFIRE performance on representative wildfire types.

2. METHODS

The SMARTFIRE algorithm can be divided into two pieces, reconciliation and prediction. The reconciliation algorithm is responsible for merging the input fire data sets into a single cohesive data set of daily area burned. The prediction algorithm uses information in the SMARTFIRE database to provide likely burn locations and sizes for the next day. Next-day burn information is needed for BlueSky to perform its daily smoke predictions. Currently, the prediction algorithm is simple persistence. Next-day burn predictions are identical to the daily area-burn data from the reconciliation algorithm.

Ground-based, manually reported burning data sets record a different subset of fire incidents from satellite-derived data sets (Soja et al., 2005); however, many large fires are recorded by both. Therefore, when attempting to merge these two sources into a single data set, it is necessary to ensure that incidents are not double-counted. To achieve this data fusion, the SMARTFIRE reconciliation algorithm uses spatiotemporal proximity.

Figure 1a shows a reconciliation example for a single day (6/22/2005) of a large wildfire. The Cave Creek fire burned about 250,000 acres (~1000 km^2) in central Arizona between June 21 and July 4, 2005. The area burned over the course of the incident, shown on the map in yellow and orange is derived from the Burned Area Reflectance Classification (BARC; http://www.fs.fed.us/eng/rsac/baer/barc.html) developed by the USFS Remote Sensing Applications Center. BARC classifies post-fire vegetation condition using high spatial resolution satellite imagery and is used here as the "true" area burned. Both ICS-209 and HMS fire data are available on this day. The ICS-209 report shows the point of origin for this wildfire. The satellite data show several hot-spot pixels in the area. SMARTFIRE draws two buffers around the fire pixels. The first buffer is the daily FirePerimeter. The FirePerimeter groups nearby pixels into clusters of contiguous burning and provides an estimate of the daily area burned. The FirePerimeter buffer radius is currently set at 750 m. The FireEnvelope is then drawn 2000 m beyond each FirePerimeter. All FirePerimeters and ICS-209 reports that fall within a single envelope are associated as a single FireEvent. For example, in Figure 1a, all the satellite-detected points, their associated FirePerimeters, and the ICS-209 report point within the envelope are associated as a FireEvent. The ICS-209 point on the left edge of the map is treated as a separate fire.

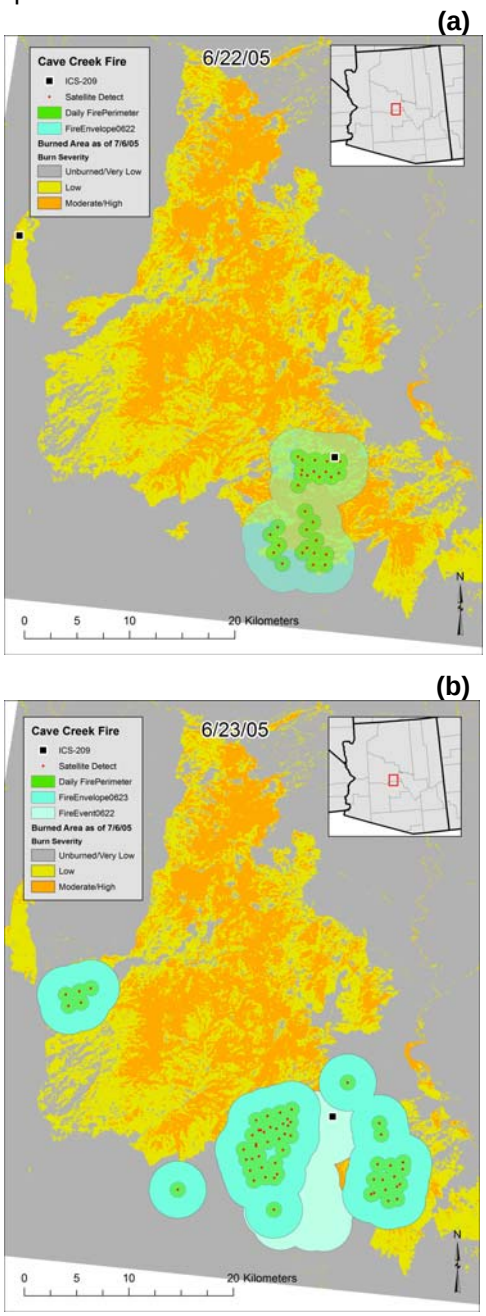

Fig 1. SMARTFIRE algorithm results for the Cave Creek wildfire on (a) the first and (b) the second day of the event.

The next day is shown in Figure 1b. The ICS-209 report has not moved, but the fire has, as seen by the HMS fire pixels. Four new FireEnvelopes were created, but two of them intersect the previous day's FireEvent. When this occurs, SMARTFIRE associates the intersecting FireEnvelopes with the preexisting FireEvent. Thus, as the fire expands away from the point of origin over time, its propagation can be tracked and recorded.

3. RESULTS AND DISCUSSION

All FirePerimeters generated by SMARTFIRE for the Cave Creek wildfire are shown in Figure 2. The total area burned according to these FirePerimeters is about 290,000 acres (1170 km2), which is about 15% higher than the estimates in the final ICS-209 report. Area is overestimated due to the overlap of FirePerimeters from different days. From these perimeters, both the daily locations and burn areas, can be extracted and fed to the BlueSky modeling framework. This improved spatial resolution is important, particularly for a large event such as Cave Creek where the fire advanced nearly 50 km from its ignition point, crossing different ecosystems and fuel types with different smoke emission characteristics.

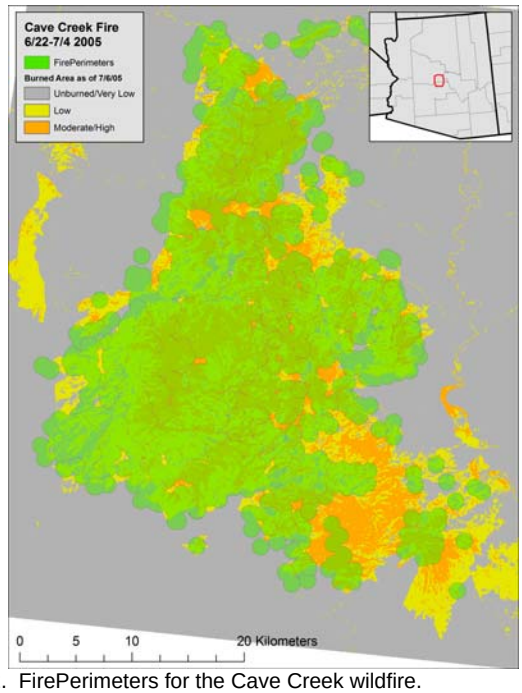

Fig 2. FirePerimeters for the Cave Creek wildfire.

The temporal profile of area burned is also important for making accurate daily smoke predictions. The School fire burned over 50,000 acres in southeastern Washington in early August 2005. Figure 3a shows the daily burned areas from ICS-209 reports, SMARTFIRE output, and the acreage modeled in the current version of BlueSky. ICS-209 reports include the total burned area of the fire up to the current day. Usually, this value increases over time as the fire spreads; however, the value sometimes decreases because the estimates of area burned are refined in subsequent days. BlueSky currently uses one-third of the area reported in the ICS-209 as its daily burn acreage. This results in both an underestimation of daily acreage during the most intense early parts of the fire, and an overestimation at the end of the burning period when the fire is dying out. The SMARTFIRE algorithm takes advantage of the daily time resolution of the satellite input data to produce a more realistic area burned temporal profile. Note that the School fire represents a best-case scenario, when ICS-209 reports are available for every day during the fire.

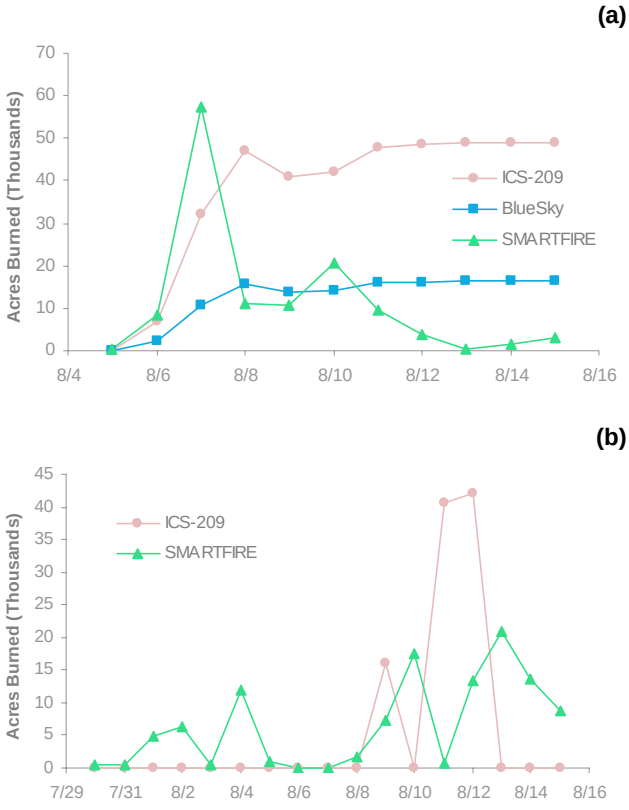

Fig 3. Time series of daily area burned for (a) the School fire and (b) the Grayling Creek fire.

Figure 3b shows the daily burned areas for the Grayling Creek fire in western Alaska, which burned in August 2005. For most of the days in the time period, there were no ICS-209 reports. The first reports on 8/9 and 8/11 represent an estimate of area burned to date, and are thus overestimates of single day burning. The current BlueSky model

would predict no smoke from this fire until 8/9, though the satellites detect substantial burning several days prior.

4. SUMMARY

The SMARTFIRE algorithm provides a method for reconciling human-reported fires with satellite-detected fires for input to the BlueSky smoke modeling framework. This merging provides a more comprehensive and spatially accurate data set than either alone, while minimizing double detection. In addition, the temporal profile of area burned is more realistic. However, the algorithm has limitations. Neither data set used in SMARTFIRE reports small fires (less than 300 acres) reliably. While the largest fires account for the majority of emissions (Soja et al., 2006), small fires are important to local $PM_{2.5}$ concentrations. Due to locational errors in the ICS-209 reports, satellite pixels may not be associated with ICS-209 reports of the same incident, even with the 2000-m buffer used to associate data into FireEvents. In these cases, SMARTFIRE will report separate incidents. This is a particular problem for large WFU complexes, which may burn in several discrete areas.

SMARTFIRE currently does not make predictions about next-day burns as required by BlueSky. The algorithm keeps all inputs used to create FireEvents, along with their associated metadata, in a relational database. This database is effectively a database of fire progression. The database will be mined in an effort to develop empirical relationships for predicting next-day burn areas based on previous days' information.

SMARTFIRE results have been verified for a limited number of cases, but have not been fully validated for all regions, ecosystems, and seasons. The parameters in the algorithm have not been optimized. The SMARTFIRE system was designed to expand as other data sets become available and desirable. Prescribed-burn reporting systems are the next data class targeted to be incorporated into the system.

5. ACKNOWLEDGMENTS

Financial support for this research was provided through a cooperative research agreement by the National Aeronautics and Space Administration (NASA) under the direction of Dr. Lawrence Friedl. In addition, the AirFire Team of the Pacific Northwest Research Station (Seattle, Washington), Forest Service of the US Department of Agriculture, provided significant in-kind contributions under the leadership of Sim Larkin and Brian Potter.

6. REFERENCES

Dozier J., 1981: A method for satellite identification of surface temperature fields of subpixel resolution. *Remote Sensing of Environment* **11** (3), 221-229.

Giglio L., 2005: MODIS collection 4 active fire product user's guide: version 2.2. Science Systems and Applications, Inc., Lanham, MD, 42 pp.

Larkin N.K., S.M. O'Neill, R. Solomon, C. Krull, S. Raffuse, M. Rorig, J. Peterson, and S.A. Ferguson, 2007: The BlueSky smoke modeling framework. (Submitted).

Soja A., J. Al-Saadi, J. Szykman, J. Kordzi, D.J. Williams T., Pace, J. Kordzi, W.R. Barnard, and B. Pierce, 2005: Using satellite-based products to enhance existing area burned data. *14th International Emission Inventory Conference, Las Vegas, NV, April 11-14*. [Available online at http://www.epa.gov/ttn/chief/conference/ei14/session12/soja_pres.pdf.]

——, Al-Saadi J., L. Giglio, D. Randall, D.J. Williams, C Kittaka., J Kordzi., T. Moore, J. Szykman, T. Pace, and B. Pierce, 2006: Comparison of satellite- to ground-based data: how well does remotely sensed data define fire? *15th Annual Emissions Inventory Conference, New Orleans, LA*. [Available online at http://www.epa.gov/ttn/chief/conference/ei15/session10/soja_pres.pdf.]

Presented at the 6th Annual CMAS Conference, Chapel Hill, NC, October 1-3, 2007

A SIMPLIFIED CMAQ EMISSION MODELING FRAMEWORK FOR CHINA'S EMISSION INVENTORY

Kebin He[1]*, Xin Yu[2], Qiang Zhang[3], David G. Streets[3], Dan Chen[1]

[1]Department of Environmental Science and Engineering, Tsinghua University, Beijing, China
[2]Green Resource Technology Company, Beijing, China
[3]Decision and Information Science Division, Argonne National Lab, Argonne, IL, USA

1. INTRODUCTION

SMOKE model has been used extensively for emission modeling process for CMAQ model in U.S. Based on National Emission Inventory (NEI) which has high spatial resolution in county-level and fixed source category code (SCC) in IDA format, SMOKE efficiently produces hourly, gridded emission data [*MCNC,* 2004]. However, for certain developing countries where the national emission inventories are not well developed, it is difficult to feed the raw inventory data into SMOKE model due to the structure difference between their national inventories and U.S. NEI inventory. Comparing to NEI, China's national emission inventory has relatively lower spatial resolution in province-level, complicated source category especially for industry and domestic sectors, thus with specific source profiles for certain sources [*Zhang et al.,* 2006]. To produce the required high resolution emission data in spatial and chemical species, we are developing a new emission modeling framework in support of applications of CMAQ model in China.

2. FRAMEWORK

The new emission modeling framework contains four main components: inventory formatting, chemistry speciation, emission gridding, and model-ready emission preparation. The framework follows the structure of current national emission inventories in China. Using China's source code table, national emission inventories are formatted into standard regional emission files. Emissions are distributed using various spatial proxies, e.g., large point sources, population, GDP, road network, land use, etc. Gridded emissions are translated to standard CMAQ model-ready files using Python and netCDF.

2.1 Inventory Formatting

Five digital source codes are used to build the China's source code table. The first three digits are for the first-level sectors. POW, IND, DOM, TRA and OTR are present for power plants, industry, domestic, transportation and other sectors respectively. The last two digits are for specific sub sectors. Annual provincial national emission inventories are formatted into standard regional emission files in CSV format. Take the VOC emission formatting file as an example, the annual VOC emissions *EVOC(i,k)* by source *i* in region *k* are given in table 1.

2.2 Chemistry Speciation

For different chemical mechanism used in CMAQ, such as CB-IV, CB-V, SAPRC99 or RADM2, the total VOC emissions are calculated into corresponding chemical species. For a certain source, the process consists of determining the portion of the volatile organic compounds in profile and transferring the regular compounds into chemical species.

Speciate 4.0 dataset [*U.S. EPA,* 2006] is the repository of VOC speciation profiles of variety sources, however limited source profiles are suitable for developing countries. We carried out comprehensive literature investigation and 25 latest measured source profiles are reviewed and integrated into the Speciate 4.0 dataset. Especially for Chinese specific sources, such as domestic stove and biofuel burning, China measured profile is used [*S. Tsai et al.*, 2003]. For a given source, appropriate profile category in new Speciate 4.0 dataset is defined and the profile number is given to each source in table 1.

**Corresponding author:* Kebin He, Department of Environmental Science and Engineering, Tsinghua University, Beijing, China,100084; E-mail: hekb@tsinghua.edu.cn

Table 1 Formatted VOC Emission inventory

	Profile	1178	90001	…
Region	Source	POWER	DOMST	…
10134	Anhui	23.5	12.6	…
10111	Beijing	6.7	8.0	…
…	…	…	…	…

For a certain chemical mechanism, the emission of chemical species *m* by source *i* in region *j*, *EVOC(i,j,m)* is then calculated by following equation:

$$EVOC(i,k,m) = \sum_{j=1}^{n}[\frac{EVOC(i,k) \times X(i,j)}{mol(j)} \times C(j,m)]$$

The weight percentage *X(i,j)* for a given volatile organic compounds *j* in source *i* and the molecular weight *mol(j)* are given in the MDB Access file in Speciate 4.0 dataset. The mapping factor from compounds *j* to chemical specie *m*, *C(j,m)* is given in the XLS file format [*Carter et al.,* 2007].

Interfaces between MDB Access file and CSV file is developed by Python. From the formatted emission inventory in table 1 as input file, emissions either by sector, region, compounds or chemical species are easily calculated as output files in CSV format.

2.3 Emission Gridding

We distribute the emission to high resolutions using various spatial proxies, according to certain principles listed in Table 2. The spatial analysis function in ArcGIS is substituted in Python by direct operation to the CSV emission files and the spatial proxies files. According to the resolution of current spatial proxies resources, 2 min gridded emission file in ASC format are generated. The original emissions are then combined and projected for user-defined modeling domain and scales. The results can be also expressed using geographical information system (GIS).

Table 2 Spatial distribution principles

Type of sources	Principles
Large point sources	Detail location
Vehicles	Road nets
Household cooking and heating	Population distribution
Industrial area sources	GDP
Fugitive dust	Land use

2.4 Model-Ready emission preparation

The gridded emission ASC files are translated to standard CMAQ model-ready files using Python and netCDF. It is also very easy to create emission files for scenario simulation by editing the imported variables in the Python files in this step.

3. ONGOING WORK

The emission modeling framework is an important part of the Regional Emission Inventory Data Platform. We will further develop the dynamical analysis and process module to import and update the emissions for various sources, build emission inventory coupling module to better overlap regional and urban emission inventory and make close coupling to the air quality modeling systems and visualization tools.

4. AKNOWLEDGEMENT

This research is funded by the National High Technology Research and Development Program of China (2006AA06A305).

5. REFERENCE

Carter, 2007, SAROAD assignments, http://www.cert.ucr.edu/~carter/emitdb/emitdb.xls

MCNC. User Mannual for Sparse Matrix Operator Kernel Emissions Modeling System (SMOKE) v.2.1. 2004

Stella Manchun Tsai, Junfeng Zhang, Kirk R. Smith, Yuqing Ma, R. A. Rasmussen, and M.A.K. Khalil Characterization of Non-methane Hydrocarbons Emitted from Various Cookstoves Used in China. Environ. Sci. Technol. 2003, 37, 2869-2877

U.S. EPA, 2006, Speciate Version 4.0, http://www.epa.gov/ttn/chief/software/speciate/index.html

Zhang, Q., Z. Klimont, D.G. Streets, H. Huo, and K. He (2006), An anthropogenic PM emission model for China and emission inventory for the year 2001, Progress in Natural Science, 16, 223-231 (in Chinese).

Presented at the 6th Annual CMAS Conference, Chapel Hill, NC, October 1-3, 2007

A SIMPLIFIED CMAQ EMISSION MODELING FRAMEWORK FOR CHINA'S EMISSION INVENTORY

Kebin He[1]*, Xin Yu[2], Qiang Zhang[3], David G. Streets[3], Dan Chen[1]

[1]Department of Environmental Science and Engineering, Tsinghua University, Beijing, China
[2]Green Resource Technology Company, Beijing, China
[3]Decision and Information Science Division, Argonne National Lab, Argonne, IL, USA

1. INTRODUCTION

SMOKE model has been used extensively for emission modeling process for CMAQ model in U.S. Based on National Emission Inventory (NEI) which has high spatial resolution in county-level and fixed source category code (SCC) in IDA format, SMOKE efficiently produces hourly, gridded emission data [*MCNC,* 2004]. However, for certain developing countries where the national emission inventories are not well developed, it is difficult to feed the raw inventory data into SMOKE model due to the structure difference between their national inventories and U.S. NEI inventory. Comparing to NEI, China's national emission inventory has relatively lower spatial resolution in province-level, complicated source category especially for industry and domestic sectors, thus with specific source profiles for certain sources [*Zhang et al.,* 2006]. To produce the required high resolution emission data in spatial and chemical species, we are developing a new emission modeling framework in support of applications of CMAQ model in China.

2. FRAMEWORK

The new emission modeling framework contains four main components: inventory formatting, chemistry speciation, emission gridding, and model-ready emission preparation. The framework follows the structure of current national emission inventories in China. Using China's source code table, national emission inventories are formatted into standard regional emission files. Emissions are distributed using various spatial proxies, e.g., large point sources, population, GDP, road network, land use, etc. Gridded emissions are translated to standard CMAQ model-ready files using Python and netCDF.

2.1 Inventory Formatting

Five digital source codes are used to build the China's source code table. The first three digits are for the first-level sectors. POW, IND, DOM, TRA and OTR are present for power plants, industry, domestic, transportation and other sectors respectively. The last two digits are for specific sub sectors. Annual provincial national emission inventories are formatted into standard regional emission files in CSV format. Take the VOC emission formatting file as an example, the annual VOC emissions *EVOC(i,k)* by source *i* in region *k* are given in table 1.

2.2 Chemistry Speciation

For different chemical mechanism used in CMAQ, such as CB-IV, CB-V, SAPRC99 or RADM2, the total VOC emissions are calculated into corresponding chemical species. For a certain source, the process consists of determining the portion of the volatile organic compounds in profile and transferring the regular compounds into chemical species.

Speciate 4.0 dataset [*U.S. EPA,* 2006] is the repository of VOC speciation profiles of variety sources, however limited source profiles are suitable for developing countries. We carried out comprehensive literature investigation and 25 latest measured source profiles are reviewed and integrated into the Speciate 4.0 dataset. Especially for Chinese specific sources, such as domestic stove and biofuel burning, China measured profile is used [*S. Tsai et al.*, 2003]. For a given source, appropriate profile category in new Speciate 4.0 dataset is defined and the profile number is given to each source in table 1.

**Corresponding author:* Kebin He, Department of Environmental Science and Engineering, Tsinghua University, Beijing, China,100084; E-mail: hekb@tsinghua.edu.cn

Table 1 Formatted VOC Emission inventory

	Profile	1178	90001	…
Region	Source	POWER	DOMST	…
10134	Anhui	23.5	12.6	…
10111	Beijing	6.7	8.0	…
…	…	…	…	…

For a certain chemical mechanism, the emission of chemical species *m* by source *i* in region *j*, *EVOC(i,j,m)* is then calculated by following equation:

$$EVOC(i,k,m) = \sum_{j=1}^{n}[\frac{EVOC(i,k) \times X(i,j)}{mol(j)} \times C(j,m)]$$

The weight percentage *X(i,j)* for a given volatile organic compounds *j* in source *i* and the molecular weight *mol(j)* are given in the MDB Access file in Speciate 4.0 dataset. The mapping factor from compounds *j* to chemical specie *m*, *C(j,m)* is given in the XLS file format [*Carter et al.,* 2007].

Interfaces between MDB Access file and CSV file is developed by Python. From the formatted emission inventory in table 1 as input file, emissions either by sector, region, compounds or chemical species are easily calculated as output files in CSV format.

2.3 Emission Gridding

We distribute the emission to high resolutions using various spatial proxies, according to certain principles listed in Table 2. The spatial analysis function in ArcGIS is substituted in Python by direct operation to the CSV emission files and the spatial proxies files. According to the resolution of current spatial proxies resources, 2 min gridded emission file in ASC format are generated. The original emissions are then combined and projected for user-defined modeling domain and scales. The results can be also expressed using geographical information system (GIS).

Table 2 Spatial distribution principles

Type of sources	Principles
Large point sources	Detail location
Vehicles	Road nets
Household cooking and heating	Population distribution
Industrial area sources	GDP
Fugitive dust	Land use

2.4 Model-Ready emission preparation

The gridded emission ASC files are translated to standard CMAQ model-ready files using Python and netCDF. It is also very easy to create emission files for scenario simulation by editing the imported variables in the Python files in this step.

3. ONGOING WORK

The emission modeling framework is an important part of the Regional Emission Inventory Data Platform. We will further develop the dynamical analysis and process module to import and update the emissions for various sources, build emission inventory coupling module to better overlap regional and urban emission inventory and make close coupling to the air quality modeling systems and visualization tools.

4. AKNOWLEDGEMENT

This research is funded by the National High Technology Research and Development Program of China (2006AA06A305).

5. REFERENCE

Carter, 2007, SAROAD assignments, http://www.cert.ucr.edu/~carter/emitdb/emitdb.xls

MCNC. User Mannual for Sparse Matrix Operator Kernel Emissions Modeling System (SMOKE) v.2.1. 2004

Stella Manchun Tsai, Junfeng Zhang, Kirk R. Smith, Yuqing Ma, R. A. Rasmussen, and M.A.K. Khalil Characterization of Non-methane Hydrocarbons Emitted from Various Cookstoves Used in China. Environ. Sci. Technol. 2003, 37, 2869-2877

U.S. EPA, 2006, Speciate Version 4.0, http://www.epa.gov/ttn/chief/software/speciate/index.html

Zhang, Q., Z. Klimont, D.G. Streets, H. Huo, and K. He (2006), An anthropogenic PM emission model for China and emission inventory for the year 2001, Progress in Natural Science, 16, 223-231 (in Chinese).

A NEW ATHROPOGENIC EMISSION INVENTORY SYSTEM FOR ASIA IN SUPPORT OF ATMOSPHERIC MODELING

Qiang Zhang [1,*], David G. Streets[1], Kebin He[2], Shekar Reddy[3], Akiyoshi Kannari[4], Il-Soo Park[5], Joshua S. Fu[6], and Zbigniew Klimont[7]

[1]Decision and Information Science Division, Argonne National Lab, Argonne, IL, USA
[2]Department of Environmental Science and Engineering, Tsinghua University, Beijing, China
[3]UK Met Office Hadley Centre, Exeter, UK
[4]Independent Researcher, Tokyo, Japan
[5]Meteorological Research Institute, Seoul, Republic of Korea
[6]University of Tennessee, Knoxville, TN, USA
[7]International Institute for Applied Systems Analysis, Laxenburg, Austria

1. INTRODUCTION

A regional inventory for Asia for the year 2000 was developed by *Streets et al*. [2003] and widely examined during and following the TRACE-P experiment. However, because of the dramatic economic growth in East Asia since 2000, that inventory no longer represents the level of present-day emissions in East Asia, especially for China. China's gross domestic product (GDP) increased ~10% annually and coal consumption increased ~15% annually during the past 5 years. Atmospheric emissions are also thought to have increased markedly from space-based observations [*Richter et al*., 2005]. In addition, some shortcomings in previous inventories were found, as a result of reanalysis of the inventories themselves and validation tests against forward and inverse modeling results and satellite retrievals. A true representation of trans-Pacific transport and the import of pollution into North America requires a revision of these emission estimates. A technology based, bottom-up methodology is developed to build a new anthropogenic emission inventory for Asia for the year 2006 in support of NASA's INTEX-B experiment.

2. METHODOLOGY

We are adopting a new strategy for this work, as follows: (a) use the TRACE-P inventory both as the foundation of the new dataset and as a default for work still in progress; (b) update China's emissions to the most recent year for which activity data are available, using an improved methodology documented in *Streets et al*. [2006] and *Zhang et al*. [2007a]; (c) incorporate the best available datasets for selected regions where national inventories exist and are thought to be more reliable than the TRACE-P inventory; (d) for other regions in Asia, extrapolate the TRACE-P estimates to the most recent year based on updated activity statistics; (e) extrapolate the emission estimates to the year 2006 based on growth factors; and (f) check for consistency among the different datasets, choose an appropriate level of precision for the final product, fill gaps with the TRACE-P inventory, and finally export the dataset for the whole of Asia in a uniform data format. So far, under item (c), we have built in the following datasets: the India inventory from Dr. Reddy, the Japan inventory from Dr. Kannari, the Republic of Korea inventory from Dr. Park, a Taiwan inventory from the Taiwan EPB, and a Far East Russia inventory from IIASA.

China is still the focus of our new Asia inventory. The general approach used to build China's new regional emission inventory is described in *Streets et al*. [2006] and *Zhang et al*. [2006, 2007a]. We have implemented a new technology-based methodology in order to be able to reflect the types of technology presently operating in China. We have also implemented an anthropogenic PM emission model to calculate primary PM emissions, including PM_{10} and $PM_{2.5}$, which the TRACE-P inventory did not address [*Zhang et al*., 2006, 2007b]. We are also in the process of adding mercury to the list of species covered [*Streets et al*., 2005]. Activity data are obtained from statistics published by a variety of government agencies. Fuel consumption by sector and by province is

**Corresponding author:* Qiang Zhang, Argonne National Laboratory; Tel: 630-252-9853; Fax: 630-252-5217; e-mail: zhangq@anl.gov.

derived from the China Energy Statistical Yearbook. Technology distributions within each sector are obtained from a variety of Chinese technology reports, as well as an energy demand approach. Emission factors are mainly based on measurements in China or estimations based on the actual technology level and practice. In some cases, where local information is lacking, we use adjusted emission factors for similar activities from international databases.

3. RESULTS

We are currently releasing the first version of the modeling system through INTEX-B website. The components of this version are shown in Table 1. We finally extrapolate the inventory to the year 2006 and consolidate the different datasets to a uniform spatial resolution of 30 min × 30 min. As a sample, Figure 1 shows the updated gridded NO_x and $PM_{2.5}$ emissions over Asia for the year 2006.

We estimate total Asian anthropogenic emissions in the year 2006 as follows: 47.1 Tg SO_2, 36.7 Tg NO_x, 298.2 Tg CO, 54.6 Tg NMVOC, 29.2 Tg PM_{10}, 22.2 Tg $PM_{2.5}$, 2.97 Tg BC, and 6.57 Tg OC. Compared with TRACE-P inventory for the year 2000, the SO2, NOx. CO, NMVOC and BC emissions in Asia were increased by 43.4%, 61.8%, 41.1%, 35.7%, and 46.9% separately, while OC emissions were decreased by 6.6%. The emission changes between the two inventories reflect a combination of: (a) actual growth in emissions due to increasing economic development, (b) the effects of replacing the TRACE-P inventory by local inventories in several countries, and (c) improvements and corrections made to the original TRACE-P inventory. The changes should not be viewed solely as real emissions growth. The 2006 inventory values are considered to be a reasonable reflection of the absolute magnitude of emissions in that year, pending re-calculation with actual activity statistics when they become available.

China shows significant emission increases in the past several years. Based on the methodology described above, we have generated three years of estimates for China, 2001, 2003 and 2004, and projected the 2004 emissions to the year 2006. We calculate that anthropogenic emissions in China in 2004 were 28.3 Tg SO_2, 18.6 Tg NO_x, 158 Tg CO, 21.5 Tg VOC, 18.2 Tg PM_{10}, 13.3 Tg $PM_{2.5}$, 1.7 Tg BC, 3.2 Tg OC, and 696 Mg Hg. we also finished a new analysis of China's NOx emissions, including an emission trend analysis for 1995-2004 and a comparison with GOME and SCIAMACHY satellite retrieval trends [*Zhang et al.*, 2007a]. We found both the emission inventory data and the satellite observations indicate a continuous and accelerating growth rate between 1996 and 2004 over East Central China. However, the growth rate from the emission inventory is lower than that from the satellite observations.

:

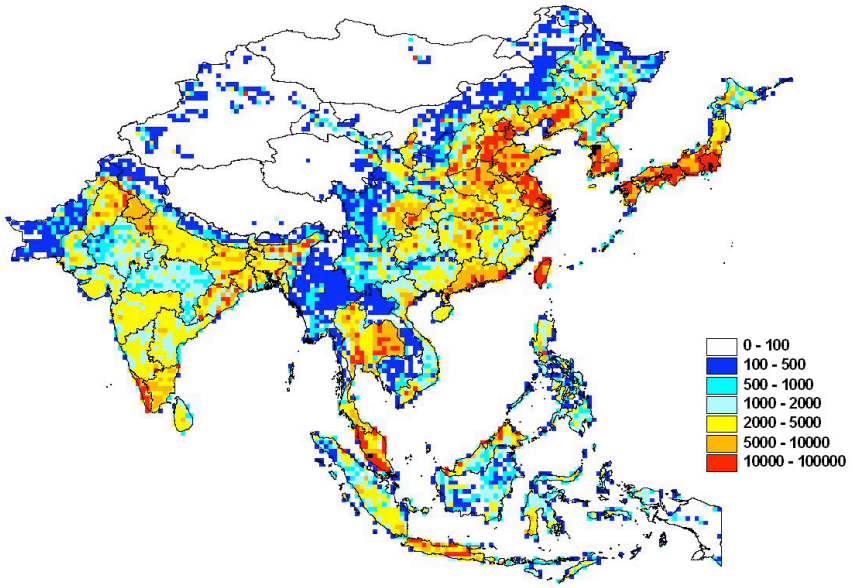

NOx

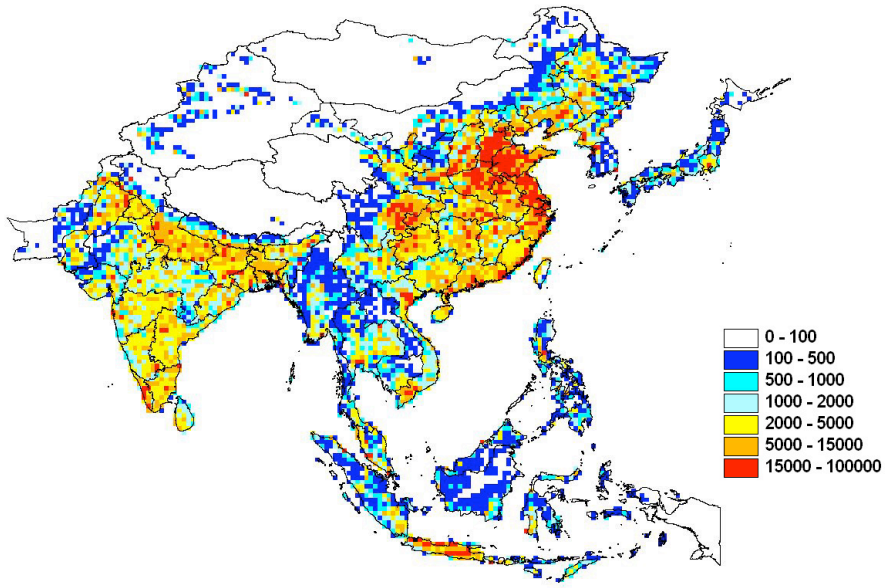

PM2.5

Fig. 1. Gridded emissions of NOx and PM2.5 at 0.5 degree resolution. Upper: NOx, lower: PM2.5. Unit: tons/yr per grid cell.

Table 1. Components of new Asian emission inventory

Region		China	Japan	South Korea	Taiwan	Far East Russia	Other Regions
Reference Year		2004	2000	2003	2003	2000	2004
Species	**SO_2**	1	2	2	2	2	3
	NO_x	1	2	2	2	2	3
	CO	1	2	2	2	2	3
	VOC	1	2	2	2	N/A	3
	PM_{10}	1	2	2	2	2	5
	$PM_{2.5}$	1	2	5	2	2	5
	BC	1	4	4	4	N/A	3
	OC	1	4	4	4	N/A	3
	NH_3	4	2	2	4	N/A	4
	Hg	1	N/A	N/A	N/A	N/A	N/A

1 = estimates made with the new methodology
2 = estimates incorporated from other datasets
3 = estimates extrapolated to the reference year from the TRACE-P inventory
4 = estimates use TRACE-P inventory values as a default for now
5 = rough estimates
N/A = estimates not presently available, but will be added later

4. REFERENCES

Streets, D.G., T.C. Bond, G.R. Carmichael, S.D. Fernandes, Q. Fu, D. He, Z. Klimont, S.M. Nelson, N.Y. Tsai, M.Q. Wang, J.-H. Woo, and K.F. Yarber (2003), An inventory of gaseous and primary aerosol emissions in Asia in the year 2000, *J. Geophys. Res*., *108*(D21), 8809, doi:10.1029/2002JD003093.

Streets, D.G., J. Hao, Y. Wu, J. Jiang, M. Chan, H. Tian, and X. Feng (2005), Anthropogenic mercury emissions in China, *Atmos. Environ*., *39*, 7789-7806.

Streets, D.G., Q. Zhang, L Wang, K. He, J. Hao, Y Wu, Y. Tang, and G.R. Carmichael (2006), Revisiting China's CO emissions after TRACE-P: Synthesis of inventories, atmospheric modeling, and observations, *J. Geophys. Res*., *111*, D14306, doi: 10.1029/2006JD007118.

Zhang, Q., Z. Klimont, D.G. Streets, H. Huo, and K. He (2006), An anthropogenic PM emission model for China and emission inventory for the year 2001, *Progress in Natural Science*, *16*, 223-231 (in Chinese).

Zhang, Q., D.G. Streets, K. He, Y.X. Wang, A. Richter, J.P. Burrows, I. Uno, C.J. Jang, D. Chen, Z. Yao, and Y. Lei (2007a), NO_x emission trends for China, 1995-2004: The view from the ground and the view from space, *J. Geophys. Res*., in press

Zhang, Q., D.G. Streets, K. He, and Z. Klimont (2007b), Major component of China's anthropogenic primary particulate emissions, *Environ. Res. Lett.*, submitted

APPLICATION OF THE CMAQ PARTICLE AND PRECURSOR TAGGING METHODOLOGY (PPTM) TO SUPPORT WATER QUALITY PLANNING FOR THE VIRGINIA MERCURY STUDY

Sharon Douglas*, Tom Myers, Yihua Wei and Jay Haney
ICF International, San Rafael, CA, USA

Michael Kiss and Patricia Buonviri
Virginia Department of Environmental Quality, Richmond, VA, USA

1. INTRODUCTION

CMAQ is being applied in this study to assess the contribution of mercury sources within Virginia and surrounding states to impaired waterways. A key component of this study is the use of the CMAQ Particle and Precursor Tagging Methodology (PPTM) which allows one to track the emission, dispersion, chemical reaction, and deposition of mercury from particular sources, source categories, or source regions throughout the simulation. The PPTM technique is being used to quantify the contributions of individual sources and source categories for a base year of 2001 and several future years. The modeling will be used to evaluate the effectiveness of emissions reductions expected as part of the Clean Air Mercury Rule (CAMR) and whether additional control measures will be needed in Virginia to meet applicable water quality criteria. Another important objective of the modeling analysis is to provide information that will enable VDEQ to conduct Total Maximum Daily Load (TMDL) studies for mercury of various Virginia waterways.

2. BACKGROUND

In the U.S., more than 8,500 individual bodies of water have been identified as mercury impaired and the primary source of mercury to these water bodies is believed to be atmospheric deposition. Mercury deposition affects the viability of aquatic ecosystems in a number of different ways. The sustainability of marine life, recreational and commercial fishing, and human health can be directly or indirectly affected by mercury deposition and the build up of mercury in lakes, streams, rivers, and wetland areas. In certain bodies of water such as those with low dissolved oxygen, high organic matter content, and low acidity, mercury deposition can lead to the formation and build up of the highly bio-accumulative form of mercury (methyl mercury).

Human exposure to mercury is most commonly associated with the consumption of contaminated fish. Due to measured high levels of mercury in fish, at least 44 U.S. states have, in recent years, issued fish consumption advisories. These advisories cover more than 2000 individual bodies of water and may suggest limits on the consumption of certain types of fish or recommend limiting or not eating fish from certain bodies of water because of unsafe levels of mercury contamination.

Within Virginia, fish consumption advisories have been issued for several bodies of water for which atmospheric deposition is thought to be the primary source of mercury. These are primarily located along the coastal plain, and have characteristics that are consistent with mercury methylation and bioaccumulation of mercury in fish.

Global, regional, and local sources of air mercury emissions contribute to the deposition, and understanding these contributions is an important step toward identifying measures that will effectively reduce mercury deposition and environmental mercury levels.

3. CONCEPTUAL MODEL

Analysis of observed mercury deposition, meteorological and emissions data as well as recent modeling results provides insight into the nature of mercury deposition in Virginia. The resulting conceptual model is being used to guide certain aspects of the modeling analysis including the modeling domain, sensitivity simulations, model evaluation, and PPTM sources as discussed in this section.

**Corresponding author:* Sharon G. Douglas, ICF International, 101 Lucas Valley Road, Suite 260, San Rafael, CA 94903; e-mail: sdouglas@icfi.com.

There are three Mercury Deposition Network (MDN) monitoring sites in Virginia: Culpeper (located in central Virginia), Shenandoah National Park (in northwestern Virginia), and Harcum (near the Chesapeake Bay in coastal Virginia). Wet mercury deposition is monitored at these sites and has an annual cycle, with higher deposition amounts during the second and third calendar quarters.

A number of different meteorological factors influence wet mercury deposition at these sites. Key factors include precipitation, temperature, wind speed, and the potential for recirculation. There are different types of meteorological conditions and combinations of parameters that lead to high deposition.

Precipitation is an important mechanism for wet mercury deposition. Mercury wet deposition is correlated with rainfall, but rainfall amount does not fully explain the observed variations in deposition. This suggests that any examination of the sensitivity of CMAQ to the meteorological inputs should include but should not be limited to precipitation.

The period of record for the MDN sites in Virginia is limited to recent years, 2002 and later. However, for each of the Virginia MDN sites, it is possible to identify a longer term monitoring site (from a neighboring state) that has similar deposition characteristics to supplement the model performance evaluation for 2001.

Annual deposition amounts that have been adjusted to account for variations in meteorology are consistent with changes in the emissions for Virginia. Thus some sensitivity to changes in local emissions is expected in the modeling. For the Culpeper and Shenandoah sites, the adjusted deposition values indicate a slight downward trend.

Monitoring data and prior modeling results suggest that for all three Virginia sites, dry deposition is a significant contributing factor to total mercury deposition. This finding may also aid the evaluation of the modeling results.

4. OVERVIEW OF CMAQ PPTM

Version 4.6 of the CMAQ model is being used for this study. CMAQ supports the detailed simulation of the emission, chemical transformation, transport, and wet and dry deposition of elemental, divalent, and particulate forms of mercury.

The CMAQ model includes three mercury (Hg) species; elemental mercury (Hg^0), reactive gaseous mercury (RGM), and particulate mercury (PHg). RGM and PHg are primarily comprised of divalent mercury.

Mercury simulation capabilities were first incorporated into the CMAQ model by adding gaseous and aqueous chemical reactions involving mercury to the CMAQ chemical mechanism (Bullock and Brehme, 2002). Since that time, the chemical mechanism has been further updated to include additional reactions and updated information on reaction rates. The most recent changes to CMAQ for mercury include an improved dry deposition algorithm and the incorporation of natural mercury emissions.

In addition to the state-of-the science chemical mechanism for mercury, other key features of the CMAQ model in simulating mercury deposition include state-of-the-science advection, dispersion and deposition algorithms, the latest version of the Carbon Bond chemical mechanism (CB05), and the CMAQ Particle and Precursor Tagging Methodology (PPTM).

PPTM for mercury (Douglas et al., 2006) provides detailed, quantitative information about the contribution of selected sources, source categories, and/or source regions to simulated mercury concentrations and (wet and dry) deposition. Mercury emissions from selected sources, source categories, or source regions are (numerically) tagged and then tracked throughout a simulation, and the contribution from each tag to the resulting simulated concentration or deposition for any given location can be quantified. By tracking the emissions from selected sources or source locations, the methodology also provides information on the fate of the emissions from these sources.

PPTM for mercury tracks emitted mass from its source through the modeling system processes. The emissions from each selected source, source category, or grouping are tagged in the simulation and each grouping is referred to as a “tag.” Typically, each tag includes all of the species necessary to keep track of the mercury emissions from a particular source or source grouping, but, the different species that comprise mercury emissions (e.g., elemental, divalent, and particulate) can also be tagged separately. The tagged species are differentiated from the regular species used in the CMAQ model by a suffix

added to the species name. Each individual species from a given source or source grouping is tagged and the combination of all of the individual species represents the tag. As an example, in order to track the mercury emissions from waste incinerators, the species HG_t1, HGIIGAS_t1, and PHGI_t1, referring to elemental (HG), divalent (HGII), and particulate (PHG) emissions from incinerators, will be created. The "t" refers to tagging and the number one is the tag number. Collectively, these species (and the other species used in CMAQ to represent other forms of mercury, such as APHGI_t1 and APHGJ_t1) are referred to as the waste incinerator tag.

PPTM was developed to utilize model algorithms as much as possible to track simulated tag species concentrations. Processes that are linear, or independent of species, utilize the model algorithms to calculate the changes in species concentrations. An example of this type of process is advection. Other processes that are potentially non-linear or involve interactions with other species, are given a special treatment and are calculated for the overall (or base) species and apportioned to the tagged species. An example of this type of process is aqueous phase chemistry.

In the following section, we describe the methodology used to allocate changes to tags for each of the major processes in the CMAQ model.

4.1 Advection, Diffusion and Dry Deposition

Advection, diffusion and dry deposition of the tag species is accomplished using the standard algorithms in CMAQ. Deposition velocities for the tagged species are based on those for the corresponding standard species.

4.2 Gas Phase Chemistry

The current gas phase chemical mechanism in CMAQ causes a gradual conversion of elemental mercury (HG) to divalent forms in gas phase (HGIIGAS) and aerosol form (HGIIAER). There is no reaction to form elemental mercury from the other forms, and there are no reactions that form one type of divalent from the other. We have used this information to develop a simple method to allocate the divalent mercury formed during the gas phase chemistry step to the tags.

At the beginning of the gas phase chemistry step, the initial amount of HG, HGIIGAS, and HGIIAER are saved (HG_{init}, $HGIIGAS_{init}$, and $HGIIAER_{init}$). The initial amounts of each tag species are also saved. The gas phase chemistry module is called with the standard set of gas phase species (i.e., without tag species). Once the gas phase chemistry has completed a step, we calculate the following ratios:

$$HGG_{ratio} = (HGIIGAS - HGIIGAS_{init}) / HG_{init} \quad (1)$$

and

$$HGA_{ratio} = (HGIIAER - HGIIAER_{init}) / HG_{init} \quad (2)$$

where HGIIGAS and HGIIAER are the final values of the divalent forms of mercury. Effectively, these ratios give the amount divalent mercury of each form produced per unit elemental mercury.

The new concentrations for each tag species are then calculated as follows:

$$HGIIGAS_s = HGIIGAS_{init,s} + HG_{init,s}*HGG_{ratio} \quad (3)$$

$$HGIIAER_s = HGIIAER_{init,s} + HGinit,s*HGA_{ratio} \quad (4)$$

$$HG_s = HG_{init,s}*HG/HG_{init} \quad (5)$$

where s indicates the tag number and HG is the final concentration of elemental mercury.

4.3 Aerosol Dynamics

Two aerosol dynamics processes are simulated for mercury in CMAQ: 1) the formation of particulate mercury via gas phase reaction of elemental mercury, and 2) the transition of some fraction of the Aitken mode particulate mercury to accumulation mode particulate mercury.

The rate of formation of particulate mercury from gas phase reactions is determined, as described above, in the gas phase chemistry, for both the overall particulate mercury and for each of the particulate mercury tags.

The rate of accumulation of Aitken-mode particles into accumulation-mode particles is calculated by CMAQ for all particles. The rate is then applied to each of the constituent particulate species, including particulate mercury. In order to determine the changes in particulate mercury for each of the tags, each equation for particulate mercury has been emulated for the tag species.

4.4 Cloud Processes

Wet scavenging of pollutants and aqueous-phase chemistry are applied for both convective and resolved clouds by CMAQ. In PPTM, the tagged species concentrations are updated following the cloud scavenging and removal processes.

For the purpose of calculating the scavenging of each of the tag species, it is assumed that the fraction of each tag species removed will be the same as the fraction of the corresponding overall species removed. The scavenging is calculated as usual for the standard CMAQ species. After the scavenging, the fraction of each mercury species removed is calculated.

The aqueous chemistry is called in the usual way for standard species including mercury, and the concentrations of the standard species are updated. The aqueous chemistry routine is called again to calculate the chemical changes for each tag.

5. CMAQ/PPTM MODELING FOR THE VIRGINIA MERCURY STUDY

5.1 Application Procedures

The CMAQ model is being applied for the calendar year 2001. Selection of the simulation period considered meteorological and emissions database availability and meteorological representativeness.

The modeling domain includes a 36-km resolution outer grid and a 12-km inner grid. The outer grid encompasses the entire contiguous U.S. as well as portions of Canada and Mexico and, therefore, all or nearly all mercury emissions sources in North America. The inner grid covers the eastern two-thirds of the U.S. with a horizontal grid resolution of 12 km. Thus, the modeling domain supports 12-km horizontal grid resolution over Virginia.

The emissions inventory incorporates the latest mercury emission data for point sources in Virginia (for 2002 and 2005). Mercury emissions for all other areas and source categories were obtained from Version 3 of the 2002 National Emissions Inventory (NEI).

5.2 Preliminary Results

A baseline simulation and two preliminary PPTM simulations have been completed to date. The first PPTM run examines the contribution to mercury deposition from mercury sources in Virginia and compares this with the contribution from all sources outside of the state. The second run examines the contributions from 1) Electric Generating Unit (EGU) sources in Virginia 2) EGU sources in the remainder of the 12-km domain, and 3) all other mercury sources in the 12-km domain. Figure 1 shown simulated wet and dry mercury deposition for baseline simulation for the month of July for the 12-km domain.

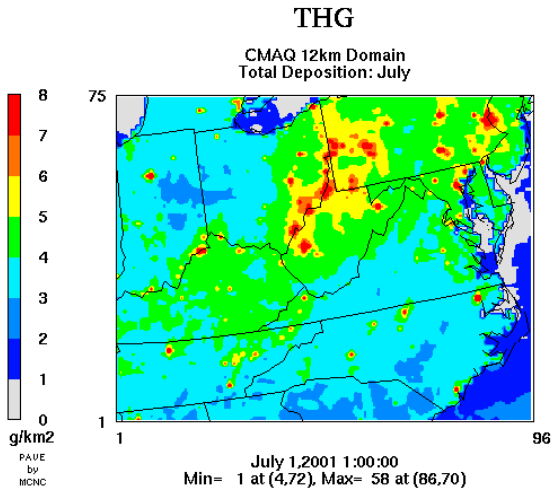

Fig. 1. Simulated wet and dry total mercury deposition for July 2001. .

Additional CMAQ and PPTM results will be displayed and discussed at the conference, with emphasis on the use of the CMAQ PPTM tool for the assessment of mercury deposition and to support environmental decision making.

6. REFERENCES

Bullock, O.R. and Brehme, K.A. 2002. Atmospheric mercury simulation using the CMAQ model: formulation description and analysis of wet deposition results. *Atmos. Environ.* 36, 2135–2146.

Douglas, S., T. Myers, and Y. Wei. 2006. "Implementation of Mercury Tagging in the Community Multi-scale Air Quality Model." Prepared for the U.S. EPA, OAQPS, Research Triangle Park, North Carolina. Prepared by ICF International, San Rafael, California (06-051).

OBSERVED AND HIGH RESOLUTION MODELED POLLUTANT FIELDS USING FINE SCALE AND HYBRID MODELING APPROACHES FOR WILMINGTON, DELAWARE

Mohammed A Majeed*

Air Quality Management Section, DNREC, New Castle, DE

1. INTRODUCTION

Characterizing the spatial variability of air pollutants in an urban setting is critical for improved air toxics exposure assessments (Isakov et al., 2006; Touma et al., 2006), for model evaluation studies (Ching et al.,, 2006b), and for air quality regulatory applications. Photochemical air quality simulation models provide gridded concentration fields for air quality assessments and for air quality regulatory applications (Byun and Ching (1999). However, outputs of air quality models are grid size dependent. For urban applications, information is needed at fine scales for exposure assessments. For such applications, in principle, this need is met by applying nesting methods to grid models such as Community Multiscale Air Quality (CMAQ) model and other such models to the desired resolution. This approach has constraints; computational expenses increase as grid size decreases, and models are not recommended for running at grids smaller than ~1 km. Yet, it is known that significant spatial variability (hereinafter, sub-grid variability or SGV) occurs even at scales smaller than 1 km (Ching et al., 2006a & 2006b, 2005, Isakov et al., 2006, and Majeed et al., 2004,) due to various reasons including the presence of within-grid sources as well as photochemical-dynamic interactions. CMAQ provides multiscale, grid resolved concentrations. Modeling at neighborhood-scale is valuable when significant variability is present at that scale, but may still underestimate variability. Therefore, SGV should be derived from a combination of - fine-scale modeling with models such as CMAQ, modeling of local sources, and also from photochemistry in turbulent flows. SGV treated as concentration probability density functions (PDFs) are appropriate and provide essential information for improved human exposure assessments.

*Corresponding author: Mohammed A Majeed, Air Quality Management Section, Delaware Department of Natural Resources and Environmental Control, 715 Grantham Lane, New Castle, DE 19720;
Phone: (302) 323-4542
Fax: (302) 323-4598
e-mail: Mohammed.Majeed@state.de.us

2. OBJECTIVE OF STUDY

Previously, as discussed in Ching et al., 2005; et al., 2006a, b, there are various types of applications for which the introduction of SGV information would be a useful adjoint to the concentrations from air quality modeling results. They suggested relaxing grid model outputs from its current fully deterministic state to quasi stochastic fields in which the gridded fields are weighted with statistical parameters of the SGV. Simple examples could include such parameters as Coefficient of Variation (COV), a user specified percentile of the distribution, peak (or maximum) values or its comparable max-to-min range values. Several approaches are being investigated in parameterizing the SGV characteristics for applications in exposure assessments - running CMAQ at urban scales (Ching et al.,2004a), developing a hybrid approach that combines local scale dispersion modeling with CMAQ, application of Large Eddy Simulation with Chemistry models (e.g., LESChem (Herwehe, 2000) and incorporating outputs from building scale and physical modeling studies. Once such SGV information is derived, however, an approach to incorporate SGV for the CMAQ modeled concentration is needed. We present an approach here.

Let *Cg* be defined as the CMAQ gridded concentration values and *CSGV*, the *SGV* concentration distribution about its grid cell value. Now, define the two additional terms - concentration adjusted for *SGV* effects (*SAC*), and a non-dimensional weighting factor $f_1(CSGV)$ derived from modeling or monitoring. Furthermore, we introduce two additional factors – a factor f_2 which is a function dependent on surrogate exposure parameters (e.g., population residence distributions by distance for roadways, in the case

of mobile sources) and another factor f_3 which is a function dependent on photochemical dynamical contributions.

$$SAC = C_g * f_1(CSGV) * f_2 * f_3 \qquad (1)$$

Function f_1 *(CSGV)* is the focus of current investigation. f_1 *(CSGV)* can be expressed in a number of ways. In principle, it would be desirable for each cell's CSGV to reflect the properties of its *SGV* distribution function (DF). However, preliminary evidence suggests that the distribution function for *SGVs* differ throughout the modeling domain (Herwehe et al., 2004). Here we use limited statistical descriptions that can still provide a representative metric for each grid cell's DF.

We explore the following three options for the non--dimensional weighting factor:

$$f_1(CSGV) = 1 + COV \qquad (2a)$$

$$f_1(CSGV) = 1 + 95^{th}\,\text{Percentile/GridValue} \qquad (2b)$$

$$f_1(CSGV) = 1 + \text{Peak/GridValue} \qquad (2c)$$

where *COV* is the standard deviation/grid value called the Coefficient of Variation, 95th (or other) percentile of the distribution/grid value and peak of the distribution/grid value. The factor in (2a), differs from (2b) and (2c) because it is computed about its grid mean value, (2b) and (2c) refer to the distribution itself.

The SGV within a regional-scale modeling grid exists for all the pollutants that are being modeled. For the pollutants that have primary and secondary components, SGVs do exist for each of them. The local-scale dispersion modeling is one of the tools available to us for assessing the SGV of primary components that exists within regional-scale modeling grids (Isakov et al., 2006; Touma et al., 2006). For this study we examine the use of local-scale dispersion models (AERMOD in this case) for assessing the SGV within the regional-scale modeling grids that result from various local sources. We are also interested in comparing such results against observations and for this purpose, we utilize data from the Enhanced Delaware Air Toxics and Assessment Study, E-DATAS (DNREC Report, 2006). Also, given that traffic is a major emissions source in urban areas, and because such emissions within a city have a high degree of complexity in their spatial distributions and source strengths, we expect them to contribute to a significant fraction of each model grid's SGV. For this study, we choose to examine the SGV of modeled formaldehyde (HCHO).

3. APPROACH

Our study involves using a hybrid modeling approach (Isakov et al., 2006; Touma et al., 2006) for determining the fine scale details of concentration fields and the E-DATAS database for corroboration. The E-DATAS was conducted in the Wilmington, Delaware (DNREC Report, 2006). During intensive fields study campaigns, a special set of continuous measurements of several air pollutant species including formaldehyde, ozone, Cr^{6+} and fine particles were made on board an instrumented van deployed in mobile transects of downtown Wilmington. Repeated sets of transects were performed, over a set, criss-cross type course that covered many of the streets; each transect taking approximately one hour to complete. Figure 1 shows the modeling domain and the sampling route of the mobile van. The sampling route provides a bases for spatial details of air pollutant characterization on scales finer than 1 km. (In this figure, the continuous data were binned at 100m intervals, and 3 hour averages computed from the morning runs. Such data provides information useful to compare with SGVs from model calculations.

Fine scale concentration measurements using a mobile sampling van

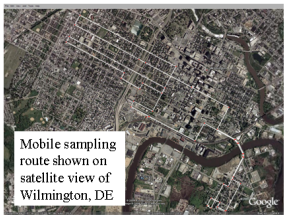

Example transect of Formaldehyde (Units?)

Domain size is 4km x 4km
Pixels are 100m averages
Three hour averages for
August 03, 2005 morning

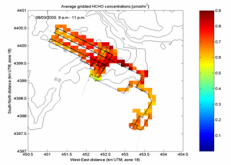

RESEARCH & DEVELOPMENT
Building a scientific foundation for sound environmental decisions

Fig. 1. Mobile sampling during E-DATAS. Study area is Wilmington, Delaware.

We performed a set of CMAQ simulations for 12km with nests at 4 km and 1 km grid sizes. The air toxics version of CMAQ that was used for this study utilized SAPRC-99 chemical mechanism for a Lambert-Conformal projection. The 1999 emissions inventory and 2001 meteorological datasets were utilized for the CMAQ runs. For the SGV, we hereinafter, only consider the primary sources; we model its contributions using a local scale model, AERMOD, to provide the fine scale distribution for CMAQ (Isakov et al., 2006). Local-scale modeling was conducted for all source categories; for the mobile sources the AERMOD was applied to link-based traffic emissions data. A comprehensive emissions inventory developed for calendar year 2003 was utilized for this purpose. However, the modeling was conducted for the calendar year 2001 so that the regional- and local-scale modeling can be related. While the CMAQ modeling is performed for Lambert Conformal and AERMOD for UTM projections, the 4 x 4 km CMAQ grid cell and the AERMOD 4 x 4 km modeling area overlap significantly. We then compute and compare distributions between model simulations and the mobile sampling data. Additionally, although the actual sampling (July-August, 2005) and the modeling period (July 2001) differed, it is assumed that the differences would be relatively small since (a) we do not expect the emissions to change significantly between 2001 and 2005 and (b) the simulations are for a month, and the sampling results are a one week average to minimize day-to-day variations.

4. RESULTS

Figure 2 is the result of CMAQ runs nested down to 4 km grid size. The 4X4 km cell is located over downtown Wilmington., DE. The results shown are the average diurnal variation Formaldehyde (HCHO) for July 2001. For formaldehyde, both primary and total HCHO are depicted for that 4X4 cell. We see the contribution of primary emissions for this cell ranging from to be about 1/5 to 1/3 of the total during the early morning to noon period with strong increases after sunrise from traffic and industry. The strong increase in the ratio of total to primary concentrations in the afternoon is a result of the increase in the height of the mixing layer. Also, photo-chemistry and regional transport processes becomes dominant factors in the afternoon; the total and the ratio show large increases and decreases respectively.

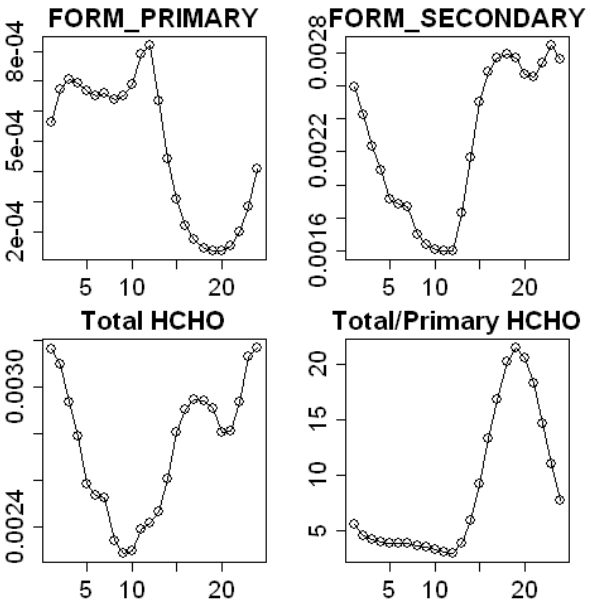

Fig. 2. Results of CMAQ simulations for July 2001 showing sample diurnal variations for a 4X4 km grid cell over downtown Wilmington, DE.

Figure 3 shows an example of the AERMOD model results for HCHO. Values shown are normalized to the modeled peak value of the month. The AERMOD simulations shown are for receptor grids of 200m in UTM coordinates for a domain of approximately 10X10 km. The figure also shows the mobile sampling route implemented during the E-DATAS. The primary sources include all point, area and line sources; the latter from road link-based emissions data. The results shown are the July 2001 average for 1200 EDT, 2001. For the total concentration field, one would need to incorporate the primary contribution from AERMOD with the CMAQ results (Isakov, et al., 2006). The AERMOD simulation shown is arbitrarily chosen for 1200 EDT. While the magnitudes changed over the course of a day, only slight changes in the spatial patterns are noted over the course of a day. From the AERMOD simulation, we observe a significant amount of spatial variability. Variability at this scale is not possible using CMAQ alone for typical urban scale applications of 1 km grid size for CMAQ. The results show clearly, the significant contributions from the highway sources to the variability pattern. Additionally local hot spots of emissions are apparent.

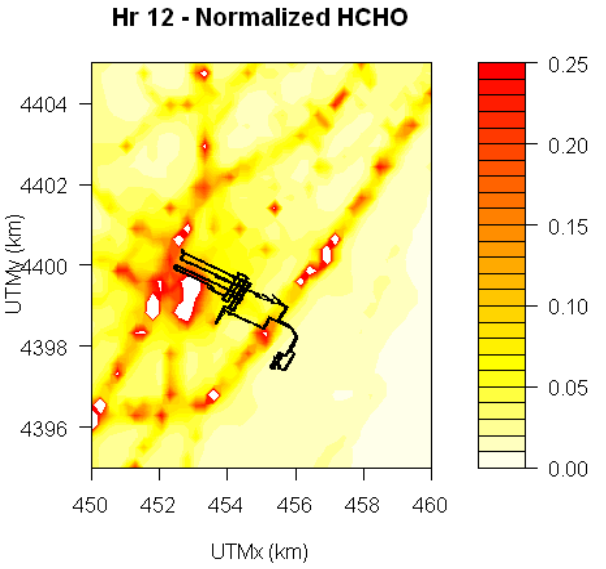

Fig. 3. AERMOD simulation of primary emissions of HCHO in the Wilmington, DE area. The mobile sampling route in the E-DATAS project is indicated. The simulations were made in UTM coordinates for July 2001 @ 1200 EDT.

Figure 4 presents time series plots for three SGVs as defined by (2a), (2b) and (2c) for the mobile van measurements made during the summer 2005 campaign July 31st through August 5th. These measurements were made during the hours of 8 am through 5 pm. The mean, 95 percentile and peak concentrations utilized in the estimation of these SGVs are based on the hourly datasets, that is, measurements for the hours of 8 am to 5 pm. Van measurements indicate that the SGVs based on COV can be as high as [1.1, 1.4], SGVs based on 1+ 95 Percentile/Mean can be as high as [2.1, 2.6], and those based on 1 + Peak/Mean can be as high as [2.1, 3.0].

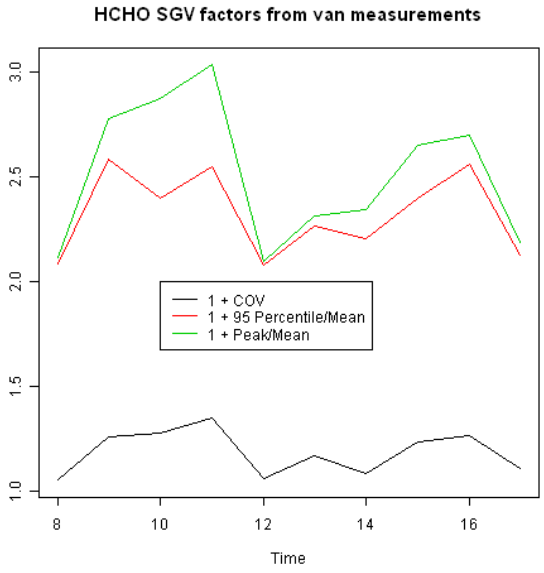

Fig. 4. Three different forms of SGV parameterization derived from mobile van measurements during the July 31 – August 5, 2005 summer campaign

The type of results shown in Figure 4 will, in principle, be an indicator of the magnitude and characteristics of the sub-grid variability of a grid model of 4X4 km size over Wilmington, DE. Figure 5 displays time series of three possible parameters representing SGV (top) and the SGV adjusted concentrations, SACs, grid concentrations influenced or adjusted fields (bottom) based on the SGV parameters from local scale modeling. The SACS shown here are the adjusted CMAQ results shown in Figure 2 for HCHO. Each of the SACs shown is defined using the CMAQ mean for the hour. This introduces a sensitivity resulting in large SACs when the mean is small, especially for example, the example of peak-to-mean. Other definitions may be more satisfactory and are being explored. We can also note that the SGVs estimated from the van measurements and modeling are comparable.

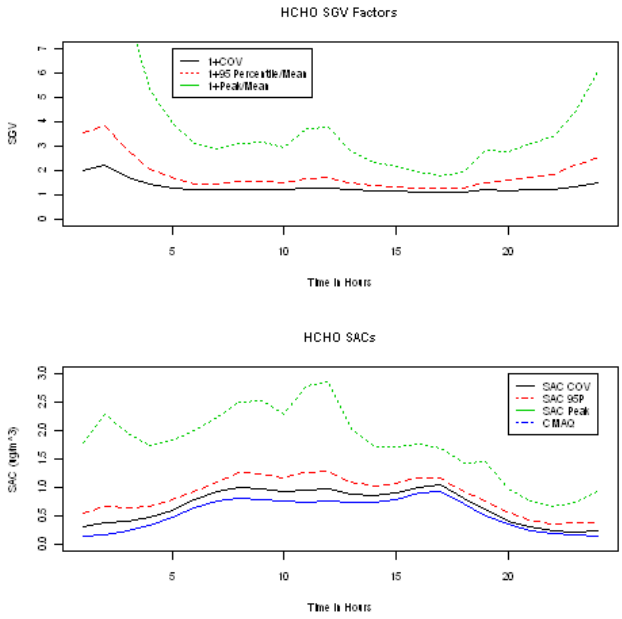

Fig.5. Three different forms of SGV parameterization derived from results of AERMOD modeling of the 4X4 km cell over Wilmington DE for HCHO for July 2001 (top). SGV weighted HCHO concentrations from CMAQ using corresponding SGV parameterizations.

5. DISCUSSIONS AND SUMMARY

We recognize that variability exists at scales smaller than can be resolved with photochemical grid models. Under the assumption that such variability can be important in exposure assessments, we have been attempting to develop modeling tools that will provide this additional dimension of information. To this end, this paper has applied local scale modeling (AERMOD) to provide an estimate of variability from primary emissions. The results of this study substantiates our hypotheses that significant amounts of spatial variability do exist; that application of dispersion models can provide a means to characterize and estimate such variabilities for a primary pollutant species, here HCHO. We note, however, that the modeling results and comparisons with observations noted here have invoked many assumptions, e.g., model and measurement periods differed. Local scale modeling will be inadequate for reactive species and thus, we still see a need for modeling tools such as coupled Large-Eddy Simulations with photoChemistry models (e.g., LESChem, Herwehe, 2000) or local-scale models capable of addressing chemistry to assess secondary components correctly as to provide a greater range of SGVs than can be obtained using local scale and fine scale CMAQ modeling alone. Future efforts will utilize the SGVs from these various modeling tools to applications that include exposure assessments, model evaluations and weight-of-evidence analyses in regulatory models. Regarding SACs, the examples shown here show that sensitivity to some definitions e.g., peak/mean may be excessive; thus, the SAC definitions shown here are to be considered preliminary. Clearly, this situation is to be considered an opportunity for the air quality communities to provide input and guidance on appropriate SAC definitions for different applications.

ACKNOWLEDGEMENTS

The author would like to thank Dr. Jason Ching (EPA Atmospheric Modeling Division) for his review and comment of this manuscript.

REFERENCES

Byun, D.W., and Ching, J.K.S. (Eds.): *Science algorithms of the EPA Models-3 Community Multiscale Air Quality (CMAQ) modeling system.* EPA-600/R-99/030, National Exposure Research Laboratory, U.S. Environmental Protection Agency. Research Triangle Park, NC (1999).

Ching, J., S. DuPont, J. Herwehe, T. Otte, A.Lacser, D. Byun, and R. Tang, 2004a: Air quality modeling at coarse-to-fine scales in urban areas. *Preprints, Sixth Conference on Atmospheric Chemistry: Air Quality in Megacities, January 11-15, 2004, Seattle, Washington*. American Meteorological Society, Boston.

Ching, Jason, V. Isakov, J. Herwehe, M. Majeed, 2005: Incorporating sub-grid variability concentration distributions with CMAQ, 4th *Annual Models-3 User's Conference*, Sep 26-28, 2005, UNC-Chapel Hill, NC Community Modeling and Analysis System.

Ching, Jason, V. Isakov and M. Majeed, 2006a: "Approach for incorporating sub-grid variability (SGV) information into air quality modeling" 14th Joint conference on the Applications of Air Pollution Meteorology with the Air and Waste Management Association, Atlanta, GA Jan 30-Feb 2, 2006.

Ching, Jason, J. Herwehe and J. Swall, 2006b: On joint deterministic grid modeling and sub-grid Variability conceptual framework for model evaluation, *Atmospheric Environment*, 40 (2006) 4935-4945.

DNREC Report: Enhanced Delaware Air Toxics Assessment Study E-DATAS, Editor, Project Report by Delaware Natural Resources and Environmental Conservation to EPA Region 3, September 2006.

Herwehe, J.A., 2000: A numerical study of the effects of large eddies on trace gas measurements and photochemistry in the convective boundary layer. PhD dissertation, Department of Atmospheric Sciences, University of Alabama in Huntsville

Isakov, Vlad., John. S. Irwin and Jason Ching**,** Using CMAQ for Exposure Modeling and Characterizing the Sub-Grid Variability for Exposure Estimates, Accepted for publication in *Golden Jubilee Special Issue of JAMC* (2006)

Majeed, M, J. Ching, T. Otte, L. Reynolds and R.Tang, (2004): CMAQ Modeling for Air Toxics at Fine Scales: A Prototype Study, . Preprints, *3rd Annual Models-3 User's Conference*, October 18-20, 2004, Chapel Hill, NC Community Modeling and Analysis System, CD ROM 5.2 (2004).

Touma, J. S., V. Isakov, J. Ching, and C. Seigneur, 2006: Air quality modeling of hazardous pollutants: current status and future directions. *Journal of the Air &Waste Management Association.* **56**: 547-558.

METEOROLOGICAL AND CHEMICAL PREDICTION WEB BASED SYSTEM USING RAMS AND CAMx NUMERICAL MODELS

,
Nestor W. Alvarez Villa and
(UPB)
Circ. 1a 70-01,.
E-mail: nestor.alvarez@upb.edu.co

M. Victoria. Toro*
Environmental Research Group, Bolivariana Pontifical University, Medellin, Colombia

J Nestor W. Alvarez Villa
Environmental Research Group, Bolivariana Pontifical University, Medellin, Colombia

Carlos G. Sanchez Toro
Environmental Research Group, Bolivariana Pontifical University, Medellin, Colombia

1. INTRODUCTION

The main purpose of the prediction system is to inform the users, in real time, about the air quality and meteorological conditions in a defined domain. The system can give air quality and meteorology related information of any point inside the domain, in a graphical and plain text format.

The whole prediction system is indeed a Web Application that is based on tools developed for the visualization and the handling of information product of Meteorological and Chemical Forecasting. The nucleus of the whole system is conformed by a Meteorological Forecasting Model, RAMS (www.atmet.com), and by a Chemical Forecasting Model, CAMx (www.camx.com). A diagram of the entire application can be seen on Fig. 1.

When the models have finished making their forecasts, these are generally stored in Data Base which is the central part of the system (see Figure 1), because from this point flows of information towards the graphical tools, and towards the end user of the system. The storage technique for the forecast data depends on the data base capacity, as the growth is exponential.

**Corresponding author:* M. Victoria. Toro, Environmental Research Group (GIA) Bolivariana Pontifical University (UPB) Circ. 1 No 70-01, Medellin, Colombia. Tel:5744159084e-mail: victoria.toro@upb.edu.co

The system visualizes its results by means of specific visualization tools, designed specifically for the type of information thrown by the system - weather & air quality forecast information. These tools are:

- Vis5d (http://www.ssec.wisc.edu/~billh/vis5d.html),
- NCARG (http://ngwww.ucar.edu/ng4.4/index.html),
- PyNGL (http://www.pyngl.ucar.edu/).

All these tools work under the UNIX like Operating system, as well as the Forecast Models. The interface between all these tools and the web page was constructed using PHP (Hypertext Preprocessor, www.php.net) programming language.

Finally, the system end user accedes to all the information through a Web Browser. By means of this, the user can obtain graphical, binary and plain text forecast data related to a point inside the global domain. Detailed an up-to-date information about the system can be obtained at http://simeca.metropol.gov.co.

2. SYSTEM ARCHITECTURE

The system is basically conformed by three modules: 1) Forecast Cluster, 2) the Web server, and 3) a Data Base.

The communication between the Forecast Cluster and the Web server is established using the SSH (Secure Shell) protocol. SSH is a set of network standards and protocols that allow to establish a safe communication channel between two computers. SSH typically is used to accede to a remote computer and to execute commands, also allows file transfer by means of the associated protocols SFTP (Secure File Transfer Protocol) or SCP (Secure Copy). Using SSH, the Data Base Server obtains the final forecast files from the Forecast Cluster, the Web Server processes them in order to turn them into graphs, plain data and animations (dynamically, depending on user request); and then gives the data to the end user as he requested.

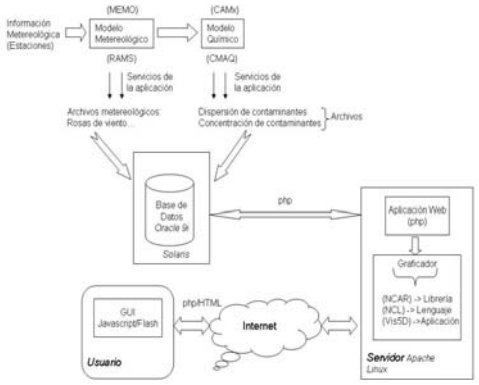

Fig. 1 General System Diagram.

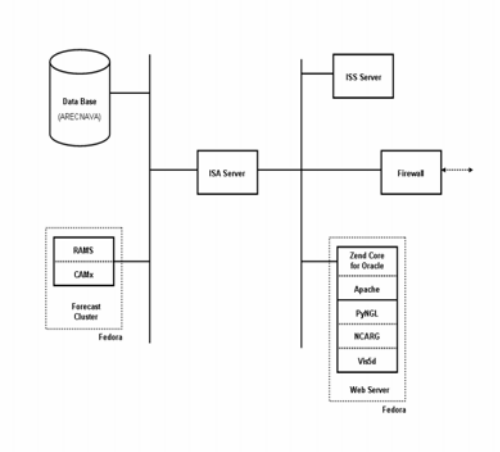

Fig. 2 General System Architecture.

The Figure 2 shows the general system architecture. It's a typical Web Application Architecture. In some blocks, the applications used are shown.

The Communication between the Web server and the Data Base Server is established by means of a client-server session, where the Web Server acts as client via the "Zend for Core Oracle" Application. Zend Core™ for Oracle® allows the use of PHP (Preprocessor Hypertext, http://www.php.net/) with the Oracle DBMS (Data Base Management System) in Web Applications; In fact, Zend Core™ for Oracle® is a PHP Development Environment that allows a complete integration with Oracle data bases.

The system Web services are implemented by means of the conjunction use of the Apache Web Server application (http://www.apache.org/) and PHP as an Application Server. Both, PHP and Apache, run under the Fedora UNIX distribution (http://fedora.redhat.com/). The system access the graphical tools (PyNGL, NCARG, Vis5d) services using PHP, they allow the system to generate the graphics it needs dynamically and in Real Time.

3. SYSTEM CHARACTERISTICS

As it was insinuated before, the main system is made up of three subsystems: 1) *Forecast Models Module*, 2) *Data Base Module* and 3) *Web Services Module*.

The Forecast Module was implemented in a Cluster. The Forecast Models (RAMS & CAMx) are installed on this machine which runs the Fedora Core 4 Operating System. The Forecast Module generates binary archives containing forecast information about the geographical domain selected. These archives are processed by the others modules so that all the services of the system are provided to the end user. All the information output by this module is stored on backup disks. The Module's Cluster is operated via a Front End Machine, usually the slowest machine of the set or any other low resources machine, who allows an operator to control the entire cluster and run the numerical models.

The binary archives obtained from de Forecast Module are used by the Web Services Module to generate graphs, animation and plain text data dynamically. All this is done via the models post-processing tools and state of the art scientific graphical tools. Also, the plain text data can be stored in a Data Base using PHP Programming Language. The binary files are also stored in a repository way for future analysis, they can also be stored in a Data Base or in Backup Disks either magnetic (tapes) or optical disks.

As mentioned early, The Web Services Module was implemented using the Apache Web Server Application in conjunction with a PHP Application Server. Trough PHP scripts and several different tools, the Web Services Module obtain the necessary data from the Forecast Module's output binary files to generate the data or graphical information requested by the system's end user from a given Web Page. After the user request, the information is displayed to the end user in real time, and all the data requested is generated dynamically.

Modules Information Flow

The scheme shown in Fig. 1 allows to observe how would be the information flow in the entire system. On first place, all the Meteorological Forecasts are done using Reanalysis Data obtained from different Global Models Runs. Then, the data generated for the Meteorological Forecast Model is saved on a data base and used as input to the Chemical Model. All the data is stored in a repository from where the Web Services Module can transform it into graphical and plain text data as end user request. The end user defines the required data characteristic trough a Web Form that is served by a PHP script who transforms the binary data into the format specified by the web page user. The PHP scripts trust on tools as PyNGL, vis5d and REVU (RAMS postprocessor tool) to give the end user the requested data.

System Services Request Procedure

The end user can access all the services supported by the system trough a typical web page (see Fig. 3). On this web page the user will find a brief system explanation, system usage tutorials and other useful documentation, and web links. Also, from the system home page the end user can access several web forms from where to interact with the system, one of this web forms is shown on

Fig. 4. Then in the web form, the end user can define the geographical point of interest (inside the model forecast domain) by clicking one point over a map who represents the models forecast domain or by entering the interest point coordinates (latitude, longitude) in decimal degrees using the web form.

Once the end user have interacted with one of the several web forms, he will be redirected to a web page where all the requested forecast products will be shown, all the products are related to the point first defined by the end user. For a given geographical point, the end user can request products like: XY Plots of a predefined forecast variable, Meteograms, Soundings, among other system products. Also, the end user can choose the final format of the system products requested, it can be graphs, XY plots, 3D animations or plaint text data. At the end of the process, the end user will obtain the required data, in the requested format.

4. BRIEF TOOLS DESCRIPTION BY MODULE

Above in this article where described the several modules that conforms the system, now it will be described the various tools that are grouped into each module.

Fig. 3. System Home Web Page.

Fig. 4. Meteorological Forecast Web Form with an interactive map.

Forecast Models Module

This Module is conformed by 2 numerical forecast models and their post-processing & pre-processing tools. Several of the post & pre-processing tools where developed by us in order to accomplish all the functional system requirements.

Regional Atmospheric Modeling System (RAMS)

The Regional Atmospheric Modeling System, is a numerical model developed by scientists at Colorado State University and the ASTER division of Mission Research Corporation for simulating and forecasting meteorological phenomena, and for depicting the results. Its major components are:

(1) an atmospheric model which performs the actual simulations,
(2) a data analysis package which prepares initial data for the atmospheric model from observed meteorological data, and
(3) a post-processing model visualization and analysis package which interfaces the atmospheric model output with a variety of visualization software and other utilities.

RAMS is most often used as a limited area model, and many of its parameterizations have been designed for mesoscale or high resolution cloud scale grids. However, RAMS may also operate as a global scale model for simulating large-scale systems by configuring two hemispheric grids, which use a polar stereographic projection and continually exchange boundary data between them. There is no lower limit to the domain size or to the mesh cell size of the model's finite difference grid; microscale phenomena such as tornadoes and boundary layer eddies, as well as sub-microscale turbulent flow over buildings and in a wind tunnel, have been simulated with this code. For more information see www.atmet.com.

Comprehensive Air quality Model with extensions (CAMx)

The Comprehensive Air quality Model with extensions is a publicly available open-source computer modeling system for the integrated assessment of gaseous and particulate air pollution. Built on today's understanding that air quality issues are complex, interrelated, and reach beyond the urban scale, CAMx is designed to:

- Simulate air quality over many geographic scales
- Treat a wide variety of inert and chemically active pollutants: Ozone, Inorganic and organic PM2.5/PM10; Mercury and toxics.
- Provide source-receptor, sensitivity, and process analyses.
- Be computationally efficient and easy to use

The U.S. EPA has approved the use of CAMx for numerous ozone and PM State Implementation Plans throughout the U.S, and has used this model to evaluate regional mitigation strategies. For more information see www.camx.com.

Data Base Module

The Forecast Models Module generates great volumes of information that must be stored. All this information is stored in two ways: In a relational Data Base or in a binary files repository.

To implement the data base we used the Oracle DBMS (Data Base Management System), more precisely Oracle Database 10g. Other DBMS can be used to implement this module; we use this particular DBMS due to platform requirements. To fill the data base, we create a PHP script that generates ASCII files from the binary files resulting from both numerical models runs. Then, these ASCII files are introduced to the data base using SQL statements invoked by a PHP script. After this, the Web Services Module can obtain the data it needs via the data base or the binary files repository. For more information about Oracle DBMS see www.oracle.com.

Web Services Module

Through this module the system can publish all its products and interact with the end user. This module also interacts with the Data Base Module to obtain the information the end user may need.

The system was implemented using the Apache Web Server Application (www.apache.org) and a special tool for Web Applications named Zend Core™ for Oracle® (www.zend.com). Zend Core™ for Oracle® supports businesses using PHP with Oracle Database for business-critical Web applications. It provides a stable, high performance, easy-to-

install and supported PHP development and production environment fully integrated with the Oracle Database. Zend Core™ for Oracle® was designed to support Oracle Database 10g, and Apache 2.0.x which is ideal for our Information System requirements.

REFERENCES

Sellers, P.J., 1992. "Canopy reflectance, photosynthesis and transpiration. Part III: Areanalysis using enzyme kinetics-electron transport models of leaf physiology.Remote Sens." Environ., 42, 187-216.

Sellers, P.J., D.A. Randall, G.J. Collatz, J.A. Berry, C.B. Field, D.A. Dazlich, C. Zhang, G.D. Collelo, and L. Bounoua, 1996. "A revised land surface parameterization (SiB2) for atmospheric GCMs. Part I: Model formulation." J. Climate, 9, 676-705.

Walko, R.L., L.E. Band, J. Baron, T.G.F. Kittel, R. Lammers, T.J. Lee, D. Ojima, R.A. Pielke, C. Taylor, C. Tague, C.J. Tremback, and P.L. Vidale, 2000. "Coupled atmosphere-biophysics-hydrology models for environmental modeling." J. Appl. Meteor., 39, 931-944.

Jacobs, C.A. J.P. Pandolfo and M.A. Atwater, 1974. "A description of a three dimensional numerical simulation model of a coupled air-water and/or air-land boundary layer." IFGYL final report. CEM report No. 5131-509a.

Mesinger, F. and A. Arakawa, 1976. "Numerical Metods used in atmospheric Models." GARP Publication series, No. 14, WMO/ICSU Joint Organizing Committee. 64 pp.

Tremback C. J., Walko R. L. and Bell M. J. 2001 *RAMS/HYPACT Evaluation and Visualization Utilities (REVU) Version 2.3.1*. User's Guide, *ASTER Division Mission Research Corporation. P.O. Box 466, Fort Collins, CO 80525-0466.

Walko R. L. and Tremback C. J. *Regional Atmospheric Modeling System MODEL INPUT NAMELIST PARAMETERS Version 4.3/4.4*. [Online] www.atmet.com.

ENVIRON International Corporation. 2006. *Comprehensive Air Quality Model with extensions User's guide*. ENVIRON International Corporation, 101 Rowland Way, Suite 220. Novato, California 94945-5010.

AUTHOR BIOGRAPHIES

MARIA V. TORO was born in Medellin, Colombia and went to the Bolivariana Pontifical University of Medellin, where she studied Chemical Engineering and obtained his degree in 1988. Then, she worked for the Bolivariana Pontifical University R&D Institute, specifically at the Environmental Research Group (GIA) as Researcher. In 1991, he went to the Polytechnical University of Madrid, where she obtains a MsC. degree in Environmental Contamination. Later, she returns to the Pontifical University of Medellin where she worked as the director of the Environmental Research Group (GIA) until 1999. The she returns to Spain and obtains a PhD degree in the Polytechnical University of Catalonia in 2004. Since then, she works for the Pontifical University of Medellin as director of the Atmospherical Research Study Line of the Environmental Research Group (GIA). His e-mail address is: victoria.toro@upb.edu.co.

NESTOR W. ALVAREZ was born in Medellin, Colombia and went to the Bolivariana Pontifical University of Medellin, where he studied Electronic Engineering and obtained his degree in 2002. Since then, he works for the Bolivariana Pontifical University R&D Institute, specifically at the Environmental Research Group (GIA) in his Atmospherical Research Study Line. Here he dedicates to implement platforms for various types of numerical weather forecast models (RAMS, MEMO, MARS, CAMx, and MM5). His e-mail address is: nestor.alvarez@upb.edu.co and his Web-page can be found at http://www.waldyd.8m.com/.

CARLOS G. SANCHEZ TORO was born in Medellin, Colombia, and went to the Bolivariana Pontifical University of Medellin, where he studied Electronic Engineering and obtained his degree in 2004. In 2005, he began to work at the Environmental Research Group (GIA) of the same university, focus himself in software development and web programming through several research projects. His e-mail address is: cg2100@hotmail.com.

plot of observed ozone concentrations at grid cell (25,20,1) compared with maximum and minimum modeled variable ozone concentrations.

AIR QUALITY AND HEALTH BENEFITS FROM FUTURE AIR POLLUTION CONTROL IN CHINA

Litao Wang*, Kebin He, Lei Yu
Department of Environmental Science and Engineering, Tsinghua University, Beijing, 100084, China
Carey Jang, Scott Voorhees
U.S. Environmental Protection Agency, Research Triangle Park, NC, USA
Qiang Zhang, David Streets
Decision and Information Sciences Division, Argonne National Laboratory, Argonne, IL 60439, USA
Joshua Fu, Nicky Lam
Department of Civil and Environmental Engineering, University of Tennessee, TN 37996, USA
Jerry Lin
Department of Civil Engineering, Lamar University, Beaumont, TX 77710, USA
Yang Zhang, Kai Wang
Department of Marine, Earth and Environmental Science, NC State University, Raleigh, NC 27695, USA

1. INTRODUCTION

China is making great effort in air pollution control and energy saving in resent years. Chinese government have set the goals of 10% reduction from 2005 SO_2 emissions in 11th Five-Year-Plan (FYP) (2006-2010). To evaluate the environmental benefit from these efforts, MM5-Models-3/CMAQ modeling system was applied in China in air quality prediction for future years. Multi-pollutants assessment of key air quality issues, including particulate matter, ozone, acid rains, visibility, and mercury and nitrogen deposition were pursued in base year and 2010 of both BAU (Business As Usual) and emission control scenarios. Environmental and health benefit resulting from various emission control scenarios were assessed with BenMap (Environmental Benefits Mapping and Analysis Program) Model. Active energy policies and pollution control activities can bring both local and regional environmental benefits, as well as significant health benefits.

2. MODEL CONFIGURATION AND INPUT

2.1 Domain and Episode

The modeling domain covers Entire China and part of East Asia with 36 x 36 km grids, as shown in Figure 1. Lambert projection with the two true latitudes of 25 ° N and 40 ° N was used. The domain origin was 34 ° N, 110 ° E, and the coordinates of the bottom left corner were (x=-2934 km, y=-1728 km). Fourteen vertical layers from the surface to the tropopause were employed, with denser layers in the lower atmosphere. The corresponding sigma levels were 0.995, 0.988, 0.980, 0.970, 0.956, 0.938, 0.893, 0.839, 0.777, 0.702, 0.582, 0.400, 0.200 and 0.000.

The modeling periods selected were January, April, July and August, 2005. A spin-up period of six days was used to eliminate the influence of initial conditions.

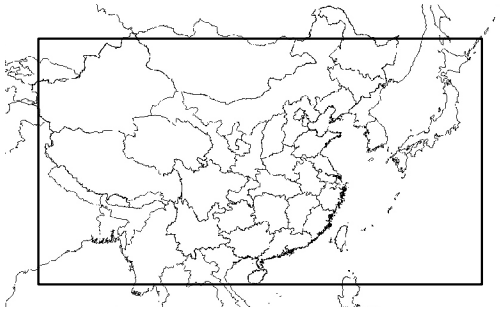

Fig. 1. Domain in Models-3/CMAQ modeling: size = 164×97 cells with 36 km resolution. MM5 domains are three grids broader on each side of each domain.

2.2 Emission

The general methodology used to build the new China regional emission inventory has been described in Streets et al. (2003, 2006) and Zhang et al. (2007). Using the same general approach, we have implemented an improved technology-based methodology, in order to be able to reflect the types of technology presently operating in China. We also implemented a new anthropogenic

*Corresponding author: Litao Wang, Department of Environmental Science and Engineering, Tsinghua University, Beijing, 100084, China. e-mail: wlt@tsinghua.edu.cn

PM emission model (Zhang et al., 2006) to calculate primary PM emissions, including PM10 and PM2.5, which the TRACE-P inventory did not address. Activity data are obtained from statistics published by a variety of government agencies of China. Fuel consumptions by sector and by province are derived from the China Energy Statistical Yearbook. Technology distributions within each sector are obtained from a wide variety of Chinese technology reports and energy demand modeling approach. Emission factors are mainly based on measurements in China or estimations based on the actual technology level and practice. In some cases, where local information is lacking, we use adjusted emission factors for similar activities from international database.

With the updated methodology, we constructed a new emission inventory for China for the year 2004 based on official government statistics. The new inventory includes the four major gaseous species (SO2, NOx, CO, and NMVOC) and four primary aerosol species (PM10, PM2.5, BC and OC). A new set of growth algorithms was developed to extend the statistics-based 2004 inventory to 2005. The extrapolated emissions in China in 2005 were 28.3 Tg SO2, 19.8 Tg NOx, 163.7 Tg CO, 22.4 Tg VOC, 18.3 Tg PM10, 13.4 Tg PM2.5, 1.8 Tg BC, and 3.2 Tg OC.

To support CMAQ modeling, emissions are distributed into 36km × 36km grids using various spatial proxies at 1 km × 1 km resolution (Streets et al., 2003; Woo et al., 2003). VOC emissions are further decomposed to 17 chemical species based on CB05 chemical mechanism. The new speciated VOC emissions are is thought to be much improved from previous versions like TRACE-P since we counted every VOC species from emissions (~1500 species total) and mapped each of them to CB05 species based on a very detailed chemical reaction mapping table. The remain uncertainties is now mainly from VOC profile of each source: there are very limit local measurements in China and we have to heavily rely on EPA's SPECIATE database.

2.3 Meteorology

MM5 model Version 3.7 was used to generate the meteorological fields. The pressure at top surface was 100 mb, and 23 vertical layers were used. The terrain and landuse data came from the U.S. Geological Survey (USGS) database. The National Center for Environmental Prediction (NCEP) final analysis datasets were used to generate the first guess field. The NCEP Automated Data Processing (ADP) data was used in the objective analysis scheme. The four dimensional data assimilation (FDDA) technique was employed.

The physics options were: the Kain-Fritsch 2 cumulus schemes (Kain and Fritsch, 1993; Kain, 2002), the high resolution Blackadar PBL scheme (Zhang and Anthes, 1982), the mixed phase (Reisner 1) explicit moisture schemes (Reisner et al., 1998), the RRTM longwave radiation scheme (Mlawer et al, 1997) and the force/restore (Blackadar) surface scheme (Blackadar, 1976; Deardorff, 1978).

2.4 CMAQ configuration

This study used Models-3/CMAQ version 4.6.1. The Carbon Bond 05 (CB05) module with aqueous and aerosol extensions, and the Aero 4 model derived from the Regional Particulate Model (RPM) (Binkowski and Shankar, 1995) were chosen for gas-phase chemistry and aerosol module. Particulates are described using the modal approach with two modes: fine (particles with diameters below 2.5 μm) and coarse particles (particles with diameters between 2.5 and 10 μm).

The Meteorology-Chemistry Interface Processor (MCIP) version 3.2 was applied to process the meteorological data. The initial conditions (ICON) for each period were prepared by running the model for six days before the first simulation day. The boundary conditions (BCON) were extracted from GEOS-CHEM model. The total ozone column data from Total Ozone Mapping Spectrometer (TOMS) were used in the photolysis rates processor (JPROC).

3. MODELING RESULTS EVALUATION

3.1 MM5

Table 1 summarized the performance statistics of observed and predicted temperature, wind speed, pressure, wind direction and precipitation at eight cities in China in July 2005. It can be seen that the meteorological field was well represented by the model.

Table 1. Statistical summary of the observed and predicted parameters at eight sites* in China in July 2005.

	Temperature	Wind Speed	Wind Direction	Pressure	Precipitation
RMSE	<2.5K	<1.8m/s	<120^{o}	<850Pa	<0.14cm/hr
MB	<±1.5K	<±0.6m/s	<±45^{o}	<±500Pa	<±0.04cm/hr

NMB	<±0.4%	<±30%	<±30%	<±0.8%	<±50%
NME	<0.8%	<60%	<45%	<0.8%	<30%

*: Shenyang, Beijing, Nanjing, Shanghai, Wuhan, Hangzhou, Changsha, and Guangzhou.

RMSE: root mean square error.

MB: mean bias.

NMB: normalized mean bias.

NME: normalized mean error.

3.2 CMAQ

(Ongoing)

4. RESULTS AND DISCUSSION

(Ongoing)

5. REFERENCES

Streets, D.G., T.C. Bond, G.R. Carmichael, S.D. Fernandes, Q. Fu, D. He, Z. Klimont, S.M. Nelson, N.Y. Tsai, M.Q. Wang, J.-H. Woo, and K.F. Yarber, An inventory of gaseous and primary aerosol emissions in Asia in the year 2000, J. Geophys. Res., 108(D21), 8809, doi:10.1029/2002JD003093, 2003.

Streets, D.G., Q. Zhang, L Wang, K. He, J. Hao, Y Wu, Y. Tang, and G.R. Carmichael (2006), Revisiting China's CO emissions after TRACE-P: Synthesis of inventories, atmospheric modeling, and observations, J. Geophys. Res., 111, D14306, doi: 10.1029/2006JD007118.

Woo, J.-H., J.M. Baek, J.-W. Kim, G.R. Carmichael, N. Thongboonchoo, S.T. Kim, and J.H. An (2003), Development of a multi-resolution emission inventory and its impact on sulfur distribution for Northeast Asia, Water Air Soil Pollut., 148, 259-278.

Zhang, Q., Z. Klimont, Streets, D.G., H. Huo, and K He (2006), An anthropogenic PM emission model for China and emission inventory for the year 2001, Progress in Natural Science, 16(2): 223-231 (in Chinese)

Zhang, Q., D.G. Streets, K. He, Y.X. Wang, A. Richter, J.P. Burrows, I. Uno, C.J. Jang, D. Chen, Z. Yao, and Y. Lei (2007), NOx emission trends for China, 1995-2004: The view from the ground and the view from space, submitted to J. Geophys. Res.

Binkowski, F. S., and Shankar, U., 1995. The regional particulate model. 1. Model description and preliminary results. J. Geophys. Res., 100, D12, 26191-26209.

Kain, J. S., 2002: The Kain-Fritsch convective parameterization: An update. J. Appl. Meteor., 43, 170-181.

Mlawer, E. J., S. J. Taubman, P. D. Brown, M. J. Iacono, and S. A. Clough, 1997: Radiative transfer for inhomogeneous atmosphere: RRTM, a validated correlated-k model for the longwave. J. Geophys. Res., 102 (D14), 16663-16682.

Kain, J. S., and J. M. Fritsch, 1993. Convective parameterization for mesoscale models: The Kain-Fritsch scheme. The representation of cumulus convection in numerical models, K. A. Emanuel and D. J. Raymond, Eds., Amer. Meteor. Soc., 246 pp.

Zhang, D. L., R. A. Anthes., 1982. A high-resolution model of the planetary boundary layer - sensitive tests and comparisons with SESAME-79 data. J . Appl . Meteor., 21: 1594-1609.

Reisner, J., R. J. Rasmussen, R. T. Bruintjes, 1998. Explicit forecasting of supercooled liquid water in winter storms using the MM5 mesoscale model. Quart. J. Roy. Meteor. Soc., 124B: 1071-1107.

Blackadar, A. K., 1976. Modeling the Nocturnal Boundary Layer. Proc. Third Symp. on Atmospheric Turbulence, Diffusion and Air Quality. Boston, Amer. Meteor. Soc., 1976: 46-49.

Deardorff, J. W., 1978. Efficient prediction of ground surface temperature and moisture, with inclusion of a layer of vegetation. J. Geophys. Res., 83: 1889-1903.

DEVELOPMENT AND OPERATION OF NATIONAL CMAQ-BASED $PM_{2.5}$ FORECAST SYSTEM FOR FIRE MANAGEMENT

Kenneth J. Craig*, Neil J. M. Wheeler, Stephen B. Reid, Erin K. Gilliland, and Dana Coe Sullivan
Sonoma Technology, Inc., Petaluma, CA, USA

1. INTRODUCTION

The BlueSky smoke modeling framework is a tool developed by the U.S. Department of Agriculture-Forest Service (USFS) for modeling the cumulative impacts of $PM_{2.5}$ emitted from multiple fires (Larkin et al., 2007). The BlueSky Framework (BSF) uses the Lagrangian CALPUFF model (Scire et al., 2000) to calculate local-scale transport and dispersion of smoke produced by wildfires and prescribed burns. While this approach is appropriate at a local scale in the vicinity of individual fires, it is computationally burdensome to use a Lagrangian model to track smoke from fires on a national scale, or to carry over predicted smoke concentrations from previous simulations into the current and future-day predictions.

The BlueSky Framework has been recently upgraded and redesigned. Among the high-level development goals in improving the BlueSky Framework version 3 (BSF3) was to build a reliable, operational system that provides national forecasts of emissions and smoke. To fulfill this goal, we designed and implemented the BlueSky National Smoke Modeling System, or BlueSky National. BlueSky National is an operational $PM_{2.5}$ forecasting system for the United States based on the Pennsylvania State University/National Center for Atmospheric Research Mesoscale Model, Version 5 (MM5) (Grell et al., 1994) and the Community Multiscale Air Quality (CMAQ) model (U.S. Environmental Protection Agency, 1998; National Exposure Research Laboratory, 1999). The BlueSky National system provides a low-resolution (36 km) national forecast of ground-level $PM_{2.5}$ concentrations caused by anthropogenic, biogenic, and fire emissions. BlueSky National also models carryover smoke from previous days' emissions and other sources to provide a more realistic national $PM_{2.5}$ background. These national forecasts will be used by the various Fire Consortia for the Advanced Modeling of Meteorology and Smoke (FCAMMS) to improve their regional high-resolution CALPUFF simulations.

This paper describes the details of the Bluesky National Smoke Modeling System. A retrospective simulation is performed to demonstrate the BlueSky National system.

* *Corresponding author:* Kenneth Craig, Sonoma Technology, Inc., 1360 Redwood Way, Suite C, Petaluma, CA 94954-1169; e-mail: kcraig@sonomatech.com.

2. SMOKE MODELING FRAMEWORK

2.1 Modeling System Overview

BlueSky National is based on BlueSky Framework version 3, MM5 version 3.7, and CMAQ version 4.5.1 (March 17, 2006 release). Forecasts from the North American Mesoscale (NAM) model are used to provide initial and boundary conditions for the MM5 simulations. Hourly meteorological data from MM5 is prepared for use in CMAQ with the Community Multiscale Air Quality Model Meteorology-Chemistry Interface Processor (MCIP) version 3.1. Non-fire emissions are based on the 2002 National Emission Inventory (NEI) version 3 (U.S. Environmental Protection Agency, 2006) projected to the current year, and average meteorological conditions for the current month. Emissions from fires are developed by the Satellite Mapping Automatic Reanalysis Tool for Fire Incident Reconciliation (SMARTFIRE) and BSF3 (Raffuse et al., 2006). The overall process is illustrated in Figure 1.

The modeling domain is the 36-km national Regional Planning Organization (RPO) grid, which covers the continental United States and much of southern Canada and northern Mexico. MM5 modeling is performed on a 29-layer vertical grid. Vertical resolution is 50 to 75 m in the boundary layer, and gradually stretches to coarser resolution up to the model top (approximately 20 km). CMAQ uses a 17-layer grid, which maps exactly to the MM5 vertical grid in the lowest 250 m, then averages every two MM5 layers up to the model top.

BlueSky National provides 72-hr forecasts of $PM_{2.5}$ concentrations caused by anthropogenic, biogenic, and fire emissions. Daily simulations are initialized off predicted concentration fields from the previous day, thereby providing national

background $PM_{2.5}$ concentrations that include carryover from previous days' emissions.

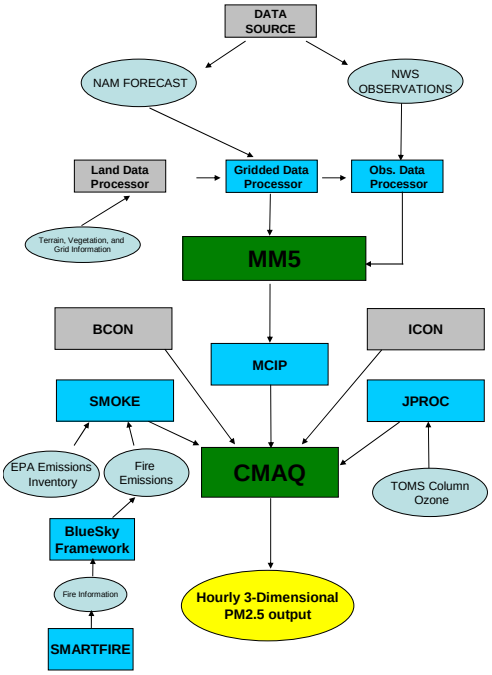

Fig. 1. Overview of data and processes involved in the BlueSky National Smoke Modeling System.

2.2 Emissions Modeling

A new tool, SMARTFIRE, was developed to provide burn-area predictions for the BlueSky Framework. SMARTFIRE integrates and reconciles human-recorded wildfire incident data from Incident Status Summary (ICS-209) reports with satellite-detected fire data. This merging provides a more comprehensive and spatially accurate data set than either tool alone, while minimizing double reports. The method also provides a more realistic temporal profile of area burned.

Burn-area predictions from SMARTFIRE are fed into the BlueSky Framework, which runs a fuel-loading model, a fire consumption model, and an emission model to develop a prediction for $PM_{2.5}$ emissions caused by fires. These emissions are merged with day-specific biogenic and non-fire anthropogenic emissions to produce the final merged emissions input files for CMAQ.

Emission files for biogenic and non-fire anthropogenic sources are developed off-line using version 2.3 of the Sparse Matrix Operator Kernel Emissions Modeling System (SMOKE) (Coats, 1996; Houyoux and Vukovich, 1999; Houyoux et al., 2000; Houyoux and Adelman, 2001). Emission estimates from the 2002 NEI are processed through SMOKE and projected to the current year using growth factors generated by the U.S. Environmental Protection Agency's Economic Growth Analysis System version 4.0 (E.H. Pechan & Associates, 2001). Average meteorological conditions for the current month are used in the preparation of emissions data for sources that are temperature-dependent, such as on-road mobile sources and biogenic sources.

2.3 Fire Tracer Species

A series of aerosol tracers have been implemented in CMAQ to separately track the evolution of primary $PM_{2.5}$ generated from wildfires, agricultural burns, and prescribed burns within BlueSky National (Table 1). Separate variables are also created to differentiate between $PM_{2.5}$ generated from the current day's run, and carryover $PM_{2.5}$ from the previous day's run. Primary $PM_{2.5}$ emissions from fires are assigned to unique tracer variables within SMOKE and are emitted into the CMAQ grid only through the special aerosol tracer variables. These fire aerosols are chemically inert but are subject to transport, dispersion, and deposition. Primary $PM_{2.5}$ emissions from non-fire anthropogenic sources are processed through SMOKE, chemically speciated, and introduced into CMAQ in the standard way. They are carried through CMAQ via the standard $PM_{2.5}$ species and are subject to secondary formation and destruction processes.

Table 1. Aerosol species introduced into CMAQ to track fires in the national smoke modeling system.

Tracer ID	Species Name
F1	Wild fires (today's run)
F2	Wild fires (yesterday's run)
F3	Prescribed fires (today's run)
F4	Prescribed fires (yesterday's run)
F5	Agricultural fires (today's run)
F6	Agricultural fires (yesterday's run)
F7	Planned prescribed fires
F8	Planned agricultural fires

The standard version of CMAQ supports the inclusion of chemically inert tracers, but they are assumed to be in the *gaseous* phase. Tracers are carried through the modeling system in volume-

based units (ppm), dry deposition of tracers is described by a gas-phase deposition velocity, and wet deposition and scavenging are based on Henry's Law of Equilibrium. Several modifications to the standard CMAQ source code were necessary to properly model the new $PM_{2.5}$ tracer species. These modifications are described below.

Because CMAQ assumes that inert tracers are gases, it also expects emission rates for inert tracers to be in units of moles/s, which are subsequently converted to ppm within CMAQ. However, the emissions processing software generates emission rates for aerosols in units of grams per second. To inject the proper aerosol tracer mass into the model, it was necessary to convert the emission rates to moles/s using the tracer molecular weight. Since the $PM_{2.5}$ aerosols produced from fires are primarily carbonaceous in nature, we assumed that the molecular weight of the aerosol tracers was that of carbon (12 g/mol).

Dry deposition for CMAQ tracers by default is determined by the gas-phase deposition velocity, which ordinarily is calculated by MCIP and provided to CMAQ through an MCIP file. Dry deposition velocity is not valid for aerosol tracers. Aerosol dry deposition is complex—an entire physics module (aero_depv) is devoted to this process. Though it was outside the scope of the effort to develop a full aerosol tracer deposition model, aerosol deposition parameters calculated for the native CMAQ aerosol species can be used to estimate deposition for the aerosol tracer species. The RDDEPV.F routine in CMAQ was modified to use the dry deposition velocity for accumulation mode (J-mode) aerosol calculated by the aerosol dry deposition module.

Tracer scavenging and wet deposition in CMAQ is based on Henry's Law of Equilibrium for gases, which is clearly not applicable for aerosol scavenging and wet deposition. The SCAVWDEP.F routine in CMAQ was modified to use calculations that are consistent with those used for aerosols in the accumulation-mode.

2.4 Operational Implementation

The operational BlueSky National Smoke Modeling System will be executed three times daily. The first execution initializes off the 1800 UTC NAM run during the afternoon and evening hours of the previous day. This "early bird" run uses fire emissions information generated only from preliminary (i.e., unverified) satellite-derived fire-location data to provide a preliminary early morning $PM_{2.5}$ forecast. The second run initializes off the 0000 UTC NAM run of the current forecast day, and executes during the overnight hours. This run still uses fire emissions generated from preliminary satellite-derived fire-location data, but the data are augmented with information from ICS-209 reports, which are made available by 2300 MDT. The third and final run is based on the same meteorological data as the previous run, but incorporates the best estimate of fire emissions generated from finalized (i.e., human-verified) satellite-derived fire-location data augmented with ICS-209 reports. Output from this final run will be archived for use in future research applications.

3. DEMONSTRATION

During the last week of June 2005, numerous wildfires were burning in the western United States. Among these were several clusters of fires located north and east of Las Vegas, Nevada, near the confluence of the Nevada, Utah, and Arizona state boundaries (Figure 2). Smoke from these fires impacted the air quality in Las Vegas and Salt Lake City (SLC) during this time period. The abundance of fires combined with the potential to impact air quality in major metropolitan areas makes this time period an interesting test case to demonstrate BlueSky National. Thus, a full test simulation was run from June 27, 2005, at 1200 UTC, through July 1 at 0000 UTC.

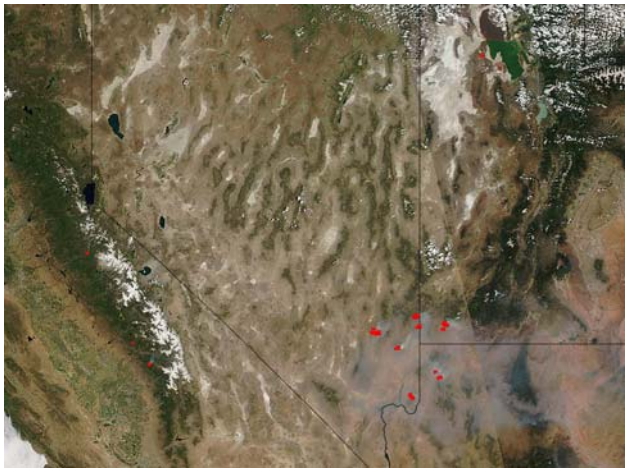

Fig. 2. MODIS-Aqua satellite image from June 29, 2005. Red markers indicate satellite-detected "hot spots", indicating fire locations.

On June 26 through the morning of June 28, southwesterly flow at the surface and aloft advected wildfire smoke northeast toward SLC.

Elevated levels (15 to 45 µg/m^3) of $PM_{2.5}$ were observed at several monitoring stations in the SLC area during this time period, including the Hawthorne site (Figure 3) located in SLC. High $PM_{2.5}$ concentrations in this region occur infrequently during the summer months. A HYSPLIT trajectory analysis confirmed that the air passing through SLC at this time originated from the fire complexes to the southwest. Note that $PM_{2.5}$ concentrations remained low (less than 10 µg/m^3) in Las Vegas, despite its proximity to the fires.

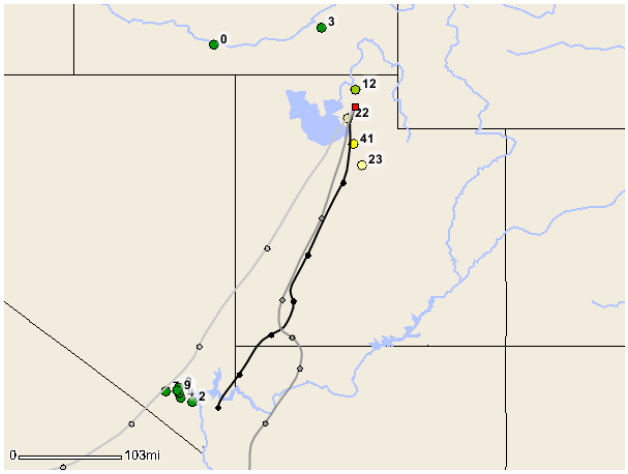

Fig. 3. Observed $PM_{2.5}$ concentrations and 36-hr HYSPLIT backward trajectories on June 28, 2005, at 0800 UTC. Trajectories originate at 250 m, 500 m, and 1000 m.

Spatial distributions of predicted ground-level fire $PM_{2.5}$ from June 27 and 28 show a distinct plume that originates from the fire complexes and stretches northeast across Utah and into southwest Wyoming. Figure 4 shows a snapshot of the predicted smoke plume at 0800 UTC on June 28 as it passes through SLC. BlueSky National predicted a ground-level fire impact of 7 to 8 µg/m^3 in the SLC area at the same time that elevated concentrations were observed. Figure 5 shows predicted $PM_{2.5}$ concentrations caused by anthropogenic and wildfire sources at the Hawthorne site, along with the observed total $PM_{2.5}$ concentrations during the modeling episode. Recall that CMAQ within BlueSky National is configured to separately track $PM_{2.5}$ emitted by fires from $PM_{2.5}$ resulting from anthropogenic activities. The observations show a 10-hr period starting June 27 at 1900 PST during which $PM_{2.5}$ concentrations were at or above 15 µg/m^3. During the same time period, predicted wildfire $PM_{2.5}$ concentrations are nonzero. Once the smoke plume passed though SLC, observed $PM_{2.5}$ fell below 10 µg/m^3 for the remainder of the modeling period, while predicted fire $PM_{2.5}$ dropped to and remained zero. BlueSky National captures the timing, as well as the transient nature of the smoke plume passing through SLC. However, the model underestimates the peak magnitude of the impact at Hawthorne, as the observed peak was 42 µg/m^3 while the predicted peak (fire plus anthropogenic) was 12.2 µg/m^3.

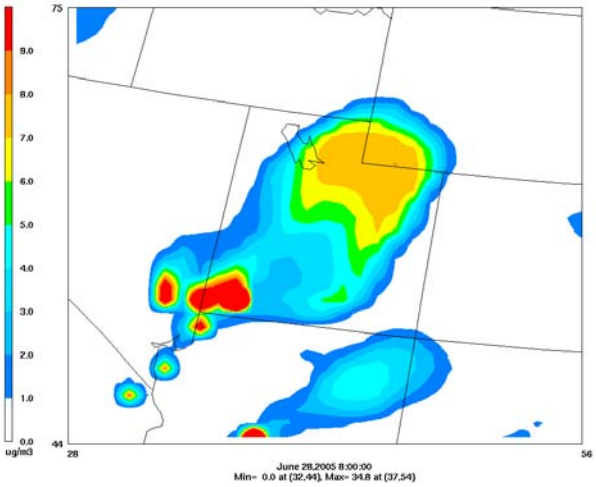

Fig. 4. Simulated ground level $PM_{2.5}$ concentration due to fires on June 28, 2005 at 0800 UTC.

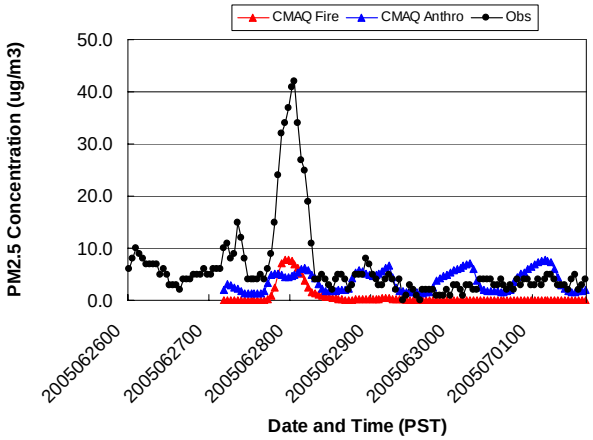

Fig. 5. Observed total $PM_{2.5}$ and predicted ground-level wildfire and anthropogenic $PM_{2.5}$ concentrations from June 26 through July 1, 2005, at Hawthorne, located in SLC.

BlueSky National predicted little or no fire $PM_{2.5}$ over the Las Vegas area. Though it is unknown how much of the observed $PM_{2.5}$ at this time was due to smoke, based on concentrations observed in subsequent days, it is reasonable to assume a minimal fire impact during this time. Therefore BlueSky National correctly predicted a minimal fire impact on Las Vegas.

During the afternoon and evening on June 28, the regional-scale wind flow shifted from southwesterly to westerly. This change in wind flow shifted the wildfire smoke plume away from SLC on June 29, and observed $PM_{2.5}$ levels dropped accordingly (Figure 6). Satellite imagery from June 29 shows a smoke plume originating from the fires and stretching eastward across northern Arizona and southern Utah, well south of SLC (Figure 2). BlueSky National also showed a plume of ground-level $PM_{2.5}$ over the same region at the same time (Figure 7). The modeled plume extends more northward into Utah than the satellite indicates, but the fire impact remains well south of SLC, as observed.

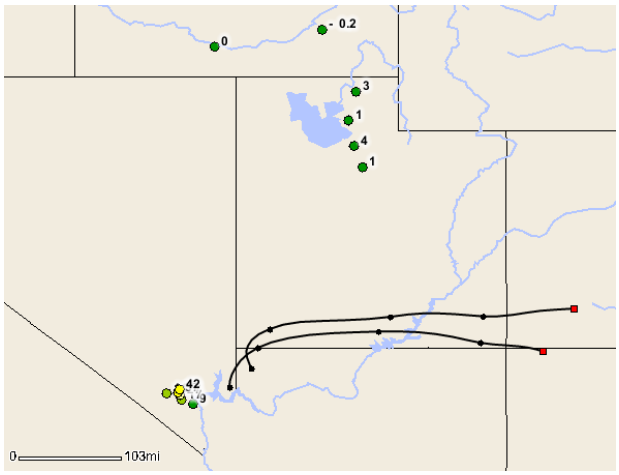

Fig. 6. Observed $PM_{2.5}$ concentrations and 24-hr HYSPLIT forward trajectories on June 29, 2005, at 1600 UTC. Trajectories originate on June 28 at 1600 UTC at 500 m agl from two of the observed fire complexes.

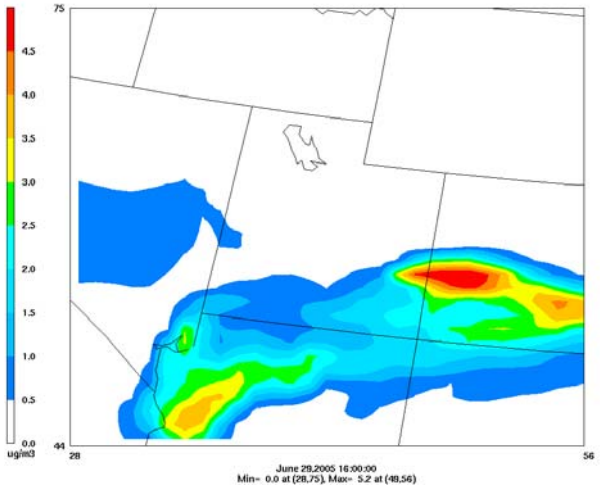

Fig. 7. Simulated ground level $PM_{2.5}$ concentration caused by fires on June 29, 2005, at 1600 UTC.

Unlike the previous day, BlueSky National incorrectly predicted a minimal fire $PM_{2.5}$ impact in Las Vegas. The satellite images show smoke persisting over Las Vegas and much of southern Nevada, and observed $PM_{2.5}$ concentrations at some Las Vegas monitoring sites exceeded 35 $\mu g/m^3$ for much of June 29; however, the western edge of the predicted smoke $PM_{2.5}$ plume remained just east of Las Vegas. On June 30, a day with weak regional surface wind flows, observed $PM_{2.5}$ concentrations remained high (peak 1-hr concentration of 85 $\mu g/m^3$). And though BlueSky National predicted a peak fire $PM_{2.5}$ concentration of 55 $\mu g/m^3$ in southern Nevada, most of the predicted $PM_{2.5}$ still remained east of Las Vegas.

4. DISCUSSION

The BlueSky National Smoke Modeling System has been described, and a test case was performed to demonstrate its performance and capabilities. The test case involved modeling $PM_{2.5}$ emissions from several wildfires in the western United States in June 2005. Smoke from these wildfires impacted SLC, which was 250 to 300 miles downwind of the fires, and Las Vegas, which was just 50 miles west of fires in southern Nevada. Satellite imagery, hourly $PM_{2.5}$ observations, and HYSPLIT trajectory analyses were used to evaluate model performance.

SLC was impacted on one day by a transient smoke plume transported from the fires by southwest winds. BlueSky National accurately depicted the timing of the smoke impact at SLC, even though the model underpredicted peak concentrations. As the smoke plume passed through SLC and the regional wind flow shifted, BlueSky National accurately depicted the shifted smoke plume and no longer predicted an impact on SLC.

Model performance was not as good near the fires themselves. During days when southwest winds were stronger, BlueSky National accurately predicted a minimal impact on $PM_{2.5}$ concentrations in Las Vegas as smoke was advected downwind. But on days when regional wind flows were light, BlueSky National did not predict a fire $PM_{2.5}$ impact on Las Vegas, while satellite imagery and hourly observations both indicated that smoke from the nearby fires was indeed impacting Las Vegas. Our findings are consistent with a previous evaluation of the

original BlueSky Framework (Raffuse et al., 2006), in which model performance degraded near fires.

The real power of BlueSky National is its ability to combine both fire and anthropogenic (primary and secondary) contributions of $PM_{2.5}$ and carry those predictions into future-day simulations. This system will provide national background $PM_{2.5}$ concentration fields that individual FCAMMS will use in their own regional high-resolution BSF3 runs. The result will be more accurate depictions of smoke impacts from wildfires and prescribed burns, and an improved smoke prediction tool for use by decision makes.

5. ACKNOWLEDGMENTS

Financial support was provided through a cooperative research agreement by the National Aeronautics and Space Administration (NASA) under the direction of Lawrence Friedl. In addition, the AirFire Team of the Pacific Northwest Research Station (Seattle, Washington), Forest Service of the U.S. Department of Agriculture, provided significant in-kind contributions under the leadership of Sim Larkin and Brian Potter. Robert Solomon from the AirFire Team provided invaluable support for the BlueSky Framework.

6. REFERENCES

Coats C.J., 1996: High performance algorithms in the sparse matrix operator kernel emissions modeling system. *Proc. Ninth Joint Conference on Applications of Air Pollution Meteorology of the American Meteorological Society and the Air and Waste Management Association, Atlanta, GA.*

E.H. Pechan & Associates, Inc., 2001: Economic Growth Analysis System: Version 4.0 Reference Manual. Emission Factor and Inventory Group, Emissions, Monitoring, and Analysis Division, Office of Air Quality Planning and Standards, U.S. Environmental Protection Agency, Research Triangle Park, NC.

Grell G.A., J. Dudhia, and D.R. Stauffer, 1994: A description of the fifth-generation Penn State/NCAR mesoscale model (MM5). National Center for Atmospheric Research, Boulder, CO, Tech. Note NCAR/TN-398.

Houyoux M.R. and J.M. Vukovich, 1999: Updates to the Sparse Matrix Operator Kernel Emissions (SMOKE) modeling system and integration with Models-3. *Air & Waste Management Association's The Emission Inventory: Regional Strategies for the Future, Raleigh, NC, October 26-28*.

——, and Z. Adelman, 2001: Quality assurance enhancements to the SMOKE Modeling System. *U.S. Environmental Protection Agency's International Emission Inventory Conference: One Atmosphere, One Inventory, Many Challenges, Denver, CO, May 1-3*.

——, J. Vukovich, and J. Brandmeyer, (2000) Sparse Matrix Operator Kernel Emissions Modeling System (SMOKE) user manual. MCNC-North Carolina Supercomputing Center, Environmental Programs, Research Triangle Park, NC.

Larkin N.K., S.M. O'Neill, R. Solomon, C. Krull, S. Raffuse, M. Rorig, J. Peterson, and S.A. Ferguson, 2007: The BlueSky smoke modeling framework. (Submitted).

National Exposure Research Laboratory, 1999: Science algorithms of the EPA Models-3 Community Multiscale Air Quality (CMAQ) modeling system. National Exposure Research Laboratory, Research Triangle Park, NC, EPA/600/R-99/030 (peer reviewed), March.

Raffuse S., L. Chinkin, D. Sullivan, and N. Larkin, 2006: Applications of a GIS-based fire emissions model - or - BlueSky SMARTFIRE. *Third International Fire Ecology & Management Congress, San Diego, CA, November 18*.

Scire J.S., D.G. Strimaitis, and R.J. Yamartino, 2000: A user's guide for the CALPUFF dispersion model, version 5. Earth Tech, Inc., Concord, MA, January.

U.S. Environmental Protection Agency, 1998: EPA third-generation air quality modeling system, Models-3, Volume 9B: user manual. National Exposure Research Laboratory, Office of Research and Development, U.S. Environmental Protection Agency, Research Triangle Park, NC, EPA-600/R-98/069(a).

U.S. Environmental Protection Agency, 2006: 2002 National Emissions Inventory data & documentation [updated August 2, 2007]. [Available online at <http://www.epa.gov/ttn/chief/net/2002inventory.html>.

VERIFICATION OF NOAA-EPA DEVELOPMENTAL AEROSOL FORECASTS

Jerry Gorline[1] and Pius Lee[2]
[1]Meteorological Development Laboratory
National Weather Service, NOAA
Silver Spring, Maryland
[2]Scientific Applications International Corporation
Beltsville, Maryland

1. INTRODUCTION

Since July 2006, the Meteorological Development Laboratory (MDL) has provided categorical verification metrics for aerosol forecasts. The Air Quality Forecasting (AQF) system links the National Centers for Environmental Prediction's (NCEP) North American Mesoscale (NAM) model with EPA's Community Multiscale Air Quality (CMAQ) modeling system to produce gridded 1-h ground-level aerosol predictions for the developmental (5x) conterminous U.S. (CONUS) domain (Binkowski and Roselle 2003). We used bilinear interpolation to calculate predicted daily maximum values at the locations of the observation sites. We compared these interpolated predicted values to the observed daily maximum to produce 2x2 contingency tables, with a threshold of 40 μgm/m^3. Our verification metrics included Percent Correct (PC), Threat Score (TS) or Critical Success Index (CSI), Probability of Detection (POD), and the False Alarm Rate (FAR). We populated two-by-two contingency tables as follows:

	Observed
Forecast	| a | b |
	| c | d |

where, a = forecast, observed (yes/yes)
b = forecast, no observed (yes/no)
c = no forecast, observed (no/yes)
d = no forecast, no observed (no/no).

The corresponding scores were computed as follows:

$$PC = (a + d)/(a + b + c + d) \quad (1)$$
$$TS = a/(a + b + c) \quad (2)$$
$$POD = a/(a + c) \quad (3)$$
$$FAR = b/(a + b) \quad (4).$$

For a more detailed discussion about 2x2 contingency table analyses, see Wilks (1995).

We computed weekly statistics displayed in the form of bar charts, scatterplots, and graphs. Spatial maps showed daily maximum predicted aerosol values overlaid with the corresponding point observations.

In this paper we describe how the CMAQ model was configured to handle aerosol predictions. We evaluated the daily maximum of 1-h average predictions over the CONUS and over six sub-CONUS regions. We also provide verification results of the daily maximum of the 24-h running average over the CONUS.

2. AEROSOLS

CMAQ's aerosol module takes a modal approach to represent the particles suspended in air (Binkowski and Roselle, 2003 and Mebust et al., 2003). The module uses the superposition of 3 log-normal sub-distributions to represent the size distribution of these particles. Aerosols are represented by two of these sub-distributions called the Aitken (i) particles with diameters up to 0.1 μm, and the accumulation (j) particles with diameters between 0.1 and 2.5 μm. The third modal sub-distribution represents particles of the coarse mode, particles with diameters between 2.5 to 10 μm. Table 1 shows the types of the particles in the i- and j-modes. The i-mode particles usually represent particles freshly formed from nucleation or from direct emission, whereas the larger j-mode particles represent aged particles.

The model approach treats the interaction between the fine modes and the coarse mode as follows. When the fine mode particles grow beyond 2.5 μm in diameter, they are merged into the coarse mode. But once the fine mode particles are merged into the coarse mode, they can not go back to the fine modes again. In the CMAQ model, there

[1]*Corresponding author:* Jerry L. Gorline, Meteorological Development Laboratory, NWS, 1325 East West Highway, Silver Spring, MD. 20910; fax: 301-713-9316; phone: 301-713-1768; e-mail: jerry.gorline@noaa.gov

is no mechanism for fine particles to coagulate with coarse particles nor is there a mechanism for fine particles to be transferred to the coarse mode via condensational growth. These processes are thought to be of minor importance.

Table 1. Speciation and variable name used in the CMAQ aerosol module.

Species description	Name
Accumulation mode sulfate mass	ASO4J
Aitken mode sulfate mass	ASO4I
Accumulation mode ammonium mass	ANH4J
Aitken mode ammonium mass	ANH4I
Accumulation mode nitrate mass	ANO3J
Aitken mode nitrate mass	ANO3I
Accumulation mode anthropogenic secondary organic mass	AORGAJ
Aitken mode anthropogenic secondary organic mass	AORGAI
Accumulation mode primary organic mass	AORGPAJ
Aitken mode primary organic mass	AORGPAI
Accumulation mode secondary biogenic organic mass	AORGBJ
Aitken mode secondary biogenic organic mass	AORGBI
Accumulation mode elemental carbon mass	ACEJ
Aitken mode elemental carbon mass	ACEI
Accumulation mode unspecified anthropogenic mass	A25J
Aitken mode unspecified anthropogenic mass	A25I
Accumulation mode water mass	AH2OJ
Aitken mode water mass	AH2OI

Justification of such a simplification is discussed in Binkowski and Roselle (2003). The coarse mode modeling has not been emphasized due to the large uncertainty in the determination of its emissions. By the same token, the current CMAQ model does not include coarse mode particles in its visual range calculations. The fine mode particles also participate in cloud micro-physics. The assumptions of the CMAQ aerosol module in relation to cloud activity are: (1) the i-mode particles form the aerosols subjected to in-cloud scavenging, (2) the j-mode particles form cloud condensation nuclei which are subjected to redistribution within the cloud water, (3) all new sulfate mass produced by aqueous phase production is added to the j-mode, (4) the shape of the j-mode size distribution, quantified by the geometric standard deviation σ_g, stays constant throughout a cloud's lifetime, and (5) the i-mode and j-mode particles are wet removed in proportion to that of sulfate wet scavenging.

In the aerosol module, the sulfate, nitrate, ammonium, and water system is considered to be in equilibrium. This assumption is used due to the large uncertainty about the sea salt and soil particle data to validate a more vigorous methodology.

For the purpose of comparing modeled values to observed (2.5 μm) mass, predicted (2.5 μm) mass is derived by summing the masses of the species from Table 1. Here, (2.5 μm) is defined as particulate matter with diameter less than or equal to 2.5 μm. Particle bound water (i.e., AH2OI and AH2OJ) is excluded from this derivation of predicted (2.5 μm) mass.

3. AEROSOL VERIFICATION FOR CONUS

During 2007, MDL generated categorical verification metrics for the CONUS developmental (5x) domain. All daily maxima of 1-h average aerosol predictions or observations that were equal to or greater than the threshold during a predefined 24-h period were counted as exceedances. The 24-h window for counting exceedances was midnight to midnight, beginning at hour 22 for the 0600 UTC CMAQ forecast period. The EPA provided ozone observations for 661 sites within the CONUS domain. If an observation or interpolated model prediction for a station was missing, we excluded that station from our calculations.

Fig. 1 shows a comparison of the percent correct of the daily maximum of 1-h average predictions (in blue) and the daily number of observed exceedances (in red), for May 29–August 30, 2007. There were several drops below 80%. Comparing the two plots in Fig. 1, we can see that decreases in the percent correct were associated with elevated aerosol episodes. There were six days in the sample period where 100 or more observed exceedances occurred, namely, June 1, June 18, June 26, July 4, August 3, and August 16. On these days, the percent correct dropped below 80%. During elevated aerosol episodes, there is

greater potential for false alarms and missed exceedance predictions.

Fig. 2 is a map of aerosol predictions and observations, for the daily maximum of the 1-h average for August 3, 2007. The predicted exceedances are shown in dark blue and the observed exceedances as red points. Table 2 shows monthly scores derived from contingency tables for March–August, 2007. The total number of cases for May was below 10,000 because observations were missing for May 20–28, 2007.

4. REGIONAL AEROSOL VERIFICATION

Fig. 3 shows a map of the CONUS broken into six regions (Mathur, 2006). This map was previously used for regional analyses of CMAQ ozone predictions. We evaluated the CMAQ aerosol forecasts for these six regions. We compared monthly verification results for the Pacific Coast (PC), Rocky Mountains (RM), Lower Midwest (LM), Upper Midwest (UM), South East (SE), and Northeast (NE). Fig. 4 shows the monthly TS for the six regions for March–August, 2007. The Pacific Coast (PC) had the highest TS in June but it dropped in August because of a high FAR. Table 3 shows the regional contingency table for June, 2007. The CMAQ model seemed to handle the aerosol activity in the PC region better than in the other regions. Fig. 5 shows a scatterplot for the PC region for June, 2007. Vertical and horizontal pink lines at 40 $\mu gm/m^3$ split the scatterplot into four quadrants. Under-forecasts of exceedance predictions are shown in the upper left quadrant. Over-forecasts are shown in the lower right quadrant. Except for a cluster of under-forecasts for predictions < 15 $\mu gm/m^3$, the model showed some degree of skill. There were a few more over-forecasts of predictions > 40 $\mu gm/m^3$, than under-forecasts.

5. DAILY MAXIMUM OF 24-H RUNNING AVERAGE

MDL used one hour average model predictions to produce spatial maps of the daily maximum of the 24-h running average. We evaluated these model predictions by generating 24-h running averages from the 1-h average observations provided by the EPA. We produced 2x2 contingency tables using a threshold of 40 $\mu gm/m^3$.

Fig. 6 shows a comparison of the percent correct of the daily maximum of the 24-h running average predictions (in blue) and the daily number of observed exceedances (in red), for June 2-August 30, 2007. Notice that there are fewer observed exceedances in Fig. 6 than Fig. 1. Fig. 6 shows similar behavior to Fig. 1, decreases in the percent correct were associated with elevated aerosol episodes. We can see that except for August 5 (percent correct = 89.4), the percent correct of the daily maximum of the 24-h running average predictions stayed above 90% for the entire period. The daily maximum of the 24-h running average predictions had better percent correct scores than the daily maximum of the 1-h average because the 24-h running average predictions contained much fewer observed threshold exceedances than the 1-h average predictions. MDL also produced spatial maps of the daily maximum of the 24-h running average, which are not shown because of space constraints.

6. CONCLUSIONS

The CMAQ model was configured to produce gridded 1-h ground-level aerosol predictions for the 5x CONUS domain. MDL computed verification metrics of the daily maximum of the 1-h aerosol predictions over the CONUS as well as for six regions. MDL derived the daily maximum of the 24-h running average predictions from 1-h aerosol predictions over the CONUS domain. We evaluated these predictions by deriving 24-h running averages from the 1-h average observations provided by the EPA. State and local authorities are interested in the 1-h average aerosol predictions and the 24-h running average predictions. Daily maps of the 1-h average and 24-h running average were provided to aid the modelers in their development. The maps showed where missed exceedance predictions were located. This information was useful for investigating systematic under prediction or over prediction issues in selected geographic areas.

7. ACKNOWLEDGMENTS

This paper was prepared in cooperation with development activities carried out under the auspices of the NWS National Air Quality Forecast Capability. We would like to thank NCEP for providing the surface aerosol concentration forecasts and the EPA for providing the associated verifying observations. Thanks to Rohit Mather, from NOAA/EPA, Research Triangle Park, North Carolina, for providing the map used for our aerosol regional analyses. Thank you Valery Dagostaro, MDL, for guidance in modification of the software for the 24-h running average verification.

8. REFERENCES

Binkowski, F. S. and S. J. Roselle, 2003: Models-3 Community Multiscale Air Quality (CMAQ) model aerosol component: 1: Model description, *J. Geophys. Res*., 108(D6), 4183, doi:10.1029/2001JD001409, 2003.

Mathur, R., NOAA Air Quality Forecasting Focus Group, 2006 (personal communication).

Mebust, M. R., B. K. Eder, F. S. Binkowski and S. J. Roselle, 2003: Models-3 Community Multiscale Air Quality (CMAQ) model aerosol component: 2: Model evaluation, *J. Geophys. Res*., 108(D6), 4184, doi:10.1029/2001JD001410, 2003.

Wilks, D. S., 1995: *Statistical Methods in the Atmosphic Sciences: An Introduction.* Academic Press, 238 – 241.

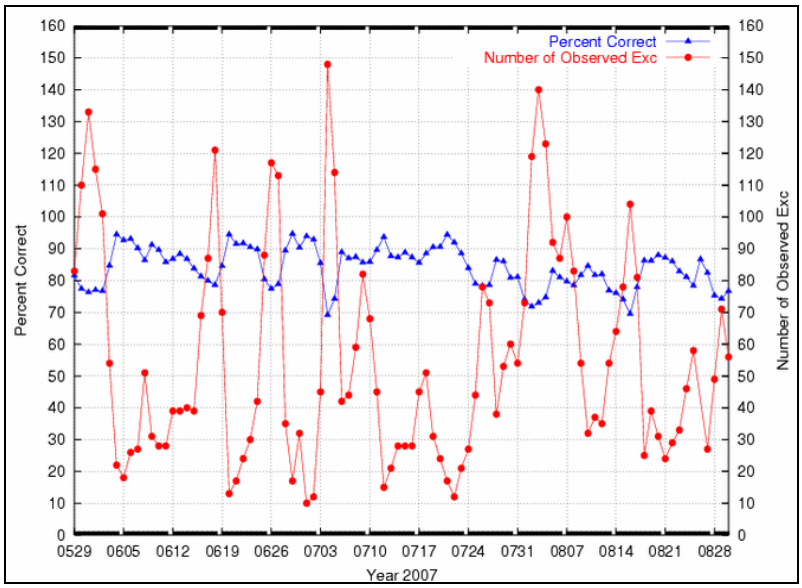

Figure 1. Percent correct vs. number of observed exceedances, daily maximum of 1-h average aerosol predictions, May 29–Aug 30, 2007.

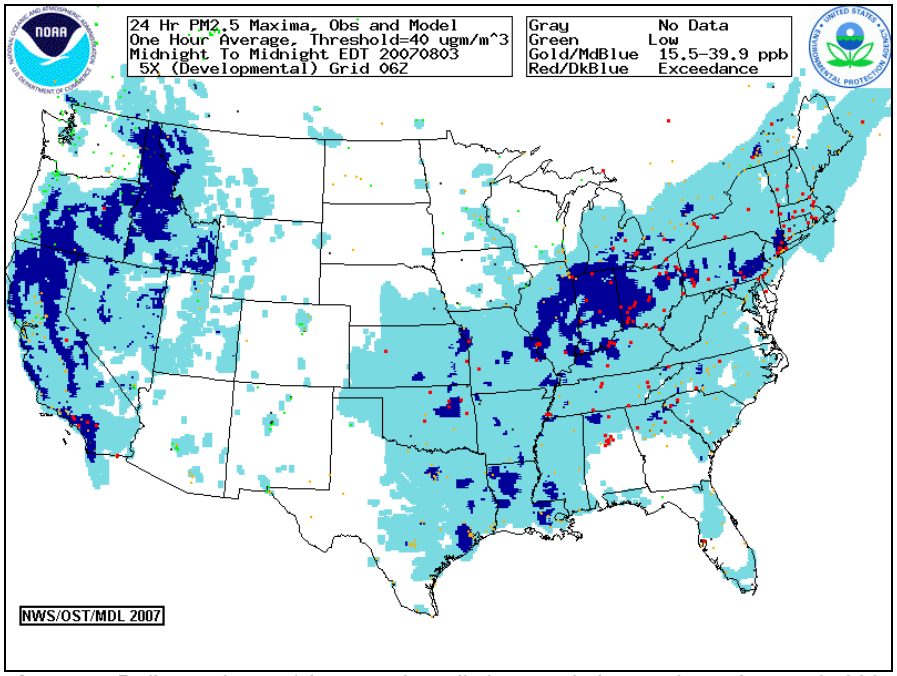

Figure 2. Daily maximum 1-h aerosol predictions and observations, August 3, 2007.

Table 2. Contingency table results for CONUS, 2007, daily maximum of 1-h average aerosol predictions.

SCORE	March	April	May	June	July	August
a	247	79	147	347	309	524
b	542	358	431	761	1019	1686
c	862	469	701	1081	1098	1318
d	12430	13006	8575	12285	12547	11264
PC	0.900	0.941	0.885	0.873	0.859	0.797
TS	0.150	0.087	0.115	0.159	0.127	0.149
POD	0.223	0.144	0.173	0.243	0.220	0.284
FAR	0.687	0.819	0.746	0.687	0.767	0.763

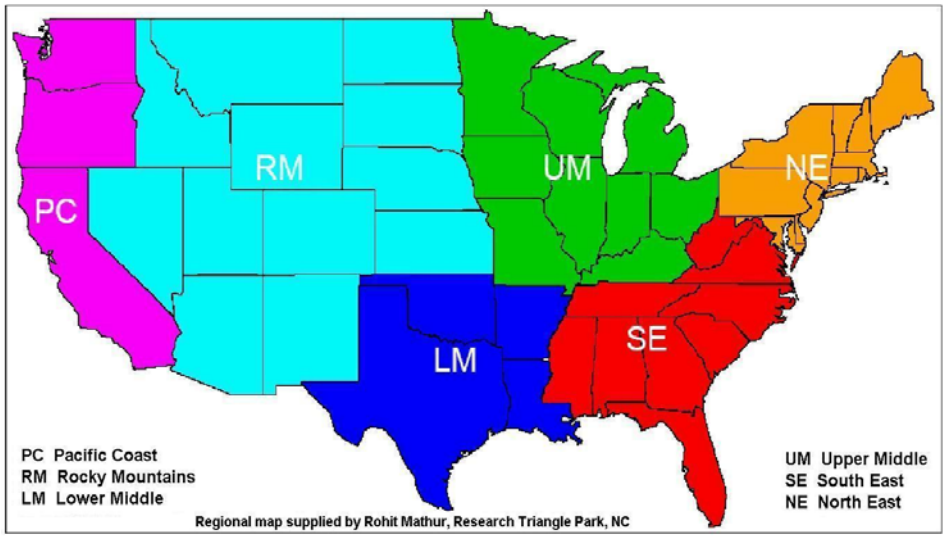

Figure 3. Map of the U.S. showing six regions, Pacific Coast (PC), Rocky Mountains (RM), Lower Midwest (LM), Upper Midwest (UM), South East (SE), and Northeast (NE).

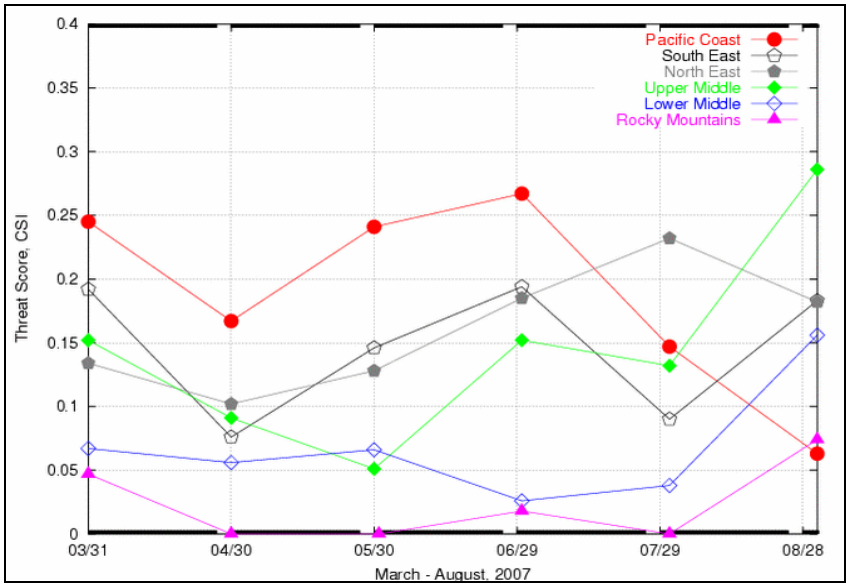

Figure 4. , Monthly average, threat score for the six regions, Mar–Aug, 2007.

Table 3. Regional contingency table results, June, 2007, daily maximum of 1-h average predictions.

SCORE	CONUS	LM	NE	PC	RM	SE	UM
a	347	4	89	52	3	95	75
b	761	104	105	68	98	194	90
c	1081	44	286	75	68	201	329
d	12285	1407	1361	2300	1390	1644	2181
PC	0.873	0.905	0.788	0.943	0.894	0.815	0.843
TS	0.159	0.026	0.185	0.267	0.018	0.194	0.152
POD	0.243	0.083	0.237	0.409	0.042	0.321	0.186
FAR	0.687	0.963	0.541	0.567	0.970	0.671	0.545

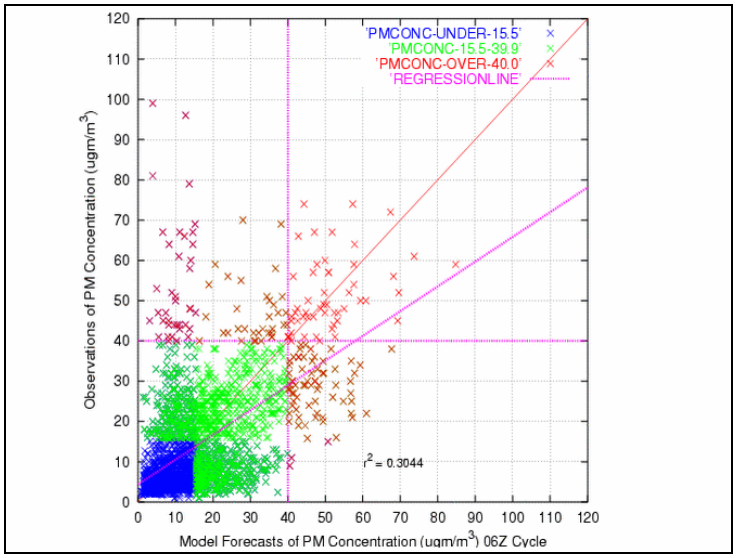

Figure 5. Scatterplot for Pacific Coast (PC) region, June, 2007, daily maximum of 1-h average predictions.

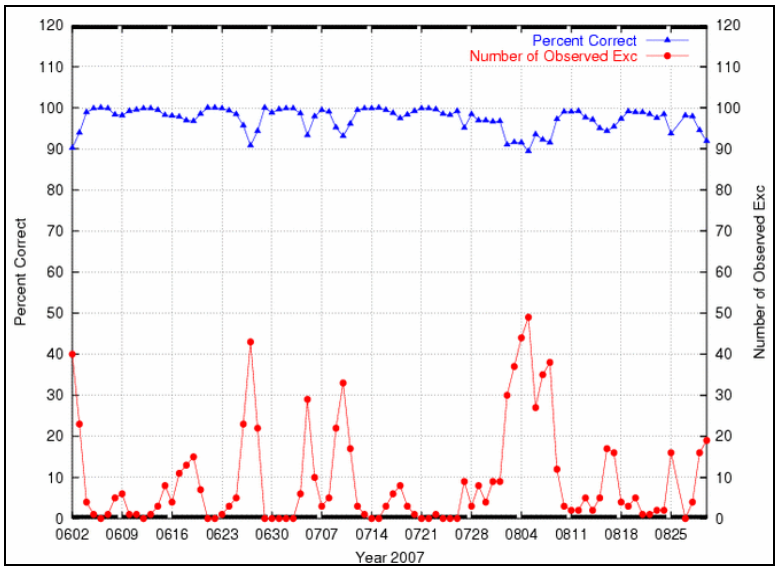

Figure 6. Percent correct vs. observed exceedances, daily maximum of 24-h running average aerosol predictions, Jun 2–Aug 30, 2007.

Forecasting the Impacts of Wildland Fires

Yongtao Hu*[1], M. Talat Odman[1], William Jackson[2], Armistead G. Russell[1]
[1]School of Civil and Environmental Engineering, Georgia Institute of Technology
[2]USDA Forest Service, Asheville, North Carolina 28801
e-mail: **yh29@mail.gatech.edu**
Telephone (404) 894-1854 Fax (404) 894-8266

We utilize Hi-Res, a regional forecasting system which provides local air quality forecasts for the metro Atlanta area since 2006, to predict the air quality impacts from wildland fires. As extensions to the Hi-Res system, the Consume and FEPS models are used to estimate the fire emissions from potential fire events. Brute-force or DDM methods are used to calculate the air quality contributions from the fires. We have tested this tool to predict air quality impacts from Jasper County prescribed fires on February 28, 2007 and the Georgia-Florida wildfires which occurred during April-May, 2007.

1. INTRODUCTION

Wildland fires (wild and prescribed fires) burned about 9 million acres nationwide in the United States each year on average during the last three years. Burning of wildland vegetation increases the emissions of air pollutants such as fine particulate matter ($PM_{2.5}$), carbon monoxide (CO), volatile organic compounds (VOC) and nitrogen oxides (NO_x), which impact air quality, visibility and potentially public health. Especially, a severe wildland fire such as the prescribed fires on February 28, 2007 in Jasper County Georgia and later the Georgia-Florida wildfires lasting from April through May that hit Atlanta metro area with thick smoke clouds, could cause rapid increases of both ozone (O_3) and $PM_{2.5}$ to extremely high levels and cause exposure of urban population to unhealthy air for hours or even days sometimes.

Of interest is to what degree the air quality impacts from wildland fires can be forecast. For prescribed burning, the air quality forecast ahead of the actual igniting would help plan and conduct burns; for wildfires, the air quality forecast would warn people to avoid unhealthy air exposures.

Here we develop a fire-impacts forecasting system based on the Hi-Res air quality forecast framework which is serving the Atlanta metro area since 2006. We then apply this fire-impacts forecast tool to predict the February 28, 2007 prescribed fire event as well as another smoke event caused by the Georgia-Florida wildfires that hit Atlanta metro area on May 22, 2007. The forecast of the occurrence of wildfire is not intended here.

Fig. 1 Hi-Res modeling domains and Atlanta metro area.

2. THE FORECASTING SYSTEM

2.1 Hi-Res

We utilize the framework of Hi-Res to forecast fire-impacts on air quality. Hi-Res uses the Weather Research and Forecasting model (WRF, version 2.2) for forecasting meteorology (wrf-model.org), the Sparse Matrix Operator Kernel Emissions model (SMOKE, version 2.1) for emissions and the Community Multiscale Air Quality model (CMAQ, version 4.6) for chemistry and transport updated with strict mass conservation and equipped with the SAPRC-99 chemical mechanism. Hi-Res nests its 4-km forecasting grid in a 12-km mother grid covering Georgia and portions of neighboring states and uses a 36-km outer grid over the eastern U.S. to provide air quality boundary conditions (Figure 1). Hi-Res first simulates a 77-h (3 days plus 5 hours) period starting from 00Z on the 36-km grid. WRF is initialized and constrained at the boundaries using 00Z 84-h forecast products from the North American Mesoscale (NAM)

- *Corresponding author:* Yongtao Hu, 311 Ferst Drive, Atlanta, GA, 30332-0512

model (nomads.ncdc.noaa.gov) and CMAQ is initialized from the previous forecasting cycle and uses "clean" boundary conditions. Then Hi-Res simulates the same 77-h period on the 12-km grid and nests down to the 4-km grid for the last 32 hours. This time WRF is initialized and constrained at the boundaries also using 00Z NAM forecasts, while CMAQ is initialized from the previous forecasting cycle and uses the 36-km forecasts for air quality boundary conditions. The simulations take about 12 hours on 6 dedicated CPUs. The Hi-Res forecast cycle (Fig. 2) allows sufficient time for extra efforts on fire-impacts forecast. "Background" fire emissions' impacts are included in Hi-Res' everyday forecasts by utilizing averaged historical fire events to represent typical fire emissions driving a forecasting day, in essence smoothing individual, more intense events both spatially and temporally. Like other air quality forecasting systems currently operational in the United States at either national or regional levels, Hi-Res has enjoyed reasonable forecasting accuracy.

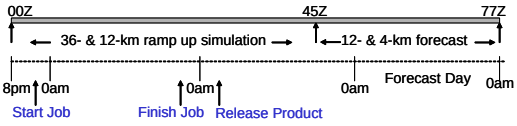

Fig. 2 The Hi-Res cycle.

2.2 Estimating Potential Fire Emissions and Calculating Air Quality Contribution

The extra efforts for fire-impacts forecast beyond the current Hi-Res framework are mainly first the emissions estimation of the potential fires and second the calculation of these emissions' contribution to the air quality.

For potential prescribed fires we estimate the emissions using information collected from the burning plans prepared in advance by the technical staff of wildland owner. Pre-burning information includes the acreage of the planned burning area, approximate locations, fuel load descriptions and operation schedules. We estimate the potential fuel consumption by using the Consume model version 3.0 (http://www.fs.fed.us/pnw/fera/research/smoke/consume/index.shtml). Since there is a lack of information for separating flaming and smoldering stages during the estimation of emissions, we use fuel consumption, emission factors and a temporal profile that merge the two stages together. We calculate emissions using the Fire Emission Production Simulator (FEPS) for each criteria pollutant and allocate them to the 12- and 4-km grid cells according to the approximate fire locations. Vertical distribution of fire emissions are based on the FEPS' typical plume rise calculated for a fair day in the season by using default fire temperature information. Gridded fire emissions are then added to other emissions for the Hi-Res standard forecast.

For existing/ongoing wildfire we forecast the potential impacts from continuing fires for the following days. We first determine the most likely fire locations on the following days according to the analysis of forecast meteorological conditions combined with the information on previous days' burning locations. We then estimate and collect other fire information including approximate acreage of burning area, fuel load and fire temperatures, and calculate the wildfire emissions through the same procedures as stated above for prescribed fires.

There are two ways to calculate the fire emission's contributions to the air quality. When there are only a couple of potential fires we choose the brute-force method, i.e., we first run Hi-Res at its standard configuration with "typical" emissions, then re-run Hi-Res' CMAQ only on the 12- and 4-km grids with the emissions from the potential wildland fires added in. The difference between simulated air quality fields from the above two Hi-Res runs is the contribution of the potential fire emissions. When there are multiple potential fires, as would be the case particularly in prescribed burning applications, a more efficient way to estimate contribution from each individual fire is by calculating emission sensitivities using Decoupled Direct Method (DDM) with the Hi-Res system. For this kind of application, the Hi-Res system is required to run only once with wildland fires' emissions added on top of the Hi-Res "typical" emissions.

We extend the function of this fire-impacts forecast system to estimate the total population of potential polluted air exposures, which is calculated by adding up the population (Census 2000, www.census.gov) living in the grid cell that has a predicted ambient $PM_{2.5}$ concentration higher than 35μg m^{-3}, the current 24-hr National Ambient Air Quality Standard (NAAQS), during the potential fire event when the fire emissions are added in.

3. APPLICATION AND RESULTS

3.1 The February 28, 2007 Prescribed Fire

On February 28 2007, thick smoke hit the Atlanta, Georgia metro area. Within a couple of hours, starting around 4 p.m., monitored hourly concentration of $PM_{2.5}$ soared up to almost 150 μg m^{-3} at several sites. Ultimately the monitored 24-hr concentration (midnight to midnight) of $PM_{2.5}$ in Atlanta, i.e. 37.8 μg m^{-3}, exceeded the NAAQS of 35 μg m^{-3}. At the same time, hourly O_3 concentrations jumped by up to 30 ppb. Two prescribed fires in adjacent wildlands about 80 km southeast, one in the Oconee National Forest (Oconee NF) and the other in the Piedmont National Wildlife Refuge (Piedmont NWR) (called Fire O and P hereafter, Figure 3), together totaling about 12 km^2, were blamed for "smoking out" metro Atlanta at the time "commuters headed home and ball teams took to the fields". Asthma attacks, apparently triggered by the smoke or ozone, were reported by asthmatics that were able to self-medicate, as well as pediatric clinics that were receiving pulmonary patients the next day.

Fig.3 Smoke detected near the Atlanta metro area at 1:15 and 1:45 pm Eastern Standard Time (EST) on February 28th, 2007 by using the Geostationary Satellite (GOES) data (received from National Oceanic and Atmospheric Administration), which originated from the prescribed fires within the Oconee NF and Piedmont NWR.

To test our fire-impact forecast system we apply the system at its forecast mode to simulate the air quality impacts from Fires O and P together. Emissions are estimated (Table 1) using information collected from the prescribed fire plans prepared in advance by the technical staff on the Oconee NF and Piedmont NWR. We first run Hi-Res starting from February 26th 00Z through March 1st 05Z at Hi-Res standard configuration with "typical" emissions, then re-run Hi-Res' CMAQ only for the last 32 hours on the 12- and 4-km grids with the emissions from Fires O and P added in. This second run takes an extra 2.5-h simulation time. To further assess the predictive capability of this system on specific fire-impacts and identify key weaknesses we also conducted a hindcast of this prescribed-fire-caused smoke event. At hindcast mode, reanalysis products from NAM are utilized to initialize WRF, constrain boundary conditions and nudge simulated fields at 6-h intervals. The Fires O and P emissions are re-estimated (Table 1) using actual and extra information collected and prepared after the burns, including the actual acreage burned each hour, fuel moisture information, fuel consumption information and hourly flaming/smoldering stage information, plus local meteorology and fire temperature information for estimating hourly plume rise. In addition, sensitivity tests found increased VOC emissions from trees due to exposure to fire and its elevated temperatures that is recommended to be included in the future forecasting of fire caused photochemical smoke events, as well as current inventories (Hu et.al 2007).

Table 1 Fires O and P estimated emissions (10^6g)

Pollutants		CO	VOC	NO_x	NH_3	SO_2	$PM_{2.5}$	PMC
Forecast Fire O		877	41.2	18.9	4.1	5.2	73.2	12.2
Forecast Fire P		708	37.6	17.2	3.7	4.8	66.8	11.1
Hindcast Fire O	Flaming	586	34.1*	30.2	1.4	0.3	48.0	8.6
	Smoldering	737	58.1*	5.8	2.6	0.5	57.5	10.4
Hindcast Fire P	Flaming	109	6.3*	5.6	0.3	0.1	8.9	1.6
	Smoldering	343	27.0*	2.7	1.2	0.2	26.8	4.8

* Biogenic emissions from pine needles induced by fire are not included in the totals. Sensitivity tests suggest the enhanced VOC emissions amount to about 368 and 133 × 10^6g for Fires O and P, respectively.

Our "forecast" simulated that Fires O and P scheduled on February 28, 2007 together significantly impacted air quality of Atlanta lasting from late afternoon through midnight. The fire impact reached its maximum between 10:00 and 11:00 p.m., when over 1 million Atlantans were estimated to have potential 1-hr exposures to 35 μg m^{-3} or higher $PM_{2.5}$ concentrations (the current 24-hr NAQQS). The maximum predicted increase was 94 μg m^{-3} in the Atlanta urban area (defined as having a population density higher than 5,000 per square mile [www.census.gov]), driving up ambient $PM_{2.5}$ concentrations to a peak of 121 μg m^{-3} between 8:00-9:00 p.m. (Fig. 4a). While the highest observed 1-h concentration was 152μg m^{-3}. Albeit large numbers of population with potentially unhealthy 1-h $PM_{2.5}$ exposures, our "forecast" simulated

that only 380 thousand Atlantans were having potential 24-hr exposures to 35 μg m^{-3} or higher $PM_{2.5}$ concentrations on February 28th, 2007. The simulated maximum 24-hr $PM_{2.5}$ concentration in Atlanta urban area is 47.5 μg m^{-3} compared to the observed 37.8 μg m^{-3}.

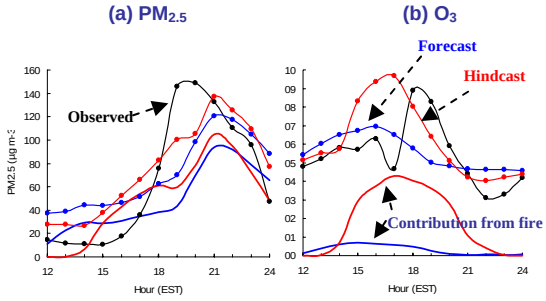

Fig.4 Predicted maximum ambient $PM_{2.5}$ (a) and O_3 (b) concentrations and maximum Fires O and P contributions within the Atlanta urban area versus observed maximum among the Atlanta urban sites.

With extra historic information and the enhanced biogenic emissions, our hindcast simulated more Atlantans would be potentially impacted by the fires. The fire impact reached its maximum between 7:00-8:00 p.m., when population of potential 1-hr exposure to $PM_{2.5}$ levels greater than 35 μg m^{-3} would increase to 1.8 million. This predicted peaking time (three hours earlier than the "forecast" prediction) is consistent with the peak $PM_{2.5}$ observations (Fig. 4a). The hourly burning information collected after the fire significantly improves timing. Note that the hindcast reproduces the "forecast" $PM_{2.5}$ peaking time, i.e. between 8:00-9:00 p.m. and 1-hr later than the measurements, but predicts the peak value at 137μg m^{-3}. In contrast to the "forecast" which doesn't include the enhanced VOC emissions, hindcast results capture the observed O_3 increases very well (Fig. 4b). The hindcast predicts a maximum jump in O_3 concentration of 40 ppb in the urban area due to the enhanced biogenic VOC emissions. The hindcast results also improve significantly in terms of Organic Matter (OM). The increased predicted OM drives the $PM_{2.5}$ prediction up to over 100 μg m^{-3} between 6:00-7:00 p.m., compared to around 70μg m^{-3} predicted by the forecast at that time (Fig. 4a). We also plot the spatial distribution of the "forecast" and the hindcast $PM_{2.5}$ plumes along with peak observations, which suggest a spatial extent for the observed plume (not shown). We calculated that there is about a 20 degree prediction error of the $PM_{2.5}$ plume direction in the "forecast" while a 10 degree error remains in the hindcast. This suggests that reanalysis data utilized with nudging technology improved simulated surface wind fields, though to a limited degree.

3.2 The Georgia-Florida Wildfire: First Attempt

The Georgia-Florida wildfires (G-F fires) started on April 16, 2007, burned about half million acres through the end of May, and continued to burn into the first week of June. The G-F fires have caused dozens of hazy days in Atlanta, GA, Miami, FL and Birmingham, AL. We apply the forecast system to simulate the May 18 -23, episode, during which the wildfire plume hit Atlanta, GA and surrounding areas with records high 24-hr $PM_{2.5}$ concentration of 76 μg m^{-3} and 1-hr $PM_{2.5}$ concentration of 365 μg m^{-3}.

A wildfire could burn much larger area of wild land, cause much higher increases of temperature and last for much longer time period, compared to a prescribed fire which is under control to burn the forest floor only. Because of these features that complicate the growth and movement of wildfire plume, there are large uncertainties in prediction of wildfire impacts. Our first attempt to simulate G-F fires totally missed the plume reaching Atlanta which according to satellite imagery occurred through long-range transport through Alabama under easterly winds on the previous day that turned to westerly on the day of the event (not shown). The possible reasons could be the missing of the surface thermal changes caused by the fire from the meteorological model, the coarse vertical resolution above 1-km from the ground in CMAQ.

4. CONCLUSIONS

We have developed and tested a modeling framework to forecast fire-impacts on air quality in Atlanta, Georgia. Application of the tool to the prescribed fires on February 28, 2007 was successful and indicates that the wildland fires could be reasonably well estimated using the system. The "forecast" predictions are in good agreement with $PM_{2.5}$ observations, though with extra historic information, the hindcast improves the predictions significantly on timing and location, and slightly on peak level. However, more efforts are needed to improve the capability of the system to simulate wildfires.

5. REFERENCES

Byun, D. W.; Ching, J. K. S., Science algorithms of the EPA Models-3 Community Multiscale Air Quality (CMAQ) Modeling System, pp, Publisher, 1999.

CEP, Sparse Matrix Operator Kernel Emissions Modeling System (SMOKE) User Manual; Carolina Environmental Program - The University of North Carolina at Chapel Hill, Chapel Hill, NC, 2003.

Hu, Y. et. al., Simulation of Air Quality Impacts from Prescribed Fire on an Urban Area: Analysis of the February 28th, 2007 Episode, Submitted to Environmental Science & Technology 2007

Odman, M. T.; Hu, Y.; Chang, M. E.; Russell, A. G. Forecasting ozone and PM2.5 in southeastern U.S. In Developments in Environmental Science, Volume 6; Borrego, C., Renner, E., Eds.; Elsevier Ltd., 2007; pp 219-288.

A CORRECTION TO MCIP CALCULATION OF VERTICAL CONTRAVARIANT VELOCITY OF NON-HYDROSTATIC MM5 IN MCIP AND ITS IMPACT ON AIR QUALITY SIMULATION

Fuquan Yang*, Jack Chen, Weimin Jiang, Helmut Roth, Steven C. Smyth,
Institute for Chemical Process and Environment Technology, National Research Council of Canada, Ottawa, Ontario, Canada

1. INTRODUCTION

The contravariant vertical velocity used in the Community Multi-scale Air Quality (CMAQ) Model is calculated by the Meteorology-Chemistry Interface Processor (MCIP). It is a key parameter in controlling vertical advection and describing the static stability of atmosphere. Large errors in the vertical wind can significantly deteriorate the consistency between the air density and wind fields. Such consistency is a fundamental requirement to ensure mass consistency in air quality modeling studies (Byun, 1999).

Recently, we found an error in MCIP (version 3.2 and its earlier versions) in the computation of the contravariant vertical wind velocity. Instead of using the surface reference state pressure, the total surface pressure from the first time period processed by MCIP was mistakenly used in the calculation of contravariant vertical velocity.

The error led to unphysical contravariant vertical wind fields, caused exaggerated perception of air mass inconsistency within the non-hydrostatic MM5 meteorological model outputs, and affected the advection scheme analysis. After the error was reported, it was subsequently corrected in the current release of MCIP version 3.3.

This paper presents a detailed analysis of the error and the correction. It also shows the impacts of the correction on the extent of CMAQ mass consistency adjustment and advected tracer concentration.

2. CORRECTION OF THE CONTRAVARIANT VERTICAL VELOCITY ERROR

**Corresponding author:* Fuquan Yang, National Research Council of Canada, Room 233, M2,1200 Montreal Road, Ottawa, Ontario, Canada K1A 0R6; e-mail: Fuquan.Yang@nrc-cnrc.gc.ca

2.1 Calculation of the contravariant vertical velocity in MCIP

In MCIP, the contravariant vertical wind velocity should be calculated as (Byun, 1999):

$$\dot{\xi} = \left[\frac{\sigma_{p0}}{p^*}\frac{\partial p_0^*}{\partial \hat{x}^1}\right](mu) + \left[\frac{\sigma_{p0}}{p^*}\frac{\partial p_0^*}{\partial \hat{x}^2}\right](mv) + \frac{\rho_0 g}{p^*}w \quad (1)$$

where, $\dot{\xi}$ is the contravariant vertical wind velocity, mu and mv are map scaled wind velocities along the $\hat{x}^1$ and $\hat{x}^2$ direction, w is the normal vertical wind velocity component from non-hydrostatic MM5, σ_{p0} is the sigma value, ρ_0 is the reference state air density, g is gravitational acceleration constant, and p^* is the difference between the reference state surface pressure (p_{s0}) and the model top pressure (p_t) , i.e.,

$$p^* = p_{s0} - p_t \quad (2)$$

The reference state surface pressure can be calculated from:

$$p_{s0} = p_{00}\exp\left(\sqrt{\left(\frac{T_{00}}{A}\right)^2 - \frac{2gH}{RA}} - \left(\frac{T_{00}}{A}\right)\right) \quad (3)$$

where R is the gas constant for dry air , H is the terrain height, P_{00} is the sea level pressure (100,000Pa), T_{00} is the temperature at P_{00} (290 K), and A is the temperature lapse rate (50K), representing the temperature difference between P_{00} and P_{00}/e = 36788 Pa. The model reference state does not change with time in the simulation.

2.2 Error in the calculation of the contravariant vertical velocity in previous MCIP versions

In the previous MCIP versions (version 3.2 and earlier), the p^* in equation (1) was incorrectly calculated as the difference between the total

surface pressure from the first time period processed by MCIP (p_s) and the pressure at the model top, i.e.,

$$p^*_{incorrect} = p_s - p_t \,. \quad (4)$$

The total surface pressure, p_s , in Eq. (4) is calculated by adding the perturbation pressure p' from the first time period processed by MCIP to the surface reference state pressure, i.e.,

$$p_s = p_{s0} + p' \quad (5)$$

where $p' << p_{s0}$. From Eqs. (4) and (5), we can get:

$$p^*_{incorrect} = p_{s0} + p' - p_t \,. \quad (6)$$

From Eqs.(2) and (6), it can be easily seen that the perturbation pressure from the first time period processed by MCIP was introduced into the calculation of the incorrect p^* in Eq. (4). The incorrect p^* was then used to calculate the contravaraint vertical velocity in Eq. (1).

Note that this error exists only when the non-hydrostatic MM5 results are processed by MCIP and the vertical contravariant wind velocity generated by MCIP is used in CMAQ. It does not exist for the calculation of contravariant vertical velocity with hydrostatic MM5 and has no impact on CMAQ simulations that use the Yamartino scheme where the contravariant vertical velocity is recalculated in CMAQ.

2.3 Mathematical differences between the incorrect and the correct contravariant vertical velocities

Mathematically, the difference between the incorrect and the correct contravariant vertical wind velocities can be expressed as:

$$\dot{\xi}_{incorrect} - \dot{\xi} = \left[\frac{\sigma_{p0}}{p^*_{incorrect}} \frac{\partial p^*_{incorrect}}{\partial \hat{x}^1} - \frac{\sigma_{p0}}{p^*} \frac{\partial p^*}{\partial \hat{x}^1} \right] (mu) + \left[\frac{\sigma_{p0}}{p^*_{incorrect}} \frac{\partial p^*_{incorrect}}{\partial \hat{x}^2} - \frac{\sigma_{p0}}{p^*} \frac{\partial p^*}{\partial \hat{x}^2} \right] (mv) + \left(\frac{\rho_0 g}{p^*_{incorrect}} - \frac{\rho_0 g}{p^*} \right) w \quad (7)$$

where $\dot{\xi}_{incorrect}$ and $\dot{\xi}$ are the contravariant vertical velocities calculated by the previous (v3.2 and older) and the current (v3.3) MCIP versions, respectively.

The three terms on the right-hand side can be approximated as:

$$\left[\frac{\sigma_{p0}}{p^*_{incorrect}} \frac{\partial p^*_{incorrect}}{\partial \hat{x}^1} - \frac{\sigma_{p0}}{p^*} \frac{\partial p^*}{\partial \hat{x}^1} \right] (mu) \cong \frac{\sigma_{p0}}{p^*} \frac{\partial p'}{\partial \hat{x}^1} (mu) \quad (8)$$

$$\left[\frac{\sigma_{p0}}{p^*_{incorrect}} \frac{\partial p^*_{incorrect}}{\partial \hat{x}^2} - \frac{\sigma_{p0}}{p^*} \frac{\partial p^*}{\partial \hat{x}^2} \right] (mv) \cong \frac{\sigma_{p0}}{p^*} \frac{\partial p'}{\partial \hat{x}^2} (mv) \quad (9)$$

$$\left(\frac{\rho_0 g}{p^*_{incorrect}} - \frac{\rho_0 g}{p^*} \right) w \cong 0 \quad (10)$$

The derivation processes for the above equations are not given here for brevity.

From Eqs. (8), (9) and (10), it can be seen that the difference of the contravariant vertical wind velocity at a specified time is largely produced by the contravariant horizontal wind velocity (mu, mv) at that time and the gradient of perturbation pressure ($\frac{\partial p'}{\partial \hat{x}^1}$ and $\frac{\partial p'}{\partial \hat{x}^2}$) from the first time period processed by MCIP.

The perturbation pressure from the first time period processed by MCIP is kept to be constant in the incorrect MCIP run and is used to calculate the contravariant vertical velocity. Even for the same non-hydrostatic MM5 output, the errors of the contravariant vertical velocity generated by different runs of the incorrect MCIP are different if the runs start from different times.

Since the magnitude of formula Eq. (10) approximates zero, the sign of the left hand side of Eq. (7) is determined by the relative magnitudes of the first two terms in the right hand side of the equation, which can then be calculated approximately by Eqs. (8) and (9).

There are two ideal situations in which the sign of the left hand side of Eq. (7) can be determined. First, when the signs of Eqs. (8) and (9) are positive, a net positive upward contravariant vertical wind is generated ($\dot{\xi}_{incorrect} - \dot{\xi} > 0$). This can occur at grid cells which are located southwest of a high perturbation pressure center with southwest wind ($\frac{\partial p'}{\partial \hat{x}^1} > 0, u > 0$; $\frac{\partial p'}{\partial \hat{x}^2} > 0, v > 0$). Second, when the

signs of both Eqs. (8) and (9) are negative, a net negative downward contravariant vertical wind is produced ($\dot{\xi}_{incorrect} - \dot{\xi} < 0$). This can occur at grid cells which are located at the northeast of a low perturbation pressure center with northeast wind ($\frac{\partial p'}{\partial \hat{x}^1} > 0, u < 0$; $\frac{\partial p'}{\partial \hat{x}^2} > 0, v < 0$).

When the signs of Eqs. (8) and (9) are different, the sign of the left hand side of Eq. (7) has to be determined by the relative magnitude of Eqs. (8) and (9).

Since both the gradients of perturbation pressure and horizontal winds are weak for high perturbation pressure systems, the large differences of vertical wind velocities are much more pronounced in the low perturbation pressure centers than that in the high perturbation pressure centers

3. IMPACTS OF THE CORRECTION ON THE CONTRAVARIANT VERTICAL VELOCITIES GENERATED BY MCIP

3.1. Correlation of the vertical velocity error with weather pattern

To investigate the contravariant vertical wind velocity error and the impacts of the correction, the non-hydrostatic MM5 was run for a 42-km grid domain covering North America with 34 half-sigma levels for July 15-20 2002. MM5 output was processed with MCIPv3.2 (incorrect MCIP) and MCIPv3.3 (correct MCIP). The Jacobian and air density weighted contravariant vertical wind velocity (WHAT_JD) from MCIPv3.2 is referred to as the "incorrect vertical velocity" and that from MCIPv3.3 is referred to as the "correct vertical velocity". Both MCIPv3.2 and MCIPv3.3 collapsed the 34 layers in MM5 to 15 layers in MCIP.

As an example, Fig. 1(a) shows the surface perturbation pressure at 00UTC July 16, which is the beginning of the MCIP calculation, and the horizontal wind vector at 06UTC, July 16, 2002, and Fig. 1(b) shows the difference between the incorrect and correct WHAT_JD (incorrect minus correct values) at 06UTC, July 16. There are high correlations between the locations of the low perturbation pressure centers with strong western winds and those grid cells where there are large differences of vertical wind velocities. One deep low perturbation pressure center with large vertical wind difference can be seen over the northwestern Atlantic Ocean. The scattered small scale low perturbation pressure centers caused by high elevation terrains in the southwest of the domain also generate large differences of WHAT_JD.

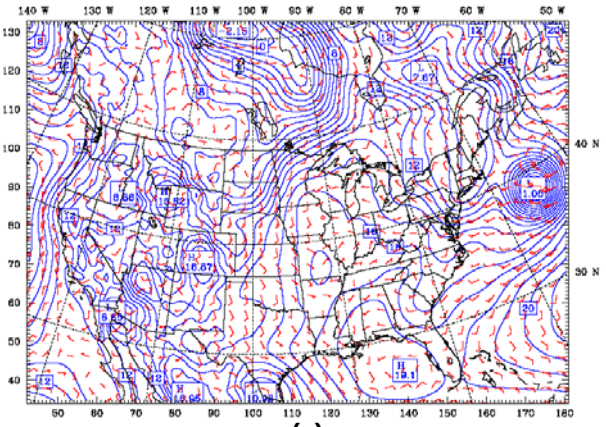

(a)

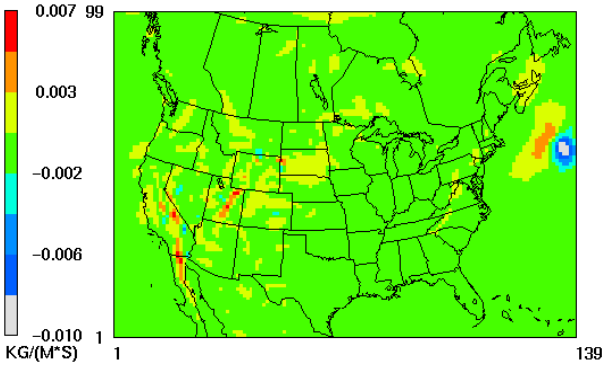

(b)

Fig. 1(a). Surface perturbation pressure at 00UTC, July, 16, and horizontal wind velocity vector at 06UTC, July 16 **(b)**. difference of Jacobian and air density weighted contravariant vertical velocity (incorrect minus correct values) at for 06UTC, July, 16.

3.2 Impact of the correction on the vertical velocity when surface front passes

A weak surface front passes southern Ontario around 18UTC (2pm EST), July 18 and terminates a three-day ozone pollution episode. Fig. 2(a) shows the hourly WHAT_JD values for the two cases, and their difference (incorrect minus correct) in the grid cell (99, 56), which is centered near Hamilton in southern Ontario. Fig. 2(b) shows the perturbation pressure at the first time step of the MCIP run and surface horizontal wind fields at 18UTC (2pm EST), July 18, 2002 for the southern Ontario areas. The upward vertical velocity is weakest at 07UTC (3am EST), but regains its peak value at 14UTC (10am EST). It weakens

again quickly after 18UTC (2pm EST) when the front passes with intrusion of cold air (Fig. 2(a)).

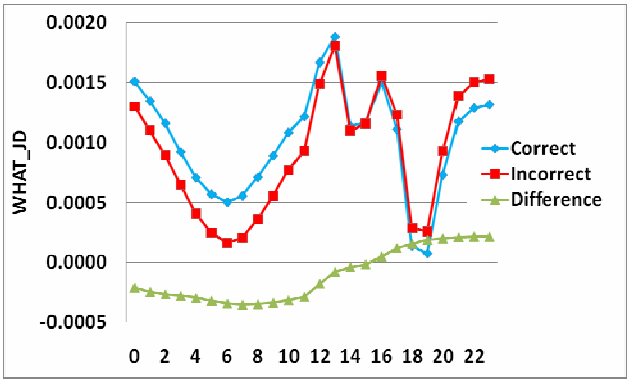

(a)

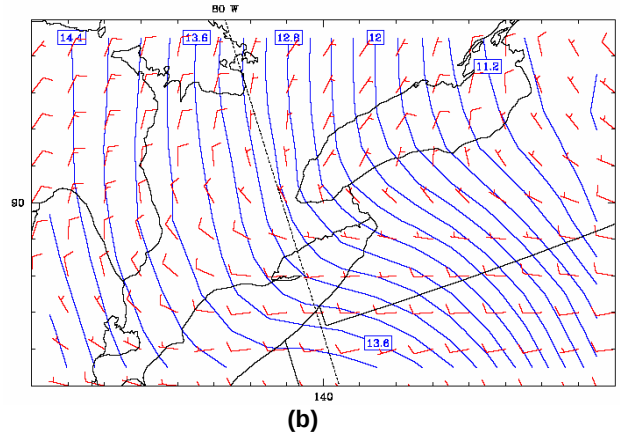

(b)

Fig. 2. (a) Hourly time series of the vertical wind velocity for July 18, 2002 for grid (99,56), which is centered with Hamilton, Southern Ontario; **(b).** Surface horizontal wind vector at 2pm EST (18UTC), July 18, 2002 and perturbation pressure for 00UTC, 16, July, 2002 in the same grid cell

Before the fontal pass, there is a negative difference in the vertical velocity because $\frac{\partial p'}{\partial \hat{x}^1} < 0, u > 0$, $\frac{\partial p'}{\partial \hat{x}^2} \cong 0, v \cong 0$ (Fig. 2(b)). The correct MCIP gave larger vertical wind velocities than the incorrect version. During the frontal passage, the vertical velocity difference diminishes because $\frac{\partial p'}{\partial \hat{x}^1} < 0, u \cong 0$ and $\frac{\partial p'}{\partial \hat{x}^2} \cong 0, v < 0$. The difference gradually shifts to positive after the front passed because $\frac{\partial p'}{\partial \hat{x}^1} < 0, u < 0$, $\frac{\partial p'}{\partial \hat{x}^2} \cong 0, v > 0$.

4. IMPACTS OF THE CORRECTION ON CMAQ RESULTS

4.1. Impact on air density advection results

Air density is advected at each time step and its ratio to the interpolated air density is used to calibrate the mixing ratio of other species at each step.

After 24 hours of advection, the incorrect vertical wind velocity produces unphysical air density with the domain maximum 6.9kg/m^3 and minimum 0.06kg/m^3. In contrast, the correct vertical wind velocity produces more reasonable air density, with the domain maximum 1.3 kg/m^3 and minimum 0.44 kg/m^3 (not shown).

4.2. Impact on Mass Consistency Adjustment

Hourly outputs from both the incorrect and correct MCIP are used in CMAQ to quantify the impact of the correction on mass consistency adjustments required by the Parabolic Piecewise Method (PPM) advection scheme used in CMAQ.

CMAQ employs two mass adjustment approaches. The default "YAMO" approach recalculates the vertical wind field with MCIP horizontal contravariant wind components. The MCIP error reported here does not affect the advection results using this method.

The "DENRATE" approach in CMAQ corrects concentration fields based on the ratio of advected and interpolated air density, called mass-adjustment ratio, at each advection time step. The error in MCIP vertical contravariant velocity significantly alters the mass consistency adjustment ratio due to incorrect transport of the air density 'tracer'.

Fig. 3(a) and Fig. 3(b) show the spatial distribution of the mass-adjustment ratio calculated with the incorrect and correct MCIP, respectively, after a 24 hour simulation. The air density tracer is advected over 24 hours rather than being updated at every advection time step. Significant differences are observed both spatially and in magnitude. Using the incorrect MCIP, the adjustment ratio is more chaotic with magnitude ranging from 0.17 to 22. In contrast, the correct MCIP gives the ratio ranging from 0.76 to 2.5, with few cells exceeding 1.5. The grid cells with high ratios are mostly at the high elevation terrain areas.

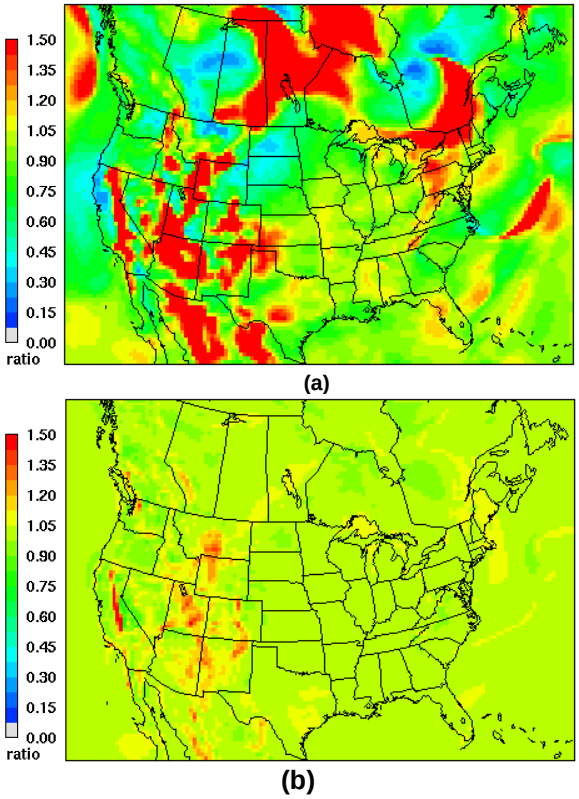

Fig. 3. Mass adjustment ratios after 24-hour advection with **(a)** the incorrect MCIP and **(b)** the correct MCIP simulation. Note the great differences in Northeast USA and Southern Ontario, Canada; in the provinces of Manitoba and Ontario and some grid cells on open sea.

Fig. 4 shows the hourly values of domain maximum and minimum mass-adjustment ratios generated by using the two MCIP versions for the first 24-hour period. The mass-adjustment ratios associated with the incorrect MCIP diverge and the adjustment required is an order of magnitude larger than that associated with the correct MCIP case. With the vertical velocity correction, the mass-adjustment ratios are generally in the range of 0.75 and 2.5, which is much closer to unity than that without the correction.

The results demonstrate that the mass inconsistency errors in the CMAQ advection scheme using the non-hydrostatic MM5 wind field and air density are not as serious as perceptions based on some previous studies e.g., (Lee, 2004) .

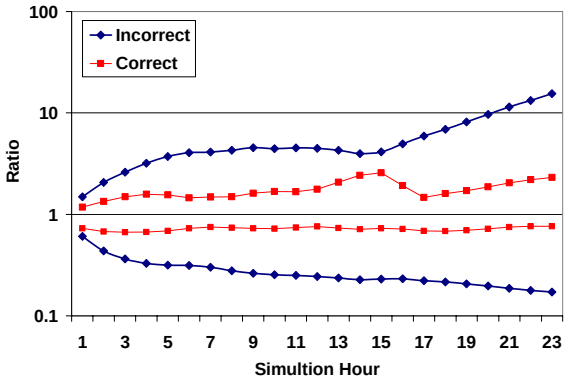

Fig. 4. Hourly time series of the domain maximum and minimum mass-adjustment ratio for correct and incorrect MCIP simulations.

4.3. Impact on Tracer Concentrations

A tracer with unit concentration (1 ppmv) was incorporated in a CMAQ simulation with advection process only. There was no mass adjustment to correct the mass inconsistency caused by the advection. Deviations from the unit concentration would indicate the extent of the mass-inconsistency caused by CMAQ advection.

The advection results after 24 hours show that the mass consistency error associated with the incorrect MCIP is sporadic, resulting in domain maximum concentration of 4.4 ppmv (Fig. 5(a)). In contrast, the domain maximum concentration is only 1.4 ppmv when the the correct MCIP results are used in the simulation, and most grid cells with large errors are in the high elevation terrain areas (Fig. 5(b)).

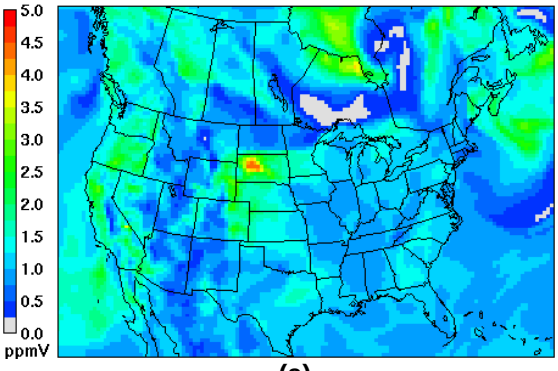

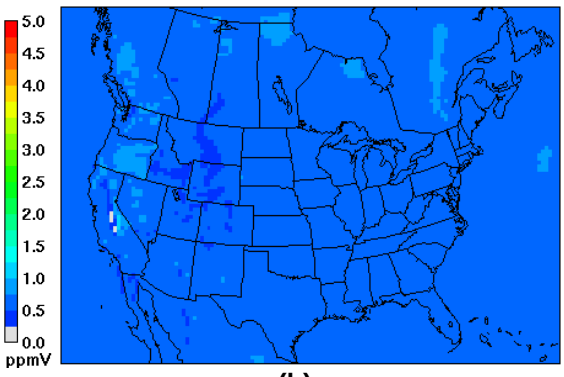

(b)

Fig. 5. Tracer concentrations after 24-hour advection when **(a)** the incorrect and **(b)** the correct MCIP results are used in the simulation.

5. CONCLUSION AND DISCUSSION

The mass inconsistency problem associated with using non-hydrostatic MM5 and MCIP results is not as serious as it has been previously regarded. The problem is partly caused by a mistake in calculating the contravariant vertical wind velocity in MCIP. This error caused incorrect tracer advection and exaggerated the mass inconsistency ratios associated with the non-hydrostatic MM5 results. The error has now been corrected in MCIP3.3.

Although the sigma formulation in non-hydrostatic MM5 allow the propagation of its individual terrain features upward to all sigma levels, even to the model top, this study shows that the mass adjustment ratios at the middle layers of CMAQ simulations are very close to unity (see Fig. 6). When developing new advection schemes, this consistency between air density and wind fields in the middle layers need to be carefully maintained and should not be disturbed without sound physical basis. Efforts should be spent to avoid propagating the errors at the lowest sigma layers upward, which would destroy the good mass consistency at the middle layers.

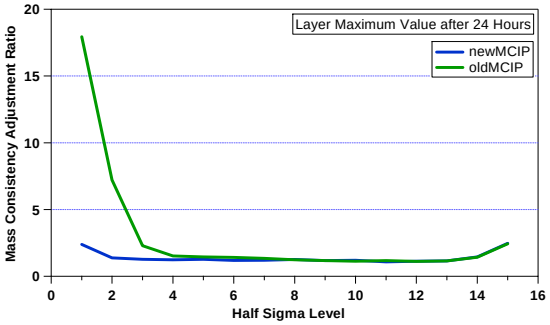

Fig. 6. Domain maximum mass adjustment ratios at the model vertical half sigma layers

6. REFERENCES

Anthes, R.A. and T.T. Warner, 1978: Development of hydrodynamic models suitable for air pollution and other mesometeorological studies. *Mon. Wea. Rev.,* 106, 1045-1078.

Byun, D. W., 1999a: Dynamically consistent formulations in meteorological and air quality models for multiscale atmospheric studies. Part I. Governing equations in a generalized coordinate system. *J. Atmos. Sci.,* **56**, 3789-3807.

Byun, D. W., 1999b: Dynamically consistent formulations in meteorological and air quality, models for multiscale atmospheric studies. Part II: Mass conservations issues. *J. Atmos Sci.,* **56**, 3808-3820.

Byun, D.W., and Ching, J.K.S., 1999: Science algorithms of the EPA Models-3 Community Multiscale Air Quality (CMAQ) Modeling System, U.S. EPA/600/R-99/030.

Dudhia, J., 1993: A nonhydrostatic version of the Penn State–NCAR, Mesoscale Model: Validation tests. *Mon. Wea. Rev.,* **121,** 1493–1513.

Dudhia J., Dave Gill, Kevin Manning, and Wei Wang, 2005: PSU/NCAR Mesoscale Modeling System Tutorial Class Notes and User's Guide: *MM5 Modeling System, Version 3*

Grell, G.A., J. Dudhia, and D.R. Stauffer, 1994: A Description of the Fifth-Generation PENN STATE/NCAR Mesoscale Model (MM5), NCAR Technical Note, NCAR/TN-398+*STR*

Kitada, T., 1987: Effect of non-zero divergence wind fields on atmospheric transport calculations. *Atmos. Environ.,* **21,** 785–788

Klaus P. Hoinka and Günther Zängl., 2004: The influence of the Vertical Coordinate on Simulations of a PV Streamer Crossing the Alps; *Mon Wea Rev*, 1860–1867

Lee, S.M., Yoon, S.C., and Byun D.W., 2004: The effect of mass inconsistency of the meteorological field generated by a common meteorological model on air quality modeling. *Atmos. Environ*. ,38, 2917-2926.

Murry L. Salby, 1996: Atmospheric physics, p166-194

Pielke, R. A., 2002: *Mesoscale Meteorological Modeling.* Academic Press, p122-160

Yin, D., 2004: A Description of the Extension for Using Canadian GEM data in MCIP and a Brief User's Guide for GEM-MCIP. ICPET, National Research Council of Canada.

EFFECTS OF USING HIGH-RESOLUTION URBAN LAND-USE AND BUILDING MORPHOLOGICAL DATA SETS ON THE WRF/URBAN COUPLED MODEL SIMULATIONS FOR THE HOUSTON-GALVESTON AREAS

Fei Chen*, Shiguang Miao, Mukul Tewari
Research Applications Laboratory, NCAR, Boulder, CO, USA

Jason Ching
U.S. Environmental Protection Agency, Research Triangle Park, NC, USA

1. INTRODUCTION

Today's mesoscale numerical weather prediction (NWP) models are routinely executed at a grid spacing of 1~4 km and used to provide meteorological conditions for air quality, transport and dispersion model forecast for urban areas. It is critical for these high-resolution NWP models to capture influences of urban forcing on variations of wind, temperature, and humidity in the atmospheric boundary layer (ABL), so that air dispersion and quality models can benefit from improved prediction of the urban meteorological conditions. One daunting challenges in mesoscale urban modeling is the description of urban surfaces, which are highly heterogeneous even at small scales. The efforts in developing gridded fine-scale data sets of buildings, vegetation cover, and other morphological features in metropolitan areas, under the National Urban Database and Access Portal Tools (NUDAPT), provide an excellent opportunity to address this challenge. This paper describes an investigation of influences of incorporating the NUDAPT data set in the coupled Weather Research and Forecast (WRF)–urban canopy modeling system on short-term simulations for selected high ozone-pollution events of 30-31 August 2000 over the Houston-Galveston areas. Subsequently, the output from this simulation will be used to drive the Community Multiscale Air Quality (CMAQ) model so that the effects of utilizing building morphological data on air pollution can be also assessed.

2. WRF/NOAH/UCM MODELING SYSTEM

The community mesoscale WRF, coupled to the Noah land surface model and to a single-layer urban canopy model (UCM) [Chen et al., 2006], was used to simulate the evolution of the PBL in this study. This UCM is based on Kusaka et al. [2001] and takes the urban geometry into account in its surface energy budgets and wind shear calculations. Radiative, thermal, moisture effects and canopy flow model are accounted for in the UCM, which includes: 1) 2-D street canyons that are parameterized to represent the effects of urban geometry on urban canyon heat distribution; 2) shadowing from buildings and reflection of radiation in the canopy layer; 3) the canyon orientation and diurnal cycle of solar azimuth angle, 4) man-made surface consists of eight canyons with different orientation; 5) Inoue's model for canopy flows [Inoue, 1963]; 6) the multi-layer heat equation for the roof, wall, and road interior temperatures; 7) anthropogenic heating associated with energy consumption by human activities; and 8) a very thin bucket model for evaporation and runoff from road surface.

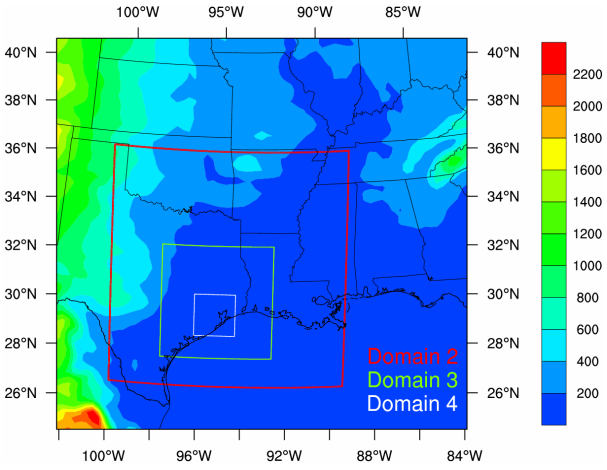

Fig. 1. Domain configuration (resolutions are 27km, 9km, 3km and 1km respectively).

**Corresponding author:* Fei Chen, Research Applications Laboratory, NCAR, PO Box 3000, Boulder, CO 80307-3000; Tel. 303-497-8454; Fax. 303-497-8401; e-mail: feichen@ucar.edu

3. WRF MODEL CONFIGURATION AND NUDAPT DATA USED IN THIS CASE STUDY

WRF/Noah/UCM modeling system was run for a 36-hour simulation initialized at 00Z on 30 August 2000 with four two-way nested domains (Fig. 1). This case was selected because it represents a severe air-pollution day.

Three WRF modeling experiments were conducted: 1) CTRL: use the traditional approach of specifying urban parameters through a look-up table in WRF; 2) BD2D: ingest gridded building morphological data from NUDAPT; and 3) AH2D: ingest gridded anthropogenic heating data from NUDAPT.

Significant differences, between look-up table and 2D data from NUDAPT, in horizontal distributions and magnitudes of building height and anthropogenic heating rate are shown in Fig. 2 and 3.

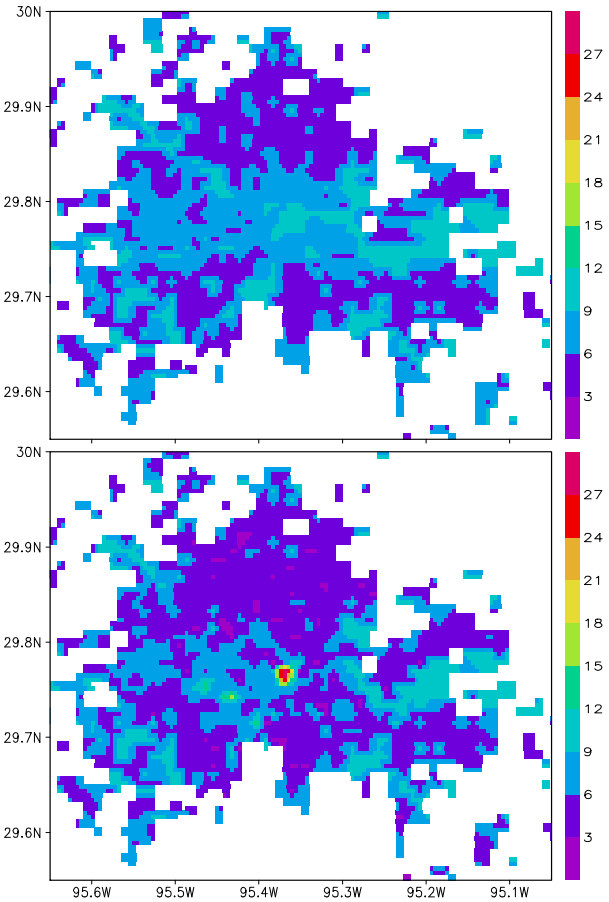

Fig. 2. Horizontal distribution of building height in meter for (a) case CTRL and (b) case BD2D.

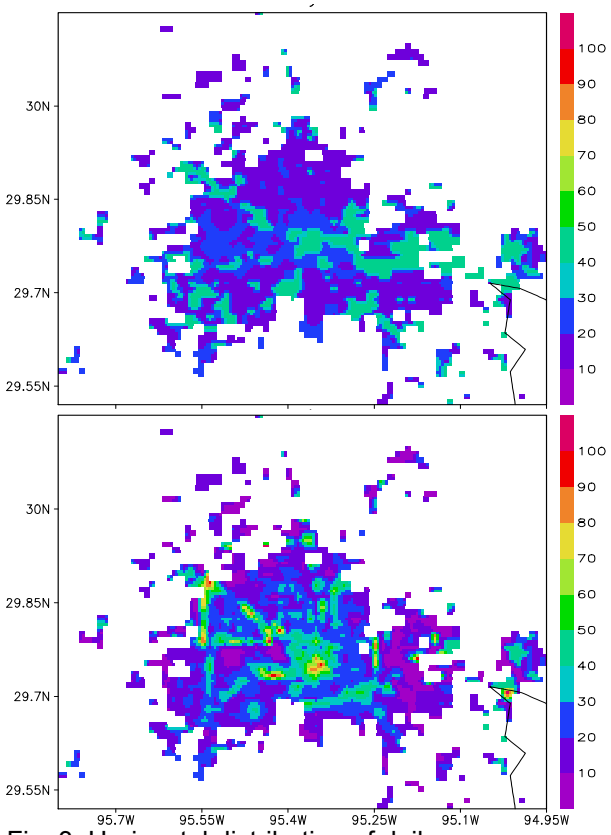

Fig. 3. Horizontal distribution of daily mean anthropogenic heating rate (in W m^{-2}) for August in (a) case CTRL and (b) case AH2D.

4. RESULTS AND ANALYSES

Compared with look-up table, building heights from NUDAPT are larger in downtown area (CBD) and smaller in other urban area. Therefore, surface wind speed from the case BD2D is lower in CBD and higher in other urban area than that in the case CTRL. Also, 2-m temperature from the case BD2D is lower than that in the CTRL case, especially in nighttime (Fig. 4).

The effect of 2D anthropogenic heating data is similar to that of 2D building morphological data. 2-m temperature from the case AH2D is lower than that in the case CTRL, especially in nighttime (Fig. 5).

At 2000LST Aug 30, 2000, the return flow simulated in the cases BD2D and AH2D at the height of 1-km is weaker than that in the CTRL case (Fig. 6), and the PBL height of AH2D is lower than that for other two cases, which would affect the mixing processes in transport and dispersion models.

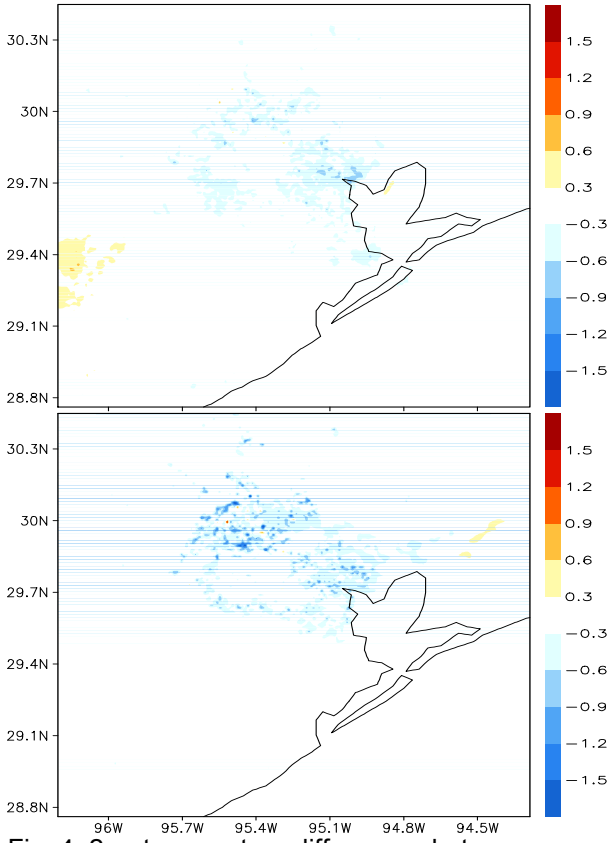

Fig. 4. 2-m temperature differences between BD2D and CTRL: (a) averaged for daytime and (b) averaged for nighttime.

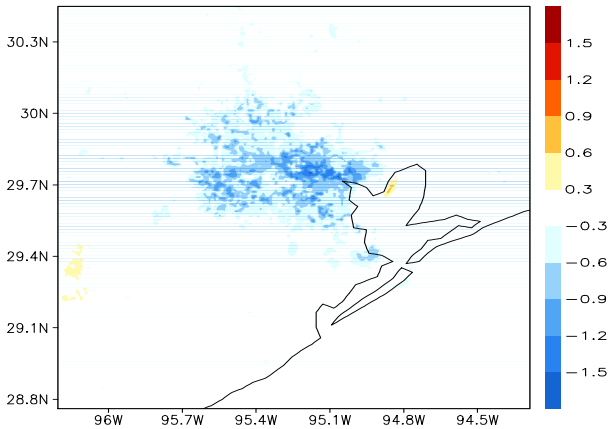

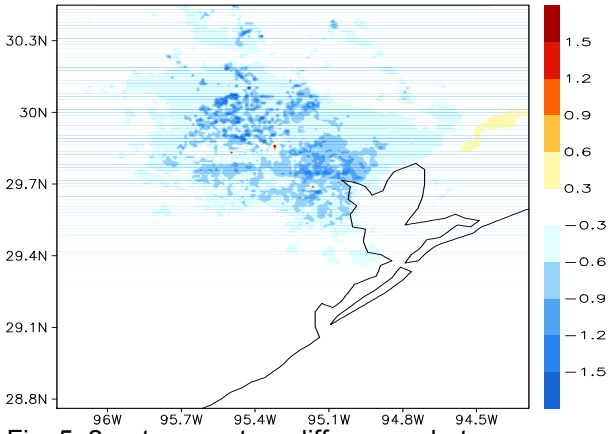

Fig. 5. 2-m temperature differences between AH2D and CTRL: (a) averaged for daytime and (b) averaged for nighttime.

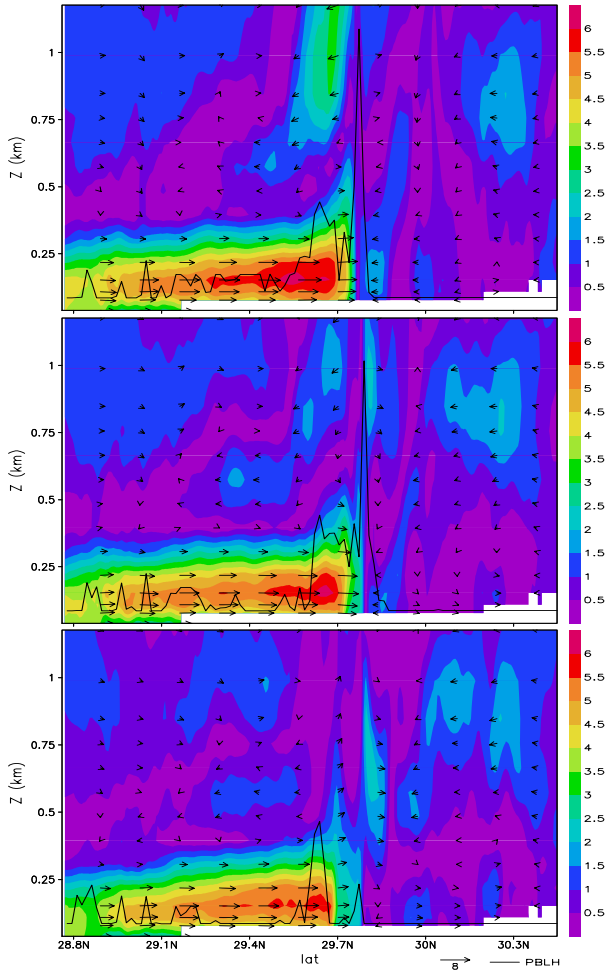

Fig. 6. North-south cross section plane, along lon=95.372W, of wind speed (shaded) and flow field (vector, v;w*10): (a) CTRL, (b) BD2D and (c) AH2D at 2000LST Aug 30, 2000.

5. SUMMARY

Preliminary results show that utilizing high-resolution urban data, e.g. urban morphological data and anthropogenic heating data from NUDAPT, alter WF simulated PBL properties and land-sea breeze circulations, which are important for air quality modeling.

Nevertheless, our results may be limited due to the single-layer urban canopy model used in this study. The consistency in urban data sets and the average approach should be further investigated.

Acknowledgements

This work was funded by the NCAR FY07 Opportunity Fund, DTRA Coastal-urban project (CDR Stephanie Hamilton and Chris Kiley), and Institute of Urban Meteorology, China Meteorological Administration.

References

Chen F., M. Tewari, H. Kusaka, and T. T. Warner (2006), Current status of urban modeling in the community Weather Research and Forecast (WRF) model, paper presented at Joint Session with Sixth Symposium on the Urban Environment and AMS Forum: Managing our Physical and Natural Resources: Successes and Challenges, The 86th AMS Annual Meeting, AMS, Atlanta, GA, 28 January – 3 February.

Kusaka, H., et al. (2001), A simple single-layer urban canopy model for atmospheric models: Comparison with multi-layer and slab models. Bound.-Layer Meteorol., 101, 329-358.

PROJECT OVERVIEW: NATIONAL URBAN DATABASE AND ACCESS PORTAL TOOLS (NUDAPT)

Jason Ching*
Atmospheric Science Modeling Division, ARL, NOAA, RTP, NC,
(In partnership with EPA's National Exposure Research Laboratory)

1. INTRODUCTION

Based on the need for advanced treatments of high resolution urban morphological features in meteorological, dispersion, air quality and human exposure modeling systems for future urban applications, a new project was launched called the National Urban Database and Access Portal Tool (NUDAPT). The initial NUDAPT prototype is a project sponsored by the United States Environmental Protection Agency (USEPA) and involves active collaborations and contributions from many groups from federal and state agencies, and from private and academic institutions. NUDAPT will produce gridded outputs of urban parameters capable of driving current (Dupont et al., 2004, Otte et al, 2004, Chen et al., 2006, 2007a, b, Park et al., 2007, Taha et al., 2007a, b, Ching et al., 2004) and future advanced urban meteorological (Martilli, 2007, Martilli and Schmitz, 2007) and air quality models. Additionally, ancillary data will be included such as gridded population, energy usage and traffic (Burian et al., 2007b) so as to encourage and facilitate linkages to air quality and human exposure models. Portal technology is incorporated to enable NUDAPT to be a "Community" based system, an important core-design feature. This web-based technology will facilitate data retrievals and handling based on data federation concepts. Houston Texas will serve as NUDAPT's initial prototype; it will feature advanced urban canopy implementations of the Mesoscale Meteorological model, Version 5 (MM5) as well as the Weather Research and Forceast (WRF) models; thus serving to demonstrate the NUDAPT features, including scope of the data and processing methodologies for eventual extension to all other cities.

2. APPROACH

In this paper, we describe a prototype operational template of this database. In principle, the Prototype will eventually provide a nation-wide resource for the model user community engaged in developing and applying advanced atmospheric transport and dispersion and air quality models. The value of using high resolution urban data in meteorological and air quality simulations has been demonstrated from sensitivity studies, Dupont, et al., (2004); Ching et al., (2004); Chen et al., (2006) and other application studies including urban heat island (UHI) modification studies based on mesoscale modeling system that incorporate urban canopy parameters, Taha (2007a,b). NUDAPT supports assessment studies needed to inform decision makers on health risk from exposure to poor air quality. Further, it addresses homeland security issues regarding the transport and dispersion of toxic releases.

We have selected Houston, the fourth largest city in the USA, as the initial prototype for demonstrating the NUDAPT features. A set of lidar-derived building data for Houston is available for unrestricted use (Figure 1), as are several derived products, and sets of air quality data available from major intensive field studies. Houston has active emissions management programs to address its poor air quality and associated health effects. The NUDAPT prototype will include: (1) primary data sets such as (three-dimensional building and geo-morphological data, roads and their linkages;(b) activity data including census data, traffic, and industrial outputs, (c) land surface characteristics data; (2) derived daughter products including model specific UCPs, diurnal gridded population data, gridded anthropogenic energy inputs (Sailor et al., 2007), and gridded traffic emissions; and (3) selected illustrative examples of model outputs and analyses to demonstrate a range of applications. This initial prototype will feature advanced urban implementations; in MM5 (Ching et al, 2004) and WRF (Chen et al., 2006) and other modeling systems.

3. FEATURES OF NUDAPT

* *Corresponding Author Address:* Jason Ching, MS E243-04, NERL, USEPA, 109 TW Alexander Dr, RTP, NC 27709; email: ching.jason@epa.gov

3.1: Morphology databases and urban canopy parameters

An important feature of NUDAPT is the provision to incorporate urban structure data and their derivative urban parameters that can be used by mesoscale meteorology models. For example, the urbanized version of MM5, makes use of UCPs introduced to account for building and vegetation influences on the drag, the partitioning of the surface energy budget components, and the generation of turbulence of the flow in the surface boundary layer. The set of UCPs listed in Table 1 (8 of which vary with height) used in the Dupont modeling system (Dupont et al., 2004) has been calculated for each grid in the modeling domain (Burian et al., 2004, 2007b). The data to derive this set of UCPs were primarily from an airborne based LiDAR system that collects data for the Digital Elevation Model (DEM) and Digital Terrain Model (DTM). Differencing the digital elevation and terrain signals provides the building and tree information, an example of which is shown in Fig. 1a. High altitude aircraft and municipal property data provide information to complement the LiDAR database. Such data and the derived UCPs (example shown in Figure 1b) are incorporated into the Houston Prototype.

Geospatial databases similar to that used in Houston that consist of detailed building and other urban morphological structures imagery information at pixel resolution of order 1 m are being acquired for 133 urban centers in the USA. This is in response to the Homeland Security Infrastructure Program (HSIP). The Nunn-Lugar-Dominici Act (Defense Against Weapons of Mass Destruction Act of 1996) established a project by which DOD was tasked to help respond to chemical, biological and nuclear (CBN) incidences in the 133 urban centers. These data (together with the National Map Project of the US Geological Survey) provide the foundation for a national scale database. Of course, even higher resolution descriptions of building data exist. In principle, the NUDAPT can incorporate such data if it can be made available.

Currently, a second generation National Building Statistics Database (NBSD2) consisting of sets of UCPs similar to the set shown in Table 1 (but without vegetation parameterizations have been created using the Urban Morphological Analyses Processor, UMAP, Burian et.al., (2007a). These gridded fields are created at 250m and 1 km grid sizes for urban areas shown in Figure 2. These datasets are available in NUDAPT courtesy of S.Burian and M. Brown.

3.2 Relevant Ancillary data

Gridded UCP and land use data sets obtained from NUDAPT are expected to improve meteorological fields for air quality, homeland security, and planning purposes. NUDAPT will also include links to other sources of relevant data including various activities and land-use data such as roads and their linkages, and activity data including census data, traffic, industrial outputs, and land surface characteristics data from which gridded products useful for models will be derived. In addition, NUDAPT will include gridded population data for the USA, e.g., day-night populations (see Figure 3), indoor-outdoor populations, sensitive population groups and population mobility matrix. These data are made available to NUDAPT courtesy of T. McPherson and M. Brown. These data is useful to exposure and consequence management assessments. Such data are being generated for the prototype at latitude-longitude (lat-long) coordinates with a spatial resolution of 250 m (McPherson, et al., 2003a,b, 2004, 2006). Additionally, gridded anthropogenic heating rates (also at 250m grid size) are available in NUDAPT courtesy of David Sailor. These data replace crude assumptions used in previous urban meteorological modeling studies. Details are provided in Sailor et al., (2004, 2006), an example of this product is shown in Figure 4.

3.3. NUDAPT Design concept

NUDAPT is structured as a two level web-enabled database that provides ready access to the various datasets, both primary or source data and processed data to users. The first level of the framework is the primary data and includes the high resolution building data. Access to this level is limited; it can be granted for those interested in creating new or modified UCP datasets. The second level provides unrestricted access; users can query the database for relevant data, retrieve data in a form that can be readily assimilated into models such as MM5, and submit model results for further analysis. The database is federated, i.e., the database will act as a repository for multiple, heterogeneous datasets that all adhere to a consistent format and metadata specification. This framework allows for analysis by the scientific community by providing an efficient means of sharing observed and modeled data. The

community provides the means for detailed analysis and knowledge integration. The data-sharing concept in NUDAPT can facilitate researcher efforts to improve models of the urban environment. For example, a researcher wishes to compare their model results with another simulation that used a different set of UCPs. This is easily accomplished by a query to the database, retrieval of the model run of interest, and analysis accomplished at the user end. Once researchers utilize these UCPs in their modeling, more knowledge integration will occur through enhanced model evaluations leading to improved models.

Datasets will either reside on the NUDAPT portal server or, where available, for public download elsewhere. The portal will provide a link to facilitate the appropriate download. Because the site is expected to act as a data repository rather than an active transaction-heavy database, there does not appear to be a need to utilize database software to manage the datasets in question. Instead the datasets will exist as stand-alone files in the file system. The initial Prototype will use the ArcGIS 9.2 server that provides the desired functionality needed to handle both vector and raster data formats.

4. DISCUSSION AND SUMMARY

Initial sensitivity studies of air quality (and other) applications using outputs of advanced meteorological models that incorporate data such as those available from NUDAPT are being performed. Figure 5 contrasts the mixed layer simulations from MM5 with and without UCP. The urban area of Houston is categorized with one urban land use category in the standard version of MM5. Figure 6 illustrates the sensitivity of Community Multiscale Air Quality (CMAQ) model to MM5 versions with and without detailed urban canopy feature. In this instance, significant differences are seen, serving as a motivation for advancements in urban modeling.

The development of NUDAPT represents a promising resource to address many of the emerging problems in urban areas. NUDAPT provides a platform for accessing and developing data and for sharing information with the user community. Primary data in NUDAPT will include physical and morphological data prepared and collected under various conventional and unconventional systems. The preparation of NUDAPT daughter products, which are closely directed to urban gridded modeling applications, will need to consider various map projections that are used in typical meteorological and air quality modeling applications. Due to the various grid sizes and map projects of applications that will potentially be used by various modelers, provisions are made in NUDAPT to include or contain methodologies for re-projecting and re-gridding these daughter products.

The Portal also includes a site (called Quickplace) designed to facilitate collaborations between NUDAPT current and future Collaborators. Rooms are set up in the name of a individual and all Collaborator's. Once registered, collaborators can engage in various model development and application studies, generation of new parameters etc.

Currently, a database for Houston Texas is serving as the focus city of the NUDAPT prototype. Eventually, the goal for NUDAPT is to be extended to all major urban areas within the United States.

5. REFERENCES

Burian, S.J., Stetson, S.W., Han, W., Ching, J. and Byun, D., 2004: High-resolution dataset of urban canopy parameters for Houston, Texas. Preprint proceedings, Fifth Symposium on the Urban Environment, AMS, 23-26 August, Vancouver, BC, Canada, 9 pp.

Burian, S.J., Brown, M.J., McPherson, T.N., Hartman, J., Han, W., Jeyachandran, I., and Rush, J., 2006: Emerging urban databases for meteorological and dispersion. *Sixth Symposium on the Urban Environment, Atlanta GA Jan28-Feb 2, 2006*. American Meteorological Society, Boston, Paper 5.2.

Burian, S.J., Brown, M.J., Augustus, N., 2007a: Development and assessment of the second generation National Building Statistics database. *Seventh Symposium on the Urban Environment, San Diego, CA Sep 10-13, 2007*. American Meteorological Society, Boston, Paper 5.4.

Burian, S.J., Brown, M.J., Sailor, D.J., Cionco, R.M., Ellefsen, R., Estes, M., and Hultgren, T., 2007b: Database features of the National Urban Database and Access Portal Tools(NUDAPT). *Seventh Symposium on the Urban Environment, San Diego, CA Sep 10-13, 2007*. American Meteorological Society, Boston, Paper 6.2.

Chen, F., M. Tewari, H. Kusaka and T. L. Warner: Current status of urban modeling in the community Weather Research and Forecast (WRF) model. *Sixth AMS Symposium on the Urban Environment, Atlanta GA, January 2006.*

Chen, F., Tewari, M., Miao, S., Liu,Y., Ching, J., and Kusaka, H., 2007a: Challenges in developing advanced urban parameterization

schemes for the community WRF model, *Seventh Symposium on the Urban Environment, San Diego, CA, Sep 10-13, 2007* American Meteorological Society, Boston, paper J3.2.

Chen, F., Tewari, M., and Ching, J., 2007b: Effects of high resolution building and urban data sets on the WRF/urban coupled model simulations for the Houston-Galveston areas. *Seventh Symposium on the Urban Environment, San Diego, CA, Sep 10-13, 2007* American Meteorological Society, Boston, paper 6.5.

Ching, J.K.S., S. Dupont, R. Gilliam, S. Burian, and R. Tang, (2004): Neighborhood scale air quality modeling in Houston using urban canopy parameters in MM5 and CMAQ with improved characterization of mesoscale lake-land breeze circulation. *Fifth Symposium on the Urban Environment, Vancouver BC, Canada, August 23-26, 2004*. American Meteorological Society, Boston, Paper 9.2.

Dupont, S., T. L. Otte, and J. K.S. Ching, 2004: Simulation of meteorological fields within and above urban and rural canopies with a mesoscale model (MM5) Boundary Layer Meteor., 113: 111-158.

Martilli, A., 2007: An overview of advanced urbanization of mesoscale models, *Seventh Symposium on the Urban Environment, San Diego, CA Sep 10-13, 2007*. American Meteorological Society, Boston, Paper J3.1.

Martilli, A., and Schmitz, R., 2007: Implementation of an Urban Canopy Parameterization in WRF-chem. Preliminary results, *Seventh Symposium on the Urban Environment, San Diego, CA Sep 10-13, 2007*. American Meteorological Society, Boston, Paper 5.3.

McPherson T.N., and Brown, M.J., 2003a: Estimating daytime and nighttime population distributions in U.S. cities for emergency response activities, Preprint, 84th AMS Annual Meeting, Seattle WA.

McPherson, T. and M. Brown, 2003b: U.S. day and night population database (Revision 2.0) – Description of methodology, LA-CP-03-0722, 30 pp.

McPherson, T. N., Ivey, A. and M. J. Brown, 2004: *Determination of the spatial and temporal distribution of population for air toxics exposure assessments*5th AMS Urban Env. Conf., Vancouver, B.C.

McPherson T., J. Rush, H. Khalsa, A. Ivey, and M. Brown, 2006: A day-night population exchange model for better exposure and consequence management assessments, 6th AMS Urb. Env. Symp., Atlanta, GA, LA-UR-05-, 6 pp.

Office of the Federal Coordinator for Meteorology (2005): Proceedings from the Forum on Urban Meteorology. www.ofcm.gov/homepage/text/pub.htm

Otte, T. L., A. Lacser, S. Dupont, and J. K. S. Ching, 2004: Implementation of an urban canopy parameterization in a mesoscale meteorological model. J. Appl. Meteor., 43, 1648-1665.

Park, K., and Fernando, H.J.S., 2007: Influence of urban effects on air quality in Phoenix urban area simulated by modified MM5/Urbanized, *Seventh Symposium on the Urban Environment, San Diego, CA Sep 10-13, 2007*. American Meteorological Society, Boston, Paper 6.6.

Sailor, D.J., Lu. L., 2004: A top-down methodology for developing diurnal and seasonal anthropogenic heating profiles for urban areas. Atmospheric Environment 38(17) 2737-2748.

Sailor, D.J, Hart, M., 2006: An anthropogenic heating database for major U.S. cities, *Sixth Symposium on the Urban Environment, Atlanta GA Jan 28-Feb 2, 2006*. American Meteorological Society, Boston, Paper 5.6.

Taha, H., and R. Bornstein, R., 2007a: Mesoscale and meso-urban modeling of heat islands and control: Evaluation of potential ozone air-quality impacts in California, . *Seventh Symposium on the Urban Environment, San Diego, CA Sep 10-13, 2007*. American Meteorological Society, Boston, Paper 1.8.

Taha, H., and Ching, J.K.S., 2007b: UCP / MM5 Modeling in conjunction with NUDAPT: Model requirements, updates, and applications, . *Seventh Symposium on the Urban Environment, San Diego, CA Sep 10-13, 2007*. American Meteorological Society, Boston, Paper 6.4

Acknowledgements: The Author gratefully acknowledges Steve Burian for his inputs on the National Building Statistics database, to Tim McPherson and Michael Brown for their inputs on day-night population data and to David Sailor for his inputs on anthropogenic heating data.

Disclaimer: *The research presented here was performed under the Memorandum of Understanding between the U.S. Environmental Protection Agency (EPA) and the U.S. Department of Commerce's National Oceanic and Atmospheric Administration (NOAA) and under agreement number* DW13921548. *This work constitutes a contribution to the NOAA Air Quality Program. Although it has been reviewed by EPA and NOAA and approved for publication, it does not necessarily reflect their policies or views.*

Table 1: Gridded UCPs from lidar-derived building and vegetation data for urbanized MM5 model.

Canopy UCPs:	Building UCPs:	Vegetation, Other UCPs:
Mean canopy height Canopy plan area density Canopy top area density Canopy frontal area density Roughness length Displacement height Sky view factor	Mean building height Standard deviation of building height Building height histograms Building wall-to-plan area ratio Building height-to-width ratio Building plan area density Building rooftop area density Building frontal area density	Mean vegetation height Vegetation plan area density Vegetation top area density Vegetation frontal area density Mean orientation of streets Plan area fraction surface covers Percent directly connected impervious area Building material fraction

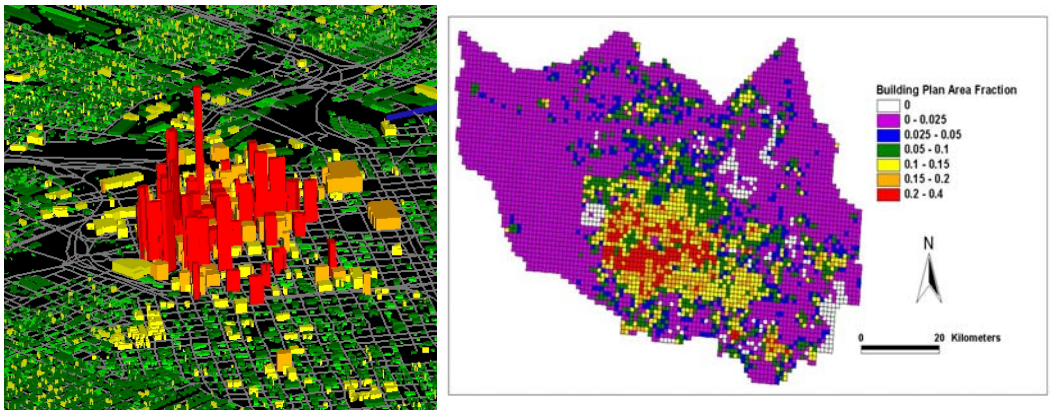

Fig. 1(a) Left: Three dimensional building data derived from airborne lidar platform for 1x1 km section of downtown Houston. (b) Right: Building plan area density, an example of a UCP for Harris County (Houston Metropolitan area) (cf Table 1)

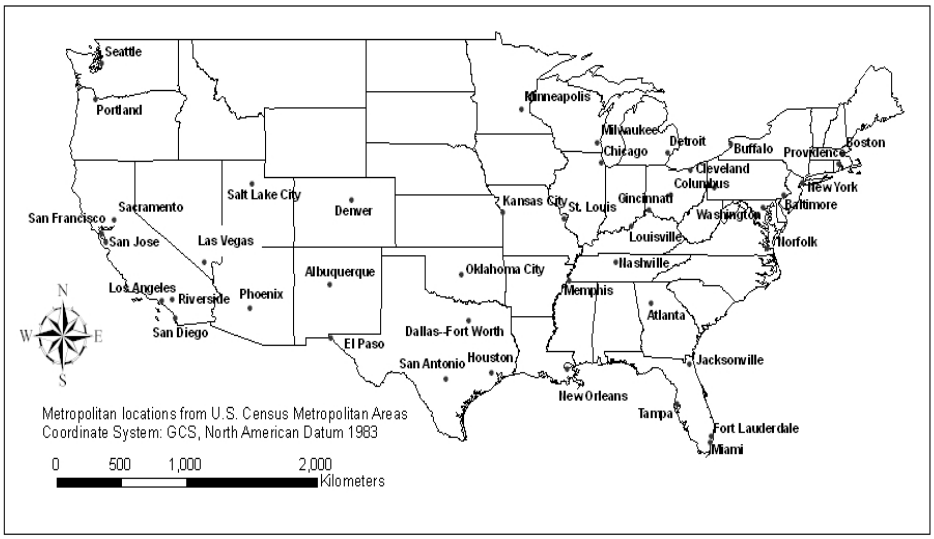

Figure 2 (a) National Building Statistics Database ((Version 2.0) (47 + Cities))

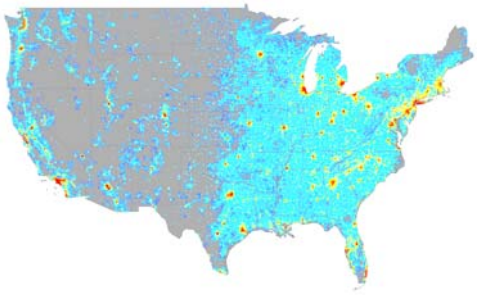

Figure 3 Gridded Day-Night Population database (Courtesy of McPherson and Brown)

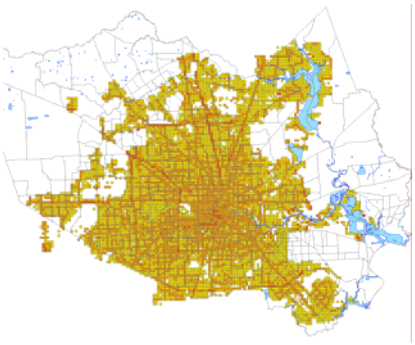

Figure 4: Anthropogenic heating: Houston August, 2000 CDT (Courtesy of David Sailor)

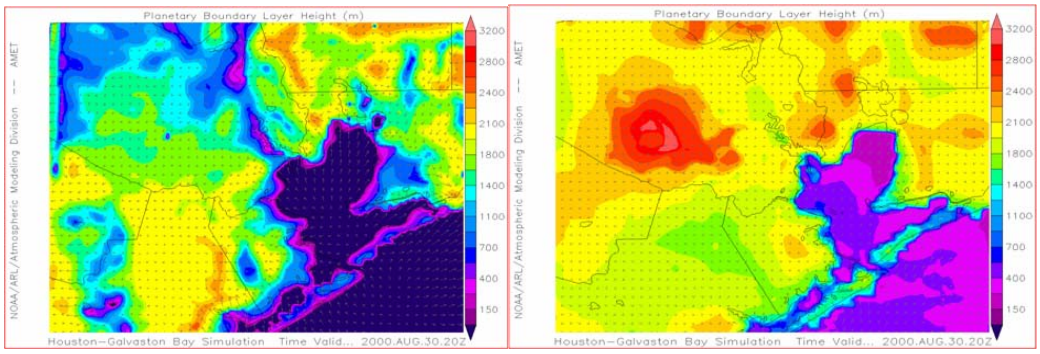

Figure 5. Simulations of mixed layer heights size for 2100 GMT, August 30, 2000. MM5 with UCP (left) and standard version of MM5 (right) at 1 km grid.

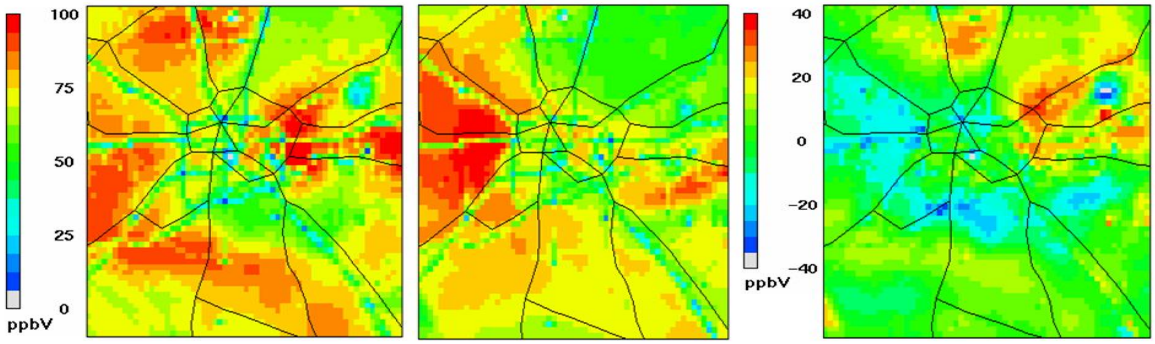

Figure 6: Simulations of surface ozone using CMAQ driven by UCP (left) and No-UCP (center) versions of MM5 (see Figure 2). Differences are shown on right panel.

Diagnostic and Operational Evaluation of 2002 and 2005 Estimated 8-hr Ozone to Support Model Attainment Demonstrations

Kirk Baker*
Lake Michigan Air Directors Consortium, Rosemont, IL, USA

Donna Kenski
Lake Michigan Air Directors Consortium, Rosemont, IL, USA

1. INTRODUCTION

The United States Environmental Protection Agency (US EPA) promulgated nonattainment area designations for the 8-hour ozone National Ambient Air Quality Standard on April 15, 2004 (69 CFR 23858, April 30, 2004). State Implementation Plans will include modeling the impacts of emission control scenarios with 3-D Eulerian photochemical transport models. Several photochemical models, including the Comprehensive Air Quality Model with Extensions (CAMx4), treat the physical processes and chemistry that form ozone. Model performance is typically evaluated on an operational basis and rarely to support a diagnostic assessment. Operational evaluations for ozone modeling purposes include matching model estimates with observation data for ozone, nitrogen oxides (NO_X), and total volatile organic compounds (VOC).

A diagnostic evaluation assesses how appropriately the modeling system responds to emissions adjustments. Since the modeled attainment demonstration includes modeling current and future year emissions it is important to have confidence that the model will predict ozone concentrations appropriately when emissions change (US EPA, 2007). This type of evaluation includes modeling two different ozone episodes that are separated by enough years that large emissions differences exist. The diagnostic evaluation is an important assessment to make in addition to an operational evaluation because it is directly linked to the end use of the model, which is modeling the change in ozone concentrations after emissions adjustments.

A comparison between observed and estimated ozone for the summers of 2002 and 2005 is useful for a diagnostic assessment because high quality emission inventories were developed for each year and a large NO_X emissions reduction occurred between these years due in part to NO_X SIP Call compliance.

Modeling two full summer seasons provides an opportunity to make another diagnostic evaluation which assesses model performance for high ozone by day of the week. Emissions change substantially from weekday to weekend and having two full summers provides enough days with high ozone on each day of the week to make this type of evaluation useful.

A comparison of a typical summer day emission inventory used for this modeling application for the 5 State Midwest region (IL, IN, OH, MI, WI) is shown in Table 1.

Table 1. Typical July weekday emissions (tpd) for 2002 and 2005.

	VOC 2002	VOC 2005	NOX 2002	NOX 2005
Nonroad Mobile	1,167	1,558	1,875	1,843
Other Area	2,555	2,637	255	283
Onroad Mobile	2,185	1,829	4,035	3,402
EGU Point	35	28	3,422	1,712
Non-EGU Point	751	635	1,085	1,021
5 State Total	6,693	6,687	10,672	8,260

NO_X emissions over the Upper Midwest 5 State region decrease from 10,672 tpd to 8,260 tpd between 2002 and 2005. Most of this difference is attributable to a 1,710 tpd decrease in emissions from electrical generating utilities (EGUs) and a 633 tpd decrease in onroad motor vehicle emissions. Total VOC emissions are very similar between 2002 and 2005 for these 5 States. Emissions change between weekday and weekend in terms of total mass for VOC and NO_X, but they change in different directions which makes the mix of pre-cursors available on weekends different from weekdays. VOC emissions generally increase about 20% from weekday to

weekend due in large part to increases in off-road mobile source emissions. NO_X emissions decrease by 20% largely due to decreases in on-road mobile source and some decreases in electrical generating utility emissions.

The Midwest region experienced meteorology that is generally conducive for ozone formation in the summer of 2002 and 2005. A Classification and Regression Tree (CART) analysis was done examining meteorological data at certain locations in the Midwest United States to characterize how ozone conducive the summers of 2002 and 2005 were compared to other recent summers. CART is a non-parametric method that is advantageous because it is insensitive to distributions of variables, which means it is insensitive to missing data and outliers. CART classifies days into groups (or bins) based on meteorological characteristics associated with observed ozone from 1990 to 2006. The index is estimated based on the number of days in high ozone groups each year compared to the average number of days in those groups. A higher index value means the summer was more conducive to ozone formation. A zero value indicates that the summer was average in terms of meteorological characteristics conducive to ozone formation.

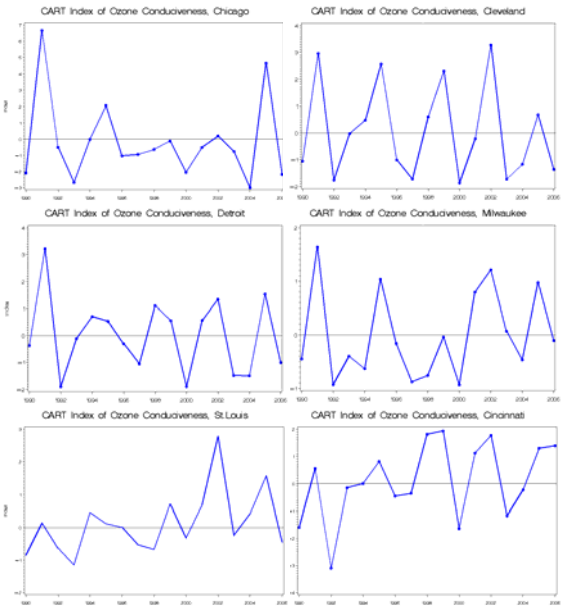

Fig. 1. CART ozone conducive index.

Figure 1 shows the estimated ozone conducive index from 1990 to 2006 at several locations: Chicago, Milwaukee, Cleveland, Cincinnati, Detroit, and St. Louis. At each of these locations the summers of 2002 and 2005 are at least typical in terms of ozone conduciveness and often have meteorological characteristics that are more conducive to ozone formation than a typical summer. This increases confidence that model estimates will largely be a response to differences in emissions rather than meteorology.

2. METHODS

The Comprehensive Air Quality Model with Extensions (CAMx) version 4.30 uses state of the science routines to model ozone formation and removal processes over regional and urban scales (Nobel et al, 2002; Chen et al, 2003; Morris et al, 2005). The model is applied with an updated carbon-bond IV (CB4) gas phase chemistry module (ENVIRON, 2006; Carter, 1996). CAMx is applied using the PPM horizontal transport scheme and an implicit vertical transport scheme with the fast CMC chemistry solver (ENVIRON, 2006). The photochemical model is initiated at midnight Eastern Standard Time and run for 24 hours for each episode day. The summer simulations are initiated on June 2 and run through August 31. The first 11 days of the simulation are not used in any analysis to minimize the influence of initial concentrations (Baker, 2007).

Boundary conditions represent pollution inflow into the model from the lateral edges of the grid and initial conditions provide an estimation of pollution that already exists. The initial and boundary conditions are based on monthly averaged species output from an annual (calendar year 2002) application of the GEOS-CHEM global chemical transport model (Jacob et al, 2002; Bey et al, 2001). Boundary conditions vary by month and in the horizontal and vertical direction. Where an initial or boundary concentration is not specified for a pollutant the model will default to a near-zero concentration.

The meteorological, emissions, and photochemical models are applied with a

Lambert projection centered at (-97, 40) and true latitudes at 33 and 45. The 36 km photochemical modeling domain consists of 97 cells in the X direction and 90 cells in the Y direction covering the central and eastern United States (Figure 2). The 2-way nested 12 km domain covers most of the upper Midwest region with 131 cells in the X and Y directions. CAMx is applied with the vertical atmosphere resolved with 16 layers up to approximately 15 kilometers above ground level.

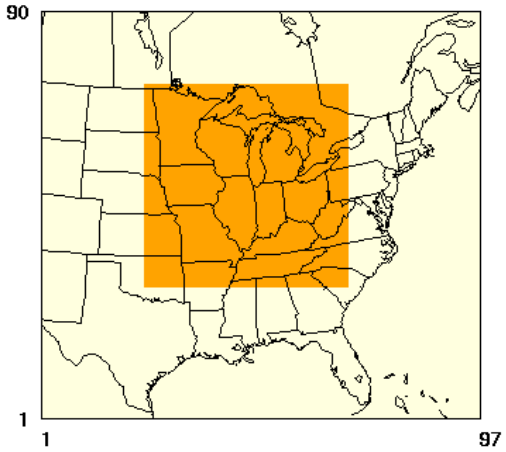

Fig. 2. 36 km (large box) and 12 km (small dark box) modeling domain.

Meteorological input data for the photochemical modeling runs are processed using the National Center for Atmospheric Research (NCAR) 5th generation Mesoscale Model (MM5) version 3.6.1 (Dudhia, 1993; Grell et al, 1994). Important MM5 parameterizations and physics options include mixed phase (Reisner 1) microphysics, Kain-Fritsch 2 cumulus scheme, Rapid Radiative Transfer Model, Pleim-Chang planetary boundary layer (PBL), and the Pleim-Xiu land surface module. Analysis nudging for temperature and moisture is only applied above the boundary layer. Analysis nudging of the wind field is applied above and below the boundary layer. These parameters and options are selected as an optimal configuration for the central United States based on multiple MM5 simulations using a variety of physics and configuration options (Johnson, 2003; Baker, 2004).

Emissions data is processed using EMS-2003. In addition to extensive quality assurance and control capabilities, EMS-2003 performs basic emissions processes such as chemical speciation, spatial allocation, and temporal allocation (Janssen and Hua, 2007; Wilkinson et al, 1994). Anthropogenic emission estimates are made for a weekday, Saturday, and Sunday for each month. The biogenic emissions are day-specific. Volatile organic compounds are speciated to the Carbon Bond IV (CB4) chemical speciation profile (Gery et al, 1989). Biogenic emissions are estimated with EMS-2003 using a variation of the BEIS3 model (Guenther et al, 2000). The BELD3 land use dataset is input to the biogenic model for fractional land-use and vegetative speciation information (US EPA, 2006; Kinnee et al, 1997). Other inputs to the biogenic emissions model include hourly satellite photosynthetically activated radiation (PAR) and 15 m (above ground level) temperature data output from MM5 (Pinker and Laszlo, 1992).

3. RESULTS & DISCUSSION

The ozone design value is the 4th highest maximum 8-hr ozone concentration over a summer averaged over 3 consecutive summers. The 95th percentile ozone concentration over each summer of 2002 and 2005 was chosen as a value similar to averaging 3 consecutive 98th percentile values together. The 95th percentile daily maximum 8-hr ozone observation for each monitor over each summer is paired with model estimates. The mean bias of 8-hr maximum ozone greater than the 95th percentile averaged over all stations in the 12 km domain is -13 ppb for 2002 (N=1,385) and -9 ppb for 2005 (N=1,677). The mean error of 95th percentile 8-hr maximum ozone is 15 ppb for 2002 and 12 ppb for 2005. NO_X and total VOC are only measured at a few sites in the region. In general, the modeling system shows little bias in estimating NO_X and total VOC in 2002 and has a slight over-estimation tendency of VOC in 2005.

The correlation coefficient is estimated to determine the relationship between the change in 95th percentile observations between 2002 and 2005 and the change in the paired model predictions between the

same years. This approach is designed to determine if the change in high ozone observed at each monitor location between 2002 and 2005 is similar to the change in model estimates of high ozone between 2002 and 2005 at the same location. If observed ozone decreases but the modeling system predicts similar values or an increase between years then the relationship would be weak. However, if the model predictions change similarly to the observed values then the relationship would be strong. The relationship in bias between 2005 and 2002 observations and the bias between paired predictions is strong (r=.64, r^2=.41, N=240). This indicates that the modeling system generally replicates the direction ozone observations are changing between 2002 and 2005 at upper Midwest monitor locations.

Another way to assess model response to emissions changes is to examine how well the model estimates high ozone by day of the week. Mean bias and mean error of days in each summer with 8-hr ozone greater than 80 ppb is shown in Table 2.

Table 2. Mean bias and mean error of days with 8-hr ozone > 80 ppb in 2002 and 2005.

Day of Week	N	Bias	Error
Monday	16	-11.8	18.1
Tuesday	14	-12.4	15.4
Wednesday	17	-15.5	18.2
Thursday	16	-13.8	17.4
Friday	17	-16.1	19.4
Saturday	14	-7.6	17.4
Sunday	16	-11.6	16.0

The benefit of simulating 2 summer seasons is that there are enough days with high ozone to assess model performance by day of the week. The results in Table 2 show consistent model performance by day of the week. The weekend days clearly do not perform any worse than weekday days. Again, the model seems to be responding appropriately to changes in the emission inventory.

4. CONCLUSION

The operational evaluation suggests high ozone is slightly under-predicted in both summers. The diagnostic approaches used in this study suggests the modeling system will appropriately respond to emissions adjustments, which is important since a relative modeling approach is required to estimate future year ozone values for ozone attainment demonstrations. Many different approaches may provide information useful to assess how appropriately the modeling system responds to emissions adjustments. Future research should explore other methods of diagnostic evaluation. One alternative approach involves modeling 2002 and 2005 anthropogenic emissions using 2002 meteorology and using the relative reduction factor approached detailed in the US EPA modeling guidance document to project 2005 values. These projected 2005 values could then be compared to observed values.

5. REFERENCES

Baker, K. Ozone Source Apportionment Results for Receptors in Non-Attainment Counties in the Great Lakes Region. 2007. AWMA Annual Conference. Pittsburgh, PA.

Baker, K. Meteorological Modeling Protocol For Application to PM2.5/Haze/Ozone Modeling Projects, 2004. http://www.ladco.org/tech/photo/photochemical.html

Bey, I.; Jacob, D; Yantosca, R.; Logan, J.; Field, B.; Fiore, A.;Li, Q.; Liu, H.; Mickley, L.; Schultz, M. Global modeling of tropospheric chemistry with assimilated meteorology: Model description and evaluation, *J. Geophys. Res*., **2001**, *106*, 073-096.

Carter, W.P.L. Condensed Atmospheric Photooxidation Mechanisms for Isoprene. *Atmos. Environ*., **1996**, *30*, 4275-4290.

Chen, K. S.; Ho Y.T.; Lai C.H.; Photochemical modeling and analysis of meteorological parameters during ozone episodes in Kaohsiung, Taiwan, *Atmospheric Environment*, **2003**, *37(13),* 1811-1823.

Dudhia, J. A nonhydrostatic version of the Penn State/NCAR mesoscale model:

Validation tests and simulation of an Atlantic cyclone and cold front, *Mon. Wea. Rev.*, **1993**, *121*, 1493-1513.

ENVIRON International Corporation. User's Guide Comprehensive Air Quality Model with Extensions (CAMx) Version 4.30; ENVIRON International Corporation: Novato, CA, 2006. www.camx.com

Gery, M.W.; Whitten, G.Z.; Killus, J.P.; Dodge, M.C. A photochemical kinetics mechanism for urban and regional scale computer modeling. *Journal of Geophysical Research*, **1989**, *94*, 12925–12956.

Grell, G. A.; Dudhia, J.; Stauffer, D. A description of the Fifth Generation Penn State/NCAR Mesoscale Model (MM5), NCAR Tech. Note, 1994; NCAR TN-398-STR.

Guenther A.; Geron C.; Pierce T.; Lamb; Harley P.; Fall R. Natural emissions of non-methane volatile organic compounds; carbon monoxide, and oxides of nitrogen from North America, *Atmos. Environ*., **2000**, *34*, 2205-2230.

Jacob, D.; Park, R.; Logan, J., Documentation and evaluation of the Geos-Chem simulation for 2002 provided to the Vistas Group. June 24, 2005. djacob@fas.harvard.edu.

Janssen, M.; Hua., C. Emissions Modeling System-95 User's Guide. Lake Michigan Air Directors Consortium: Rosemont, IL. See http://www.ladco.org/emis/guide/ems95.html

Johnson, M. Meteorological Modeling Protocol: IDNR 2002 Annual MM5 Application, 2003.

Kinnee, E.; Geron C.; Pierce T. United States land use inventory for estimating biogenic ozone precursor emissions. *Ecological Applications*, **1997**, *7(1)*, 46-58.

Morris, R.E.; Mansell G.; Tai. E. Air Quality Modeling Analysis for the Denver Early Action Ozone Compact. Prepared for Denver Regional Air Quality Council, Denver, CO. ENVIRON International Corporation, Novato, California, 2005.

Nobel, C. E.; McDonald-Buller E.C.; Kimura, Y.; Lumbley, K.E.; Allen, D.T. Influence of population density and temporal variations in emissions on the air quality benefits of NOx emission trading, *Environmental Science & Technology*, **2002**, *36*, 3465-3473.

Pinker, R.T.; Laszlo I. Modeling surface solar irradiance for satellite applications on a global scale. *J. Appl. Meteor*., **1992**, *31*, 194-211.

U. S. Environmental Protection Agency. See http://www.epa.gov/ttn/chief/emch/biogenic/ (accessed August 9, 2006).

U. S. Environmental Protection Agency, *Guidance on the Use of Models and Other Analyses for Demonstrating Attainment of Air Quality Goals for Ozone, PM2.5, and Regional Haze.* April 2007. EPA -454/B-07-002.

Wilkinson, J.; Loomis, C.; Emigh, R.; McNalley, D.; Tesche, T., Technical Formulation Document: SARMAP/LMOS Emissions Modeling System (EMS-95). Final Report prepared for Lake Michigan Air Directors Consortium (Rosemont, IL) and Valley Air Pollution Study Agency (Sacramento, CA), 1994.

RESULTS OF IMPLEMENTING A SUB-GRID SCALE TERRAIN EFFECTS PARAMETERIZATION UPON EMISSIONS AND DRY DEPOSITION IN CAMX

Saswati Datta*
Data and Image Processing Consultants LLC, Morrisville, NC, USA

Carlie J. Coats Jr.
Baron Advanced Meteorological Systems, Candler, NC, USA

M. Talat Odman
School of Civil and Environmental Engineering, Georgia Institute of Technology, Atlanta, GA, USA

1. INTRODUCTION

The mathematical formulation of certain algorithms in any atmospheric and air quality models may be based on assumptions and simplifications that can lead to incomplete treatment of mass conservation (Byun, 1999a and 1999b; Odman and Russell, 2000). Air quality models combine emissions with meteorological fields to track the transport, transformation and removal of air pollutants. Problems of mass inconsistency or mass distribution in the air quality models arises due to

- Using inconsistent meteorological field generated by the meteorological model.
- Inconsistency in the otherwise correct meteorological fields introduced during translating the grid and time step to the air quality model.
- Terrain height discrepancies in the meteorological models due to numerical stability issues in the dynamics.

The mass inconsistency problem can be handled by modifying the wind and density field used or by using other mass adjustment methods or using a combination of these methods. But, the terrain height problem is not currently addressed in any operational meteorological, emission, or air quality model.

A project funded by Central California Ozone Study (CCOS) addressed that issue by implementing parameterized sub grid scale terrain effects on emission and dry deposition processes in CAMx air quality model.

**Corresponding author:* Saswati Datta, Data and Image Processing Consultants, 504 Willingham Road, Morrisville, NC 27560; e-mail: swati@baronams.com

Section 2 gives a brief description of the problem and the approach to solve it. Section 3 describes the modeling domain, time period and basis of the sensitivity analysis presented in section 4. The final section (5) summarizes the main findings of the study.

2. SUB GRID SCALE TERRAIN EFFECT

In search of sources of mass distribution problems, CAMx model formulations are examined to realistically simulate interactions with complex terrain such as found in California. Existing Baron Advanced Meteorological Systems (BAMS) tools show that when high-resolution United States Geological Survey (USGS) 30 arc-sec terrain data are averaged over 4km CCOS grid in CAMx, the standard deviation of the terrain height within the grid cells exceeds 200 m for most of the State of California, with a maximum of 515 m. Such differences in terrain height would have substantial impacts on model simulations. For example, emission sources and their plumes may be placed at a very different altitude in the model than the actual atmosphere. Again, deposition processes may be removing very different amounts of mass in the model than the actual atmosphere. This further implies, the volume of air subject to emission and dry deposition needs to be corrected to account for the sub-grid scale terrain effect.

The problem is approached from two perspectives.

- Sub-grid scale correction to effective stack height for point source plume rise. This will have substantial effect on emissions near static point sources and resulting air quality behavior.
- Devise a better sub-grid scale terrain parameterization. There are at least two different approaches available,

the 'naive' approach and the 'reference-mass-conservative' approach described by Coats (2005).

The primary variables for the sub-grid scale terrain effects are the number of model layers PLAYS into which terrain is allowed to penetrate, and a 3-D array of layer fractions LFRAC, which gives the fraction of each layer of each horizontal grid cell in contact with the terrain. The details of correction approach are described in another accompanying paper (Coats et. al, 2007) in this conference. In brief, the sub grid scale terrain effects are parameterized via modified layer fraction (the fraction of each layer of each horizontal grid cell in contact with the terrain) and a stack height adjustment technique.

3. MODELING SETUP

The modeling domain for this exercise is shown in Figure 1 below.

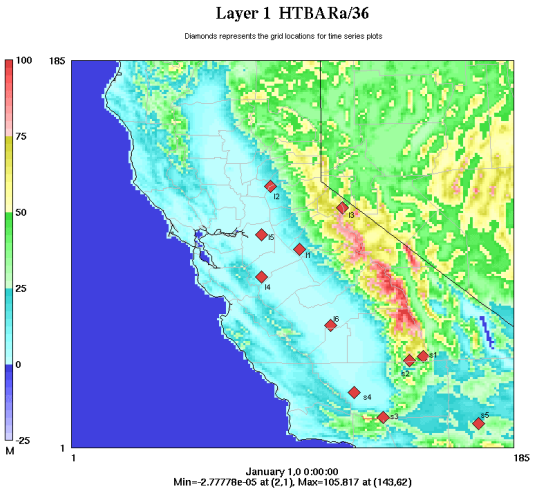

Figure 1: CCOS CAMx modeling domain with terrain height. The diamonds represent selected grid cells for which some detailed analysis are performed.

The time period of interest is July 29, 2000 to August 02, 2000. The horizontal resolution is 4 km and the temporal resolution is 1 hour. The time stamps in CAMx runs are local standard time, which in our case is Pacific Daylight Time (PDT). For this analysis, only layer 1 ozone (PPM) is considered. Table 1 below describes the base case and scenario case runs that have been made.

Table 1: List of model runs for CCOS

Case	***Description***
Base	Default Version, this is the reference case
Lfrac_em	Introduce layer fraction with emission effects only
Lfrac_dif	Introduce layer fraction with deposition consideration only
Lfrac	Introduce layer fraction with both emission and deposition consideration
Stk	Introduce stack height adjustment
Lfrac_stk	Introduce layer fraction and stack height adjustment together

4. RESULTS OF THE SENSITIVITY ANALYSIS

The base case layer ozone varies from near 0 to 0.267 PPM with a definite diurnal pattern in it. A plume is found to develop around 11 AM local time at and near grid cell (147, 52) every day from 07/29/ 2000 to 7/31/2000 (see Figure 2).

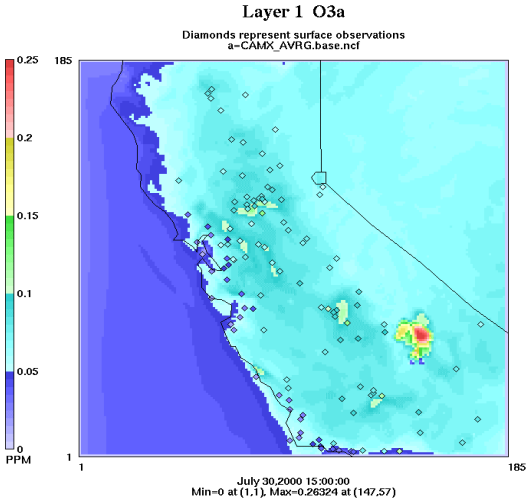

Figure 2: July 30, 2000 3:00 PM surface ozone simulation with surface observation overlay. No surface observation is available to support the hot plume in the southeastern section of the modeling domain.

The plume has a NNE to Northerly movement which disperses by 6 to 8 PM local time. On 7/31, 8/1 and 8/2 some more activity is also noted in the central valley region. The introduction of layer fraction with emission only does not seem to affect the simulation, but the introduction of layer fraction with deposition, affects the result significantly. Figures 3 a-c depicts the effect for July 30, 2000 3:00 PM simulation.

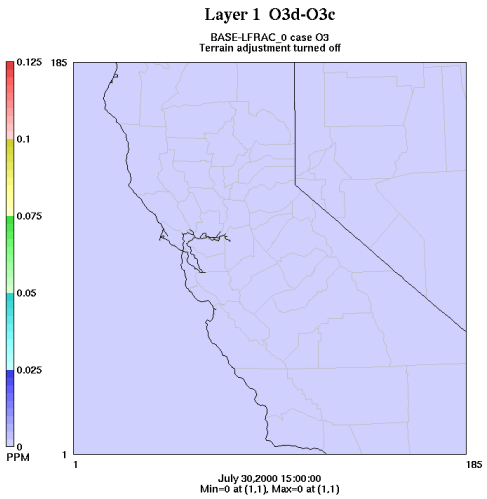

Figure 3a: No Correction applied, the reference.

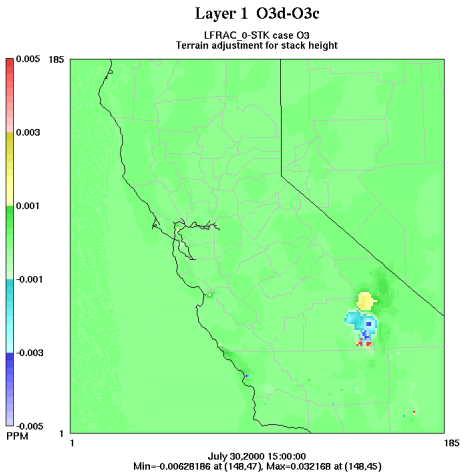

Figure 3b: Effect of introducing stack height adjustment

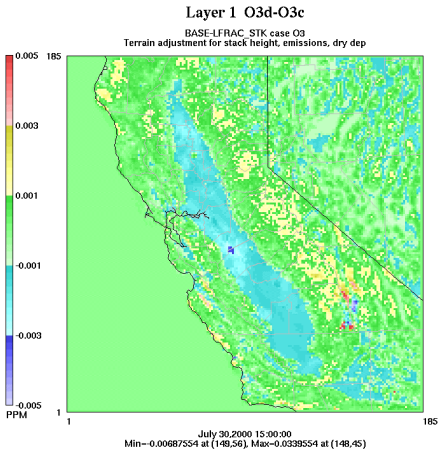

Figure 3c: Effect of introducing layer fraction and stack height adjustment

The stack height adjustment effect (Figure 3b) is pronounced only near a significant point source. But as, the layer fraction correction is introduced, more widespread effects are noted (Figure 3c) mainly due to corrected deposition. The effects are more pronounced over and close by mountains and very less to negligible in the plain valley.

In order to assess, the performance of these simulations, the model output is compared against surface observation. Diamonds in Figure 2 shows the locations of some of the surface ozone monitoring sites in California. For the performance analysis the entire domain is split in 3 windows. The Northern window covers 38.8° N, 122.8°W to 40.0° N, 121.8° W. The Central window covers 37.7° N , 122.3° W to 38.7°N, 121.4°W; and the Southern window covers 37.1°N, 120.6°W to 37.4°N, 119.7°W. For each window the model and observation pairs are selected for morning hours between 8 to 10 AM local time and evening hours between 4 to 6 PM local time. These 6 cases are marked as NM, NE, CM, CE and SM, SE cases respectively. The effect of different scenario case simulation is assessed via the improvement (or deterioration) of the correlation coefficient between model and observation with respect to base case run. Figure 4 shows a bar plot with improvements in correlation coefficient for different scenario cases with respect to the base case run. Negative numbers indicate the correlation is improved towards 1.0 and positive numbers indicate correlation worsens away from 1.0.

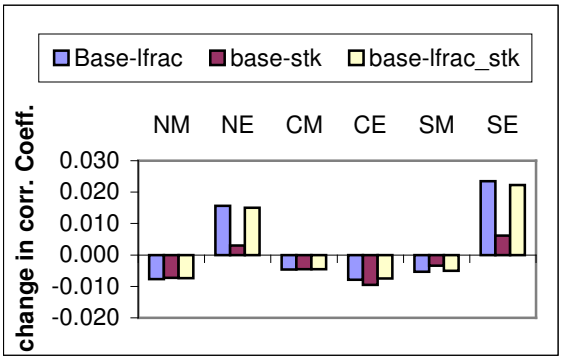

Figure 4: Bar plot for improvements in correlation coefficient

It is observed the layer fraction correction has significant impact in both southern and northern window in the evening. The central part does not show any significant change.

To investigate further how different adjustments impact over the base case, a time series analysis is performed over selected grid cells. 11 points are selected (see Figure 1).

The time series analysis show, the lfrac correction seem to smooth the temporal gradient

of the field particularly around the evening hours. For locations in the plain valley, l5 and l6, (see figure 1) the effects are negligible (Figures 5 and 6).

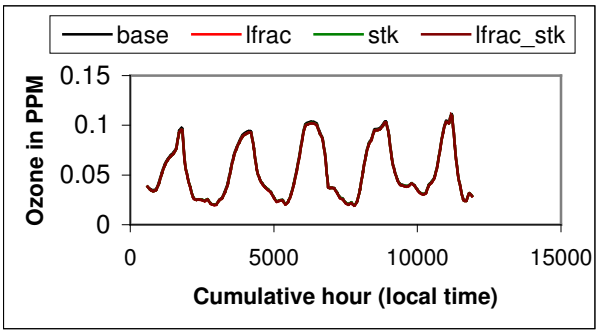

Figure 5: Time-series for grid cell l5

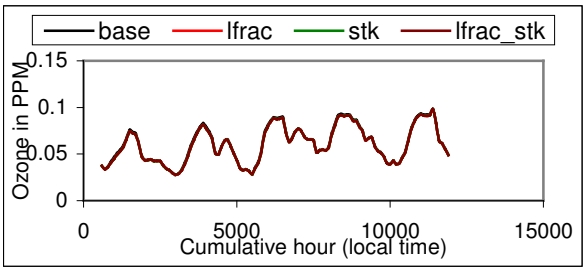

Figure 6: Time-series for grid cell l6

Some interesting features are noted during the time series analysis for grid cells s4 and s5, where there are significant effect of stack height correction. Again, those cells being on top or near mountains, the layer fraction effect is also quite pronounced. As a result, when both lfrac and stk are applied together, for point s4 (Figure 7), the opposite impacts are balanced out and in case of point s5 (Figure 8), similar impacts are added up resulting more temporal smoothing.

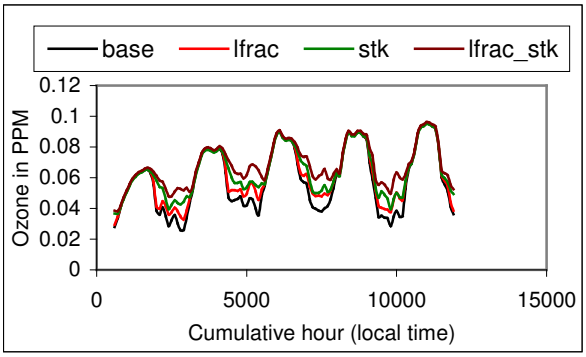

Figure 7: Time-series for grid cell s4.

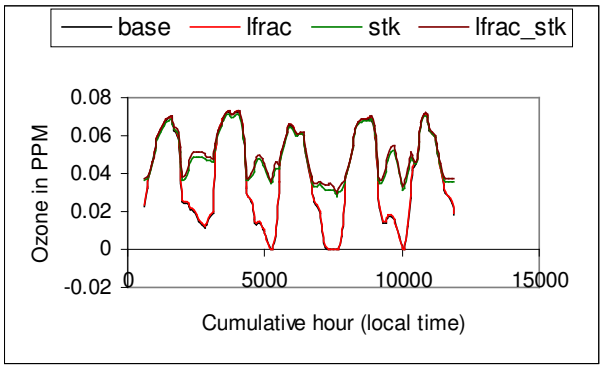

Figure 8: Time-series for grid cell s5.

5. SUMMARY

This paper discussed the result of applying sub-grid scale terrain correction to CAMx model in layer 1 ozone simulation over the State of California. It is found that adjusting stack height has significant but localized impact on air quality simulation near static point sources. It can be as high as 0.05 ppm at some locations. Introducing a layer fraction based terrain parameterization has a more wide spread effect, mostly near the mountains. The maximum effect noted is about 0.035 ppm. The valley region does not have much impact as expected due to flatter terrain.

6. REFERENCES

Byun D. W., 1999a. Dynamically consistent formulations in meteorological and air quality models for multi-scale atmospheric studies, Part I: Governing equations in a generalized co-ordinate system. *J. Atmos. Sci.*, **56**, 3789-3807.

Byun D. W., 1999b. Dynamically consistent formulations in meteorological and air quality models for multi-scale atmospheric studies, Part II: Mass conservation issues. *J. Atmos. Sci.*, **56**, 3808-3820.

Coats C. J., 2005. A conservative framework for sub-grid scale terrain effects in air quality forecast models. 7th Conference on Atmospheric Chemistry, American Meteorological Society, San Diego, CA, January 2005.

Coats C.J., Datta S. and Odman M. T., 2007. Implementation of a parameterization of sub-grid scale terrain effects upon emissions and dry deposition in CAMx. 6th Annual CMAS Conference, Chapel Hill, NC, October 1-3, 2007.

Odman M. T. and Russell A. G, 2000. Mass conservative coupling of non-hydrostatic meteorological models with air quality models, in *Air Pollution Modeling and Its Application XIII*, eds., S. –E. Gryuing and E. Batchvarova, Kulwer Academic/Plenum Publishers, New York, 651-660.

AERMOD-HPC A HIGH PERFORMANCE COMPUTING VERSION OF AERMOD

George Delic *
HiPERiSM Consulting, LLC, Durham, NC, USA

Arnold R. Srackangast
AS1MET Services, Blanco TX, USA

1. INTRODUCTION

HiPERiSM **C**onsulting, LLC, (Durham, North Carolina) has **l**inked with **AS1**MET Services (Blanco, Texas) to form a joint venture, **HiCLAS1** (http://www.hiclas1.com), dedicated to bringing High Performance Computing (HPC) capability to Environmental Modeling. The HiCLAS1 mission is to develop (or enhance) software and improve performance on current and future computers for legacy Air Quality Models (AQM). The first model chosen for performance enhancement by HiCLAS1 is the U.S. EPA's AERMOD developed by the U.S. EPA Office of Air Quality Planning and Standards (OAQPS), Emissions Monitoring and Analysis Division (EMAD), at the U.S. EPA in Research Triangle Park, North Carolina, U.S.A (SCRAM). In-house Quality assurance testing and results from Beta testers show performance of the serial version of AERMOD-HPC that is 1.95 to 3.43 times faster than the EPA distribution of AERMOD. The purpose of this presentation is to provide quantitative evidence of the measured hardware performance metrics to demonstrate how the improvements in efficiency are achieved. Results with the serial version of AERMOD-HPC are presented for Intel Pentium Xeon processors. The subject of numerical differences is taken up in technical reports available on-line (HiCLAS1).

2. CHOICE OF HARDWARE AND OPERATING SYSTEM

The hardware used for the results reported here is the Intel Pentium 4 Xeon processor with separate platforms using the Linux™ operating systems for both 32-bit and 64-bit platforms, respectively. The hardware used for the results reported here is the Intel Pentium 4 Xeon (P4) and Pentium Xeon 64EMT (P4e) processors.

* *Corresponding author address:* George Delic, HiPERiSM Consulting, LLC, P.O. Box 569, Chapel Hill, NC 27514-0569. Email: george@hiclas1.com

The operating system (OS) is HiPERiSM Consulting, LLC's modification of the Linux™ 2.6.9 kernel to include a patch that enables access to hardware performance counters. This modification allows the use of the Performance Application Programming Interface performance event library (PAPI, 2005) to collect hardware performance counter values as the code executes. Results for selected performance metrics are presented with a view to giving insight into how the application is mapped to the architectural resources by an un-named compiler.

3. BENCHMARK TIMINGS

Four benchmarks are used with the number of sources varying from 10 to 963, number of receptors from 771 to 916, and the number of meteorological hours from 2160 to 8760. Details on the benchmarks are available elsewhere (HiCLAS1). Two version of the U.S. EPA's AERMOD model are used here: the executable distribution, designated AERMOD-EPA, and the version compiled from the (unmodified) source distribution designated as AERMOD-EPA/SRC. The U.S. EPA source and executable are available on-line (SCRAM).

To create the High Performance Computing (HPC) version of AERMOD the source code for the U.S. EPA distribution was progressively modified to enhance performance. Speedup of the HPC version over the EPA model is shown in Fig. 1 (AERMOD-HPCS versus AERMOD-EPA) and Fig. 2 (AERMOD-HPCS versus AERMOD-EPA/SRC). The results of Fig. 2 are for both versions compiled from source with identical compiler options.

Whether comparing against the U.S. EPA executable or source code compiled with the same compiler options AERMOD-HPCS always delivers superior performance. The remainder of this report gives some in reasons as to why this is the case.

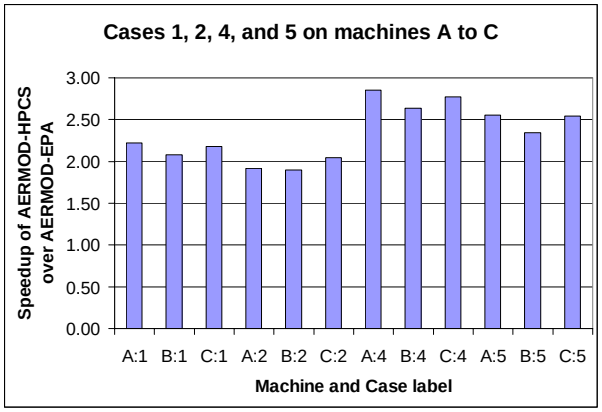

Fig. 1 displays the ratio of runtimes for AERMOD-HPCS and AERMOD-EPA for three Pentium 4 Xeon machines (A to C) with a 32-bit Windows OS. This shows that, for four Cases, performance enhancement ranges from 1.9 to 2.77 times faster than AERMOD-EPA (depending on the platform and data set used in the benchmark).

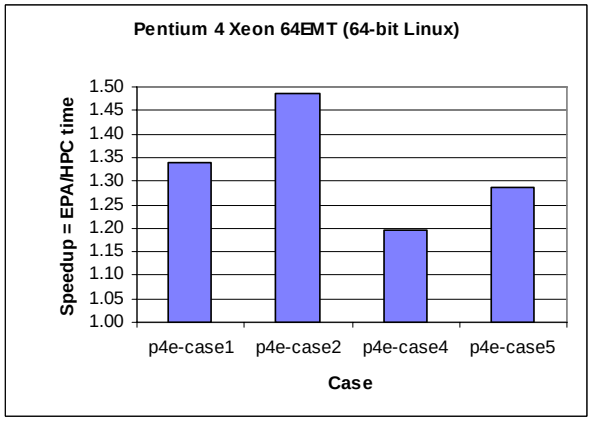

Fig.2. Speedup of AERMOD-HPCS as measured by the ratio of the wall clock time for the U.S. EPA AERMOD version (compiled from source code) divided by the wall clock time for AERMOD-HPCS for the same compiler options for four cases.

4. HARDWARE PERFORMANCE EVENTS

The hardware used for the results reported here is the Intel Pentium 4 Xeon (P4) and Pentium Xeon 64EMT (P4e) processors. For this hardware performance counters were used to measure performance metrics and some values are summarized below.

4.1 Operations and instructions

AERMOD-HPCS delivers higher Mflops rates as is shown in Fig. 3 for the 64-bit Linux case.

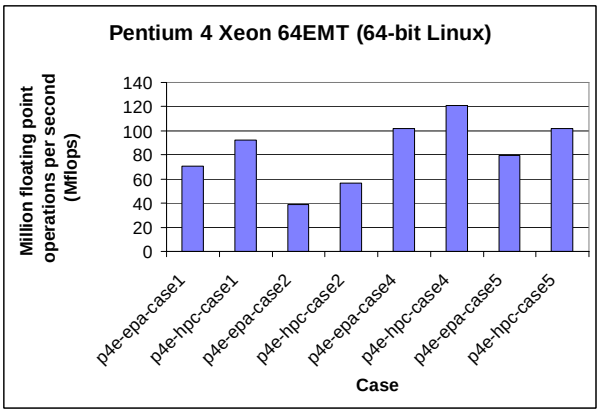

Fig. 3 Mflops for AERMOD in EPA (epa) and HPCS (hpc) versions for four cases.

One important contributing factor to higher Mflops is that AERMOD-HPCS delivers higher vector/SSE instruction rates as shown in Fig. 4. However, performance gains for AERMOD from enhanced vector instructions alone is limited because of the lack of vector loop structure and the predominance of control transfer instructions. These stall the vector pipeline and cycles are lost to loading of new instructions.

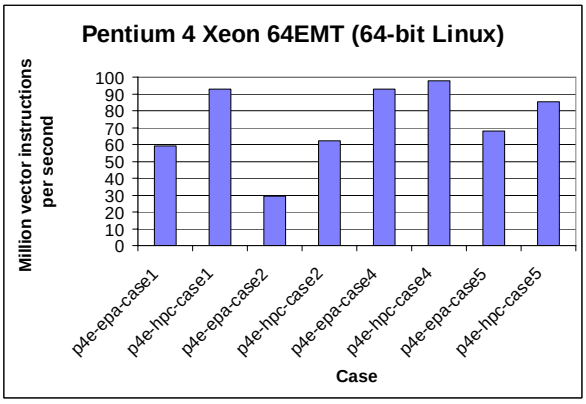

Fig. 4 Vector instruction rates for AERMOD in EPA (epa) and HPCS (hpc) versions for four cases.

4.2 Memory footprint

For AERMOD in general, the rate of total memory instructions issued is voluminous. The consequence of AERMOD's memory footprint is that the path to memory becomes a critical performance bottle-neck. This bottle-neck is somewhat ameliorated in AERMOD-HPCS compared to AERMOD-EPA as is described in the following.

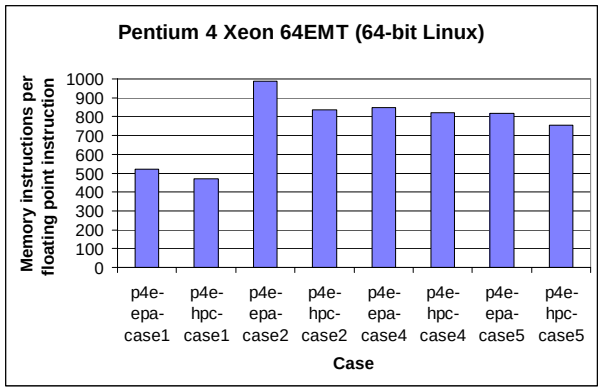

Fig. 5 Memory instructions per floating point instruction for AERMOD-HPCS (hpc) compared to that for the U.S. EPA's distribution (epa) for four cases.

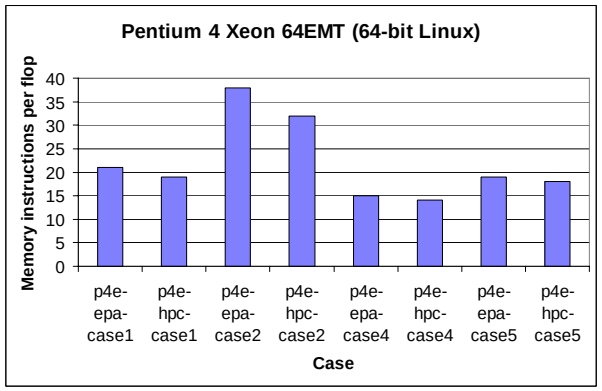

Fig. 6 Memory instructions per flop for AERMOD-HPCS (hpc) compared to that for the U.S. EPA's distribution (epa) for four cases.

Fig. 5 shows the load balance of memory versus floating point instructions and demonstrates the extent to which AERMOD is a memory-bound application. As a consequence, AERMOD is extremely sensitive to any inefficiency in memory access. It is notable that AERMOD-HPCS reduced this load imbalance somewhat, but it is still critical. Fig. 6 shows that for each flop there are more then 14 memory instructions in all cases on either P4 (not shown) or P4e platforms. This is a gross imbalance suggesting that the CPU is starved of data and spends excessive cycles in an idle state.

4.3 Branching instructions

Control transfer instructions are a significant source of lost CPU cycles in AERMOD and chief among these are branch instructions. Mispredicted branch instructions on deep pipelined processors are an important cause of lost performance, because instructions in the mispredicted path are cancelled and operations are not completed. The pipeline is flushed and new instructions are loaded with the result that cycles are lost to arithmetic performance. Fig. 7 shows that in all cases, on both 32-bit (not shown) and 64-bit platforms, AERMOD-HPCS has reduced mispredicted branch instruction rates and this correlates positively with higher Mflops.

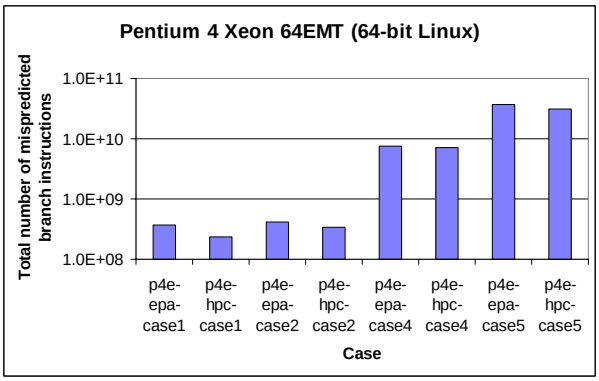

Fig. 7 Logarithm of total number of mispredicted branch instructions for AERMOD-HPCS (hpc) compared to that for the U.S. EPA's distribution (epa) for four cases.

4.4 TLB Cache usage

The translation lookaside buffer (TLB) is a small buffer (or cache) to which the processor presents a virtual memory address and looks up a table for a translation to a physical memory address. If the address is found in the TLB table then there is a hit (no translation is computed) and the processor continues. The TLB buffer is usually small, and efficiency depends on hit rates as high as 98%. If the translation is not found (a TLB miss) then several cycles are lost while the physical address is translated. Therefore TLB misses degrade performance. In the case of AERMOD it is the instruction TLB misses that are critical. Higher instruction TLB miss rates suggest that the processor pipeline stalls more frequently because of a higher rate of control transfer instructions. This is due to numerous procedure calls and voluminous mispredicted branch instruction rates.

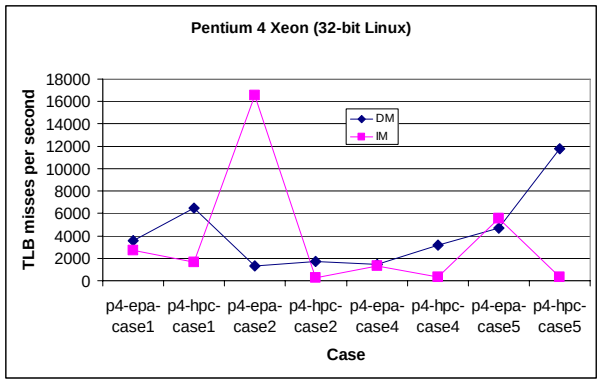

Fig. 8 TLB misses per second for AERMOD-HPCS (hpc) compared to that for the U.S. EPA's distribution (epa). Note that the instruction misses (IM) are reduced in AERMOD-HPCS for each of four cases.

While the TLB data miss rates (DM) have increased in AERMOD-HPCS relative to the EPA version, performance has improved, suggesting that it is the TLB instruction miss rates that are important for performance in AERMOD. The AERMOD-HPCS version is more efficient in reducing instruction TLB miss rates (IM) through optimization and resource allocation compared to the EPA version. The most dramatic reduction is in Case 2 for the 32-bit platform, as shown in Fig. 8, and this explains (in part) why AERMOD-HPCS has so much better performance compared to the EPA version (see Case 2 in Fig. 2).

4.5 L1 Cache usage

A cache miss occurs when data or instructions are not found in the cache and an excursion to higher level cache, or memory, is necessitated. Cache misses result in lost performance because of increasing latency in the memory hierarchy. Memory latency is smallest at the register level and increases by an order of magnitude for a L1 cache reference, and another order of magnitude to access L2 cache. In the case of AERMOD this analysis will focus on the L1 cache behavior. Fig. 9 shows L1 cache miss rates for data (DCM) and instructions (ICM). Even though the ICM rate has been scaled the reduction for AERMOD-HPCS versus the EPA version is evident and has a positive correlation with the TLB instruction miss rate reduction shown in Fig. 8.

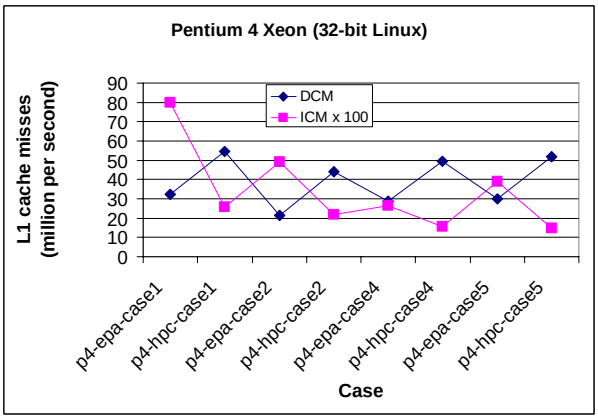

Fig. 9 Million L1 cache misses per second for AERMOD-HPCS (hpc) compared to that for the U.S. EPA's distribution (epa) for four cases.

5. WHY IS AERMOD-HPC FASTER?

The code transformation applied in AERMOD-HPCS take cognizance of procedures occurring at the leaves of a deep calling tree. Such procedures invariably have no loop structure but consist of simple arithmetic statements and conditional code blocks. The most frequently called procedures typically have little arithmetic work. These are some of the reasons for lack of vectorizable loops and the high rates of branching instructions in the U.S. EPA version of AERMOD. As a result the extremely high instruction TLB misses for AERMOD are a critical source of performance limitations. High memory instruction rates are due to high TLB instruction miss rates and also to correlated L1 instruction cache miss rates. This behavior is ameliorated by the improved efficiency of the AERMOD-HPCS version in reducing the performance consequences of this behavior. AERMOD-HPCS is faster than the U.S. EPA version AERMOD-EPA/SRC because it delivers:

- Higher Mflops rates
- Lower number of memory instructions per floating point instruction
- Lower mispredicted branch instruction rates
- Lower instruction TLB miss rates
- Lower L1 instruction cache miss rates

6. CONCLUSIONS

This performance analysis of the U.S. EPA version of AERMOD, shows that it is a memory intensive application with large rates of control transfer instructions such as branching logic and procedure calling overhead. These features result in large observed rates for branching instructions and instruction TLB misses. These, in turn, result in stalled pipelines and cycles lost to arithmetic operations. In combination these characteristics of the AERMOD code place a limit on the optimal performance possible from it on commodity platforms. This is because, by design, commodity hardware solutions offer a cost effective compromise between processor clock rates, cache size, and bandwidth (or latency) to memory.

The AERMOD-HPCS version goes some way to ameliorate these performance limitations. As a result gains in computational efficiency translate into reduced wall clock time. However, there is still scope for further improvements and progress will be reported in subsequent reports at the HiCLAS1 URL where the AERMOD-HPCS version of AERMOD is available at the download pages (HiCLAS1).

References

HiCLAS1: Further details are available from the HiCLAS1 URL at http://www.hiclas1.com.

PAPI, 2005: *Performance Application Programming Interface*, http://icl.cs.utk.edu/papi. Note that the use of PAPI requires a Linux kernel patch (as described in the distribution).

SCRAM: AERMOD is available at U.S. EPA, Technology Transfer Network, Support Center for Regulatory Air Models http://www.epa.gov/scram001/.

USE OF AIR QUALITY FORECASTING AS A DIAGNOSTIC TOOL OVER THE NORTHEASTERN US

Prakash Doraiswamy[1,$,*], Christian Hogrefe[1,2], Winston Hao[2], Kevin Civerolo[2], J.-Y. Ku[2], Robert Henry[2] and Gopal Sistla[2]

[1]Atmospheric Sciences Research Center, University at Albany, Albany, NY
[2]Bureau of Air Quality Analysis and Research (BAQAR), New York State Department of Environmental Conservation (NYSDEC), Albany, NY
[$] On assignment to BAQAR, NYSDEC

1. INTRODUCTION

Typical air quality simulations involve modeling selected episodes retrospectively based on time periods of interest. This limits the ability of evaluating the performance of a model beyond the episodic periods or select years, and to identify issues that may not be apparent. Since June 2005, the research group at the Bureau of Air Quality Analysis and Research (BAQAR) at New York State Department of Environmental Conservation (NYSDEC) has been conducting daily air quality forecasting of ozone and fine particles ($PM_{2.5}$) using the Community Multi-scale Air Quality Model (CMAQ) on a pilot-scale, in collaboration with EPA and NOAA. These simulations have been (and continue to be) archived providing a dataset for varied air quality applications. As an example, this study focuses on the archived hourly concentration fields for isoprene during June through August 2005 and compares its performance to measured concentrations on a diurnal scale at locations in the northeastern part of the US. The overall objective is to assess the utility of the forecast based simulations as a diagnostic tool by using a combination of analyses on the response of the model to biogenic, anthropogenic and secondary species.

2. MODEL AND OBSERVATIONAL DATABASE

2.1. Model Set-Up and Archived Database

The data used in this study were from the archived air quality forecast simulations conducted by NYSDEC for the summer of 2005. The modeling system used during that time period has been described elsewhere (Hogrefe et al. 2006; 2007). Briefly, it consisted of the ETA meteorological model, the PREMAQ (Otte et al. 2004; 2005) emissions and meteorology preprocessor, and the CMAQ (Byun and Ching 1999) photochemical model (v4.4), operated in a forecasting mode. The PREMAQ processor included BEIS3.12 for the biogenic emissions processing. The simulation was started on June 1, 2005, which was initialized using default conditions in CMAQ. Each CMAQ simulation was performed for 48 hours starting at 12:00 Greenwich Mean Time (GMT). Simulations for every day thereafter were initialized using modeled concentration fields from the previous day. Time-invariant boundary conditions were used. In this analysis, results for June 1-11, 2005 are excluded to eliminate the effects of initial conditions. The modeling domain covered almost the entire Eastern U.S with a 12 km horizontal grid resolution. All emission and meteorological inputs processed by PREMAQ, and the CMAQ-processed concentration fields of all model species for layer 1 (i.e., ground level surface layer, ~35 m height above ground level [agl]) and selected species for the lowest 14 layers (~2750 m agl) are archived regularly, among other custom analyses. The predicted concentration fields from these files are used in this analysis.

This study focuses on diurnal predictions of isoprene concentrations during June-August of 2005, the dominant time period in 2005 for which observational data were available for most sites.

2.2. Observational Database

Measured concentrations of isoprene were obtained from the EPA Air Quality System (AQS) for all monitors in the New England and Mid-Atlantic State region comprising of Maine, Vermont, New Hampshire, New York, Massachusetts, Connecticut, Rhode Island, Pennsylvania, New Jersey, Maryland, Delaware and District of Columbia. Table 1 lists the sites with hourly

[*] *Corresponding author:* Prakash Doraiswamy, BAQAR, New York State Department of Environmental Conservation, 625 Broadway, Albany, NY 12233-3259; Phone: (518) 402-8402; Fax: (518) 402-9035; Email: pdorai@gmail.com

isoprene measurements that were used in this analysis. In addition to isoprene, hourly concentrations of ethylene (anthropogenic and biogenic origin), ozone (product of photochemical reaction) and nitrogen dioxide (anthropogenic and chemical production) were also obtained, where available, for the same sites, to serve as supplemental information in the evaluation of model performance.

3. DATA ANALYSIS, RESULTS AND DISCUSSION

Hourly model predictions were compared with measured concentrations of isoprene. Various statistical measures of performance, including the correlation coefficient (r), root mean square error (RMSE), normalized mean gross error (NMGE) and normalized mean bias (NMB) were calculated for each site utilizing hourly data. In addition to the traditional statistical measures, diurnal concentrations averaged by hour for each month were calculated and plotted for both observed and model-predicted concentrations.

Table 2 lists the statistical summary for the 2.5-month period (June 12-August 31, 2005) for each site. Correlations for that period ranged from 0.25 to 0.63. Sites in NJ, PA, MD, DC and one site in CT showed a net over-prediction as shown by a positive NMB, while other sites showed a net under-prediction. While the results presented in Table 2 provide a good overall summary of the model behavior over the entire summer period, an examination of observed and simulated diurnal profiles is presented as further focus of this study. First, the correlation between hourly observed and simulated concentrations were calculated separately for each day utilizing all available data within each 24-hour period, and box plots were constructed displaying the distribution of these correlations at all sites (Figure 1). As seen, the distribution of daily correlations differed between sites. Some sites exhibit zero to negative correlations indicating poor to inverse agreement. Median daily correlations ranged from 0.24 to 0.72. The upper end of whiskers of all sites was typically above 0.8, indicating days of excellent agreement of diurnal profiles. Since the focus of the study is the Mid-Atlantic Region, the following sites are further examined in this study: an urban site in NY (SI:360050083) located at NY Botanical Gardens (NYBG), Bronx, NY, a suburban site in NJ (SI:340210005) located at Rider College (NJRC) and a rural site in PA (SI:420010001), which is a NARSTO site located at Arendtsville, PA (PANARSTO).

Figure 2 presents the distribution of the hourly bias (CMAQ-predicted minus Observed) at each of the three sites. At the NYBG, the predictions differ from observations during mid-day hours. The bias (negative, implying an under-prediction) starts to deviate from zero at about 8 am local standard time, reaches a maximum around 2 pm, and then decreases back to zero around 7 pm. The suburban NJRC site showed zero bias until 5am, then a constant positive bias until 5 pm, and a peak between 6 pm to 9 pm. The rural PANARSTO site also shows similar pattern, with zero bias till 5 am, then near-zero bias until 1 pm, followed by a pronounced positive bias between 5 pm and 9 pm. Figure 3 (left panel) shows the corresponding average diurnal plots for the three sites. The urban and suburban sites show a pronounced dual peak in the predicted concentrations, which is present in measured concentrations at the suburban site, but not at the urban site. The rural site shows a less pronounced morning peak, while still possessing the evening peak. The questions of interest are: why do we see dual peaks in predicted concentration at an urban site, when the measurements do not; and is it possible to identify causes for agreement/ disagreement seen at the sites?

The answers to the above questions lie in analyzing the possible sources and sinks of isoprene, which will determine the ultimate shape of the profile. To aid in this analysis, CMAQ-predicted nitrogen dioxide (NO_2) (top half of each chart in left panel, Figure 3), ozone (O_3) (middle panel) and ethylene (C_2H_4) (right panel) concentrations were also compared to observations at these sites. Model-predicted HO_2 radical concentrations are also plotted as an indicator of products of isoprene reactions. In addition, estimated planetary boundary layer (PBL) heights were analyzed. All these plots are displayed in Figure 3. Based on these plots, the following hypotheses can be made: For the NYBG site, the NO_2 concentrations are over-predicted, which is consistent with predicted night-time ozone concentrations being lower than observed (due to scavenging by oxides of nitrogen, NO_x). It is possible that the over-prediction in NO_2 concentrations (possibly resulting from overestimation of emissions of NO_x) resulted in more OH radical formation which consumed isoprene. For the NJRC and PANARSTO sites, it could be hypothesized that the emission rate of isoprene is overestimated. The predicted ethylene concentrations (plotted on right y-axis, right panel of Figure 3), while being overestimated by more than 2 times, have a profile similar to observed

concentrations, except at PANARSTO between midnight and 5 am.

To further test the hypotheses, the time period under consideration was re-run using CMAQv4.6 and enabling the process analysis feature. Figure 4 presents the diurnal average of integrated process rates (IPR) for the first layer (surface) at NYBG as reported by the process analysis module. While the diurnal profile of the predicted concentrations varied between the three sites, the IPR profiles were similar at all three sites. For the surface layer, the dominating processes contributing to an increase in the isoprene concentrations are emissions followed by horizontal advection, while those contributing to a depletion of isoprene are losses by diffusion in the vertical direction followed by consumption by chemical reactions. From this, it is obvious that the resultant profile is primarily a balance between the emissions, advection, chemistry and vertical diffusion processes. The previously shown differences in predicted versus observed diurnal profiles at NYBG, that is, a depression in predicted profiles during mid-day hours, could imply that the predictions are either overestimating the chemical or diffusion losses or underestimating additional sources. For upper layers (not shown), chemical reactions appear to be the major and dominant pathway for depletion of isoprene, while the source of isoprene was diffusion from lower layers. Although the chemistry effect is smaller than the diffusion loss, it is potentially large enough (~ -0.5 ppb/hr) to partially explain the differences between observed and simulated diurnal profiles. For the other two sites, the process analyses confirmed emissions to be the major source of isoprene. Given the reasonable agreement in the shape of the predicted versus observed diurnal profiles of ozone and ethylene during mid-day hours at these two sites, it appears that the mixing processes (i.e., PBL height, vertical mixing) are modeled satisfactorily, and could not be solely responsible for the over-prediction of isoprene. It is likely that the emissions are overestimated, resulting in a positive bias. However, measurements at the individual process level (emissions, isoprene flux, etc.) would be needed to corroborate these findings.

The predicted peak in the evening is around 8-9 pm for the urban site, while it is around 6pm for the suburban and rural sites. At NYBG, an analysis of the IPRs, shows that horizontal advection of isoprene is the dominant process that contributes to the addition of isoprene in upper layers, and approximately 40% of the source term at the surface layer at that 8-9 PM. However, at NJRC and PANARSTO, while horizontal advection contributed to addition of isoprene, it was not the major source at 6 PM when the peak was observed. Although process analyses parameters for ethylene were not computed, the fact that the shape of the predicted diurnal profile of ethylene closely resembles measured profiles suggests that the horizontal advection process is treated adequately, and is unlikely to be the sole cause of the secondary peak in CMAQ-predicted isoprene profiles, which is either absent (at NYBG) or less pronounced (at NJRC and PANARSTO) in observations. At NYBG, this could mean a slight underestimation of night-time isoprene consumption in reactions. The physical and chemical mechanisms that result in loss of isoprene at night are highly uncertain and have been the subject of extensive research (Faloona et al. 2001; Goldan et al. 1995; Sillman et al. 2002; Starn et al. 1998). In CMAQ, the reaction between isoprene and nitrate radical is the only major reaction that contributes to nighttime depletion of isoprene. This in turn could imply an underestimation of production of nitrate radical concentrations. Starn et al. (1998) found that the rapid decrease in observed isoprene concentrations was associated with conditions when the product, $[O_3]*[NO_2] > 300$ ppb^2. At NYBG, while the observed $[O_3]*[NO_2]$ product dropped from 657 to 382 ppb^2 between 7 pm and 11 pm, the CMAQ predicted value was 395 ppb^2 at 7 pm, which dropped to 152-145 ppb^2 between 8 pm and 11pm. This is consistent with the theory that overestimated NO emissions resulted in scavenging of ozone, and over-prediction of NO_2. The cause of the peak at the other two sites could be related to a combination of overestimated isoprene emissions and possibly lack of surface emissions/sinks; however more research is needed to verify this.

4. CONCLUSIONS

Analyses of archived air quality forecasting simulations present a unique opportunity to evaluate the model under varied atmospheric conditions. This study presented an example of isoprene analysis based on a combination of techniques. Overall, the model appeared to track the diurnal profile as demonstrated by median correlations typically greater than 0.5 at most sites. Causes of model performance discrepancies do not seem to be universal, but appear to differ by site. The analyses revealed possible overestimation of isoprene emissions at NJRC and PANARSTO sites, and an over-prediction of NO_x emissions at NYBG site. Process analysis enabled confirming

initial hypotheses derived from analyzing isoprene and other supporting species.

5. DISCLAIMER

This research was funded in part by the U.S. Environmental Protection Agency (EPA) and the National Oceanic Atmospheric Administration (NOAA). The results presented here have not been reviewed by the funding agencies. The views expressed in this paper are those of the authors and do not necessarily reflect the views or policies of NYSDEC.

6. REFERENCES

Byun, D. W. and J. K. S. Ching (1999). Science algorithms of the EPA MODELS-3 community multiscale air quality (CMAQ) modeling system. Washington, DC, Office of Research and Development, U.S. Environmental Protection Agency.

Faloona, I., D. Tan, W. Brune, J. Hurst, D. Barket, T. L. Couch, P. Shepson, E. Apel, D. Riemer, T. Thornberry, M. A. Carroll, S. Sillman, G. J. Keeler, J. Sagady, D. Hooper and K. Paterson (2001). "Nighttime observations of anomalously high levels of hydroxyl radicals above a deciduous forest canopy." Journal of Geophysical Research **106**(D20): 24315-24333.

Goldan, P. D., W. C. Kuster, F. C. Fehsenfeld and S. A. Montzka (1995). "Hydrocarbon measurements in the southern United States: The Rural Oxidants in the Southern Environment (ROSE) Program 1990." Journal of Geophysical Research **100**(25): 945-963.

Hogrefe, C., W. Hao, K. Civerolo, J.-Y. Ku and G. Sistla (2006). Exploring Approaches to Integrate Observations and CMAQ Simulations for Improved Air Quality Forecasts. Models-3 Users' Workshop. Chapel Hill, NC.

Hogrefe, C., W. Hao, K. Civerolo, J.-Y. Ku, G. Sistla, R. S. Gaza, L. Sedefian, K. Schere, A. Gilliland and R. Mathur (2007). "Daily Simulation of Ozone and Fine Particulates over New York State: Findings and Challenges." Journal of Applied Meteorology **46**(NOAA/EPA Golden Jubilee Special Issue): 961-979.

Otte, T. L., G. Pouliot and J. E. Pleim (2004). PREMAQ: A New Pre-Processor to CMAQ for Air Quality Forecasting. Models-3 Conference. Chapel Hill, NC.

Otte, T. L., G. Pouliot, J. E. Pleim, J. O. Young, K. L. Schere, D. C. Wong, P. C. S. Lee, M. Tsidulko, J. T. McQueen, P. Davidson, R. Mathur, H. Y. Chuang, G. DiMego and N. L. Seaman (2005). "Linking the Eta Model with the Community Multiscale Air Quality (CMAQ) Modeling System to Build a National Air Quality Forecasting System." Weather and Forcasting **20** (3): 367-384.

Sillman, S., M. A. Carroll, T. Thornberry, B. K. Lamb, H. Westberg, W. H. Brune, I. Faloona, D. Tan, P. B. Shepson, A. L. Sumner, D. R. Hastie, C. M. Mihele, E. C. Apel, D. D. Riemer and R. G. Zika (2002). "Loss of isoprene and sources of nighttime OH radicals at a rural site in the United States: Results from photochemical models." Journal of Geophysical Research **107**(D5).

Starn, T. K., P. B. Shepson, S. B. Bertman, D. D. Riemer, R. G. Zika and K. Olszyna (1998). "Nighttime isoprene chemistry at an urban-impacted forest site." Journal of Geophysical Research **103**(D17): 22437-22448.

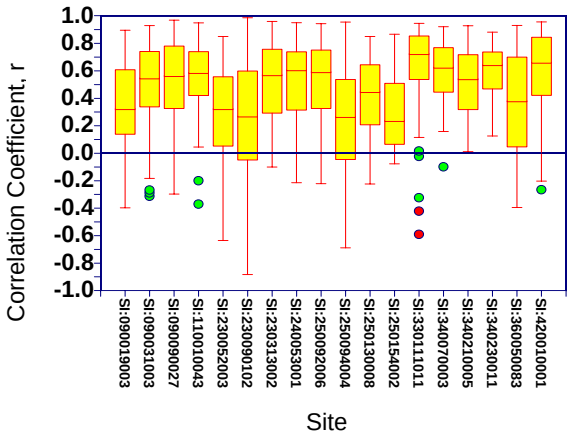

Figure 1. Daily Correlation Coefficients by Site during June 12-August 31, 2005. Only days with valid data for 18 hours or more (i.e., 75% of 24 hours) are included in the above plot. The box indicates the 25th, 50th and 75th percentiles. The upper (or lower) whiskers represent the largest (or the lowest) observation that is less than or equal to the 75th percentile plus 1.5 times the inter-quartile range [IQR] (or greater than or equal to the 25th percentile minus 1.5 times IQR). Data that fall outside the whiskers are outliers. Green dots are mild outliers (within 3 times IQR from the end of whiskers), while red dots are "severe" outliers (> 3 times IQR from end of whiskers).

Table 1. Sites Used in Model Evaluation

State	County	Site ID	Latitude (degrees)	Longitude (degrees)	Site Description	Land Use	Location Setting
Connecticut	Fairfield	090019003	41.1183	-73.3367	Sherwood Island State Park	Forest	Rural
Connecticut	Hartford	090031003	41.7847	-72.6317	McAuliffe Park	Residential	Suburban
Connecticut	New Haven	090090027	41.3011	-72.9028	1, James Street	Commercial	Urban city center
District of Columbia		110010043	38.9189	-77.0125	S.E. End McMillian Reservoir	Commercial	Urban city center
Maine	Cumberland	230052003	43.5608	-70.2078	Two Lights State Park	Residential	Rural
Maine	Hancock	230090102	44.3517	-68.2272	Top of Cadillac Mountain	Mobile	Rural
Maine	York	230313002	43.0833	-70.7500	Frisbee School, Goodsoe Rd	Residential	Suburban
Maryland	Baltimore	240053001	39.3108	-76.4744	Woodward and Franklin Roads, Essex	Residential	Suburban
Massachusetts	Essex	250092006	42.4744	-70.9725	390, Parkland	Commercial	Urban city center
Massachusetts	Essex	250094004	42.7894	-70.8092	Sunset Blvd	Residential	Suburban
Massachusetts	Hampden	250130008	42.1945	-72.5557	Anderson Rd, AFB	Commercial	Suburban
Massachusetts	Hampshire	250154002	42.2983	-72.3347	Quabbin Summit	Forest	Rural
New Hampshire	Hillsborough	330111011	42.7204	-71.5231	Gilson Road	Residential	Suburban
New Jersey	Camden	340070003	39.9228	-75.0972	Copewood & E. Davis Streets, Trailer	Residential	Suburban
New Jersey	Mercer	340210005	40.2828	-74.7467	Rider College, Lawrence Township	Residential	Suburban
New Jersey	Middlesex	340230011	40.4619	-74.4298	R.U. Veg Research Farm, 3 Ryders Ln	Agricultural	Rural
New York	Bronx	360050083	40.8659	-73.8808	200th Street and Southern Blvd	Commercial	Urban city center
Pennsylvania	Adams	420010001	39.9200	-77.3100	NARSTO Site, Arendtsville	Residential	Rural

Table 2. Statistical Summary of Model Performance for Isoprene Based On Hourly Data from June 12 – August 31, 2005*

Site ID	No.of Pairs	Obs.Mean (ppb)	Pred.Mean (ppb)	Correlation, r	RMSE[a] (ppb)	No.of Pairs, where Obs.> 0	NMGE[b] (%)	NMB[c] (%)
090019003	1616	0.477	0.231	0.446	0.718	1334	75.7	-53.1
090031003	1729	0.495	0.263	0.433	0.589	1714	73.8	-46.9
090090027	1865	0.260	0.284	0.525	0.433	1691	82.6	7.7
110010043	1520	0.402	0.959	0.404	1.210	1348	165.3	128.4
230052003	1831	0.183	0.219	0.255	0.516	1113	102.9	-11.6
230090102	1630	0.311	0.106	0.318	0.420	1337	81.2	-67.4
230313002	1602	0.435	0.383	0.441	0.644	1437	76.1	-13.2
240053001	803	0.429	0.524	0.544	0.575	794	75.1	22.0
250092006	1454	1.001	0.468	0.418	1.158	1428	72.1	-53.3
250094004	1606	0.491	0.196	0.351	0.805	1501	85.6	-60.2
250130008	1625	0.818	0.446	0.393	0.917	1615	71.5	-45.5
250154002	824	1.989	0.526	0.380	2.943	820	79.3	-73.6
330111011	1515	0.885	0.765	0.580	1.022	1504	63.8	-13.9
340070003	1810	0.397	1.180	0.524	1.323	1803	214.3	196.9
340210005	1796	0.439	0.697	0.502	0.716	1783	102.8	58.4
340230011	1583	0.783	1.141	0.542	1.236	1575	88.4	45.3
360050083	1526	0.769	0.300	0.272	0.922	1525	78.2	-61.0
420010001	1722	0.479	1.370	0.634	1.995	1644	211.2	185.2

* Model predictions were not available for June 1, 2005. June 2-11, 2005 were not considered to avoid effect of initial conditions. Note that there were a total of 1944 possible hours. Sites with number of pairs less than 1458 imply fewer than 75% of total possible dataset.

[a] RMSE: Root Mean Square Error = $\sqrt{\frac{1}{n}\sum_{i=1}^{n}\left(C_{pred}-C_{obs}\right)^2}$

[b] NMGE: Normalized Mean Gross Error = $\frac{100*\frac{1}{n}\sum ABS\left(C_{pred}-C_{obs}\right)}{\frac{1}{n}\sum C_{obs}}$

[c] NMB: Normalized Mean Bias = $\frac{100*\frac{1}{n}\sum\left(C_{pred}-C_{obs}\right)}{\frac{1}{n}\sum C_{obs}}$

where, C_{pred} is the CMAQ predicted concentration; C_{obs} is the measured concentration; ABS is the absolute value of the term; and n is the number of pairs of valid data for RMSE, while for NMGE and NMB, it is the number of pairs of valid data for which $C_{obs} > 0$.

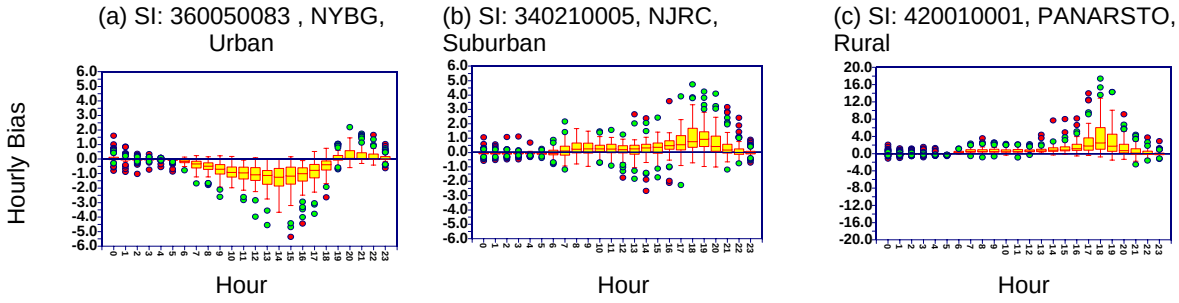

Figure 2. Hourly Bias (Predicted minus Observed) of Isoprene at Selected Sites during June 12-August 31, 2005

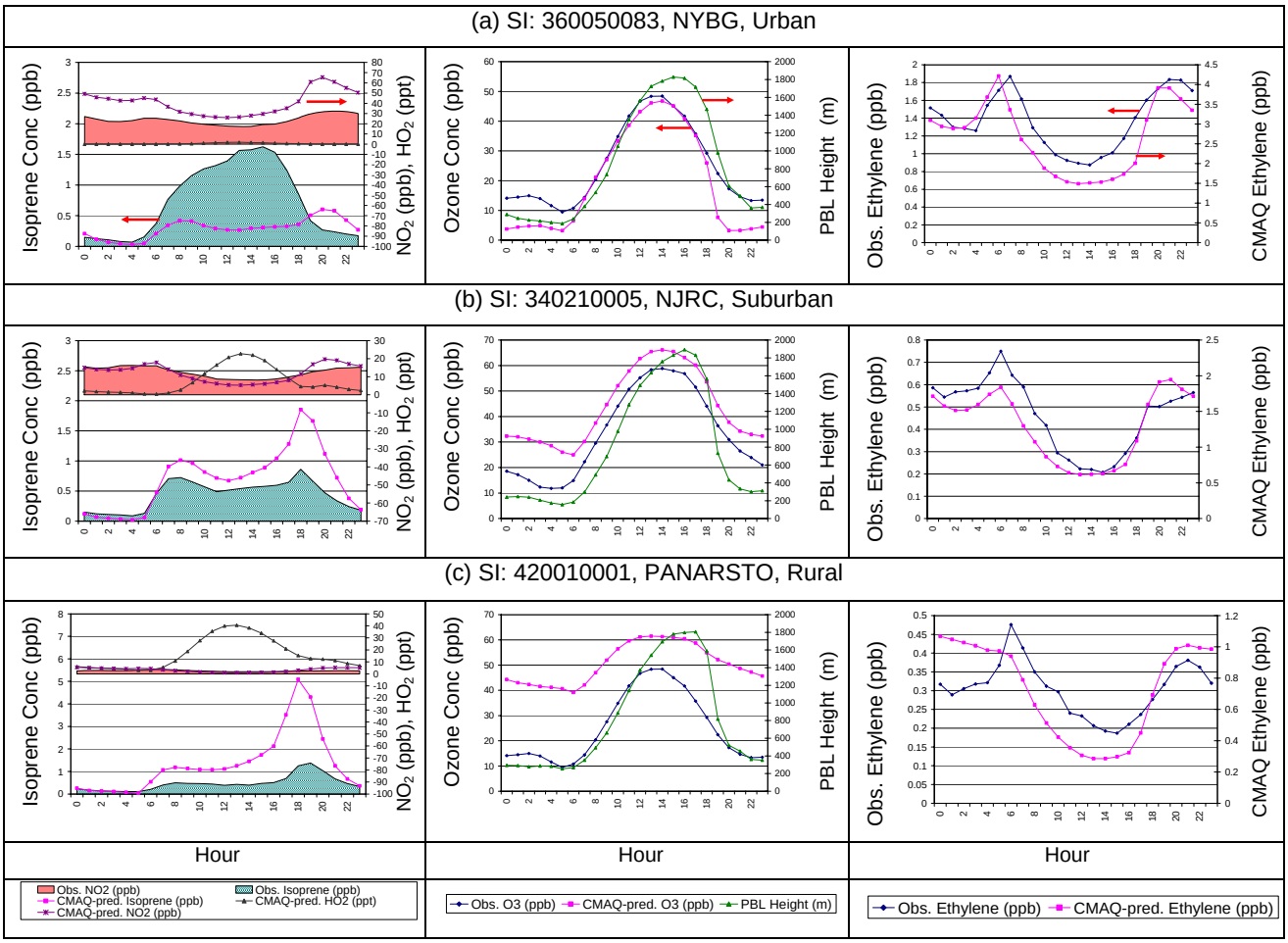

Figure 3. Average Diurnal Profile of Isoprene and Related Species during June 12-August 31, 2005. Note that certain species/parameters are plotted on the right y-axis, as indicated in the axis caption.

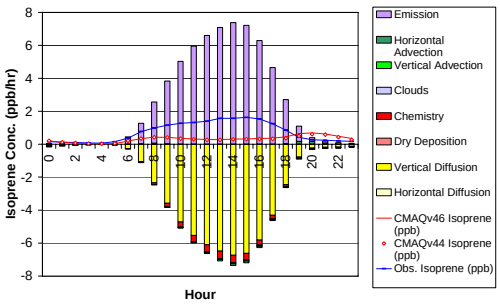

Figure 4. Diurnal Average of Integrated Process Rates Contributing to Predicted Isoprene Concentrations at NYBG during June 12 - August 31, 2005

STATISTICAL METHODS FOR MODEL EVALUATION - MOVING BEYOND THE COMPARISON OF MATCHED OBSERVATIONS AND OUTPUT FOR MODEL GRID CELLS

Jenise L. Swall and Kristen M. Foley*
Atmospheric Sciences Modeling Division, Air Resources Laboratory, National Oceanic and Atmospheric Administration, RTP, NC, 27711, USA
(In partnership with the U.S. Environmental Protection Agency, National Exposure Research Laboratory)

1. INTRODUCTION

Standard evaluations of air quality models rely heavily on a direct comparison of monitoring data matched with the model output for the grid cell containing the monitor's location (e.g. Eder and Yu 2006, Appel et al. 2007). While such techniques may be adequate for some applications, conclusions are limited by such factors as the sparseness of the available observations (limiting the number of grid cells at which the model can be evaluated), potential measurement error in the observations, and the incommensurability between volume-averages and point-referenced observations. While we focus most closely on the latter problem, we find that it cannot be addressed without some discussion of the others. Our approach uses simulated datasets to demonstrate cases in which incommensurability is more likely to adversely affect a traditional analysis. Future work will illustrate the impact on model evaluation analysis using a comparison of CMAQ simulations and observed maximum 8 hour ozone.

2. SIMULATED "PERFECT-WORLD" EXAMPLE WITH WEAK CORRELATION

For the purposes of illustration, we simulate pollutant fields with both strong and weak correlation structures. Fig. 1 shows an example of such a field with weak spatial dependence. The superimposed gray lines show where our "grid cell" boundaries are located. The circles designate 26 points chosen to represent observations in this domain. Using this field, we can find the average in each grid cell, as shown in Fig. 2.

We can now compare our hypothetical observations with the averages of the cells in which they fall. This allows us to assess the outcome of a traditional analysis technique assuming a perfect scenario in which the model output is in perfect agreement with the "true" process and there is no measurement-related or fine-scale variability in the observations. The scatterplot in Fig. 3 shows the observations vs. the grid cell averages, with a red 1:1 line shown for reference. We note that the correlation between the two is only about 0.84. This case study confirms that in a situation in which the extent of the spatial correlation is quite short-range, a traditional analysis can yield misleading results, even if the model and observations are actually in perfect agreement. However, this situation becomes much less extreme when the spatial correlation is farther-reaching, i.e. when the field is more spatially homogeneous.

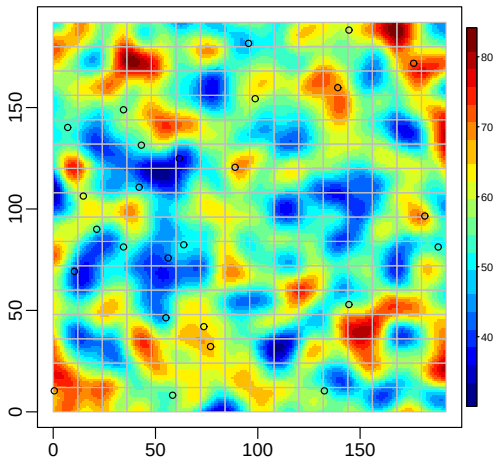

Fig. 1. Simulated data with short-range spatial dependence. In this case, the correlation between neighboring sites becomes negligible after approximately 30 units.

**Corresponding author:* Kristen M. Foley, U.S. EPA, MD E243-01, RTP, NC 27711; e-mail:foley.kristen@epa.gov

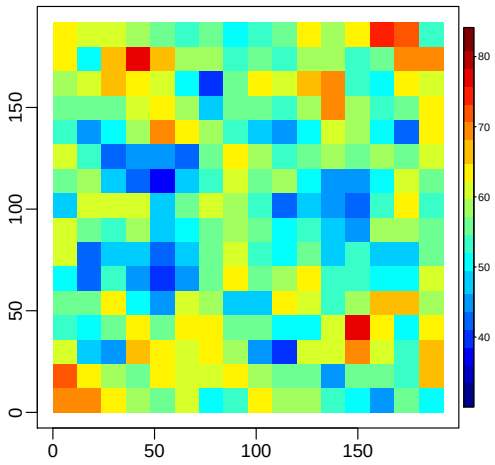

Fig. 2. Grid cell averages based on the simulated data portrayed in Fig. 1. Each grid cell is a square with a side length of 12 units.

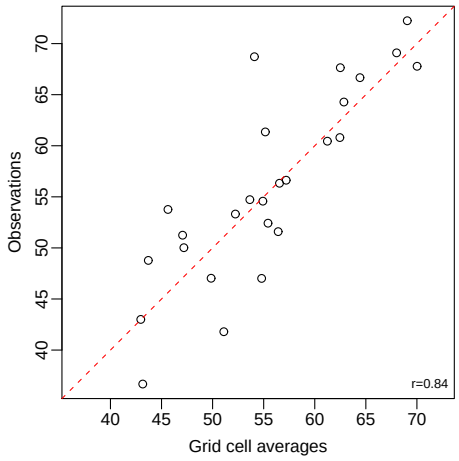

Fig. 3. Observations vs. grid cell averages, based on the data shown in Fig. 1 and Fig. 2.

3. SIMULATED EXAMPLE WITH STRONGER CORRELATION AND MEASUREMENT ERROR

Fig. 4 gives an example of simulated field with correlation that becomes effectively zero only at distances greater than about 160 units. This means that points near the center of our region are still correlated with those at the edges, at least to some extent, accounting for the smooth, homogeneous nature of the picture. Fig. 5 shows the grid cell averages calculated based on this field.

Unlike the example in the previous section, in this case we allow for a slightly more realistic situation in which the observations, while taken at the locations designated by the black circles in Fig. 4, have an additional error component to represent measurement or other fine-scale error. Note that we are still calculating the grid cell averages directly from the underlying field shown in Fig. 4, so we continue to assume that the model output is equal to this "true" simulated field, i.e. no model error.

Fig. 6 shows the observations (with error as described above) plotted against the averages for grid cells in which they fall. As before, we see substantial variability around the red 1:1 reference line, with a correlation coefficient of approximately 0.87. However, further analysis shows that in this more spatially homogeneous field, most of this variability comes from the error associated with the observations, rather than from the incommensurability issue.

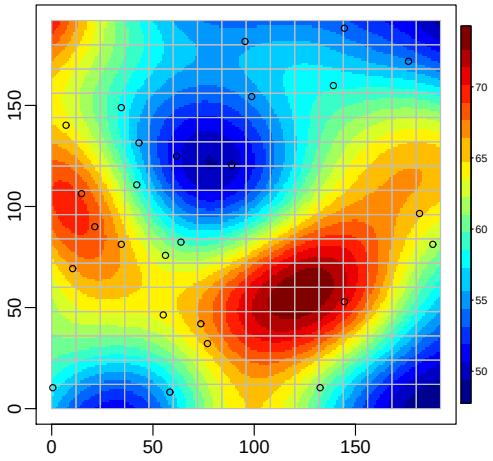

Fig. 4. Simulated data with long-range spatial correlation structure.

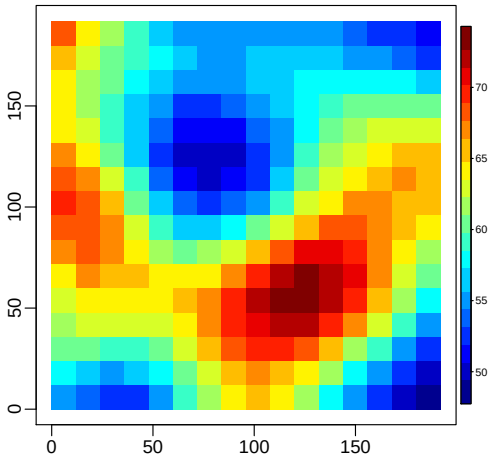

Fig. 5. Grid cell averages based on the simulated data portrayed in Fig.4. Each grid cell is a square with a side length of 12 units.

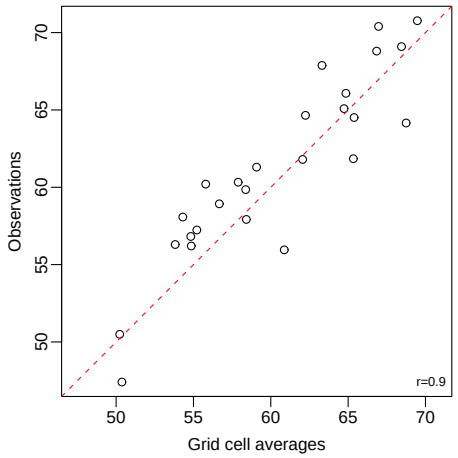

Fig. 6. Observations vs. grid cell averages, based on the data shown in Fig. 4 and Fig. 5.

4. SIMULATED EXAMPLE COMPARING KRIGING TECHNIQUES FOR USE IN MODEL ASSESSMENT

In the preceding sections, the comparison of simulated grid cell averages and observations was facilitated mostly by the scatterplots in Fig. 3 and Fig. 6. Using this approach, only grid cells which contain observations can be evaluated. As mentioned in the introduction, we are interested in investigating statistical techniques which make use of the observational data to estimate the level of the field at unobserved locations. We can then compare the grid cell averages with these estimates.

Given knowledge of or an estimate of the spatial correlation structure, kriging is a technique which can be used to make such estimates. While we are interested in other techniques as well, we focus on kriging here primarily because of its ease of use (it is available in many software packages) and its ability to provide error estimates associated with its predictions. We return to our simulations and the discussion in the preceding sections in an attempt to illustrate how incommensurability affects our choice of kriging techniques.

4.1 Kriging to the grid cell centers

A typical kriging procedure begins by assessing the correlation structure inherent in the spatial field. In our case, since the data are simulated, this correlation structure is known. In more realistic practice, this would rarely be the case, so techniques such as variogram estimation might be used to assess this structure.

The practitioner must identify the locations at which estimates are desired. In classical kriging, this would just be a series of points, most probably the centers of the grid cells to be evaluated. The kriging procedure provides the estimate at each of these points and an estimate of the standard error, based on the provided observational and correlation information.

Fig. 8 shows the kriging predictions made based on the observations shown in Fig. 7. Comparison with Fig.5, which contains the true grid cell averages for this simulation, shows that our estimates are reasonable ones for the most part. As is the case with most such estimation procedures, we see notable discrepancies where observational information is most limited, such as at the edges and in the right portion of the region. Fig. 8 also shows the well-known smoothing effect of kriging (and other similar methods), in which the extremes are not always well-captured. This is particularly noticeable in the “hot spot” in the right portion of the region, where the situation is further complicated by the relative scarcity of observational data.

We can also judge the performance of the kriging technique based on Fig. 9, which shows (for a subset of the grid cells) each kriging estimate vs. the true grid cell value (represented by points). The plot also displays 95% confidence bounds, determined using the kriging error estimates. In this case, the intervals based on kriging to the center points of all 256 grid cells (not just the subset shown), include the true value. We would expect approximately 243 (95% of 256) of the intervals to miss their target. This indicates that the error estimates are not well-calibrated for estimating spatial average, and we explore this issue further in the next section.

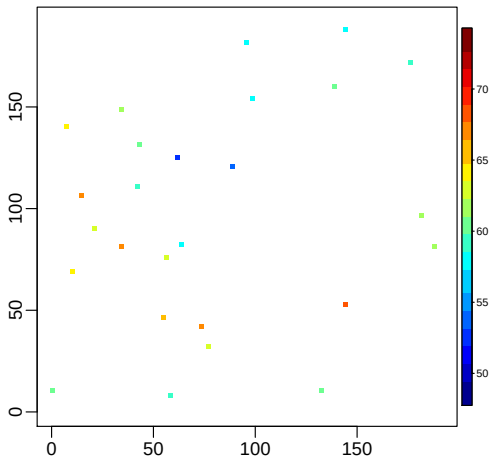

Fig. 7. Observations simulated with fine-scale error at the locations shown in Fig. 4 (long-range spatial correlation)

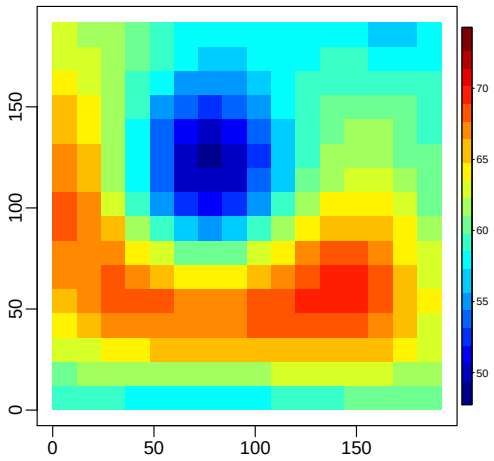

Fig. 8. Estimates yielded by kriging the observations in Fig. 7 to the grid cell centers (long-range spatial correlation)

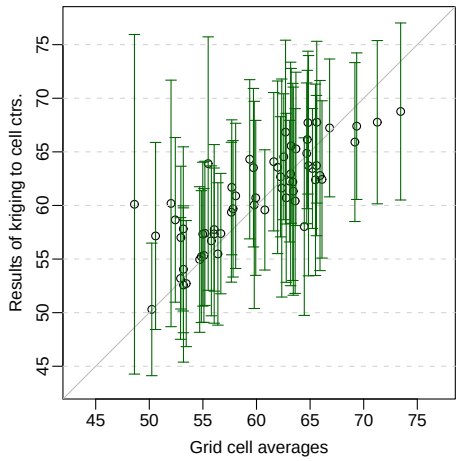

Fig. 9. Sample of results yielded by kriging to the grid cell centers (long-range spatial correlation)

4.2 Block kriging

Given our discussion of the potential problems associated with incommensurability and the calibration issues discussed in the previous section, it is reasonable to question whether we should be using the kriging technique to estimate the spatial field point-wise at the grid cell centers. Statistical reasoning (Gelfand et al. 2001) indicates that estimates of variability and error are generally sensitive to the incommensurability issue, with estimates of averages less variable than estimates for individual points. The block kriging technique (e.g., Goovaerts 1997, pg. 152) allows us to adjust for incommensurability by estimating the spatial field at a lattice of points within each of the grid cells. The estimate for the grid cell average is then given by the average of the estimates for all the lattice points, and the variance of the estimate is given by a function of the covariances among all the lattice points.

Fig. 10 shows the block kriging estimates for each grid cell, based once again on the observational data in Fig. 7. Comparison with Fig. 8 shows that the estimates given by the two kriging techniques are very similar, with only minor differences visible on close inspection. This is what we would expect, especially with the effective correlation range extending well beyond the distance spanned by not just one, but several, grid cells.

However, Fig. 11 shows that the error estimates and resulting confidence intervals (in green if the true value is captured and red otherwise) are quite different for the two kriging techniques. The confidence intervals depicted in Fig. 11 are noticeably shorter than those in Fig. 9, due to smaller errors associated with estimating an average rather than an individual location. The block kriging method showed better calibration, with 247 (about 96%) of the confidence intervals enclosing the actual grid cell average. This further indicates that the errors associated with kriging to the cell centers are estimated to be higher than what is needed for kriging to grid cell averages. Achieving a more accurate estimate of the error associated with the kriging technique allows us to better assess model performance by giving us information about differences which are more likely due to estimation error than to model error.

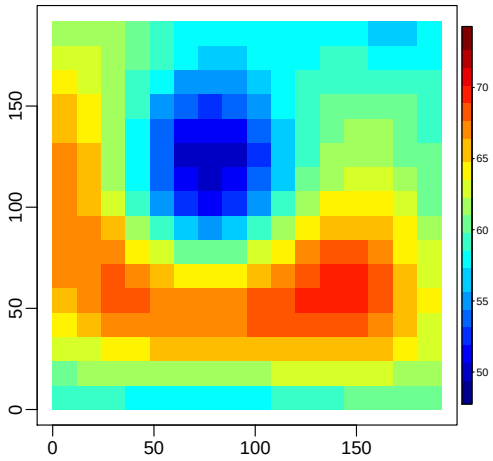

Fig. 10. Estimates yielded by block kriging the observations in Fig. 7 (long-range spatial correlation)

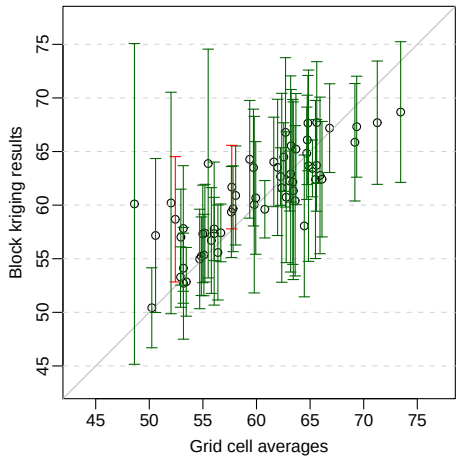

Fig. 11. Sample of results yielded by block kriging (long-range spatial correlation)

4. DISCUSSION

Analysis such as block kriging provides one approach to address the difference in variability between a point measurement and a volume-average prediction by using a statistical model to characterize sub-grid variability based on observed values. An alternative approach is to use a nested grid modeling system of fine scale features to simulate sub-grid variability as proposed by Ching et al. (2006). Although in the context of air quality modeling most evaluations have not considered this issue of incommensurability in detail, some authors have considered the problem and developed alternative methods for comparing measurements and model output (Swall and Davis 2006). The more sophisticated statistical modeling provides additional information, which is not available in a matched model to observation type comparisons. Spatial analysis of model errors is used to determine regions where model output is significantly different from observation-based estimates. These areas may be used for diagnostic evaluation to identify the source of consistent model errors. The added benefit of this extra layer of analysis will depend on the goals of a particular model evaluation. Analysis of observed and modeled ozone data will be used to further compare standard evaluation methods and more complex statistical modeling in an operational setting.

DISCLAIMER: The research presented here was performed under the Memorandum of Understanding between the U.S. Environmental Protection Agency (EPA) and the U.S. Department of Commerce's National Oceanic and Atmospheric Administration (NOAA) and under agreement number DW13921548. This work constitutes a contribution to the NOAA Air Quality Program. Although it has been reviewed by EPA and NOAA and approved for publication, it does not necessarily reflect their policies or views.

References

Appel, K. W., Gilliland, A. B., Sarwar, G. and R. C. Gilliam, 2007: Evaluation of the Coummunity Multiscale Air Quality (CMAQ) model version 4.5: Sensitivities impacting model performance; Part I – ozone, *Atmos. Envir., to appear.*

Ching, J., Herwehe, J., and J. Swall, 2006: On joint deterministic grid modeling and sub-grid variability conceptual framework for model evaluation, *Atmos. Envir.*, **40**, 4935-4945.

Eder, B., and S. Yu, 2006: A performance evaluation of the 2004 release of Models-3 CMAQ. *Atmos. Envir*., **40**, 4894-4905.

Gelfand, A. E., Zhu, L., and B. P. Carlin, 2001: On the change of support problem for spatio-temporal data, *Biostatistics*, **2,** 31-45.

Goovaerts, P. 1997: *Geostatistics for Natural Resources Evaluation*. Oxford University Press, 483 pp.

Swall, J. and J. Davis, 2006: A Bayesian Statistical Approach for Evaluation of CMAQ, *Atmos. Envir.*, **40**, 4883-4893.

Presented at the 6th Annual CMAS Conference, Chapel Hill, NC, October 1-3, 2007

DIAGNOSTIC AND MECHANISTIC EVALUATIONS OF MM5-CMAQV4.6 FOR THE SUMMER 2000 CENTRAL CALIFORNIA OZONE STUDY

Ling Jin, Nancy J. Brown*, Shaheen Tonse
Atmospheric Science Department, Lawrence Berkeley National Laboratory, Berkeley, CA, USA

Robert A. Harley,
Department of Civil and Environmental Engineering, University of California , Berkeley, CA, USA

Jian-wen Bao, Sara A. Michelson, and James Wilczak
Regional Weather and Climate Applications Division NOAA/Environmental Technology Laboratory, 325 Broadway, Mail Stop: ET7, Boulder, CO, USA

1. INTRODUCTION

Past evaluations of Community Multiscale Air Quality (CMAQ) (Byun, 2006) modeling system have focused on the eastern United States and applications of it are usually conducted for high ozone episodes that last for a few days. In our research, we seek more comprehensive model evaluation by applying MM5-CMAQ to simulating ozone formation for an entire summer season in central California, where ozone air pollution problems are severe and air districts are out of compliance with the 8-hour ozone standard.

In this study, we apply the Community Multi-Scale Air Quality model (CMAQ version 4.6) to a 15-day period contained in the summer 2000 Central California Ozone Study. Model parameters and inputs are set to reflect actual conditions of the modeling domain. We apply a variety of evaluation and diagnostic methods to assess model performance across a range of days and locations, with significant spatial and temporal variations in air quality. Effects of meteorological data assimilation are evaluated. We perform sensitivity analyses with the brute force method and Direct Decoupled method (DDM) (Dunker, 1984, 2002) to diagnose causes for discrepancies between observations and model predictions.

2. METHODS

2.1 Modeling Domain

The San Joaquin Valley is surrounded by Sierra Nevada and coastal mountain ranges. On typical summer days, westerly winds are funneled into the Central valley through gaps in the coastal range with large portions of the flow directed into the San Joaquin valley. The San Francisco Bay area and Sacramento valley are the major upwind emission sources affecting air quality in the San Joaquin valley. The study domain is gridded into 96 by 117 cells, with a horizontal resolution of 4 km. Vertically, the domain is divided into 27 layers from the surface to 100 mb (about 17 km); the near surface layers are about 20 m thick.

2.2 Emission Inputs

Model inputs were developed that describe variability in atmospheric conditions, including day-specific emission rates from both natural and anthropogenic sources. Anthropogenic emissions from area, and point sources were derived from the gridded emission inventory data provided by the California Air Resources Board. Motor vehicle emission inventory estimates describe light-duty gasoline and heavy-duty diesel vehicle activity patterns and emissions separately by time of day and day of week using the methodology developed by Harley et al. (2005). Biogenic VOC emissions (mainly isoprenes and terpenes) were estimated hourly with the BEIGIS modeling system (Scott and Benjamin, 2003, Steiner et al., 2006).

2.3 Meteorology Inputs

Gridded hourly meteorological fields were developed using the MM5 meteorological model (Grell, 1994) for the 15 day period from July 24 to August 8, 2000, using three nested grids: an outer 36 km resolution grid, within which is nested a 12 km grid, within which is nested the 4 km CCOS grid with 190 cells in each horizontal direction and 50 vertical layers. The 4 km resolution MM5 output is used to drive CMAQv4.6 simulation.

**Corresponding author:* Nancy J. Brown, Atmospheric Science Department, Lawrence Berkeley National Laboratory, Berkeley, CA 94720; e-mail: njbrown@lbl.gov.

The middle 5-day period (a high ozone episode) is characterized by an offshore pressure gradient caused by a large high-pressure system over Utah and Colorado, with reduced incoming westerly flow at the coast and stagnate conditions in the valley. Four dimensional data assimilation was conducted for this 5-day ozone episode using data from a network of surface wind observations, and radar wind profilers.

2.4 Boundary Conditions and Parameter Adjustments

Constant pollutant concentrations are set for each of the four lateral boundaries of the domain. The western inflow boundary is mostly over the ocean and its chemical species concentrations are set to clean marine background values. Vertically varying O_3 is based on averaged August ozone sonde measurements made at Trinidad Head, CA (Newchurch, 2003). Nitrogenous species (NO: 0.01 ppb; NO2: 0.03 ppb; etc.) and a suite of VOC species take values measured in the marine background free troposphere (Nowak, 2004). The other three boundaries are dominated by outflows; the same boundary values used in past studies conducted in this domain by the California Air Resources Board (Kaduwela, 2006, personal communication) are used here.

Ozone dry deposition velocity over the ocean is increased from the CMAQ default value of zero to 0.04 cm/s according to measured values (Faloona, 2006, personal communication). Minimum eddy diffusivity (Kzmin) in CMAQ default value (0.5 m/sec^2) appears too high for stable marine layers on the western boundary, and this causes excessive vertical mixing and increases surface ozone. Assuming wind speeds of about 10 m/s and surface roughness lengths for the ocean to be between the suggested values of $1.5\times10\text{-}5$ and $1.5\times10\text{-}3$ m, we calculated Kz to be between 0.0015 and 0.15 m/sec^2. Kzmin is thus set to 0.1 m/sec^2.

2.5 Evaluation and Diagnostic Tools

Different evaluation methods address model performance from various perspectives. The evaluation methods employed in this study are summarized in the following table.

Sensitivity analysis with the brute force method and Direct Decoupled method (DDM) (Hakami, 2003) are used to diagnose causes for discrepancies between observations and model predictions.

Table 1 Summary of evaluation methods.

Methods	**Usage**
Taylor's Diagram	Describe how well patterns in modeled and observed values match each other
Mean Bias	Average sign in model prediction errors
RMSE, Gross Error	Magnitude of model prediction errors
Spatial Krigging	Spatial variation in model performance
Ozone Production Efficiency	Limiting regimes presented in the observed and modeled air masses

3. MODEL SIMULATION AND EVALUATION

Our 15-day simulation is driven by the prognostic meteorology in CMAQv4.6, configured with SAPRC99 (Carter, 2000) chemical mechanism. Additional simulations for the middle 5-day ozone episode are performed using nudged meteorological fields. Highest ozone levels occur on Aug 1st and 2nd (Julian days 214 and 215).

3.1 Spatial and Temporal Trends in Model Performance

The model's ability to reproduce the variation and correct levels of observed ozone is examined with a Taylor diagram (Taylor, 2001) and normalized biases. We report daytime comparison statistics with respect to ozone. At night, when strong convective mixing is absent, observed ozone at measurement sites are often more affected by titration with NO emitted at nearby roadways. Hence we compare odd oxygen O_x (NO_2+O_3) concentrations to evaluate model performance at night.

On a Taylor diagram the correlation coefficient and the root-mean-square difference (RMSD) between the modeled and observed values, along with the ratio of the standard deviations of the two patterns are all indicated by a single point on a two-dimensional plot (Fig. 1). Across the three air basins that have the highest ozone levels, model simulation of the middle 5-day ozone episode shows a consistent better match to the observed standard deviation, while the first 5-day period shows consistent better linear correlations and root mean squared differences across the three air basins. In general, points representing modeled patterns in different air basins and time periods are clustered together, indicating a similar model

performance across time and space. All the pattern metrics indicate that model performance in the San Francisco Bay area during the last 5-day period needs improvements relative to the first two 5-day periods.

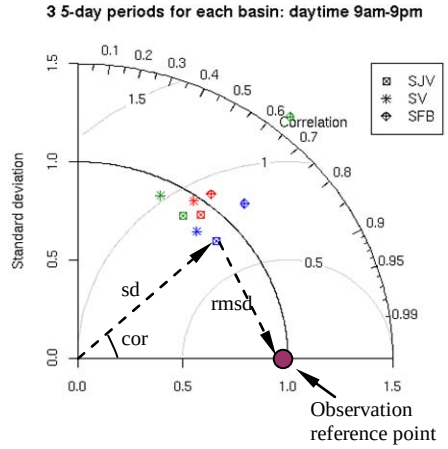

Fig. 1. Taylor diagram showing daytime evaluation statistics normalized by observed standard deviation, for July 24-29 (blue), July 29-August 2 (red), August 2-7 (green), respectively, at three air basins: the San Joaquin Valley (SJV), the Sacramento Valley (SV), and the San Francisco Bay area (SFB).

Pattern statistics are useful for comparing the anomalies in two data sets, while normalized mean bias indicates either over-prediction or under-prediction. From Fig. 2 we see that the model slightly under-predicts daytime ozone in the San Joaquin Valley and Sacramento Valley in general, but over-predicts ozone in the Bay area, especially for the first half of the simulation period. There is no clear temporal trend in model biases, but we do observe over-prediction on the last day, and this corresponds to the positive bias present in MM5 temperature fields during that day.

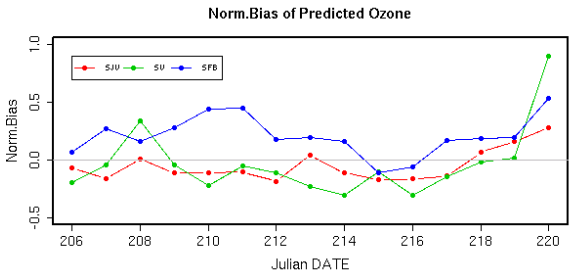

Fig. 2. Daytime normalized biases at three air basins with cutoff value of 10 ppb.

Table 2 shows evaluation metrics for modeled peak ozone, daytime NO_x, and nighttime O_x across the three 5-day periods. Gross errors suggest CMAQ does a better job in predicting peak ozone concentrations than the precursor concentrations. There is a slight improvement in peak ozone prediction over three 5-day periods, as suggested in the normalized biases. Overall, CMAQ under-predict peak ozone concentrations.

Table 2 Summary statistics for three 5-day period.

	Normalized Bias			Normalized Gross Error		
	1	2	3	1	2	3
1h Peak O_3	-10%	-7%	-4%	17%	20%	18%
8h Peak O_3	-15%	-12%	-11%	17%	17%	18%
Daytime NO_x	0%	-4%	3%	57%	60%	64%
nighttime O_x	8%	10%	8%	19%	29%	22%

Peak ozone cutoff value: 60 ppb, NO_x and O_x: 10 ppb.

3.2 Effects of Meteorology Nudging on Air Quality Simulations

Four dimensional data assimilation provides clear improvements in MM5 simulated wind fields (Fig. 3, 4), in terms of wind speed and direction at all altitudes presented here. The largest improvements appear on Day 214, when we also see the largest improvements in spatial ozone biases (Fig. 5).

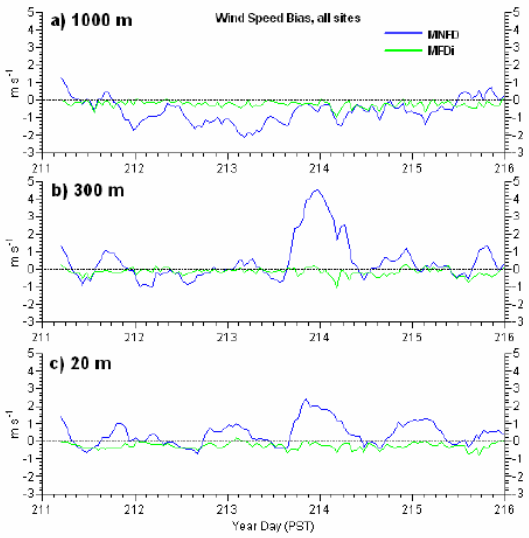

Fig. 3. Domain averaged wind speed biases with (MFDi) and without (MNFD) four dimensional data assimilation.

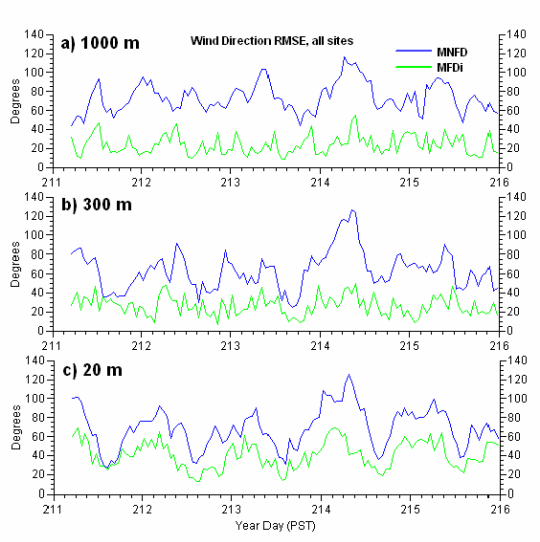

Fig. 4. Domain averaged wind direction biases with (MFDi) and without (MNFD) four dimensional data assimilation.

Improved wind speed and direction ensure better representation of chemical transport in the model, which leads to more correct localization of ozone plumes. Ozone biases on Day 214 are krigged (Cressie, 1993) to generate a continuous error surface and are shown at 3 PM local time, when ozone levels are the highest. Before wind nudging, modeled meteorology appears to have less strong westerly flows, which prevents the Bay area ozone plume from entering the San Joaquin valley, and causes excessive over prediction in the Bay area and under prediction in the northern San Joaquin valley. Another significant improvement occurs in the Sacramento valley. Before nudging, the southward winds appear to be too strong in the Sacramento valley, resulting a shorter residence time for local pollutants to build up. Thus we observe a large under-prediction of ozone in Sacramento. After observational nudging, ozone biases are reduced by about factor of two.

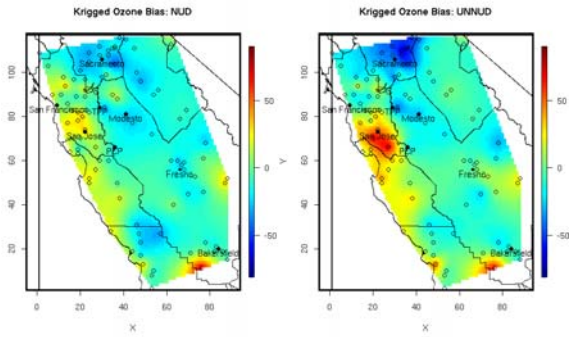

Fig. 5. Predicted ozone biases on Day214 at 3 pm PDT with (NUD) and without (UNNUD) nudged wind.

3.3 Ozone Production Efficiency

Up to now we have only examined model performance in terms of predicting individual species concentrations. Previous study related odd oxygen O_x to NO_z in terms of ozone production efficiency (OPE) (Trainer et al., 1993), which is defined here as the slope when we plot O_x against NO_z (Mena-Carrasco et al. 2007). Ozone production efficiency reflects ozone sensitivity to NO_x in the air mass of interest, and thus can be used to evaluate how well modeled ozone sensitivities match the observed ones. Sources of discrepancy between modeled and observed OPE at a particular location and time include incorrect mixtures of emission inputs, insufficient representation of ozone chemistry, and misplacement of ozone plumes by transport errors. We present weekday OPEs in the middle 5-day period, at three sites where the daytime NO_z observations are available (Fig. 6). Fortunately, ozone chemistry at these sites represents three typical air masses in terms of their distances from the major nearby emission sources. Turlock station is located in northern San Joaquin Valley, far downwind of Bay area emissions, and often experiences aged air masses (NO_x poor) transported from the Bay area. Fresno is right at the urban emission center in the middle San Joaquin valley, representing air masses of fresh emissions rich in NO_x. Arvin station in the southern San Joaquin Valley is in the intermediate downwind of Bakersfield emissions. OPE is considered separately for modeled data driven by meteorology with and without four dimensional data assimilation to investigate the effects of transport errors on predicted OPEs. In Fig 6, we see modeled OPEs with or without wind nudging are both very close to observed ones at Turlock and Fresno stations. A large OPE at Turlock station indicates efficient ozone production, typical of NO_x-limiting conditions in aged air masses. OPE at Fresno station is much lower, which reflects the fact that the air mass is very close to the emission sources. Observed OPE (6.1) at Arvin station indicates NO_x-limiting conditions, while modeled OPE (3.3) without wind nudging implies less aged air masses sampled at this station. Wind nudging brings modeled OPE from 3.3 to 5.3, much closer to the observed value. As the first two stations are either far away from or very close to the emission sources, ozone sensitivities to NO_x in the air masses there are both less affected by transport errors. In contrast, wind direction and speed determine how much Arvin station is influenced by its nearby upwind

emissions in Bakersfield. We see similar modeled and observed OPEs across all three sites when nudged wind fields are used, indicating adequate representation of ozone sensitivities in the model.

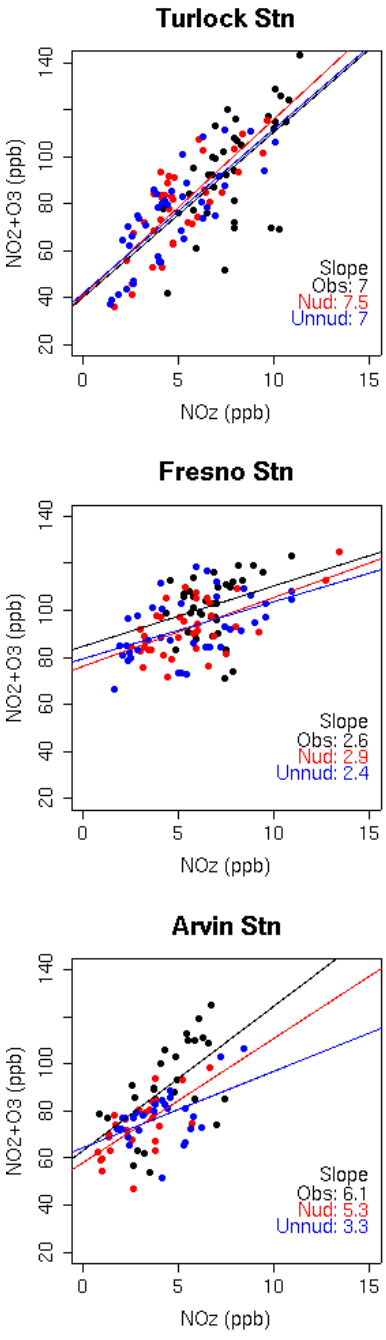

Fig. 6. Ozone production efficiency (the linearly fitted slope) at three sites evaluated for observed and modeled daytime data during weekdays in the middle 5-day period.

3.4 Sensitivity Analysis

We have seen that CMAQ generally over predicts ozone on the west coast, but under-predicts ozone in the central valley. Sensitivity analyses with brute force and decoupled direct methods are employed to determine the most influential factors of simulated ozone concentrations at various geographical locations. We evaluate ozone sensitivities to a number of input parameters: boundary conditions (ozone, volatile organic compounds (VOC), nitrogen oxides), boundary ozone at different heights, emissions of NO_x, anthropogenic VOCs (AVOC), and biogenic VOCs (BVOC). We found that the coastal areas are most sensitive to NO_x emissions and boundary ozone conditions, especially those at the surface level. The San Francisco Bay area is sensitive to both anthropogenic and biogenic emissions, as well as boundary conditions, while central valley is more sensitive to anthropogenic emissions.

4. CONCLUSIONS

In this paper, we have simulated ozone formation in the central California region with CMAQv4.6 for a 15-day period, which includes a five-day high ozone episode. We have applied a number of evaluation methods to assess model performances. Simulated ozone concentrations adequately match the observed pattern, except in the Bay area during the last 5-day period. Model performance does not degrade over time, but exhibits spatial trends in biases. CMAQ tends to over-predict ozone at coastal areas, and slightly under-predict in the central valley. Wind nudging greatly improves the chemical transport processes. When transport errors are minimized, we see similar ozone sensitivities when comparing observed and modeled ozone production efficiencies. Sensitivity analysis is performed and the most influential factors studied here are listed for different geographical regions. The Bay area is sensitive to uncertainties in all the input parameters considered here, which suggests great challenges on correct simulating ozone concentrations in this area.

5. ACKNOWLEDGMENTS

Support for this study was provided by the California Energy Commission, the California Air Resources Board, the UC Toxic Substances Research and Teaching Program Student

Fellowship, and by the Assistant Secretary for Fossil Energy, Office of Natural Gas and Petroleum Technology through the National Petroleum Technology Office under U.S. Department of Energy Contract No. DE-AC03-76SF00098. The authors thank Allison Steiner for providing the biogenic emission inventory used in this research.

6. REFERENCES

Byun, D. W.; Schere, K. L. Review of the governing equations, computational algorithms, and other components of the Models-3 Community Multiscale Air Quality (CMAQ) modeling system. *Applied Mechanics Reviews*. **2006**, Vol. 59, No. 2, p. 51-77.

Carter, W. P. L. Implementation of the SAPRC-99 Chemical Mechanism into the Models-3 Framework. University of California, Riverside, California. Report to the U.S. Environmental Protection Agency, Washington, D. C., **2000**.

Cressie, N.A.C. Statistics for Spatial Data, Wiley, New York,**1993** (revised edition) .

Dunker, A.M. The decoupled direct method for calculating sensitivity coefficients in chemical kinetics, *J. Chem. Phys.* **1984**, *81*, 2385-2393.

Dunker, A.M.; Yarwood, G.; Ortmann, J. P.; Wilson, G. M. The decoupled direct method for sensitivity analysis in a three-dimensional air quality model: Implementation, accuracy, and efficiency, *Environ. Sci. Technol.* **2002**, *36* (13), 2965 -2976.

Grell, G.A.; Dudhia, J.; Stauffer, D. R. A description of the fifth-generation Penn State/NCAR mesoscale model (MM5). NCAR Technical Note, NCAR/TN-398+STR, 122 pp., NCAR, Boulder, CO, **1994**.

Hakami, A.; Odman, M. T.; Russell, A. G. High-order, direct sensitivity analysis of multi-dimensional air quality models, *Environ. Sci. Technol.* **2003**, *37* (11), 2442-2452.

Harley, R.A.; Marr, L. C.; Lehner, J. K.; Giddings, S. N. Changes in motor vehicle emissions on diurnal to decadal time scales and effects on atmospheric composition, *Environ. Sci. and Technol.*, **2005**, 39, 5356-5362.

Mena-Carrasco, M.; Tang, Y.; Carmichael, G. R.; Chai, T.; Thongbongchoo, N.; Campbell, J. E.; Kulkarni, S.; Horowitz, L.; Vukovich, J.; Avery, M.; Brune, W.; Dibb, J. E.; Emmons, L.; Flocke, F.; Sachse, G. W.; Tan, D.; Shetter, R.; Talbot, R. W.; Streets, D. G.; Frost, G.; Blake, Donald. Improving regional ozone modeling through systematic evaluation of errors using the aircraft observations during the International Consortium for Atmospheric Research on Transport and Transformation. *J of Geophys. Res.* **2007**, Vol 112, D12S19, doi: 10.1029/2006JD007762.

Newchurch, M. J.; Ayoub, M. A.; Oltmans, S.; Johnson, B.; Schmidlin, F. J. Vertical distribution of ozone at four sites in the United States. *J. Geophys. Res.* **2003**, 108, D14031: doi: 10.1029/2002JD002059.

Scott, K. I.; Benjamin, M. T. Development of a biogenic volatile organic compound emission inventory for the SCOS97-NARSTO domain, *Atmos. Environ.*, **2003**, 37(2), S39-S49.

Steiner, A. L.; Tonse, S.; Cohen, R. C.; Goldstein, A. H.; Harley, R. A. Influence of future climate and emissions on regional air quality in California, *J. Geophys. Res.*, **2006**, 111, D18303, doi:10.1029/2005JD006935

Taylor, K.E. Summarizing multiple aspects of model performance in a single diagram. *J. of Geophys. Res*. **2001**, *106*(D7), 7183–7192.

Trainer, M.; Parrish, D. D.; Buhr, M. P.; Norton, R. B.; Fehsenfeld, F. C.; Anlauf, K. G.; Bottenheim, J. W.; Tang, Y. Z.; Wiebe, H. A.; Roberts, J. M.; Tanner, R. L.; Newman, L.; Bowersox, V. C.; Meagher, J. F.; Olszyna, K. J.; Rodgers, M. O.; Wang, T.; Berresheim, H.; Roychowdhury, U. K. Correlation of ozone with NO_y in photochemically aged air, *J. Geophys. Res.* **1993**, 98, 2917-2925.

Case Study on the High Ozone Phenomena in Seoul Metropolitan Area Using CMAQ Model

Chong Bum Lee*, Tae Hun Cheon, Su Kap Park
Dept. of Environmental Science, Kangwon National Uinversity, Chunchon, Kangwon-do, 200-701, Korea

1. Introduction

The diurnal variation of ozone in urban area shows generally high concentration in daytime and low concentration in nighttime. Ozone in Seoul Metropolitan area occurs frequently days to maintain somewhat high level of ozone during nighttime period. The purpose of this study is to understand the mechanism of ozone episodes occurred in daytime and the phenomena of high level ozone in nighttime using Model3/CMAQ. To evaluate the results of CMAQ modeling, ozone concentration calculated from CMAQ modeling were compared with ozone measured in air pollution monitoring sites of the surface level. The effects of each of mechanism attributed to the variation of ozone concentration were analysed through the process Analysis method in CMAQ on Seoul Metropolitan area.

2. Methodology

The domain of CMAQ in this study consists of 132 grid cells in east-west direction and 114 grid cells in south-north direction, with 30km x 30km horizontal resolution covering the China, Korea and Japan as shown in Fig. 1. Number of vertical layer is 15 layers and the height of lowest layer is about 80m. The meteorological data for CMAQ simulation were obtained using the MM5. The emission inventory made for ACE-ASIA project(2001) were used. The CMAQ simulation was performed during 2 months period from 1 May to 30 June, 2007.

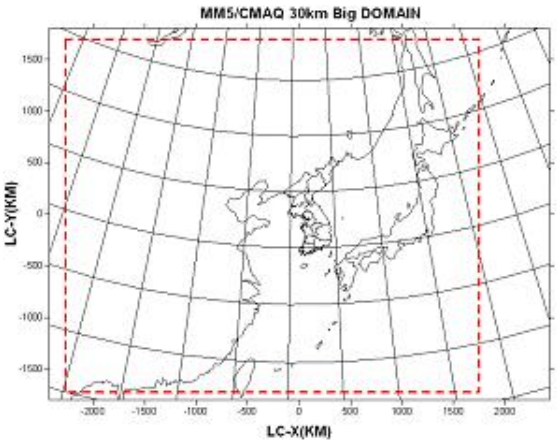

Fig. 1. Modeling domain of MM5(outer box) and CMAQ(inner dotted box). Grid size is 30km x 30km.

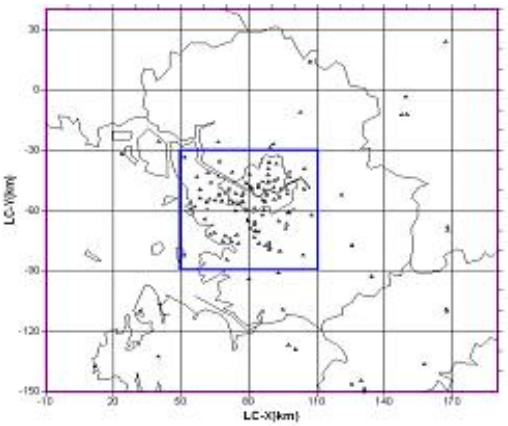

Fig. 2. 4 grid cells surrounded with thick line in 30km grid of CMAQ model domain is the target area for Process Analysis on Seoul Metropolitan area . The symbol of triangle denotes air pollution monitoring sites.

3. Results and Discussion

3.1. Evaluation of model

The comparison of observed and calculated ozone concentration during the modeling periods is presented in fig. 3. The time variation of ozone follows the trend of measured ozone very well. Table 2 shows the error measure of ozone concentration calculated by CMAQ using the algorithms in Table 1.

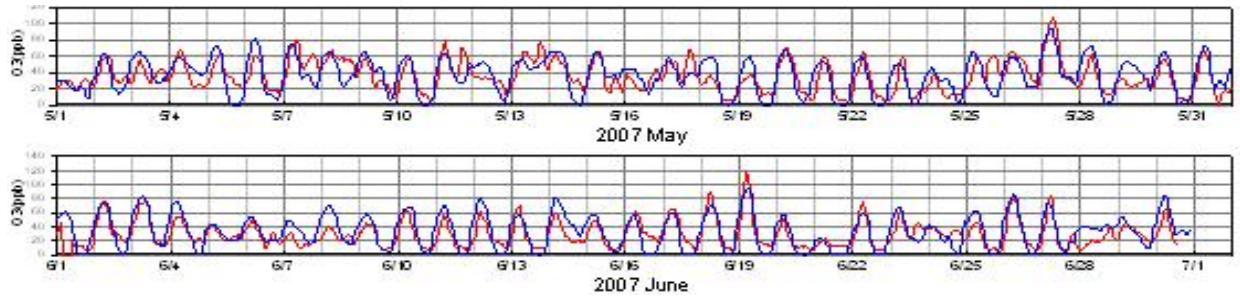

Fig. 3. Comparison of observed(thin line) and calculated(thick line) O3 concentration on May 1-June 30, 2007 in metropolitan area

Table 1. The statistics used for CAMQ evaluation

Root Mean Square Error (RMSE)	$RMSE=\sqrt{\frac{1}{N}\sum_{1}^{N}(C_p-C_O)^2}$ $RMSEs=\sqrt{\frac{1}{N}\sum_{1}^{N}(C^*-C_O)^2}$ $RMSEu=\sqrt{\frac{1}{N}\sum_{1}^{N}(C^*-C_p)^2}$ $C^*=a+bC_O$
Fractional Bias (FB)	$FB=\frac{\overline{C_p}-\overline{C_o}}{0.5(\overline{C_p}+\overline{C_o})}$
Mean Bias (MB)	$MB=\frac{1}{N}\sum_{i=1}^{N}(C_p-C_o)$

The evaluation results are provided in Table 2 and the correlation coefficient(r) between ozone observed and those calculated by CMAQ is 0.757.

Table 2. Model evaluation statistics for hourly ozone concentrations over Seoul Metropolitan area for the period of May 1-June 30, 2007.

	NO. of data	avr. obs.	avr. model	r
	1440	32.57	35.19	0.7570
RMSE	RMSEs	RMSEu	MB	FB
15.009	3.6469	14.559	2.8112	0.0826

3.2. Case studies

3.2.1 Case A

The simulated ozone concentrations and horizontal wind on fields on 13 May 2007 is showed in Fig. 4. The wind fields would be expected to affect the horizontal transport of air pollutants and their products from the Shanghai to the Seoul Metropolitan areas.

Fig. 5. shows the result of Process Analysis (PA) on 13 May 2007. We noticed that nighttime ozone was increased up to 10ppb in due to the horizontal transport (Hor. Trans).

.

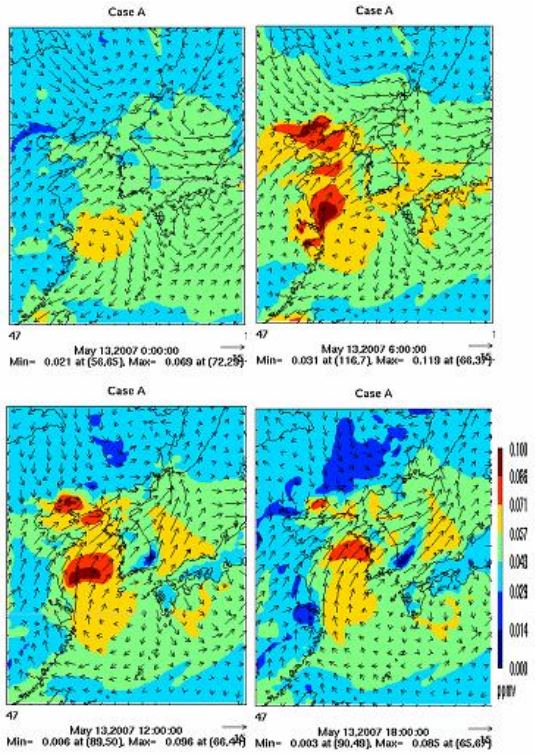

Fig. 4. Difference maps of ozone concentrations calculated by CMAQ model on May 13, 2007

3.2.2 Case B

Ozone in Seoul Metropolitan area is affected by ozone and precursor transported during 26 May, 2007. ozone production by chemical mechanism attributed to be increased more about 40ppb for 00-06 GMT on next day. Winds

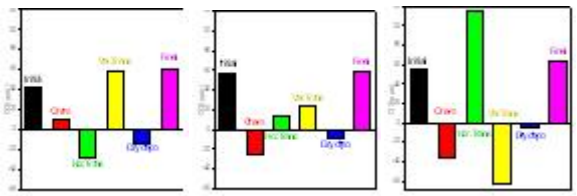

13, May 00-06GMT 13, May 06-12GMT 13, May 12-18GMT

Fig 5. Mass balance of process contribution to ozone concentration on May 13, 2007.

converge to Metropolitan area during daytime and continued to 12 GMT on 27 May 2007. As a result of Process Analysis, ozone is increased as much as 95 ppb by horizontal transport and decreased as much as 110 ppb by vertical convection.

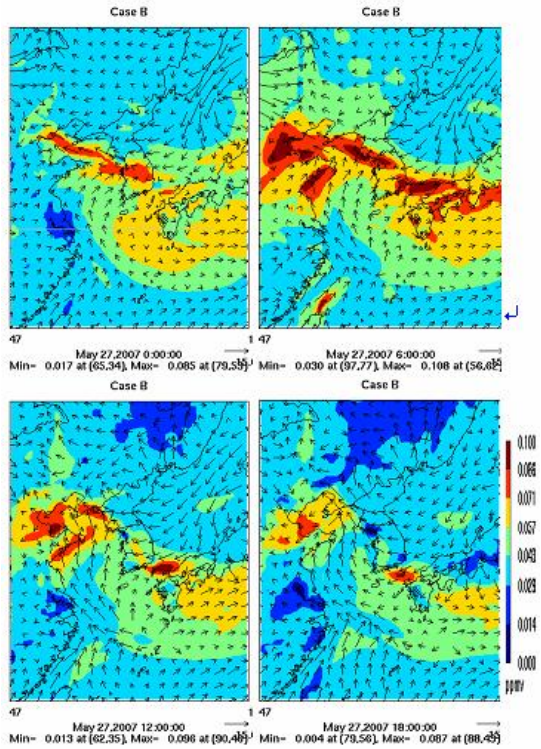

Fig. 6. Difference maps of ozone concentrations calculated by CMAQ model on May 27, 2007.

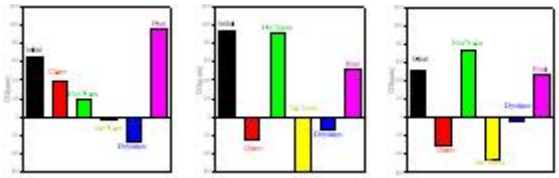

27, May 00-06GMT 27, May 06-12GMT 27, May 12-18GMT

Fig 7. Mass balance of process contribution to ozone concentration on May 27 2007.

3.2.3 Case C

On August 19 2007, ozone episode occurred in the Seoul metropolitan area. At that time, ozone over east sea area was near 60ppb and ozone in Seoul Metropolitan area was affected by the flowing of ozone converged into the Seoul metropolitan by the easterly wind from the east sea. Also, ozone was produced by local source in this period. We can notice that production of ozone by chemical reaction was 50ppb during 00~06 GMT through Process Analysis. At 06 GMT, production of ozone by chemical reaction was 100ppb. In nighttime, ozone concentrations decreased because of non-effect from China.

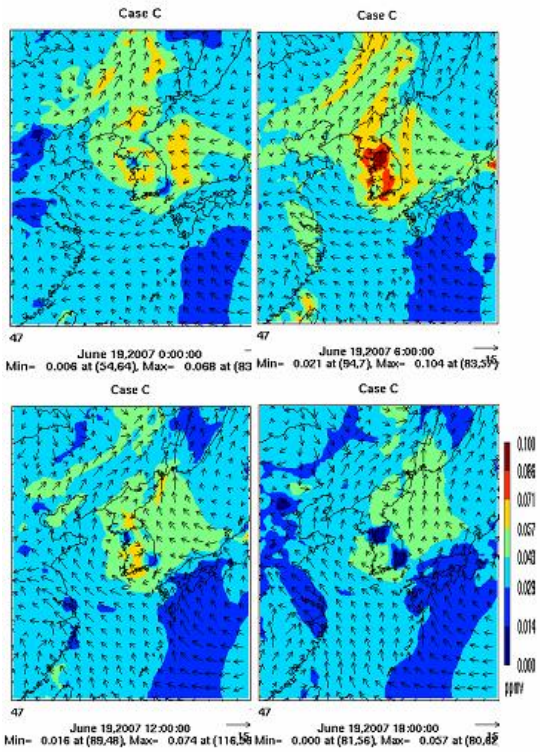

Fig. 8. Difference maps of ozone concentrations calculated by CMAQ model on June 19, 2007.

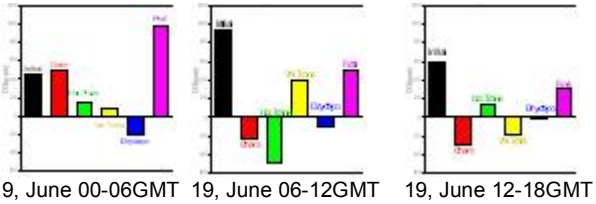

19, June 00-06GMT 19, June 06-12GMT 19, June 12-18GMT

Fig. 9. Mass balance of process contribution to ozone concentration on June 19, 2007.

4. REFERENCES

Byun, D.W., Ching J.K.S. (Eds.) 1999. Science Algorithms of the EPA Models-3 Community Multi-scale Air Quality (CMAQ) Modeling System. US EPA Report No. EPA/600/R-99030. Office of Research and Development, Washington D.C

Lin, C-J., Ho, T.C., Chu, H., Yang, H., Chandru, S., Krishmarajanagar, N., Chiou, P., Hopper J.R., 2005. Sensitivity analysis of ground-level ozone concentration to emission changes in two irban regions of southeast Texas, Journal of Environmental Management 75, 315-323.

Zhang, M., Pu, Y., Zhang, R., Han, Z., 2005. Simulation of sulfur transport and transformation in East Asia with a comprehensive chemical transport model. Environmental Modelling & Software 21, 812-820

Assessing Model Performance Using Weekday/Weekend Analysis

Jim Smith, Mark Estes, Fernando Mercado, and Jocelyn Mellberg*
Texas Commission on Environmental Quality, Austin, Texas

1. BACKGROUND AND INTRODUCTION

Comparison of photochemical air quality model predictions with observed ambient concentration data is necessary for assessing model performance. In modeling applications for the one-hour ozone standard, this comparison was often considered sufficient for determining whether the model performed well enough to predict future ozone concentrations and test proposed control strategies. Often, little or no consideration was given to the model's performance in predicting the response to emission changes.

With the advent of the new standards for eight-hour ozone and $PM_{2.5}$, EPA devised a new attainment test based on the model's relative response to emission changes (the one-hour test for ozone was based on predicted peak ozone concentrations). Thus, under the new standard, evaluating the model's response to emission changes becomes at least as important as evaluation of its ability to reproduce historically observed events. In its recently finalized guidance for demonstrating attainment under the eight-hour standard, EPA (2007) recommended several possible means of assessing model response to emission changes, but these methods are either indirect (probing tools, alternative base cases, most observation-based models) or are difficult to employ in practice (retrospective analyses). However, weekday/weekend analysis (a type of observation-based model) is relatively straightforward and offers a direct comparison between modeled and observed responses to emission changes.

Several researchers, including Blanchard and Tannenbaum (2003, 2005), Fujita, et.al. (2003), and Yarwood, et al (2003), have studied the so-called "Weekend Effect," which often leads to an increase in measured ozone concentrations on weekends compared to weekdays.

The "Weekend Effect" is somewhat counterintuitive, since emissions of NO_X, an integral component in tropospheric ozone formation, are generally lower on weekend mornings than on weekday mornings because of reduced vehicular activity. The explanation for this effect is that newly-emitted NO_X (consisting of a mixture of NO and NO_2) is primarily NO, which reacts with ozone (O_3) to form more NO_2 plus molecular oxygen ($NO + O_3 \rightarrow NO_2 + O_2$). This reaction, called *titration*, tends to reduce ozone concentrations near large NO_X sources, particularly roadways, and can serve to generally inhibit ozone buildup in urban areas. In addition, NO_X-rich areas can have ozone formation suppressed by the reaction of NO_2 with OH radicals, creating HNO_3, and preventing the radicals from participating further in the ozone formation pathway (i.e., *radical termination*). Lower motor vehicle emissions on weekends, especially in the morning, reduce the NO_X to lower concentrations. The lower NO_X concentrations may result in less ozone destruction via titration, and less radical termination. In some cases, the lower mobile NO_X emissions on the weekends can lead to higher observed ozone concentrations. It is important to note, however, that the NO_2 created during ozone titration can fuel ozone formation later as the air mass moves away from the NO_X sources, potentially raising downwind ozone concentrations and increasing background ozone levels.

If a photochemical model responds appropriately to emission changes, it should reproduce the "Weekend Effect" in its predictions. Thus, urban environments provide a natural laboratory environment in which a model's response to emission changes can be evaluated. The authors investigated the modeled response to weekday/weekend emission changes in the Houston/Galveston/ Brazoria ozone nonattainment area during the 2000 Texas Air Quality Study (TexAQS 2000).

2. METHODOLOGY

The TexAQS 2000 was a major field study of the causes of high measured ozone concentrations in eastern Texas, and in particular in the Houston-Galveston-Brazoria (HGB) ozone nonattainment area (Figure 1). The intensive field campaign ran from August 15 through September 15, 2000. For regulatory modeling, the TCEQ

**Corresponding author:* Jocelyn Mellberg, TCEQ, 12100 Park 35 Circle, Bldg. E, Austin TX 78753 jmellber@tceq.state.tx.us

selected the period from August 15 through September 6 (the meteorology during the remainder of the intensive period was not conducive to ozone formation). This period contained 24 weekdays and 6 weekend days. However, Saturday traffic patterns are notably different from those on Sunday (on Sunday, there is generally less traffic in the morning than on Saturday), and these differences appear to manifest themselves in peak ozone concentrations in the HGB area as well. Treating Saturday and Sunday separately leaves only three days of each during the period modeled, which is a very small sample to use in validating model response to daily emission changes.

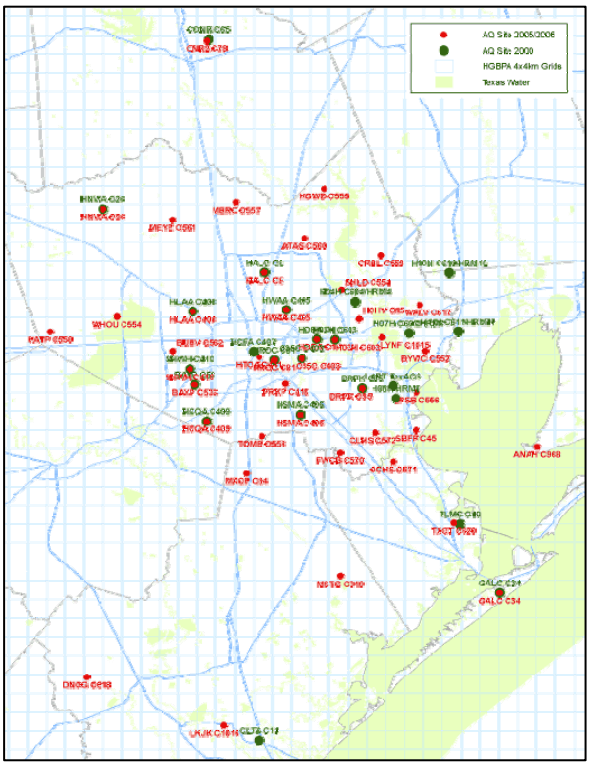

Figure 1: Monitoring Sites in the Houston-Galveston-Brazoria Ozone Nonattainment Area

To increase the sample set, we ran the entire modeling period three times, first with emissions for a Wednesday, then with Saturday emissions, and finally with Sunday emissions, which produced a set of 22 modeled ozone concentration fields for each day. In this test we allowed each day to start with the modeled concentrations from the previous day, which in this case had emissions from the same day of the week. A more rigorous application would re-initialize the hour zero concentrations with modeled values from the preceding day (i.e., start each Saturday using modeled concentrations simulated with Friday emissions).

Modeled daily peak eight-hour concentrations were extracted at each of 18 monitors in the HGB area and averaged across the 22 days of the simulation. These were compared with measured concentrations from the same monitors averaged across all ozone season (June-September) days in 2000 through 2003 that saw at least one monitor exceeding the eight-hour standard. Because the modeled period was specifically chosen to represent periods of higher ozone concentrations, it would not be appropriate to include low-ozone days (many of which are windy, cloudy, or rainy) in the comparison.

3. RESULTS

Figure 2 shows observed average 6 AM concentrations of NO_X at eleven HGB-area monitors as a percentage of each monitor's Wednesday average. The legend lists all 16 monitors used in the ozone comparison, but not all of these measured NO_X. All but two sites (GALC and CONR) show a distinct pattern of concentrations that are lower on Saturday than on Wednesday, and all show a drop from Saturday to Sunday.

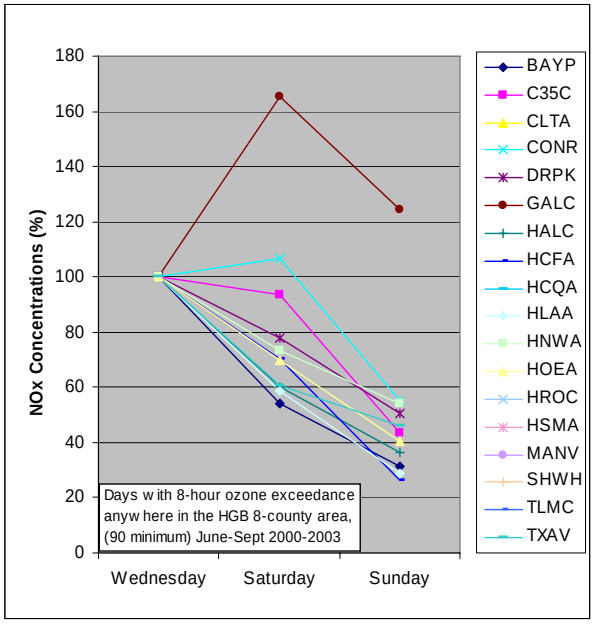

Figure 2: 6 AM Observed NOx Concentrations as a % of Wednesday

The GALC monitor is somewhat unique since it is located on Galveston Island, a popular destination for vacations and weekend excursions. The modeled NO_X concentrations shown in Figure

3 show a similar pattern, although there is more spread in the Sunday concentrations. This may be partially attributable to a smaller sample (22 days vs. at least 90 days for each monitor with measured data). Overall, modeled concentrations on Saturday tend to be lower than observed, while Sunday modeled concentrations are closer to observed. One possible explanation for this finding is that there may be residual NO_X left over from Friday evening, but which was not modeled in this exercise.

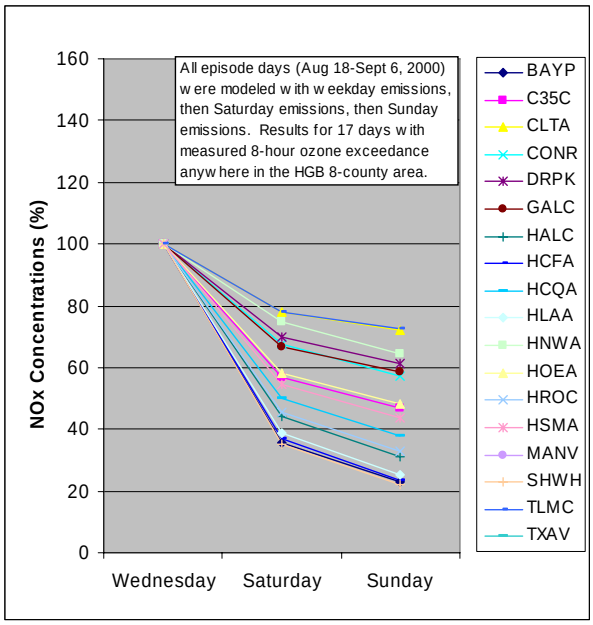

Figure 3: 6 AM Modeled NOx Concentrations as a % of Wednesday

Figure 4 shows average monitored peak eight-hour ozone concentrations at all 18 monitors. Here the picture is much different from that for NO_X, with some monitors increasing from Wednesday through Sunday, some declining from Wednesday through Sunday, and some peaking on Saturday with a decline on Sunday. The first pattern is suggestive of VOC limitation, the second of NO_X limitation, and the third (Saturday peak) of VOC-limited leaning to transitional.

The model (Figure 5) shows much less variability, with either no change or a slight decline from Wednesday through Sunday, and it appears that the model does not respond to the weekend emission changes in the same way as the monitors. However, the TexAQS 2000 was notable for including a period characterized by extreme meteorology Between August 30 and

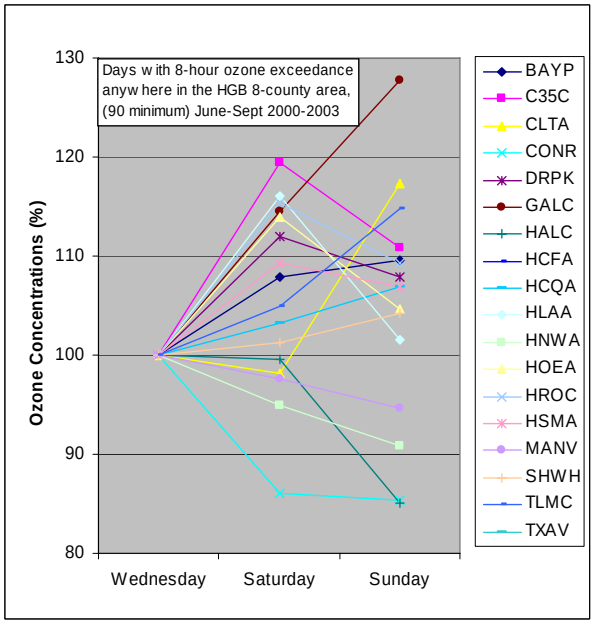

Figure 4: Mean Daily Observed Peak 8-Hour Ozone Concentrations as a % of Wednesday Peak

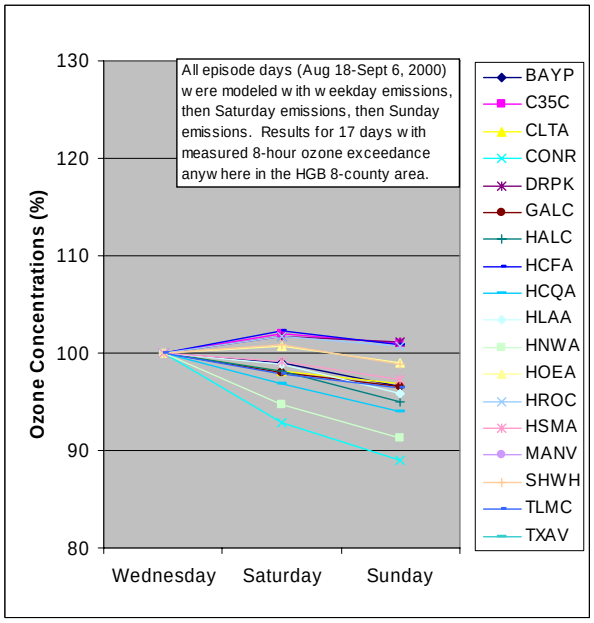

Figure 5: Mean Daily Modeled Peak 8-Hour Ozone Concnetrations as a % of Wednesday Peak

September 6, 2000 the HGB area saw some of the hottest temperatures ever recorded in the area, associated with winds with an uncharacteristically westerly component which brought in hot, dry air from the desert southwest. To illustrate how extreme this period was, in the 57-year period from 1942 through 2003, Houston Hobby airport saw temperatures exceeding 104° F on nine days. Five of these days occurred between August 30 and September 6, 2000, including the two hottest

temperatures ever recorded there: 108° on September 4 followed by 107° on September 5. These days, not surprisingly, also recorded most of the highest eight-hour ozone concentrations seen during the period modeled (see TCEQ, 2004). Modeled peak ozone concentrations on these days were similarly much higher than those in the remainder of the modeling period, and these concentrations dominated the average values shown in Figure 5.

To see if the inclusion of the highly unusual meteorological event of August 30 – September 6, 2000 influenced the model's response to weekday-weekend emissions changes, we divided the modeled period into a "typical" period (Aug. 18-29) and an "extreme" period (Aug. 30 – Sept. 6). The results are shown in Figures 6 and 7 below. The model results resemble the monitored values much more closely from the "typical" conditions than for the "extreme" conditions. One notable difference between the "typical" modeled concentrations and the monitored concentrations is the former's lack of Saturday peaks which characterize the monitored values at many urban and industrial monitor sites.

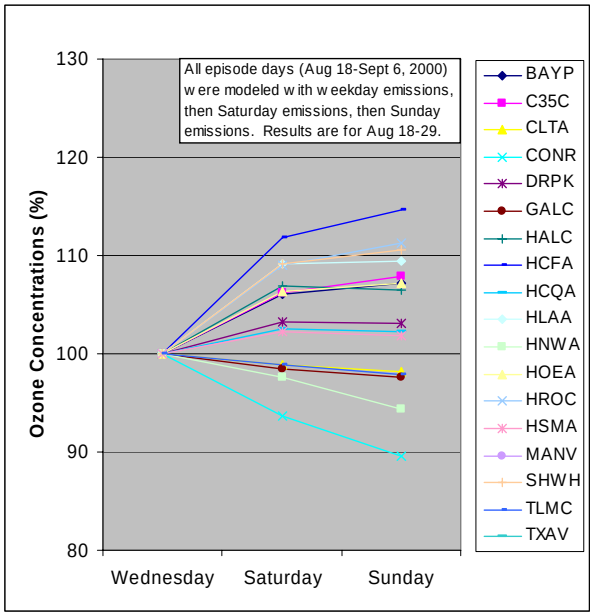

Figure 6: Mean Daily Modeled Peak 8-Hour Ozone Concentration as a % of Wednesday Peak, Aug 18-29, 2000

4. SUMMARY

Overall, model response to the weekday/weekend effect is reasonably consistent with observations, at least in the first part of the episode. The lack of a Saturday peak in modeled ozone at urban/industrial sites may indicate that the model has too much surface-level NO_X, and may be less responsive to NO_X reductions than the real atmosphere.

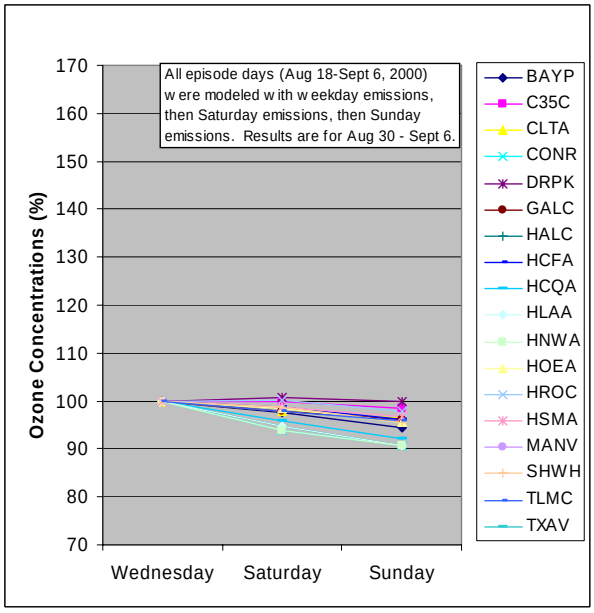

Figure 7: Mean Daily Modeled Peak Ozone Concentration as a % of Wednesday, Aug. 30 - Sept 6, 2000

The latter part of the episode shows little response to weekday/weekend emission changes, which probably dampens overall model response. Note that while the modeled behavior during this period is not consistent with long-term measured trends, there is no reason to believe the model is not correctly characterizing the response to emission changes for these types of days.

5. NOTES AND CAVEATS

A rigorous analysis would ensure that each day modeled used appropriate Hour 0 starting concentrations, such as Friday night prior to Saturday morning. Lack of residual NO_X may have affected some of the analyses.

Note also that because of limited sample sizes, trends in the data were not tested for statistical significance. The analysis presented here relies on visual identification of patterns in the data and is therefore subjective.

6. REFERENCES

EPA 2007 Guidance on the Use of Models and Other Analyses for Demonstrating Attainment of Air Quality Goals for Ozone, PM2.5, and Regional Haze, http://www.epa.gov/scram001/guidance/guide/final-03-pm-rh-guidance.pdf

Blanchard C.L. and Tannenbaum S.J. 2003. Differences between weekday and weekend air pollutant levels in southern California. J. Air Waste Manage. Assoc. 53: 816-828.

Blanchard C.L. and Tannenbaum S.J. 2005. Final Report: Weekday/Weekend Differences in Ambient Concentrations of Primary and Secondary Air Pollutants in Atlanta, Baltimore, Chicago, Dallas-Fort Worth, Denver, Houston, New York, Phoenix, Washington, and Surrounding Areas, NREL Project ES04-1 NREL Subcontract No. LDX-4-44213-01

Fujita E.M, Stockwell WR, Campbell D.E., Keislar R.E., and Lawson D.R.. 2003a. Evolution of the magnitude and spatial extent of the weekend ozone effect in California's South Coast Air Basin. J. Air Waste Manage. Assoc. 53: 802-815.

Yarwood G., Stoeckenius T.E., Heiken J. G. , and Dunker A.M. 2003. Modeling weekday/weekend ozone differences in the Los Angeles region for 1997. J. Air Waste Manage. Assoc. 53: 864-875.

TCEQ. 2004, Revisions to the State Implementation Plan (SIP) for the Control of Ozone Air Pollution: HOUSTON/GALVESTON/ BRAZORIA OZONE NONATTAINMENT AREA, http://www.tceq.state.tx.us/implementation/air/sip/dec2004hgb_mcr.html

USE OF HYBRID PLUME/GRID MODELING AND THE ST. LOUIS SUPER SITE DATA TO MODEL $PM_{2.5}$ CONCENTRATIONS IN THE ST. LOUIS AREA

Ralph Morris*, Bonyoung Koo, Jeremiah Johnson and Greg Yarwood
ENVIRON International Corporation, Novato, CA, USA

Jay Turner and Jennifer Garlock
Washington University, St. Louis, MO, USA

Calvin Ku, Wendy Vit, Adel Alsharafi and Jeff Bennett
Missouri Department of Natural Resources, Jefferson City, MO, USA

1. INTRODUCTION

The St. Louis region was designated as nonattainment for both the 8-hour ozone and $PM_{2.5}$ National Ambient Air Quality Standards (NAAQSs) by the U.S. Environmental Protection Agency (EPA). The Illinois Environmental Protection Agency (IEPA) and Missouri Department of Natural Resources (MDNR) are developing common 8-hour ozone and $PM_{2.5}$ emission control plans for the St. Louis region with a 2010 attainment date. ENVIRON International Corporation was retained by the MDNR to assist in the 8-hour ozone and $PM_{2.5}$ modeling for the St. Louis State Implementation Plan(SIP). During Phase I of the work effort, that was mainly performed in 2005, ENVIRON assisted in the development 36/12/4 km CMAQ and CAMx ozone modeling databases for three episodes from 2002. Under Phase II in 2006, ENVIRON assisted in the completion of the 8-hour ozone modeling for the three 2002 episodes, performed the final 2009 8-hour ozone attainment demonstration modeling and wrote the air quality Technical Support Document (TSD) that was included with the St. Louis 8-hour ozone SIP submitted in June 2007. Phase III of the work (2007) is focusing on the development of an annual 2002 36/12 km $PM_{2.5}$ regional modeling database to be used for the $PM_{2.5}$ SIP due April 2008.

2. $PM_{2.5}$ NONATTAINMENT PROBLEM IN ST. LOUIS

The St. Louis region has been designated nonattainment for $PM_{2.5}$ based on measured violations of the annual $PM_{2.5}$ NAAQS. The annual $PM_{2.5}$ NAAQS is based on the $PM_{2.5}$ Design Value that is the three year average of annual $PM_{2.5}$ concentrations with a threshold of 15.0 $\mu g/m^3$. Figure 1 displays the 2003-2005 $PM_{2.5}$ Design Values for the St. Louis area. There are two monitoring sites that violate the annual $PM_{2.5}$ NAAQS: Granite City and East St. Louis that have 2003-2005 PM Design Values of 17.0 and 15.5 $\mu g/m^3$, respectively. Both of these monitors are in the Illinois portion of the St. Louis nonattainment area.

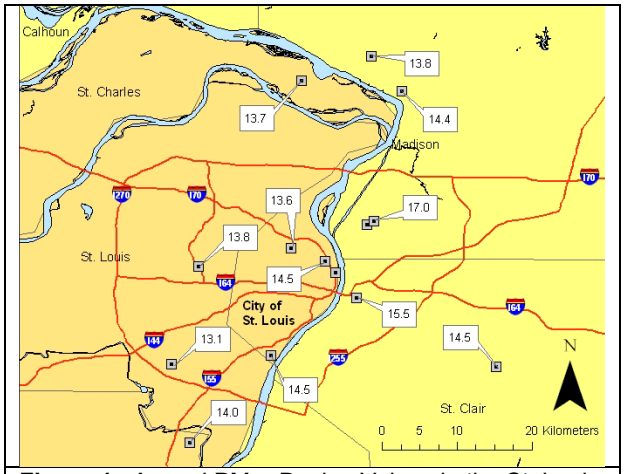

Figure 1. Annual $PM_{2.5}$ Design Values in the St. Louis region based on 2003-20005 monitoring data (Source: Turner and Garlock, 2007).

3. REGIONAL $PM_{2.5}$ MODELING FOR ST. LOUIS

ENVIRON and MDNR are developing a regional 36/12 km $PM_{2.5}$ modeling database for the 2002 annual period and the St. Louis region. Figure 2 displays the 36/12 km grid structure used in the St. Louis regional-scale modeling; the larger 12 km grid is being used. The SMOKE emissions

*_Corresponding author:_ Ralph Morris, ENVIRON International Corporation, 101 Rowland Way, Novato, CA USA 94945. e-mail: rmorris@environcorp.com. (415) 899-0708; FAX: (415) 899-0707

model is being used to generate emissions for the 36/12 km grid and a 2002 base case. The CMAQ and CAMx models were used to model 2002 and 2009 using the Base D emissions. The Base 4 emissions were updated to Base G and CMAQ was rerun for the 2002 and 2009 base case Base G emission scenarios. The CMAQ and CAMx Base D and CMAQ Base G 2002 and 2009 modeling results were used to project $PM_{2.5}$ Design Values for comparisons with the 15.0 $\mu g/m^3$ annual $PM_{2.5}$ standard. Two sites, Granite City and East St. Louis, are projected to still violate the annual $PM_{2.5}$ NAAQS in 2009. The 2009 $PM_{2.5}$ Design Value at Granite City is projected to be 1 to 1½ $\mu g/m^3$ higher than the annual standard. Because it will be difficult to implement additional controls in time to achieve attainment by 2009, the MDNR is pursuing modeling of the 2012 period.

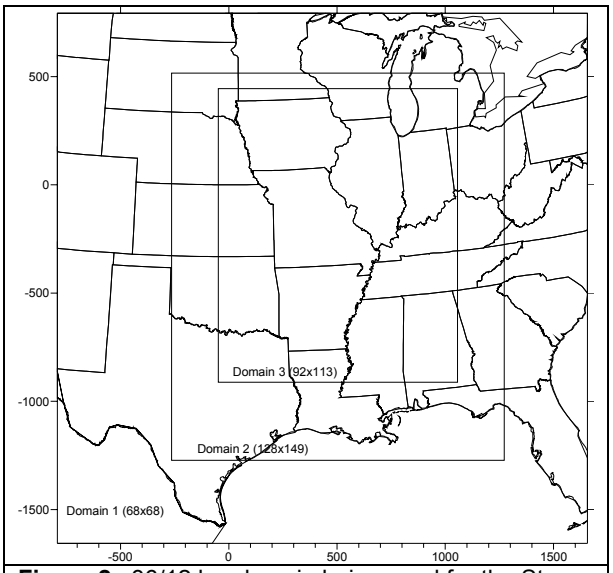

Figure 2. 36/12 km domain being used for the St. Louis 2002 annual $PM_{2.5}$ regional-scale modeling.

4. DATA ANALYSIS USING ST. LOUIS PM SUPER SITE DATA

The St. Louis Super Site has collected detailed PM measurements in the St. Louis area for several years, including 2002, that has allowed the use of advanced data analysis techniques to better understand the $PM_{2.5}$ problem in St. Louis. Figure 2 shows the results of $PM_{2.5}$ source apportionment modeling using the Positive Matrix Factor (PMF) receptor model and the St. Louis Super Site East St. Louis monitoring data. PMF decomposes the measured $PM_{2.5}$ into "factors" that are then associated with "source types". The largest factors identified by PMF are secondary sulfate, secondary nitrate, organic carbon plus secondary sulfate, urban carbon (mobile) and biomass burning. These factors are primarily regional in nature. Steel production is also identified as a significant source of the East St. Louis $PM_{2.5}$ contributing 1.28 $\mu g/m^3$ of the annual value (7.2%) with smaller contributions due to Zinc and Lead smelting (approximately 0.3 $\mu g/m^3$ each). These factors are more related to local sources.

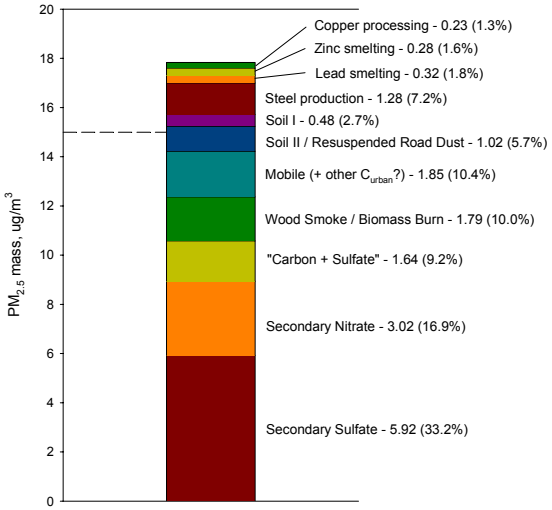

Figure 3. $PM_{2.5}$ source apportionment at East St. Louis (Source: Turner and Garlock, 2007).

Figure 4 displays another PMF analysis that combines the PMF analysis for the Industrial Point Source #1 factor with wind data at East St. Louis and indicates that the largest $PM_{2.5}$ contributions associated with this factor at the East St. Louis monitor are coming from the north, which is the direction of Granite City. Turner and Garlock (2007) also performed an analysis of the local versus regional contributions of $PM_{2.5}$ at the Granite City monitor which is summarized in Figure 5. Also shown in Figure 5 is the outline of the U.S. Steel Granite City Works (GCW) facility, with the steel production in the western and coke ovens in the eastern portion of the facility.

The data analysis using the advanced St. Louis Super Site PM data clearly shows that the $PM_{2.5}$ problem in St. Louis is a combination of regional (Figure 3) and local (Figures 4 and 5) sources. Consequently a hybrid modeling approach is needed that accounts for PM contributions from the local-scale using a plume

model and at the regional scale using a full chemistry photochemical grid model.

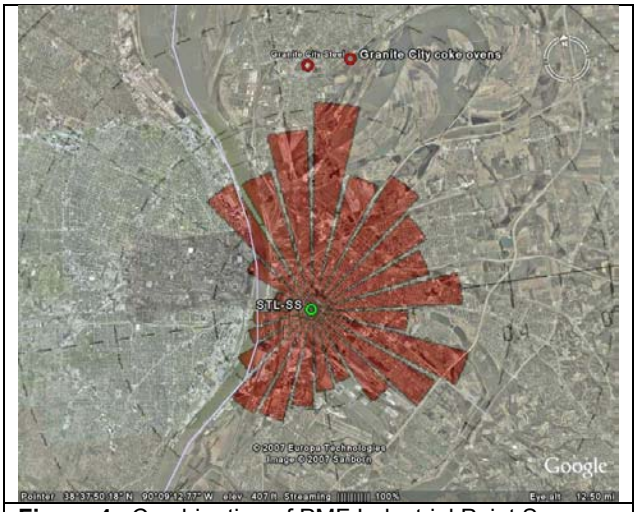

Figure 4. Combination of PMF Industrial Point Source #1 factor with wind data (Source: Turner and Garlock, 2007).

Figure 5. Wind analysis showing predominate wind directions when $PM_{2.5}$ concentrations at the Granite City monitor (location B) exceed the regional background $PM_{2.5}$ levels and outline of U.S. Steel Granite City Works facility (Source: Turner and Garlock, 2007).

5. HYBRID PLUME/GRID MODELNG APPROACH

5.1 Alternative Plume/Grid Hybrid Modeling Approaches

The regional 2002 36/12 km CMAQ/CAMx database can not address the local-scale contributions to $PM_{2.5}$ concentrations at Granite City. Thus, four approaches for treating local-scale impacts within the overall context of the 2002 36/12 km CMAQ/CAMx modeling were considered:

1. Hybrid Modeling using Regional Photochemical Grid Model and Local-Scale Gaussian Plume Model: In this approach a regional model (e.g., CMAQ and CAMx) would be used to represent the regional and urban scale contribution and a plume model, such as AERMOD or CALPUFF, that would be used to represent the contribution of local sources.

2. Use CAMx with the Subgrid-Scale Plume-in-Grid (PiG) Model for Local Sources: CAMx includes a subgrid-scale Plume-in-Grid (PiG) module to model the near-source transport, dispersion and chemistry of point sources. When the PiG plume size is commensurate with the grid cell size or chemical maturity is reached in the plume, the mass in the plume is released to the grid model for further tracking. The CAMx PiG module has been updated to work with a receptor sampling grid to obtain subgrid-scale concentrations at user-specified receptor locations. CMAQ also includes a Plume-in-Grid (PinG) module but it is designed for large power plant plumes not local contributions of point sources.

3. Use CMAQ or CAMx with Finer Grids (e.g., 1 km or smaller): Finer grid spacing using either CMAQ or CAMx models would also better represent the impacts of local sources. However, even a 1 km grid would not to be sufficient to represent the separation between the GCW facility and the Granite City monitor.

4. Use CAMx with Both Finer Grids and PiG: This approach combined the approaches listed in 2 and 3 above.

Because the CMAQ/CAMx regional grid models are designed to be accurate and the AERMOD/CALPUFF models are designed to be conservative, a hybrid plume/grid modeling approach mixing these two types of models is problematic. EPA guidance (EPA, 2007) suggests splitting the $PM_{2.5}$ Design Value into a regional and local component and then using the grid and plume models to project the separate component. However, how the Design Value is split is somewhat arbitrary. Thus, the IEPA and MDNR decided to explore the fourth approach to use an integrated hybrid grid/plume model to account for local as well as regional primary and secondary PM impacts within a single integrated unified modeling system.

5.2 Integrated Hybrid Plume/Grid Modeling approach

The St. Louis integrated hybrid plume/grid model would be based on the Comprehensive Air Quality Model with extensions (CAMx; ENVIRON, 2006) that incorporates a subgrid-scale Plume-in-Grid (PiG) model. The CAMx PiG has been recently updated to include second order closure (SOC) dispersion coefficients and the ability to use a receptor file to allow the subgrid-scale sampling of the PiG plumes. CAMx would be set up on a 12/4/1 km nested-grid configuration, like that shown in Figure 6. Boundary conditions (BCs) for the outer edges of the 12 km domain in Figure 6 would be based on a regional CMAQ or CAMx simulation on the St. Louis 36/12 km grid (see Figure 2). The feasibility of using a fourth grid nest finer than 1 km will be investigated (e.g., 333 m), however modifications to the horizontal diffusion coefficient algorithms would likely be needed (e.g., use of the SOC dispersion values). The 12/4/1 km and possibly 333 m grids would be run using fully interactive two-way grid nesting.

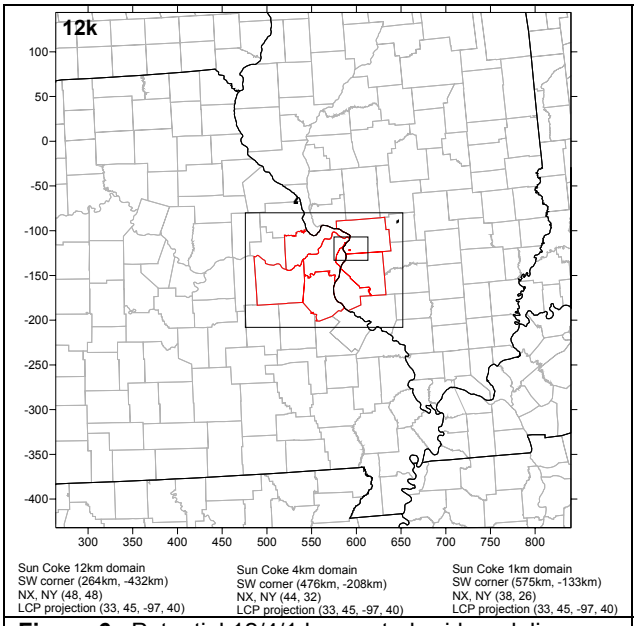

Figure 6. Potential 12/4/1 km nested-grid modeling domain for St. Louis $PM_{2.5}$ modeling.

6. CONCLUSIONS

Exceedances of the $PM_{2.5}$ NAAQS in St. Louis are due to the combination of regional and local sources. Thus, to demonstrate attainment of the $PM_{2.5}$ standard will require addressing the contributions and effects of controls at several scales. The unified multi-scale CAMx photochemical grid/plume model will be used to address this issue. It includes a full-chemistry Plume-in-Grid (PiG) plume model with second order closure dispersion and receptor sampling capabilities.

7. REFERENCES

ENVIRON. 2006. User's Guide – Comprehensive Air-quality Model with extensions, Version 4.40. ENVIRON International Corporation, Novato, California. (www.camx.com).

EPA. 2007. "Guidance on the Use of Models and Other Analyses for Demonstrating Attainment of Air Quality Goals for Ozone, $PM_{2.5}$ and Regional Haze", U.S. Environmental Protection Agency, Research Triangle Park, NC. EPA-454/B-07-002. April.

Turner, J. and J. Garlock. 2007. Observational Data Analysis to Support PM 2.5 SIP Development. Department of Energy, Environment and Chemical Engineering, Washington University. Presented at Modeling and Control Strategies Joint Workgroup Meeting, St. Louis, MO. June 4.

USE OF HYBRID PLUME/GRID MODELING AND THE ST. LOUIS SUPER SITE DATA TO MODEL $PM_{2.5}$ CONCENTRATIONS IN THE ST. LOUIS AREA

Ralph Morris*, Bonyoung Koo, Jeremiah Johnson and Greg Yarwood
ENVIRON International Corporation, Novato, CA, USA

Jay Turner and Jennifer Garlock
Washington University, St. Louis, MO, USA

Calvin Ku, Wendy Vit, Adel Alsharafi and Jeff Bennett
Missouri Department of Natural Resources, Jefferson City, MO, USA

1. INTRODUCTION

The St. Louis region was designated as nonattainment for both the 8-hour ozone and $PM_{2.5}$ National Ambient Air Quality Standards (NAAQSs) by the U.S. Environmental Protection Agency (EPA). The Illinois Environmental Protection Agency (IEPA) and Missouri Department of Natural Resources (MDNR) are developing common 8-hour ozone and $PM_{2.5}$ emission control plans for the St. Louis region with a 2010 attainment date. ENVIRON International Corporation was retained by the MDNR to assist in the 8-hour ozone and $PM_{2.5}$ modeling for the St. Louis State Implementation Plan(SIP). During Phase I of the work effort, that was mainly performed in 2005, ENVIRON assisted in the development 36/12/4 km CMAQ and CAMx ozone modeling databases for three episodes from 2002. Under Phase II in 2006, ENVIRON assisted in the completion of the 8-hour ozone modeling for the three 2002 episodes, performed the final 2009 8-hour ozone attainment demonstration modeling and wrote the air quality Technical Support Document (TSD) that was included with the St. Louis 8-hour ozone SIP submitted in June 2007. Phase III of the work (2007) is focusing on the development of an annual 2002 36/12 km $PM_{2.5}$ regional modeling database to be used for the $PM_{2.5}$ SIP due April 2008.

2. $PM_{2.5}$ NONATTAINMENT PROBLEM IN ST. LOUIS

The St. Louis region has been designated nonattainment for $PM_{2.5}$ based on measured violations of the annual $PM_{2.5}$ NAAQS. The annual $PM_{2.5}$ NAAQS is based on the $PM_{2.5}$ Design Value that is the three year average of annual $PM_{2.5}$ concentrations with a threshold of 15.0 $\mu g/m^3$. Figure 1 displays the 2003-2005 $PM_{2.5}$ Design Values for the St. Louis area. There are two monitoring sites that violate the annual $PM_{2.5}$ NAAQS: Granite City and East St. Louis that have 2003-2005 PM Design Values of 17.0 and 15.5 $\mu g/m^3$, respectively. Both of these monitors are in the Illinois portion of the St. Louis nonattainment area.

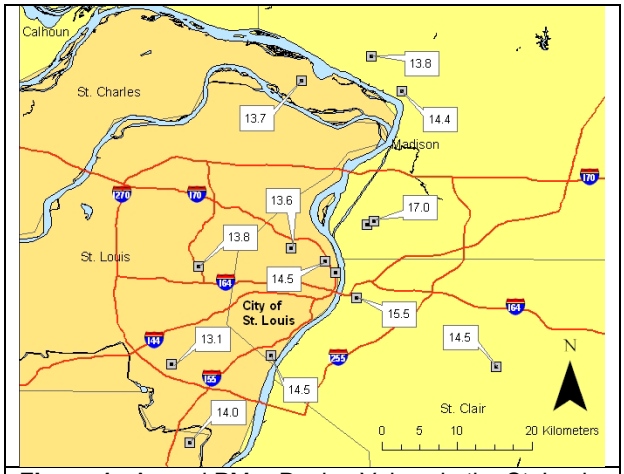

Figure 1. Annual $PM_{2.5}$ Design Values in the St. Louis region based on 2003-20005 monitoring data (Source: Turner and Garlock, 2007).

3. REGIONAL $PM_{2.5}$ MODELING FOR ST. LOUIS

ENVIRON and MDNR are developing a regional 36/12 km $PM_{2.5}$ modeling database for the 2002 annual period and the St. Louis region. Figure 2 displays the 36/12 km grid structure used in the St. Louis regional-scale modeling; the larger 12 km grid is being used. The SMOKE emissions

*_Corresponding author:_ Ralph Morris, ENVIRON International Corporation, 101 Rowland Way, Novato, CA USA 94945. e-mail: rmorris@environcorp.com. (415) 899-0708; FAX: (415) 899-0707

model is being used to generate emissions for the 36/12 km grid and a 2002 base case. The CMAQ and CAMx models were used to model 2002 and 2009 using the Base D emissions. The Base 4 emissions were updated to Base G and CMAQ was rerun for the 2002 and 2009 base case Base G emission scenarios. The CMAQ and CAMx Base D and CMAQ Base G 2002 and 2009 modeling results were used to project $PM_{2.5}$ Design Values for comparisons with the 15.0 $\mu g/m^3$ annual $PM_{2.5}$ standard. Two sites, Granite City and East St. Louis, are projected to still violate the annual $PM_{2.5}$ NAAQS in 2009. The 2009 $PM_{2.5}$ Design Value at Granite City is projected to be 1 to 1½ $\mu g/m^3$ higher than the annual standard. Because it will be difficult to implement additional controls in time to achieve attainment by 2009, the MDNR is pursuing modeling of the 2012 period.

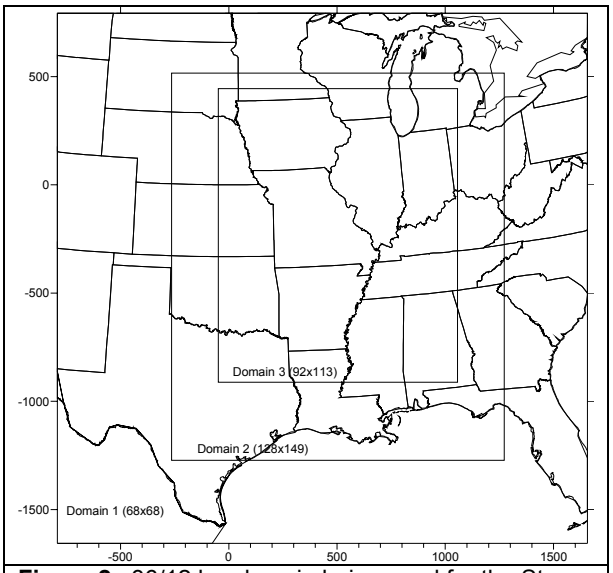

Figure 2. 36/12 km domain being used for the St. Louis 2002 annual $PM_{2.5}$ regional-scale modeling.

4. DATA ANALYSIS USING ST. LOUIS PM SUPER SITE DATA

The St. Louis Super Site has collected detailed PM measurements in the St. Louis area for several years, including 2002, that has allowed the use of advanced data analysis techniques to better understand the $PM_{2.5}$ problem in St. Louis. Figure 2 shows the results of $PM_{2.5}$ source apportionment modeling using the Positive Matrix Factor (PMF) receptor model and the St. Louis Super Site East St. Louis monitoring data. PMF decomposes the measured $PM_{2.5}$ into "factors" that are then associated with "source types". The largest factors identified by PMF are secondary sulfate, secondary nitrate, organic carbon plus secondary sulfate, urban carbon (mobile) and biomass burning. These factors are primarily regional in nature. Steel production is also identified as a significant source of the East St. Louis $PM_{2.5}$ contributing 1.28 $\mu g/m^3$ of the annual value (7.2%) with smaller contributions due to Zinc and Lead smelting (approximately 0.3 $\mu g/m^3$ each). These factors are more related to local sources.

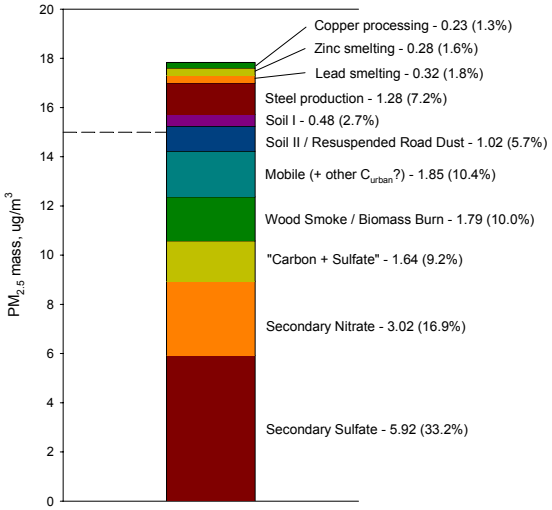

Figure 3. $PM_{2.5}$ source apportionment at East St. Louis (Source: Turner and Garlock, 2007).

Figure 4 displays another PMF analysis that combines the PMF analysis for the Industrial Point Source #1 factor with wind data at East St. Louis and indicates that the largest $PM_{2.5}$ contributions associated with this factor at the East St. Louis monitor are coming from the north, which is the direction of Granite City. Turner and Garlock (2007) also performed an analysis of the local versus regional contributions of $PM_{2.5}$ at the Granite City monitor which is summarized in Figure 5. Also shown in Figure 5 is the outline of the U.S. Steel Granite City Works (GCW) facility, with the steel production in the western and coke ovens in the eastern portion of the facility.

The data analysis using the advanced St. Louis Super Site PM data clearly shows that the $PM_{2.5}$ problem in St. Louis is a combination of regional (Figure 3) and local (Figures 4 and 5) sources. Consequently a hybrid modeling approach is needed that accounts for PM contributions from the local-scale using a plume

model and at the regional scale using a full chemistry photochemical grid model.

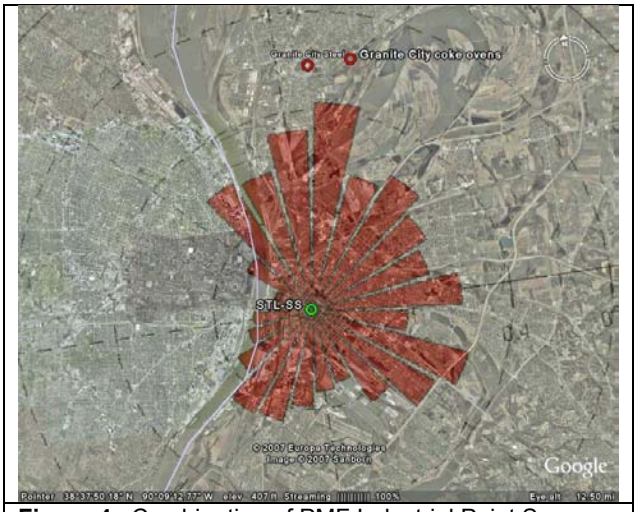

Figure 4. Combination of PMF Industrial Point Source #1 factor with wind data (Source: Turner and Garlock, 2007).

Figure 5. Wind analysis showing predominate wind directions when $PM_{2.5}$ concentrations at the Granite City monitor (location B) exceed the regional background $PM_{2.5}$ levels and outline of U.S. Steel Granite City Works facility (Source: Turner and Garlock, 2007).

5. HYBRID PLUME/GRID MODELNG APPROACH

5.1 Alternative Plume/Grid Hybrid Modeling Approaches

The regional 2002 36/12 km CMAQ/CAMx database can not address the local-scale contributions to $PM_{2.5}$ concentrations at Granite City. Thus, four approaches for treating local-scale impacts within the overall context of the 2002 36/12 km CMAQ/CAMx modeling were considered:

1. Hybrid Modeling using Regional Photochemical Grid Model and Local-Scale Gaussian Plume Model: In this approach a regional model (e.g., CMAQ and CAMx) would be used to represent the regional and urban scale contribution and a plume model, such as AERMOD or CALPUFF, that would be used to represent the contribution of local sources.

2. Use CAMx with the Subgrid-Scale Plume-in-Grid (PiG) Model for Local Sources: CAMx includes a subgrid-scale Plume-in-Grid (PiG) module to model the near-source transport, dispersion and chemistry of point sources. When the PiG plume size is commensurate with the grid cell size or chemical maturity is reached in the plume, the mass in the plume is released to the grid model for further tracking. The CAMx PiG module has been updated to work with a receptor sampling grid to obtain subgrid-scale concentrations at user-specified receptor locations. CMAQ also includes a Plume-in-Grid (PinG) module but it is designed for large power plant plumes not local contributions of point sources.

3. Use CMAQ or CAMx with Finer Grids (e.g., 1 km or smaller): Finer grid spacing using either CMAQ or CAMx models would also better represent the impacts of local sources. However, even a 1 km grid would not to be sufficient to represent the separation between the GCW facility and the Granite City monitor.

4. Use CAMx with Both Finer Grids and PiG: This approach combined the approaches listed in 2 and 3 above.

Because the CMAQ/CAMx regional grid models are designed to be accurate and the AERMOD/CALPUFF models are designed to be conservative, a hybrid plume/grid modeling approach mixing these two types of models is problematic. EPA guidance (EPA, 2007) suggests splitting the $PM_{2.5}$ Design Value into a regional and local component and then using the grid and plume models to project the separate component. However, how the Design Value is split is somewhat arbitrary. Thus, the IEPA and MDNR decided to explore the fourth approach to use an integrated hybrid grid/plume model to account for local as well as regional primary and secondary PM impacts within a single integrated unified modeling system.

5.2 Integrated Hybrid Plume/Grid Modeling approach

The St. Louis integrated hybrid plume/grid model would be based on the Comprehensive Air Quality Model with extensions (CAMx; ENVIRON, 2006) that incorporates a subgrid-scale Plume-in-Grid (PiG) model. The CAMx PiG has been recently updated to include second order closure (SOC) dispersion coefficients and the ability to use a receptor file to allow the subgrid-scale sampling of the PiG plumes. CAMx would be set up on a 12/4/1 km nested-grid configuration, like that shown in Figure 6. Boundary conditions (BCs) for the outer edges of the 12 km domain in Figure 6 would be based on a regional CMAQ or CAMx simulation on the St. Louis 36/12 km grid (see Figure 2). The feasibility of using a fourth grid nest finer than 1 km will be investigated (e.g., 333 m), however modifications to the horizontal diffusion coefficient algorithms would likely be needed (e.g., use of the SOC dispersion values). The 12/4/1 km and possibly 333 m grids would be run using fully interactive two-way grid nesting.

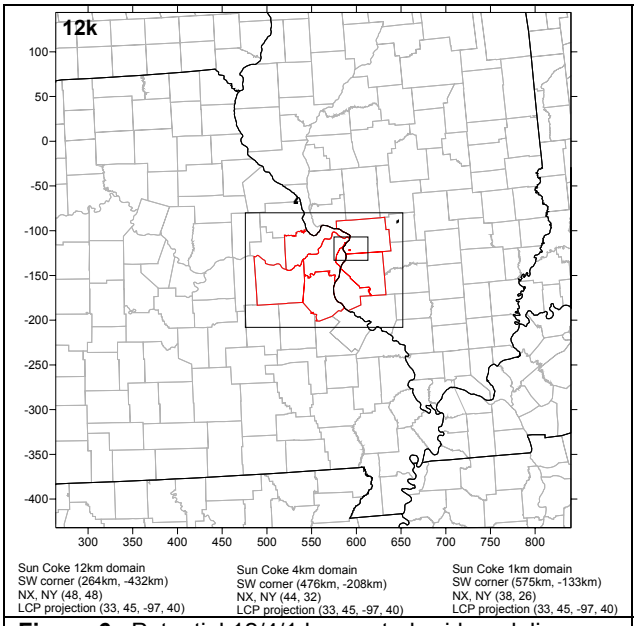

Figure 6. Potential 12/4/1 km nested-grid modeling domain for St. Louis $PM_{2.5}$ modeling.

6. CONCLUSIONS

Exceedances of the $PM_{2.5}$ NAAQS in St. Louis are due to the combination of regional and local sources. Thus, to demonstrate attainment of the $PM_{2.5}$ standard will require addressing the contributions and effects of controls at several scales. The unified multi-scale CAMx photochemical grid/plume model will be used to address this issue. It includes a full-chemistry Plume-in-Grid (PiG) plume model with second order closure dispersion and receptor sampling capabilities.

7. REFERENCES

ENVIRON. 2006. User's Guide – Comprehensive Air-quality Model with extensions, Version 4.40. ENVIRON International Corporation, Novato, California. (www.camx.com).

EPA. 2007. "Guidance on the Use of Models and Other Analyses for Demonstrating Attainment of Air Quality Goals for Ozone, $PM_{2.5}$ and Regional Haze", U.S. Environmental Protection Agency, Research Triangle Park, NC. EPA-454/B-07-002. April.

Turner, J. and J. Garlock. 2007. Observational Data Analysis to Support PM 2.5 SIP Development. Department of Energy, Environment and Chemical Engineering, Washington University. Presented at Modeling and Control Strategies Joint Workgroup Meeting, St. Louis, MO. June 4.

AEROSOL MODELING AT REGIONAL AND CONTINENTAL SCALES

Karine Sartelet*, Edouard Debry, Marilyne Tombette, Yelva Roustan, Bruno Sportisse
CEREA, Joint Research Laboratory, École Nationale des Ponts et Chaussées / EDF R&D, France

This talk aims at presenting two aerosol models that are part of the air-quality modeling system Polyphemus : SIREAM (SIze Resolved Aerosol Model) based on a sectional description of the aerosol distribution and MAM (Modal Aerosol Model) based on a modal discretization. The models are first described, as well as their coupling to the chemistry-transport model Polair3D of Polyphemus. Validations were made at the regional scale over Paris and Tokyo, and at the continental scales over Europe and over Asia in the framework of MICS (Model Inter-Comparison Study). Sensitivity of aerosol concentrations to configuration choices used in the aerosol models, such as whether or not the assumption of thermodynamic equilibrium is made for coarse aerosols, is briefly presented.

1 MODELING

The models SIREAM and MAM are described in details in Debry et al. [2007] and Sartelet et al. [2006]. SIREAM (SIze Resolved Aerosol Model) based on a sectional description of the aerosol distribution and MAM (Modal Aerosol Model) based on a modal discretization. The models share physical parameterizations. They both assume internal mixing of inert (mineral dust, elemental carbon), inorganic (sodium, chloride, nitrate, sulfate and ammonium) and organic species (primary organics and secondary organics following Schell et al. [2001]). The following processes are modeled : ternary nucleation following Napari et al. [2002], Brownian coagulation, condensation/evaporation solved using ISORROPIA (Nenes et al. [1998]). Mass transfer can be solved either assuming thermodynamic equilibrium (bulk equilibrium approach) or dynamically. In addition, a hybrid approach can be used in which thermodynamic equilibrium is assumed for the smallest sections/modes and mass transfer is computed dynamically for the largest sections/modes. In the framework of the air quality modeling system Polyphemus, SIREAM/MAM are coupled to the chemistry transport model Polair3D (Mallet et al. [2007]). Heterogeneous reactions : $HO_2 \rightarrow 0.5\ H_2O_2$, $NO_2 \rightarrow 0.5\ HONO + 0.5\ HNO_3$, $NO_3 \rightarrow HNO_3$, $N_2O_5 \rightarrow 2\ HNO_3$ are modeled following Jacob [2000] with the reaction probabilities $\gamma_{HO_2} = 0.1$, $\gamma_{NO_2} = 10^{-6}$, $\gamma_{NO_3} = 2.10^{-4}$, $\gamma_{N_2O_5} = 0.01$, except when specified. When the liquid water content of the cell exceeds a threshold value of 0.05g m^{-3}, the grid cell is assumed to contain a cloud, and a model for aqueous phase chemistry for cloud dropets (based on the Variable Size Resolved Model VSRM of Fahey and Pandis [2003]) is called instead of SIREAM/MAM.

*Corresponding author : sartelet@cerea.enpc.fr

2 VALIDATION AND SENSITIVITY STUDIES

The validation of Polyphemus-SIREAM or Polyphemus-MAM was done at the regional scale over Paris (Tombette and Sportisse [2007]), Greater Tokyo (Sartelet et al. [2007b]), at the regional scale over Asia (Sartelet et al. [2007c]) and over Europe (Sartelet et al. [2007a]). The domain and input data are not detailed here, and the comparisons to measurements are only briefly summarized. The scores obtained for PM_{10} and inorganic aerosols (sulfate and nitrate) are presented (measured and simulated mean, correlation, normalized mean error NME and normalized mean bias NMB, see Sartelet et al. [2007c] for a definition of these statistics). Different assumptions can be made in the modeling and different parameterizations can be used. To test the impact of aerosol processes and modeling assumptions on aerosol concentrations, sensitivity studies were carried out for each validation. The reference simulation is the simulation used to compute the scores. The reference simulation is compared to simulations where only one aerosol process differ from the reference simulation. The comparison is done by computing the NME between the reference simulation and the other simulations. Although the impact of aerosol processes on aerosol concentrations differ depending on local conditions and the chemical component studied, comparisons of the different sensitivity studies allow us to point out common features and differences.

2.1 At the regional scale

2.1.1 over Greater Paris

Over Greater Paris, Tombette and Sportisse [2007] run a simulation for 5 months, from 1 May 2001 to 30 September 2001, using 10 sections in the range 0.01μm - 10μm. The scores for PM_{10} averaged over 8 stations are given in table 1.

A sensitivity study was conducted over the first 15 days of July. All the discretization points in the domain of study are taken into account when computing the statistics. Three simulations are considered in the sensitivity study : a run without heterogeneous reaction (the reaction probabilities are ta-

TAB. 1 – Scores for PM_{10} over Greater Paris

Meas. mean	Sim. mean	Corr	NMB	NME
23.0	23.9	59.5	4.0	32.4

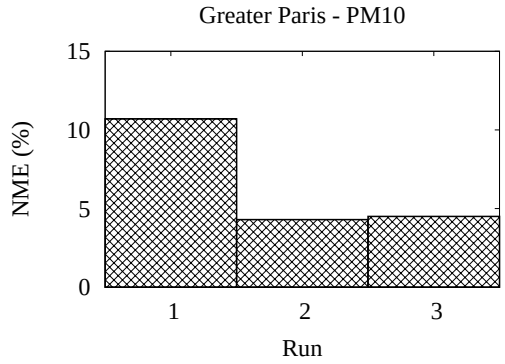

FIG. 1 – Over Greater Paris, for PM_{10}, differences between the reference run and a run without heterogeneous reaction (1), bulk equilibrium (2) and dynamic mass transfer (3)

ken as $\gamma_{HO_2} = 0.2$, $\gamma_{NO_2} = 10^{-5}$, $\gamma_{NO_3} = 10^{-3}$, $\gamma_{N_2O_5} = 0.03$ in the reference run), a run assuming bulk equilibrium for all sections instead of computing dynamically the largest 3 sections (i.e. sections of diameter larger than 1.25μm), and a run where all sections are computed dynamically. As shown in Figure 1, PM_{10} concentrations were found to be very sensitive to heterogeneous reaction with a NME of 11$\%$ but less sensitive to whether mass transfer is computed dynamically or assuming bulk equilibrium (the NME is about 4$\%$).

2.1.2 over Greater Tokyo

Over Greater Tokyo, Sartelet et al. [2007b] use Polyphemus-MAM to simulate two high-pollution episodes : one in winter (9 and 10 December 1999) and one in summer (31 July and 1 August 2001). The 4 modes lie in the diameter range 0.001μm and 10μm.

The scores are given in table 2 for inorganic $PM_{2.5}$ (sulfate and nitrate) at 4 stations for the winter episode and two stations for the summer episode. Better scores are generally observed for sulfate than nitrate.

Only the concentrations at the location of measurements were considered in the sensitivity study. In the reference run, condensation assuming thermodynamic equilibrium, dry deposition, nucleation and coagulation are taken into account, heterogeneous reactions are ignored. Eight simulations were conducted : without condensation, using the hybrid scheme (thermodynamic equilibrium is assumed only for the smallest mode instead of the four

TAB. 2 – Scores for sulfate and nitrate over Tokyo in the winter episode (first 2 lines) and in the summer episode (last 2 lines)

	Meas.	Sim.	Corr	NMB	NME
sulfate	2.6	3.3	66.2	-26	41
nitrate	4.5	4.1	44.5	8	111
sulfate	13.3	14.1	-2	-7	34
nitrate	5.7	2.1	34	62	67

modes), with heterogeneous reactions (the reaction probabilities are taken as $\gamma_{HO_2} = 0.2$, $\gamma_{NO_2} = 10^{-4}$, $\gamma_{NO_3} = 10^{-3}$, $\gamma_{N_2O_5} = 0.03$ in the reference run), without deposition, without nucleation, without coagulation, using SIREAM instead of MAM (i.e. using the sectional distribution instead of the modal distribution), using CMAQ instead of Polyphemus-MAM. Because CMAQ models the same processes as Polyphemus-MAM, comparison of the reference run to CMAQ allows us to have a rough idea of the sensitivity to parameterizations in and outside the aerosol module.

Comparisons of the NME between each of these simulations and the reference run is shown in Figure 2. For sulfate, in the summer episode, the impact of long-range transport dominates because the close by Mount Oyama of Miyake Island was in eruption at that time. This is illustrated by the fact that the highest sensitivity is observed when CMAQ is used (with a NME of 42$\%$ against 12$\%$ for condensation). In the winter episode, sulfate is mostly impacted by condensation (21$\%$), CMAQ (20$\%$), coagulation (17$\%$), and deposition to a lesser extent(10$\%$). Whereas nucleation and coagulation are negligible in the summer episode (1$\%$), they are not in the winter episode (17$\%$ and 5$\%$). The impact of coagulation is larger in the winter episode than in the summer episode, because the number of small particles is higher in the winter episode as a consequence of higher nucleation.

For nitrate, the impacts of condensation, heterogeneous reactions and CMAQ dominate (66$\%$, 190$\%$ and 100$\%$ respectively in the winter episode and 99$\%$, 119$\%$ and 251$\%$ in the summer episode). The impact of the thermodynamic equilibrium assumption is limited (12$\%$ in the winter episode and 49$\%$ in the summer episode).

For both sulfate and nitrate, the impact of dry deposition is limited (8 to 10$\%$).

The impact of using a sectional representation of the size distribution is small, also not negligible, and it is higher for nitrate (8-18$\%$) than for sulfate (6-8$\%$).

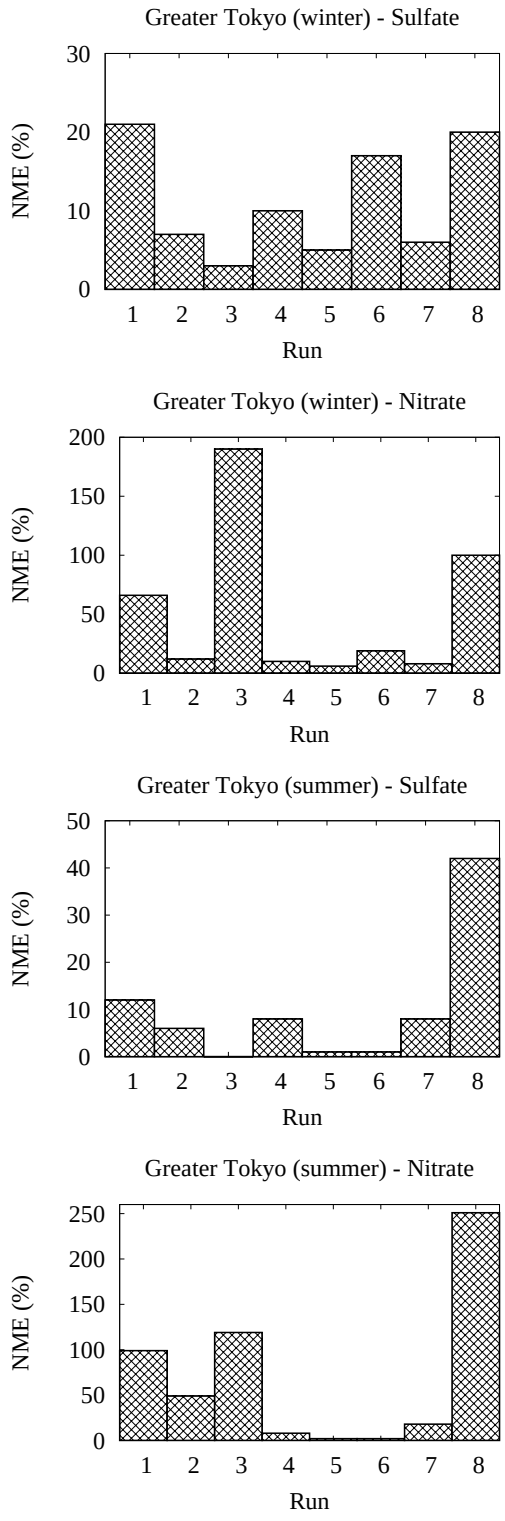

FIG. 2 – Over Greater Tokyo, for sulfate and nitrate, differences between the reference run and a run without condensation (1), using the hybrid scheme (2), with heterogeneous reaction (3), without dry deposition (4), without nucleation (5), without coagulation (6), SIREAM (7), CMAQ (8)

TAB. 3 – Scores for sulfate and nitrate over 24 stations of East Asia in March 2001

	Meas.	Sim.	NMB	NME
sulfate	4.9	5.2	13	13
nitrate	0.9	1.8	24	27

2.2 At the continental scale

2.2.1 over East Asia

The validation of Polyphemus-SIREAM over East Asia was done in the framework of the model intercomparison study–Asia Phase II (MICS2).The sensitivity study was conducted only for March 2001. The scores for sulfate and nitrate over 24 stations are given in table 3. In the reference run, 10 sections in the range 0.01μm - 10μm are used, thermodynamic equilibrium is assumed, heterogeneous reactions and cloud chemistry are ignored. Only the concentrations at the location of measurements were considered in the sensitivity study. Seven simulations were conducted : with 3 sections instead of 10, with the hybrid scheme (with a cutoff diameter of 0.6μm, i.e. the finest 6 sections are computed with the full equilibrium approach), without coagulation, with heterogeneous reaction ($\gamma_{HO_2} = 0.2$, $\gamma_{NO_2} = 10^{-4}$, $\gamma_{NO_3} = 10^{-3}$, $\gamma_{N_2O_5} = 0.03$), with cloud chemistry, using CMAQ instead of Polyphemus-SIREAM.

As shown in Figure 3, sulfate is mostly impacted by CMAQ (34$\%$), and by cloud chemistry (17$\%$), heterogeneous reaction (15$\%$) and coagulation (11$\%$) to a lesser extent. For nitrate, the impact of heterogeneous reactions is very large (99$\%$) followed by CMAQ (71$\%$). The number of sections, the hybrid scheme and coagulation have much smaller impacts although they are not negligeable (15$\%$, 13$\%$ and 15$\%$ respectively).

2.2.2 over Europe

Sartelet et al. [2007a] presented a validation of multi-pollutants over Europe with a focus on aerosols for the year 2001 (see the scores in table 4 evaluated with three different databases (EMEP, AirBase and BDQA). A sensitivity study was conducted over 1 month in summer (between 15 July and 14 August 2001) and 1 month in winter (between 15 November and 14 December 2001).

All the discretization points in the domain of study are considered when computing the statistics. In the reference run, 5 sections in the range 0.01μm - 10μm are used, thermodynamic equilibrium is assumed, heterogeneous reactions and cloud chemistry are taken into account, nucleation is ignored. Twelve other simulations were conducted : with 10 sections instead of 5, with dynamic mass transfer for all sec-

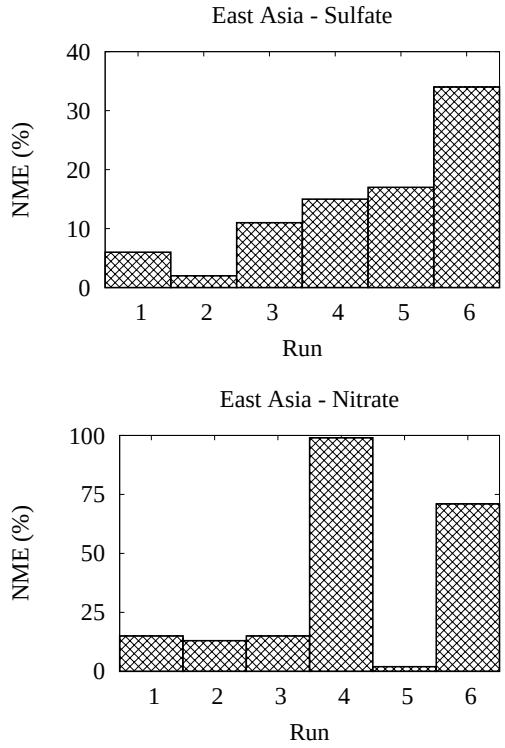

FIG. 3 – Over East Asia, for sulfate and nitrate, differences between the reference run and a run with 3 sections instead of 10 (1), with the hybrid scheme (2), without coagulation (3), with heterogeneous reaction (4), with cloud chemistry (5), using CMAQ instead of Polyphemus-SIREAM (6)

TAB. 4 – Scores for PM_{10}, sulfate and nitrate over Europe 2001. E refers to the EMEP database, A to the airbase database and B to the bdqa database.

	Meas.	Sim.	Corr	NMB	NME
PM_{10} (E)	16.9	15.6	55	-1	51
PM_{10} (A)	24.9	15.4	44	-33	49
PM_{10} (B)	19.8	15.8	57	-19	36
sulfate (E)	2.5	2.1	56	-5	51
sulfate (A)	1.9	2.4	51	73	105
nitrate (E)	2.6	4.1	41	91	122
nitrate (A)	3.5	4.4	72	27	56

tions, without the heterogeneous reaction for N_2O_5, with varying reaction probability for the heterogeneous reaction N_2O_5 (following Evans and Jacob [2005] and Riemer et al. [2003]), with nucleation (by adding 2 bins between 0.001μm and 0.01μm), with the criterion LWC (liquid water content) < 0.07g m^{-3} instead of LWC < 0.05g m^{-3} to call the aqueous model VSRM, with a different criterion to call the aqueous model VSRM (VSRM is called when the cloud fraction is greater than 20%), with different parameterizations of the diameter and falling velocity of raindrops (instead of the parameterizations of Loosmore and Cederwall [2004], the parameterization of Seinfeld [1985] is used for the falling velocity of raindrops and the one of Pruppacher and Klett [1998] is used for the diameter of raindrops), with monthly boundary conditions from Mozart version 2.4 (Horowitz [2003]) instead of daily boundary conditions from Gocart (Chin et al. [2000])), with the parameterization of Louis (Louis [1979]) rather than Troen Mahrt (Troen and Mahrt [1986]) for vertical diffusion.

As shown in Figure 4 for the winter run and Figure 5 for the summer run, PM_{10}, sulfate and nitrate are strongly impacted by the parameterization used for vertical diffusion (for PM_{10}, it corresponds to the highest sensitivity with a NME of 20% in winter and 29% in summer). For PM_{10}, sulfate and nitrate, low sensitivity is observed to the number of sections used, to whether the reaction probability of the heterogeneous reaction N_2O_5 varies or not, to nucleation and the threshold used for LWC. In winter, PM_{10} is sensitive to whether LWC or a cloud criterion is used to call VSRM, to the parameterization of scavenging, to boundary conditions and to the heterogeneous reaction of N_2O_5 (NMEs of about 10%). In summer, PM_{10} is sensitive to boundary conditions (NME = 16%) and to the parameterization used for scavenging (NME = 8%). For sulfate, the highest sensitivity in both winter and summer corresponds to boudary condition (with a NME of 22 and 19%). Sulfate is also sensitive to the criterion used to call VSRM (with a NME of 10 and 8%), and to the heterogeneous reaction N_2O_5 in winter (NME = 8%). For nitrate, there is a high sensitivity to the heterogeneous reaction N_2O_5 (with a NME of 63 and 24%) and to the dynamic mass transfer (with a NME of 17 and 27%). To a lesser extent, nitrate is also sensitive to the cloud criterion use to call VSRM (with a NME of 11 and 16%).

3 CONCLUSION

The chemistry transport model Polyphemus with the aerosol module MAM or SIREAM performs reasonnably well at the regional scale over Paris, Tokyo and at the continental scale over Europe and Asia. For each validation, sensitivity studies were conducted. As expected, PM_{10} is sensitive to configuration

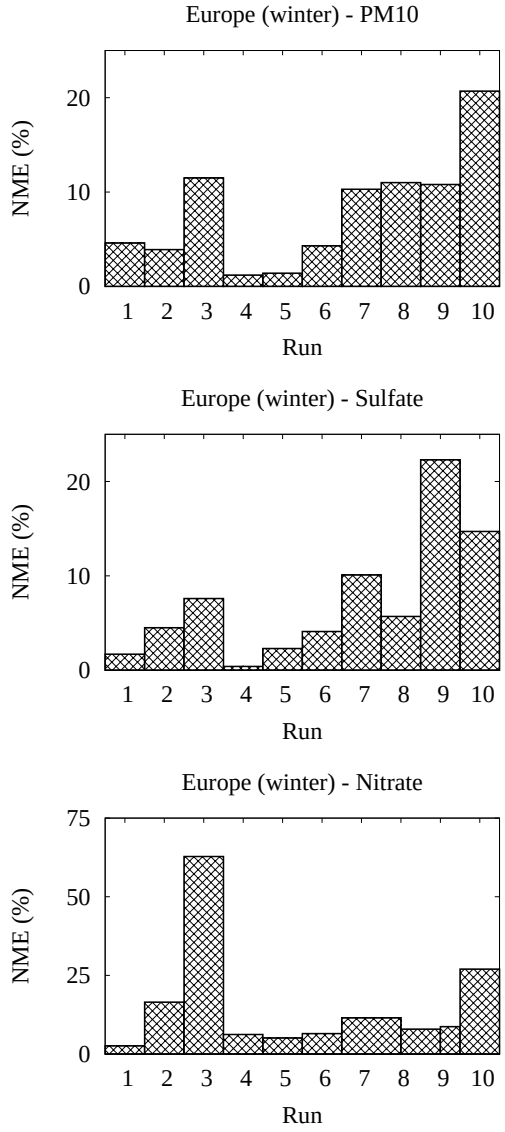

FIG. 4 – Over Europe, for PM_{10}, sulfate and nitrate, differences between the reference run and a run with 10 sections (1), with dynamic mass transfer (2), without the heterogeneous reaction N_2O_5 (3), with varying reaction probability for the heterogeneous reaction N_2O_5 (4), with nucleation (5), with the criterion LWC $< 0.07\mu$g m^{-3} to call the aqueous model VSRM (6), with the cloud fraction to diagnose when to call VSRM (7), with a different parameterization for scavenging (8), with different boundary conditions (9), with a different parameterization for vertical diffusion (10).

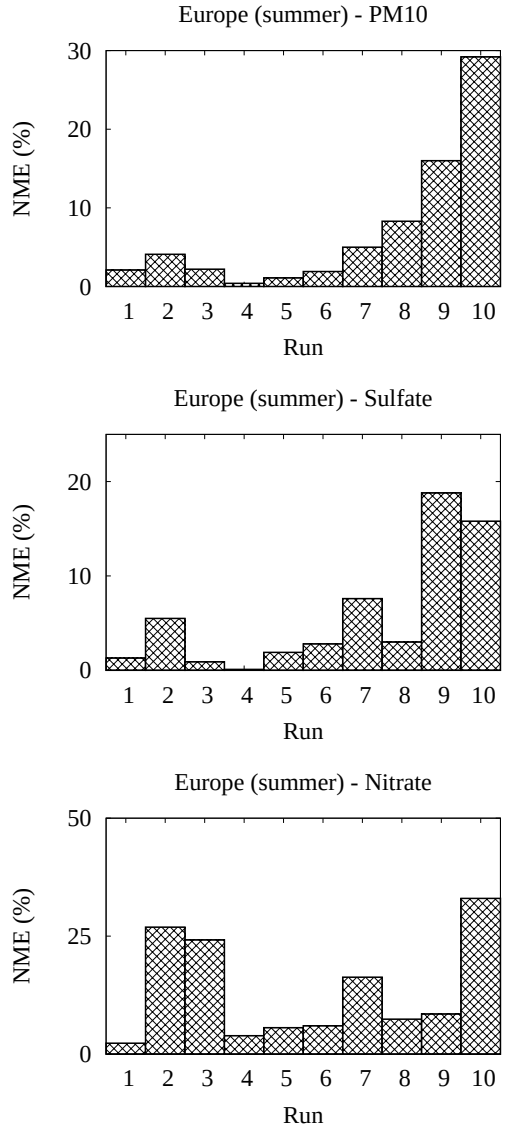

FIG. 5 – Over Europe, for PM_{10}, sulfate and nitrate, differences between the reference run and the other runs of the sensitivity study (see caption of Figure 4).

choices outside the aerosol module, such as vertical diffusion and boundary conditions, but also to parameterizations inside the aerosol module, such as scavenging or heterogeneous reactions. Size distribution, coagulation and nucleation have lower sensitivities. Sulfate is sensitive to boundary conditions, to the criterion used to diagnose clouds. For nitrate, high sensitivity to the heterogeneous reaction of N_2O_5 was observed, although the sensitivity becomes low in the european runs when the reaction probability varies with the aerosol composition, temperature and relative humidity following Evans and Jacob [2005] and Riemer et al. [2003]. The sensitivity to the dynamic mass transfer varies depending on conditions.

RÉFÉRENCES

Chin, M., Rood, R., Lin, S.-J., Muller, J., and Thomspon, A. (2000). Atmospheric sulfur cycle in the global model GOCART : Model description and global properties. *Journal of Geophysical Research*, 105 :24671–24687, 10.1029/2000JD900384.

Debry, E., Fahey, K., Sartelet, K., Sportisse, B., and Tombette, M. (2007). Technical note : A new SIze REsolved Aerosol Model : SIREAM. *Atmos. Chem. Phys.*, 7 :1537–1547.

Evans, M. and Jacob, D. (2005). Impact of new laboratory studies of N2O5 hydrolysis on global model budgets of tropospheric nitrogen oxides, ozone, and oh. *Geophysical Research Letters*, 32 :L09813, doi :10.1029/2005GL022469.

Fahey, K. and Pandis, S. (2003). Size-resolved aqueous-phase chemistry in a three-dimensional chemical transport model. *Journal of Geophysical Research*, 108 :4690.

Horowitz, L. a. (2003). A global simulation of tropospheric ozone and related tracers : description and evaluation of mozart, version 2. *Journal of Geophysical Research*, 108(D24).

Jacob, D. (2000). Heterogeneous chemistry and tropospheric ozone. *Atmospheric Environment*, 34 :2131–2159.

Loosmore, G. and Cederwall, R. (2004). Precipitation scavenging of atmospheric aerosols for emergency response applications : testing an updated model with new real-time data. *Atmospheric Environment*, 38 :993–1003.

Louis, J. (1979). A parametric model of vertical eddy fluxes in the atmosphere. *Boundary Layer Met.*, 17 :187 :202.

Mallet, V., Quelo, D., Sportisse, B., Ahmed de Biasi, M., Debry, E., Korsakissok, I., Wu, L., Roustan, Y., Sartelet, K., Tombette, M., and Foudhil, H. (2007). Technical Note : the air quality modeling system Polyphemus. *Atmos. Chem. Phys. Discuss.*, 7 :6459–6486.

Napari, I., Noppel, M., Vehkamaki, H., and Kulmala, M. (2002). Parametrization of ternary nucleation rates for h_2so_4-nh_3-h_2o vapors. *Journal of Geophysical Research*, 107 (D19) :doi :10.1029/2002JD002132.

Nenes, A., Pandis, S., and Pilinis, C. (1998). Isorropia : A new thermodynamic equilibrium model for multicomponent inorganic aerosols. *Aquatic geochemistry*, 4 :123–152.

Pruppacher, H. and Klett, J. (1998). *Microphysics of Clouds and Precipitation*. Kluwer Academic Publishers.

Riemer, N., Vogel, H., Vogel, B., Schell, B., Ackermann, I., Kessler, C., and Hass, H. (2003). Impact of heterogeneous hydrolysis of n2o5 on chemistry and nitrate aerosol formation in the lower troposphere under photosmog conditions. *Journal of Geophysical Research*, 108(D4, 4144) :doi :10.1029/2002JD002436.

Sartelet, K., Debry, E., Fahey, K., Roustan, Y., Tombette, M., and Sportisse, B. (2007a). Simulation of aerosols and gas-phase species over Europe with the POLYPHEMUS system. part I : model-to-data comparison for 2001. *Atmospheric Environment*. doi :10.1016/j.atmosenv.2007.04.024, in press.

Sartelet, K., Hayami, H., Albriet, B., and Sportisse, B. (2006). Development and preliminary validation of a modal aerosol model for tropospheric chemistry : Mam. *Aerosol Science and Technology*, 40(2) :118–127. doi : 10.1080/02786820500485948.

Sartelet, K., Hayami, H., and Sportisse, B. (2007b). Dominant aerosol processes during high-pollution episodes over Greater Tokyo. *Journal of Geophysical Research*, 112(D14214) :doi :10.1029/2006JD007885.

Sartelet, K., Hayami, H., and Sportisse, B. (2007c). MICS-Asia Phase II : sensitivity to the aerosol module. *Atmospheric Environment*. doi :10.1016/j.atmosenv.2007.03.005, In press.

Schell, B., Ackermann, I., Hass, H., Binkowski, F., and Ebel, A. (2001). Modeling the formation of secondary organic aerosol within a comprehensive air quality model system. *Journal of Geophysical Research*, 106(D22) :28275–28293.

Seinfeld, J. (1985). *Atmospheric physics and chemistry of Air Pollution*. Wiley.

Tombette, M. and Sportisse, B. (2007). Aerosol modeling at regional scale : Model-to-data comparison and sensitivity analysis over Greater Paris. *Atmospheric Environment*. doi :10.1016/j.atmosenv.2006.10.037.

Troen, I. and Mahrt, L. (1986). A simple model of the atmospheric boundary layer : sensitivity to surface evaporation. *Boundary-Layer Meteorology*, 37 :129–148.

A New Tool for Analyzing CMAQ Modeling Results: Visualization Environment for Rich Data Interpretation (VERDI)

Donna Schwede*
Atmospheric Science Modeling Division, NOAA/EPA, Research Triangle Park, NC, USA

Nicholson Collier, Jayne Dolph, Mary Ann Bitz Widing, Thomas Howe
Argonne National Laboratory, Decision and Information Sciences Division, Argonne, IL, USA

1. INTRODUCTION

The Community Multiscale Air Quality Model (CMAQ) produces files of gridded concentration and deposition fields. Users have the need to visualize these data both spatial and temporally. Historically, CMAQ users have used the Package for Analysis and Visualization of Environmental data (PAVE) for visualizing CMAQ output. PAVE was first developed in 1996 and is written in C and Motif. The aging PAVE platform has presented some challenges with current computers and operating systems. The last release of PAVE was in 2004 and no further development is planned. In recent years, there has been a rapid increase in the availability of open source Java libraries for producing graphical output. A development effort was initiated to build a replacement for PAVE that uses these updated software libraries. That effort has resulted in the development of the Visualization Environment for Rich Data Interpretation (VERDI). This new tool is useful for viewing CMAQ files as well as other environmental data.

2. SYSTEM REQUIREMENTS AND INSTALLATION

VERDI requires version 6 of the Java Runtime Environment (JRE). At this time, JRE 6 is available from Sun for Windows XP, Vista and 2000, as well as Linux and Solaris. The full JRE 6 is not currently available for Mac OS X but should appear in the next version of Mac OS X (Leopard) due before the end of 2007.

VERDI's memory and CPU requirements are largely dependant on the size of the datasets to be rendered. Small datasets can be rendered and manipulated in less than 512 megabytes while larger datasets may need considerably more. Similarly, slower CPUs can quickly render and animate smaller datasets whereas larger datasets can take longer. VERDI has been run satisfactorily on older Intel Core Duo and later model Pentium processors as well as on the latest Core 2 Duos and comparable AMD chips using both Windows and Linux operating systems. Three dimensional contour plots require a graphics processor with OpenGL or DirectX capability.

Installation on Windows operating systems is accomplished via a dedicated install program. On Unix based platforms, VERDI is distributed as a gzipped tarball that contains the executable application. When JRE 6 for Mac OS X is available, an application bundle for Mac OS X will be made as well.

3. SOFTWARE DESIGN

One of the goals in the development of VERDI was to use a language that would allow platform independence and eliminate the need for the software bus currently needed when running PAVE. Java was selected as the programming language since it met this requirement and is widely used. Additionally, numerous open-source Java graphical libraries are available which expedited the development. The code is modular in design and well-documented which will facilitate further modifications. A generalized reader was programmed that allows a number of input file formats and is easily extensible to other file types.

In interactive operation, VERDI opens as a single window with data and plot sub-windows accessible as tabs (Figure 1). These windows can be undocked to allow them to be moved into separate windows. Dataset lists and associated formulas may be saved as a project for later reuse. VERDI commands can also be issued directly from the command line or via a script to allow batch processing.

* *Corresponding author:* Donna B. Schwede, NOAA/AMD 109 Alexander Drive, Research Triangle Park, NC 27709; e-mail: donna.schwede@noaa.gov

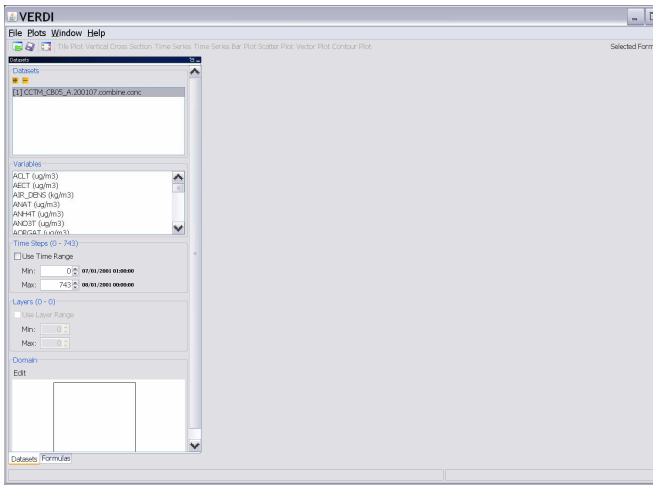

Figure 1. Screen shot showing the VERDI interface with the window open for adding datasets and selecting variables.

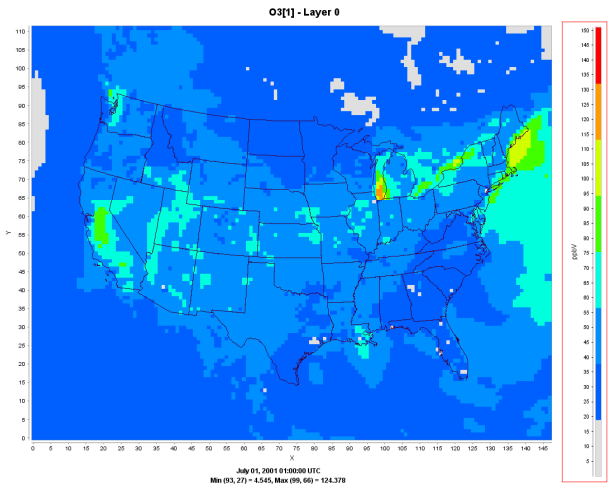

Figure 2. Tile plot exported in PNG format.

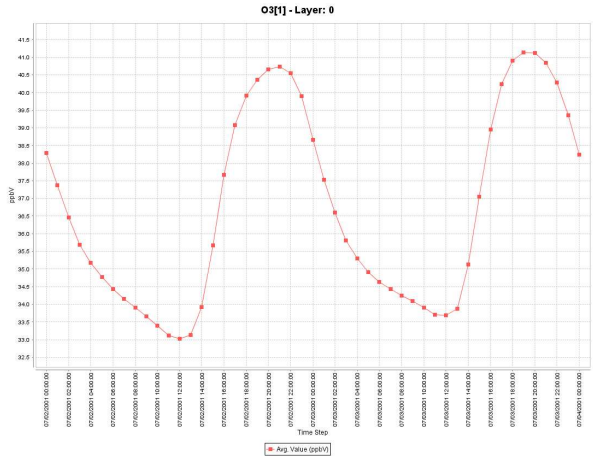

Figure 3. Time series plot exported in PNG format.

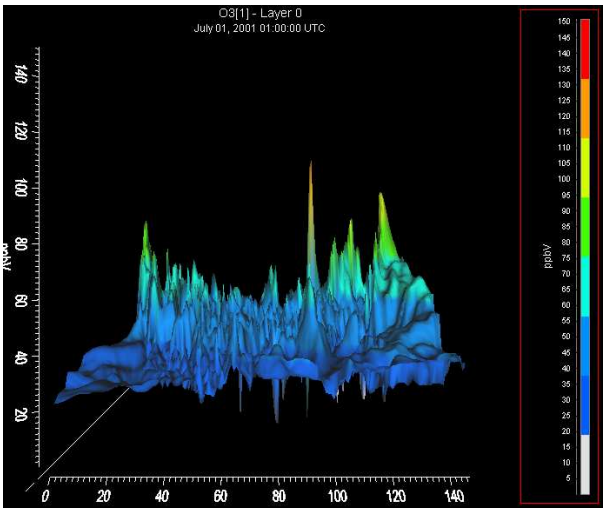

Figure 4. Contour plot exported in PNG format.

4. DATA FORMATS AND PLOT TYPES

VERDI was designed to have all of the functionality of PAVE as well as new features. Currently supported input file formats include Models-3 IOAPI, WRF IOAPI, and netCDF, however additional formats can easily be added to the code. Once a dataset is loaded, users have the option to select variables for plotting and may use formulas to create new variables. Data can also be windowed by selecting a time range and/or layer range and/or domain.

A number of plot types are available including smoothed tile (Figure 2), time series line (Figure 3), time series bar, vertical cross section, scatter, vector, and contour (Figure 4). Plots are full configurable to change scale, color maps, symbols, and text. Plots can be probed to obtain the value of a particular point and can be zoomed to examine an area in detail. Tile and contour plots can be animated to view a time series. Contour plots are displayed in 3-D and may be rotated to achieve different view angles.

A number of output file formats are provided. Results from probing a plot can be saved as a text file. Plots can be saved as a PNG, JPEG, BMP, or TIFF file. Animations can be saved as an animated GIF or a movie.

5. FUTURE IMPROVEMENTS

VERDI is intended to be a community based visualization tool with strong user involvement. The source code will be made available to the public. Users may contribute modules that they have developed and feel may be useful to the modeling community. Examples include readers for additional file formats and modules for additional plot types. Data analysis routines could be added. The development directions will respond to the needs expressed by the modeling community. EPA is also continuing some limited development of VERDI as resources permit. One targeted area for improvement is speed of operation. In particular, slow rendering speeds have been noted when using Secure Shell. EPA also intends to add the spatial analysis capability found in the Watershed Deposition Tool (Dennis and Schwede, 2006) to VERDI. The Watershed Deposition tool takes gridded atmospheric deposition estimates from CMAQ and allocates them to 8-digit HUC's (hydrologic cataloging units of rivers and streams) within a watershed, State or Region.

6. REFERENCES

Dennis, R., 2006: The Watershed Deposition Tool: A Means to Link Atmospheric Deposition to Watersheds, Proceedings, National Atmospheric Deposition Program, 24-26 October, Norfolk, VA, p 69.

Thorpe, S., J. Ambrosiano, C. Coats, A. Eyth, S. Fine, D. Hils, T. Smith, A. Trayanov, R. Balay, M. Vouk, and T. Turner, 1996: The package for analysis and visualization of environmental data. Proceedings, Computing in Environmental Resource Management, 2-4 December, Research Triangle Park, NC, pp 241-249.

7. DISCLAIMER

The research presented here was performed under the Memorandum of Understanding between the U.S. Environmental Protection Agency (EPA) and the U.S. Department of Commerce's National Oceanic and Atmospheric Administration (NOAA) and under agreement number DW13921548. This work constitutes a contribution to the NOAA Air Quality and Global Climate Programs. Although it has been reviewed by EPA and NOAA and approved for publication, it does not necessarily reflect their policies or views. Argonne National Laboratory's work was supported by the U.S. Environmental Protection Agency (EPA) though U.S. Department of Energy contract DE-AC02-06CH11357.

Ozone Episodes in US-Mexico Boarder Cities: Inferences based on Simulations and Satellite/Surface Data

Chune Shi[1*] and H.J.S. Fernando

Department of Mechanical and Aerospace Engineering, Environment Fluid Dynamics Program, Arizona State University, Tempe, AZ, U.S.A.

Edmund Y.W. Seto

School of Public Health, University of California, Berkeley, CA, U.S.A

1. INTRODUCTION

Chemical transport models (CTM) are usually evaluated using surface measurements, but increasing availability of space-borne remote sensing products offers a new and powerful tool to conduct such evaluations. Extensive geographical coverage and frequent observations of satellite measurements are particularly attractive in this context as they minimize the necessity of interpolations among point surface measurements. The study reported herein assesses the usefulness of tropospheric satellite data, in combination with those of surface monitoring networks, in evaluating ozone predictions of an air quality model. The motivation was to investigate the feasibility of utilizing satellite data to improve the extent, severity and episodes of ozone pollution in the Southwestern US.

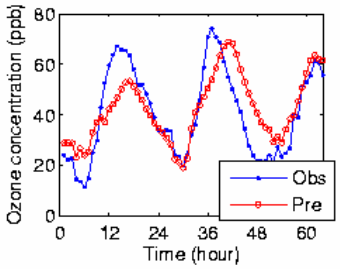

Figure 1 Time series of ozone concentration at San Diego

The design of the study was centered on an ozone episode over South California, including US-Mexico boarder in San Diego, on August 8-10, 2006, recorded by the EPA's Aerometric Information Retrieval System (AIRS). The maximum 1-hr/8hr ozone concentration exceeded 120ppb/80ppb at several sites in San Diego. The episode was particularly striking on the 9th August, and hourly variation of ozone concentration (averaged over all observational sites on San Diego) is given in Figure 1. The time begins at 00LT on August 8, 2006.

[1]Permanent affiliation: Anhui Institute of Meteorological Sciences, Hefei, China

**Corresponding author: Chune Shi*, Arizona State University, Email: shichune@sina.com

2. DESCRIPTIONS OF THE MODELING SYSTEMS AND DATA

2.1 Model configuration and input data

The simulations were conducted for the design days August 8-10, 2006 using the regional air quality model system of Models-3 (MM5v3.7/SMOKEv2.3/CMAQv4.5.1). Two nested grids with horizontal resolutions of 36km and 12km and centers coinciding at (97ºW, 40ºN) were used for MM5/SMOKE/CMAQ. For CMAQ and SMOKE runs, the outer domain covered the Southwestern U.S. with 74×70 horizontal grid cells. The inner domain with 120×110 grid cells mainly included California, Arizona, Nevada and Utah. The coarse domain for MM5 covers the whole North American continent. The troposphere from ground to 100hPa was divided into 29 model sigma layers, with 16 unevenly distributed vertical layers within the lower 2000m. The lowest layer near the ground was 7m, and highest resolution was maintained near the ground to better capture boundary-layer processes. The data for initialization and side boundary conditions were from NCEP/ETA model, NCEP global surface observations and NCEP global upper air observations. The National Emissions Inventory (NEI) databases of 2001 (for the US) and 1999 (MEXICO) were used for air quality simulations. For runs with default initial/boundary conditions, the simulation began at 00GMT on August 4 and ended at 00GMT on August 11. The results of the first 4 days were discarded to account for the spin-up.

2.2 Data for Model Evaluation

The surface data used for CMAQ evaluation were from the AIRS; and for MM5 evaluation were from the California Air Resources Board (http://www.arb.ca.gov/aqmis2/paqdselect.php). The satellite data included: SCanning Imaging Absorption Spectrometer for Atmospheric Chartography (SCIAMACHY) (Bovensman et al. 1999), Ozone Monitoring Instrument (OMI)

(Pieternel et al. 2006) and Tropospheric Emission Spectrometer (TES) (Beer et al. 2001). SCIAMACHY provides tropospheric NO_2 vertical column densities (VCDs) with a resolution of 30km×60km at about 10:30LT; OMI provides tropospheric NO_2 VCDs with a resolution of 13km×24km at about 14:00LT; TES provides ozone profiles in troposphere with a higher resolution.

3. COMPARISON METHODS

3.1 Tropospheric NO_2 VCDs

For consistent comparisons both spatially and temporally, the simulated concentrations were integrated from the bottom to the model top and then integrated to the satellite pixel by the area-weighted method exactly at the time where SCIAMACHY/OMI data were collected. Some commonly used statistical parameters were calculated, which include: correlation coefficient (R), Mean Bias (MB) and Normalized Mean Bias (NMB). Considering that satellite data have gross retrieval errors (GRE), mean absolute bias (MAB) with CAMQ and mean gross retrieval error (MGRE) were calculated as:

$$MAB = \frac{1}{N}\sum_{i=1}^{N}(VCD_{CMAQ,i} - VCD_{SATT,i})$$

$$MGRE = \frac{1}{N}\sum_{i=1}^{N} GRE_i \ .$$

Here, $VCD_{CMAQ,i}$ and $VCD_{SATT,i}$ are the simulated and satellite-observed tropospheric NO_2 vertical column densities (VCDs) in the i^{th} pixel. GRE_i is the gross retrieval error for the i^{th} Pixel. N is the total pixel number.

3.2 Ground level O_3

The methods used to evaluate the model based on ground-level ozone include:
(1) Graphical procedure: Preparing scatter plot for all hourly prediction-observation pairs for all sites for each simulation, as recommended by the USEPA (1991) for model evaluations.
(2)Statistical Evaluations: The use of commonly used statistical parameters as discussed in section 3.1 for all model cells containing the observational sites

4. VALIDATION OF MODELING RESULTS

4.1 MM5

Bilinear interpolation was used to obtain simulated ground level parameters for each site in San Diego and Imperial Valley. In general, MM5 could capture the hourly variation of surface temperature very well. The average correlation coefficients for temperature in San Diego and Imperial Valley are 0.938 (range from 0.866 to 0.967, over 7 sites) and 0.885 (0.843 to 0.913, over 6 sites), respectively. However, the model generally overestimates the surface temperature all the time for San Diego and at night for Imperial Valley. The correlation for wind speed comparison is not as good as that for temperature; e.g., 0.457 for San Diego (ranging from 0.146 to 0.665; 8 stations) and lesser for Imperial Valley. The dominant surface wind direction generally changes twice a day, and modeled wind direction lags behind the data for San Diego whereas the model did not capture well the wind direction at Imperial well.

4.2 CMAQ

(i) Comparisons of surface O_3

The average statistical results for all model cells in the U.S. containing observational sites for the two domains are included in Table 1. For ozone in the coarse/finer domain, the correlation coefficient is larger than 0.6 for majority of cells. The NMB is between -25% and 25% at more than half of the cells. In the coarse domain, aside from two minuses, the positive correlation coefficient ranges from 0.13 to 0.95.

Table 1 Statistical results of ground Ozone between AIRS and CMAQ

Parameters	Coarse Domain	Finer Domain	TES-BC -Coarser
correlation	0.51	0.43	0.498
Slope	0.47	0.39	0.499
Intercept (ppb)	21.9	22.5	23.4
NMB(%)	6.5	-2.3	13.99
MB(ppb)	-6.8	-3.2	2.67
Sample(r>0)	194	237	192
No(r>0.6)	149	146	144
No(|nmb|<25%	133	147	135
No (r<0)	4	2	6

Here: the linear equation is Y=A×X + B, where X, Y, A and B refer to observed ozone, modeled ozone, slope and intercept.

As for Mexico, data from nine observational

sites located in 6 different coarse model grids are available. The correlation of O_3 ranges from 0.29 to 0.76, with an average of 0.62. The model over-predicted the surface O_3 at most sites.

The performance (as quantified by the correlation coefficient) of coarse domain simulations is better than that of finer domain simulations. As for the twin cities with ozone episode, the temporal correlations in San Diego are quite good, but the simulated ozone maxima lagged the observations about 3 to 4 hours (Figure 1). Figure 2 shows a scatter plot for all (hourly) observations-simulations pairs in coarse domain.

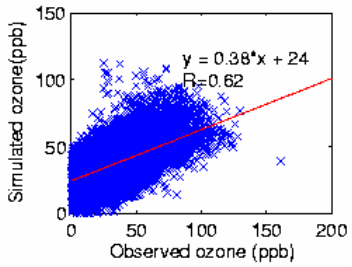

Figure 2 Scatter plot of hourly ozone

(ii) Comparison of NO_2 VCDs between SCIAMACHY and CMAQ

Composite distributions of NO_2 VCDs from SCIAMACHY and CMAQ for the coarse domain are shown in Figure 3, indicating that the model can reproduce the observed characteristics of NO_2 VCDs in the morning (around 10:30LT), especially for hot spots in areas such as Los Angeles and San Diego. Statistical results for the two domains are tabulated in Table 2. Table 2 indicate that the simulated NO_2 VCDs are highly correlated with SCIAMACHY observations, although the model under-predicted the tropospheric NO_2 columns approximately 57% of the time in coarse domain and 33% of the time in finer domain. However, MAB is somewhat smaller than MGRE in two domains.

(iii) Comparison of NO_2 VCDs between OMI and CMAQ

Composite distributions of NO_2 VCDs from OMI and CMAQ for the coarse domain are shown in Figure 4, which shows that the model can replicate the observed characteristics of NO_2 VCDs, especially those hot spots of high NO_2 columns. The statistics of comparisons are shown in Table 2, which shows that the simulated NO_2 VCDs correlates reasonably well with OMI. The model, however, under-predicts the tropospheric NO_2 column content in approximately 75% of the stations in the coarse domain and 68% in the finer domain. For OMI, the MAB is larger than MGRE.

The above comparisons show that the model predicts better the spatial distribution of tropospheric NO_2 VCDs in the finer domain, perhaps due to increased resolution of the pollution inventory. In addition, the model under-predicts NO_2 when compared with both SCIAMACHY in the morning and OMI at ~ 14.00LT, but the negative bias in the latter is larger. The anachronous pollution inventory is perceived to be a large source of uncertainty, and an updating of the available inventory is recommended for better results.

5. THE USE OF TES DATA FOR CMAQ/INITIAL/BOUNDARY CONDITIONS

To assess the usefulness of satellite data of the troposphere in CMAQ calculations, the TES -based ozone profiles (obtained at 06:00 UTC, August 4) were interpolated to the 3D model grids of 36km resolution to implement as the initial condition for CMAQ (in lieu of CMAQ default initial condition). Also, the TES data at 06:00 UTC on August 4 and 8 were interpolated to boundary grids to implement as boundary conditions. The data of August 4 were used for August 4-7 and of August 8 were used for August 8-10. The statistical results with surface ozone and satellite observations were compared with those obtained with default boundary/initial conditions of CMAQ.

5.1 Surface Ozone

Statistics of comparisons for surface ozone concentrations between observations and CAMQ simulations (with and without TES data ingestion) are tabulated in Table 1. Accordingly, the differences between the two simulations are negligible for most cases.

5.2 Comparison with Tropospheric NO_2 (OMI and SCIAMACHY)

Statistical comparisons between simulated (with TES initial and boundary conditions) and SCIAMACHY and OMI observations are tabulated in Table 2. There is either very little or no change of performance of CMAQ when TES data are ingested as initial/boundary conditions.

5.3 Comparison of tropospheric O_3

profiles

Simulations with default initial/boundary conditions under-predicted ozone in the upper troposphere in different land use divisions considered in this study. For heights above 8km, the simulated ozone concentration was ~ 70ppb, which is close to the default no-flux boundary conditions of CMAQ (70ppb) at the model top. In the lower troposphere, however, the predicted and TES-measured ozone showed better agreement. Also note that CMAQ employs zero-gradient (Neumann) boundary condition in the lateral direction, thus making the effects of side boundaries weaker.

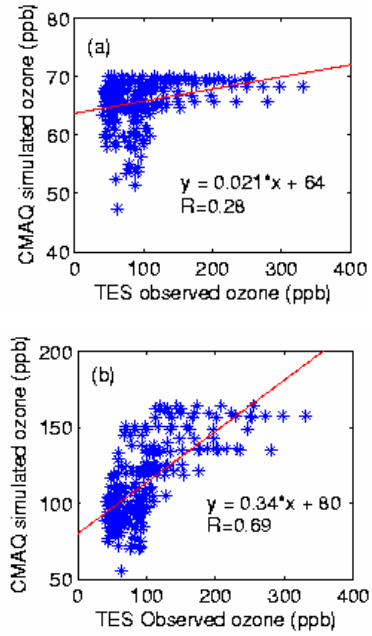

Figure 5 Comparisons of ozone concentration in the upper troposphere (over 500mb) between CMAQ and TES ((a): Simulations without TES input data; (b) Simulations with TES input for initialization)

For cases where TES data were used for initial/boundary conditions, a significant improvement was noted in CMAQ predictions for the upper troposphere when compared with subsequent TES observations, which can be seen from the plots shown in Figure 5. Here the correlation coefficient changed from 0.28 to 0.69. Similar plots were also made for the lower troposphere, but the correlation was low, for both default and TES based initializations.

6. CONCLUSIONS

Models-3 (MM5/SMOKE/CMAQ) with emissions from the National Emissions Inventory (NEI) database of 2001 for the US and 1999 for MEXICO was applied to simulate an ozone episode in San Diego area occurred on August 9, 2006. Ground level observations of ozone and satellite observations of tropospheric NO_2 column contents and ozone profiles were used to evaluate the model performance. The modeled NO_2 VCDs were correlated well with SCIAMACHY measurements. The correlation between OMI and CMAQ are not as good as that between SCIAMACHY and CMAQ. The model underpredicted the tropospheric NO_2 column in terms of comparing with both satellites measurements.

In general, in most observational sites, the diurnal patterns of ozone were reproduced satisfactorily by CMAQ. For coarser and larger domains, two thirds of model cells containing surface observations showed a correlation larger than 0.6 and a NMB between -25% and 25% when (AIRS) and CMAQ (lowest level) are compared. In the case of comparisons for finer and smaller domains, similar levels of correlation and NMB were also shown by more than two thirds of model cells containing surface observations. The correlation for all hourly prediction-observation pairs in the coarse domain is 0.62.

The sensitivity tests with TES data as initial/boundary conditions did not show, when viewed in terms of correlation coefficients, an appreciable improvement in the predictions of surface ozone concentrations (AIRS observations); tropospheric NO_2 columns (SCIAMACHY and OMI); and ozone concentration in the lower troposphere (TES). This modification, however, did show a significant improvement in the correlation coefficient between CMAQ predictions and TES observations of the upper-tropospheric ozone.

Acknowledgement: The support of Advanced Monitoring Initiative of the U.S. EPA is greatly acknowledged.

References:

Beer, R., T. A. Glavich, and D. M. Rider, Tropospheric Emission Spectrometer for the Earth Observing System's AURA satellite. *Appl. Opt.*, 40, 2356-2367,2001

Bovensmann H, Burrow J P, Buchwitz M, et al. SCIAMACHY: Mission objectives and measurement modes. Journal of the Atmospheric Sciences, 1999, 56(2): 127-150

Pieternel F. Levelt, Gijsbertus H. J. van den Oord, Marcel R. Dobber, Anssi Malkki, Huib Visser, Johan de Viries, Piet Stammes, Jens O. V. Lundell, and Heikki Saari: The Ozone Monitoring Instrument, IEEE Transactions on

geoscience and remote sensing, vol. 44, NO. 5, May 2006

US EPA, 1991. Guideline for regulatory application of the urban airshead model. US EPA Report No. EPA-450/4-91-013. Office of Air Quality Planning and Standards Technical Support Division Source Receptor Analysis Branch, Research Triangle Park, NC27711

Table 2 Statistics of comparison between Satellite (SCIAMACHY/OMI) measurements and CMAQ simulations for the tropospheric NO_2 column content

Parameters	SCIAMACHY			OMI		
	Coarse	Finer	TES-BC	Coarse	Finer	TES-BC
Correlation(r)	0.775	0.812	0.618	0.4761	0.561	0.442
Slope	0.4313	0.6251	0.4813	0.1607	0.2997	0.228
Intercept	0.0736	0.0682	0.0657	0.1753	0.0335	0.0918
MB	-0.63	-0.51	-0.59	-1.12	-1.35	-1.15
NMB(%)	-51	-33	-46.7	-73	-68	-71.4
MAB	0.79	0.95	0.859	1.19	1.447	1.22
MGRE	0.81	1.02	0.82	0.75	0.878	0.76
Total Pixels	1607	371	1622	29637	6196	32496

Here: the linear equation is Y=A×X + B, where X, Y, A and B refer to satellite measured NO_2 column, modeled NO_2 column, slope and intercept. The units of MB, MAB and MGRE are 10^{15}moleculaes/cm^2

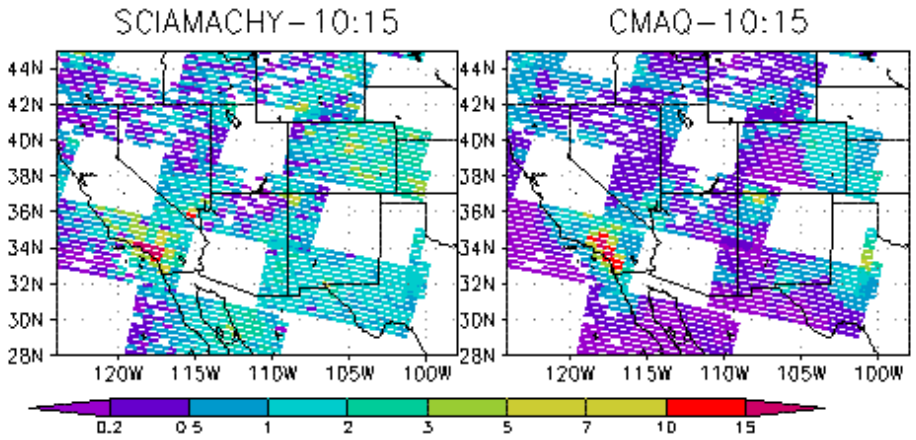

Figure 3 Distributions of tropospheric NO_2 columns from SCIAMACHY and CMAQ

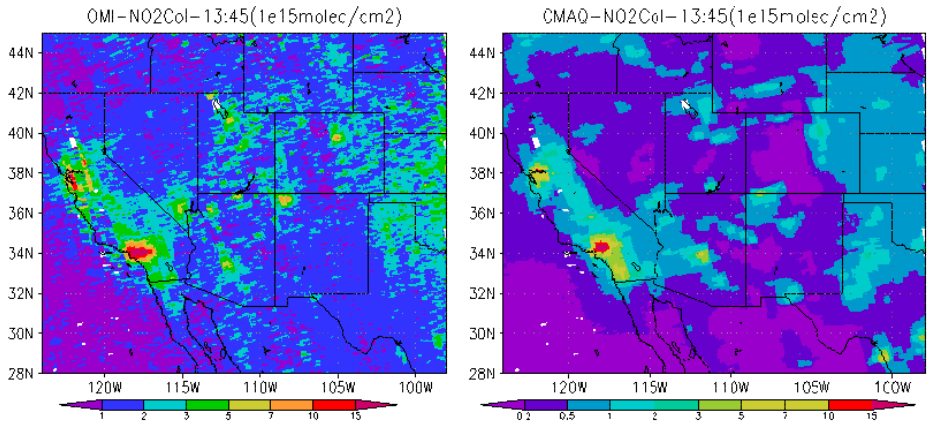

Figure 4 Distribution of tropospheric NO_2 columns from OMI and CMAQ

A COMPARATIVE PERFORMANCE EVALUATION OF THE AURAMS AND CMAQ AIR QUALITY MODELLING SYSTEMS

Steven C. Smyth*, Weimin Jiang, Helmut Roth, and Fuquan Yang
ICPET, National Research Council of Canada, Ottawa, Ontario, Canada

Véronique S. Bouchet, Michael D. Moran, Hugo Landry, and Paul A. Makar
Environment Canada, Toronto, Ontario, Canada and Montréal, Québec, Canada

1. INTRODUCTION

A comparative performance evaluation has been conducted for the AURAMS (A Unified Regional Air-quality Modelling System) and CMAQ air-quality (AQ) modelling systems, developed by Environment Canada (EC) and the U.S. Environmental Protection Agency (EPA), respectively. This study was unique in that many aspects of the AURAMS and CMAQ simulations were purposefully "aligned" in order to reduce some of the common sources of differences between the models.

The two AQ models were run for a 696-hour period starting at 0100 UTC 1 July 2002 and ending at 0000 UTC 30 July 2002 over a continental North American domain. Each model used 42-km horizontal grid spacing and the model domains cover approximately the same land area. Emission files were generated from the same Canadian, U.S., and Mexican raw emissions inventories and the same biogenic emissions model (BEISv3.09). The raw emissions were processed using the SMOKE (Sparse Matrix Operator Kernel Emissions) emissions processing system, developed by the Carolina Environmental Program (CEP). Meteorological fields generated by the EC GEM (Global Environmental Multiscale) meteorological model were used as input to both the emissions processor and the two chemical transport models (CTMs).

Both AQ models were run in their "native" states to provide a baseline comparison of the two sets of modelling results. Despite the best-possible alignment of the two models, there still exist many differences between the "native" states of the models. Some key differences related to the model setup and operation include differences in "native" map projections, vertical coordinate systems, gas phase chemical mechanisms, aerosol representations, meteorological pre-processors, and emissions processing methods. In addition, there are also numerous differences in detailed scientific processes embedded in the models. All of these differences contribute to each models' behaviour and performance.

Our methodology, however, precludes or greatly reduces the impacts of the other components of the system aside from the CTMs themselves, and gives us more confidence that the observed differences result from the AQ models, as opposed to the meteorological and/or emissions inputs to those models.

*Corresponding author: Steven C. Smyth, Institute for Chemical Process and Environmental Technology, National Research Council of Canada, 1200 Montreal Road, Bldg M-2, Ottawa, ON, Canada K1A 0R6; e-mail: steve.smyth@nrc-cnrc.gc.ca

2. MODELLING SYSTEMS DESCRIPTION

2.1. The AURAMS Modelling System

AURAMS is an AQ modelling system with size- and composition-resolved particulate matter (PM) representation. The AURAMS modelling system consists of three major components: an emissions processor; a meteorological driver; and a CTM (Gong et al., 2006). The AURAMS system also contains pre-processors that calculate biogenic emissions using the Biogenic Emissions Inventory System v3.09 (BEISv3.09) and transform emissions and meteorological data into a form useable by the CTM.

Emissions are processed using the SMOKE processor/model (CEP, 2005) and converted from I/O API format to Recherche en Prévision Numérique (RPN) standard format (Chartier, 1995) for use in AURAMS.

Predicted meteorological fields from the GEM model (Côté et al., 1998a,b) stored at every AURAMS advection time step (15 min) are used to drive the AURAMS CTM after transformation by the AURAMS meteorological pre-processor (Cousineau, 2003).

AURAMS was designed to be a "one atmosphere" or "unified" model in order to address a variety of interconnected tropospheric air pollution problems ranging from ground-level ozone (O_3) to PM to acid rain. As such, AURAMS treats gas-phase species and PM formation and evolution with time, as well as their interactions through gaseous, aqueous, and heterogeneous reactions and physical processes.

Nine chemical components, are considered to contribute to PM composition: sulphate (SU), nitrate (NI), ammonium (AM), black carbon (EC), primary organic aerosol (PC), secondary organic aerosol (OC), crustal material (CM), sea salt (SE), and particle-bound water (WA). AURAMS represents the PM size distribution using 12 size bins, ranging from 0.01 to 40.96 µm in diameter, with the PM chemical components assumed to be internally mixed in each size bin.

The gas phase chemistry is modelled using a modified version of the ADOM-II (Acid Deposition and Oxidant Model) chemical mechanism (Stockwell and Lurmann, 1989; Lurmann et al., 1986). Although AURAMS includes sea-salt emissions, sea-salt chemistry is not considered. Organic aerosol chemistry is modelled using the approach of Odum et al. (1996), and Jiang (2003). Inorganic aerosol calculations are performed using multiple chemical domain activity coefficient iterations (Makar et al, 2003). Aqueous-phase processes in AURAMS include size-resolved aerosol activation, aqueous-phase chemistry and wet deposition (Gong et al., 2006).

For this comparative modelling study, AURAMS v1.3.1b was run with 12-hour restarts for the complete 696-hour simulation period.

2.2. The CMAQ Modelling System

Similar to the AURAMS modelling system, the CMAQ modelling system (Byun and Ching, 1999) consists of three major components: an emissions processing system; a meteorological driver; and a CTM. The CMAQ modelling system also contains three other pre-processors for initial conditions, boundary conditions, and photolysis rates.

As with AURAMS, emissions files are generated by the SMOKE processor/model. In contrast to AURAMS, the emissions files are used directly by CMAQ without file format conversion.

GEM was used as the meteorological driver in CMAQ in order to align with the AURAMS modelling system. The GEM meteorological fields are processed by the GEM Meteorology Chemistry Interface Program (GEM-MCIP) (Yin, 2004), developed in-house at the National Research Council of Canada (NRC), to transform the GEM fields into a form useable by SMOKE and CMAQ.

In CMAQ, particle size distributions are represented as a superposition of three log-normal sub-distributions or modes: Aitken or i-mode; accumulation or j-mode; and coarse or c-mode (Binkowski and Roselle, 2003). The PM concentrations generated by CMAQ cover the complete log-normal distributions and are not directly comparable with size-resolved measurement data. In this study, the PMx postprocessor, developed in-house at NRC (Jiang and Yin, 2001; Jiang et al., 2006b), is used to calculate particle size distribution parameters and PM concentrations within required particle size ranges. Calculations are done on the basis of classical aerodynamic diameter (Jiang et al., 2006a) to facilitate comparison with field measurement data (Jiang et al., 2006b).

CMAQ considers 12 species to contribute to PM composition: sulphate (ASO4), nitrate (ANO3), ammonium (ANH4), primary anthropogenic organics (AORGPA), secondary anthropogenic organics (AORGA), secondary biogenic organics (AORGB), elemental carbon (AEC), other fine PM mass (A25), aerosol water (AH2O), soil derived dust (ASOIL), other coarse mass (ACORS), and sea-salt (ACL and ANA).

CMAQ v4.6 was run for the 696-hour simulation period using 24-hour restarts, the SAPRC-99 chemical mechanism (Carter, 2000a,b), and the AERO4 aerosol module.

A more detailed description of the AURAMS and CMAQ AQ modelling systems, including CTM science components and 3-D grid definition, is available in Smyth et al. (2007).

2.3. Comparison of the AURAMS and CMAQ Grids

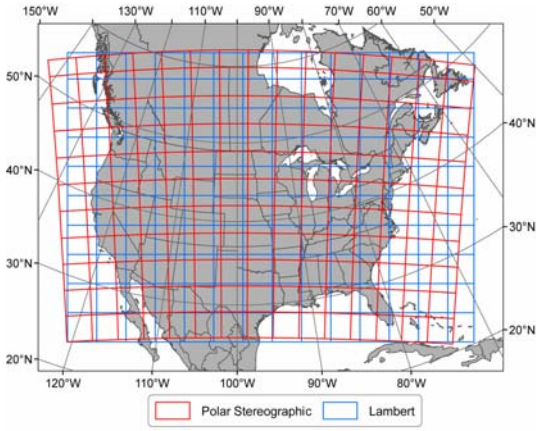

Fig. 1. The AURAMS polar stereographic domain and CMAQ Lambert conformal conic domain, displayed on the Lambert projection map.

The AURAMS modelling system uses a polar stereographic (PS) map projection as the basis for defining the horizontal grid. For this study, the Environment Canada “cont42” PS domain was adopted, consisting of 150 columns and 106 rows, with 42-km grid resolution.

The CMAQ modelling system uses a Lambert conformal conic (LCC) map projection in its “native” state. For this study, the LCC domain was

defined to "match" the AURAMS PS domain. The developed LCC grid consists of 139 columns and 99 rows with 42-km grid resolution and covers approximately the same geographical area as the PS grid as shown in Fig. 1.

3. COMPARISON OF METEOROLOGICAL AND EMISSIONS INPUTS

Evaluation of the processed meteorological fields input into each AQ modelling system showed minor differences in surface temperature, pressure, and specific humidity with normalized mean errors (NME) ranging from 0.25% to 3.8% when calculated over all over-lapping surface grid cells and the entire simulation period. These differences result from differences in the meteorological pre-processors and differences in map projections, which affect grid alignment.

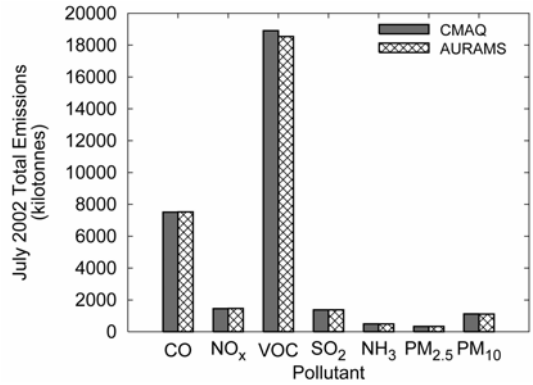

Fig. 2. Comparison of AURAMS and CMAQ anthropogenic and biogenic emissions totalled over the simulation period and respective domains.

Fig. 2 shows the comparison AURAMS and CMAQ anthropogenic and biogenic emissions totalled over each respective domain, all vertical levels, and the entire simulation period. The total emissions are similar for all criteria contaminants. More detailed analysis showed that total anthropogenic emissions were virtually identical for the two modelling systems, while there were slight differences in biogenic emissions of NO and VOCs. Since only minor variations in input temperature and pressure were present and identical biogenic emission factors were used, it is likely that the differences in biogenic emissions result from differences in solar radiation, BELD3 land-use data, and/or the implementation of the BEISv3.09 model in the modelling systems.

Analysis of temporal and spatial emission patterns (not shown) suggested that differences in input emissions can be caused by differences in speciation profiles, differences in processing major-point sources, and the differences in "true" grid cell size. The PS domain uses 15 900 42-km grid cells to cover approximately the same land area as the LCC domain which uses 13 761 42-km grid cells, meaning that the average PS grid cells are slightly smaller in "true" size than average LCC grid cells. Because of this, an average LCC grid cell contains more emission sources than a corresponding average PS grid cell.

4. COMPARISON OF O_3 PERFORMANCE

Performance statistics for AURAMS- and CMAQ-modelled ground-level ozone (O_3) in comparison with measurement data are summarized in Table 1. Hourly measurement data was taken from the National Air Pollution Surveillance (NAPS) and Air Quality Service (AQS) networks, administered by EC and the U.S. EPA, respectively.

Both models over-predicted O_3 concentrations. AURAMS had a lower bias than CMAQ with a normalized mean bias (NMB) of 17.9% versus 44.5% for CMAQ. In terms of error, the models' performance was more similar, with AURAMS performing slightly better with a NME of 45.6% versus 52.8% for CMAQ. In terms of correlation, the AURAMS r^2 of 0.39 was slightly lower than the CMAQ value of 0.44.

Table 1. AURAMS and CMAQ O_3 and daily peak O_3 statistics for 3-30 July 2002.

performance statistics	O_3 (ppb)		daily peak O_3 (ppb)	
	AURAMS	**CMAQ**	**AURAMS**	**CMAQ**
no. sites	1245	1247	1245	1247
n	774 946	776 154	20 599	20 635
meas. mean	35.64	35.62	60.77	60.72
mod. mean	42.03	51.46	66.66	70.16
MB	6.38	15.85	5.89	9.44
NMB (%)	17.91	44.50	9.68	15.56
ME	16.25	18.82	16.38	14.29
NME (%)	45.59	52.83	26.96	23.54
% within factor of 2	71.3	70.3	94.5	96.2
r^2	0.393	0.438	0.350	0.505

CMAQ's larger O_3 errors were largely due to its inability to correctly predict night-time lows, as shown in Fig. 3, which shows the time-series' of observed as well as AURAMS-, and CMAQ-modelled O_3 concentrations averaged over all O_3 measurement sites.

Performance statistics for daily peak O_3 is also shown in Table 1. Both models over-predicted the daily peaks with AURAMS having a slightly better NMB of 9.7%, whereas CMAQ had a NMB of 15.6%. In contrast, CMAQ had a slightly lower NME and a higher r^2. Both models did well in

predicting the time of the daily peaks, with AURAMS daily peak concentrations within 3-hours of the measured daily peak 65.2% of the time, while CMAQ was slightly better with a value of 68.8%.

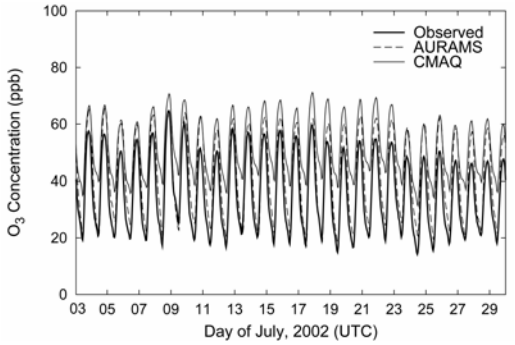

Fig. 3. Site-averaged observed as well as AURAMS-, and CMAQ-modelled O_3 concentrations.

5. COMPARISON OF TOTAL $PM_{2.5}$ PERFORMANCE

Hourly measurement data was taken from the NAPS and AQS networks to evaluate the performance of total $PM_{2.5}$. Statistics are presented in Table 2. Both models under-predicted total $PM_{2.5}$, although AURAMS' under-prediction was much less than CMAQ with a NMB of -15.4% versus -64.5% for CMAQ. However, just as with O_3, the models' errors were more similar, with NMEs of 67.1% and 70.6% for AURAMS and CMAQ, respectively. The similarity in error shows that there was cancellation of positive and negative biases in the AURAMS results, which contributed to the better NMB.

Table 2. AURAMS and CMAQ total $PM_{2.5}$ and daily peak total $PM_{2.5}$ statistics for 3-30 July 2002.

performance statistics	$PM_{2.5}$ ($\mu g\ m^{-3}$)		daily peak $PM_{2.5}$ ($\mu g\ m^{-3}$)	
	AURAMS	CMAQ	AURAMS	CMAQ
no. sites	350	354	350	354
n	211 141	213 707	7444	7538
meas. mean	14.43	14.40	28.26	28.14
mod. mean	12.21	5.11	21.65	9.12
MB	-2.23	-9.29	-6.60	-19.02
NMB (%)	-15.42	-64.52	-23.38	-67.59
ME	9.69	10.16	16.32	19.47
NME (%)	67.12	70.59	57.74	69.18
% within factor of 2	49.8	29.5	59.5	25.8
r^2	0.074	0.151	0.040	0.086

Table 2 also shows the performance statistics for daily peak $PM_{2.5}$. AURAMS performed better with a NMB of -23.4% and NME of 57.7% while CMAQ had a NMB of -67.6% and a NME of 69.2%. CMAQ did slightly better in predicting the time of the daily peaks with 34.2% of modelled $PM_{2.5}$ daily peaks within 3-hours of the measured daily peak, while AURAMS had a value of 28.7%. Station representativeness likely influenced the under-prediction of $PM_{2.5}$ concentrations for both models as most measurement sites were located in urban areas. In addition, the relatively large 42-km grid cells likely caused a "dilution" of $PM_{2.5}$, especially when comparing the modelled concentrations to the high localised concentrations expected around urban centres.

6. COMPARISON OF SPECIATED $PM_{2.5}$ PERFORMANCE

Speciated $PM_{2.5}$ performance was evaluated using 24-hr averaged measurement data from the NAPS network and the U.S. EPA administered Speciation Trends Network (STN).

As shown in Table 3, AURAMS bias was much better than CMAQ for $PM_{2.5}$ sulphate (SO4), ammonium (NH4), and total organic aerosols (TOA), and somewhat worse for nitrate (NO3) and elemental carbon (EC). For NO3, AURAMS over-predicted by approximately 121% while CMAQ under-predicted by approximately 71%. Both models significantly under-predicted TOA concentrations. However, the AURAMS modelled station-mean was over 4 times larger than the CMAQ value, showing better overall TOA performance. This difference was likely due to differences in secondary organic aerosol (SOA) schemes. In addition, the under-prediction in both models was partly due to forest fire emissions not being included in the emissions processing. The inclusion of forest fire emissions would likely improve performance for total PM and TOA.

In terms of error, the AURAMS and CMAQ results were very similar for $PM_{2.5}$ SO4, NH4, and EC, while AURAMS' NME for NO3 was much larger than CMAQ's. For TOA, AURAMS had a better NME of 65.6% versus 91.2% for CMAQ. In terms of correlation, r^2 values for the two models were generally close but CMAQ's were higher.

It is interesting to note that the poor correlation coefficients for both models for total $PM_{2.5}$ (Table 2) may be largely due to their inability in accurately predicting the organic component (Table 3). A large portion of the measured aerosol mass is TOA, while the correlation coefficient for this component is poor for both models.

The differences in AURAMS and CMAQ $PM_{2.5}$ species are likely due to a number of reasons, including differences in the speciation of PM emissions, aerosol chemistry, wet/dry removal mechanisms, and chemical boundary conditions.

Table 3. AURAMS and CMAQ performance statistics for $PM_{2.5}$ sulphate (SO4), nitrate (NO3), ammonium (NH4), elemental carbon (EC), and total organic aerosols (TOA) for 3-30 July 2002.

$PM_{2.5}$ Species	model	no. sites	n	meas. mean ($\mu g\ m^{-3}$)	mod. mean ($\mu g\ m^{-3}$)	MB ($\mu g\ m^{-3}$)	NMB (%)	ME ($\mu g\ m^{-3}$)	NME (%)	% within factor of 2	r^2
SO4	AURAMS	221	1229	5.03	5.31	0.29	5.72	3.03	60.34	57.8	0.367
	CMAQ				2.44	-2.59	-51.51	2.83	56.26	47.2	0.524
NO3	AURAMS	204	1112	0.902	2.00	1.09	121.2	1.58	174.7	30.0	0.397
	CMAQ				0.263	-0.64	-70.87	0.71	79.00	14.8	0.437
NH4	AURAMS	221	1230	1.63	1.64	0.009	0.58	0.885	54.20	60.9	0.428
	CMAQ				0.821	-0.811	-49.68	0.929	56.90	51.2	0.458
EC	AURAMS	205	1180	0.524	0.284	-0.240	-45.83	0.302	57.55	44.7	0.166
	CMAQ				0.338	-0.187	-35.59	0.306	58.42	45.7	0.204
TOA	AURAMS	205	1180	10.56	3.92	-6.64	-62.85	6.93	65.64	33.1	0.0005
	CMAQ				0.928	-9.64	-91.22	9.64	91.25	2.0	0.0066

7. COMPARISON OF PM COMPOSITION

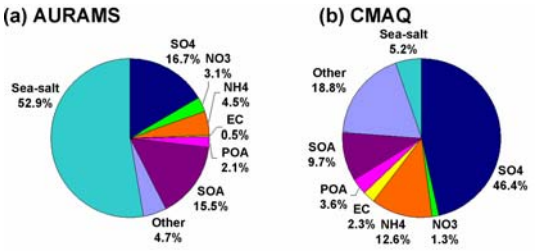

Fig. 4. Average $PM_{2.5}$ composition over all grid cells and last 648 hours of simulation period for (a) AURAMS and (b) CMAQ.

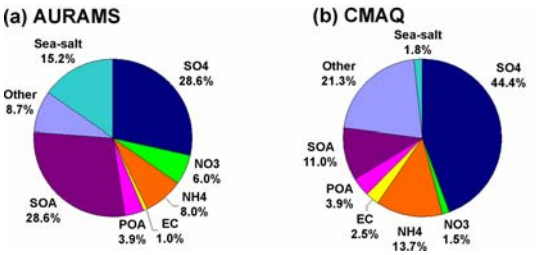

Fig. 5. Average $PM_{2.5}$ composition over land grid cells only and last 648 hours of simulation period for (a) AURAMS and (b) CMAQ.

Fig. 4 shows the average $PM_{2.5}$ composition of AURAMS and CMAQ averaged over all grid cells of their respective domains. The results show very different PM compositions between the models with over 50% of $PM_{2.5}$ mass coming from sea-salt aerosols in AURAMS, whereas only 5.2% of CMAQ's $PM_{2.5}$ mass is from sea-salt aerosols.

As shown in Fig. 5, when the average $PM_{2.5}$ composition is calculated by averaging over land grid cells only, the contribution of sea-salt aerosols to the total mass decreases to 15.2% for AURAMS and 1.8% for CMAQ, showing that sea-salt aerosols contribute a much larger amount to the total PM mass in AURAMS than they do in CMAQ, even if only land grid cells are considered.

8. SUMMARY AND CONCLUSIONS

In general, the two modelling systems showed similar levels of error for O_3, total $PM_{2.5}$, and most $PM_{2.5}$ species. However, in terms of bias, AURAMS performed better for all investigated species, except for $PM_{2.5}$ nitrate. This enhanced bias performance was somewhat due to the cancellation of positive and negative biases as indicated by the similar levels of error.

This study reflects the best effort up to now to closely align many operational aspects of the two modelling systems. However, due to the complexity of the model structures and the numerous interconnected science processes, it is difficult to assess the contributions of individual science processes to the differences in model performance. Improved modularity at the process level would make such scientific process assessment more feasible.

9. NOTE

Results from the brief abstract submitted before and the extended abstract here differ substantially due to incorrect land-use fields generated for the previous AURAMS run. A new AURAMS run was conducted with the correct land-use fields supplied by Environment Canada (EC), and the results are reported in this extended abstract. Investigation is underway to determine the source of the processing error.

10. ACKNOWLEDGEMENTS

The authors acknowledge Radenko Pavlovic and Sylvain Ménard of EC for their efforts in transferring data and code to NRC and for their support in helping to understand the various AURAMS related material. Also, we thank Wanmin Gong of EC for her comments and help in identifying the problem in land-use data.

Several organizations provided information and/or funding support to this project and their contributions are greatly appreciated. The Pollution Data Division of EC supplied the Canadian raw emissions inventories used in this modelling study. The U.S. EPA provided U.S. raw emissions data and the Carolina Environmental Program distributed CMAQ, and SMOKE. Colorado State University developed the VIEWS database and the Meteorological Service of Canada operates the NAtChem database, both of which were used to obtain measurement data. Funding was provided by EC and by the Program of Energy Research and Development (PERD).

11. REFERENCES

Binkowski, F.S., and S.J. Roselle, 2003: Models-3 community multiscale air quality (CMAQ) model aerosol component 1. Model description. *J. Geophy. Res.*, **108**, No. D6, 4183.

Byun, D.W., and J.K.S. Ching, 1999: Science algorithms of the EPA Models-3 Community Multiscale Air Quality (CMAQ) modelling system. U.S. EPA Report EPA/600/R-99/030.

Carolina Environmental Program, 2005: SMOKE User Manual Version 2.2. [Available online at http://cf.unc.edu/cep/empd/products/smoke/version2.2/manual.pdf]

Carter, W.P.L., 2000a: Documentation of the SAPRC-99 chemical mechanism for VOC reactivity assessment. Final Report to California Air Resources Board Contract 92-329 and Contract 95-308. [http://pah.cert.ucr.edu/~carter/reactdat.htm.]

Carter, W.P.L., 2000b: Implementation of the SAPRC-99 chemical mechanism into the Models-3 framework. Report to the United States Environmental Protection Agency. [http://pah.cert.ucr.edu/~carter/reactdat.htm.]

Chartier, Y., 1995. An Introduction to RPN Standard Files. Section informatique, Recherche en Prévision Numérique, Atmospheric Environment Service, Environment Canada, 41 pp.

Côté, J., J.-G. Desmarais, S. Gravel, A. Méthot , A. Patoine, M. Roch and A. Staniforth, 1998a: The operational CMC/MRB Global Environmental Multiscale (GEM) model. Part 1: Design considerations and formulation. *Mon. Wea. Rev.*, **126**, 1373-1395.

Côté, J., J.-G. Desmarais, S. Gravel, A. Méthot, A. Patoine, M. Roch, and A. Staniforth, 1998b: The operational CMC-MRB Global Environment Multiscale (GEM) model. Part II: Results. *Mon. Wea. Rev.*, **126**, 1397-1418.

Cousineau, S., 2003: All you need to know about the AURAMS Meteorological Post Processor (AMPP) version 2.1 – Purpose, installation, description. Air Quality Modelling Applications Group Operations Branch, Canadian Meteorological Centre, Montréal, Québec.

Gong, W., A.P. Dastoor, V.S. Bouchet, S. Gong, P.A. Makar, M.D. Moran, B. Pabla, S. Ménard, L-P. Crevier, S. Cousineau, and S. Venkatesh, 2006: Cloud processing of gases and aerosols in a regional air quality model (AURAMS). *Atmos. Res.*, **82**, 248-275.

Jiang, W., and D. Yin, 2001: Development and application of the PM_x software package for converting CMAQ modal particulate matter results into size-resolved quantities. Institute for Chemical Process and Environmental Technology Tech. Rep. PET-1497-01S, 44 pp.

Jiang, W., 2003: Instantaneous secondary organic aerosol yields and their comparison with overall aerosol yields for aromatic and biogenic hydrocarbons. *Atmos. Environ.* **37**, 5439-5444.

Jiang, W., É. Giroux, H. Roth, and D. Yin, 2006a: Evaluation of CMAQ PM results using size-resolved field measurement data: the particle diameter issue and its impact on model performance assessment. *Air Pollution Modeling and Its Applications XVII*, 571-579.

Jiang, W., S. Smyth, É. Giroux, H. Roth, and D. Yin, 2006b: Differences between CMAQ fine mode particle and PM2.5 concentrations and their impact on model performance in the Lower Fraser Valley. *Atmos. Environ.* **40**, 4973-4985.

Lurmann, F.W., A.C. Lloyd, and R. Atkinson, 1986: A chemical mechanism for use in long-range transport/acid deposition computer modeling. *J. Geophys. Res.*, **91**, 10905-10936.

Makar, P.A., V.S. Bouchet, A. Nenes, 2003 : Inorganic chemistry calculations using HETV – a vectorized solver for the SO_4^{2-}—NO_3^-—NH_4^+ system based on the ISORROPIA algorithms. *Atmos. Environ.* **37**, 2279-2294.

Odum, J.R., T. Hoffman, F. Bowman, D. Collins, R.C. Flagan and J.H. Seinfeld, 1996: Gas/particle partitioning and secondary organic aerosol yields, *Environ. Sci. Technol.,* **30**, 2580-2585.

Smyth, S.C., W. Jiang, H. Roth, and F. Yang, 2007: A comparative performance evaluation of the AURAMS and CMAQ air quality modelling systems – REVISED. Report Number PET-1572-07S, ICPET, NRC, Ottawa, ON.

Stockwell, W.R., and F.W. Lurmann, 1989: Intercomparison of the ADOM and RADM Gas-Phase Chemical Mechanisms. Electrical Power Research Institute Topical Report, EPRI, 3412 Hillview Avenue, Palo Alto, Ca., 254 pp.

Yin, D., 2004: A Description of the Extension for Using Canadian GEM data in MCIP and a Brief User's Guide for GEM-MCIP. Institute for Chemical Processing and Environmental Technology, 44 pp.

The Impact of Lateral Boundary Conditions on CMAQ Predictions over the Continental US: a Sensitivity Study Compared to Ozonsonde Data

Youhua Tang*, Pius Lee, Marina Tsidulko, Ho-Chun Huang,
Scientific Applications International Corporation, Camp Springs, Maryland

Jeffery T. McQueen, Geoffrey J. DiMego
NOAA/NWS/National Centers for Environmental Prediction, Camp Springs, Maryland.

Louisa K. Emmons
National Center for Atmospheric Research, Boulder, Colorado

Robert B. Pierce
NOAA/NESDIS Advanced Satellite Products Branch, Madison, Wisconsin

Hsin-Mu Lin, Daiwen Kang, Daniel Tong, Shao-cai Yu
Science and Technology Corporation, Hampton, VA.

Rohit Mathur, Jonathan E. Pleim, Tanya L. Otte, George Pouliot, Jeffrey O. Young, Kenneth L. Schere
NOAA-OAR/ARL, Research Triangle Park, NC. (On assignment to the National Exposure Research Laboratory, U.S.E.P.A.)

and Paula M. Davidson
Office of Science and Technology, NOAA/National Weather Service, Silver Spring, MD.

1. Introductions

The offline coupled WRF-Non Hydrostatic Mesoscale model (NMM)/ Community Model for Air Quality (CMAQ) system is the current operational air quality forecast system (AQFS) used at NOAA/NWS/NCEP. This system uses a static profile as the lateral boundary condition (BC) for air quality prediction over the continental USA, since real-time boundary conditions are not commonly available. The simple-profile BC has been widely used in the case when external influences from transport outside the CMAQ domain are relatively weak compared to emissions within the model domain. However, the validity of using a static BC is difficult to assess since the importance of the external influence is very uncertain. Over the continental USA , the major inflows include Asian pollutants transported across the Pacific which usually becomes strong during springtime (Jacob et al., 2001; Jaffe et al., 2003), Mexican pollutants impacting the south border, and Northern influx from Canadian emissions and occasionally Canadian and Alaskan wildfire plumes. Sahara desert dust storm could also reach the U.S. crossing the Atlantic. The fixed BC cannot reflect these influences related to certain events. An alternative approach for addressing this uncertainty is to use global model predictions as the lateral boundary conditions. It should be noted that the global models may also introduce uncertainties from their own model errors. In this study, we perform sensitivity studies with 3 global boundary conditions and existing fixed boundary conditions to evaluate the influences due to BCs.

* Corresponding Author: Youhua Tang,
NOAA/NWS/NCEP/EMC, W/NP22 Room 207,
5200 Auth Road, Camp Springs, MD 20746-4304
youhua.tang@noaa.gov

2. Models and Boundary Conditions

The operational CMAQ system with Carbon Bond Mechanism-4 (CBM4) chemical mechanism (Gery et al., 1989) at 12km horizontal resolution covering continental US is used in this study, with 22 vertical layers up to 100hPa. It uses vertical diffusivity and dry deposition based on Pleim and Xu (2001), scale J-table for photolysis attenuation due to cloud, and Asymmeric Convective Scheme (ACM) (Pleim and Chang, 1992). The detailed operational CMAQ configuration can be found in

Lee et al (2007b). This air quality prediction is driven by hourly meteorological forecasts from the operational North America Mesoscale (NAM) WRF-NMM prediction system. The NAM prediction is run with 60 sigma-pressure hybrid layers up to 2hPa; Noah unified 5-layer land and surface model; Mellor-Yamada-Janjic planetary boundary layer closure scheme; Ferrier cloud microphysics; and Betts-Miller-Janjic convective mixing scheme.

In this sensitivity study, all simulations use the same emissions, meteorology and other configurations except for lateral boundary conditions. To investigate the influence of BC, we employ 3 global models (Table 1) for the time-varied boundary conditions. It should be noted that all these global models integrate satellite data, though in different methods. Among these global models, the MOZART (Model for OZone And Related chemical Tracers) model (version 4, updated from Horowitz et al., 2003) has the most detailed reactions and related chemical species (97 species), including bulk sulfate, ammonium, organic and soot aerosols, and size-resolved dust and sea salts (e.g., Pfister et al., 2005). The RAQMS (Real-time Air Quality Modeling System) (Pierce et al., 2003) model used in this study has only gaseous chemistry. GFS (Global Forecast System) O_3 boundary condition is provided by NCEP's operational GFS that treats O_3 as a 3-D prognostic variable (Moorthi and Iredell, 1998; NCEP, 2004). The O_3 prediction in GFS is initialized with Solar Backscatter Ultra-Violet (SBUV-2) satellite observations, and advected as a trace species with simple zonally averaged climatological derived production and depletion mechanism (Rood et al. 1991). Since SBUV-2 can only provide O_3 data above 250hPa, GFS-O_3 BC is applied to the CMAQ simulation above 10km, while the other two global models provide CMAQ with full-profile O_3, CO, sulfur oxidants, nitrogen oxidants and volatile organic compounds (VOCs). Table 2 shows the species mapping tables used in this study from RAQMS/MOZART to CMAQ's CBM-IV chemical mechanism. These models have similar inorganic gaseous species. RAQMS's mechanism is modified from CBM-IV. It added explicitly treated ethane (C2H6), and uses different lumping method for alkenes. MOZART chemical mechanism has more explicit VOCs. For most of them, we simply split into paraffin (PAR) and olefin (OLE) carbon bonds.

Figure 1 shows the mean O_3 BCs from July 21 to Aug 5, 2006. Above 10 km, GFS O_3 BC has the highest mean O_3 concentration, but its values below 10km are same as those with static BC. RAQMS and MOZART provide similar O_3 BCs in the upper troposphere, and their major difference appears in the middle troposphere as the RAQMS has more high-concentrated ozone bands extended from upper layers to lower layers. Below 1 km, RAQMS and MOZART have lower mean O_3 BC than the static BCs. Four simulations with different BCs are performed starting from 12Z, July 21, with the same initial conditions and other configurations. Simulated results are compared with IONS (INTEX Ozonesonde Network Study http://croc.gsfc.nasa.gov/intexb/ions06.html) ozonesonde data and EPA AIRNOW surface O_3 data. IONS sites for our research period are shown in Figure 2. It should be noted that NOAA Research Ship Ron Brown cruised over Gulf of Mexico, and had time-varied locations.

3. Comparison to Ozonesondes

Figure 3 shows the model prediction compared to IONS ozonesonde measurements over 5 sites on August 3, 2006. These site locations can also be seen in Figure 4. Over Beltsville, Maryland, most simulations yielded similar ozone profiles, except when using GFS O_3 BC, which captured the high ozone event in the upper troposphere, with less underprediction. Similar behaviors are also evident at Huntsville, Alabama and Boulder, Colorado. However at Boulder, the use of GFS O_3 BC led to overestimation of O_3 above 7km. Below 6km, differences between the simulations are less than 10 ppbv over Boulder. These four simulations usually yielded similar result in low altitudes, except in Trinidad Head, the site facing Pacific inflow. Here, using RAQMS BC (Figure 3) resulted in better agreement below 8km, especially between 1km and 6km. Other simulations are about 20 to 40 ppbv lower than the observations. Bratt's Lake, Saskatchewan, Canada is near the model's north boundary. Over this site, all simulations have similar O_3 prediction below 4km. In the altitudes above 10km, using GFS O_3 yielded higher ozone than RAQMS BC which yielded higher ozone than MOZART BC, with all experiments yielding larger ozone than using a static profile. Winds at Bratt's Lake were mainly westerly (Figure 4A). Figure 4 shows that in most areas of continental USA, global model BCs tend to cause higher O_3 prediction than that using Fixed BC in upper troposphere, which is simply due to their boundary condition difference (Figure 1). In other stations near the domain's north and northwest boundaries, such as Kelowna, British Columbia , Canada, we also found GFS O_3 >

RAQMS > MOZART > Fixed BC during this period. Most high differences appeared north of 40°N driven by the west wind. It should be noted that these time-varied BC sometimes also yielded lower ozone concentrations than that with fixed BC, such as the outflow near middle Atlantic coast. In general, these global BCs brought more time-dependent variations to CMAQ.

During August 1 to 5, 2006, there are 15 IONS ozonesonde profiles available for comparison within the CMAQ domain (Figure 2). Figure 5 shows observed vs predicted diagrams between the four simulations for all of these 15 profiles during the 5 days. The MOZART-BC simulation has the highest correlation coefficient R in Figure 5, indicating that this configuration best captured variation trends from lateral boundaries. The RAQMS BC yielded similar statistical correlations. Among these simulations, GFS-O_3 BC had the most reasonable correlation slope, reflecting its good skill for predicting variation in magnitudes. The Fixed BC yielded the worst performance in the upper troposphere, as expected. In the lower troposphere, the differences between experiments are small (Figure 6). Therefore, for most cases, the BC variations mainly affect the model predictions for the middle and upper troposphere. Near the surface, some regional or local factors may play a more important role on ozone. However, the relative importance of each influencing factor also depends on the locations and scenarios. For instance, using time-varied BCs from RAQMS did improve overall and low-altitude O_3 prediction (Figure 5B & 5B), over Trinidad Head, because it is located at the west edge of Northern California and facing Pacific inflow. On the other hand, global BCs did not show significant advantage over Houston at either high altitudes (except for GFS O_3) or low altitudes (Figures 4C, 5C) as other factors probably dominated. The use of different BCs had a moderate impact over Yarmouth, Nova Scotia as it is located in the Northeast of the CMAQ domain and is affected by both emitted pollutants over the continent and less frequently by BCs when transport is from the northwest. The use of real-time global BCs yielded better correlations slopes (Figure 6D) below 2km over Yarmouth, but did not show an advantage at upper levels (Figure 5D).

4. Comparison to AIRNOW data

The previous section emphasized that the importance of lateral boundary conditions depended on site location and weather conditions. Also, choice of boundary conditions on model predictions was more important at higher altitudes. For air quality prediction, verification with surface measurements is a primary performance indicator. EPA AIRNOW (http://airnow.gov) data provides operational surface ozone measurement in hourly temporal resolution. In this study, we selected 1635 AIRNOW stations within the CMAQ's CONUS domain to compare BC impacts. Table 3 shows the statistical results. Real-time boundary conditions do yield statistical improvements when compared against all AIRNOW sites except correlation slopes, implying that real-time BCs could improve the model prediction for ozone variation magnitudes. In this scenario, CMAQ prediction had a high bias. It is possible that the use of global BCs sometimes could exaggerate the CMAQ overprediction (Lee, et al., 2007a). The impact becomes stronger when evaluations are done for stations just west of -115°W (includes California, Oregon, Washington, Nevada, and western Idaho). Figure 7 shows the O_3 mean biases of the 4 simulations superposed on their predicted mean O_3 or O_3 differences. The use of MOZART BC shows the best improvement by reducing the mean bias by 2.5 ppbv and increasing the correlation coefficient/slope (Table 3). The major improvement occurred in Northwest of this domain (Figure 7B) and California coastal regions. The RAQMS BC experiment has the best correlation slope, but it also tends to increase the mean bias (Table 3). It should be noted that the highest RAQMS impact of high biases occurred not along the coast, but further inland, like Idaho (Figure 7C), which could be caused by transport from upper layers. That transport also depends on WRF-NMM and CMAQ's prediction for vertical exchange, affected by boundary layer height and convection etc. The change caused by GFS O_3 BC is relatively small over this region it is used only above 10 km and needs longer transport time/distance to affect surface ozone (Table 3 and Figure 7D). The GFS O_3 BC experiment has a stronger impact when evaluated in a region north of 43°N where tropopause folds around fronts are more prevalent. For this area, all global boundary conditions improve the correlation slopes, but only the MOZART BC reduces the mean bias and has the highest correlation coefficient/slope.

5. Conclusion

Boundary conditions can have an impact on any regional model performance. This study investigated the impacts of lateral boundary conditions from global models on ozone prediction

over continental USA. The simulation period from late July to early August has several high-ozone events due to regional and local photochemical activities. It is not a typical strong inflow period, nor a noticeable scenario for Asian pollutants or biomass burning plumes to reach North America. However, time-varying global boundary conditions still show a strong impact on ozone prediction at all altitudes. Depending on locations and scenarios, the simulations with global BCs did not always yield better results than that with static BC. The error could be caused by global model performance, or CMAQ regional prediction. Previous studies (Lee, et al., 2007a) have shown that high ozone aloft can often be mixed downward too quickly by CMAQ, thereby increasing model errors in the lower troposphere.

At high altitudes, ozone predictions are mainly related to stratospheric influence, in which using GFS O_3 for LBCs show reasonable performance on capturing strong transport events, perhaps due in part to its high spatial resolution. For some events, GFS O_3 also tends to overpredict upper-troposphere ozone. It could be due to that its simplified ozone treatment does not consider photolysis loss, or the SBUV-2 satellite assimilation lacks of vertical resolution. In this study, we did not test the use of global simulations for the top boundary condition as Tang et al. (2007) did, which could yield even stronger impacts on upper atmospheric prediction. Compared to GFS O_3 BC, RAQMS and MOZART can provide full-layer BCs with more species. These species include long-lifetime CO and NO_y, which can be transported from long ranges and possibly affect regional ozone production. Therefore, the more detailed chemical boundary conditions provided from MOZART and RAQMS tended to have strong impacts on surface ozone prediction than GFS O_3 BC, especially in U.S west coast. The chemical transformation of boundary conditions needs to be evaluated in the future. The MOZART BC experiments also yielded the largest improvements for reducing the CMAQ ozone high bias, which could be due to its lower O_3 BC (Figure 1B) in low altitudes at the north and west boundaries. Finally, this study has highlighted how improvements in global air quality models could yield better results for regional air quality prediction

Reference:

Gery, M. W., G. Z. Whitten, J. P. Killus, and M. C. Dodge. 1989: A Photochemical Kinetics Mechanism for Urban and Regional Scale Computer Modeling. *J. Geophys. Res*., 94, 925-956.

Granier, C., et al., 2004, Present and future surface emissions of atmospheric compounds, *Rep. EVK 2199900011, Eur. Comm., Brussels*.

Horowitz, L. W., et al. 200: A global simulation of tropospheric ozone and related tracers: Description and evaluation of MOZART, version 2, *J. Geophys. Res.*, *108*(D24), 4784, doi:10.1029/2002JD002853.

Jacob, D. J., J. A. Logan, and P. P. Murti, 2001: Effect of rising Asian emissions on surface ozone in the United States, *Geophys. Res. Let.*, 26 (14): 2175-2178.

Jaffe, D., H. Price, D. Parrish, A. Goldstein, and J. Harris, 2003: Increasing background ozone during spring on the west coast of North America, *Geophys. Res. Let.*, 30 (12).

Lee, P., R. Mathur, J. McQueen, J. Pleim, D. Wong, D. Kang, S. Kondragunta, G. Pouliot, M. Tsidulko, G. DiMego, T. L. Otte, J. O. Young, K. L. Schere, and P. Davidson, 2007a: Impact of Domain Size on Modeled Ozone Forecasts for the Northeastern U.S., *J. Appl. Meteorol., in press*.

Lee, P., S. McKeen, J. McQueen, D. Kang, M. Tsidulk, S. Lu, H.-M. Lin, G. DiMego, N. Seaman and P. Davidson, 2007b: Air Quality forecast using WRF/NMM-CMAQ during the TexAQS, Preprints, Ninth Conf. on Atmos. Chem./, Amer. Met. Soc., San Antonio, TX, 15-18, Jan 2007. pp1.6.

McLinden, C.A., S.C. Olsen, B. Hannegan, O. Wild, and M. J. Prather 2000, Stratospheric ozone in 3-D models: A simple chemistry and the cross-tropopause flux, *J. Geophys. Res., 105(D11), 14,653-14,665.*

Moorthi, S., and Iredell, M., 1998, Prognostic Ozone: Changes to the 1998 NCEP Operational MRF Model Analysis/Forecast System: The Use of TOVS Level 1-b Radiances and Increased Vertical Diffusion. [Available at http://www.nws.noaa.gov/om/tpb/449.htm from the National Weather Service, Office of Meteorology, 1325 East-West Highway, Silver Spring, MD 20910].

NCEP, 2004c: GFS – Global data assimilation, [Available at http://wwwt.emc.ncep.noaa.gov/gmb/gdas/]

Pierce, R. B., et al., 2003, Regional Air Quality Modeling System (RAQMS) predictions of the tropospheric ozone budget over east Asia, *J. Geophys. Res., 108(D21), 8825, doi:10.1029/2002JD003176*.

Pfister, G., P. G. Hess, L. K. Emmons, J.-F. Lamarque, C. Wiedinmyer, D. P. Edwards, G. Pétron, J. C. Gille, and G. W. Sachse, 2005, Quantifying CO emissions from the 2004 Alaskan wildfires using MOPITT CO data, *Geophys. Res. Lett.*, *32*, L11809, doi:10.1029/2005GL022995.

Pierce, R. B., et al., 2007, Chemical data assimilation estimates of continental US ozone and nitrogen budgets during the Intercontinental Chemical Transport Experiment-North America, *J. Geophys. Res., 112(D12S21), doi:10.1029/2006JD007722.*

Pleim, J. E., and J. Chang, 1992: A non-local closure model for vertical mixing in the convective boundary layer. *Atmos. Envi.*, 26A, 965-981.

Pleim, J. E., A. Xiu, P. L. Finkelstein, and T. L. Otte, 2001, A coupled land-surface and dry deposition model and comparison to field measurements of surface heat, moisture, and ozone fluxes. *Water Air Soil Pollut.*, *Focus*, **1**, 243-252.

Rood, R., A. R. Douglas, J. A. Kaye, M. A. Geller, C. Y. Chen, D. J. Allen, E. M. Larsen, E. R. Nash, J. E. Nielsen, 1991: Three-dimensional simulations of wintertime ozone variability in the lower stratosphere. *J. Geophys. Res.*, 96, D3, 5055-5071.

Streets, D. G., et al., 2003, An inventory of gaseous and primary aerosol emissions in Asia in the year 2000, *J. Geophys. Res., 108 (D21), 8809, doi:10.1029/2002JD003093*.

Tang, Y., et al. 2007, Influence of lateral and top boundary conditions on regional air quality prediction: A multiscale study coupling regional and global chemical transport models, *J. Geophys. Res.*, 112, D10S18, doi:10.1029/2006JD007515.

van der Werf, G.R., J.T. Randerson, L. Giglio, G.J. Collatz, P.S. Kasibhatla, and A.F. Arellano, Jr., 2006, Interannual variability in global biomass burning emissions from 1997 to 2004, *Atmos. Chem. Physics, 6*, 3423-3441

Table 1, Global models and their configurations in this study

	MOZART	RAQMS	GFS O_3
Horizontal Resolution	2.8°×2.8°	2°×2°	0.31°×0.31°
Meteorology	GFS analysis	GFS analysis	GFS forecasts
Anthropogenic emissions	Granier et al., 2004	GEIA/EDGAR inventory with updated Asian emission (Streets et al. 2003)	Not applicable
Biomass burning emissions	GFED-v2 (van der Werf, 2006)	ecosystem/severity based	Not applicable
stratospheric ozone	synthetic ozone constraint (McLinden et al., 2000)	OMI/TES assimilation (Pierce et al., 2007)	Initialized by SBUV-2

Table 2, Species mapping tables between RAQMS (left)/MOZART (right) species and CMAQ CBM-IV

RAQMS Species	**CMAQ CBM-IV**
CH3OOH	UMHP
HNO4	PNA
C2H6	2* PAR
OLET (terminal alkenes)	OLE1+PAR
OLEI (internal alkenes)	OLE2 + 2*PAR

MOZART Species	**CMAQ CBM-IV**
CH3OOH	UMHP
HNO4	PNA
CH3CHO	ALD2
C2H6	2* PAR
C3H8	3*PAR
BIGALK (higher alkanes)	4*PAR
C3H6	OLE + 2*PAR
BIGENE (higher alkenes)	OLE + 3*PAR
C10H16 (terpene)	OLE + 9*PAR

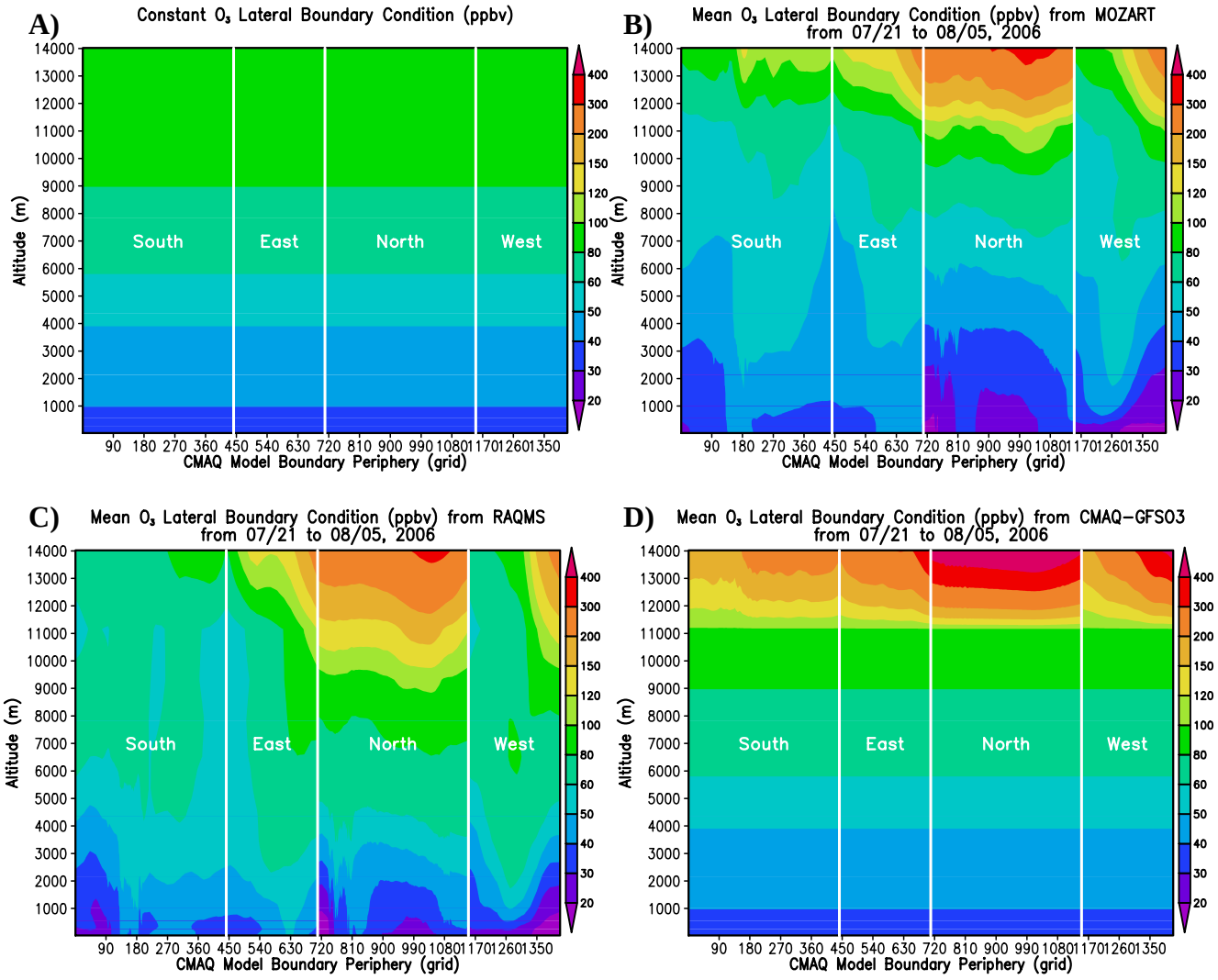

Figure 1, Mean O_3 lateral boundary conditions along the boundaries of CMAQ 442×265 (12km horizontal resolution) CONUS domain.

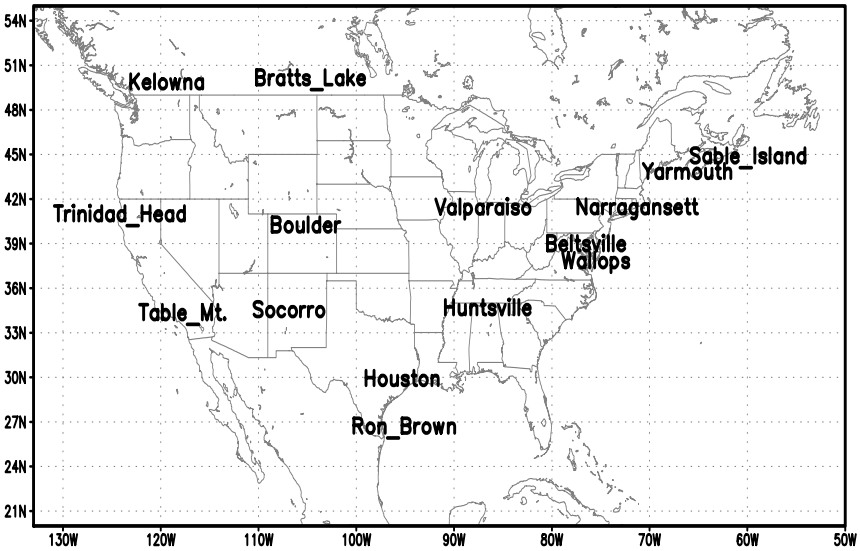

Figure 2. IONS ozonesonde sites during Aug 1-5, 2006.

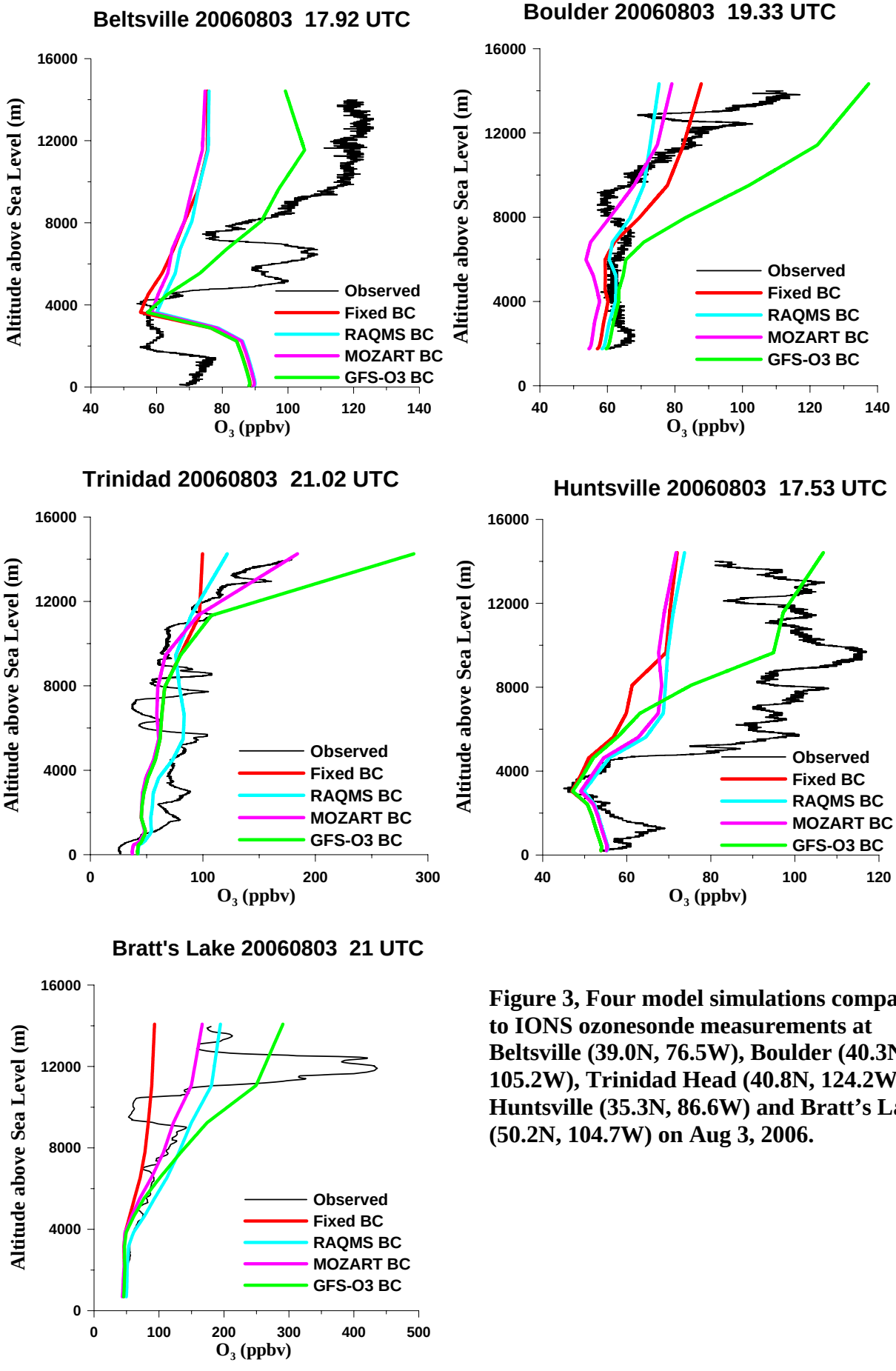

Figure 3, Four model simulations compared to IONS ozonesonde measurements at Beltsville (39.0N, 76.5W), Boulder (40.3N, 105.2W), Trinidad Head (40.8N, 124.2W), Huntsville (35.3N, 86.6W) and Bratt's Lake (50.2N, 104.7W) on Aug 3, 2006.

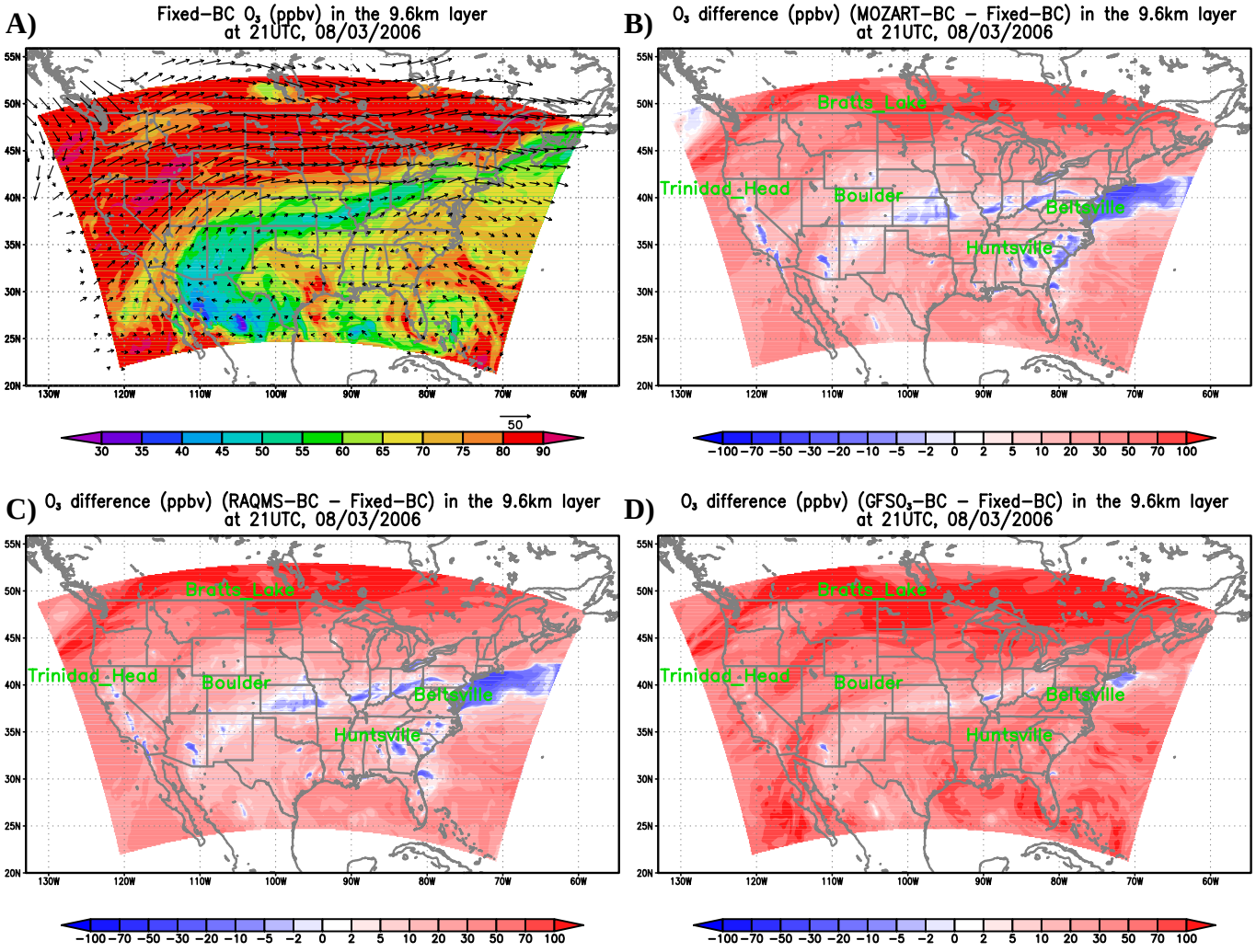

Figure 4, Model simulated ozone (A for Fixed-BC) and their differences (B, C, D) in the model's 9.6km layer at 21Z, Aug 3, 2006.

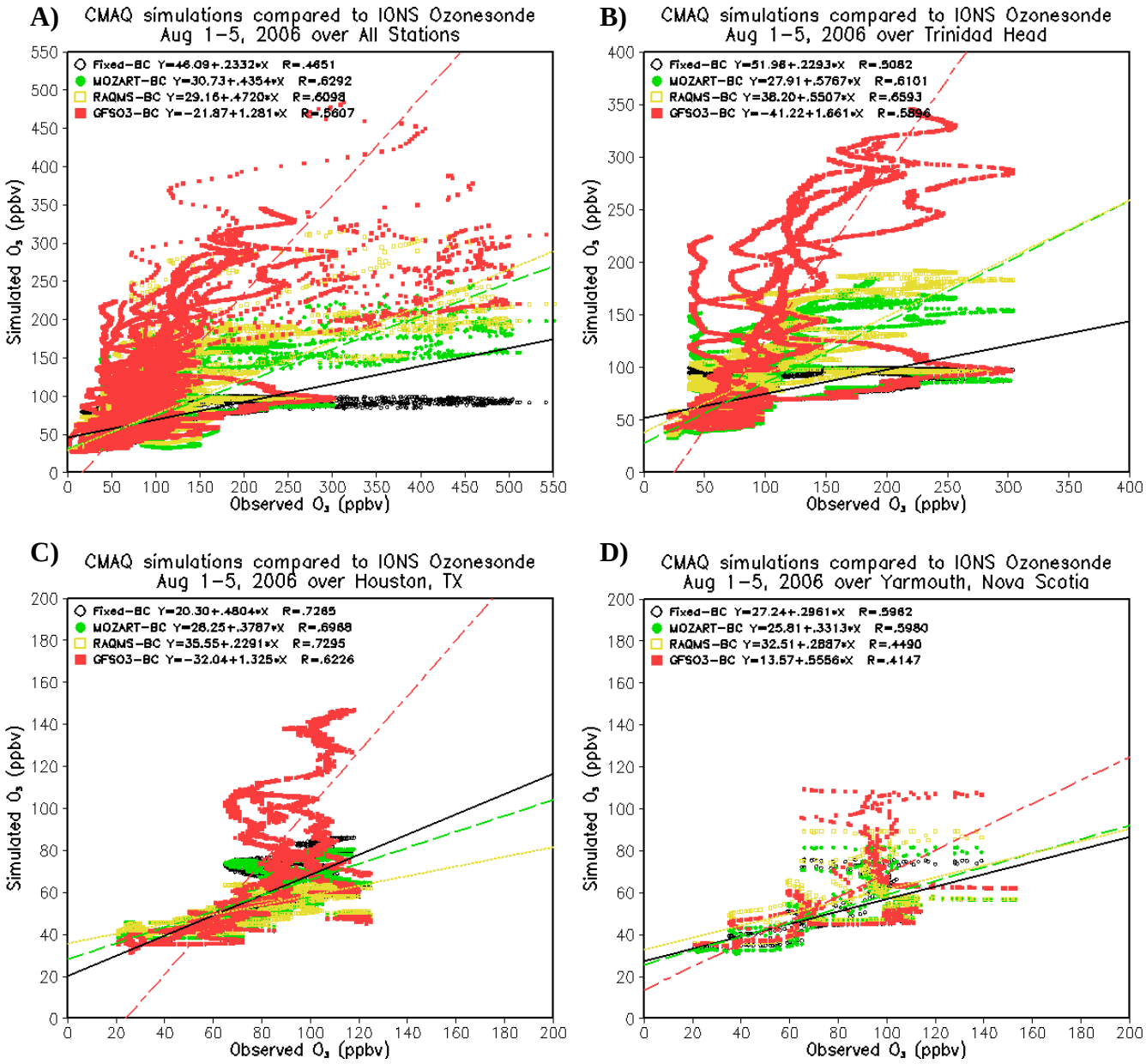

Figure 5, Statistical Correlations between the simulations and measurement over IONS stations from August 1 to August 5, 2006.

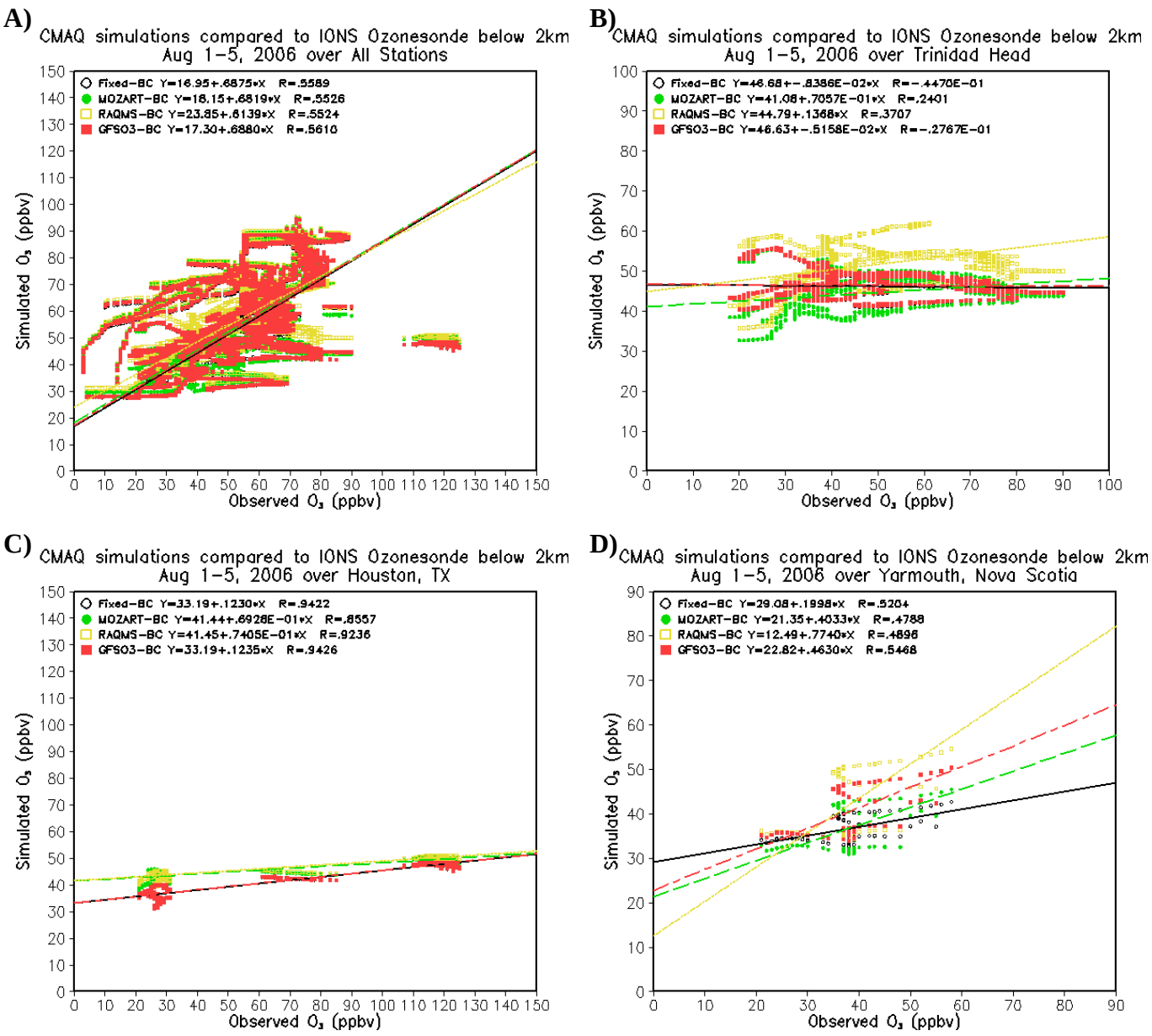

Figure 6, Same as Figure 5 but only for the altitudes below 2km.

Table 3, CMAQ simulations compared to AIRNOW hourly O_3 data from Aug 1 to 5

	All AIRNOW Stations	**West of -115°W**	**North of 43°N**
Fixed BC	S=0.887 R=0.714 MB=8.0 ppbv	S=0.804 R=0.691 MB=4.7 ppbv	S=0.873 R=0.737 MB=7.5 ppbv
RAQMS BC	S=0.911 R=0.718 MB=10.0 ppbv	S=0.914 R=0.703 MB=7.1 ppbv	S=0.942 R=0.742 MB=10.0 ppbv
MOZART BC	S=0.941 R=0.716 MB=8.2 ppbv	S=0.872 R=0.730 MB=2.2 ppbv	S=0.985 R=0.743 MB=6.9 ppbv
GFS O_3 BC	S=0.935 R=0.714 MB=9.2 ppbv	S=0.820 R=0.697 MB=4.8 ppbv	S=0.922 R=0.724 MB=9.0 ppbv

*S is correlation slope, R is correlation coefficient, and MB is mean bias.

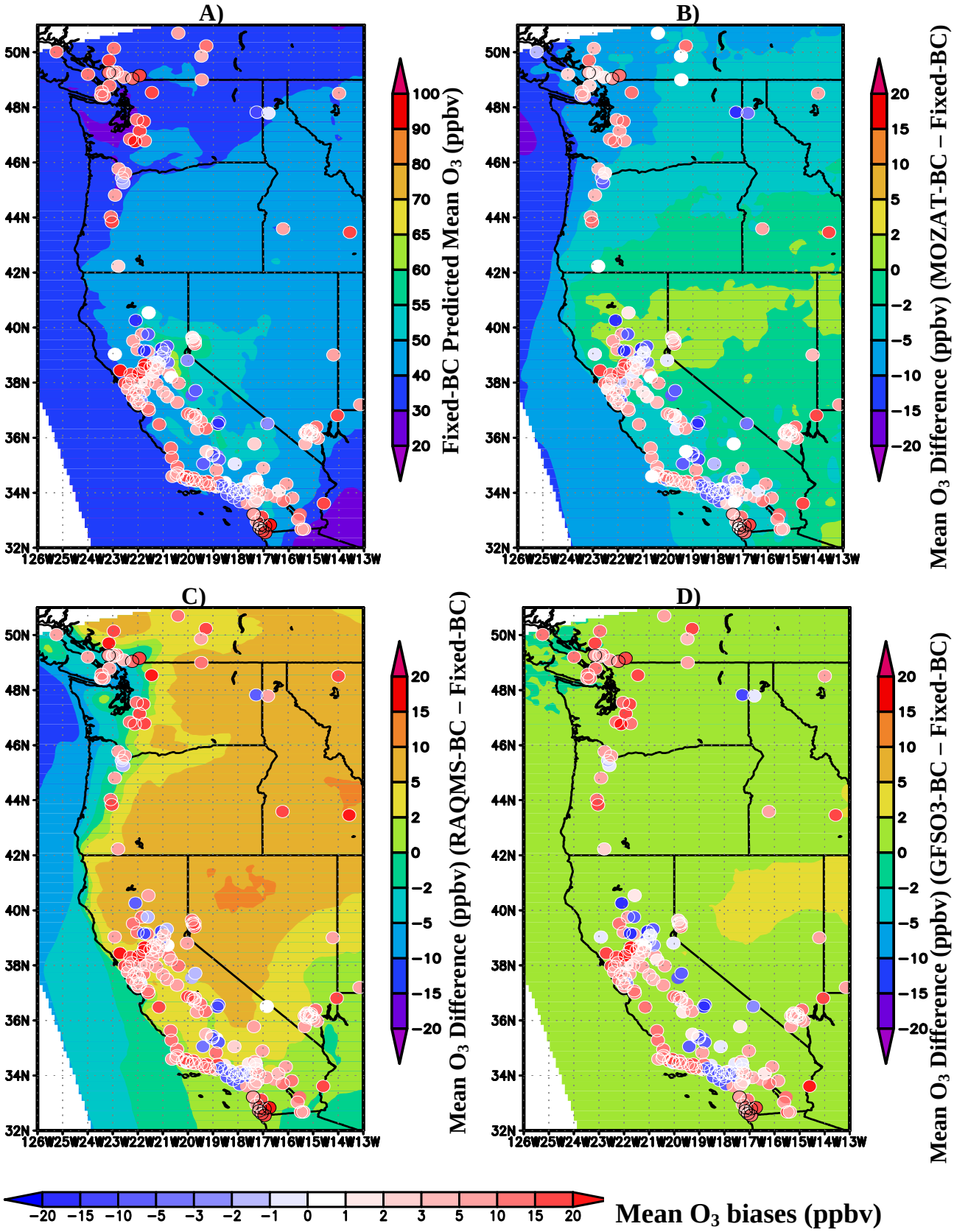

Figure 7, Mean surface O_3 prediction (plot A for Fixed-BC), mean O_3 prediction differences (B for MOZAR-BC, C for RAQMS-BC, D for GFS O_3 BC) and their mean biases from AIRNOW observations during Aug 1 to 5, 2006.

Presented at the 6th Annual CMAS Conference, Chapel Hill, NC, October 1-3, 2007

An Exploration of Model Concentration Differences Between CMAQ and CAMx

Brian Timin*, Karen Wesson, Patrick Dolwick, Norm Possiel, Sharon Phillips
U.S. Environmental Protection Agency, Office of Air Quality Planning and Standards, Research Triangle Park, NC, USA

1. INTRODUCTION

The majority of State Implementation Plan (SIP) modeling for the ozone and PM2.5 National Ambient Air Quality Standards (NAAQS) will be conducted with the CMAQ and CAMx air quality models. This paper explores the differences in base case concentrations predicted by the two models, given similar inputs.

Both models were run for a 2001 base case period using similar emissions and meteorological inputs. Significant differences were seen in the predicted model concentrations, especially for ozone and gaseous photochemical by-products. Several aspects of the modeling systems were explored to determine why the model predictions were dissimilar.

Among the inputs examined were vertical diffusion coefficients (Kv's), dry deposition velocities, photolysis rates, and cloud attenuation of photolysis rates. Several sensitivity runs were completed in an effort to further understand the cause of the concentration differences. The analyses uncovered fundamental differences between the two models and can qualitatively explain many of the concentration differences seen between the models.

2. OVERVIEW OF MODELING

CMAQ version 4.5 (Byun, 2006) and CAMx version 4.31 (Environ, 2006) were run for the July 2001 period (with a 10 day spin-up period at the end of June). Both models were driven with the same raw emissions and meteorological data. Both models were run with CB-IV chemistry. The emissions data were processed through SMOKE for both models. The CMAQ meteorological input data were processed through MCIP version 3.1 and the CAMx meteorological input data were processed through MM5CAMX. Both models used identical vertical structures. The 34 layer MM5 vertical structure was collapsed to 14 layers, with ~7 layers below the daytime boundary layer (less than 3100 meters). Both models had a 12km Eastern U.S. domain[1] nested inside of a 36km continental U.S. domain. All results shown are for the 12km nested domain.

2.1 Examination of CMAQ and CAMx Outputs

Comparisons of model output concentrations revealed large differences in predicted ozone concentrations. Figures 1 and 2 show the predicted layer 1 ozone concentrations at 2100 GMT on July 17th 2001.

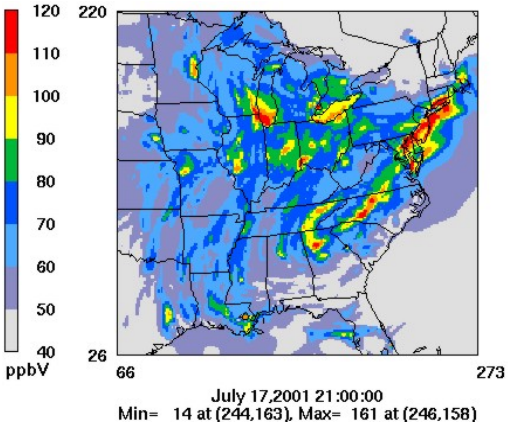

Fig. 1. CAMx 12km grid modeled ozone concentrations on July 17th, 2001 at 2100 GMT.

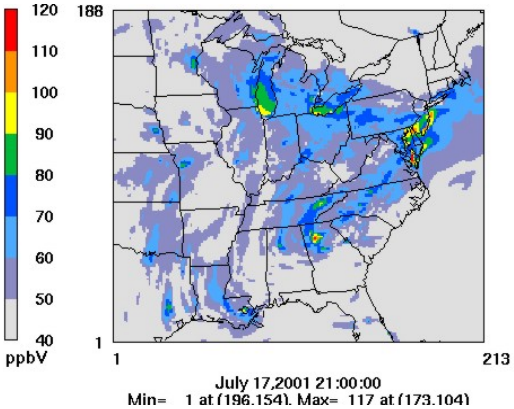

Fig. 2. CMAQ 12km grid modeled ozone concentrations on July 17th, 2001 at 2100 GMT.

As can be seen from figures 1 and 2, the predicted ozone concentrations in CAMx were significantly higher than those predicted by CMAQ. Afternoon peak ozone concentrations were often

**Corresponding author:*, Brian Timin, U.S. EPA, OAQPS, C431-01, RTP, NC 27711; e-mail: timin.brian@epa.gov .

[1] The CAMx 12km domain is larger (220 X 273) than the CMAQ 12km domain (188 X 212). The CAMx plots in this paper are cropped to produce approximately equal size plots.

20 to 30 ppb higher in CAMx (at the same time and location).

Additional species were examined to see if similar patterns existed, especially for ozone precursors.

While examination of species such as NO and NO_2 did not reveal any obvious differences, examination of CO revealed a very large systematic difference between the models. Figures 3 and 4 show the layer 1 CO concentrations for the two models for the same time period shown for ozone in figures 1 and 2.

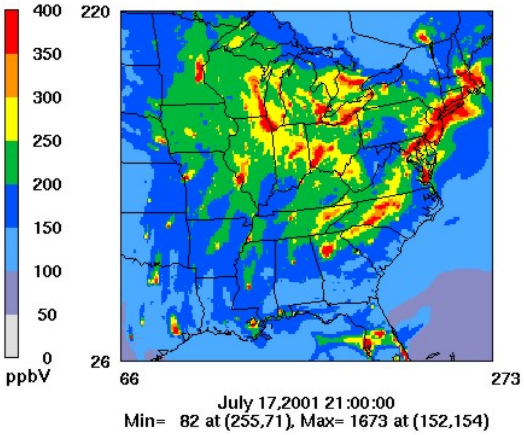

Fig. 3. CAMx layer 1 12km grid modeled CO concentrations on July 17th, 2001 at 2100 GMT

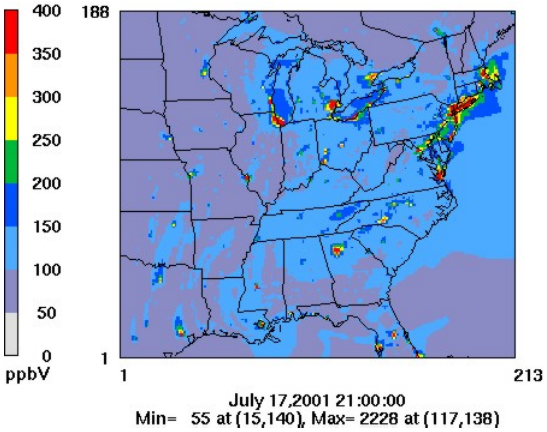

Fig. 4. CMAQ layer 1 12km grid modeled CO concentrations on July 17th, 2001 at 2100 GMT

The predicted CO concentrations are vastly different between the two models. The CO concentrations in CAMx are as much as twice the CMAQ CO concentrations in rural areas. However, in the largest urban areas, the concentrations are similar. The example plots only show one hour of one day, but the same pattern exists for all hours and all days during the simulation.

Additional species examined included formaldehyde (FORM), higher aldehydes (ALD2), hydrogen peroxide (H2O2), and various CB-IV VOC species (ISOP, PAR, OLE). In general, species with large secondary formation differed the most between the models. These include FORM, ALD2, and H2O2. Figures 5 and 6 illustrate the differences seen for formaldehyde (FORM).

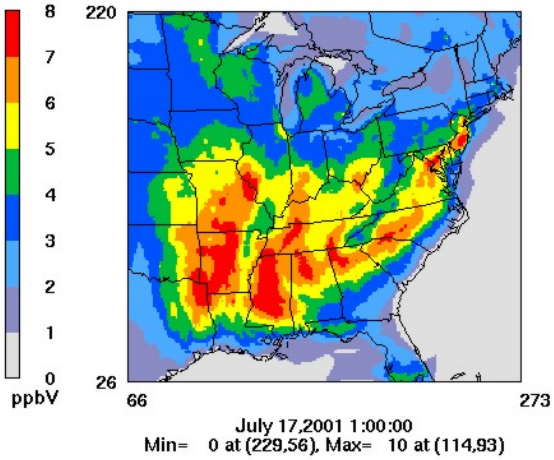

Fig. 5. CAMx layer 1 12km grid modeled FORM concentrations on July 17th, 2001 (24-hour average).

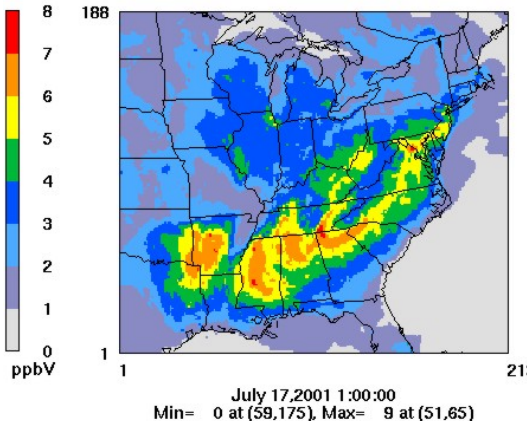

Fig. 6. CMAQ layer 1 12km grid modeled FORM concentrations on July 17th, 2001 (24-hour average).

Again, the CAMx concentrations were significantly higher than those seen in CMAQ for the same location and time period.

As a result of these findings, additional analyses and sensitivity studies were completed in an effort to better understand the large differences between the two models.

3. SENSITIVITY STUDIES

Several avenues were explored in the analysis of the model concentration differences. First, existing information and studies were examined to look for clues to differences in the models. Both models were run with CB-IV chemistry. However, the implementation of the chemistry in the models

is somewhat different. Some differences between the models include: 1) CAMx version 4.31 was run with "Mechanism 4" which contains additional reactions beyond the base CB-IV mechanism. 2) Both models use different pre-processors to calculate photolysis rates. 3) Both models use different schemes to calculate the attenuation of photolysis by clouds.

Upon review of each of these differences, it was found that none were likely the cause of the large differences in ozone, CO, and secondary gases. This is discussed below.

3.1 Chemical mechanism

Additional CMAQ runs were completed with a newer version of CMAQ (v4.6) which contained the CB-05 mechanism (Yarwood, 2006). CB-05 contains many of the same "additional" reactions as CAMx "Mechanism 4" ("CB-IV+" mechanism). The CB-05 mechanism was expected to produce higher ozone (~5 ppb) in CMAQ and it did. But, given that this change in chemical mechanisms (going from CB-IV to CB-05) gave a relatively modest increase in ozone, we believe it is unlikely that the additional reactions in CAMx CB-IV+ were a major cause of ozone concentration differences between CAMx (CB-IV+) and CMAQ ("standard" CB-IV).

3.2 Photolysis rates

The clear skies photolysis rates were examined in both models. The CAMx CB-IV rates for NO2 and ozone photolysis were slightly higher than the CMAQ CB-IV rates, but the CMAQ CB-05 rates were higher than the CAMx CB-IV rates. Since the increase in ozone concentrations from CMAQ CB-05 was not nearly as large as the difference in ozone concentrations between the models, it is not likely that the differences in photolysis rates are a major cause of concentration differences between the two models.

3.3 Cloud attenuation of photolysis rates

The differences in cloud attenuation between the models have previously been explored in (Dolwick, 2007). The study found that there tended to be less attenuation of UV radiation in CAMx, which caused small areas of higher ozone in CAMx. However, the overall ozone differences were constrained to small areas and did not account for the large regional ozone differences between the two models.

4. SENSITIVITY RUNS

Several additional model runs were completed in order to test differences in vertical mixing and dry deposition. For vertical mixing, we implement two different vertical mixing schemes in CAMx and compare the results to CMAQ. These tests help us understand the impact of vertical mixing on model concentrations. For the deposition sensitivity tests, we explore the different schemes used by the two models. Our CAMx run used a "Wesely" based dry deposition scheme (Wesely, 1989), while CMAQ was run with a more up to date dry deposition scheme called "M3Dry".

4.1 Vertical mixing

CAMx uses vertical diffusion coefficients (Kv's) as an input to the model. The Kv's are generated in the postprocessing of the MM5 meteorological data (using the MM5CAMX program). There are two options for generating CAMx Kv's: an O'Brien scheme and a "CMAQ-like" scheme. The "CMAQ like" scheme is designed to replicate the CMAQ methodology[2] for generating Kv's. The initial version of CAMx was run with the O'Brien vertical mixing scheme.

We ran CAMx for the July 2001 period with the "CMAQ-like" Kv's in order to estimate the impact of differences in vertical mixing between the models. The "CMAQ-like" Kv's almost always were higher than the O'Brien Kv's, and therefore generated more vigorous daytime mixing.

Figure 7 shows an example of the vertical Kv patterns between the schemes. The plot is for hour 2000 GMT on July 19th for a grid cell over Atlanta. The differences between O'Brien and "CMAQ-like" Kv's in this plot are typical of an afternoon peach hour for most areas in the domain. The "CMAQ-like" Kv's are always higher than O'Brien throughout the mixing layer. And the O'Brien Kv's usually begin to fall off at a lower layer than the "CMAQ like" Kv's. This indicates less vigorous mixing (to a lower height) in CAMx with O'Brien Kv's.

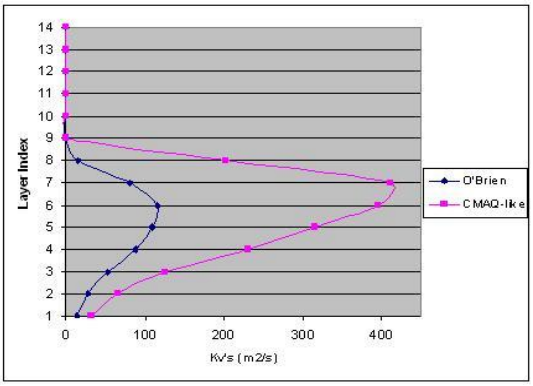

Fig. 7. Vertical Kv profile (layers 1-14) in CAMx for a grid cell over Atlanta on July 19th, 2001 at 2000 GMT. The pink profile is for the "CMAQ-like" Kv's and the blue profile is for the O'Brien Kv's.

[2] We have examined the actual Kv's from a CMAQ model run to see how they correspond to the "CMAQ like" Kv's produced by CAMx. The two sets of Kv's were very similar.

We would expect the increased mixing with the "CMAQ-like" Kv's to produce less ozone compared to the O'Brien Kv's. This was verified with the CAMx sensitivity run. Figure 8 shows the ozone differences in CAMx for the two Kv schemes. The differences are shown for the same hour that is plotted in figure 7 and show a mixture of ozone increases and decreases. In general, ozone went down (with "CMAQ-like" Kv's) by up to 10-15 ppb in areas with high ozone in the O'Brien case. Ozone went up in areas that were oxidant limited and therefore, increased mixing led to less titration of ozone and higher concentrations. This pattern is typical of most late afternoon hours on most days.

This sensitivity run clearly shows that CAMx run with the O'Brien mixing scheme produces more peak ozone compared to the CMAQ scheme. This likely accounts for at least part of the higher ozone seen in CAMx compared to CMAQ.

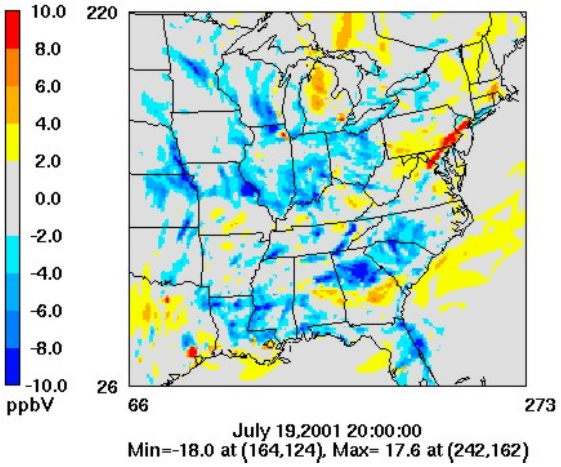

Fig. 8. One hour average ozone difference between CAMx run with O'Brien and "CMAQ like" Kv's (CMAQ-like – O'Brien) on July 19th, 2001 at 20Z. Negative values are ozone reductions due to "CMAQ like" Kv's.

4.2 Dry Deposition

CAMx uses a Wesely based dry deposition scheme (Wesely, 1989) that has been used in photochemical models for over 15 years. A similar scheme is available in CMAQ, called the RADM dry deposition scheme. CMAQ model runs over the last ~4 years have generally used a more recent dry deposition scheme called M3Dry (Pleim, 2001). M3Dry contains many improvements over previous schemes. M3Dry has updated resistance values based on more recent literature and field studies and it is also closely coupled with the Pleim-Xiu land surface model (used in MM5). M3Dry is able to use leaf area index and meteorological information to estimate canopy wetness, and it uses canopy wetness information to enhance dry deposition velocities for soluble gases (when surfaces are wet).

4.2.1 Dry deposition velocities

Dry deposition velocities (Vd) in CMAQ and CAMx were compared for several species to determine if major differences existed between the models. Among the species examined, large differences were noted for CO and NO, and smaller (but significant) differences were seen for other species including ozone, formaldehyde, NO_2, and hydrogen peroxide. In general, CMAQ deposition velocities were always higher than those seen in CAMx.

There are several differences that were seen. For CO and NO, CMAQ deposition velocities (using M3Dry) were 2-4 orders of magnitude higher than CAMx. For non-soluble gases, CMAQ deposition velocities were generally 20-100% higher than CAMx. For soluble gases (NH3, formaldehyde, etc.), CMAQ deposition velocities were several times higher than CAMx when modeled surfaces were wet.

Figures 9 and 10 show the deposition velocities for CO from CAMx and CMAQ on July 17th at 1600 GMT. This represents typical peak early afternoon deposition velocities. As can be seen in the figures, the CO Vd in CAMx is near zero while the CMAQ Vd (using M3Dry) ranges from 0.4-1.4 cm/s.

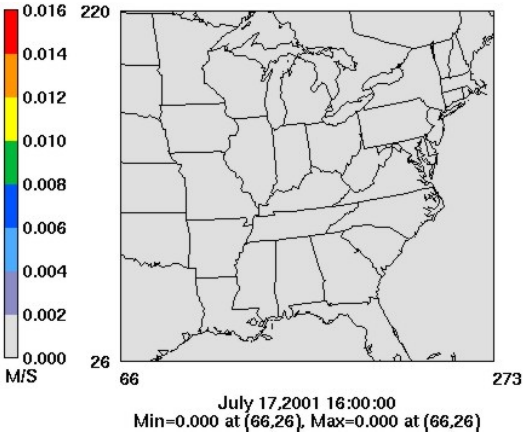

Fig. 9. CAMx 12km grid deposition velocity (Vd) for CO on July 17th, 2001 at 1600 GMT.

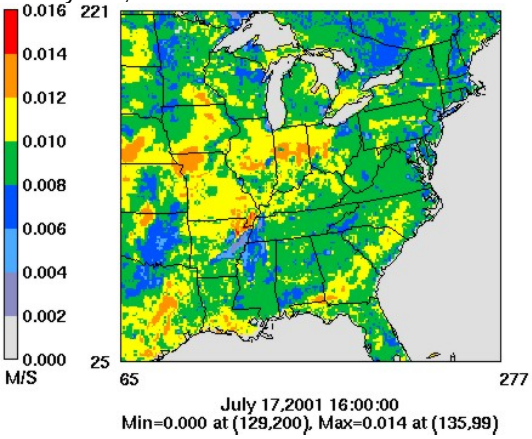

Fig. 10. CMAQ 12km grid deposition velocity (Vd) for CO (M3Dry) on July 17th, 2001 at 1600 GMT.

Figures 11 and 12 show ozone deposition velocities for the same time period. The CMAQ Vd values are generally 20-50% higher than those seen in CAMx.

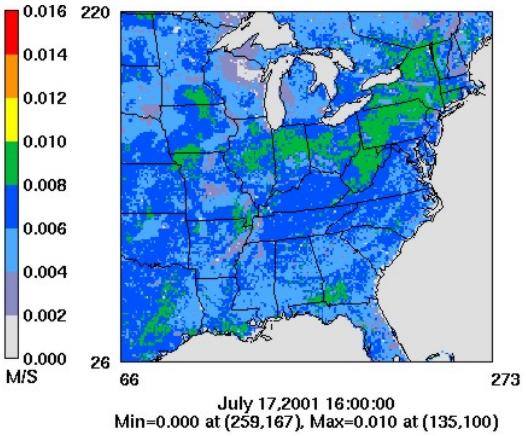

Fig. 11. CAMx 12km grid deposition velocity (Vd) for O3 on July 17th, 2001 at 1600 GMT.

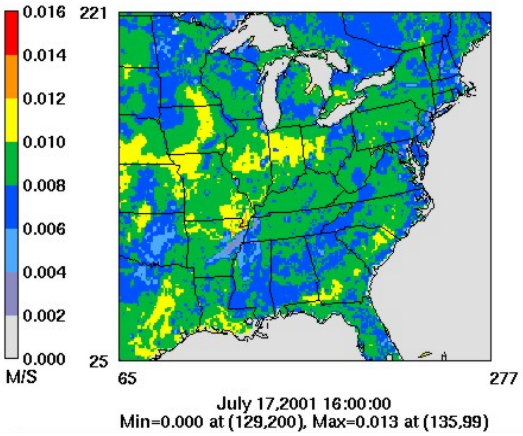

Fig. 12. CMAQ 12km grid deposition velocity (Vd) for O3 (M3Dry) on July 17th, 2001 at 1600 GMT.

4.2.2 Dry deposition sensitivities

Two CMAQ sensitivity runs were completed in order to examine the ozone response to dry deposition schemes. Both sensitivity runs were completed for a short time period with a more recent CMAQ platform. The platform used CMAQ v4.6 with CB-05 chemistry and 2002 emissions and meteorology. We ran CMAQ for the August 1-15th, 2002 period, with a 7 day ramp-up period. There were several high ozone episodes in the East during this period.

The first sensitivity run investigated the CO, NO, and NO_2 deposition velocities in order to better understand the differences between CMAQ and CAMx. The second sensitivity run looked at CMAQ ozone using the older RADM dry deposition scheme, in an effort to emulate the dry deposition scheme in CAMx. We then compared the ozone predictions in CMAQ using RADM back to the concentrations from the M3Dry model run.

4.2.2.1 Mesophyll resistance sensitivity

In our first sensitivity test of deposition, it was found that the Vd values for CO, NO, and NO_2 (especially CO and NO) were too high in M3Dry. A resistance value was added to M3Dry to represent mesophyll resistance for these three species and this resulted in CO and NO Vd values which were ~2 orders of magnitude lower than the original values in M3Dry. The rural CMAQ CO concentrations went up by a large amount and compared better to what was predicted by CAMx. We concluded that the mesophyll resistance values had a large impact on CO concentrations. The impact on ozone concentrations was small. Daily peak ozone concentrations went up by 1 or 2 ppb in many areas in the East.

4.2.2.2 RADM dry deposition sensitivity

Substituting the RADM dry deposition scheme for the M3Dry scheme in CMAQ had a large impact on modeled concentrations. The RADM deposition velocities were generally lower than M3Dry. The spatial patterns and magnitude of the RADM deposition velocities looked qualitatively similar to the deposition velocities from CAMx. This was expected, due to the common origin of both schemes (Wesely).

Figure 13 shows the 8-hour average ozone maximum on August 5th, 2002 from the base CMAQ v4.6 model run (using M3Dry). Figure 14 shows the increase in ozone on the same day as a result of switching to the RADM dry deposition scheme (everything else in the model runs were held constant). Ozone concentrations increased by 8-24 ppb (8-hour average) over large portions of the domain. Ozone increases were largest where peak values were seen in the base case.

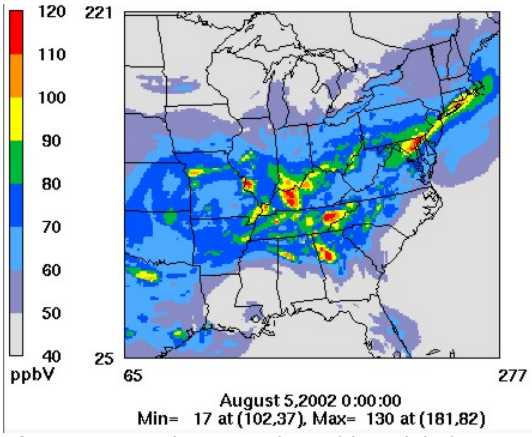

Fig. 13. CMAQ layer 1 12km grid modeled ozone concentrations on August 5th, 2002 (8-hour average).

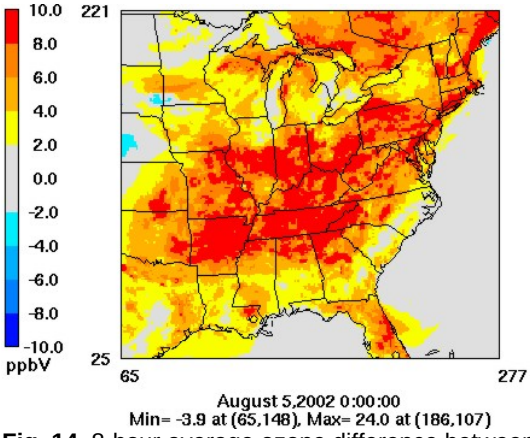

Fig. 14. 8-hour average ozone difference between CMAQ with RADM dry and M3Dry (RADM – M3Dry) on August 5th, 2002. Positive values are ozone increases due to RADM dry deposition.

5. CONCLUSIONS

Through sensitivity testing of CAMx and CMAQ we were able to account for most of the major concentration differences between the two models. We concluded that the largest difference in ozone concentrations in the two models is due to differences in the dry deposition schemes. Ozone increased by 10-20 ppb when a dry deposition scheme similar to the CAMx scheme is used in CMAQ. There were also problems identified in the CO and NO deposition velocities in M3Dry in CMAQ. Adding a value for mesophyll resistance for CO has a large impact on CO concentrations in CMAQ, though a somewhat small impact on daily ozone concentrations.

Sensitivity testing of vertical mixing schemes within CAMx revealed that inserting a "CMAQ-like" mixing scheme in CAMx leads to increased mixing and generally lower peak ozone concentrations (by up to 15-20 ppb).

Although difficult to precisely quantify, the combined effects of vertical mixing and dry deposition differences in CAMx and CMAQ likely account for the vast majority of the ozone concentration differences between the two models. These model formulation issues also account for differences in predicted concentrations of secondary aerosols (e.g. sulfate) and other photochemical precursors and by-products.

6. RECOMMENDED FOLLOW-UP

Further work is needed to examine the vertical mixing and dry deposition schemes in both CAMx and CMAQ. Vertical mixing in the models should be compared to mixing height observations to determine which scheme is most appropriate. Dry deposition velocities should be compared to published literature and fields studies to determine potential deficiencies in the current schemes. We stress that the models should not be compared to observed ozone concentrations to determine the appropriate mixing and deposition schemes. Conclusions based solely on an operational evaluation for ozone can lead to and/or perpetuate compensating errors in the modeling system.

7. REFERENCES

Byun, D., and K. L. Schere, 2006: Review of the governing equations, computational algorithms, and other components of the Models-3 Community Multiscale Air Quality (CMAQ) modeling system. *Appl. Mech. Rev.*, **59**, 51–77.

Dolwick, P., 2007: The effects of cloud attenuation on air quality: A comparison of model treatments. Presented at the 87th AMS Annual Meeting, San Antonio, TX.

ENVIRON International Corporation. User's Guide Comprehensive Air Quality Model with Extensions (CAMx) Version 4.30; ENVIRON International Corporation: Novato, CA, 2006. www.camx.com

Pleim, J. E., A. Xiu, P. L. Finkelstein, and T. L. Otte, 2001: A coupled land-surface and dry deposition model and comparison to field measurements of surface heat, moisture, and ozone fluxes. *Water Air Soil Pollut.* Focus, 1, 243–252.

Wesely, M. L., 1989: Parameterization of surface resistances to gaseous dry deposition in regional-scale numerical models. *Atmos. Environ*., **23**, 1293–1304.

Yarwood, G., S. Rao, M. Yocke, and G. Whitten, 2005: Updates to the carbon bond chemical mechanism: CB05. Final report to the US EPA, RT-0400675. Available at www.camx.com

8. ACKNOWLEDGEMENTS

We want to thank CSC for running CMAQ and CAMx; Jon Pleim for assistance on dry deposition issues (including recommendations for mesophyll resistance values); Environ for CAMx help and Kirk Baker of LADCO for CAMx assistance.

VOC/NO_X SENSITIVITY ANALYSIS FOR OZONE PRODUCTION USING CMAQ PROCESS ANALYSIS FOR THE PACIFIC NORTHWEST

Ying Xie*, Brian Lamb, and Tom Jobson
Department of Civil and Environmental Engineering, Washington State University, Pullman, WA, USA

1. INTRODUCTION

The Cascadia region of the Pacific Northwest periodically experiences elevated ozone levels downwind of major urban areas. Most of the modeling studies conducted in the region have involved direct comparisons of predicted and measured ozone levels (Barna et al., 2000). It is well known that photochemical production of ozone is a highly nonlinear system where the predicted peak ozone level is not dependent on a unique set of VOC and NO_x concentrations, and therefore, the model might predict incorrect sensitivities to changes in precursors even while correctly predicting ozone levels (Sillman, 1995). The uncertainties in ozone sensitivity have led to the development of various chemical indicators for ozone sensitivity to changes in VOC and NO_x emissions (Sillman, 1995; Kleinman et al., 1997, 2005; Tonnesen and Dennis, 2000a, 2000b). The general thought is that those measurable indicators would have different values related to NO_x sensitive and VOC sensitive conditions, so that model predicted sensitivity could be evaluated by comparing to measured indicator values or ozone sensitivity could be evaluated directly from measurements. Although there have been a number of studies (Kleinman et al., 1997; Lu and Chang, 1998; Sillman and He, 2002; Sillman et al., 2003) of these indicators, there is considerable uncertainty about how the indicators might behave under different conditions, and with different models and photochemical mechanisms. For the Pacific Northwest region, these indicators haven't been widely tested, and therefore it is unclear about their effectiveness and whether the ranges of values related to ozone sensitivity are similar or different compared to other urban areas.

The goal of this study is 1) to investigate ozone production rate ($P(O_3)$) and its relationship with precursors, namely NO_x, VOC reactivity, and radical production rate in the Pacific Northwest, 2) to investigate the behavior of local indicators for instantaneous odd oxygen production rate ($P(O_x)$), and 3) to evaluate $P(O_x)$ sensitivity to changes in VOC and NO_x emissions in the region using these indicators.

**Corresponding author:* Ying Xie, Department of Civil & Environmental Engineering, Sloan Hall 101, Spokane Street, Washington State University, Pullman, WA 99164-2910; e-mail: ying_xie@wsu.edu

2. METHODOLOGY

The VOC/NO_x sensitivity analysis for ozone production was studied by using the MM5/SMOKE/CMAQ modeling system with 4 km grid size for a region encompassing the I-5 corridor of western Washington and Oregon for an ozone episode that occurred in July, 1998. The integrated reaction rate analysis (IRR) (Gipson, 1999) was used to output production rate of selected species such as ozone, odd oxygen (O_x), new radical (Q), as well as important propagation and termination pathways. Model output within the Portland sub-domain at 13 LST from July 26 to July 28, 1998 was selected for data analysis, which correspond to the periods when maximum ozone production rates ($P(O_3)$) were predicted. This sub-domain (as shown in the black box in Figure 1) covers Portland urban area and downwind regions with high $P(O_3)$.

To investigate ozone production rate ($P(O_3)$) and its relationship with precursors, $P(O_3)$ and radical production rate (Q) from process analysis along with NO_x and total VOC reactivity (VOC_R) were analyzed. Radical production rate (Q) is the sum of production rate of new radicals ($OH+RO_2+HO_2$). Total VOC reactivity (VOC_R) was calculated based on OH reactivity.

To investigate the behavior of local indicators for instantaneous odd oxygen production rate ($P(O_x)$), two model sensitivity runs were conducted by decreasing the anthropogenic VOC and NO_x emissions by 30% from the base case. The grid cells are related to VOC or NO_x sensitive regimes according to the following criteria. Grid cells with $\partial P(O_x)/\partial E_{NOx} = 0$ are close to ridgeline conditions. NO_x sensitive cells are associated with $\partial P(O_x)/\partial E_{NOx} > 0$, whereas VOC sensitive cells are linked to $\partial P(O_x)/\partial E_{NOx} < 0$. Equal sensitivity is thought to

occur in these grid cells when $\partial P(O_x)/\partial E_{NOx} = \partial P(O_x)/\partial E_{VOC}$.

The five indicators (f_{OH+HC}, f_{HO2+NO}, $P(H_2O_2)/P(HNO_3)$, O_3/NO_x, and L_N/Q) are defined using similar definition as Tonnesen and Dennis (2000a) and Kleinman et al. (1997, 2005).

3. OZONE PRODUCTION RATE AND ITS PRECURSORS

Contour maps of model predicted ozone production rate is plotted in Figure 1 at 13 LST on July 27, 1998. As shown in Figure 1, maximum ozone production rate close to 35 ppb hr^{-1} was predicted downwind of the Portland and Seattle urban area. For the urban cores, negative values were predicted as a result of high NO_x concentrations.

Ozone production rate as a function of total VOC reactivity and NO_x concentration is plotted in Figure 2 as color-coded symbols using data within the Portland sub-domain at 13 LST from July 26 to July 28, 1998. For $P(O_3)$ > 20 ppb h^{-1}, the data points (red and pink) appear to generally follow an upward slope, indicating similar VOC_R/NO_x ratios between those data points. For the data points with $P(O_3)$ >30 ppb h^{-1}, VOC_R ranges mostly between 8-12 s^{-1} and NO_x ranges mostly between 5-15 ppb. There is much more scatter for the low $P(O_3)$ data points (<10 ppb h^{-1}) which exist at both low and high end of VOC_R and NO_x values.

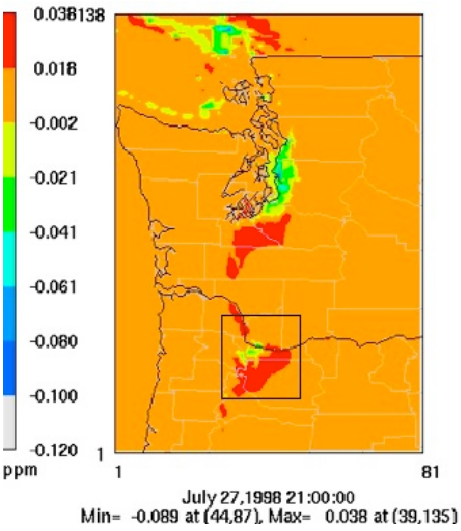

Figure 1. Surface $P(O_3)$ contours at 13 LST on July 27,1998 for the entire modeling domain. The inner black box shows the location of Portland sub-domain.

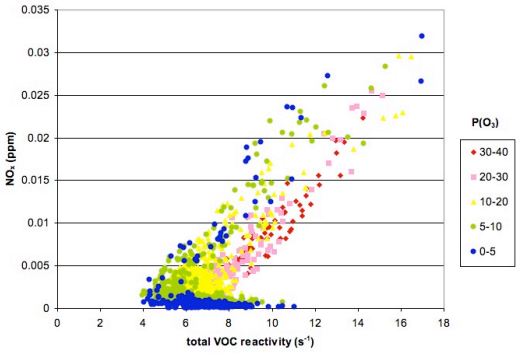

Figure 2. Ozone production rate as a function of NO_x and total VOC reactivity at 13 LST on July 26-28, 1998 within the Portland sub-domain.

4. THE BEHAVIOR OF LOCAL INDICATORS FOR $P(O_X)$

Figure 3 shows $\partial P(O_x)/\partial E$ as a function of f_{HO2+NO} in the base case at 13 LST on July 26-28, 1998 within the Portland sub-domain. There is a narrow range f_{HO2+NO} values associated with $\partial P(O_x)/\partial E_{NOx}$ =0, primarily between 0.96-0.97 indicating ridgeline values. Here cells with values greater than 0.97 are mainly VOC limited, whereas cells with values less than 0.92 are mostly NO_x limited. Values between 0.92-0.95 are linked to cells having equal sensitivity to VOC and NO_x. The other four indicators (f_{OH+HC}, $P(H_2O_2)/P(HNO_3)$, O_3/NO_x, and L_N/Q) also appear to be able to clearly distinguish NO_x and VOC sensitive conditions (not shown).

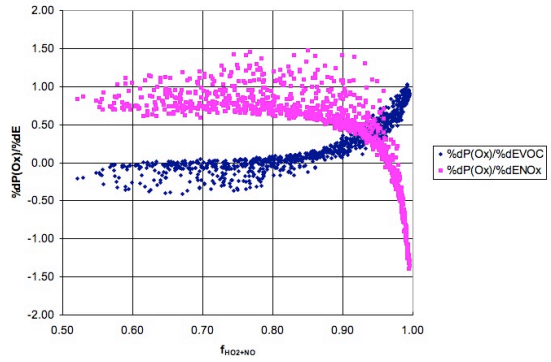

Figure 3. $\partial P(O_x)/\partial E$ as a function of f_{HO2+NO} at 13 LST on July 26-28, 1998 within the Portland sub-domain.

5. SENSITIVITY TO VOC/NO_X CHANGES BASED ON INDICATORS

Contour plot for f_{HO2+NO} is plotted at 13 LST on July 27, 1998 for the entire modeling domain as shown in Figure 4. On the maps, the color tiles around the ridgeline value are plotted in black and white, so that the intersection zone of the two colors could be viewed as where the ridgeline approximately sits. Both Portland and Seattle urban cores appear to be VOC limited in that hour, with Seattle being further more limited by radicals. Cells with high $P(O_3)$ (as shown in Figure 1) are primarily NO_x limited, but not far from the ridgeline. The contour plots of other indicators show very consistent patterns regarding to VOC and NO_x sensitive regions (not shown here).

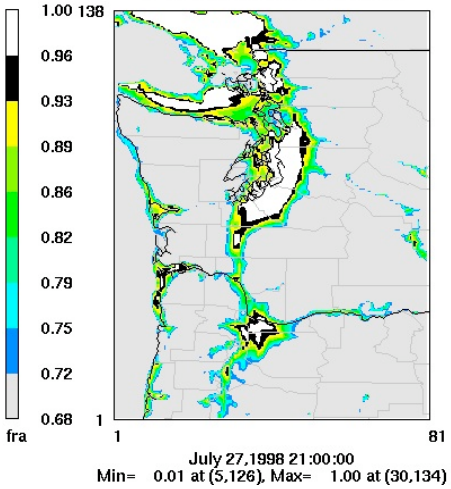

Figure 4. Surface contour plot of f_{HO2+NO} at 13 LST on July 27, 1998.

6. CONCLUSIONS

Maximum ozone production rate was found to be 30-40 ppb hr^{-1}, with NO_x concentrations of 5-15 ppb and total VOC reactivity of 8-12 s^{-1}. All five indicators (f_{OH+HC}, f_{HO2+NO}, $P(H_2O_2)/P(HNO_3)$, O_3/NO_x, and L_N/Q) appear to be able to distinguish NO_x and VOC sensitive conditions and suggest similar results regarding the location of ozone ridgeline. When $P(O_3)$ reaches maximum levels, Portland and Seattle urban cores both appear to be VOC limited; the grid cells with maximum $P(O_3)$ are located downwind of the urban core and mainly NO_x limited based on the indicator values. Further analysis using selected indicators is underway to compare model predicted ozone sensitivity with observations using aircraft and ground based measurements from PNW2001 field study.

7. REFERENCES

Barna, M. G., and B. K. Lamb, 2000: Improving ozone modeling in the regions of complex terrain using observational nudging in a prognostic meteorological model, *Atmos. Environ*., **34**, 4889- 4906.

Gipson, G. L., 1999: Process Analysis, *Science Algorithms of the EPA Models-3 Community Multiscale Air Quality (CMAQ) Modeling System*, D. W. Byun and J. K. S. Ching, eds., National Exposure Research Laboratory, U.S. EPA, Research Triangle Park, NC, Chap. 16.

Kleinman, L. I., P. H. Daum, J. H. Lee, Y.-N. Lee, L. J. Nunnermacker, S. R. Springston, L. Newman, J. Weinstein-Lloyd, and S. Sillman, 1997: Dependence of ozone production on NO and hydrocarbons in the troposphere, *Geophys Res. Lett.*, **24**, 2299– 2302.

Kleinman, L. I., 2005: The dependence of tropospheric ozone production rate on ozone precursors, *Atmos. Environ*., **39**, 575-586.

Lu, C.-H., and J. Chang, 1998: On the indicator-based approach to assess ozone sensitivities and emission features, *J. Geophys. Res*., **103**, 3453–3462.

O'Neill, S. M. and B. K. Lamb, 2005: Intercomparison of the Community Multiscale Air Quality Model and Calgrid Using Process Analysis, *Environ. Sci. Technol*., **39**, 5742-5753.

Sillman, S., 1995: The use of NO_y, HCHO, H_2O_2, and HNO_3 as indicators for ozone-NO_x-hydrocarbon sensitivity in urban locations, *J. Geophys. Res*., **100**, 14175-14188.

Sillman, S., and D. He, 2002: Some theoretical results concerning O_3-NO_x-VOC chemistry and NO_x-VOC indicators, *J. Geophys.Res.,***107**(D22), 4659, doi:10.1029/2001JD001123.

Sillman, S., R. Vautard, L. Menut, and D. Kley, 2003: O_3-NO_x-VOC sensitivity and NO_x-VOC indicators in Paris: Results from models and atmospheric pollution over the Paris area (ESQUIF) measurements, *J. Geophys. Res*., **108**(D17), 8563, doi:10.1029/2002JD001561.

Tonnesen, G. S., and R. L. Dennis, 2000a: Analysis of radical propagation efficiency to assess ozone sensitivity to hydrocarbons and NO_x, 1, Local indicators of instantaneous odd oxygen production sensitivity, *J. Geophys. Res*., **105**, 9213-9226.

Tonnesen, G. S., and R. L. Dennis, 2000b: Analysis of radical propagation efficiency to assess ozone sensitivity to hydrocarbons and NO_x, 2, Longlived species as indicators of ozone concentration sensitivity, *J. Geophys. Res*., **105**, 9227-9242.

IMPACT OF HIGH RESOLUTION MODELING ON OZONE PREDICTIONS IN THE CASCADIA REGION

Ying Xie* and Brian Lamb
Department of Civil and Environmental Engineering, Washington State University, Pullman, WA, USA

1. INTRODUCTION

Air quality in the Pacific Northwest is strongly influenced by complex terrain and unique meteorological conditions within and near the Columbia River Gorge and the Cascade Mountain range. Topographical features interact closely with the regional flow, and therefore have an important impact on the dispersion of pollutants. In addition, unresolved subgrid variability in precursor emissions within the metropolitan areas also suggests the need for high resolution in photochemical modeling.

Despite the need for high resolution modeling, weather forecasting and air quality simulations in the region have been and are routinely applied with grid sizes of 36, 12 and/or 4 km (Mass et al., 2002; O'Neill et al., 2005). There have been only a few meteorological modeling studies conducted with horizontal grid sizes near or less than 1 km (Colle and Mass, 1998a and 2000a; Sharp and Mass, 2002); the effect of high model resolution on air quality simulations and ozone predictions remains unknown. It is also not clear whether high resolution meteorological input or emissions will have a larger impact on air quality simulations if not applied simultaneously.

In this study, the MM5/SMOKE/CMAQ modeling system was used for nested 4 km and 1 km domains encompassing the Portland metropolitan area and the Columbia River Gorge for an ozone episode that occurred at July, 1998 to investigate the impact of high resolution meteorological and photochemical modeling on ozone predictions for the region. The effects of high resolution meteorological input were compared with those of high resolution emissions by running CMAQ at 1 km with two scenarios: one with 1 km MM5 but 4 km emissions and the other with both MM5 and emissions at 1 km.

For emissions sources, spatial surrogates at 4 km resolution were used to allocate the emissions for the 4 km domain and some source categories in the 1 km domain when surrogates at finer resolution weren't available. Surrogate available at 1 km resolution included population, mileage on roadways, major airport, livestock, and Oregon drycleaners.

**Corresponding author:* Ying Xie, Department of Civil & Environmental Engineering, Sloan Hall 101, Spokane Street, Washington State University, Pullman, WA 99164-2910; e-mail: ying_xie@wsu.edu

2. HIGH RESOLUTION MM5 RUN

The run with 1 km MM5 but 4 km emissions was compared with the 4 km run first to investigate the impact of high resolution meteorological input. Ozone surface contour plots at 15 LST on July 27 are shown in 1a and 1b for the 4 km run and 1 km run, respectively, with the difference plot (1b-1a) shown in 1c. Here the 1 km run ozone contours (1b) are the gridded means aggregated from 1 km to 4 km grid cells, so that they can be compared with the 4 km results.

Similar ozone peaks were predicted by the two runs on that ozone episode day. When using high resolution MM5, the areas with elevated ozone are reduced in size and shifted slightly further downwind. The maximum ozone increases occur along the Columbia River Gorge and the foothills of Cascades where the terrain effects are substantial. For example, transport of ozone along the Gorge can be clearly identified, with ozone increases around 20 ppb compared to the 4 km run. On the other hand, ozone decreases, mostly around 10-20 ppb, were predicted closer to the source region when high resolution MM5 was used.

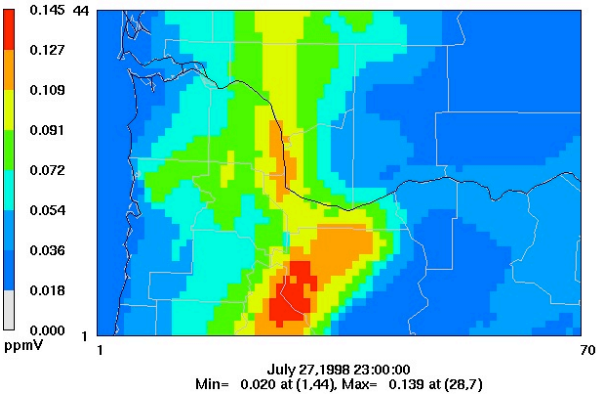

Fig. 1a. Surface ozone contours from CMAQ at 15 LST on July 27, 1998 from the 4 km run.

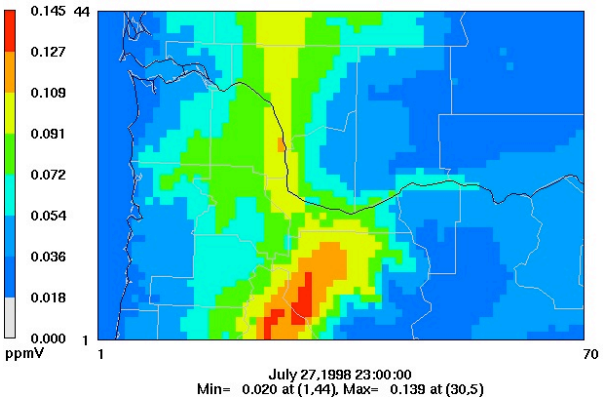

Fig. 1b. Surface ozone contours from CMAQ at 15 LST on July 27, 1998 from the 1 km run using 1 km MM5 but 4 km emissions.

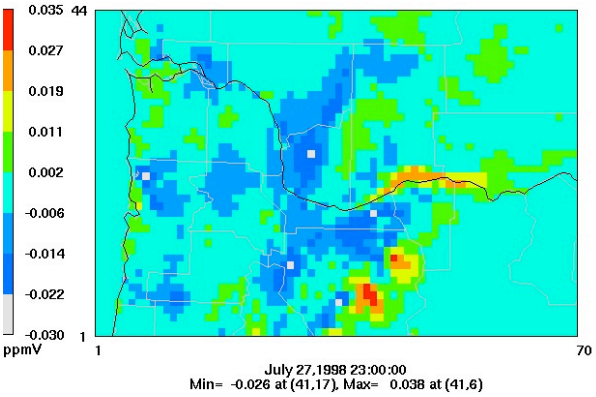

Fig. 1c. Difference plots of "1b-1a".

3. HIGH RESOLUTION EMISSIONS RUN

The run with 1 km MM5 but 4 km emissions was further compared with the run in which both high resolution MM5 and emissions were used. Ozone surface contour plot at 15 LST on July 27 are shown in Figure 2a for the run with high resolution MM5 only. Figure 2b shows similar contours for the run with both 1 km MM5 and emissions, with the difference plot (2b-2a) shown in 1c.

The overall pattern and ozone peaks are fairly similar between the two runs, but the run with both high resolution MM5 and emissions shows small-scale features which are missing when coarser emissions were used. Most of the differences occur close to the source region such as along the I-5 corridor and within the Portland urban area with both increases and decreases in ozone levels.

Ozone decreases (mostly less than 15 ppb) mainly occur at the grid cells with large roadway emissions, where NO titration effects are better represented with fine-scale emissions. Ozone increases (mostly less than 10 ppb) were predicted in the surrounding cells next to these roadway emissions, where NO emissions were artificially diluted when using 4 km emission surrogates. Increases in ozone were also predicted further downwind of the source region, although the changes are mostly below 5 ppb.

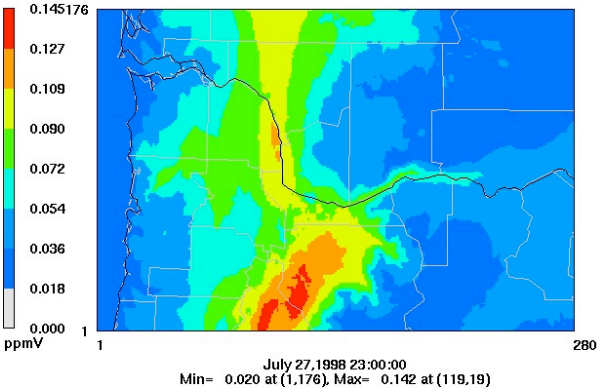

Fig. 2a. Surface ozone contours from CMAQ at 15 LST on July 27, 1998 from the 1 km run using 1 km MM5 but 4 km emissions.

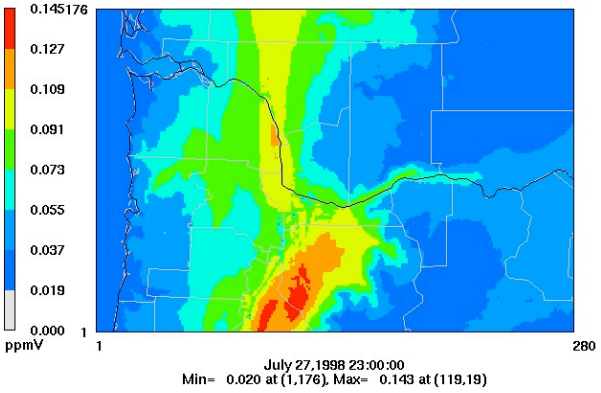

Fig. 2b. Surface ozone contours from CMAQ at 15 LST on July 27, 1998 from the 1 km run using both 1 km MM5 and emissions.

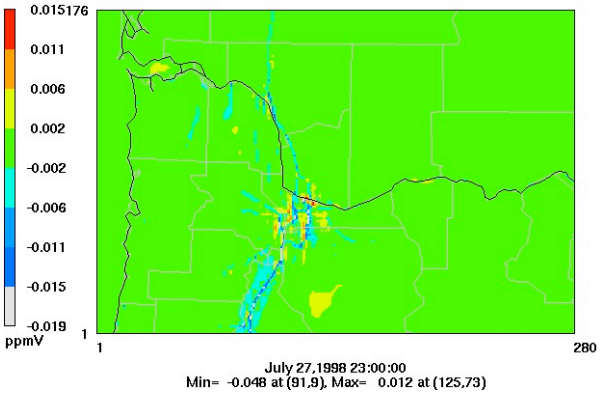

Fig. 2c. Difference plots of "2b-2a".

4. CONCLUSIONS

Using high resolution meteorological input alone appeared to have a larger impact on ozone predictions in terms of the position and peak levels of the ozone plume. Ozone concentrations were higher in the 1 km case compared to the 4 km case in areas along the Columbia River Gorge and the foothills of Cascades where the terrain effects are substantial. Using high resolution emissions appeared to affect small-scale features in ozone concentration patterns mainly within the urban area. In that case both ozone increases and decreases could be identified which were missing when using coarse resolution emissions.

5. REFERENCES

Colle, B. A., and C. F. Mass, 1998a: Windstorms along the western side of the Washington Cascade Mountains. Part I: A high resolution observational and modeling study of the 12 February 1995 event, *Mon. Wea. Rev*., **126**, 28–52.

Colle, B. A., and C. F. Mass, 2000a: High-resolution observations and numerical simulations of easterly gap flow through the Strait of Juan de Fuca on 9–10 December 1995, *Mon. Wea. Rev*., **128**, 2398–2422.

Mass, C. F., D. Ovens, K. Westrick, and B. A. Colle, 2002: Does Increasing Horizontal Resolution Produce More Skillful Forecasts?, *Bull. Amer. Meteor. Soc*., **83**, 407-430.

O'Neill, S. M. and B. K. Lamb, 2005: Intercomparison of the Community Multiscale Air Quality Model and Calgrid Using Process Analysis, *Environ. Sci. Technol.,* **39**, 5742-5753.

Sharp, J., and C. Mass, 2002: Columbia Gorge gap flow: Insights from observational analysis and ultra-High-Resolution Simulation, *Bull. Amer. Meteor. Soc*., **83**, 1757-1762.

THE EXPERIMENTS OF MODIFYING THE CMAQ PRODUCTS BY USING THE CMAQ-MOS AND THE CMAQ-ANNs

Hong Zhao
College of Information Technical Science, Nankai University, Tianjin,China

Zhen-ling Wu and Yi-yang Xie
Meteorological Institute of Tianjin, Tianjin,China

Zhi-peng Bai
College of Environmental Science and Engineering, Nankai University, Tianjin,China

Chi Zhang
College of Information Technical Science, Nankai University, Tianjin,China

1. INTRODUCTION

The Models-3 Community Multiscale Air Quality (CMAQ) model owns better capability in forecasting the spatial distribution and the trends of the distribution of multiple pollutants in different scales. Due to the complexity of the spatial and temporal features of the pollution emission，it is difficult to describe the time-space variation of the pollution source intensities finely or accurately and objectively in the forecast regions. Comparing with the monitoring values, the estimated values of CMAQ products, which are similar to values using other models, are significantly lowered by systematic errors. Take the example of Tianjin, China, the estimated values of SO_2 and NO_2 using the CMAQ model are two orders of magnitude lower than the monitoring values, which means that the CMAQ products are far to reach the requirements of daily operation.

2. CMAQ-MOS AND ITS FORECASE EXPERIMENT

In order to correct the systematic errors produced by the average amount of pollutant emission inventory, Jianming Xu, Xiangde Xu[1] and others analyzed the monitoring data of the air pollutants. The monitoring data were from September 2004 to March 2005 and were collected at 8 observation sites in the urban and suburban areas of Beijing. The study revealed the synchronal and in-phase characteristics in the time-space variation of the air pollutants at different sites on a city-proper scale. It also described the seasonal differences in the pollutant emission influence between the heating and non-heating periods. The monitoring data from the urban and suburban sites also showed significant regional features that the spatial distributions of the air pollutants were closely related with the pollutant emission influence. Therefore the study proposed the employment of a statistical correction model--CMAQ-MOS, which was a combination of dynamics and statistics used for air quality forecast.

The CMAQ-MOS model utilized the early monitoring data of the atmosphere and combined the forecast values of the CMAQ products on the forecast date to predict the pollutant concentrations, which would correct the deviation of the air quality forecast in the city due to the subjectivity of the pollutant emission sources. The monitoring data of the atmosphere included in the CMAQ-MOS were: the monitoring data of meteorological elements and multiple pollutants; the CMAQ products: the output of multiple pollutants using the CMAQ model. The mathematical model of CMAQ-MOS is demonstrated as follows:

$$S^{n} = \tilde{G}_{m} + \tilde{S}_{M+N+L} \times \tilde{A}_{m}^{M+N+L}$$

where

S^{n} is the forecast object which represents the concentration of a particular pollutant on the forecasting day (the n^{th} day)

$\tilde{A}_{m}^{L+M+N}$ are coefficient matrices; m represents different phases

and $\tilde{G}_{m}$

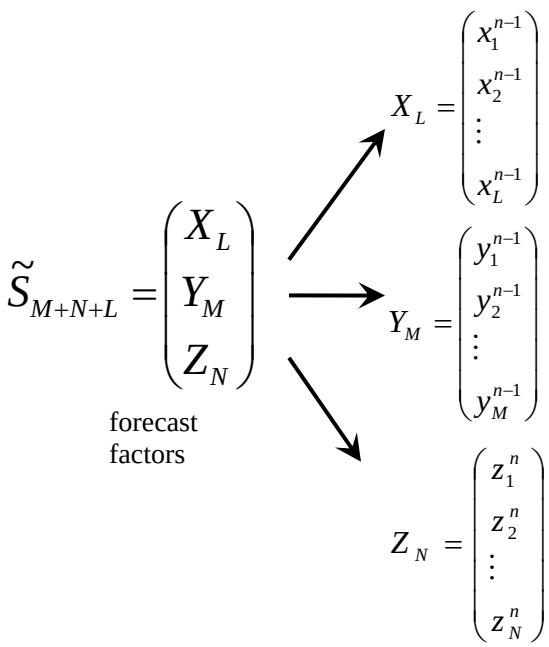

The monitoring data of the pollutants:
PM_{10}, SO_2, NO_2
The monitoring data of the meteorological elements:
wind field(U,V),temperature field(Ts), relative humidity(RH)
The CMAQ products:
$PM_{2.5}$、PM_{10}、SO_2、NO_2、O_3

X_L represents the monitoring values of L types of pollutant concentrations on the starting forecasting day

Y_M represents the monitoring values of M types of atmospheric elements on the starting forecasting day

Z_N represents the forecast values of N types of pollutant concentrations on the forecasting day

2.1 The Description of CMAQ-MOS Experiment

We took the city of Tianjin, China as the research object, used the CMAQ products and the monitoring data of the meteorological elements from March 2006 to April 2006, employed the CMAQ-MOS method to forecast the pollution concentration in May 2006, compared the results of the CMAQ-MOS method with the CMAQ products as well as the monitoring values, and analyzed the actual forecast performance of the CMAQ-MOS. Due to the limited data sources of the monitoring materials and the CMAQ products, and considering the demands of the daily operations, all the data waiting for input were daily averaged to keep unity.

The longitude and latitude range of Tianjin:

latitude 39 degrees 3 minutes to 39 degrees 25 minutes N

longitude 117 degrees 9 minutes to 117 degrees 32 minutes E

For the CMAQ forecast model, the experiment selected the average of 7 grid points in the longitude range between 117 degrees 9 minutes to 117 degrees 29 minutes E, and the latitude range between 39 degrees 3 minutes to 39 degrees 35 minutes N.

The Materials for CMAQ-MOS experiment included:

We used the materials above to build equations on 12 observation sites respectively to forecast the concentrations of PM_{10}、SO_2、NO_2.

$$\begin{aligned} <PC> = g &+ a_1\times[PM_{10}]_1 + a_2\times[SO_2]_1 + a_3\times[NO_2]_1 \\ &+ a_4\times[PM_{10}]_2 + a_5\times[SO_2]_2 + a_6\times[NO_2]_2 \\ &+ b_1\times[Ts] + b_2\times[U] + b_3\times[V] + b_4\times[RH] \\ &+ c_1\times\{PM_{2.5}\} + c_2\times\{PM_{10}\} + c_3\times\{SO_2\} \\ &+ c_4\times\{NO_2\} + c_5\times\{O_3\} \end{aligned}$$

where

PC stands for pollutant concentration

<> represents the forecast value of the pollutant concentrations.

[] represents the monitoring values on the starting forecasting day (1 represents the average concentration of the whole city area, 2 represents the average concentration of a single observation site) and the monitoring values of meteorological elements.

{} represents the CMAQ products on the forecast date

$a_1 \ldots a_n$, $b_1 \ldots b_m$, $c_1 \ldots c_l$ are coefficients and are found through mathematical methods.

We used the forecast equation established to forecast the pollutant concentrations of the whole

city area, the values of the pollutant concentrations represented the average forecast values of 12 observation sites.

2.2 The Results of CMAQ-MOS Experiment

Figure 1 illustrates the condition of pollutant forecast concentrations about PM_{10} and NO_2 in May, employing the equation established by the pollutant concentration data in April. "CMAQ" represents the CMAQ products. "Real" represents the monitoring values which are two orders of magnitude higher than the CMAQ products. "CMAQ-MOS-4" represents the pollutant forecast concentrations of PM_{10} and NO_2 in May using the forecast equation established by the pollutant concentration data in April. The values are approximately on the same order of magnitude as the monitoring values, but it contains relatively big errors, for example the average relative error of the "CMAQ-MOS-4" forecast values for NO_2 is 42.91%.

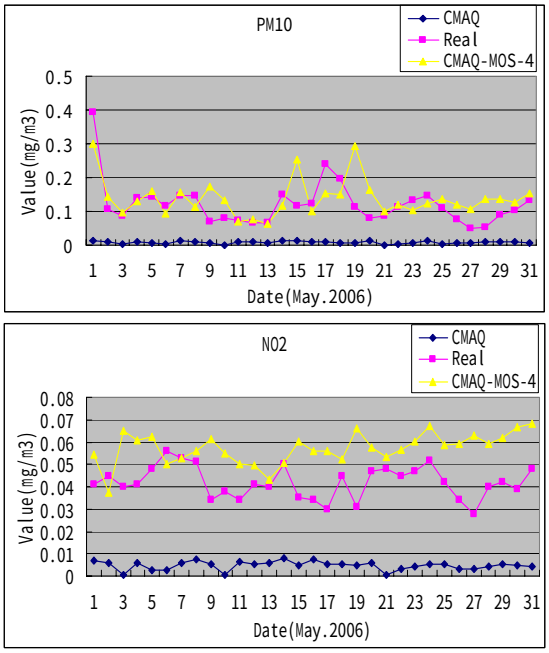

Fig1.Forecasting Results of Pollutant Concentration in May Using Statistical Model Established in April

Figure 2 illustrates the comparison between the pollutant concentration condition of PM_{10} and NO_2 in May using the forecast equation established by the pollutant concentration data in April and in March. "Real" represents the monitoring values. "CMAQ-MOS-3" represents the forecast values of PM_{10} and NO_2 in May using the forecast equation established by the pollutant concentration data in March,"CMAQ-MOS-4" represents the forecast values of PM_{10} and NO_2 in May using the forecast equation established by the pollutant concentration data in April.

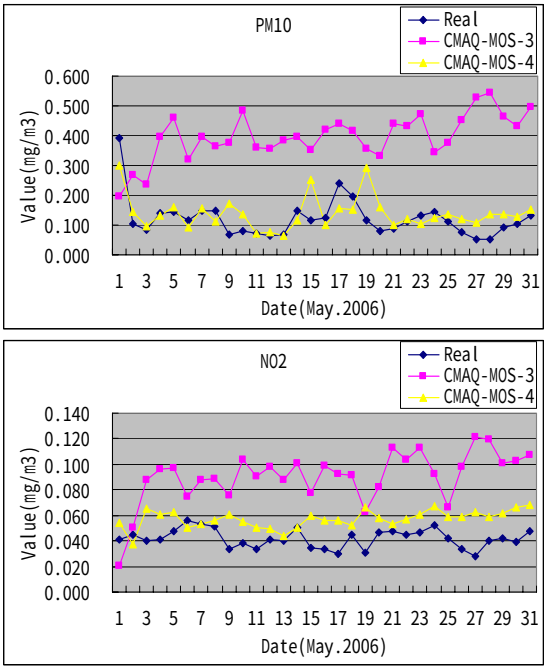

Fig2.Comparison of Forecasting Results between the Statistical Models Established Respectively in March and in April

Because the month March is in the transition from heating period to non-heating period, the heating equipments in some areas are still being used in the last ten days of this month, and the pollutant sources are obviously more in March than in April and May, which causes an ineffective simulation in May using the forecast equation established by the pollutant concentration data in March. The forecast values are higher, for example the average relative error of the CMAQ-MOS-3 values of NO_2 can be as big as 125.72%. Therefore, using split-season method or rolling method to build the MOS forecast equation will be more effective.

3. CMAQ-ANNs AND ITS FORECASE EXPERIMENT

Artificial neural networks have drawn the attention of the scholars in various fields for its self-learning, self-organizing, relatively good error tolerance and excellent non-linear approximating ability. Generally speaking, ANN has no superiority over classical computational methods. However, it will only show its superiority when the problem can not be solved or can not be solved

effectively using conventional methods. It is often the best tool especially when the mechanism of the problems, such as troubleshooting and feature extraction and prediction, are not quite clear or when the system can not be demonstrated using mathematical models. On the other hand, ANN shows great flexibility and self-adaptation in handling massive bodies of raw monitoring data and dealing with problems which can not be demonstrated using regulations and formulae.

Due to the excellent non-linear approximating ability, BP neural networks have been widely applied to the evaluation and forecasting of the environment quality in environmental science and engineering field, the deployment optimization of the observation points, the degradation and liberation of the pollutant chemicals and the simulation and prediction of water(treatment, ecology)-system as well as other aspects. CMAQ-ANNs employed BP neural networks to correct the CMAQ products.

3.1 The Description of CMAQ-ANNs Experiment

In the CMAQ-ANNs experiment, there were three hidden layers that constructed the neural network. Each layer used linear functions as transition functions. The weight and threshold values were all initialized randomly between -1 and 1. The number of the hidden layer neurons was set to 5.

The training samples were data gathered from March 2006 to April 2006, totally 61 days. The testing samples were data from each day in May. Experimental materials included:

Monitoring data of meteorological elements: wind field (U, V).temperature field (Ts) and relative humidity (RH)

CMAQ products: $PM_{2.5}$, PM_{10}, SO_2, NO_2 and O_3

The objective vector of the training samples: monitoring data of the pollutants PM_{10}, SO_2 and NO_2.

The CMAQ-ANNs method was to use the 61 training samples from March to April to build the BP neural network, input the atmospheric sounding data observed each day(wind field(U,V), temperature field(T),relative humidity(RH)) and the CMAQ products(SO_2, NO_2, O_3 ,$PM_{2.5}$, PM_{10}) to this neural network in order to find the forecast values of the pollution concentration in May, compare the forecast values of CMAQ-ANNs with CMAQ products and monitoring values, and analyze the performance of the CMAQ-ANNs.

In order to understand the impact of using different types of data on the forecast quality, we built several neural networks with different numbers of input neurons and output neurons.

3.2 The Results of CMAQ-ANNs Experiment

Figure 3 illustrates the neural network which contains three inputs and three outputs. The CMAQ products(PM_{10}、 SO_2 and NO_2) are inputted to the network, while the network outputs another three variables(PM_{10}、 SO_2 and NO_2). We used this neural network to forecast the conditions of pollutant concentrations of SO_2 and PM_{10} in May 2006. In the figure the CMAQ curve shows the values of the CMAQ products and the REAL curve shows the monitoring values of the pollutant concentration. The CMAQ-ANNs curve shows the corrected CMAQ products using the neural network method. The figure indicates that the CMAQ-ANNs is able to correct the CMAQ product to the same order of magnitude as the monitoring values, and its curve has in most cases the same crest and trough to the one of monitoring values, that is to say, to have similar trends as the curve of the monitoring values. But obviously it contains bigger errors, the minimum value of the relative error of SO_2 is 2.37% while the maximum reaches 89.15%, the average is 31.21%. For PM_{10} the average of the relative error reaches up to 100.25%.

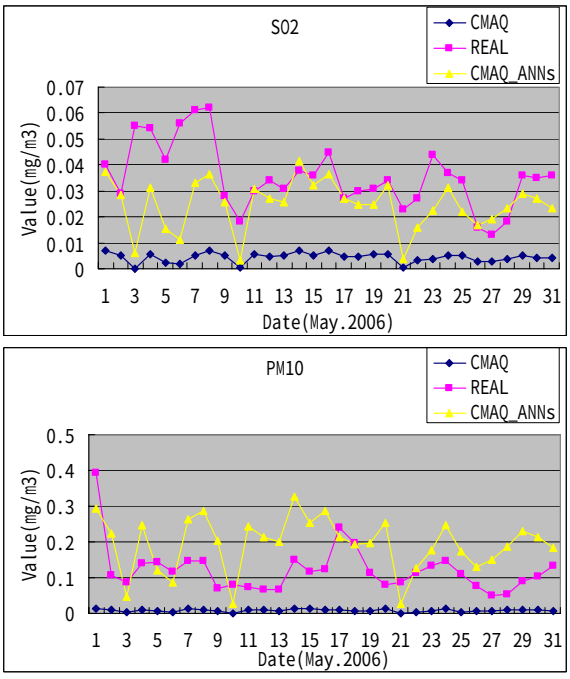

Fig3. Forecast Results of the Pollutant Concentrations Using the Neural Network with 3 Inputs and 3 Outputs

Figure 4 illustrates the neural networks built for forecasting pollutants PM_{10}、SO_2 and NO_2 respectively which uses the CMAQ products(PM_{10}、SO_2 and NO_2)as input variables and output only one variable. We used two out of the three networks to forecast the pollutant concentration of SO_2 and NO_2 in May 2006. The forecast performance is almost the same as the neural networks using 3 inputs and 3 outputs. CMAQ-ANNs-3 represents the neural network with 3 outputs and CMAQ-ANNs-1 represents the neural network with only 1 output. From the figure it shows that the two curves almost overlap with each other. And this indicates that the forecast quality has no significant difference between the two networks.

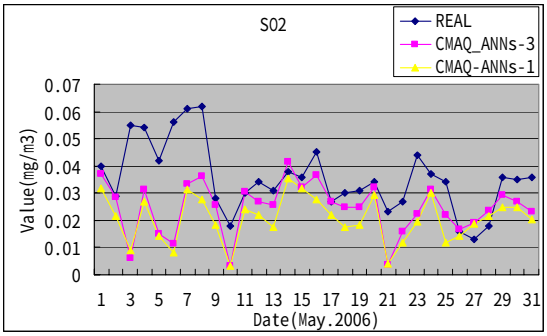

Fig4.Comparison of Forecast Quality between the Neural Network with 3 Inputs and 3 Outputs and the Neural Network with 3 Inputs and 1 Outputs

Figure 5 illustrates the neural network which uses the CMAQ products ($PM_{2.5}$、PM_{10}、SO_2、NO_2 and O_3) as input variables and outputs three (PM_{10}、SO_2 and NO_2) variables. We use this neural network to forecast the pollutant concentrations of SO_2 and NO_2 in May 2006. The minimum value of the relative error of SO_2 was 2.27% while the maximum reaches 290.86%, the average is 77.45%. For PM_{10} the average of the relative error reaches up to 32.49%.

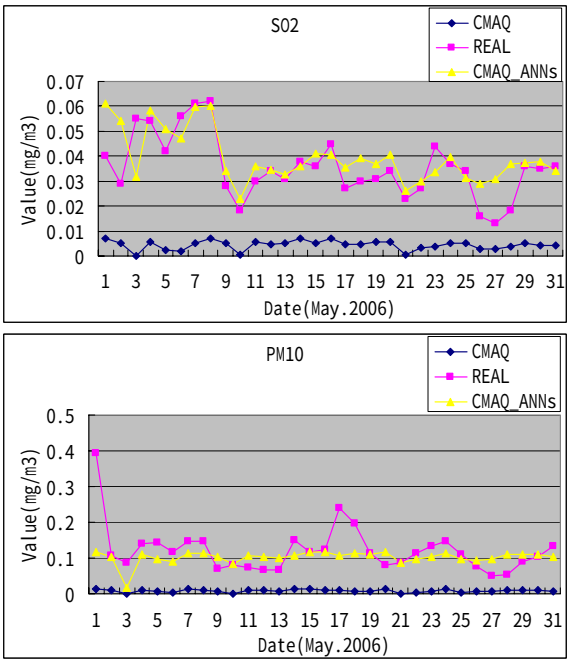

Fig5. Forecast Results of the Pollutant Concentrations Using the Neural Network with 5 Inputs and 3 Outputs

Figure 6 illustrates the neural network which uses the meteorological elements (wind field(U), wind field(V)、temperature field(Ts)and relative humidity(RH))and CMAQ products (PM_{10}、SO_2、NO_2)as seven input variables and outputs three (PM_{10}、SO_2 and NO_2)variables. We use this neural network to forecast the pollutant concentrations of SO_2 and NO_2 in May, 2006. The minimum value of the relative error of SO_2 is 2.28% while the maximum reached 96.8%, the average was 53.08%. For PM_{10} the average of the relative error reaches 56.72%.

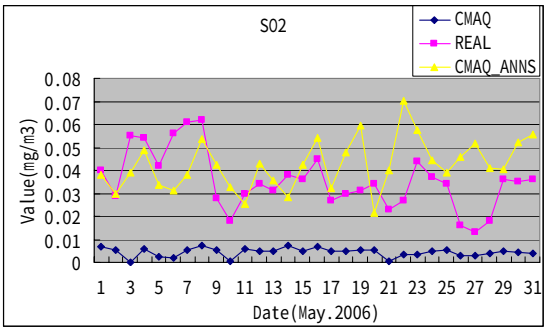

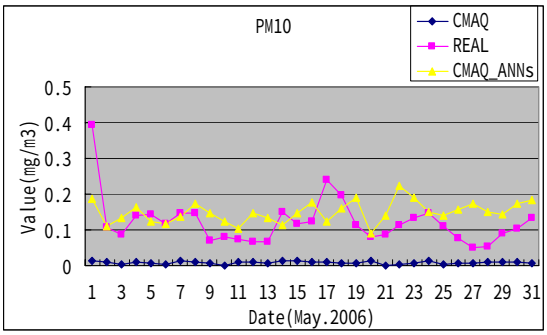

Fig6. Forecast Results of the Pollutant Concentrations Using the Neural Network with 7 Inputs

Figure 7 illustrates the neural networks which outputs 3 variables(PM_{10}、SO_2 and NO_2) and inputs 3, 5 or 7 variables. We compared the forecast pollutant concentration results of SO_2 in May, 2006 generated from the three networks. From the figure it shows that the estimated results of the 3 CMAQ-ANNs experiments are able to correct CMAQ products to the same order of magnitude as the monitoring values. The results can also form similar curves as the monitoring values, though all the results have relatively big errors. The values corrected by the neural network which used the CMAQ products($PM_{2.5}$、PM_{10}、SO_2、NO_2 and O_3) as input variables are closer to the monitoring values，both of the neural networks which use meteorological elements (wind field(U)，wind field(V)、temperature field(Ts)and relative humidity(RH))and CMAQ products (PM_{10}、SO_2、NO_2) as seven input variables and the one which uses the CMAQ products (PM_{10}、SO_2 and NO_2)as input variables are more sensitive to the input of the CMAQ products.

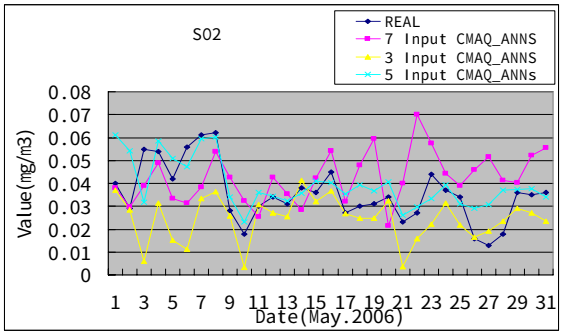

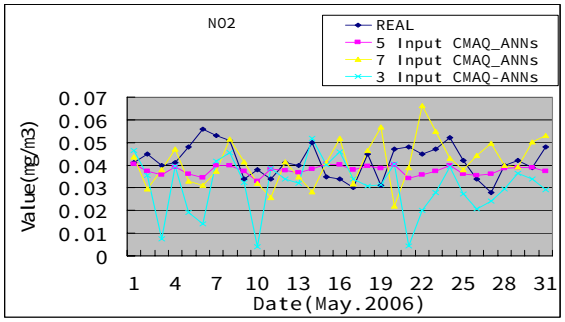

Fig7.Comparison of Forecast Results among the 3 Neural Networks

4. CONCLUSION

The paper has only made some tentative experiments. Although CMAQ-MOS and CMAQ-ANNs methods are capable of correcting the CMAQ products to the same order of magnitude as the monitoring values, relatively big errors still exist. The forecast curve of the CMAQ-ANNs experiment is the same or similar in the alteration as the curve of the monitoring values, which indicates that CMAQ-ANNs handles the internal law of the relationship between CMAQ products and the monitoring values better.

Due to the factors such as the limitation of the experimental data, the input errors from all sorts of data, the internal randomness of the atmospheric process and that of the numeric models, as well as the uncertainty of the discharge concentration and that of the source parameters of the pollution sources, it is fairly difficult to find and grasp the true internal law of the relationship between CMAQ products and the monitoring values. Therefore, to find a measurable law which is the way to fundamentally solve the problem of the model's uncertainty, it needs for deeper research into the impact of these factors on the uncertainty of the air quality forecast model. It is also the working priority and major point of future research.

References

[1]XU Jianming, XU Xiangde, LIU Yu. Study of statistically correcting model CMAQ-MOS for forecasting regional air quality, SCIENCE IN CHINA SERIES D (EARTH SCIENCES), 2

[2] J. Ma, J. A. van Aardenne. Impact of different emission inventories on simulated tropospheric ozone over China: a regional chemical transport model evaluation. Atmospheric Chemistry and Physics, 4, 877–887, 2004

[3] Source of CMAQ: http://www.CMAScenter.org

CMAQ APPLICATION TO THE OZONE POLLUTION IN PEARL RIVER DELTA OF CHINA

Wei Zhou[1,2], Yuanhang Zhang1*, Xuesong Wang1, Daniel Cohan[2]
[1] College of Environmental Science and Engineering, Peking University, Beijng, China
[2] Department of Civil and Environmental Engineering, Rice University, Houston, TX

1. INTRODUCTION

The Pearl River Delta (PRD) was one of the very first areas of rapid economic development in China. Program of Regional Integrated Experiments of Air Quality over Pear River Delta (PRIDE-PRD) was developed to provide as comprehensive as possible descriptions of the air pollution in this quickly developing South-Eastern region of China. Based on the result of field observation in PRIDE-PRD2004 campaign, maximum ozone concentration in most sites which had its observation was higher than China's national ambient air quality standard. Especially, the down wind area of PRD and Pearl River Estuary (PRE) had high ozone concentration record. The maximum ozone concentration observed at the monitoring site –Donghu (the site of B in Fig.1).

To better understand the serious ozone pollution in PRD, the third generation of air quality model (Models-3/CMAQ) was applied to simulate the ozone episode in October 2004, regional ozone distribution and the related meteorological features of PRD were analyzed. Cities in PRD and monitoring sites were shown in Fig1. Site A was located in Guangzhou City, site B was a coastal site of PRE. In this study, the inland PRD was controlled by the northeast wind, therefore site C was the down wind of Guangzhou, which was the largest pollutant emission source in PRD.

Figure-1. Pearl River Delta of China (A, B,C –the monitoring sites for the model performance test)

**Corresponding author:* Yuanhang Zhang, College of Environmental Science and Engineering, Peking University, Beijing, China, 100871; email: yhzhang@pku.edu.cn

2. PRIMARY RESULTS OF OZONE SIMULATION OVER PRD

This modeling system using MM5, SMOKE, CMAQ was run with a configuration of three nested domains as shown in Fig2. The resolution was 36km over the domain1- China, 12km over the domain2- south China, and 4km over the domain3-PRD. The emission data for the domain1 was based on the TRACE-P emission inventory in 2000(Streets DG et al., 2003). Those of 12km and 4km were prepared on the basis of the PRD emission inventory–2001 from Hong Kong EPD and updated (Song Xiang-yu et al., 2006, Zhao Jing et al., 2006). The chemical mechanism used in this modeling study was SAPRC-99. As an initial modeling study, the simulation was run from 17th to 23rd October 2004 with two days for a spin-up.

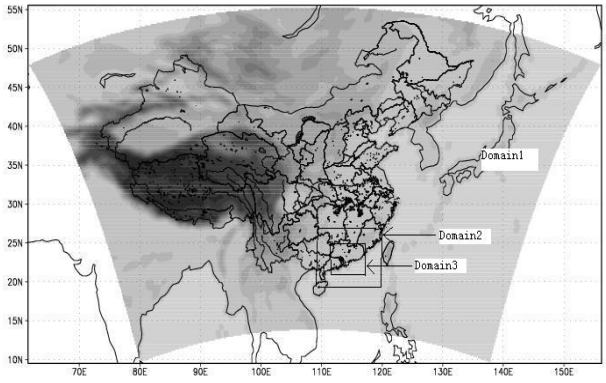

Figure-2. Three nested domains of this modeling study

In this modeling study, three monitoring sites (the three marked sites in Fig1) were chosen for testing the model performance. Model predictions were compared with observed data of three monitoring sites. Generally, the simulation can capture the variation of ozone at the monitoring sites. High ozone concentration was found at the southwest of PRD- the site of Donghu, while the site of Xiken over the PRE has also recorded a high ozone concentration.

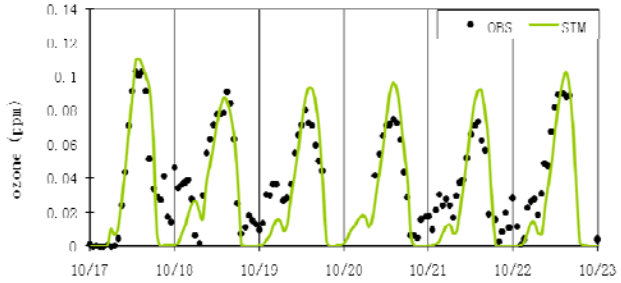

Figure-3. Observation and simulation ozone concentration at the monitoring site of Luhu (A in Fig.1)

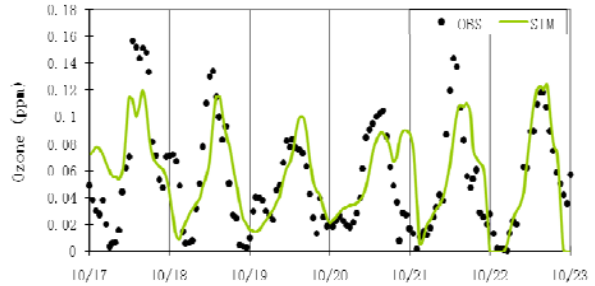

Figure-4. Observation and simulation ozone concentration at the monitoring site of Xinken (B in Fig.1)

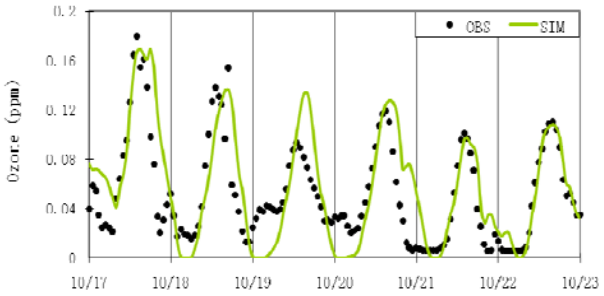

Figure-5. Observation and simulation ozone concentration at the monitoring site of Donghu (C in Fig.1)

3. RESULT ANALYSIS AND DISCUSSION

3.1 Regional Distribution of Ozone Pollution

In the following study, we focus on the features of ozone distribution and meteorology at 14:00 17th October, as their features were similar everyday. As shown in Fig6, was the ozone concentration distribution over PRD at 14:00 17th October. High ozone concentration was found at the site B, which might be strongly influenced by the emission source of Guangzhou. Meanwhile the coastal areas at both sides of PRE also had high ozone concentration.

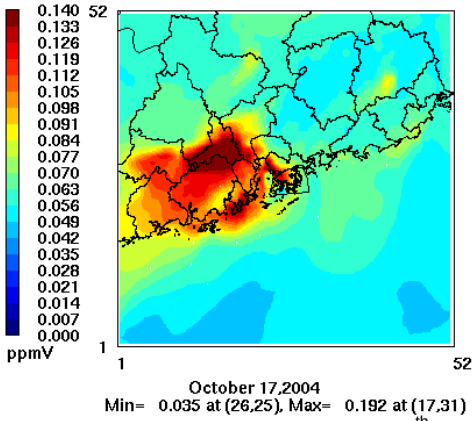

Figure-6. Ozone concentration at 14:00, 17th October

3.2 Meteorological Features over PRE

Land sea breezes play an important role in transporting air pollution over PRD (Lo JCF et al., 2006, Ding A et al., 2004). During 17th to 23th October, land sea breezes were predominant over PRE. As showed in Fig7, a band-shaped area of a low wind speed (<1.0 m/s) was formed, which might lead to the accumulation of pollutants transported from the emission sources, when land wind and sea wind encountered in the afternoon. To further examine the structure of land sea breezes, the vertical wind stream was plotted. Fig8-(a) presents a cross-section (latitude-sigma level) of u-w wind stream, and Fig8-(b) shows a cross-section (longitude-sigma level) of v-w wind stream, both of which were taken over the monitoring site of Xinken (Longitude:113.6^0, Latitude: 22.6^0). Fig7 and Fig8 revealed that strong air circulations existed over PRE. This pattern of air circulation and land sea breeze were frequently captured during the simulation. In Fig8-(a) and Fig8-(b), the axis of Y showed the sigma levels, the minimum sigma level is approximately equal to the height of 1700m. The height of the air circulation in Fig8 was about 700m. As shown in Fig8, there was a up-down air flow at the monitoring site of Xinken, which was formed by the air circulation over PRE.

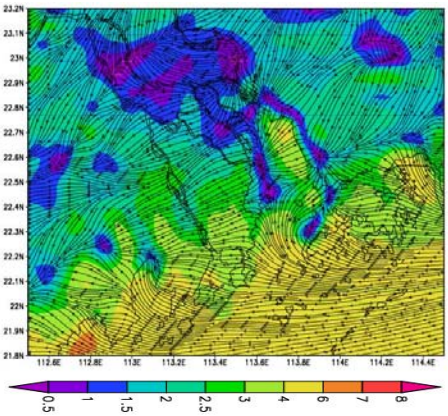

Figure-7. Horizontal distribution of surface wind stream at 14:00 17th October(colors show the horizontal wind, unit: m/s).

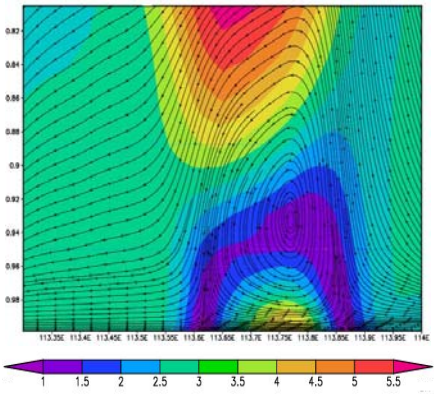

(a)

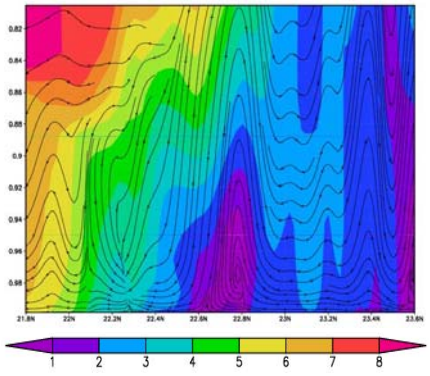

(b)

Figure-8. Vertical cross sections of wind stream taken over the monitoring site of Xinken at 14:00 17th October (a: u-w, b: v-w, colors show the horizontal wind, unit: m/s)

3.3 Vertical Ozone Profile over PRE

Fig9 showed the vertical ozone profile (vertical layer of CMAQ), which were taken over PRE. In both vertical profiles, the maximum ozone concentration was located at the sixth layer of CMAQ, approximately equal to the vertical height of 800m. And the distribution of vertical high ozone concentration had a similar shape with the vertical cross section of low wind speed area in Fig8. The high ozone concentration on the ground was dominated at both sides of PRE, which were also the locations of the band-shaped areas with the low wind speed (as shown in Fig8).

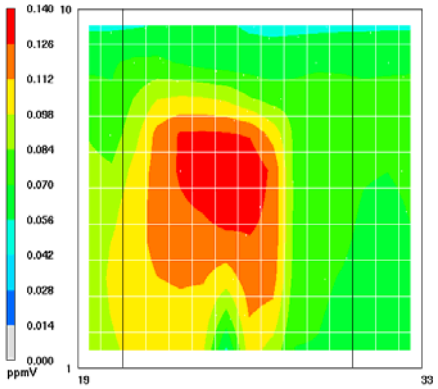

(a)

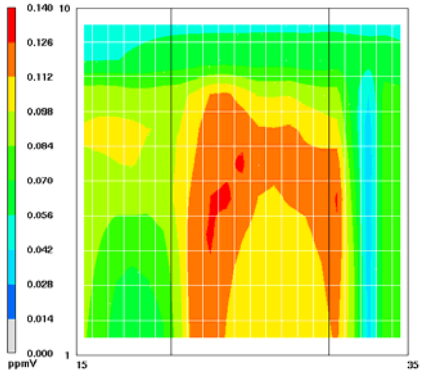

(b)

Figure-9. Vertical ozone concentration of Xinken at 14:00 17th Ocoter (a: latitude-vertical layer, b: longitude-vertical layer)

3.4 Process Analysis of Ozone over Xinken

To further analyze the ozone formation and transport over PRE, process analysis(PR) of ozone was carried out for Xinken. As shown in Fig10, most ozone concentration at the monitoring site of Xinken was contributed by vertical advection and vertical diffusion,while horizontal advection is the greatest process to consume ozone. Vertical and horizontal transport contribution of ozone can be revealed from Fig-8 and Fig9. As compared to transportation processes, chemical reactions contribute relatively less ozone concentration.

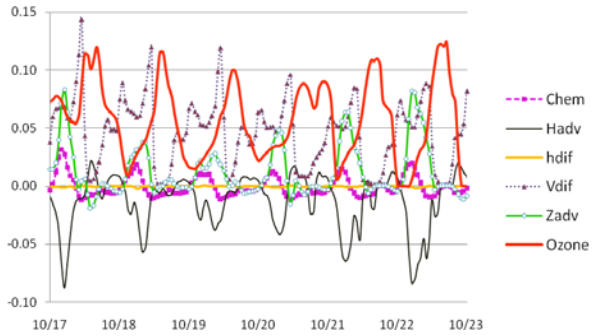

Figure-10. The contribution of various processes to ozone concentration at the monitoring site of Xinken (Chem- Chemistry reaction, Hadv- Horizontal advection, Hdif – Horizontal diffusion, Vdif- Vertical diffusioin, Zadv- Vertical advection)

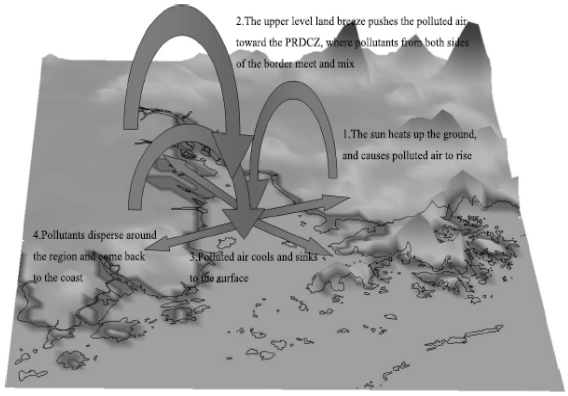

Figure-10. Schema of cross-section air pollutant transport and trapping mechanism by the air circulation over PRE (Lo JCF et al., 2006)

3.5 Conceptual Model

To better clarify the process of ozone transport and formation over PRE, a conceptual model was presented. Fig11 is a schematic picture showing the air pollutant transport and trapping mechanism over PRE. Pollutants are routinely emitted from power plants, vehicles, as well as from industrial commercial or residential buildings. In the sunny afternoon with weak background winds, the coastal urban areas can have temperature a few degrees higher than the surrounding oceanic areas. Air tends to rise over the urban areas because of higher temperature; thereby drawing in air from the oceanic areas, resulting in a convergent inflow at the lower levels into the inland urban areas during the day (the band-shaped areas with low wind speed shown along PRE in Fig7.). However, the air typically will only rise up to about one to two kilometers, and then it will spread out in the horizontal, and eventually sinks back in the nearby oceanic areas, forming a closed vertical circulation (as the ones shown in Fig8.) These land-sea breeze circulations are significant for air pollutant transport, as the air pollutant can come back to the inland area through the returning branch of the air circulation, leading to the trapping of air pollutants.

4. CONCLUSION

The models-3/CMAQ system was applied to simulate the ozone episode over PRD in October 2004. Comparison between the observed and simulated ozone concentration from three monitoring sites, indicated that the model prediction was in agreement with the measurement. The regional high ozone concentration was distributed at the southwest of Guangzhou, and the coastal areas at both sides of PRE also had high ozone concentration. There was a band-shaped low wind speed area over PRE, which was formed by the land-sea breeze. The air circulation over PRE was revealed by the vertical analysis of wind stream, vertical ozone profile and process analysis of ozone concentration at the monitoring site of Xinken indicated that the air circulation over PRE played an important role in transport and trapping ozone and its precursors at the coastal areas, then subsequently lead to high ozone concentration in these area.

5. ACKNOWLEGDGEMENT

This study was supported by China National Basic Research and Development Programs 2002CB410801. We would like to thank Daniel Cohan for covering the registration and travel of this presentation. And many thanks also extend to Yongtao Hu and Russell in setting up the coarse domain modeling of this study.

6. REFERENCE

Ding A et al,. 2004. Simulation of sea-land breezes and a discussion of their implications on

the transport of air pollution during a multi-day ozone episode in the Pearl River Delta of China. Atmospheric Environment. 38 (39): 6737-6750

Lo JCF et al., 2006. Investigation of enhanced cross-city transport and trapping of air pollutants by coastal and urban land-sea breeze circulations. Journal of Geophysical Research – Atmospheric 111(D14): Art. No. D14104.

Streets DG et al., 2003. An inventory of gaseous and primary aerosol emissions in Asia in the year 2000. Journal of Geophysical Research – Atmospheres 108 (D21): Art. No. 8809.

Song Xiang-yu et al., 2006. Development of Vehicular Emission Inventory in China, Chinese Journal of Environmental Science, Vol.27 No.6.

Zhao Jing et al., 2006. Studies on the emission rates of plants' VOCs in China. China Environmental Science, Vol.24 No.6.

****

These are the short abstracts from the 2007 CMAS Conference for presentations that did not submit extended abstracts

Implementing an Updated Carbon Bond Mechanism into the Community Multiscale Air Quality Model

Golam Sarwar and Deborah Luecken - National Exposure Research Laboratory, U.S. Environmental Protection Agency, Research Triangle Park, NC 27711

Greg Yarwood - ENVIRON International Corporation, 101 Rowland Way, Suite 220, Novato, CA 94945-5010

Gary Z. Whitten - Smog Reyes, PO Box 518, 112 Mesa Road, Point Reyes Station, CA 94956

William P. L. Carter - CE-CERT, University of California, Riverside, California 92521

An updated Carbon Bond (CB-05) Mechanism has been developed for the Community Multiscale Air Quality (CMAQ) model. It has been expanded to be appropriate for use as a general tropospheric chemistry mechanism so that conditions like pristine areas, winter temperatures, and high altitudes can be more accurately simulated. Additional species in the mechanism include ethane, internal olefins, terpenes, acetaldehyde, higher aldehydes (C3+ species), formic acid, acetic acid, methanol, ethanol, peroxyacetic acid, higher alkyl peroxy acetyl nitrate analogues, methylhydroperoxide, methylperoxy radical, acetyl peroxy radical, higher peroxy acyl radical (C3+ species). The mechanism contains 156 reactions and 51 chemical species. Rate constants for all reactions have been updated using the latest kinetic data recommended by the National Aeronautics and Space Administration/Jet Propulsion Laboratory and the International Union of Physical and Analytical Chemists. It has been validated by comparing simulation results with smog chamber data from the University of North Carolina, Chapel Hill and the University of California, Riverside. The CB-05 mechanism was incorporated into the CMAQ model and a new Euler Backward Iterative (EBI) solver for the mechanism was developed. Model simulations were performed using the CB-05 and CB-IV mechanisms for selected summer days in 2001. The modeling domain was the continental United States consisting of 148 x 112 horizontal grid cells with a 36 kilometer resolution. The Sparse Matrix Operator Kernel Emission (SMOKE) model was used to generate model ready emissions for the CB-05 and CB-IV mechanisms. The meteorological data for the study were derived from the mesoscale model (MM5). The predefined clean air vertical profiles for initial and boundary conditions were used for this study. The accompanying article provides a comparison of the predicted concentrations of selected model species.

DISCLAIMER
The research presented here was performed under the Memorandum of Understanding between the U.S. Environmental Protection Agency (EPA) and the U.S. Department of Commerce's National Oceanic and Atmospheric Administration (NOAA) and under agreement number DW13921548. This work constitutes a contribution to the NOAA Air Quality Program. Although it has been reviewed by EPA and NOAA and approved for publication, it does not necessarily reflect their policies or views.

MODELS-3/SMOKE UPDATES AND DEVELOPMENTS TO RUN CMAQ FOR US-CANADA MODELLING DOMAIN

An. Chtcherbakov, R. Bloxam, N. Reid, S. Wong, Ontario Ministry of the Environment, Toronto, Canada

CMAQ modelling results could be very sensitive to the emissions. Models-3 emission processor SMOKE was designed to process mostly US-specific input data. The completeness and the quality of the inventory and supplementary SMOKE files for Canada can be different for the USA. It demands serious updates and developments in the emission processing for Canadian portion of any US-Canada modelling domain. The procedure involves splitting the domain in two to process Canadian and US parts separately, using different sets of input files and then merging CMAQ-ready emission files together at the last processing step. The most important Canada-specific files which were generated /updated include: land-use file for the complete set of species/land-use types used in BEIS and with high spatial resolution; spatial surrogates and temporal profiles, stack characteristics, input mobile files, ammonia inventory file, holidays file; and usage of MOBILE6.2C (Canadian version of MOBILE6.2).

Multi-Pollutant Response Surface Modeling Using CMAQ: Development of an Innovative Policy Support Tool

Carey Jang, Sharon Phillips, Pat Dolwick, Bryan Hubbell, Tyler Fox

Over the last two decades, U.S. EPA has devoted significant efforts to developing air quality models for the assessment of regulatory impacts and designs of effective emissions control strategies. From O3 and PM control strategies assessment to evaluation of acid deposition and air toxics, photochemical air quality models are widely used to support policy analysis as part of decision-making process. Air quality models can be a powerful regulatory tool for comparing the efficacy of various emissions control strategies and policy decisions. However, due to the often enormous computational costs and the complication of the required emission inputs and processing, using complex air quality models to generate outputs to meet time-pressing requirement of policy analysis always present a challenge and is typically inefficient, if not ineffective. A promising tool for addressing this issue, Response Surface Modeling (RSM), has been developed by utilizing advanced statistical techniques to characterize the relationship between model outputs and input parameters in a highly economical manner. The RSM is a model of the model (i.e., air quality model); it is a reduced form prediction model using relatively simple polynomial representations to approximate model functions through the design of complex multi-dimension experiments. The RSM technique has recently been successfully tested and evaluated for PM 2.5 and ozone, respectively. In this paper we describe the development of multi-pollutant RSM application using Community Multi-Scale Air Quality (CMAQ) Modeling System developed at EPA. The processes involved in developing multi-pollutant RSM application using CMAQ will be discussed, including the selection of modeling domain and configuration, evaluation of the need of computer resources, development of multi-dimension experimental design for control strategies, development of CMAQ/SMOKE interface program to expedite model runs and eliminate massive emission inputs and processing needs, and implementation and verification of RSM technique.

Impact of Highway Networks on the Ambient Ozone Concentrations

Der-Min Tsai, Yee-Lin Wu, Department of Environmental Engineering, National Cheng Kung University, Ching-Ho Lin, Department of Environmental Engineering & Science, Fooyin University, and Hsin-Chih Lai, Education Center for Teacher, Chang-Jung Christian University

Ozone is one of major pollutants exceeding the ambient air quality standard in the southern Taiwan. The fractions of days each year exceeding the ambient air quality standard due to ozone have increased from 2.9% in 2000 to 4.6% in 2004. The contributions of mobile sources to NOx and NMHC were 44.7% and 17.6%, respectively, based on the emission inventory from Taiwan EPA. Note that the contributions from highways are significantly greater for NOx than those for NMHC and they are 14.7% and 1.6%, respectively. In this study, the effects of emissions from Highways 1 and 3 on the ambient air quality were evaluated by using CMAQ. The impacts were evaluated by comparing the results from different scenarios for spatial distributions with the same total emissions. The period December 12 to 16, 2002 of high ozone concentrations and extensive field measurement data was used in the following study. Two different scenarios were examined: H1 and H2 were for emissions from only Highway 1 and Highway 3, respectively. The model simulated results were compared with the observed data to evaluate the model performance. The mean error for upaired peak ozone concentration were generally less than 17%; those for paired ozone and NOx concentrations were less than 25%. Therefore, the model simulated results were in good agreement with observed data. The simulated results showed that the ambient O3 concentrations generally increased more than 2 ppb, with hourly increment up to 6 ppb, for both scenarios. Although the total emissions were the same, significant changes in the ambient air quality were found due to the difference in emission locations. The ozone concentrations decrease along the highway due to the effect of NO titration, if the emission from highway was increased. However, greater ozone concentrations were found at further downwind sites. Therefore, the ozone concentrations may have significant changes for different highway networks under the same total emission. The differences in ozone concentrations were due to the changes in emission locations.

A Performance Evaluation of the 2005 Release of Models-3 CMAQ

K. Wyat Appel and Brian Eder, NOAA/ARL/AMD

The Clean Air Act and its subsequent Amendments require the United States Environmental Protection Agency (EPA) to establish National Ambient Air Quality Standards (NAAQS) for pollutants such as ozone and particulate matter and to evaluate current and future air quality standards in order to protect human health and welfare. The best tools available for performing these current and future assessments are air quality models, such as the Community Multiscale Air Quality (CMAQ) model. The CMAQ model is an Eulerian grid model which incorporates meteorology, emissions and an air chemistry model to provide a one-atmosphere approach to modeling many atmospheric pollutants, including ozone, particulate matter and air toxics on both the regional and urban scales. CMAQ employs first principles to simulate concurrently the various atmospheric and land processes affecting the formation, transport and deposition of air pollutants and their precursors. As with any model, it is necessary to compare the model simulation against observations in order to understand the strengths and weaknesses of the model. This is particularly true of CMAQ due to its extensive use in the air quality community and in the development of

regulations and policies within the EPA. Therefore, an extensive and exhaustive evaluation of the 2005 release of the CMAQ model will be performed using data from several observational networks including: the Air Quality System (AQS) from which hourly observations of ozone data will be obtained from over 700 stations; the Clean Air Status and Trends Network which will provide weekly average concentrations of sulfate, nitrate, ammonium, and nitric acid (µg/m3); the Interagency Monitoring of PROtected Visual Environments (IMPROVE) network which will provide observations of sulfate, nitrate, PM2.5, and organic and elemental carbon (µg/m3) every third day for some 50 rural sites. Also utilized will be weekly averaged wet concentration (mg/l) and wet deposition (kg/ha) observations of sulfate, nitrate, and ammonium from the National Acid Deposition Network (NADP) from over 200 sites across the United States. When available, data from the Southern Aerosol Research and Characterization Study (SEARCH) will be utilized as well. The evaluation will include various spatial and statistical plots and summary statistics for model simulations at 12km horizontal grid spacing, along with some model to model comparisons.

An Operational Evaluation of the Eta-CMAQ Air Quality Forecast Model
Brian Eder, Daiwen Kang, Rohit Mathur, Shaocai Yu, Kenneth Schere

The National Oceanic and Atmospheric Administration (NOAA), in partnership with the Environmental Protection Agency (EPA), have been developing an operational Air Quality Forecasting System for the United States. The system, which couples NOAA s Eta meteorological model with EPA s Community Multiscale Air Quality (CMAQ) model, will be providing public forecasts of hourly, peak 1- and 8-hour ozone (O3) concentrations over the contiguous United States throughout the summer of 2005. An important component of this Air Quality Forecasting Program will be the development and implementation of an evaluation protocol. Accordingly, a suite of statistical metrics that facilitates evaluation of both discrete-type forecasts (observed versus modeled concentrations of O3) and categorical-type forecasts (observed versus modeled exceedances of both the maximum 1-hr and 8-hr standards for O3) will be developed and applied in order to characterize the performance of this model system. The metrics will be applied over various temporal and spatial resolutions, as well as over different concentration ranges. O3 data from more than 1000 monitors obtained from EPA s AIRNOW monitoring network will be used in the evaluation.

Annual Model Simulations and Evaluation of Particulate Matter and Ozone at 36 and 12 km Grid Resolutions
Sharon Phillips, Carey Jang, Norman Possiel, Patrick Dolwick, Brian Timin, Tom Braverman, Binyu Wang, Marc Houyoux, and Tyler Fox; EPA/OAQPS

An annual model application and evaluation study was performed for the continental United States using the U.S. EPA s Community Multi-scale Air Quality (CMAQ) modeling system. Annual model simulations for 2001 were conducted over the continental U.S. using a 36 km grid resolution. In addition, annual simulations at a 12km resolution were also performed for the Eastern U.S. The focus of this effort is to evaluate model predictions of PM2.5 component species and precursor gases (including ozone), and deposition of sulfate and nitrate. Based on the 36 km 2001 simulation, sulfate predictions compare very well with measurements over the summer months in the eastern U.S. where sulfate is the dominant PM2.5 species. The model appears to simulate the total nitrate (nitrate

PM and nitric acid, HNO3) fairly well, but the partitioning between nitrate PM and HNO3 leads to a modest overestimate of nitrate PM. The results indicate that the predictions of nitrate PM and HNO3 are highly sensitive to (1) the amount of ammonia (NH3) emissions, (2) dry deposition of HNO3 and NH3, (3) night time chemistry of N2O5 and HNO3, and (4) the diffusivity of night time atmospheric chemistry. In this paper the model performance results from the 36 km run are compared to those from the 12 km run to determine the importance of using finer resolution modeling for predicting PM2.5 species and deposition. Preliminary results show that at the 12 km grid resolution, the model is sensitive to finer resolution of meteorological processes, specifically cloud processes and wet deposition. These characterizations and relationships between the 36 km and 12km grid resolutions are further explored in this paper.

PERFORMANCE METRICS FOR AIR QUALITY MODELS ON COMMODITY PLATFORMS

George Delic, HiPERiSM Consulting, LLC, P.O. Box 569, Chapel Hill, NC 27514

This report examines performance of CMAQ (and other Air Quality Models) with two compilers on both the Intel Pentium 4 Xeon and Intel Pentium 64EMT processors for both 32-bit and 64-bit Linux operating systems. Our modification of the Linux kernel on these platforms allows the use of a performance event library to collect hardware performance counter values as the code executes. More than two dozen performance events were studied in categories such as floating point operations, instruction counting, conditional branching, cache access, data access, and TLB operations. The results helped to identify which performance metrics best indicate performance inhibiting factors for CMAQ during code execution. The metrics were also used to measure the effects of compiler optimization switches in improving performance and how performance changes when model data sets changed. The analysis of the results allowed a complete characterization of CMAQ performance as a function of the model under study. Some parallel performance results with specialized MPI tracing software were also collected. The consequences for expected performance ranges and work-load throughput on commodity platforms such as the Intel Xeon 64EMT are discussed in detail and a prognosis for performance on future commodity architectures is presented.

Development of a comprehensive mercury model in the parallel CMAQ framework: New science implementation and testing over the Continental United States

Che-Jen Lin, Pruek Pongprueksa, Thomas C. Ho, Taruna Vanjani and Hsing-wei Chu, Lamar University; Carey Jang, EPA OAQPS

The Mercury Model of the Community Multiscale Air Quality modeling system (CMAQ-Hg, Bullock and Brehme, 2002) has been modified to simulate the emission, transport, transformation and deposition of atmospheric mercury (Hg) in three different forms: gaseous elemental mercury (GEM), reactive gaseous mercury (RGM), and particulate mercury (PHG). The modified mercury model is incorporated into the framework of the CMAQ V4.4. In this paper, we evaluate implemented mercury science and update/modify the science components in the model. The new science components include (1) a new deposition velocity scheme for both GEM, RGM and PHg based on Wesley s formulation of dry deposition, (2) product speciation and distribution of gaseous phase oxidation of GEM, (3)

modification of aqueous phase sorption of dissolved Hg(II) to the insoluble particulate in atmospheric droplets, and (4) inclusion of vegetative emission in emission inventory processing, and (5) inclusion of additional gaseous phase oxidation by reactive halogens for future model implementation when emission inventory becomes available. For testing of the modified model, monthly simulations are performed with the NEI99 emission inventory estimates (for mercury and criterion pollutants) and USEPA July 2001 meteorology over 36-km Lambert Conformal grids covering the continental United State. With identical meteorology and anthropogenic emission inventory, the impact of the new science components is assessed in terms of the average gaseous concentration of GEM, RGM and PHg, as well as the total mercury dry and wet deposition flux in July 2001. The performance of the modified CMAQ-Hg is also evaluated using the mercury wet deposition data recorded by Mercury Deposition Network (MDN). Recommendations on future mercury model improvement are made based on the model evaluation analysis.

Study of the Impact of Dry Deposition Schemes in MCIP v2.3 on the Deposition Velocity and Concentration of Gaseous Pollutants Using CMAQ
Che-Jen Lin, Santosh Chandru, Thomas Ho and Hsing-wei Chu

Two dry deposition schemes, i.e., RADM and M3DRY, in the MCIPv2.3 are analyzed to investigate the impact of dry deposition schemes in MCIP v2.3 on the deposition velocity and concentration of gaseous pollutants in southeast Texas using CMAQ. In the analysis, MM5 outputs are processed using the two different deposition schemes for generating the deposition velocities of various gaseous pollutants. CMAQ simulations are then performed for the two deposition scenarios using identical emission inventory data (NEI99) and metrological fields (2002 MM5 output) in a 36-km CONUS domain. The simulated results are compared to the TCEQ air quality monitoring data in Houston-Galveston (HGA) and Beaumont-Port Arthur (BPT) non-attainment areas during the September 9-15, 2002 ozone episode. It is found that dry deposition of O3 and SO2 is controlled by the aerodynamic resistance in the urban areas of HGA and BPA, while the stomatal resistance is more important in the rural areas. Dry deposition velocities estimated by RADM do not exhibit strong diurnal variations and have similar magnitudes in both urban and rural areas of the studied domain, predominantly due to the high stomatal resistance. M3DRY-predicted deposition velocities show strong diurnal variations, and are strongly affected by soil moisture (thus the buoyant fluxes). The ozone concentrations obtained by M3DRY compare more closely to the observed ozone levels. Difference in calculated ozone deposition fluxes up to 10 and 5 g km-2 hr-1 during midday in the urban and rural areas, respectively, is observed between the two deposition schemes. Modeled concentrations of SO2 using RADM scheme are consistently higher than the concentrations using M3DRY scheme by 1-2 ppbv. Dry deposition of NO2, NO, PAN, PAA, N2O5, HONO, HNO3 is not the major removal pathway for these species in the domain based on the model results.

Trans-Pacific Transport of Air Pollutants and its impact on the Continental United States
Carey Jang, Binyu Wang, Sharon Phillips, David Streets, Adel Hanna, Jeff Vukovich, Aijun Xiu, Zac Adelman, Jung-Hun Woo, Joshua Fu, and Dennis Doll

There is increasing evidence that air pollutants originating from regions outside of

North America such as Asia could impact U.S. domestic air quality. A pioneer modeling project, the Intercontinental Transport and Climatic Effects of Air Pollutants (ICAP) project, has been undertaken at U.S EPA to help understand and assess these impacts associated with the intercontinental transport of air pollutants, including particulate matter (PM), ozone (O3), and mercury (Hg). A series of intercontinental modeling and emissions efforts have been undertaken over the pacific regions, including a 2001 Base year simulation, future (2030) scenarios, and several sensitivity studies (e.g., removal of man-made Asian emissions and North America emissions, etc.). The key modeling tool utilized in this project is U.S. EPA s Community Multi-scale Air Quality (CMAQ) modeling system. The trans-Pacific modeling results revealed that PM 2.5 and O3 can be transported across the Pacific Ocean over a time period of 5 to 10 days before reaching North America and the U.S. A sensitivity study by removing the Asian man-made emissions showed that the impact of Asian man-made emissions on North America appeared to be persistent through the entire year, although exhibiting seasonal variations. The spring (April) had higher impact for PM 2.5, up to 2~2.5 ug/m3 (monthly average) in the western U.S. and up to 1~1.5 ug/m3 in the eastern U.S., while the summer (July) and spring (April) has comparable impacts for O3, up to 5~6 ppb (daily max) in the western U.S. and up to 2 ppb in the eastern U.S. The continental influxes of air pollutants into the U.S. simulated by ICAP trans-Pacific modeling have also been compared to those by a global chemistry/transport model (GEOS-CHEM) and the conventional default static influxes (static boundary conditions) used in continental U.S. modeling. The results showed that the continental influxes provided by the ICAP trans-Pacific modeling was able to provide a better model performance in the western United States when compared against observed CASTNet and IMPROVE network data.

Development and Application of Two Advanced Plume-in-Grid PM Models, CMAQ-PM-APT and CMAQ-MADRID-APT

P. Karamchandani, K. Vijayaraghavan, S.-Y. Chen and C. Seigneur, AER, Inc.

Three-dimensional grid models, such as CMAQ, are frequently used to predict emission control impacts on concentrations of pollutants such as ozone and fine particulate matter (PM2.5). However, such models are limited in their ability to correctly represent the near-source transport and chemistry of emissions from elevated sources. These limitations are due to the inability of grid models, with typical horizontal resolutions of a few kilometers to tens of kilometers, to resolve stack plumes with initial dimensions of tens of meters. A common approach to address these limitations is to use Plume-in-Grid (PiG) modeling, in which a subgrid-scale representation of stack plumes is imbedded in the 3-D model. This approach has traditionally been used in ozone modeling studies. However, the errors associated with the gridded representation of point source plumes are just as important for PM2.5 as they are for ozone, since the chemistry leading to the formation of PM2.5 constituents, such as sulfate and nitrate, is significantly slower in the plume of a large NOx point source than it is in the background. This is particularly true in the initial stages of plume dispersion, when the plume dimensions are small relative to the grid resolution. Thus, using a purely grid-based approach can potentially lead to incorrect estimation of the impacts of large SOx and NOx point sources on ambient PM2.5 concentrations. We have previously developed an advanced PiG model for ozone based on CMAQ. This model is referred to as CMAQ-APT (CMAQ with Advanced Plume Treatment), and includes a state-of-the-science reactive puff model, SCICHEM, to resolve stack

plumes within CMAQ (Version 4.4, released in October 2004). Here, we present the extension of SCICHEM and CMAQ-APT to include two alternative treatments for particulate matter. In the first treatment, the PM algorithms from CMAQ are incorporated in SCICHEM, and the resulting model, SCICHEM-PM, is imbedded into CMAQ to develop CMAQ-PM-APT. In the second treatment, the PM algorithms from CMAQ-MADRID are used to develop SCICHEM-MADRID, which is then incorporated in CMAQ-MADRID, resulting in CMAQ-MADRID-APT. The primary differences between these two treatments are in their representation of the particle size distribution and the formation of secondary organic aerosols. We also present the results from the applications of the two models for January and July 2002 in the southeastern United States. The modeling data sets from the Visibility Improvement State and Tribal Association of the Southeast (VISTAS) Study are used in the simulations. We present the impacts of using a PiG treatment on predicted ozone and PM2.5 concentrations as well as a comparative performance evaluation of the base and PiG models.

On the Possibility of Off-line Diagnostic Analysis of CMAQ Model Performance Using an Efficient Positive Matrix Factorization Method

Jinyou Liang, Bruce Jackson, Planning and Technical Support Division, Air Resources Board, California Environmental Protection Agency, and Ajith Kaduwela, Planning and Technical Support Division, Air Resources Board, California Environmental Protection Agency, and Department of Land, Air and Water Resources, University of California at Davis

Grid-based photochemical air quality models, such as CMAQ, often require a large amount of input data and generate large amount of output data. Due to the large volume of input/output data, the error diagnostics has become a demanding task. Implementation of process analysis in CMAQ was shown to provide some helpful information on certain processes. However, it has to be run on-line and thus reducing the computational efficiency. A complementary off-line diagnostic tool is desirable especially if the computational efficiency is an issue as is the case in northern California. Receptor-based analysis, such as positive matrix factorization (PMF), may be useful as an off-line diagnostic tool in model performance analysis. We have conducted a multi-week simulation of particulate matter using CMAQ in central California for a 2000-2001 winter episodes captured during the California Regional PM10/PM2.5 Air Quality Study (CRPAQS). Using an efficient PMF method developed recently by Liang and Fairley, we explored the advantages of factorizing a large data set that includes hourly averaged concentrations of gaseous and PM pollutants, meteorological parameters, and emissions from/for CMAQ simulations. The implications of this exercise will be discussed, in terms of possible diagnostic analysis of CMAQ model performance evaluation for the 2000-2001 winter CRPAQS episode.

CMAQ Size Distributions in the Pacific Northwest with Ternary Nucleation

David S. Covert and Clifford F. Mass, University of Washington; Jack Chen, Washington State University

Several investigators have tested CMAQ's prediction of PM2.5, but little attention has been paid to its representation of the entire size distribution. Evaluation of CMAQ version 4.4 has shown an under-prediction of aerosol number by a factor of 10 to 100, especially in the Aitken mode (i.e., ultrafine or less than 100 nm diameter). This error was consistent in space and time and not obviously related

to an error in gaseous concentrations, meteorological input, or aerosol mass. While many factors could be responsible for this error, the binary H2SO4-H2O nucleation parameterization in the model is not appropriate for the sulfate-poor Pacific Northwest environment. Therefore, a ternary H2SO4-H2O-NH3 parameterization was implemented in CMAQ. Performance will be presented by comparison to the binary parameterization and to number and size distribution measurements from the Pacific Northwest 2001 (PNW2001) and Pacific 2001 field campaigns.

Development of an Improved Process-Based Ammonia Model for Agricultural Sources

Zion Wang (UCR), Ruihong Zhang (UCD), Gerard Mansell (ENVIRON), James Fadel (UCD), Tom Rumsey (UCD), Jactone Arogo (VT), Hongwei Xin (ISU)

Ammonia is an important atmospheric pollutant that combines with sulfuric acid and nitric acid to form aerosol sulfates and nitrate, respectively. These aerosol species are major components of fine particulate matter (PM) and contribute significantly to visibility impairment. In the United States, an estimated 55% of total ammonia emissions come from livestock and 24% from fertilizer use. Estimates of ammonia emissions factors are both highly variable and uncertain. Emissions factors vary depending on meteorological conditions and seasonal and regional differences in farming practices. Previous ammonia emissions inventories have not adequately characterized seasonal and geographical variations in emissions factors. In addition, recent chemical transport modeling suggests that daily and hourly variability in ammonia emissions is required to model accurately the formation of ammonium nitrate and ammonium sulfates. Because of difference among animals and farming practices it is necessary to develop animal specific models for the major livestock categories including: dairy cows, beef cattle, hogs, chickens, and turkeys. An improved processed-based ammonia model was developed to consider each of the processes occurring on a typical livestock farm, and calculates the resulting ammonia emissions. By tracking the amount of manure through each stage at the farm and using mass conservation, the total ammonia emissions for each process and for the farm as a whole is estimated. The main processes treated in the model include the nitrogen excretion from the animals, animal housing, feedlot operation, manure storage and land application of manure. Comparisons of the new ammonia emission estimates with existing ammonia emission inventories will be presented.

Development of the CMAQ-UCD sectional aerosol model

K. Max Zhang and Anthony S. Wexler, University of California at Davis

In collaboration with USEPA Atmospheric Modeling Division, we incorporated a sectional, dynamic partitioning aerosol module into the USEPA CMAQ framework and developed a new model named CMAQ-UCD. CMAQ-UCD is currently being employed to simulate aerosol dynamics in two locations, Tampa Bay, FL, and the San Joaquin Valley, CA -- these results are discussed in companion presentations. The former simulation emphasizes formation of coarse nitrate particles, and the latter investigates the severe secondary ammonium nitrate formation in fine particles. This talk serves as a general introduction to CMAQ-UCD, including modeling structure, aerosol thermodynamics, particle size and aerosol dynamic representations, and numerical integration using an Asynchronous Time-stepping (ATS) scheme.

Implementation and Testing of EQUISOLV II in the CMAQ Modeling System
Yang Zhang, North Carolina State University; Mark Z. Jacobson, Stanford University

Although numerous aerosol thermodynamic modules have been developed in the past two decades, numerical accuracy and computational efficiency remain challenges in simulating gas-particle partitioning and chemical equilibrium in three-dimensional (3-D) air quality models (AQMs). Most modules that are currently used in 3-D AQMs are computationally efficient but numerically less accurate and vice versa. In this study, a detailed aerosol thermodynamic module, EQUISOLV II, was first compared with ISORROPIA that is currently used in the U.S. EPA Models-3/Community Multiscale Air Quality (CMAQ) modeling system over 560 typical ambient conditions. The relative accuracy and computational speed of EQUISOLV II were studied by changing its physical options (e.g., metastable vs. stable) and varying the number of iterations for activity coefficients, water equation, and equilibrium equations to determine an optimal configuration that provides the best compromise between accuracy and efficiency. EQUISOLV II with the optimal configuration will then be implemented into a 3-D host model (e.g., CMAQ and/or CMAQ-MADRID) to further test its accuracy and efficiency using available observational data. Its performance will be examined and discussed.

Simulating with CMAQ the transport of PAHs over Europe
Armin Aulinger, Volker Matthias, Markus Quante, GKSS Research Centre Geesthacht, Germany

PAHs have been recognized as significant air borne carcinogens for several decades. They are hardly decomposed and can be transported over large distances. However, it is not yet possible to precisely quantify the risk of human exposure to those compounds due to missing long-term studies about ambient air concentations and depositions that can only be performed with the aid of numerical models. Most of these carcinogenic substances have a low vapor pressure at ambient air temperatures that are common in Middle-Europe and are, thus, mainly transported in the atmosphere bound to particles. To achieve our goal of doing long-term studies about PAHs and other POPs with a focus on coastal regions it is necessary to have a numerical modeling system with an advanced aerosol chemistry and aerosol dynamics module that allows modeling both in coarse and fine spatial resolution and the possibility of easily incorporating new chemical mechanisms. All these prerequisites are fullfilled by the Models-3 Community Multiscale Air Quality (CMAQ) modeling system. CMAQ 4.4 has been modified to read the emission species Benzo(a)Pyrene (BaP) as example PAH. The split between the modes, transport and deposition of aerosol bound BaP is processed equal to the primary organic aerosols. To account for the partitioning between gas and aerosol phase a new module was added to the model. The algorithm is based on the Junge Equation. The entire model domain covers the European continent at a grid cell size of 54x54 km2. A smaller domain that covers the North Sea coast from the Netherlands to Denmark with a cell size of 18x18 km2 was nested into the large domain. Within this region first model runs of an episode in September 2001 were carried out. The resulting concentration fields have been compared to measured monthly means, which suggested a reasonably well performance of the model.

Layer Dependent Horizontal Advection in CMAQ

Jeffrey Young and Jonathan Pleim, NOAA

A layer dependent horizontal advection scheme has been developed that allows for multiple advection steps per synchronization step in upper layers dominated by high winds. Results from both the standard CMAQ Piece-wise Parabolic Method for advection and a new, explicit mass-conserving scheme are demonstrated.

Examining the Role of in-situ Aircraft Emissions on Photolysis Rates with a Prototype Inline photolysis module within CMAQ
Frank Binkowski*, Sarav Arunachalam*, Zac Adelman*, and Joe Pinto**; *Carolina Environmental Program, The university of North Carolina at Chapel Hill, **US EPA, Research Triangle Park

An inline photolysis module has been developed for CMAQ. The module calculates actinic fluxes at every vertical level in each of seven intervals from 291 to 850 nm as well as the total surface irradiance within each interval. Aircraft emit vapors as well as particles. This study concentrates on the effect of carbon particles emitted by aircraft at all flight altitudes on the actinic flux, the surface irradiance, and the photolysis rate for NO2 in the lowest layer.

A proposed coupling of natural mercury emissions and deposition in CMAQ
Jesse Bash, Thomas Meyer, Patricia Bresnahan, David Miller

It is known that mercury is readily re/emitted from and deposited to natural surfaces. Recent measurements have shown that there is a dynamic interaction between the deposition and emissions from vegetative surfaces. However, current emission and deposition models usually calculate emissions and depositions separately, often in different models. By coupling natural emissions models and depositions in an air quality model, flux dynamics can be approximated more realistically and strict conservation laws can be applied to the surface mercury pool. We will outline a newly developed model for predicting the bidirectional flux of mercury across the leaf stomatal interface, the leaf surface, soil surfaces, and surface water to be developed in the CMAQ model framework. Conservation laws will be applied to the ground water, soil, surface water, and vegetative pools of mercury allowing the model to predict sinks and sources of mercury at the surface interface.

Modelling Toxic Air Contaminants from Ethanol Blend Fuels using a Modified SAPRC-99 Chemical Mechanism
Xin Qiu, RWDI AIR INC.; William P. L. Carter, Chao-Jung Chien, University of California, Riverside; Mike Lepage, RWDI AIR Inc.; Zion Wang, University of California, Riverside; Wayne Boulton, Martin Gautier, RWDI AIR Inc

To model toxic air contaminants and the associated health impacts with ethanol blend fuels, the authors undertook a study and introduced a new version of the SAPRC-99 condensed chemical mechanism. This mechanism with explicit 1,3-butadiene and benzene chemical species were implemented into the Models-3 system. The upgrades to the Models-3 system included: the creation of a new set of SAPRC-99 speciation programs and speciation database; the integration of the new speciation database with SMOKE (v1.3); and the modification of the SAPRC-99 chemical mechanism in CMAQ (v4.3). The study included the application of the new SMOKE/CMAQ system to model the effects of on-road vehicles operating on 10% ethanol blend gasoline (E10) on toxic and photochemical pollutants in two

distinct regions in Canada. Emissions were calculated using an updated and Canadianized version of the MOBILE model (Mobile6.2C+) to account for better understanding of emissions about toxic species and ethanol permeation / NOX effects. These data were then integrated into the regional emission inventories for SMOKE emission processing. Based on the application of the new modelling system, it was possible to explicitly identify concentration changes of toxic species such as 1,3-butadiene, benzene, acetaldehyde, formaldehyde, along with carbon monoxide nitric oxide, nitrogen dioxide and ozone, etc. for different emission scenarios. Deposition rates and aerosol concentrations were also simulated. The results from this work are currently being integrated into comprehensive health impact studies performed by Health Canada.

Revised treatment of N2O5 hydrolysis in CMAQ
Prakash Bhave, Golam Sarwar, Wyat Appel, and Robin Dennis

The treatments of homogeneous and heterogeneous hydrolysis of dinitrogen pentoxide (N2O5) will be updated in the Community Multiscale Air Quality (CMAQ) model version 4.6 based on recent reports in the scientific literature. In CMAQ v4.3 - v4.5.1, the heterogeneous reaction probability (gN2O5) ranged from 0.002 to 0.02 as a function of aerosol sulfate and nitrate concentrations. Recent laboratory studies suggest that gN2O5 is also affected by temperature (T) and relative humidity (RH). By adding T and RH dependence, gN2O5 values will decrease over most of the U.S. in the winter and increase slightly in the summer. Recent studies also suggest that nitric acid (HNO3) can be produced via gas-phase reactions involving N2O5 and water (H2O). These reactions, which had been shut off since CMAQ v4.3, will be activated in the Carbon Bond 2005 (CB05) and Statewide Air Pollution Research Center (SAPRC99) mechanisms released with CMAQ v4.6. Model simulations using the new hydrolysis treatments will be performed using the CB05 mechanism for selected months in 2001. Preliminary results suggest that the revised treatments decrease total nitrate concentrations during winter and have mixed effects in the summer. The effects on ozone concentrations were found to be small. Comparisons of the modeled results with observations will be presented. [Editorial note: the character "g" in "gN2O5" above was intended to be the Greek letter, gamma.]

MCIPv3: Using WRF-EM Output with CMAQ
Tanya L. Otte and Jonathan E. Pleim (NOAA/ARL/ASMD and EPA/ORD/NERL/AMD)

The Meteorology-Chemistry Interface Processor (MCIP) has been upgraded to include the capability to process output from the Weather Research and Forecast (WRF) Model using the Eulerian Mass (EM) core (also known as the Advanced Research WRF (ARW) core or the National Center for Atmospheric Research (NCAR) core). The new version of MCIP, which will be known as MCIPv3, will be released to the CMAQ community in conjunction with CMAQv4.5 in Fall 2005. This paper reports on the technical upgrades that were included in MCIPv3 to add the WRF processing capability. In addition, a preliminary evaluation of the WRF output for CMAQ will be presented. Disclaimer: The research presented here was performed under the Memorandum of Understanding between the U.S. Environmental Protection Agency (EPA) and the U.S. Department of Commerce s National Oceanic and Atmospheric Administration (NOAA) and under agreement number DW13921548. Although it has been reviewed by EPA and NOAA and

approved for publication, it does not necessarily reflect their views or policies.

CMAQ model development for PCBs and PCDD/Fs and its Applictaion in the Simulation of Transport, Transformation and Deposition of PCBs and PCDD/Fs in North America

Fan Meng, Baoning Zhang, Philip Gbor, Deyong Wen, Chune Shi, Fuquan Yang, James Sloan, Waterloo Center for Atmospheric Sciences, University of Waterloo

PCBs, PCDDs and PCDFs are persistent, bioaccumulative, and toxic pollutants. Some of them are semi-volatile and can, in both gaseous and aerosol phases, be transported long distances in the atmosphere and deposit by dry and wet processes to the surface, where they can bio-accumulate in the food chain. WCAS has developed model system for PCBs and PCDD/Fs based on the U.S. EPA s SMOKE/CMAQ system. In this model system, PCBs and PCDD/Fs have been speciated into 22 and 17 congeners respectively using the SMOKE emission preprocessing model. CMAQ has been modified to simulate the transport, diffusion and deposition of the speciated PCBs and new CMAQ model components have been created to describe gas/particle partitioning and chemical reactions between OH radicals. The CMAQ-PCBs and CMAQ-PCDD/Fs models have applied to simulate the transport, transformation and deposition over North America domain for 2000. The model results have been compared with monitoring data.

Development and testing of a module for estimating spatio-temporal dynamic pollen emission rates

1Christos Efstathiou, 1Nilesh Lahoti, 2Alper Unal, and 1Panos Georgopoulos 1Environmental and Occupational Health Sciences Institute (EOHSI), a joint Institute of UMDNJ - Robert Wood Johnson Medical School and Rutgers University, Piscataway, NJ 2MACTEC, Trenton, NJ

Allergic diseases represent a complex health problem that is receiving increased attention. Europe has succeeded in unifying a network of 400 monitoring stations that share pollen counts through the European Aeroallergen Network (EAN) pollen database. Similarly, the emission and dispersion of particles of biogenic origin, such as aeroallergens, is getting an increasing interest. There is strong evidence supporting the hypothesis that in urban areas, the synergism of pollen and other air pollutants exacerbates respiratory diseases like asthma and allergic rhinitis. A prototype algorithm for simulating the emissions of allergenic particles originating from major tree families of the New York/New Jersey region was developed by extending the approach used for estimating biogenic gas emissions in the Biogenic Emission Inventory System (BEIS). A spatio-temporal vegetation map was derived from a number of different remote sensing sources. Ground level measurements of pollen levels were analyzed and correlated with environmental conditions in order to establish source strengths and the temporal extent of the pollen-shedding period. Photosynthetically Active Radiation (PAR), the absorbed fraction of radiation, which is a major indicator of the state and productivity of vegetation, was closely examined. A preliminary comparison of results derived from simulations utilizing the new pollen emission model is presented: PAR estimates from the 5th generation Mesoscale Model (MM5) and the Community Multiscale Air Quality (CMAQ) model are compared with observations from the Surface Radiation monitoring network (SURFRAD) and with estimates derived from the Moderate Resolution Imaging Spectroradiometer (MODIS). Finally, a framework for aerobiological modeling applications is introduced and its

advantages are discussed vis-à-vis the limitations posed by the lack of temporally resolved dynamic vegetation mapping and of a modern, automated pollen monitoring network for the US. This work is funded in part by a University Partnership Agreement between USEPA and EOHSI. Viewpoints expressed here are do not necessarily reflect views of the USEPA or its contractors.

Efficient Techniques for Sensitivity and Uncertainty Analysis of Multiscale Air Quality Models

Sastry Isukapalli, Sheng-Wei Wang, Nilesh Lahoti, and Panos Georgopoulos; Environmental and Occupational Health Sciences Institute (EOHSI), a joint Institute of UMDNJ - Robert Wood Johnson Medical School and Rutgers University, Piscataway, NJ

Ambient air quality modeling, using numerical simulation systems such as the Community Multiscale Air Quality model (CMAQ), involves uncertainties of multiple origins, including uncertainties in the modeling of meteorology, emissions, and chemical interactions. Therefore, uncertainty propagation and identification of contributions of input uncertainties to output uncertainties are important tasks. Traditional techniques such as Monte Carlo and Latin Hypercube Sampling impose significant computational demands, typically requiring several hundreds to thousands of simulations to obtain combined sensitivity and uncertainty information. Recently developed, computationally efficient, alternative techniques include the Stochastic Response Surface Method (SRSM) and the High Dimensional Model Response (HDMR), which have been implemented as modules of the MENTOR system (Modeling ENvironment for TOtal Risk studies). SRSM approximates model outputs as probabilistic response surfaces involving orthogonal polynomials of random variables ("polynomial chaos"), whereas HDMR approximates model responses in terms of orthogonal polynomials in the deterministic space. This presentation focuses on the implementation and evaluation of the SRSM and HDMR to the assessment of the impacts of uncertainties in emissions estimates on different CMAQ model outputs of concern, as well as on other important metrics such as population-weighted mean concentrations, and number of exceedances of ambient concentration standards. The SRSM and HDMR are evaluated from the perspective of (a) estimating output uncertainties, (b) assessing contributions of individual input uncertainties, (c) computational efficiency, and (d) ability to provide an approximate model. This work is funded in part by a University Partnership Agreement between USEPA and EOHSI. Viewpoints expressed here do not necessarily reflect the views of USEPA or its contractors.

Regional/Urban Air Quality Modeling in Beijing and Shanghai

Joshua Fu, The University of Tennessee, Carey Jang, USEPA OAQPS, David Streets, Argonne National Laboratory, Zuopan Li, The University of Tennessee, Kebin He, Tsinghau University, Litao Wang, Tsinghua University, Qiang Zhang, Tsinghua University, Jung-Hun Woo, NESCAUM

Air pollution has become one of the most important problems of megacities such as Beijing and Shanghai and has serious impacts on public health, causes urban and regional haze. The Models-3/CMAQ modeling application that has been conducted to simulate multi-pollutants in China is presented. The modeling domains cover East Asia (36-kmx36-km) including Japan, South Korea, Korea DPR, Indonesia, Thailand, India and Mongolia, East China (12-kmx12-km) and

Beijing/Tianjing, Shanghai (4-kmx4-km). For this study, the Asian emission inventory based on the emission estimates of the year 2000 that supported the NASA TRACE-P program is used. However, the TRACE-P emission inventory was developed for a different purpose such as global modeling. TRACE-P emission inventory may not be practical in urban area. There is no China national emission inventory available. Therefore, TRACE-P emission inventory is used on the East Asia and East China domains. The 8 districts of Beijing and Shanghai local emissions inventory are used to replace TRACE-P in the area of the 4-km domains, respectively. The meteorological data for the Models-3/CMAQ run are extracted from MM5. The model simulation is performed in four seasons (January, April, July and October) in 2001. The model results are shown O3 concentrations are in the range of 80 120 ppb in the urban area. Lower urban O3 concentrations are shown in Beijing areas, possibly due to underestimation of urban man-made VOC emissions in the TRACE-P inventory and local inventory. High PM2.5 (~75ug/m3 in summer and 150ug/m3 in winter) were simulated over metropolitan & downwind areas with significant secondary constituents. More comprehensive simulations in the Beijing, Shanghai areas are presented with sensitivity analysis. A comparison against available ozone and PM measurement data such as weekly average of PM2.5 and PM10 in Beijing, Shanghai is presented. The local emission inventory improvement in China is to be suggested to investigate. The modeling configuration of the Beijing 4-km x 4-km domain is to demonstrate the development of cost-effective control strategies for the air pollution control of the air quality management plan for 2008 Olympic Game in Beijing and 2010 World Exhibition in Shanghai.

Modifications to SMOKE for WRF-Chem and Real-Time Forecasting
Coats, C.J., Condrey, J.W., and Vukovich, J, BAMS

Numerous changes were necessary to the meteorologically modulated parts of SMOKE in order for it to function as part of thw WRF-Chem system, and more generally for air quality forecasting applications. These changes are described, and the reasons for them are given.

Sub-Grid Scale Terrain Effects in Air Quality Modeling
Coats, C.J., Condrey, J.W., and Vukovich, J, BAMS

A methodology is presented for the parameterization of sub-grid scale terrain effects upon emissions and dry deposition, and for correcting grid-scale met-model terrain error due to met-model terrain smoothing, with associated modeling results.

The Roadmap for MADRID: Model Development for the Next Release and Beyond
Betty K. Pun, Krish Vijayaraghavan, Prakash Karamchandani, Christian Seigneur, Robert J. Griffin, James F. Pankow, Donald Dabdub, John H. Seinfeld, Eladio M. Knipping, Leonard Levin, Naresh Kumar

The Model of Aerosol Dynamics, Reaction, Ionization, and Dissolution (MADRID) implemented within the CMAQ modeling framework, provides an alternative, sectional treatment for simulating the formation and fate of particulate matter (PM) in the atmosphere. This presentation reviews recent model development efforts focused on improving the simulation of organic PM in CMAQ-MADRID and segues into an overview of development goals for the next MADRID release and

beyond. The recently optimized secondary organic aerosol (SOA) module used in MADRID 1 is based on empirical data from environmental chamber experiments. Anthropogenic SOA precursor gases are represented by two aromatic compound and two additional anthropogenic precursors have been added to represent SOA formation from long-chain alkanes and PAH species. Biogenic SOA precursors are represented by five monoterpenes and a sesquiterpene. The presence of water in an organic PM mixture affects the characteristics of the mixture including the average molecular weight of the absorbing medium and the activity coefficients of the condensed compounds. The role of water on the partitioning of SOA has been investigated and the relative humidity (RH) dependence of the partitioning coefficients is now parameterized in the model. The CMAQ-MADRID framework includes an option for detailed treatment of mercury chemistry and deposition, as well as the Advanced Plume Treatment (APT) plume-in-grid algorithm. The APT algorithm can also be run wholly within the CMAQ framework, i.e. without the MADRID modules. Model development goals for the next release include the parallelization of all components of the CMAQ-MADRID framework. Development goals for future release include the development of a computationally efficient MADRID 2 option based on the Caltech Atmospheric Chemistry Mechanism (CACM), the Model to Predict Multiphase Partitioning of Organics (MPMPO), and the Ionic-UNIFAC.2 activity coefficient model for inorganic/organic mixtures.

WRF[-Chem], the Models-3 I/O API, and SMOKE: a Coupled-System Implementation
Coats, C.J., Condrey, J.W., and McHenry, J.N., BAMS

By implementing the Models-3 I/O API into WRF and using its "Coupling Moder", we construct a coupled WRF-Chem/SMOKE integrated meteorology/air quality modeling system.

Development and Application of CMAQ-MADRID-Mercury
Krish Vijayaraghavan, Prakash Karamchandani, Shu-Yun Chen and Christian Seigneur, AER

CMAQ-MADRID (CMAQ with the Model of Aerosol Dynamics, Reaction, Ionization and Dissolution, MADRID) is a version of CMAQ that is publicly available and currently distributed by CMAS. We present here the incorporation of atmospheric mercury processes into CMAQ-MADRID. Mercury chemical transformations, dry deposition and wet deposition are based on the formulation used in the Trace Element Analysis Model (TEAM). The resulting model, CMAQ-MADRID-Hg, is a one-atmosphere model that can be used to evaluate the co-benefits of emission controls on ozone and PM ambient concentrations, and mercury deposition. The results of a simulation of mercury deposition over North America for 1996 are presented. Model simulation results are evaluated with 1996 wet deposition data from the Mercury Deposition Network (MDN). Simulated precipitation was identified as a significant source of uncertainty, particularly in the Carolinas and Texas. After the mercury wet deposition results were scaled with the observed/simulated precipitation amount ratios, model performance improved significantly. The coefficient of determination (r2) is 0.41, the normalized bias is 29% and the normalized error is 40%.

Development and Application of the CMAQ Plume-in-Grid Model

A plume-in-grid (PinG) treatment has been an integral component of the CMAQ

modeling system. The PinG approach was specifically developed to simulate the relevant processes governing pollutant concentrations in subgrid scale plumes released from major point sources within the CMAQ grid modeling domain. Since excessive dilution occurs when high NOx or SOx point source emissions are instantly emitted into large volumes of Eulerian grid cells defined for typical regional modeling domains, chemical processes and pollutant concentration levels from point source emissions are greatly impacted. Consequently, the PinG approach models the meteorological, photochemical, and aerosol processes at the appropriate spatial dimension by allowing for the realistic, gradual horizontal/vertical growth of each subgrid scale plume. The PinG treatment has been fully integrated into the CMAQ chemical transport model (CTM) and is applied during a CTM model simulation. A description of the technical approaches and capabilities of the key PinG science algorithms, the Plume Dynamics Model (PDM) processor program and the Lagrangian plume model (PinG module), will be provided. These modeling algorithms simulate plume rise, transport and dispersion in the horizontal and vertical, dry deposition, and chemical and aerosol processes in the plume sections released from multiple point sources. The PinG module simulates gas-phase chemistry and aerosol formation processes with the same algorithms applied in the CMAQ/CTM. The effort to adapt and incorporate the photochemical and aerosol algorithms into PinG will also be described. In addition, the decisions and processing procedures needed to apply the CMAQ/PinG treatment will be outlined. Results will also be presented from a model application during a summer period for a continental domain with a 32 km grid cell size where 53 of the largest point sources were subjected to the PinG treatment. Disclaimer: The research presented here was performed under the Memorandum of Understanding between the U.S. Environmental Protection Agency (EPA) and the U.S. Department of Commerce's National Oceanic and Atmospheric Administration (NOAA) and under agreement number DW13921548. This work constitutes a contribution to the NOAA Air Quality Program. Although it has been reviewed by EPA and NOAA and approved for publication, it does not necessarily reflect their policies or views.

Dispersion modeling of carbon monoxide during the COPP Study (2001)
Matthew Simpson and Sethu Raman

Observations of carbon monoxide during the COPP Study (2001) show higher concentrations along the roadside than at rural locations. Carbon monoxide concentrations were greatest along the roadside when wind speeds were weak. There is little difference between carbon monoxide concentrations along the roadside and the ambient locations when wind speeds are strong. A coupled mesoscale and Gaussian dispersion model is used to simulate the dispersion of carbon monoxide from road sources in Wake County, North Carolina. Major roads in Wake County are treated as line sources and emission rates are assigned a scaling factor depending on average traffic counts. Episodes of high simulated CO concentrations are associated with periods of light wind over the study domain. Strong winds episodes result in much lower daytime CO concentrations. Highest CO concentrations are simulated during the late afternoon hours when traffic and emission rates are greatest. During the night, concentrations are lower due to smaller emission rates. Regions of simulated low-level convergence result in high CO concentrations.

New Developments in Community Multiscale Air Quality (CMAQ) Model

Jonathan Pleim, Shawn Roselle, Jeffrey Young, Donna Schwede, and Prakash Bhave, Atmospheric Sciences Modeling Division, NOAA

An overview of recent developments in the CMAQ model will be presented. The focus will be on new features of the physical processes in the model system. A new PBL model, called the Asymmetric Convective Model version 2 (ACM2), which combines non-local and local closure techniques will be described. A modified subgrid convective cloud scheme that corrects some of the shortcomings of the current scheme will also be described. We will also present the latest updates to dry deposition, particularly some important modifications to aerosol dry deposition velocities. In addition, modifications of the cloud radiation attenuation algorithm are being investigated. The new release of CMAQ will have a new scheme for ensuring mass continuity and a new algorithm for specifying minimum vertical eddy diffusivity. Sensitivity tests of each of these updated model components will be presented with some simple evaluation against observed values. Aerosol processes will be only briefly outlined since this area will be covered in another presentation.

An overview of the NAM-CMAQ Air Quality Forecast Model Forecasts run at NOAA/NWS/NCEP operations

Jeff McQueen, Pius Lee, Marina Tsidulko and Geoff DiMego (NOAA/NWS/NCEP), Rohit Mathur, Jon Pleim, George Pouliout and Ken Schere (NOAA/ARL/ASMD), Paula Davidson (NOAA/NWS/OST)

NOAA and EPA have developed and operationally implemented a new ozone forecast capability, in response to Congressional direction. The NWS/ National Centers for Environmental Prediction (NCEP) North American Model (NAM) Eta model at 12 km is used to provide meteorological predictions for the EPA Community Multi-scale Air Quality (CMAQ) model to produce 48 h ozone predictions. The CMAQ system simulates various chemical and physical processes that are important for modeling atmospheric trace gas transformations and distributions. This paper describes the improvements to and performance of the NOAA NAM-CMAQ modeling system that are run on the NWS/NCEP operational computer center for real-time air quality forecasting. Two systems are tested and evaluated in the Summer 2005; the Eastern U.S domain and CONUS runs. The Eastern U.S. domain is run twice per day at 12 km resolution at 06 and 12 UTC with forecasts to 48 hours. This year the system was run with updates to the both the Eta-12 and CMAQ modeling systems including 6 hour cycling for initial CMAQ conditions, use of the NCEP Global Forecast System (GFS) ozone predictions (Lee, et al, 2004) to prescribe CMAQ upper lateral boundary conditions, and updates to the CMAQ model cloud scheme and emissions. Both experimental and developmental systems were run with gas-phase chemistry only, however, research runs were made over the Eastern U.S. with aerosols turned on. The NAM land surface model and cloud physics were also upgraded. These effects on air quality forecasts will be summarized.

The Nonlinear Response of Nitrate Replacement that Mitigates Sulfate Reductions: Gas Ratio as Indicator and Sensitivity to Errors to Total Ammonia and Total Nitrate

Robin L. Dennis and Prakash Bhave, NOAA/EPA, Atmospheric Modeling Division

There is concern that the possible nitrate nonlinear response of replacing sulfate when sulfate is reduced will greatly mitigate sulfate reduction benefits. The

particulate NO3- relative response factor (RRF) would be positive. An assessment with CMAQ shows that positive nitrate RRFs are predicted to occur when sulfate is decreased in the eastern U.S. We know from previous work that there are model input uncertainties or errors that introduce uncertainty in the nitrate predictions of the model. The objectives of this study are: 1) see if there is an indicator for the nonlinear nitrate replacement of sulfate that can be constructed from current ambient air concentrations, and 2) characterize how the nitrate RRF is affected by uncertainties associated with total ammonia (NHX) and total nitrate (TNO3). The analysis was carried out for the month of January 2002 using monthly averages to be consistent with model application practice. A winter period was chosen because nitrate is more stable at the colder temperatures and the nitrate replacement is an order of magnitude larger in winter than in summer. Analysis regarding the first question indicated that the Gas Ratio (GR), the ratio of free ammonia to TNO3 could be a good qualitative "predictor" of the nitrate RRF across the eastern U.S. However, the sulfate is not fully neutralized. Accounting for the degree of neutralization results in an Adjusted GR. Further analysis concluded that the Adjusted GR is the best qualitative "predictor" of the nitrate RRF. Nonetheless there is a good deal of uncertainty, i.e. 90% of the cells are within ±2 percentage points of the predicted nitrate RRF, but the trend is well captured. The analysis regarding the second question showed that the uncertainty in NHX is by far the most important contributor to uncertainty in the nitrate RRF. The uncertainty in NOX emissions, affecting TNO3, is a less important contributor and the uncertainty in the heterogeneous reaction probability to convert N2O5 to HNO3, also affecting TNO3, is a negligible contributor to the nitrate RRF uncertainty. The Adjusted GR did well at anticipating the nitrate RRF response to the NHX uncertainty, but it failed at anticipating the response to uncertainties affecting TNO3 due to other types of nonlinearities affecting response to these uncertainties.

Implementation and Initial Applications of Sea Salt Aerosol Emissions and Chemistry Algorithms in the CMAQ v4.5 - AERO4 Module

Uma Shankar*, Prakash V. Bhave**, Jeffrey M. Vukovich***, and Shawn J. Roselle**; *UNC-Carolina Environmental Program, **Atmospheric Sciences Modeling Division, Air Resources Laboratory, National Oceanic and Atmospheric Administration (on assignment to the National Exposure Research Laboratory, U.S Environmental Protection Agency), ***Baron Advanced Meteorology Systems

Sea salt aerosol constitutes an important component of the global background aerosol loading. Sea salt particles also influence the aerosol composition in coastal environments as they contribute surfaces for heterogenous chemical reactions with condensable and volatile species (H2SO4, HNO3 and NH3). Parameterizations for modeling the sea salt emission flux that have been developed and refined over the past 20 years for the open ocean source and the surf zone source applicable to 80% relative humidity (RH) and emitted particle dry radii from 0.03 - 10 um have been recently extended to the wide range of RH encountered in regional-scale modeling. The extended parameterizations have been implemented in CMAQ to simulate size-resolved and speciated sea salt emissions. The thermodynamics calculations have been appropriately modified to treat the sea salt species, and a new algorithm has been implemented in the aerosol module for the size-dependent mass transfer of the volatile species between the gas phase and the aerosol modes. Initial applications of the model for a CMAQ evaluation case over the eastern U.S. in 2001, and for a 2002 period during the Bay Regional

Atmospheric Chemistry Experiment (BRACE) campaign in Tampa Bay, FL, are described. The effects of sea salt aerosol on the fine aerosol composition are examined, and the model performance is evaluated against BRACE as well as network (IMPROVE, CASTNet, and STN) measurements.

Simulation of Texas August 2000 ozone episode using a Variable Grid Resolution air quality model
Alapaty, Arunachalam, et al.

The August 2000 ozone episode for the Houston-Galveston region was simulated using a newly developed variable grid resolution (VGR) air quality model. While the meteorological fields were interpolated to VGR grids, the emission sources were estimated using the recently developed VGR version of SMOKE system. Some of the highlights of this work are: 1. Better meteorological inputs were developed by using our surface data assimilation scheme (FASDAS) at 36, 12, and 4 km grids. 2. Satellite-derived SSTs were ingested into the MM5 simulations that used 4-km grid 3. Emission sources were estimated on the VGR grid as opposed to interpolation. 4. Horizontal diffusion and cloud process modules were developed for the VGR grids Results from a case study using the conventional (36, 12, and 4 km) and VGR simulations (36-4 km and 12-1km) will be presented.

Use of the CMAQ Modeling System for Estimating Visibility Progress in the Southeastern US for Complying with the Requirements of the Regional Haze Rule
Ralph Morris, ENVIRON International Corporation; Dennis McNally and Tom tesche, Alpine Geophysics, LLC; Gail Tonnesen, UCR; Jim Boylan, GA DNR; and Pat Brewer, VISTAS

The Visibility Improvement State and Tribal Association of the Southeast (VISTAS) is one of five Regional Planning Organizations (RPOs) that consist of states, tribal governments and federal agencies. VISTAS is charged with the management of haze, visibility and other regional air quality issues in the southeastern US. VISTAS has embarked on a multi-phase process of testing and evaluation of regional meteorological, emissions and air quality models that will be used to project visibility improvements as required by the regional haze rule. VISTAS has performed regional PM/ozone/visibility modeling of the continental US using a 36 km grid resolution and the eastern US using a 12 km grid resolution for the 2002 calendar year for a 2002 Actual and Typical base case simulation and the 2009 and 2018 future-years using the Community Multiscale Air Quality (CMAQ) modeling system. This paper discusses how the model was applied for the 2002 base case and the model performance evaluation. To improve model performance for Organic Carbon (OC) and Total Carbon Mass (TCM), the CMAQ Secondary Organic Aerosol (SOA) module was enhanced to include several important SOA processes not currently treated in CMAQ. The formulation of the updated SOA module and improvements in OC and TCM model performance are presented. The procedures used and the results of projecting visibility improvements at southeastern US Class I areas to 2018 are discussed, including which areas are estimated to achieve the Regional Haze Rule reasonable progress goal under currently mandated and expected control measures.

New Features in Version 3 of the MIMS Spatial Allocator
Alison M. Eyth, Benjamin Brunk, UNC Chapel Hill

The Multimedia Integrated Modeling System (MIMS) Spatial Allocator is open-source software for generating spatial surrogates for emissions modeling, changing the map projection of Shapefiles, and performing other types of spatial allocation without requiring the use of a commercial Geographic Information System (GIS). A new version of the Spatial Allocator was released in July, 2005. This new version can perform the following spatial allocation functions: create the inputs for biogenic emissions processing that are required by the Sparse Matrix Operator Kernel Emissions (SMOKE) modeling system; perform general spatial allocation functions, such as mapping gridded data to and from county-level data, mapping from grid to grid, and aggregating data from census tract to county levels; and print the attributes of shapes that are overlapped by a grid, bounding box, or set of polygons. Enhanced spatial surrogate related features in this version are the following: subsets of Shapefiles can be defined and used to generate surrogates or create smaller Shapefiles, surrogates can be generated based on a function of multiple attributes in one or more Shapefiles, surrogates can be generated using weighted sums of other surrogates, and new surrogates can be made by filling in the gaps of less comprehensive surrogates.

Recent Updates to the SMOKE Emissions Modeling System
Catherine Seppanen, UNC Chapel Hill

The SMOKE modeling system is used to process emission inventory data to create inputs for a variety of air quality models. Recent updates to SMOKE include processing for variable grid resolutions and integration with the Blue Skies fire emissions estimates model. Other updates to be discussed include enhancments to allow SMOKE to produce outputs for various toxics model such as ASPEN, ISCST3, and AERMOD. We anticipate that SMOKE v2.2 will be released shortly before the CMAS conference.

The CMAQ Graphical User Interface
Prashant Pai, Alison Eyth, Benjamin Brunk, Zachariah Adelman, Carolina Environmental Program, UNC Chapel Hill

The Community Multiscale Air Quality (CMAQ) Modeling System is designed to be a powerful air quality modeling and assessment tool supporting various applications ranging from regulatory assessments to scientific investigations. Due to the complex science knowledge and intricate software that constitutes CMAQ, there has always been an invisible barrier to its widespread adoption. The CMAQ Graphical User Interface (GUI) aims to lower this barrier, by providing an intuitive, easy-to-use visual interface. The CMAQ GUI is designed to simplify setting up, compiling and executing CMAQ for non-sophisticated users as well as enhance interaction for more experienced users. This paper will provide a preview of the interfaces and features included in the CMAQ GUI, and describe typical usages of the system.

Using EmisView to Quality Assure and Visualize Emission Modeling Data
Alison M. Eyth and Rajasooriyar Partheepan, UNC Chapel Hill; Marc Houyoux, U.S. EPA

EmisView is a new, open-source visualization tool that will improve the quality assurance of emissions data for use in air quality modeling efforts of states, Regional Planning Organizations (RPOs), and the U.S. Environmental Protection Agency (EPA). It works closely with emission models, including the Sparse Matrix

Operator Kernel Emissions (SMOKE) modeling system, and the CONsolidated Community Emissions Processing Tool (CONCEPT), which has been developed by the Midwest RPO. The analyses and graphics created by EmisView can be configured and repeated in an automated fashion. The first beta version of EmisView was released in June 2005, and an additional release will follow in September 2005. It will be released under a GNU Public License, which will enable modelers to examine its source code and enhance it as needed. EmisView is being developed to perform analyses that the states, RPOs, and EPA have identified as priorities. EmisView can plot emissions at various temporal and spatial resolutions with many types of plots (e.g., bar, line); display spatial plots of gridded, county, and source-level emissions; track a single source through all the stages of the emissions modeling process; and compare at least two emissions modeling runs (e.g., versions 1 and 2, or controlled versus uncontrolled). More information on the EmisView project is available at http://emisview.sourceforge.net.

Future Year Attainment Modeling in NC: An alternative look at health-related benefits

Saravanan Arunachalam and Andrew Holland, Carolina Environmental Program, University of North Carolina at Chapel Hill

Recent modeling performed for various 8-h ozone non-attainment areas in North Carolina demonstrated attainment of the National Ambient Air Quality Standard (NAAQS) in 2012 and 2017. A few monitors in the Charlotte region alone were projected to be in non-attainment for future year 2007. We used MAQSIP (a prototype model for the Models-3/CMAQ) with MM5 and SMOKE for modeling 4 different episodes in North Carolina at three different grid resolutions (36/12/4-km). To demonstrate accountability of the projected attainment, we present here results from additional analyses of health-related benefits. Specifically, we will look at impacts of modeled attainment demonstration by using a metric - potential population exposure - which takes into account population data in the areas of interest. We will also present results from using the EPA's Environmental Benefits Mapping and Analyses Program (BENMAP) to assess the health-related benefits from meeting these air quality goals.

PERFORMANCE ANALYSIS OF CAMX ON COMMODITY PLATFORMS

George Delic, HiPERiSM Consulting, LLC, Durham, NC and Byeong-Uk Kim and Harvey E. Jeffries, Department of Environmental Science and Engineering, University of North Carolina, Chapel Hill, NC

We present a performance analysis of CAMx with two compilers on both the Intel Pentium 4 Xeon and Intel Pentium 64EMT processors for both 32-bit and 64-bit Linux operating systems. Whole code performance is measured with hardware performance counters using the TCEQ 2000 Mid-course Review Scenario for the SIP with an episode from 8/22 to 8/31 in the Houston Greater Metro area. The goal of this study is to identify which hardware performance metrics best identify performance inhibiting factors for CAMX during code execution on commodity platforms. The effects of compiler switches in changing performance is investigated and reasons for differences identified by use of hardware metrics. Proposals for CAMX optimization are presented and the consequences for model throughput are summarized for current and future commodity architectures.

Diesel Particulate Matter Modeling and Inhalation Cancer Risk in Nashville, Tennessee, using Models-3/CMAQ

Luis A Diaz, Gregory D. Reed, and Joshua S. Fu

The fine and ultra fine sizes of diesel particulate matter (DPM) are of greatest health concern, which significantly contributes to the overall cancer risk from air toxics. The composition of these fine and ultra fine particles is composed principally by elemental carbon (EC) with adsorbed compounds such as VOCs, sulfate, nitrate, ammonia, metals, and other trace elements. The purpose of this research was to use EPA's Models3/CMAQ version 4.3 and CMAQ version air toxics to predict aerosol concentrations and inhalation cancer risk that come from diesel fueled sources (DFS) and air toxics respectively in the Nashville urban area, Tennessee, by linking the MM5v3 meteorological model, the Sparse Matrix Operator Kernel Emissions (SMOKE 2.0) model, and the National Mobile Inventory Model (NMIM). The national emissions inventory version 3 for the year 1999 (NEI99) was used in this analysis and the year 2003 was used as reference to compare the monitored concentrations and model performance. The modeling domain consisted of a 36 km domain. Five emissions scenarios were selected in the domain to compare the main results; base case without DFS, base case without biogenic emissions, base case without on-road DFS base case without, base case without heavy duty diesel vehicles (HDDVs), and the scenario considering the in effect regulations on mobile sources for the year 2020. The results showed that DPM contributed by almost 70% of the inhalation cancer risk that came from the total air toxics. The main DPM reductions on concentrations and cancer risk were due to not considering the HDDVs emissions and for the year 2020, which were 50% and 39% respectively. Finally, the contribution of the non-road sources on DFS also was significant.

Development and Use of a GIS Emissions Analysis Tool to Estimate the Probability of Regional Source Contributions to Haze
Sean M. Raffuse, Steve G. Brown, Dana C. Sullivan, Tami H. Funk, and Lyle R. Chinkin, Sonoma Technology, Inc.

A customized geographic information system (GIS) spatial mapping tool was developed to aid in the characterization of relationships between emissions and ambient observations. The tool, called the probability of regional source contribution to haze (PORSCH), combines back-trajectory meteorological analyses with emission inventories to calculate or visualize emissions source regions most likely to impact a user-selected site. PORSCH weights emissions geographically, temporally, and according to trajectory probability distributions. Thus, emissions that have the greatest potential to affect the location of ambient measurement are more heavily weighted in the correlation analyses. PORSCH has been used to facilitate an analysis of visibility conditions in Class I areas, and results of this analysis will be presented. This analysis can be a valuable component of integrated, corroborative research projects, which, when taken as a whole body of evidence, can be effective for developing conceptual models of regional haze phenomena, planning photochemical modeling efforts, and selecting control strategies.

A Modular System for Source-to-Dose Exposure Modeling of Co-Occurring Air Pollutants: Recent Developments and Computational Implementation
Sastry Isukapalli, Sheng-Wei Wang and Panos Georgopoulos, Environmental and Occupational Health Sciences Institute (EOHSI), a joint Institute of UMDNJ - Robert Wood Johnson Medical School and Rutgers University, Piscataway, NJ; Tom Pierce

and Jason Ching, National Exposure Research Laboratory (NERL), USEPA, Research Triangle Park, NC

The probabilistic source-to-dose modeling system, MENTOR/SHEDS-1A [Modeling ENvironment for TOtal Risk studies (MENTOR) using the Stochastic Human Exposure and Dose Simulation (SHEDS) approach in a "One Atmosphere" (1A) setting] characterizes cumulative exposures to co-occurring air pollutants by taking into account their physical and chemical interactions, and calculates exposure and dose profiles, while providing the ability to focus on time scales and subpopulations of interest. This is achieved through a sequence of steps involving (1) calculation of ambient outdoor concentrations using multiscale photochemical modeling, (2) spatiotemporal interpolation for developing census-tract level outdoor concentration fields, (3) calculation of microenvironmental concentrations that match activity patterns of the individuals in the population of each census tract considered, and (4) population-based dosimetry modeling that accounts for activity and physiological variability. The implementation of MENTOR/SHEDS-1A presented here improves upon previous versions by explicitly characterizing contributions of indoor sources, as well as effects of commuting patterns. A case study is presented focusing on modeling hourly resolved exposures over one year to ozone, formaldehyde, benzene, xylene, and toluene, for the urban Philadelphia, PA, and Camden, NJ areas. This case study utilizes the Models-3/CMAQ-AT (CMAQ-Air Toxics), which explicitly models a number of gas-phase air toxic compounds. Population exposures and doses are characterized with special focus on susceptible population groups such as the children and the elderly. The presentation focuses on methodological and computational issues relevant to implementing and optimizing the MENTOR/SHEDS-1A system for long-term population exposures. This work is funded in part by a University Partnership Agreement between USEPA and EOHSI. Viewpoints expressed here do not necessarily reflect the views of USEPA or its contractors.

Fast Spatio-Temporal Interpolation Modules for Photochemical Grid Based Air Quality Models

Sastry Isukapalli, Vikram Vyas, and Panos Georgopoulos; Environmental and Occupational Health Sciences Institute (EOHSI), a joint Institute of UMDNJ - Robert Wood Johnson Medical School and Rutgers University, Piscataway, NJ

Ambient air quality information from photochemical air quality models is often needed at resolutions higher than provided by regional scale models, such as the Models-3/Community Multiscale Air Quality (CMAQ). This is especially true for exposure assessment modeling, which requires ambient concentrations at census tract or census block levels, while the air quality models provide estimates at grid cells larger than 2 km x 2 km. Techniques such as the Spatio-Temporal Random Field (STRF) and the Bayesian Maximum Entropy (BME) have been recently used for subgrid interpolation of photochemical model estimates. These techniques are general in nature, and can be applied to both monitor data and model outputs, while not requiring a regular grid for the interpolation. However, there are significant performance limitations in using the current implementations of STRF and BME for the interpolation of massive datasets, such as the CMAQ outputs from an annual simulation; often the computational time for interpolation is of the same order of magnitude as the CMAQ simulation itself. Furthermore, there are several pre-processing steps involved in the application of the STRF and BME: (a) the CMAQ outputs have to be processed and transformed, (b) the outputs need

to be manually split into several large data sets, as the current implementations cannot handle such large data sets. This work presents recent improvements of the STRF modules available in the MENTOR (Modeling ENvironment for TOtal Risk studies) system, and provides modules for fast spatio-temporal interpolation on regular grids. These modules are designed to operate directly upon the standard formats of model outputs from several photochemical grid models, and are demonstrated by interpolating CMAQ model outputs at different scales. This work is funded in part by a University Partnership Agreement between USEPA and EOHSI. Viewpoints expressed here do not necessarily reflect the views of USEPA or its contractors.

Micro-development of CMAQ for California Regional Particulate-Matter Air Quality Study

Jinyou Liang, Air Resources Board, California Environmental Protection Agency; Ajith Kaduwela, Air Resources Board, California Environmental Protection Agency and University of California at Davis

Particulate matter (PM) episodes are frequent in central California during wintertime. The development of State Implementation Plans (SIP) to reduce ambient PM levels in this area requires the application of fine-grid photochemical PM models, such as CMAQ. However, the application of CMAQ in central California demands additions, modifications, and corrections to the model code and default parameters of the standard version of CMAQ. These developments are required due to unique topography, meteorology, and emission features found in central California. We conducted a series of 3-week simulations of ozone and PM compositions in central California during the 2000-2001 wintertime, using CMAQ with various improvement and modifications to physical and chemical processes and default parameters. We will first describe, in detail, the scientific bases for these improvements and modifications, and then present the impacts of these improvements and modifications on the PM concentrations and compositions simulated in central California. Finally, we will recommend specific improvements to CMAQ for inclusion in its future releases.

Continued Development of the CMAQ Modal Aerosol Model

Although the Community Multiscale Air Quality (CMAQ) model has been upgraded significantly in recent years, the latest aerosol module description available in the literature reflects science algorithms in CMAQ v4.0 (public release in September 2000). The purpose of this paper is to report the scientific upgrades and computational-efficiency improvements that have been made in the CMAQ aerosol module during the five-year period between the public releases of CMAQ v4.0 and v4.5. These include: " The addition of secondary organic aerosol treatment and subsequent modifications for reversible partitioning. " The incorporation of the ISORROPIA thermodynamic equilibrium module and improvements to its numerical stability. " Treatment of the heterogeneous reaction between gas-phase N2O5 and aerosol-phase liquid water. " The development of a computationally-efficient method for calculating coagulation coefficients. " An improved treatment of impaction in the deposition-velocity calculations. " The addition of sea-salt emissions and the thermodynamic interactions between gas-phase inorganic molecules and sea-salt aerosol.

Particulate Matter Forecasts with the Eta-CMAQ Modeling System: Towards Development of a Real-time System and Assessment of Model Performance

Rohit Mathur (NOAA/EPA), Daiwen Kang (STC), Shaocai Yu (STC), Kenneth Schere (NOAA/EPA), Jonathan Pleim (NOAA/EPA) , Jeff Young(NOAA/EPA) , George Pouliot(NOAA/EPA) , and Tanya Otte (NOAA/EPA)

An air-quality forecasting (AQF) system based on the National Weather Service (NWS) National Centers for Environmental Prediction s (NCEP s) Eta model and the U.S. EPA s Community Multiscale Air Quality (CMAQ) Modeling System is used to simulate the distributions of tropospheric ozone and particulate matter (PM) over the eastern United States. Real-time developmental testing of the system was initiated during the summer of 2004, and has continued since then. The refinements and adaptation of the CMAQ model for PM forecast applications will be discussed. The ability of the model to forecast the co-evolution of surface level ozone and PM pollution will be assessed through comparisons with regional ozone and continuous PM2.5 measurements from the AIRNOW system. The strengths and weaknesses of the modeling system in representing the fine PM chemical constituents and their seasonal variations is analyzed through comparisons with speciated measurements from the IMPROVE, CASTNet, and STN networks as well as specialized measurements from the 2004 International Consortium for Atmospheric Research on Transport and Transformation (ICARTT) field study. The ability of the model to represent the columnar distribution of tropospheric aerosol burden is evaluated through comparison between aerosol optical depths derived from the model and satellite and ground based measurements.

CONCEPT - An Open Source Community Driven Emissions Model.
Mark Janssen - LADCO, Cyndi Loomis - Alpine Geophysics.

CONCEPT is an open source community driven emissions model. It is the next generation of emissions model and includes updated temporal, spatial, and speciation tools. It also includes a process based ammonia model.

Application of CMAQ for the Clean Air Mercury Rule (CAMR)
Thomas Braverman, US EPA

The CMAQ model was applied for the Clean Air Mercury Rule(CAMR)using full year runs for the regional area consisting of all the continental US, Southern Canada and Northern Mexico. Prior to these applications some chemistry updates for mercury were made to the CMAQ model. The meteorolgy used for these runs was MM5 generated for 2001 at 36 km grid square horizontal resolutional and 14 vertical layers. The height of the surface layer was 38 meters. The US mercury emissions inventory used for this application was the 1999 NEI updated to 2002 for only Medical Waste Incinerators. The Canadian emissions invenoty was for 2000 and the US Criteria emissions inventory was for 2001. Boundary condition inflow into to the regional modeling domain for mercury and criteria pollutant species were obtained from the GEOS-CHEM global model developed and applied at Harvard University. The boundary conditions obtained from the global model varied horizontally across the border, vertically by layer, and in 3-hour increments. The CMAQ model performance for mercury wet deposition is provided for the 2001 Mercury Deposition Network Sites. The CMAQ model was applied for a full year for the following six cases: the 2001 base case, 2001 with utility mercury emissions zeroed-out, 2001 with mercury boundary conditions zeroed-out, 2020 with the Clean Air Interstate rule (CAIR), 2020 with utility mercury emissions zeroed-out, and 2020 with CAIR and the Clean Air Mercury Rule (CAMR). This presentation presents the results of these applications. The

results include the effects of utilities on mercury deposition in 2001 and 2020. The effects of CAIR, CAMR, and CAIR and CAMR on mercury deposition are also provided for 2020. In addition the effects of the mercury bounday conditions on mercury deposition are also provided.

Development of GEOS-CHEM/CMAQ Interface and Comparison Studies Over China During the Episode July 2001

Zuopan Li1, Joshua Fu1, Carey Jang2 , Binyu Wang3, Rohit Mathur4 , Litao Wang5 ,Qiang Zhang5 Rokjin Park6 and Daniel J. Jacob6 , 1. The University of Tennessee, Knoxville (UTK) 2. USEPA/Office of Air Quality Planning & Standards 3. North Carolina State University 4. USEPA/ORD 5. Tsinghua University6. Harvard University

This paper introduces the GEOS-CHEM/CMAQ interface and its applications on the air quality studies over China during the episode July 2001. For typical CMAQ runs with multiple nesting domains, finer domains obtain initial conditions(IC) and boundary conditions(BC) from coarser domain results and the coarsest domain uses the profile IC/BC provided by CMAQ. This profile IC/BC is time independent, and usually are kept the same even with different scenarios and different episodes. A spin-out period (washout period) is usually applied to initialize the model to get more realistic results. The length of spin-out time varied with different research groups and different studies, which is usually 3, 5, 7 or even higher number of simulation days. Considering the time-consuming CCTM and the input preparation involved for CCTM, this is a kind of waste of time and resources sacrificed for more realistic results. If MM5 output is used for MCIP, more waste of time, resources and energy is expected. Despite all the efforts, there is still no much confidence in the profile IC/BC because of its unrealistic nature. In order to get more realistic IC/BC, researchers are trying to get more realistic IC/BC from outputs from other well-developed global simulation models such as GEOS-CHEM developed at Harvard University. The GEOS-CHEM/CMAQ interface was developed at the University of Tennessee, Knoxville. Detailed procedures of the GEOS-CHEM/CMAQ interface to extract IC/BC for CMAQ domains will be introduced and comparison studies of runs with GEOS-CHEM IC/BC and runs with standard profile IC/BC will be conducted over China during the episode July 2001. The predicted concentrations will be compared with limited monitored values in the Beijing rural area.

Model Performance Evaluations for Fine Particulates Using Unpaired in Space and Time Analyses

Gail Tonnesen, UC-Riverside

Air quality models are now being used in the development of State and Tribal Implementation Plans as required by the Clean Air Act Regional Haze Rule (RHR). In contrast to traditional, episodic ozone modeling studies, the completion of model performance evaluations for visibility modeling poses several special challenges. First, the RHR requires that visibility models be operated for long periods. Typically, annual simulations are used, and this makes it difficult to improve model performance through intensive efforts to fine tune the meteorological and emissions input data for each simulation day. Secondly, the RHR requires that visibility be evaluated on the very cleanest days as well as the most polluted days. It is very challenging to achieve "good" model performance both for extended time periods and for clean conditions. In fact, model

performance guidance is not yet available to provide a definition of what constitutes acceptable model performance. To address these issues we are experimenting with a variety of analysis methods for presenting model performance results for visibility models. We demonstrate two new approaches in which we relax the model evaluation criteria by allowing the comparison of model predictions and ambient data to performed either un-paired in time or un-paired in space. These analyses are used to show that the model can simulate a reasonable version of reality even while failing to accurately reproduce observed ambient data on each day at each monitoring site. We also present some of the traditional model performance metrics and we propose that model performance guidance for visibility models should include a combination of the un-paired in space and time analyses with the traditional model performance metrics.

An Update on EPA Attainment Modeling Guidance for Ozone, Particulate Matter, and Regional Haze

Brian Timin, Pat Dolwick, Norm Possiel, Sharon Phillips, Marc Houyoux, EPA

The EPA has developed two guidance documents which describe the modeling requirements for demonstrating attainment of the 8-hour ozone and PM2.5 National Ambient Air Quality Standards (NAAQS) and demonstrating reasonable progress towards the Regional Haze goals. The documents have two purposes. The first is to explain how to interpret whether modeling and other analyses support a conclusion that attainment of the NAAQS (or reasonable progress) will occur by the appropriate attainment date for an area. The second purpose is to describe how to apply an air quality model to produce results needed to support an attainment demonstration. The guidance documents consist of two major parts. Part I explains how to use the results of models and other analyses to help demonstrate attainment. It explains what is meant by a modeled attainment demonstration, a modeled attainment test, and a weight of evidence determination. Part II of the guidance describes how to apply air quality models for the purpose of showing attainment of the standards. The results of this process are then used to apply the modeled attainment test to support an attainment demonstration. The 8-hour ozone guidance document has been recently revised and is now in final form. The draft PM2.5 and Regional Haze document is currently being revised and is expected to be finalized by the end of calendar year 2005. The documents are available at http://www.epa.gov/ttn/scram/ .

Development and Evaluation of an Improved SOA Representation in the CMAQ Model

John Offenberg, Edward Edney, Tad Kleindienst, Michael Lewandowski, Mohammed Jaoui, Prakash Bhave,Chris Nolte, Golam Sarwar U.S. Environmental Protection Agency, Human Exposure Atmospheric Sciences Division, Alion Science and Technology and National Oceanic and Atmospheric Administration

Combining HYSPLIT and CMAQ to resolve urban scale features: an example of application in Houston, TX

Ariel F. Stein , Vlad Isakov , James Godowitch , and Roland R. Draxler

Resolving urban scale features is critical for air toxics modeling and exposure assessments. While grid-models (such as CMAQ) are the model platform of choice for simulation of chemically-reactive airborne pollutants on a regional scale, there

are various models that can provide detailed resolution of the spatial variations in hourly-average concentrations. In this study, we test the feasibility of developing an urban hybrid simulation system. In this combination, CMAQ provides the regional background concentrations and urban-scale photochemistry, and the Hybrid Single Particle Lagrangian Integrated Trajectory model (HYSPLIT) provides the spatially resolved concentrations due to local emission sources. Furthermore, multiple HYSPLIT simulations with varying model inputs and physical parameters are used to create a concentration ensemble to estimate the concentration variability. In this first application, the HYSPLIT and CMAQ models are used in combination to calculate high resolution Benzene concentrations in the Houston area. The study period is from August 18th to September 4th of 2000. The Mesoscale Model 5 (MM5) is used to create meteorological fields with a horizontal resolution of 1x1 km2. Multiple HYSPLIT simulations are used to model two sources of concentration variability; one due to variability created by different particle trajectory pathways in the turbulent atmosphere and the other due to different flow regimes that might be introduced when using gridded data to represent meteorological data fields. The first series of ensemble runs consisted of 27 members, in which the particle trajectory variability in HYSPLIT is calculated by using a different seed number to estimate the random component of the particle diffusion. The concentration sensitivity to the meteorological data field is calculated by shifting the position of the meteorological field variables. In this latter series of ensemble runs, the first 9 members are created by displacing the meteorological field by one grid point in the horizontal. The other 9 have also one-grid displacements in the horizontal but with a starting height of approximately 150 m above the original starting height. The ensemble mean determined by HYSPLIT is added to the CMAQ calculated background to estimate the mean Benzene concentration and these estimated mean concentrations are compared with field measurements. Further, the HYSPLIT ensemble concentration predictions are used to estimate the variability that might be expected about mean concentration predictions to determine if the measurements could be significantly different from the model predictions.

Air Quality Modeling in Hong Kong on Particulate Episodes

Jimmy C.H.Fung, Roger Kwok, Department of Mathematics, The Hong Kong University of Science and Technology; Alexis K.H. Lau, Institute for the Environment, The Hong Kong University of Science and Technology; Joshua Fu, Department of Civil and Environmental Engineering, The University of Tennessee at Knoxville

In recent years, Hong Kong and the Pearl River Delta (PRD) of China have been experiencing air pollution problems such as episodic levels of respirable suspended particulate (RSP) matters, manifesting visibility degradation. Rapid economic development has resulted in drastic increase in anthropogenic emissions as well as urbanized area. By 2000, urbanization level reached nearly 50%. With this scale of urbanization, local scale wind circulations, including sea-land breezes and urban heat island, play a vital role in occurrences of air pollution events in Hong Kong and PRD region. MM5, SMOKE and CMAQ are used to investigate main physical and chemical processes controlling RSP episodes in Hong Kong. The high resolutions of up-to-date land use datasets replace the standard USGS land use datasets in MM5. Spatial surrogates and temporal allocation have also been updated for SMOKE to process the local emissions covering southern China, while the emissions covering other parts of China are

based on estimates by Streets China emission database. Simulation results show that although local accumulation of RSP cannot be neglected, regional transport remains the major contributor to the episodic events. Spatial uniformity of sulfates is evident from both observations and simulations. More analyses will demonstrate these phenomena.

Simulations of Diurnal Variations for Vertical Ozone Concentration Profiles within the Mixing Layer by CMAQ

Yee-Lin Wu, Department of Environmental Engineering, National Cheng Kung University, Ching-Ho Lin, Department of Environmental Engineering & Science, Fooyin University, and Hsin-Chih Lai, Education Center for Teacher, Chang-Jung Christian University

Significant diurnal variations are observed for the ozone concentrations at surface monitoring site; the peak ozone concentrations are generally at noon to 2 pm and the nighttime concentrations are generally less than 10 ppbv. However, the ozone concentrations at 600 m to 1000 m, which is the residence layer, are generally greater than 50 ppb at nighttime. The variations of ozone concentrations at the residence layer are determined by the sea-land breeze, the NO titration and surface temperature inversion at night, and the plume from major stationary sources. Extended field campaigns for vertical profiles of ozone concentrations and meteorological conditions from ground to 1500 m were conducted during 27 to 31, October 2003. Models-3/CMAQ was used to simulate the variations of vertical profile for ozone concentrations. In order to simulate the vertical profile of ozone concentrations, finer resolutions in vertical direction was used in this study and there were 20 layers from ground to 1500 m. The meteorological conditions were simulated with MM5 with four layers of nested grids and the finest grid size was 3 km by 3 km over the whole island. Therefore, all the emissions in Taiwan were included in the simulation for the finest grid size. The Taiwan emission datum system, which was compiled by Taiwan EPA, was used as the basis for emission data. The ground ozone concentrations simulated by using Models-3/CMAQ were generally in good agreement with the observed results in southern Taiwan. Nocturnal ozone residence layer was also found in the simulated vertical concentrations profiles and the results were consistent with those observed. The ozone in nocturnal residence layer was from the daytime photochemical reaction within the mixing layer. However, the simulations by CMAQ did not show the ozone depletion layer which was probably due to the NO titration from plume.

CMAQ Multi-Pollutant Response Surface Modeling: Applications of an Innovative Policy Support Tool

Sharon Phillips, Bryan Hubbell, Carey Jang, Pat Dolwick, Norm Possiel, Tyler Fox

Air quality models can be a powerful regulatory tool for comparing the efficacy of various emissions control strategies and policy decisions. However, due to the often enormous computational costs and the complication of the required emission inputs and processing, using photochemical air quality models to generate outputs to meet time-pressing requirements of policy analysis always presents a challenge and is typically inefficient, if not ineffective. A promising tool for addressing this issue, Response Surface Modeling (RSM), has been developed by utilizing advanced statistical techniques to characterize the relationship between model outputs and input parameters in a highly economical manner. The

RSM is based on a new approach known as air quality metamodeling that aggregates numerous pre-specified individual air quality modeling simulations into a multi-dimensional air quality "response surface". Simply, this metamodeling technique is a "model of the model" and can be shown to reproduce the results from an individual modeling simulation with little bias or error. The RSM incorporates statistical relationships between model inputs and outputs to provide real-time estimates of these air quality changes. The RSM provides a wide breadth of model outputs, which we can utilize to develop emissions control scenarios and allow for the rapid assessment of air quality impacts of different combinations of emissions reductions In this paper we describe the development of a multi-pollutant RSM application using the Community Multi-Scale Air Quality (CMAQ) Modeling System developed at EPA. The processes involved in developing a multi-pollutant RSM application using CMAQ will be discussed, including the selection of modeling domain and configuration, development of a multi-dimension experimental design for control strategies, development of a CMAQ/SMOKE interface program to expedite model runs and eliminate massive emission inputs and processing needs, implementation and verification (out-of-sample validation and cross validation) of the RSM technique, and an assessment of the contribution of regional versus urban controls. In addition, we describe and show how the RSM was used to estimate air quality changes for various control scenarios for the proposed PM2.5 NAAQS, and providing inputs for other types of regulatory analyses. For example, generating air quality inputs for estimating the health benefits of reductions in PM precursors and providing screening level estimates of the impacts of control strategies on NAAQS design values are functions the RSM supports. Intended policy uses should be built into the experimental design stage to ensure the ability of the RSM to appropriately address policy questions. The ability of the RSM to look at scenarios outside of the pre-defined "policy space" is a function of the deviation of the scenario of interest from the original experimental design.

Plume-in-Grid Modeling for PM and Mercury

Prakash Karamchandani, Krish Vijayaraghavan, Shu-Yun Chen and Christian Seigneur Atmospheric & Environmental Research, Inc. 2682 Bishop Drive, #120 San Ramon, CA 94583

One-atmosphere grid models are now being widely used to predict the impacts of emission controls on the concentrations and depositions of pollutants such as ozone (O3), fine particulate matter (PM2.5) and mercury (Hg). A major limitation of grid models is their inability to correctly represent the near-source transport and chemistry of emissions from elevated sources. These models typically use horizontal grid resolutions of a few kilometers to tens of kilometers, which is inadequate to resolve stack plumes with initial dimensions of tens of meters. This limitation of grid models can lead to errors in determining 1) the contribution of elevated sources to ambient concentrations and deposition fluxes, and 2) the response of the model to emissions changes from elevated point sources or to emission changes from other sources that may affect the chemistry of the elevated point source emissions. A common approach to address this limitation is to use Plume-in-Grid (PiG) modeling, in which a subgrid-scale representation of stack plumes is imbedded in the 3-D model. This approach has traditionally been used in O3 modeling studies and more recently in PM2.5 modeling studies, but has not been employed for Hg modeling. In this study, we extend an advanced PiG model for O3 and PM to incorporate a treatment of the transport, chemistry and

deposition of Hg and apply the model to the southeastern United States for the 2002 calendar year. The model uses the Model of Aerosol Dynamics, Reaction, Ionization, and Dissolution (MADRID) for PM processes, and an Advanced Plume Treatment (APT) using a state-of-the-science reactive puff model, the Second-order Closure Integrated puff model (SCIPUFF) with CHEMistry (SCICHEM), to resolve stack plumes. The model is referred to as CMAQ-MADRID-APT-Hg, and is based on the March 2006 release of CMAQ (Version 4.5.1). We present an operational performance evaluation of the model using data from national and regional ambient and deposition monitoring networks. We also compare model predictions of ambient Hg concentrations downwind of selected coal-fired power plants with measurements during several plume events. In addition, we conduct a simulation without APT and compare the results from the two simulations to show that 1) using APT results in a better representation of measured concentrations downwind of major elevated point sources, and 2) there are significant differences between the two simulations in their predictions of the impacts of these sources on downwind air quality.

Recent Updates to the SMOKE Modeling System
Bok H. Baek, Alison M. Eyth, and Any P. Holland

EPA's Office of Air Quality Planning and Standards is developing the one-model framework for toxics and criteria modeling for all air quality models used by U.S. EPA, including CMAQ, CAMx, REMSAD, and AERMOD. In addition, OAQPS is developing an Emission Modeling Framework (EMF) to provide better management, versioning, quality assurance, and tracking of data used for emissions modeling. The Sparse Matrix Operator Kernel Emissions (SMOKE) modeling system is used to prepare emissions input data for many of the models used by U.S. EPA. SMOKE has been enhanced to better support the integration with the EMF and the one-model framework, which includes the improved integration of toxics and criteria modeling. Many updates in support of this effort have been completed, and others are currently underway or planned for the remainder of FY06 and for FY07. Updates to SMOKE v2.2 include processing data for variable grid resolutions and integration with the BlueSky fire emissions estimates model. SMOKE v2.3 significantly reduces memory requirements during gridding, can model non-sequential episodes within a single run of Temporal, supports an extended one record per line (ORL) format, and includes a new approach to wildfire inventories. Additional details regarding the usage of the new versions of SMOKE are available at www.cmascenter.org under the model documentation section. Upcoming updates to be discussed include enhancements to allow SMOKE to produce outputs for various toxics models such as ASPEN, ISCST3, and AERMOD.

Recent Advancements to Quality Assurance and Case Management within the Emission Modeling Framework
A. Eyth, M. Houyoux, Q. He, R. Partheepan

The Emission Modeling Framework (EMF) has been developed over the last two years to provide data management, case management, and quality assurance for emissions modeling related input and output files. The data management component of the EMF was available for use as of Spring 2006. During the summer of 2006, updates were made to the case management portion of the EMF to provide a mechanism for collecting datasets input to and output from SMOKE modeling runs. In addition, improvements were made to the integration of quality

assurance tools such as EmisView with the EMF along with a number of improvements to EmisView itself. The uses of the EMF for data management, case management, and quality assurance of emissions modeling data will be discussed.

Using combined lagrangian and eulerian modeling approaches to improve particulate matter estimations in the Eastern US
Ariel F. Stein, Rohit Mathur, and Roland R. Draxler

The Hybrid Single Particle Lagrangian Integrated Trajectory model (HYSPLIT) and the Community Multiscale Air Quality model (CMAQ) have been used together in an attempt to improve the forecast of the distribution of particulate matter (PM) in the Eastern US. A case study covering the period from July 14th to 23rd of 2004 is used to assess the contribution from wild fire emissions located in Alaska to the PM levels in the Eastern US. In this work, HYSPLIT is used to track and quantify the transport, dispersion and deposition of primary PM from long-range Alaskan fire sources to the CMAQ domain boundary and then CMAQ is used to account for the additional PM sources within its Eastern US domain. The boundary conditions for CMAQ have been calculated by summing the ratio of the mass of each HYSPLIT particle to the volume of the CMAQ boundary grid-cell in which the particle resides. Once the CMAQ PM boundary concentration has been calculated, a speciation profile has been applied to partition the primary PM to be compatible with CMAQ s chemical mechanism. The composition of PM was assumed to be 77% organic carbon, 16% elemental carbon, 2% sulfate, 0.2% nitrate and 4.8% unspeciated PM. Two sets of CMAQ model runs have been performed to assess the effect long range transport of PM originating from wild fires in Alaska. One set including the time varying PM boundary conditions calculated from HYSPLIT and the other one with constant background concentrations.

NOAA-EPA's National Air Quality Forecast Capability: Progress and Plans
Paula Davidson, Nelson Seaman, Jeff McQueen (NOAA/NWS); Rohit Mathur (NOAA/OAR and EPA/ORD); Roland Draxler (NOAA/OAR) Richard Wayland (EPA/OAQPS)

Current Operational Capabilities: In partnership with the US EPA, NOAA has implemented the early phases of a national air quality forecast capability. The initial operational implementation in September, 2004, provided ground-level ozone predictions only for northeastern US. In August 2005, the operational domain was extended to the entire Eastern US. Predictions are generated with linked weather and air quality models run operationally at NOAA's NCEP: the NOAA-EPA Community Multiscale Air Quality CMAQ) model driven by NOAA's operational North American mesoscale weather prediction model (NAM). The capability is an end-to-end system providing twice daily predictions of hour-by-hour ground-level ozone concentrations at 12km resolution, disseminated on NWS and EPA servers. Near-real-time verification is conducted with AIRNow observations. Expanding Test Capabilities: During Summer 2006, predictions for ground-level ozone will be tested experimentally over a coast-to-coast domain. Improvements to the expanding ozone capability, along with conversion of NAM from Eta-12 to the new WRF-NMM, and updated CMAQ, include: better coupling between NAM and CMAQ, with options for increased vertical resolution; updated emissions estimates, and improved vertical mixing. In addition, efforts are underway to develop a quantitative particulate matter forecast capability. An experimental qualitative smoke forecast tool is being

tested. This tool integrates satellite information on location and extent of wildfires with USFS estimates of fire emissions, NAM weather prediction and HYSPLIT dispersion prediction to simulate smoke transport. Near real-time verification compares the aerial extent of predicted column-integrated smoke concentrations with satellite observations. Concurrently, the NOAA-EPA team is developmentally testing ground-level aerosol predictions, using a modified WRF/CMAQ capability and pollutant data from emissions inventories. Research is ongoing to develop capabilities for real-time quantitative ingest of additional emissions sources important for quantitative predictions of particulate matter. Targeted deployment of nationwide (including AK and HI) ozone forecasts within 3 years will be followed by the addition of quantitative particulate matter forecasts, and extended forecast periods - out to day 2 and beyond.

Simulating diurnal changes of speciated particulate matter in Atlanta, Georgia using CMAQ

Yongtao Hu, Jaemeen Baek, Rodney Weber*, Bo Yan*, Sangil Lee*, Evan Cobb, Amy Sullivan* and Armistead G. Russell, School of Civil and Environmental Engineering and *School of Earth and Atmospheric Sciences, Georgia Institute of Technology, Atlanta, GA, 30332

Speciated particulate matter monitored at two sites in Goergia Tech's campus in the summer of 2005 is simulated using CMAQ. One site is directly adjacent to the interstate running through the city, the other is 500 m away. Different features in PM composition were found at these two locations. Both morning and afternoon peaks of total PM2.5 were observed. CMAQ, using a 1.333 km grid, is used to simulate and explain the diurnal changes of the speciated particulate matter observed at the above locations. DDM-3D is also used to trace the contributions to organic carbon, both primary and secondary, and sulfate from the different emission sources.

CMAQ model evaluation using an ensemble of MM5 meteorological simulations

Robert W. Pinder, Robert C. Gilliam, K. Wyat Appel, Alice B. Gilliland

Users of CMAQ and MM5 have a multitude of options when selecting the submodules and mechanisms for their application. These options generate scientifically credible yet varying meteorological instantiations, each of which has an impact on the chemical and physical processes simulated by CMAQ. In this study, we examine the impact of these meteorological differences on CMAQ predictions of ozone and particulate matter. We have selected six configurations of MM5 with differing schemes for convection, planetary boundary-layer processes, and land-surface processes. These meteorological simulations are used to drive the biogenic and mobile source emission models. The emissions and meteorological fields are used as input to CMAQ for month long simulations of January and July 2002. Each individual simulation is then operationally evaluated using observations from the various EPA monitoring networks. Differences in the predicted meteorological fields (e.g. surface temperature, wind speed, PBL height) from each individual MM5 simulation are examined to find correlations with the errors in the CMAQ predictions of ozone and particulate matter. It is also important to determine if these meteorological differences impact CMAQ predictions in hypothetical emission control scenarios. We also examine the change in ozone and particulate matter due to emission changes under each meteorological instantiation. From these differences, we quantify the uncertainty

in CMAQ predictions of future emission scenarios attributable to the MM5 configuration. Disclaimer: The research presented here was performed under the Memorandum of Understanding between the U.S. Environmental Protection Agency (EPA) and the U.S. Department of Commerce's National Oceanic and Atmospheric Administration (NOAA) and under agreement number DW13921548. This work constitutes a contribution to the NOAA Air Quality Program. Although it has been reviewed by EPA and NOAA and approved for publication, it does not necessarily reflect their policies of views.

Comparison of Mercury Chemical Transport Model Between CMAQ and STEM
Li Pan, Che-Jen Lin, Gregory, R. Carmichael, Pruek Pongprueksa, Thomas, C. Ho

CMAQ-Hg and STEM-Hg are developed by US-EPA and CGRER (center for global and regional environment research) at the University of Iowa, respectively. The chemistry mechanisms of mercury in the gaseous and aqueous phase are included in both models, but are treated in different methods. For example, Hg gaseous phase reaction with ozone is assumed to produce only the particulate mercury in the STEM, but in the CMAQ both particulate Hg and reactive Hg are considered. The objects of this work are to demonstrate the differences in the performances of the two models and to understand the magnitude of uncertainty inherent to the model and mercury chemical mechanisms for reducing the uncertainties in the formulation of model formulations. Bi-monthly simulations of the two models using the same meteorology, emission inventory and IC/BCs were performed to assess the ambient concentrations and depositions of mercury in the period of June and July 2001. The model results were compared each other and as well as with the MDN observations.

Comparison Evaluation of Two Leading Photochemical Air Quality Models for Particulate Matter and Ozone: CMAQ and CAMx
Sharon Phillips, Karen Wesson Carey Jang, Norman Possiel, Patrick Dolwick, Brian Timin, Tom Braverman, Marc Houyoux, and Tyler Fox

USEPA's Air Quality Modeling Group in the Office of Air Quality Planning and Standards is performing a comparative model evaluation of the Community Multi-scale Air Quality model (CMAQ v4.5) and the Comprehensive Air Quality Model with Extensions (CAMx v4.3). Both models are state-of-the-science tools in use by the regulatory community for estimating the impacts of sources and control strategies on ozone and fine particle concentrations, deposition, and visibility. This evaluation consists of model simulations for July and January 2001 for a Continental U.S. (CONUS) domain at 36 km resolution and an Eastern US domain (EUS) at 12-km resolution. Both CMAQ and CAMx were run with the same inputs, to the extent possible given somewhat differing requirements of each model. Both models were run with a consistent 14 layer vertical structure. CAMx was run in a two-way nesting mode while CMAQ was run one-way nested for 36-km and 12-km. Common inputs for 2001 include: boundary/initial concentrations from a global chemistry model (GEOS-CHEM); emissions inventories for biogenics (BEIS 3.12) and anthropogenic sources (NEI); and meteorological data (MM5 3.6.3). For CMAQ, anthropogenic emissions were processed with SMOKE and model-ready meteorological inputs were processed with MCIP v3.0. The CMAQ emissions were input into CAMx using the emissions converter, CMAQ2CAMX. The 2001 meteorological data were processed for CAMx using MM5CAMx v4.4. The model evaluation includes graphical and statistical

comparisons of model-predicted ozone, PM2.5 species, nitrogen and sulfur deposition, and visibility to the corresponding observed data for 2001 as measured at sites in the following networks: the Clean Air Status and Trends Network (CASTNet), the Interagency Monitoring of Protected Visual Environments (IMPROVE), the Speciation Trend Network (STN), National Atmospheric Deposition Program (NADP) and the Aerometric Information Retrieval System (AIRS). Preliminary results indicate that the two models show differences in model performance, most notably for summer sulfate, winter nitrate, and summer ozone. This paper will examine the differences in model performance between the two models for multiple subregions and the extent that model performance varies between the 36 km vs 12 km simulations. Possible factors that contribute to differences in model performance will also be identified in this paper.

Developing Emission Inventories for Biomass Burning for Real-time and Retrospective Modeling

George Pouliot,Thomas Pierce,Tom Pace

The EPA uses chemical transport models to simulate historic meteorological episodes for developing air quality management strategies. In addition, chemical transport models are now being used operationally to create air quality forecasts. There are currently a number of methods and approaches to the estimation of wildland fire emissions for use in chemical transport models. We will provide an overview of these approaches and compare and contrast their merits and deficiencies. Ground-based approaches as well as satellite based approaches will be reviewed. In particular, we will be comparing different approaches to national fuel loading estimates, the accuracy of satellite derived fire events both in space and in time, and emission factors used in generating emission estimates. The goal of this review is to guide the timely development of a spatially and temporally accurate method for estimating a national inventory of wild land fire emissions. Currently, there is a need to develop national wild land fire inventories on a timely basis.

Fast Equivalent Operational Models (FEOMs) for Atmospheric Chemical Kinetics within Photochemical Air Quality Simulation Models

Sheng-Wei Wang and Panos G. Georgopoulos Ozone Research Center, Environmental and Occupational Health Sciences Institute, UMDNJ - R.W. Johnson Medical School and Rutgers University, Piscataway, NJ

Chemical kinetics calculations are often the most computationally intensive components of 3-D Photochemical Air Quality Simulation Models (PAQSMs) such as the Community Multiscale Air Quality model (CMAQ). Various approaches, such as parallel computing and efficient numerical techniques (for example, the sparse matrix vectorized Gear method and the Modified Euler Backward Iterative (MEBI) method), have been introduced to reduce simulation time. This presentation highlights an alternative to the above approaches by creating Fast Equivalent Operational Models (FEOMs) for the chemical kinetics. A FEOM is an expansion of correlated functions which capture the chemical kinetic input-output relationships. From these quantitative input-output relationships, the FEOM calculates efficiently the output species concentrations based on the initial species concentrations, employing very rapid and stable algebraic manipulations. FEOM expansion functions are constructed based on a family of High Dimensional Model Representation (HDMR) tools, which have been implemented as modules of the

Modeling ENvironment for TOtal Risk studies (MENTOR) framework. The speed of computations utilizing the FEOM expansion functions offers excellent potential for resolving the computational burden associated with long-term and multi-scenario simulations employing state-of-the-art comprehensive regional and multiscale PAQSMs such as CMAQ. A case study, which focuses on the development of FEOM as an efficient solver for atmospheric chemistry mechanisms (such as CB4) that can be utilized in PAQSMs, is presented here. Base Funding for the Ozone Research Center is provided by the New Jersey Department of Environmental Protection (NJDEP - Contract AQ05-011). This work is also funded in part by a University Partnership Agreement between the U.S. Environmental Protection Agency (USEPA) and EOHSI. Viewpoints expressed here do not necessarily reflect the views of USEPA, NJDEP, or their contractors.

Assessment of Environmental Benefits Modeling System (AEB); General Description of Project and Results

Bob Imhoff (Principal Investigator, BAMS) Stan Hadley (ORNL), Stewart Dickson (UNCA NEMAC), Jerry Condrey, Saswati Datta, Jesse O'Neal

Assessment of Environmental Benefits (AEB) Modeling System is a coupled system designed to enable state air agencies to analyze emission reductions related to energy efficiency (EE) and provide documentation to support SIP credit for these reductions. Main building blocks of this system are Oak Ridge Competitive Electricity Dispatch (ORCED) model, Sparse Matrix Operator Kernel Emission (SMOKE) system and EPA Models-3 Community Multi-scale Air Quality (CMAQ) Model version 4.5. AEB team successfully developed software tools and analytical procedures to couple these three systems in order to achieve a linkage between power dispatch analysis and air quality impacts. This research relies on the data and modeling foundation established by Visibility Improvement State and Tribal Association of Southeast (VISTAS). Both the meteorology data and future base case emissions inventory were provided by VISTAS. In the CMAQ sensitivity cases, three assumptions were tested: Demand side management (DSM) impact area, the percentage demand reduction for 2018, and the electric generating unit supply domain. In this series of modeling runs, the DSM impact area was one of, or a combination of the North Carolina, Tennessee and Georgia. The main product of the AEB modeling system is a Sensitivity Matrix: a database containing the hourly sensitivity of air quality parameters in response to change in power demand for each grid cell. This sensitivity matrix provides, for the first time, the capability for model-driven, integrated energy/air quality policy development.

Assessment of Environmental Benefits (AEB) Modeling System;Technical Review

Bob Imhoff (Principal Investigator, BAMS) Stan Hadley (ORNL), Stewart Dickson (UNCA NEMAC), Jerry Condrey, Saswati Datta, Jesse O'Neal

Assessment of Environmental Benefits (AEB) project is aimed at finding the impact of air quality resulting from implementation of Energy Efficiency (EE) technologies in Southeastern states of North Carolina, Tennessee, Georgia. This has been accomplished by coupling the Oak Ridge Competitive Electricity Dispatch (ORCED) Model with the EPA SMOKE emissions model and Models-3 Community Multi-scale Air Quality (CMAQ) model, version 4.5. The AEB research team developed the necessary software tools to make this coupling possible. The output of this coupled system is then analyzed to generate sensitivities of air quality parameters with respect to the changes in individual unit electricity

generation load predicted by ORCED for specific scenarios. The simulations are run for one complete model year using VISTAS meteorology data for 2002 and emissions inventory for 2018 (Version OTW F4). In the course of setting up and running these simulations the team faced several technical hurdles. This paper will present the technical lessons learned during the AEB modeling exercise and also present methods for visualizing selected results of the project.

Evaluation of the 2006 air quality forecasting operation in Georgia
Talat Odman Yongtao Hu Ted Russell Michael Chang Carlos Cardelino

We are developing a high-resolution air quality forecasting system for Southeastern United States. The initial version of the system is based on Weather Research and Forecasting (WRF) and Community Multiscale Air Quality (CMAQ) models. Operational forecasting of ozone and PM2.5 started on May 1, 2006. The modeling domain covers the Eastern U.S. with a 36-km grid, nested down to 12-km over the Southeast and finally to 4-km over Georgia and portions of neighboring states. Data from the North American Mesoscale (NAM) model forecasts are used in driving the WRF simulations. In addition to locally increasing the spatial resolution and extending the forecast period, the system utilizes more up-to-date land use, emissions, and monitoring data than the NOAA/EPA national forecast. Future versions of the system will include extensions developed at Georgia Tech such as the time-saving variable step algorithm, the direct decoupled method that allows calculation of emission sensitivities in addition to pollutant concentrations and the very high-resolution (~100 m) dynamic adaptive grid algorithm. In this paper, some operational issues will be discussed and the accuracy of the forecasts during the summer of 2006 will be evaluated. The performance will be compared to forecasts derived from other models such as persistence, climatology, linear regression, close neighbor and decision tree, as well as to the national forecasts. Finally, the potential applications of the systems in health-effects and air quality management areas will be described.

PBL HEIGHT VERIFICATION FROM ETA AND WRF/NMM MODELS
Marina Tsidulko, Geoff DiMego, Michael Ek, Jeff McQueen, Pius Lee

PBL heights from the ETA and WRF/NMM models are compared with boundary layer heights computed from RAOBS data. Vertical profiles of temperature, moisture and wind at RAOBS locations are compared. Richardson number approach in estimating PBL heights from radiosond data is applied, while both ETA and WRF/NMM models utilize TKE schemes in boundary layer calculations. Differences between Ri number and TKE approaches are studied. Statistical parameters of PBL height verification are computed for different geographical regions as well as for individual stations. Also, dependence of stations elevations on PBL statistics is studied. Preliminary evaluations suggest that while ETA produces less accurate PBL over high terrain, there is no such dependence in WRF/NMM model. For geographical regions, WRF/NMM produces higher than ETA boundary layer over Eastern US, and lower layer over Western US. Both models provide higher PBL than the RAOBS observations estimate. Comparison of model and RAOBS calculations with LIDAR data will be discussed. We also analyze impacts of variations in PBL height estimates from different models on ground-level ozone prediction by comparing NOAA/EPA CMAQ predictions driven by ETA and WRF/NMM models.

Numerical Aspects of the CMAQ Adjoint

K. Singh, A. Sandu, A. Hakami, D.W. Byun, P. Percell, V. Coarfa, Q. Li, J.H. Seinfeld

Chemical data assimilation is a method to obtain the best estimate of the currect concentration fields of chemical species in the atmosphere, using information from observations together with informations encapsulated in a chemical-transport model. In this paper, we present the development of the adjoint of CMAQ model-3 and demonstrate it in real applications. The chemistry is implemented using our Kinetic PreProcessor(KPP). Discrete and Continuous adjoints are implemented for transport. The checkpointing scheme has two levels. Applications on data-assimilation and receptor-oriented sensitivity analysis are shown.

Development of a Tightly Coupled WRF-NMM-CMAQ Air Quality Forecast System by using the Hybrid sigma-P Vertical Coordinate
Hsin-Mu Lin, Tanya Otte, Rohit Mathur, Pius Lee, Jonathan Pleim, Jeffery McQueen, Kenneth Schere, and Paula Davidson

In the mid 2006 major changes will be implemented in the NOAA/EPA air quality forecasting (AQF) system to incorporate the new operational North American Mesoscale (NAM) model. The NAM, currently the Eta model, will be replaced by the Weather Research and Forecasting Non-Hydrostatic Mesoscale model (WRF-NMM). The horizontal, and vertical grid, and coordinate systems used in the NAM are different from those employed in CMAQ. To reduce errors associated with interpolation of meteorological data from the WRF-NMM coordinate and grid structure to that of CMAQ, efforts are underway to improve the coupling and consistent use of data between the two models. This paper presents the first step in this effort, namely improving the coupling in the vertical direction such that the CMAQ calculations are performed with the same hybrid sigma-P vertical coordinate system that is utilized in the WRF-NMM. Since the CMAQ governing equations are cast in generalized coordinates, alternate coordinate systems can be accommodated provided the Jacobian , which encapsulates the transformations from physical to computational space, is accurately calculated. PREMAQ is an interface processor that 1) transfers various meteorological fields from the NAM's coordinate and grid structure; 2) contains the requisite functionality to ingest and process (following the SMOKE emissions processing system) emission inventory data to forms compatible with CMAQ input requirements for the NOAA-EPA AQF system. Calculations of the Jacobian and associated variables have been modified in PREMAQ to achieve this vertical tight coupling. The updated system provides more accurate representation of the 3-D meteorological fields and is expected to reduce mass inconsistency errors in chemistry/transport calculations. Numerous sensitivity tests of the new version of PREMAQ for the vertical tight linkage of WRF-NMM and CMAQ have been preformed and show agreements with the old PREMAQ and WRF-NMM from different aspects. The new version of PREMAQ processes the necessary meteorological fields from all the vertical layers of WRF-NMM and has the option for users to choose the desired vertical layers, named collapsing, that are used for CMAQ. The collapsing results are also verified from numerous sensitivity tests. The formulation of the hybrid sigma-P coordinate will be reviewed and modifications implemented in the AQF system will be presented along with results from various sensitivity and consistency testing experiments to demonstrate the working of the new coupled model.

A New Control Strategy Tool within the Emissions Modeling Framework

D. Misenheimer, A. Eyth, D. Weatherhead, M. Houyoux, L. Sorrels, Q. He, R. Partheepan

The purpose of the Emissions Modeling Framework (EMF) is to solve many of the long standing difficulties of emissions modeling at EPA. These difficulties stem from the complexity of emissions modeling, which requires emission modelers to piece together many disparate data sources including emission inventories, chemical speciation factors, temporal allocation factors, spatial allocation factors, growth factors, and control factors. These data are often generated using a variety of different tools and processes. Recently, a more integrated approach has become available for the generation of controlled inventories. The EMF can now generate emission inventories with additional controls applied on top of the base case inventory. The EMF tracks information about control measures, their costs, and to which types of sources they apply. It can also compute control strategies that match control measures to emission sources using algorithms such as maximum emissions reduction and least cost. When running a control strategy, the user can take advantage of the data versioning that is built in to the EMF by choosing a particular version of an EMF data set on which to compute the strategy. The result of a control strategy contains information that specifies the estimated cost and emission reduction achieved for each control measure-source combination. The control strategy result can be exported to a CSV file as a table; viewed in a graphical table that supports sorting, filtering, and plotting; or it can exported to an emissions inventory file that can be input to SMOKE. The object-oriented nature of the EMF will make it possible to add many new features related to control strategy development over time in a straightforward fashion. By providing this new feature integrated within the EMF, it facilitates a level of collaboration between control strategy developers and emission inventory modeling that was not previously possible.

Fine scale air quality modeling using a hybrid dispersion and CMAQ modeling approach: An example application in Wilmington DE
Jason Ching Mohameed Majeed Vlad Isakov

Characterization of spatial variability of air pollutants in an urban setting at fine scales is critical for improved air toxics exposure assessments, for model evaluation studies and also for air quality regulatory applications. For this study, we investigate an approach that supplement results of outputs from a local scale dispersion model (AERMOD) to CMAQ at regional scales for fine particulates and formaldehyde. The CMAQ runs were performed at 4 and 12 km grid sizes. Both modeling systems were run for the calendar year 2001. (A limited set of CMAQ runs were also made at 1 km grid size for July, 2001) Model results for formaldehyde, ozone and ultrafine PM are compared with observational data from a recent field study in Wilmington, DE.). Our attention will be focused on an area covered by a 12 km CMAQ grid cell (and its nine 4 km cells) centered over Wilmington DE. The ultrafine particle and formaldehyde data were collected in situ using an instrumented van deployed in a mobile sampling mode for approximately one week periods during each of four seasons in 2005-2006. (During the summer of 2005, an ozone monitor was installed and operated in the van.). The sampling consisted of mobile transects over a set course covering much of the street blocks over an areas about 1 km by 2 km of downtown Wilmington. Each set of transects took approximately an hour to complete. The concentration distributions derived from each of the time series of the individual transects and

constituted a sample which is then compared against distributions based on the modeled results.

SENSITIVITY ANALYSIS OF EMISSION GROWTH FACTORS FOR 2009 DESIGN VALUE, NORTHEAST OHIO

Myoungwoo Kim, Jhumoor Biswas, Kevin Crist, and Bill Spires

In 1997 the U.S. Environmental Protection Agency (EPA) amended the existing National Ambient Air Quality Standard for 1-hour ozone to one based on an 8-hour average. The U.S. EPA has provided guidelines for development of a State Implementation Plan (SIP) that will exhibit that the future probable mathematically determined concentrations or the design values of 8-hour averaged ozone concentrations at observational sites must be reduced to or maintained at or below the National Ambient Air Quality Standards to assume attainment. Selected counties in the Cleveland region are currently in non-attainment based on the stricter 8-hour ozone design values at their monitoring sites. In this study the photochemical model CAMx (Comprehensive Air Quality model with extensions) along with non-hydrostatic Penn State/ NCAR Mesoscale Meteorological Model (MM5) and the Emissions Modeling System (EMS) was applied to the eastern United States with special emphasis on the State of Ohio focusing on the northeastern regions of this state to study the attainment demonstration in the Cleveland region. It was also found by application of the photochemical modeling system that certain counties in the Cleveland region will still be in non-attainment of the 8-hour ozone standards for the year 2010 which is the year set by EPA for attainment demonstration for moderate non-attainment regions. Lake Michigan Air Directors Consortium (LADCO) has applied CAMx for the projected year design values in 2009 and 2012 for northeast Ohio. In this study, alternative emission growth factors were applied for specific categories such as non-EGU point sources, aircrafts-ships-locomotives non-road sources, and commercial and residential non-road sources. These emission growth factors were estimated based on Title V reporting for non-EGU point sources, evaluation of aircraft usage patterns, and economic indicators such as employment and population growth in northeast Ohio. The CAMx model results utilizing the alternative emission growth factors demonstrated a 1.4 ppb decrease in the projected design value for 2009 in the Cleveland area. This project indicates that reconsideration of emission growth factors could potentially have an impact on the projected design values.

Recent Developments in the Community Emissions Model: CONCEPT

Mark Janssen - LADCO

This presentation will include discussion of recent modifications to the Consolidated Community Emissions Processing Tool(CONCEPT). The CONCEPT Project was started by the Regional Planning Organizations and continues to have enhancements and improvements through a variety of community based projects. The two most active projects are development of link based onroad mobile inventories with CONCEPT and inclusion of updated biogenics for secondary organics using the MEGAN algorithm. The Mobile source discussion will include examples of how complex temporal information can influence emissions calculations for sensitive variables like vehicle mix and hourly profiles. The discussion of the updated biogenics model will include model performance improvements using plant species level emissions rated to calculate biogenic organic carbon emissions and its precursors.

An Evaluation of Aerosol Chemistry and Transport in the Great Lakes Region

Scott Spak and Tracey Holloway
Center for Sustainability and the Global Environment
University of Wisconsin-Madison

We employ a 2001 annual simulation with CMAQ to identify patterns in the speciation, number density, and mass concentration of PM10 and PM2.5 in the Upper Midwestern U.S. CMAQ 4.3 is run at 36 km resolution using the 2001 EPA Clean Air Interstate Rule emissions inventory, MM5 meteorology, and boundary conditions from the MOZART global atmospheric chemistry model. Results are compared to hourly and daily-average surface observations from the IMPROVE and EPA Speciation Trends networks. Effects of CMAQ model configuration (plume-in-grid dispersion, advection scheme, sectional PM) are compared, identifying common findings and model-dependent features.

A Modeling Study to Quantify the Impact of Aviation Emissions on Air Quality

Adel Hanna, Sarav Arunachalam, Andy Holland, B H Baek
University of North Carolina at Chapel Hill
Ian Waitz
Massachusetts Institute of Technology
Mohan Gupta
Federal Aviation Administration

This work is motivated by the need to better understand the relationship between airport emissions from commercial aircraft and local air quality. There objectives are: quantifying the impact of aviation on local air quality throughout the U.S. and establishing a simplified parametric relationship between emissions and air quality impacts. The results presented are preliminary and focused on the potential impacts due to emissions from commercial aircraft activities at 150 airports that are located in non-attainment areas. A sensitivity modeling study was developed by comparing baseline model concentrations to sensitivity model concentrations (excluding commercial aircraft emissions). The baseline simulation was performed for the entire mainland U.S. region and for the period May-August, 2002 using 36 km x 36 km horizontal model resolution.

The contribution of NOx emissions from commercial aircraft to all sources of emissions are in general less than 5% at most of the grid cells of airports located in non attainment areas in the U.S. The modeling analyses reveal that the removal of commercial aircraft emissions results in regional benefits for both PM2.5 and daily maximum 8-hour ozone. However for ozone, a disbenefit (increase of ozone as a result of removal of commercial aircraft emissions) is found near several urban cores. A 6-parameter fitted formula was established using modeled values at grid cells containing the location of the airports (called as radius 0) and in maximum concentration cluster of 3x3 and 5x5 grid cells centered on the airport (called as radius 1 and radius 2) respectively. The 6-parameter fitted formula shows high correlation with modeled differences of PM2.5 at radius 0. The ozone case shows much less correlation between the parameter fitted formulae and model concentrations. At radii 1 and 2, the correlations between differences of model concentrations and differences in emissions are small. Based upon the chosen grid-resolution and input databases for this study, we conclude that the air quality impact of commercial aircraft emissions quickly diminishes at locations

further away from the grid cell containing the airport.

Numerical Noise in PM Simulation in CMAQ

David C. Wong and Daniel Tong1
Atmospheric Sciences Modeling Division2
Air Resources Laboratory
1 In Partnership with US EPA
2 On Assignment from Science and Technology Corp.

Use the Eta-CMAQ air quality forecasting system to estimate crop loss from ozone damages in the United States

Daniel Tong$, Rohit Mathur+, Kenneth Schere+, Daiwen Kang$, Shaocai Yu$, George Pouliot+, Robert Mendelsohn& Atmospheric Sciences Modeling Division, Air Resources Laboratory, National Oceanic and Atmospheric Administration, RTP, NC 27711 +On assignment to NERL, U.S. Environmental Protection Agency, Research Triangle Park, NC 27711 $ On assignment from Science and Technology Corporation, 10 Basil Sawyer Drive, Hampton, VA 23666-1393 &School of Forestry and Environmental Studies, Yale University, New Haven, CT 06511

Optimistic predictions of impacts of changing environment on agriculture have been made that rising carbon-dioxide levels are likely to increase food production. Much of the work, however, has ignored the potential damage of air pollution to agricultural crops. Ozone (O3) is well documented as the air pollutant most damaging to agricultural crops. Crop damage due to exposure to O3 is of particular concern as ambient O3 concentrations remain high in many major food producing countries, such as the United States and China. Assessing O3 damage to crops is challenging due to the difficulties in determining the reduction in crop yield that results from exposure to surface O3, for which monitors are limited and mostly deployed in non-rural areas. This study presents an integrated approach that utilizes archived results from the NOAA/EPA air quality forecasting (AQF) system to estimate crop exposure to surface O3 in rural areas. We use results from the experimental nationwide air quality forecast, initialized in June 2005, and county-level crop data from USDA s National Agricultural Statistics Services to estimate crop exposure to surface O3 in the continental United States. Dose-response functions from the National Crop Loss Assessment Network (NCLAN) studies are used to convert calculated O3 exposure into damages and then resultant economic cost. We also estimate the potential benefits from agricultural crop yield if the O3 NAAQS is attained across the country. Such an integrated assessment approach, when combined with long-term continuous simulations of national air quality, can eventually provide us a more comprehensive view of impacts of environmental change on society, with food production in this particular case.

Incorporating biomass burning emissions in the 2006 air quality forecast and its implications to US air quality and public health

Daniel Tong$, Rohit Mathur+, George Pouliot+, Kenneth Schere, Shaocai Yu$, Daiwen Kang$, and Jeff Young+ Atmospheric Sciences Modeling Division, Air Resources Laboratory, National Oceanic and Atmospheric Administration, RTP, NC 27711 +On assignment to NERL, U.S. Environmental Protection Agency, Research Triangle Park, NC 27711 $ On assignment from Science and Technology Corporation, 10 Basil Sawyer Drive, Hampton, VA 23666-1393

Biomass burning, such as wildfire and prescribed burning, can contribute to local and regional air pollutant loading that impairs an area s ability to attain air quality standards designated to protect public health and welfare. Due to uncertainties associated with estimating fire emissions and their spatial and temporal occurrences, biomass burning has not been included in most regional air quality simulations. Biomass burning emissions are incorporated into the WRF-CMAQ air quality forecasting system for the 2006 operation. Since the fire emissions inventory is developed based on historic fire data, allocating the emission load temporally and spatially is difficult from an air quality forecasting perspective as burning episodes do not always reoccur at the same place during the same period for a future year. We therefore redistribute the episodic emissions from biomass burning to a level averaged over the burning season. By turning on and off biomass burning emissions, we examine the resulting impacts of biomass burning on the regional air quality in the US. We then couple the change in concentrations with population distribution and dose-response functions from epidemiological studies to calculate health impacts of the biomass burning-induced degradation in air quality.

Utilizing CMAQ Modeling to Assess Regional Impacts of Air Pollutants in Beijing Area, China

Joshua Fu, Carey Jang, David Streets, Zuopan Li, Hao Jiming, Kebin He, Litao Wang, Qiang Zhang

China is taking major steps to improve Beijing s air quality for the 2008 Olympic Games. However, concentrations of fine particulate matter and ozone in Beijing often exceed healthful levels in the summertime. The Models-3/CMAQ modeling application that has been conducted to simulate multi-pollutants in Beijing is presented. To model the regional effects of air pollution from surrounding provinces, the study domain covers East China (12-kmx12-km). For this study, the Asian emission inventory based on the emission estimates of the year 2000 that supported the NASA TRACE-P program. The 8 districts of Beijing local emissions inventory are used to replace TRACE-P in the area of the 12-km domains, respectively. The meteorological data for the Models-3/CMAQ run are extracted from MM5. The model simulation is performed in summer time for all contributions from outside of Beijing in 2001. ozone concentrations can be in the range of 60-90 ppb even with man-made Beijing emissions removed. Based on limited observational data for ozone in Beijing, we believe that the predicted concentrations of ozone in Beijing are somewhat underestimated. Our analysis of NOx/VOC ratios and ozone formation indicators (e.g., H2O2/HNO3) also lends support to this hypothesis. Further modeling studies and measurements of ozone in Beijing are called for. Sources outside Beijing contribute a consistent level of >20 ¼g m-3 to Beijing PM2.5 levels. The contribution of Beijing sources alone is >30 ¼g m-3 over a wide area of urban Beijing and >60 ¼g m-3 in the city center. Based on the U.S. EPA s Models-3/CMAQ model simulation over the Beijing region, we estimate that about 34% of PM2.5 on average and 35-60% of ozone during high ozone episodes at the Olympic Stadium site can be attributed to sources outside Beijing. Neighboring Hebei and Shandong Provinces and the Tianjin Municipality all exert significant influence on Beijing s air quality. During sustained wind flow from the south, Hebei Province can contribute 50-70% of Beijing s PM2.5 concentrations and 20-30% of ozone. Controlling only local sources in Beijing will not be sufficient to attain the air quality goal set for the Beijing Olympics. There is an urgent need for regional air quality management

studies and new emission control strategies to ensure that the air quality goals for 2008 are met.

A Study of the Dependence of VOC Reactivity on Environmental Conditions in the Houston - Galveston Area
B. Czader, D.W. Byun, S. Kim, P. Percell, B. Rappenglück

Houston - Galveston area is the region where NAAQS for ozone is often violated. The measured ozone concentrations often exceed 120 ppb, and in many occasions they surpass 200 ppb. Among the sources of ozone precursors are VOC and NOx emissions related to human activities (area and mobile sources) as well as emissions from industrial facilities that are densely located in the Houston Ship Channel area. These point source emissions make Houston air composition quite unique in comparison to other U.S. cities. The Texas Air Quality Study aimed to characterize Houston chemical and meteorological condition leading to high ozone event. However, few investigations involving reactivity estimation of individual compounds with air quality model have been carried so far for the Houston Galveston area. In this study reactivity of individual organic species toward ozone formation is calculated for the Houston Galveston air conditions. Two area of interest are chosen inside this region, one representing urban air mixture and the other dominated by industrial sources emissions. Reactivity is calculated for different days of the summer 2000 episode, and different time of the day representing distinctive emissions and meteorological conditions. An extended version of SAPRC99 mechanism, representing 26 additional individual compounds explicitly, is developed, and employed for the CMAQ model simulations. The Screening Trajectory Ozone Prediction (STOP) system is used for quick evaluation of the chemical reactivities. Dependence of reactivity of individual VOCs on air mixture composition is established.

Simulation and Analysis of Regional Climate Effects of Smoke Pollutants
Yongqiang Liu (Forestry Sciences Laboratory, USDA Forest Service, Athen, GA)

Biomass burning releases a large amount of smoke pollutants. By scattering and absorbing solar radiation, smoke pollutants, acting as atmospheric aerosols, can change atmospheric solar radiation (i.e., radiative forcing), which can further change regional climate. In this study, a regional climate model was first used to simulate direct radiative forcing of smoke pollutants and the resulting atmospheric perturbations. The simulated clouds and precipitation are reduced due to smoke, in agreement with a recent finding from satellite measurements. Smoke also leads to the enhancement of a dominant planetary-scale high system. A two-layer structure of warmer air with ascending tendency on top of cooler air with descending tendency is formed due to smoke with strong absorption. A radiative-dynamical model was then used to analyze the major factors for the atmospheric disturbances due to smoke. The model is developed by including smoke radiative forcing and turbulent heat transfer in a model for study of bio-geophysical self-feedback mechanism. Radiative forcing of smoke is expressed as atmospheric absorption and bottom boundary condition (sensible heat flux). The analytical solution of the model confirms the simulated two-layer structure in the atmospheric disturbances.

The Impact of Short-Term Climate Variations on Predicted Surface Ozone Concentrations in the Eastern US 2020 and Beyond
Shao-Hang Chu and William W. Cox

A statistical model (the CDV model) is used to characterize the short-term climate variability impact on photochemical model predictions of ozone in the eastern United States in the year 2020 due to projected emission changes resulting from existing and planned control measures and growth. In this study, the ozone design values predicted by CAMx model (version 3.1) at each ozone monitoring site was used in the analysis. The CDV model applies the ozone inter-annual variability and the difference in average design value levels between 2001 to 2020, due explicitly to meteorological influences, to predict the probability of future violation of the ozone NAAQS at 2020. The CDV prediction reveals potential problem areas which are otherwise not identified by the CAMx photochemical model predictions. The success of this hybrid modeling approach not only significantly improves the photochemical model predictability but also provides a reliable forecast tool in the study of short-term climate impact on ambient air quality in the time frame of 20-30 years.

Implementation of the Particle and Precursor Tagging Methodology (PPTM) for the CMAQ Modeling System: Mercury Tagging

Tom Braverman, USEPA, OAQPS, RTP, NC; Tom Myers, ICF International, San Rafael, CA; Dwight Atkinson, USEPA, OW, Washington, DC

Several current air quality modeling systems include mercury (Hg) as simulation species and are, thus, able to provide information on the formation, transport and deposition of mercury. The ability to estimate the contribution of airborne mercury from various sources, source categories, and source regions to wet and dry deposition at specific locations is important to air quality and water quality planning. Mercury tagging is a technique that provides this information. Each process that effects mercury species (e.g. gas phase reactions) is simulated for the overall mercury and the mercury associated with each of the tags. Since all proceses are tracked for mercury species, the deposition of mercury is provided for overall mercury species and each tag. The mercury tagging is one element of the Particle and Precursor Tagging Methodology (PPTM), which also supports sulfur and nitrogen tagging. Mercury emissions from selected sources, source categories, or source regions are (numerically) tagged and then tracked throughout a simulation and the contribution from each tag to the simulated concentration or deposition for any given location can be quantified. Tagging provides information about the contribution of the tagged sources, without modification of the simulated conditions. Tagged sources and source categories may include, for example, power plants, incinerators, motor vehicles, and simulation boundary conditions (input to the modeling domain from outside global sources). Tags can also be applied by State, geographic region or individual species of mercury. The mercury tagging procedure has recently been implemented in the Community Multiscale Air Quality (CMAQ) model. This presentation will describe the mercury tagging procedure in greater detail, discuss how the mercury tagging procedure is utilized with CMAQ, and will provide results of CMAQ mercury tagging applications.

Assessing the Effects of Emissions on Visibility in the Pacific Northwest using CMAQ.

Xin Qiu, Martin Gauthier, Mike Lepage, Jeff Lundgren, Wayne Boulton, Colin di Cenzo

Haziness or visibility impairment is strongly influenced by changes in emissions,

meteorological related phenomena and the atmospheric chemistry. Visibility impairment, expressed as DeciView (Dv), is a useful parameter that can be used to assess the air quality in a region. Since 2003, the authors have been involved in a study to set up, test, and deliver to Environment Canada a unique air quality modelling system comprised of the following components: the MC2 meteorological model, the SMOKE emission data processing system, and the CMAQ photochemistry/transport model. The initial work focused on the preparation of a comprehensive air quality modelling system that would satisfy the unique research and application needs of Environment Canada in the Pacific Northwest, which included the capability to evaluate the impacts of Canadian and U.S. emissions from anthropogenic and natural sources on: ozone, fine particulate matter, and visibility. Over the past three years, the study has involved: the preparation of MC2 meteorological data on specific projections and domains/grids, the compilation and processing of emission inventory data through SMOKE for more than 25 unique emissions scenarios, and the performance of regional air quality modelling over the study domain for typical summer and winter periods. To assist in the analysis of how visibility is affected by different emission scenarios, six Lines of Sight were defined within the CMAQ inner, 4 km resolution domain. Haziness or visibility impairment (Dv) along the six Lines of Sight was calculated from the CMAQ model results. The study revealed that Lines of Sight not only responded to emissions changes, but also to other factors such as meteorological conditions. For example, large reductions of NOx related to marine vessel emissions had only a small impact on visibility due to the presence of fog and moisture in the marine areas.

Results of the SMOKE/WRF-Chem Coupled Modeling System
Carlie J. Coats, Jr. John N. McHenry

We will show a comparison between model emissions and air quality results for WRF-Chem with in-line emissions (basically meteorology independent, except for biogenics) and for the coupled WRF/SMOKE/WRF-Chem system.

Simulation of Exposures to PM2.5 Trace Elements in Detroit during DEARS using CMAQ
Adam H. Reff, Prakash V. Bhave, Carvin Stevens, Ron Williams

The inhalation transfer factor (ITF) - defined as the fraction of a pollutant emission that is inhaled by an individual - is specific to the location, emission source, pollutant, and meteorological scenario. Population ITF (PITF) values can potentially provide an effective metric for determining the sources that most substantially contribute to human exposure, providing useful preliminary estimates with which to design effective exposure mitigation strategies (Lai et al., JA&WMA, v50, p1688). In this work, PITF values in Detroit, MI during Summer 2004 will be calculated through simulations of ambient fine particulate matter (PM2.5) and chemical constituents in Detroit, MI with the Community Multi-Scale Air Quality (CMAQ) model. Analysis of the EPA National Emissions Inventory (NEI) shows that major source categories of PM2.5 in the Detroit area include residential wood combustion (11.8% of emissions), bituminous coal combustion (11.4%), and unpaved road dust (11.3%). Subsequent dispersion of these emissions in CMAQ and calculations of PITF values will reveal the relative importance of these and other source categories to human exposure.

Deleterious health effects are known to be associated with exposure to a number a number of metals present in PM2.5. Air quality models have historically been designed to simulate only the ionic and carbonaceous fractions of PM2.5, with the remaining mass treated as an inert species. An emissions inventory of PM2.5 trace elements has recently been developed, and a modified version of CMAQ that employs the new inventory is used to simulate concentrations of a suite of 42 PM2.5 species and trace elements across the eastern U.S. for what we believe is the first time. Resulting predictions are evaluated against measurements made during the Detroit Exposure and Aerosol Research Study (DEARS) by USEPA. Population data from Detroit are then combined with the CMAQ results to calculate source- and pollutant-specific PITF values.

Diagnostic Probes of Gas- and Aerosol-phase Constituents in CMAQ-UCD Using the BRACE 2002 Aloft Data
J.R. Arnold, W.T. Luke, C.G. Nolte, R.L. Dennis

The NOAA Twin Otter is an ideal research platform for urban air quality studies: the high-wing, unpressurized airplane can carry 900 kg of payload for 4.5 h duration aloft; its operating range is 900 km; and its slow flight speed (55-60 m s-1) and excellent maneuverability facilitate high-resolution chemical and meteorological measurements. In May 2002, the Twin Otter flew science missions for the BRACE field intensive on 14 days, producing data from three to ten hours' duration generally concentrated in the photochemically-active midday period. Because the aircraft was moving along various flight paths in the Tampa Bay airhsed, it passed through a variable number of CMAQ-UCD model grid cells vertically and horizontally in each hour. Hence, comparisons to model predictions aloft were computed from the CMAQ-UCD 2 km solution as the time-weighted averages from all cells passed through by the Twin Otter, adjusted for the length of time the aircraft remained in each cell. The corresponding Twin Otter values were scaled up to one hour averages from their various underlying sampling frequencies, which ranged from 1 Hz to 15 min. CMAQ-UCD performance aloft was excellent. Means of the model-to-observation ratios for operational and diagnostic comparisons over all hours and surfaces were

New results on study of bias-adjustment techniques for Air Quality Forecasts
Daiwen Kang, Rohit Mathur, S. Trivikrama Rao, and and Shaocai Yu

Additional analysis on the application performance of bias-adjustment techniques for air quality forecasting has been conducted since last CMAS workshop. Two techniques namely a hybrid approach and a Kalman filter technique are examined. The new results include the optimization of the error ratio, which dictates the manner by which the KF responds to the variations in biases at prior steps, the KF application in combination with the Kolmogorov-Zurbenko (KZ) filter decomposed intraday components, and the characteristics of the bias-adjustment technique performance at different concentration levels. The optimum error ratios were estimated for each location based on the criterion that generates the minimum root mean square error (RMSE). However, the influence of the optimum error ratios on RMSE of the corrected forecasts was found to be small compared with that when a reasonable universal ratio was used for all the locations. The KF-KZ bias-adjustment technique is found to have a large impact on O3 forecasts at locations at California, in that it significantly improved the performance of O3 forecasts, but the KF-KZ technique

generally showed little improvement compared with the use of KF bias-adjustment technique at other locations. The limitation of the bias-adjustment techniques due to the non-linear behavior of the model will also be discussed.

An Operational Evaluation of the WRF-CMAQ

Brian Eder+, Daiwen Kang$, Shaocai Yu$, Rohit Mathur+ Atmospheric Sciences Modeling Division, NERL, U.S. Environmental Protection Agency, Research Triangle Park, NC 27711 +On assignment from Air Resources Laboratory, National Oceanic and Atmospheric Administration, RTP, NC 27711 $ On assignment from Science and Technology Corporation, 10 Basil Sawyer Drive, Hampton, VA 23666-1393

The National Oceanic and Atmospheric Administration (NOAA), in partnership with the Environmental Protection Agency (EPA), have developed an operational Air Quality Forecasting System for the United States. The system, which couples NOAA s WRF (Weather Research Forecast) meteorological model with EPA s Community Multiscale Air Quality (CMAQ) model, will be providing public forecasts of hourly, peak 1- and 8-hour ozone (O3) concentrations over the contiguous United States throughout the summer of 2007. In order to characterize the performance of the modeling system a suite of statistical metrics that facilitates evaluation of both discrete-type forecasts (observed versus modeled concentrations of O3) and categorical-type forecasts (observed versus modeled exceedances of both the maximum 1-hr and 8-hr standards for O3) will be applied over various temporal and spatial resolutions. Ozone data from more than 1000 monitors obtained from EPA s AIRNOW monitoring network will be used in the evaluation.

Effect of Heteorogeneous HONO Formation on the Ambient Ozone Concentrations

Yee-Lin Wu and Dermin Tsai Department of Environmental Engineering National Cheng Kung University Tainan, Taiwan

In addition to the ozone concentration, Wu et al. (2004) have compared the CMAQ simulated results with observed H2O2, HNO2, and HNO3 concentrations. Although the agreements were fair for the daytime HNO2 concentrations, significant underestimations of simulated results were noted and the differences were up to several orders of magnitudes. The possible missing mechanism in the CMAQ is the heterogeneous formation mechanisms for HONO. In this study, several possible heteorogeneous HONO formation mechanisms have been tested with CMAQ to evaluate its effects on the ambient HONO and O3 concentrations. Results show that significant improvement in the simulation of nighttime HONO concentration and its impact on the ozone concentration is about 10 ppb.

Uncertainty analysis of ozone formation and emission control responses using high-order sensitivities under three different meteorological conditions

Di Tian1, Dan Cohan2, Yongtao Hu, Sergey Napelenok3, and Armistead Russell School of civil and environmental engineering, Georgia Institute of Technology, Atlanta, Georgia, 30332 1 Now at Georgia Department of Natural Resources, Atlanta, Georgia, 30332 2 Now at Department of civil and environmental engineering, Rice University, Houston, TX, 77005 3 Now at Atmospheric Sciences Modeling Division, NOAA In partnership with the U.S. EPA, Research Triangle Park, NC 27711 Michael Chang School of earth and atmospheric science, Georgia Institute of Technology, Atlanta, Georgia, 30332

Uncertainties in emission inventories are regarded as one of the major sources of uncertainty in air quality modeling. Their impacts on ozone formation and emission control efficiencies during future year 2007 with three different base year episodes have been evaluated using high-order sensitivities calculated by a decoupled direct method implemented in community multiscale air quality model (CMAQ). Large emission inventory uncertainties, e.g. a factor of 1.5 for 95% confidence interval (CI) of stationary point NOX emission and a factor of 2 for 95% CI of all other emissions, lead to less than 10% uncertainties (as coefficient of variance) in ozone concentrations. Elevated ozone concentrations in Atlanta are impacted by NOX emissions from Atlanta mobile sources, point sources inside and outside Atlanta, and Atlanta anthropogenic VOC emissions in a decreasing order, with anthropogenic VOC emissions having their primary impacts in the downtown Atlanta area. Uncertainties in Atlanta mobile NOX emissions have the largest impact on uncertainties in ozone concentrations, with similar impacts of uncertainties in emissions from other source categories at a smaller scale. A large variance in the impacts of emission inventory uncertainties is found within an episode, while the variance between episodes is small. Reducing NOX emissions from Atlanta mobile source is the most efficient way to control ozone, followed by point NOX emissions inside and outside of Atlanta and anthropogenic VOC emissions. Mean emission control efficiencies with consideration of emission inventory uncertainties indicate similar ranking, with significant uncertainties associated with emission control efficiencies. Uncertainties in emissions sometimes even lead to negative emission control efficiencies, i.e. ozone concentrations increase with emission reduction. Better understanding of emissions in Atlanta is required for the development of a reliable control strategy in the Atlanta area.

An overview of the NAM-WRF CMAQ Air Quality Forecasting System run operationally during the Summer 2007.
Jeff McQueen, Pius Lee, Marina Tsidulko, Youhua Tang, Ho-Chun Huang, Sarah Lu, Rohit Mathur, Daewin Kang, Hsin-Mu Lin, Shoacai Yu, Geoff DiMego and Paula Davidson

This presentation will overview upgrades to the NOAA-EPA Regional Air Quality Forecast System for the Summer 2007 ozone season. The AQF modeling system consists Weather Research and Forecasting Nonhydrostatic Mesoscale Model (WRF-NMM) run in the NCEP North American Model (NAM) cycle slot and the EPA CMAQ to predict ozone, particulate matter and their precursers. The operational AQFS (Eastern U.S. domain w gas phase chemistry) and experimental (CONUS with gas phase chemistry) produce 48 hour forecasts twice per day (06 and 12 Z cycles) with 6 hour update cycles driven by the NAM Data Assimilation 3D variational assimilation System (NDAS). A 48 hour developmental configuration with CMAQ gas phase and aerosol chemistry is run once per day to 48 hours with 24 hour cycling. The experimental and developmental runs are configured with tight vertical coupling between NAM and CMAQ. Upgrades to point, source and mobile emissions were made and tests with various boundary layer mixing schemes were performed to improve experimental model performance over California. This paper will also overview NAM-WRF model changes that included upgrades to the model's surface layer and land surface parameterizations to help address low level moist biases. Impact of n the NAM improvements on the CMAQ foreasts will be summarized.

Generalized Numerical Approach to the Treatment of Aqueous Chemistry in CMAQ

Annmarie G. Carlton, Gerald Gipson, Shawn Roselle and Rohit Mathur

Clouds and aqueous phase processes affect atmospheric chemistry in several ways: convective mixing provides a mechanism for venting atmospheric constituents from the boundary layer to the free troposphere; aqueous chemistry in clouds can produce secondary aerosol, acid rain, fog and haze. Development of efficient and accurate numerical models to better understand the effects of clouds on the atmosphere is essential. The current cloud model in CMAQ includes an aqueous chemistry module derived from the Regional Acid Deposition Model (RADM). A new module is being developed that utilizes a generalized Rosenbrock solver for numerical solution of aqueous chemistry equations in CMAQ. Gas/aqueous partitioning, acid/base equilibria and chemical change equations are solved simultaneously. Presented box models results are compared with results from a Gear solver technique. Results from several aqueous phase chemical mechanisms are discussed.

A Nudging Strategy for Mesobeta-Scale WRF Simulations Suitable for Retrospective Air Quality Modeling

Tanya L. Otte (1) and Lara J. Reynolds (2) (1) NOAA Air Resources Laboratory, Atmospheric Sciences Modeling Division, RTP, NC (In partnership with U.S. EPA, National Exposure Research Laboratory) (2) Computer Sciences Corporation, RTP, NC

In a landmark paper, Stauffer and Seaman (1994) developed a multiscale nudging strategy for mesoalpha-scale (30-km resolution) and mesobeta-scale (10-km resolution) meteorological modeling simulations using the PSU/NCAR Mesoscale Model (MM5). Their approach was based on a combination of nudging toward gridded analyses that were regularly spaced in time (i.e., analysis nudging) and nudging toward asynoptic observations that were irregular in space and time (i.e., observation nudging). Seaman et al. (1995) extended the multiscale nudging technique to a series of MM5 runs at 36-km, 12-km, and 4-km horizontal grid spacing where analysis nudging is emphasized at the coarser horizontal resolution and there is a gradual transition to observation nudging at the finer resolution. That nudging strategy is commonly used for meteorological modeling simulations that support retrospective air quality modeling. In the mid-90's, background analyses were only archived every 12 h and at a coarse (2.5 degree) horizontal grid spacing. Those analyses, even when reanalyzed to the simulation domain using available land-based observations, often did not reflect mesoscale details in the meteorological fields. Thus, nudging toward those data at the finer scales may not have been beneficial. Today background analyses from operational models are archived with a finer temporal (i.e., 3-h or 6-h) and spatial (12-km) granularity. In addition, those analyses include remotely sensed data that complete the 3D description of the state of the atmosphere. Given these advances in modeling, as well as the upgrade from MM5 to the Weather Research and Forecasting (WRF) Model, it is timely to explore whether or not the typical nudging strategies are still appropriate. This presentation will offer preliminary findings toward the development of an effective nudging strategy using WRF that is suitable for retrospective air quality modeling at the mesobeta scale.

Evaluation of WRF/Chem-MADRID with the July 2004 New England Air Quality

Study Episode

Xiao-Ming Hu, Evelyn F. Frazier, and Yang Zhang North Carolina State University Stuart A. McKeen, Georg A. Grell, and Steven E. Peckham NOAA-Earth Systems Research Laboratory Shaocai Yu$ and Kenneth L. Schere+ Atmospheric Sciences Modeling Division, NOAA, Research Triangle Park, NC, USA $ On assignment from Science and Technology Corporation + In partnership with the U.S. Environmental Protection Agency

The Weather Research and Forecast/Chemistry Model (WRF/Chem) that simulates chemistry simultaneously with meteorology has recently been developed for real-time forecasting. As one of the six air quality models, WRF/Chem with a modal aerosol module has been applied for ozone and PM2.5 ensemble forecasts over eastern U.S. as part of the 2004 New England Air Quality Study (NEAQS) program (NEAQS-2004). Summer haze and ozone episodes in the New England area are characterized by high local emissions, large scale flow coupled with local thermal circulation (e.g., southwest flow, the Appalachian lee trough, and the nocturnal low-level jet), and regional transport from upwind areas (e.g., northern Ohio River Valley and northeast corridor). Extensive gas and aerosol measurements over this area are available for model evaluation from the 2004 International Consortium for Atmospheric Research on Transport and Transformation (ICARTT)/NEAQS field campaign. In this work, WRF/Chem with the Model of Aerosol Dynamics, Reaction, Ionization, and Dissolution (MADRID) (referred to as WRF/Chem-MADRID) will be evaluated using July NEAQS-2004 episode over eastern U.S. The evaluation will focus on several gas/particle mass transfer approaches in WRF/Chem-MADRID including newly-developed computationally-efficient kinetic and hybrid gas/particle mass transfer approaches for volatile or semi-volatile species. The model outputs will be evaluated using observations from ICARTT and four surface routine monitoring networks (i.e., AIRNow, STN, IMPROVE and CASTNet). The intercomparison between the prediction from WRF/Chem-MADRID and previous predictions from the aforementioned six models will be conducted and the difference will be interpreted and linked to different mechanisms used in each model. The accuracy and computational efficiency of different gas/particle mass transfer approaches on simulated gas and aerosol concentrations will also be examined.

Sensitivity of the Community Multiscale Air Quality (CMAQ) Model to Convective Cloud Parameterizations in the Meteorological Model

Shawn J. Roselle, Tanya L. Otte, Jonathan E. Pleim, Robert C. Gilliam, and K. Wyat Appel Atmospheric Sciences Modeling Division, Air Resources Laboratory, NOAA, Research Triangle Park, North Carolina, USA, in partnership with the National Exposure Research Laboratory, U.S. Environmental Protection Agency

Modeling air quality requires an accurate representation of the physics and chemistry of the atmosphere. Clouds are important to air quality because they transport pollutants from the boundary layer into the free troposphere, provide cloud and rainwater for aqueous chemical reactions, attenuate solar radiation impacting photochemistry, and remove pollutants through the process of wet deposition. In the current Community Multiscale Air Quality (CMAQ) modeling system, clouds are loosely connected to the meteorological driver; CMAQ develops clouds based on environmental profiles and precipitation provided by the meteorological model. To study the impact of meteorological model configurations on air quality, CMAQ has been applied to several datasets,

including: (1) a simulation with the PSU/NCAR Mesoscale Model (MM5) using the Kain-Fritsch (KF) cumulus parameterization; (2) a simulation with the Weather Research and Forecasting (WRF) model using the KF cumulus parameterization; and (3) a WRF simulation with the Grell-Devenyi ensemble cumulus scheme. An evaluation of the air quality and meteorological simulations will be presented. DISCLAIMER The research presented here was performed under the Memorandum of Understanding between the U.S. Environmental Protection Agency (EPA) and the U.S. Department of Commerce's National Oceanic and Atmospheric Administration (NOAA) and under agreement number DW13921548. Although it has been reviewed by EPA and NOAA and approved for publication, it does not necessarily reflect their policies or views.

Using CMAQ to Simulate a Dust Storm in the Southwestern United States
Daniel Tong, George Bowker, Rohit Mathur, Tom Pierce, Shaocai Yu, Dale Gillette

Airborne dust generated during windstorms from natural desert areas can have a significant impact on air quality from local to regional and, occasionally, hemispheric scales. This study uses the CMAQ) model to simulate a 2003 dust storm event in the southwestern United States. The magnitude of the sediment eroded by the wind was predicted using a stand-alone dust emission model based on the local wind speed, the threshold wind speed to initiate erosion, soil texture and moisture, land use type, and vegetation coverage. The windblown dust emitted during the storm, transported vertically and available for regional transport, was calculated to be a fraction of the total sediment eroded by the wind. The calculated dust emissions were then combined with other natural and anthropogenic emissions and fed into the CMAQ model. Finally, we compared CMAQ-predicted particulate matter (PM) concentrations with measurements collected within the dust storm and at IMPROVE sites further downwind. While results of this study are preliminary, we demonstrate here how the dust emission model and CMAQ can be used together to simulate the effects of major dust storm event on air quality. Accurate simulation of the emission and transport of windblown dust will be increasingly important to air quality management in the United States, as majority of climate models have projected an imminent transition of a more arid climate in the southwest North America. Disclaimer: The research presented here was performed under the Memorandum of Understanding between the U.S. Environmental Protection Agency (EPA) and the U.S. Department of Commerce's National Oceanic and Atmospheric Administration (NOAA) and under agreement number DW13921548. This work constitutes a contribution to the NOAA Air Quality Program. Although it has been reviewed by EPA and NOAA and approved for publication, it does not necessarily reflect their policies or views.

Comparative evaluation of the impact of WRF/NMM and WRF/ARW meteorology on CMAQ simulations for O3 and PM2.5 during the 2006 TexAQS/GoMACCS study
Shaocai Yu, Rohit Mathur, Jonathan Pleim, Daiwen Kang, Daniel Tong, Brian Eder, Kenneth Schere, S.T. Rao, Jeff McQueen, Pius Lee, Marina Tsidulko, Youhua Tang, Paula Davidson

The Weather, Research and Forecasting (WRF) model, a next generation mesoscale weather model, has been used to produce meteorological input for the Community Multiscale Air Quality (CMAQ) model. There are two available dynamical cores within the WRF modeling system. These cores are the Advanced

Research WRF (ARW) developed by the National Center for Atmospheric Research (NCAR), and the nonhydrostatic Mesoscale Model (NMM) developed by the National Centers for Environmental Prediction (NCEP). In this study, the impact of WRF/NMM and WRF/ARW meteorology on CMAQ simulations for O3, PM2.5 chemical composition (SO42-, NO3-, and NH4+), their gaseous precursors, meteorological variables (liquid water content, water vapor, temperature, wind speed and direction and pressure) has been examined in detail over the eastern U.S. with the observations obtained by aircraft, ship, ozonesonde, and lidar during the 2006 Texas Air Quality Study/Gulf of Mexico Atmospheric Composition and Climate Study (TexAQS/GoMACCS) field experiments. The influence of WRF/NMM and WRF/ARW meteorology on the simulated ground-level O3 and PM2.5 mass over the eastern U.S during this period is examined through comparison with observations from the U.S. EPA Air Quality System (AQS) network. Disclaimer: The research presented here was performed under the Memorandum of Understanding between the U.S. Environmental Protection Agency (EPA) and the U.S. Department of Commerce's National Oceanic and Atmospheric Administration (NOAA) and under agreement number DW13921548. This work constitutes a contribution to the NOAA Air Quality Program. Although it has been reviewed by EPA and NOAA and approved for publication, it does not necessarily reflect their policies or views.

A detailed evaluation of the WRF-CMAQ forecast model performance for O3, and PM2.5 during the 2006 TexAQS/GoMACCS study
Shaocai Yu, Rohit Mathur, Daiwen Kang, Jonathan Pleim, Daniel Tong, Brian Eder, Kenneth Schere

Atmospheric ozone (O3), and fine particulate matter (PM2.5; particles with diameters less than 2.5 mm) created by pollution from anthropogenic and biogenic sources can adversely affect human and ecosystem health, and are thus of major concern in the U.S. In this study, the WRF-CMAQ model s forecast performance for O3, PM2.5 chemical composition (SO42-, NO3-, and NH4+), and their gas precursors has been examined over the eastern U.S. with the observations obtained by aircraft, ship, ozonesonde, and lidar during the 2006 Texas Air Quality Study/Gulf of Mexico Atmospheric Composition and Climate Study (TexAQS/GoMACCS) field experiments. The spatial and temporal performance of the model for ground-level O3 and PM2.5 mass over the eastern U.S during this period is also examined through comparison with observations from the U.S. EPA Air Quality System (AQS) network. Disclaimer: The research presented here was performed under the Memorandum of Understanding between the U.S. Environmental Protection Agency (EPA) and the U.S. Department of Commerce's National Oceanic and Atmospheric Administration (NOAA) and under agreement number DW13921548. This work constitutes a contribution to the NOAA Air Quality Program. Although it has been reviewed by EPA and NOAA and approved for publication, it does not necessarily reflect their policies or views.

Comparison of CMAQ Aerosol Prediction Using Two Thermodynamic Modules: UHAERO V.S. ISORROPIA
Fang-Yi Cheng, Andrey V. Martynenko, Daewon Byun and Jiwen He

To predict the gas/aerosol partitioning of semi-volatile inorganic aerosol is a challenging task because complex gas, liquid and solid phase equilibrium can exist. For the application in 3D air quality models like CMAQ, an efficient numerical algorithm must be used. In this research, we conduct CMAQ simulations

to compare the inorganic aerosol formation behaviors by the UHAERO and ISORROPIA modules. The differences between the UHAERO and ISORROPIA modules can be distinguished based on three general features: (1) methods of computing activity coefficient for aerosol-phase species, (2) methods of computing the aerosol water content, and (3) the numerical techniques to determine the equilibrium state. For instance, ISORROPIA uses a priori specification of the presence of solid phases at a certain relative humidity. While these assumptions facilitate the numerical determination of the equilibrium, they sometimes fail to capture the physical behavior of the aerosol species in certain ambient conditions. On the other hand, UHAERO predicts both deliquescence and crystallization based on thermodynamics. In general, UHAERO is more complete and complex, thus requiring more computation. Comparison of two CMAQ aerosol predictions using UHAERO and ISORROPIA is carried out for a winter (2002 January) episode. The resolution is at 36-km regional scale covering continental U.S. domain. The observed CASTNET and IMPROVE datasets and super site programs at Pittsburgh are used to evaluate the model performance. The preliminary results show distinctive behavior of nitrate and ammonium over the low relative humidity and low temperature regions. The focus of this research is to resolve the differences in simulated metastable and deliquescence behaviors between two modules.

Ozone and PM 2.5 verification in NAM-CMAQ modeling system at NCEP in relation to WRF/NMM meteorology evaluation

Marina Tsidulko, Jeff McQueen, Pius Lee, Geoff DiMego, Michael Ek, Rohit Mathur, Jon Pleim and Paula Davidson

The current version of the NOAA/EPA air quality forecast system uses WRF/NMM model as the meteorological driver and the CMAQ model for predicting reactive transport of chemical species. WRF/NMM is verified in the NCEP Forecast Verification System (FVS) allowing evaluation for surface and upper air data for different time periods and for relatively small sub-domains. Wind, temperature and moisture errors in WRF/NMM model are related to ozone and particular matter CMAQ forecasts. As one of the key parameters in air quality modeling determining extent of turbulence and dispersion of pollutants, PBL height was added to FVS several years ago. PBL verification is done with radiosonde data using Richardson number approach in computing observed PBL height. Different model approaches in boundary layer depth estimations include PBL height and mixed layer height derived in TKE boundary layer scheme, and also Richardson number approach. All versions of PBL height estimations derived in WRF/NMM model are verified with radiosonde data. Verification with aircraft (ACARS) observations is expected. Accuracy of PBL forecasts has a direct impact to ozone predictions and varies rather significantly for different sub-domains and individual stations. Retrospective period of July-August 2006 is chosen to verify ozone predictions using NCEP FVS system. Ozone forecasts with TKE PBL, Ri number PBL and mixed layer height are verified using FVS statistics. The study will also evaluate the impact of WRF/NMM temperature, moisture and wind errors on CMAQ forecasts for the retrospective period.

EPA s 2002 Multipollutant Platform: Model Applications and Evaluation of Ozone, Particulate Matter, and Toxics

Sharon Phillips, Madeleine Strum, Norman Possiel, Carey Jang, Patrick Dolwick, Brian Timin, Karen Wesson, Marc Houyoux, Rich Mason and Tyler Fox

US EPA s Office of Air Quality Planning and Standards is undertaking a series of model application and evaluation efforts across multiple pollutants and over multiple (urban and regional) scales using the Community Multi-scale Air Quality (CMAQ) and the AERMOD modeling systems. This work is part of an effort to develop and demonstrate the capability of multipollutant air quality modeling analyses as part of a comprehensive air quality management process. This paper focuses on the application and evaluation of the CMAQ modeling. The 2002 National Emission Inventory includes both criteria air pollutants (CAPs) and air toxics that are classified as hazardous air pollutants (HAPs) and were processed through SMOKE for two cases: CAP only, and combined CAP and HAP emissions. For the combined case, an effort was made to integrate the HAPs that are components of VOC with the VOC emissions without double-counting the emissions, thus enabling the HAP inventory estimates to influence the chemical speciation and resulting chemistry. Annual simulations for the 2002 modeling platform were conducted for both cases over the continental U.S. using a 36 km grid resolution and a 12km grid resolution for the Eastern U.S. The series of model simulations utilize a CAP only version of CMAQ as well as a multipollutant version of the CMAQ modeling system that was developed to predict ozone, particulate matter, mercury, and 38 other HAPs within one model simulation. The focus of this effort is to evaluate model predictions and gain a better understanding of the chemical and physical interactions between concentration and deposition of ozone, PM2.5 component species (including toxics metals), and precursor gases (including gaseous toxics). In this paper the model performance evaluation results for 2002 from the CAP only model simulation and the integrated CAP and HAP model simulation are compared.

On the verification of particulate matter simulated by the NOAA-EPA Air Quality Forecast system

Ho-Chun Huang, Pius Lee, Binbin Zhou, Jian Zeng, Marina Tsidulko, You-Hua Tang, Jeff McQueen, Shobha Kondragunta, Rohit Mathur, Jon Pleim, George Pouliot, Geoff DiMego, Ken Schere, and Paula Davidson

The NOAA-EPA Air Quality Forecast (AQF) system is run in an experimental mode to predict particulate matter (PM) concentrations at the National Centers for Environmental Prediction (NCEP). Model verification collected during this developmental stage is critical for understanding model errors now so that improvements to the AQF PMs forecast can be made for potential operational implementation. The modeling system consists of the NCEP Weather Research and Forecasting Mesoscale Model Non-hydrostatic Mesoscale Model (WRF-NMM) and the US EPA Community Multiscale Air Quality (CMAQ) modeling system and covers the continental US (CONUS). This study overviews WRF-CMAQ performance from March 2007 to present using NCEP s Forecast Verification System (FVS) grid2grid package to evaluate column integrated atmospheric optical depth (AOD) derived from the daily AQF product and GOES satellite observations. The preliminary results show that the AQF does not resolve AOD < 0.1 while the satellite data often produce 1/3 of the observed grid points with AOD < 0.1. For AOD > 0.2 categories, the AQF has better skill in the eastern US (critical successful index of 0.2 ~ 0.7) than the western US (critical successful index < 0.2). Satellite observed AOD provides a near real-time and wider aerial coverage. However, the retrieval of observed AOD is greatly affected by the presence of cloud and strong surface reflectivity. This leads to an inconsistent number of grid points for daily

comparison. The number of observed points available for comparison in the eastern US often is larger than those in the western US (can be more than 4 times larger). The skill scores of different days can be biased toward a typical area such as urban and/or rural area. We will explore the relationship between the weather system, available satellite observations, and computed statistics to interpret the modeling performance.

Evaluating uncertainty predictions using an ensemble of CMAQ model configurations
Robert W. Pinder, Robert C. Gilliam, Alice B. Gilliland, K. Wyat Appel

Because all models are a simplification of the phenomenon they aim to represent, it is useful to estimate the uncertainty in a given model result. The aim of probabilistic modeling is to bound the range of likely outcomes. A common way to generate such a range is with an ensemble of deterministic models. In this work, we use an ensemble of CMAQ simulations that include differences in the type and configuration of the meteorological model, the type and parameterization of the chemical mechanism, emissions and deposition. However, this approach is subjective, because the uncertainty range is dependant on the selection of the ensemble members. It is important to evaluate these ranges using two important criteria: (1) accuracy, the observed value often falls within the bounds, and (2) stringency, the probabilistic range is no wider than necessary. Using these criteria, we assess a variety of statistical methods for probabilistic evaluation. We then use these methods to improve our estimated uncertainty range using CMAQ ensembles. We find that using a relatively small number of ensemble members, it is possible to derive robust uncertainty estimates.

CMAQ simulated oxidized nitrogen: recent findings and model enhancements
Robert W. Pinder; Prakash V. Bhave; Annmarie G. Carlton; James Godowitch; Rohit Mathur; Sergey L. Napelenok; Jon Pleim; Golam Sarwar; Shaocai Yu

Oxidized nitrogen, including NO, NO2, HONO, NO3, HNO3, HNO4, N2O5, PAN, and alkyl nitrates, contributes to tropospheric ozone, fine particulate matter, and excess nitrogen deposition to sensitive ecosystems. Since many of these compounds are difficult to measure, their relative importance to atmospheric processes has been difficult to simulate and evaluate. In this work, we evaluate CMAQ simulations of these compounds in a common framework using ground-based, aircraft, and satellite observations including established monitoring networks and recent field campaigns. We use process analysis to explain discrepancies between modeled and observed values. Our evaluation has identified several key issues including: (1) insufficient NOx lifetime, (2) under predictions of HONO concentrations, (3) over predictions of HNO3 concentrations at night, (4) insufficient nitrate wet deposition during the summer, (5) under prediction of oxidized nitrogen aloft. Sensitivity results from candidate solutions to these problems will be presented in this poster.

Resolving the sources of PM2.5 in Georgia using emissions and receptor based models
Amit Marmur, Di Tian, Byeong-Uk Kim, and James Boylan

In response to EPA's designation of several areas in Georgia as non-attainment for PM2.5, the Georgia Environmental Protection Division (GA EPD) has conducted a sensitivity analysis using the EPA's Models-3 (MM5/SMOKE/CMAQ) modeling

system. This analysis assists in understanding the sources contributing to ambient PM2.5, and guides the development of efficient control strategies. However, the certainty in PM2.5 modeling results varies between its chemical components (e.g., the chemical processes leading to sulfate formation are better understood compared to those leading to the formation of secondary organic aerosol) and between its various sources (e.g., some emission sources are better characterized than others, especially for primary PM2.5). Such uncertainties might introduce a bias when weighing several control strategies as part of policy development. To address these uncertainties in emissions-based (CMAQ) PM2.5 modeling results, the GA EPD is complementing its modeling efforts with the use of receptor-based models, predominately Positive Matrix Factorization (PMF). PMF utilizes speciated PM2.5 data collected at a monitoring site to apportion total PM2.5 back to its contributing sources. PM2.5 source-apportionment results based on CMAQ and PMF are compared at several locations throughout Georgia, with emphasis on the each modeling technique's estimate of total mass associated with each source type, and its ability to capture both the temporal and spatial patterns of source-contributions throughout the state. This analysis assists in understanding the uncertainties associates with each modeling technique, and provides useful information to for policy development.

Forecasting the Impacts of Wild Fires
Talat Odman, Yongtao Hu, Armistead Russell

May 2007 has been phenomenal in terms of smoke events experienced in Atlanta, and throughout Georgia. The scrub fires in Okefenokee Wildlife Refuge that broke out by mid April grew to the biggest wildfire of the recent decades. First on May 16, then on May 22, and later on May 26-30 record high levels of PM2.5 were recorded at several metro Atlanta locations. From the air quality modeler s point of view, the question is how accurately the air quality impacts of these wildfires can be predicted using the current forecasting systems and whether the state of the models can be advanced to improve this accuracy. In this paper, we use an air quality forecasting system operated in Atlanta regularly during the ozone season to simulate the effects of wildfires. In an accompanying paper, the same system is used to simulate a prescribed burn on February 28th, 2007. Although there are similarities in the system setup, the simulation of wildfires presents numerous new challenges. The system consists of three major components: WRF for meteorology, SMOKE for emissions, and CMAQ for air quality. NAM forecasts are used to initialize the meteorological fields. Starting with a 36-km grid over the eastern US, 12- and 4-km grids are nested consecutively over southeastern US, and Georgia. The emissions from the wildfires are estimated using the Fire Emission Production Simulator. First, the system is used in its forecasting mode strictly with forecasted meteorology and fire information from previous days. Then, a few hind-casts are analyzed to evaluate the effects of nudging reanalysis data and using actual fire information. Several issues are investigated in relation to the emissions estimates by comparing the predicted O3 and PM2.5 fields to the ground-level observations. Finally, the effects of assimilating satellite observations both in forecasting and hind-casting modes are evaluated and directions are provided for modeling the impacts of wildfires in the future.

Sensitivity of top-down correction of 2004 black carbon emissions inventory in the United States to rural-sites versus urban-sites observational networks
Yongtao Hu, Sergey L. Napelenok, M. Talat Odman and Armistead G. Russell,

School of Civil and Environmental Engineering, Georgia Institute of Technology, Atlanta, Georgia, USA

Black carbon (BC) is emitted into earth s lower atmosphere mainly through fossil fuel combustion and bio-mass combustion. BC is a significant component of fine particulate matter in ground level atmosphere and is found influential on climate radiation forcing budget with its high regional variability. BC emissions in the United States is estimated to be about 5% of the global totals (8.0 Tg) in year 1996, as the third largest country after China (~20%) and India (~9%). Inverse modeling techniques reconcile the gap between modeled and observed pollutant concentrations by multi-step adjustments of emissions. We apply an inverse method that uses DDM-3D in the Community Multiscale Air Quality model (CMAQ) at a 36-km horizontal resolution over continental North America, to correct the current estimation of U.S regional BC emissions. Fully operational BC monitoring networks, i.e. STN, IMPROVE, SEARCH and ASACA, at both urban and rural locations are utilized to constrain the BC emissions in the U.S. for the year 2004. The difference between the CMAQ simulations and the observations, along with the DDM-3D derived sensitivities of BC concentrations to each source group, are used to estimate how much BC emissions from a specific source should be adjusted to optimize the CMAQ BC performance through ridge regression. A set of scaling factors are calculated for five source categories (i.e. on-road mobile, non-road mobile, fire, wood-fuel combustion and other sources) from five RPO regions, for five months of 2004 (i.e. January, March, May, August and October). An a posteriori BC emissions inventory is then developed by implementing those scaling factors obtained from the optimization and CMAQ is re-run by using the a posteriori emissions. Here we investigate the sensitivity of the a posteriori CMAQ-run performance to rural-sites (IMPROVE) versus urban-sites (STN) networks by applying their observations separately in the inverse modeling.

Comparison and Evaluation of the ACM2 and MYJ PBL models used in both WRF/ARW and CMAQ simulations during the 2006 TexAQS/GoMACCS study
Jonathan Pleim, Robert Gilliam, Shaocai Yu

Realistic Planetary Boundary Layer (PBL) simulation of both meteorological parameters (u,v,qv,qv,qc,qi) and trace chemical species are critical components of combined meteorology and air quality model systems. Ideally, all chemical and meteorological parameters should be modeled using identical PBL modeling techniques. However, with the common practice of offline modeling, many physical processes, including PBL, are often modeled using completely different techniques that mix meteorological and chemical parameters differently and often result in different effective meteorological and chemical mixed layers. The WRF-CMAQ system is being upgraded for consistent online and offline capabilities. Thus, identical PBL simulation in both components is necessary. This study will compare two PBL models applied consistently in both WRF and CMAQ: the Mellor Yamada Janic (MYJ) TKE scheme that is used in the NCEP WRF-NMM and the Asymmetric Convective Model version 2 (ACM) that was recently added to both WRF and CMAQ. The two sets of WRF/CMAQ runs that differ only in their PBL component will be compared for the summer and early fall of 2006. A variety of observed vertical profiles of both metrological and chemical parameters from the 2006 Texas Air Quality Study/Gulf of Mexico Atmospheric Composition and Climate Study (TexAQS/GoMACCS) will be used for evaluation, including rawinsondes, ozonesondes, radar profilers, both ship borne and aircraft LIDAR,

and aircraft profiles. Several of these platforms had co-located meteorological and chemical measurements. Thus, we can perform combined evaluations of chemical and meteorological vertical profiles for the two sets of model simulations.

A GIS-based Study for Optimizing the Total Emission Control Strategy in Lanzhou City

Xingqin An12 Anqing Ma3 Daobin Liu3
1 Centre for Atmosphere Watch And Services (CAWAS), CMA
Chinese Academy of Meteorological Sciences (CAMS), 46 Zhong-Guan-Cun S. Ave., Beijing 100081, China
2 College of Environmental Sciences, Peking University, Beijing 100871, China
3 Department of Environmental Science and Engineering, Ocean University of China, Qingdao, Shandong 266003, China

A geographic information system (GIS)-based approach with spatial analysis advantages was developed to optimize the total emission control scheme on air pollution in Lanzhou, combined with Models-3 modeling system and a linear programming model. GIS system is mainly used for establishing a multifactor assessment model to quantitatively divide environmental functional zone, and also used for selecting control sites in linear programming model. The results show that most of the urban area belongs to the second type of function, which is 122.8 km2 occupying about 76.5% and the third type of about 32.9 km2 occupying 20.5%. To reach the air quality up to the national standard in the entire control area, some large-emission factories need to cut emissions from 19% to 27%. For small but low-emission height sources, the cut may be as high 40%. The improvement of the ecological environment is urgently needed for controlling the background particle pollution.

Performance Evaluation of East Texas Air Quality (ETAQS) Forecasting and Transition to the Simulations for Air Quality Assessment

Daewon W. Byun, Fong Ngan, Dae-Gyun Lee, and Xiangshang Li
dbyun@mail.uh.edu Institute for Multidimensional Air Quality Studies Department of Geosciences, University of Houston

The Eastern Texas Air Quality (ETAQ) forecasting system was employed to support the Second Texas Air Quality Study (TexAQS-II), June 2005-October 2006, whose main objective was to understand the meteorological and chemical processes of high ozone and regional haze events. The real-time forecasting was used for planning of daily field program operations, and to provide information on the suitability of particular cases for future modeling activities. The ETAQ air quality forecasting system is based on MM5/SMOKE/CMAQ. We perform 54-hour air quality forecasting simulations with the 12-km regional domain, and the 4-km domain covering both the HGA and Dallas-Fort Worth (DFW) metropolitan areas. Performance evaluation of the forecasting results for the June 2005-May 2006 period and June 2006 Oct 2006 period were performed separately to demonstrate the effects of different emissions and meteorological events. When compared with observations, certain bad forecasting events during the 2006 summer were found to be related with serious inaccurate meteorological forecasting or due to the emissions upset events. Worse, we have found that the effects of bad forecasting results could last several days because the ETAQ forecasting system currently utilizes the results of the last hour of the previous day s forecast as the initial conditions for the following simulation day. We will

discuss how a multi-stage nested four-dimensional data assimilation (MS-FDDA) method can improve the meteorological simulations to generate inputs for air quality assessment studies. The MS-FDDA is repeatedly applied at multiple nest domains to minimize the prediction errors at the target domains. The scheme needs to be refined and evaluated further but the preliminary results seem beneficial for correcting the meteorological forecasting errors and subsequent air quality simulations. With accurate meteorological inputs, uncertainties in the emissions inputs for the upset events could be studied.

Simulating Climate-Chemistry-Aerosol-Cloud-Radiation Feedbacks in WRF/Chem: Model Development and Initial Application

Yang Zhang, Xiao-Ming Hu, and Xin-Yu Wen, North Carolina State University, Raleigh, NC; Kenneth L. Schere, Atmospheric Sciences Modeling Division, NOAA, Research Triangle Park, NC(In partnership with the U.S. EPA); Carey J. Jang, Office of Air Quality Planning & Standards, the U.S. EPA, Research Triangle Park, NC

The two-way and chain feedbacks between atmospheric aerosols and meteorology/climate are very important but traditionally neglected in mesoscale meteorology and air quality modeling due largely to historical separation of meteorology, climate, and air quality communities as well as our limited understanding of mechanisms underlying those feedbacks. Some potential impacts of aerosol feedbacks include a reduction of downward solar/thermal-IR radiation (direct effect); a decrease in surface temperature and wind speed but an increase in relative humidity and atmospheric stability (semi-direct effect), a decrease in cloud drop size but an increase in drop number via serving as cloud condensation nuclei (first indirect effect), as well as an increase in liquid water content, cloud cover, and lifetime of low level clouds but a suppression of precipitation (the second indirect effect). Accurately simulating those feedbacks requires fully-coupled meteorology, climate, and chemistry models and presents significant challenges in terms of both scientific understanding and computational demand. In this work, the above feedbacks will be examined using the Weather Research and Forecast/Chemistry Model (WRF/Chem) that couples chemistry and aerosols with meteorology online. The Carbon Bond Mechanism 2005 (CB05) is being coupled with aerosol modules in WRF/Chem (e.g., the Model for Simulating Aerosol Interactions and Chemistry (MOSAIC) and the Model of Aerosol Dynamics, Reaction, Ionization, and Dissolution (MADRID)) to enable the simulation of those feedbacks. WRF/Chem-CB05-MOSAIC (or MADRID) will be applied for the July 2001 episode over the continental U.S. with a horizontal grid spacing of 36-km to demonstrate the climate-chemistry-aerosol-cloud-radiation feedbacks. Recommendations for future model development and improvement for accurately representing aerosol feedbacks will be provided based on the initial application and lessons learned from this application.

Using linked global and regional models to simulate U.S. air quality in the year 2050

Christopher G. Nolte, Alice B. Gilliland, Christian Hogrefe

The potential impact of global climate change on future air quality in the U.S. is investigated with a coupled global/regional-scale modeling system. Regional climate model scenarios developed by dynamically downscaling outputs from the Harvard/GISS global chemistry/climate model are used by CMAQ to simulate climatological air quality. CMAQ is first applied to a 5-year period representing

current climate and evaluated by comparison against measurements of surface ozone and chemically speciated fine particulate matter (PM25) concentrations. Next, the model is applied to a simulated climate for the year 2050 based on the IPCC A1B scenario. Two 5-year future simulations are conducted, one basecase simulation with anthropogenic emissions held at 2001 levels, and one with anthropogenic emissions reduced in accordance with the A1B scenario for the developed world. In both future simulations, biogenic and other climate-sensitive emissions are modulated by the simulated climate. Results indicate a substantial positive bias in the predicted daily maximum 8-h average ozone concentrations relative to current measurements. For the future basecase simulation, small increases from 2-5 ppb in summer ozone concentrations are obtained in Texas and parts of the eastern U.S., while decreases of 1-2 ug/m3 PM25 are seen in most of the eastern U.S. By contrast, substantial decreases exceeding 15 ppb ozone and 10 ug/m3 PM25 are predicted for the future control case. These results show that, under the A1B scenario, the emissions reductions envisioned for the U.S. have a much larger impact than, and are only slightly counteracted by, increases caused by climate change. Sensitivity tests conducted with methane concentrations increased by 30% yield 0.5-2 ppb higher ozone concentrations throughout most of the U.S., pointing to the need to consider changes in methane levels alongside climate change when simulating future air quality.

Application of the CMAQ-UCD Aerosol Model to a Coastal Urban Site
Christopher G. Nolte, Prakash V. Bhave, Robin L. Dennis, Jeff R. Arnold, K. Max Zhang, and Anthony S. Wexler

The University of California at Davis (UCD) aerosol module, an internally mixed, sectional aerosol model with dynamic mass transfer between the gas and particle phases, has been coupled to CMAQ. This paper describes the application of CMAQ-UCD to simulate air quality in Tampa. Modeled aerosol size and composition distributions are evaluated against 15 daily size-segregated ambient measurements of sulfate, ammonium, nitrate, sodium, and chloride collected at three Tampa-area sites during May 2002, and against semi-continuous total aerosol measurements collected at a single site. Sea salt emissions over the open ocean and the surf zone are parameterized as a function of modeled wind speed and relative humidity. The regional meteorology is accurately simulated, with a slight temperature bias but with excellent representation of complex sea breeze patterns. Modeled total aerosol sulfate and ammonium concentrations and size distributions are in good agreement with measurements, with average normalized mean bias (NMB) of -0.4 and -22.3% and normalized mean error (NME) of 44.0 and 39.8%, respectively, and generally correctly identifying the size bin in which the peak concentration is observed. Sea salt size distributions are also simulated well, with the distribution dominated by the coarse mode and total aerosol sodium and chloride NMB of -1.1 and 19.5% and NME of 31.1 and 38.8%. This good agreement indicates that sea salt emissions, advective transport, and deposition are being accurately captured, on average. However, analysis of the continuous time series measurements reveals that the model significantly overpredicts aerosol chloride concentrations at night. Aerosol nitrate is consistently significantly underpredicted by about a factor of two (NMB = -50.1%) though the model correctly identifies that nitrate is predominantly in the coarse (Dp > 2.5um) size sections. Evidence for the displacement of aerosol chloride by nitrate is discussed.

Model Inter-comparison to Evaluate Gaseous Pollutants in East Asia Using an

Advanced Modeling System: Models-3/CMAQ System

Joshua S. Fu, Carey J. Jang, David G. Streets, Zuopan Li, Roger Kwok, Rokjin Park, Zhiwei Han,

An advanced modeling system with a one-atmosphere perspective, Models-3/Community Multi-scale Air Quality (CMAQ) modeling system, driven by MM5/NCEP reanalysis data as the meteororology, and GEOS-Chem outputs as boundary values was applied to simulate the O3, and other gaseous pollutants (SO2, and NO2) evolution among other atmospheric chemicals for July 2001. Comparisons had been made with 7 models in the MICS-II exercise for the same period. Statistics of both monthly and daily means show that the model skill is very well in reproducing O3 and SO2 with small to moderate RMSE. The model species capture the day-to-day and spatial variability of the observations. The same O3 model concentrations that over-predict most of the EANET observations in the MICS-II study may have underpredicted ones from monitoring networks in Beijing area that is not included in this paper. Vertical O3 profiles at 4 ozonesonde sites are well predicted in July 2001. In fact, our model is among the best of those MICS-II models within the 2-km surface layer. The meteorology near surface and lower troposphere is well reproduced. Compared to SO2 and O3, the NO2 gas concentrations are simulated less well, but the correlation coefficient is still significant. The choice of reanalysis meteorological fields and different boundary conditions generated by different global models may result in diverse spatial patterns exhibited by MICS-II models and ours. Our spatial distributions of O3 shows a high concentration patch covering Beijing, a moderate to high pattern across Korea and Japan Sea, and a low but extensive pattern enclosing southern China, Taiwan and East Sea. Extension of the pattern to southern China coincides with the existence of pollution problems in Guangdong and Taiwan, but overprediction of O3 over the region deserves further improvement by various factors. One of them can be the grid resolution to resolve the complex orography in or close to the ocean. Another factor can be the refinement of local land use data that changes the micro-meteorology in favor of more air pollution events.

Box Model Tests of Two Mass Transfer Methods for Volatile Aerosol Species in CMAQ

Uma Shankar*, Prakash Bhave**,*UNC-Institute for the Environment, **Atmospheric Sciences Modeling Division, Air Resources Laboratory, National Oceanic and Atmospheric Administration (on assignment to the National Exposure Research Laboratory, U.S Environmental Protection Agency)

Sea salt aerosol constitutes an important component of the global background aerosol loading. Sea salt particles also influence the aerosol composition in coastal environments as they contribute surfaces for heterogeneous chemical reactions with condensable and volatile species (H2SO4, HNO3 and NH3). The mass transfer of the volatile species between the gas- and particulate phases is a size-dependent process, with the smaller particles coming to their equilibrium concentrations with the gas phase more rapidly than the larger particles. Two methods of modeling the mass transfer process have been tested in a box model version of CMAQ's aerosol module: (1) a fine-particle equilibrium method wherein the fine aerosol modes are at an instantaneous equilibrium with the gas phase with equilibrium concentrations determined by ISORROPIA based on ambient temperature and relative humidity (RH), and the coarse mode is chemically non-reactive and (2) a fully dynamic method which transfers mass between the

gas- and particulate phase at multiple substeps of the model time step, adjusting the size distribution after each mass transfer. A hybrid approach, which applies the first method to the fine modes and the second method to the coarse mode will be tested next. Test results are presented for a Los Angeles episode for a 38-hour period, which injected emissions of H2SO4, HNO3 and NH3 into an urban background in the presence of background sea salt concentrations.

Climate Impacts on Air Quality and Response to Controls: Not Such an Uncertain Future

Kuo-Jen Liao, Efthimios Tagaris, Kasemsan Manomaiphiboon, Armistead G. Russell, Jung-Hun Woo, Praveen Amar, Shan He

Uncertainties in impacts of climate change on regional air quality and emission control responses are quantified for the continental U.S. Forecasts of future climate from two global climate models, NASA s GISS model and MIT s IGSM, are downscaled using MM5. CMAQ with DDM-3D is used to simulate future (2050) regional air quality and how pollutant levels will response to emissions reductions. Three future climate scenarios: high-extreme, low-extreme and base, downscaled from GISS and IGSM, are used for regional air quality simulation. Outputs from GISS with IPCC A1B scenario are determined as the base scenario while IGSM fields are used to perturb the base scenario. Impact of climate uncertainties on summer average daily maximum 8-hr average ozone (MDA8hr O3) and summertime fourth-highest daily maximum 8-hr average ozone (4th MDA8hr O3) are found up to 6 and 10 ppbV, respectively. Differences in seasonal average daily PM2.5 are predicted to range between -1.0-1.5 µg/m3 for the three different scenarios. The differences in MDA8hr O3, 4th MDA8hr O3 and seasonal average daily PM2.5 levels and their sensitivities to precursor emissions for three scenarios are relatively small compared to the reductions in 2050 due to planned emission controls. Controls of anthropogenic NOx and SO2 will continue to be the most effective for reducing regional ozone and PM2.5 in the future. However, urban areas should be more concerned about climate uncertainties for offsetting the effectiveness of emission controls.

Uncertainty of meteorological input choices on the modeled 2009 summer ozone predictions in Atlanta, GA

Byeong-Uk Kim, Maudood Khan, Amit Marmur, James Boylan

Recently, Atlanta, GA was designated as an 8-hour ozone non-attainment area by the United States Environmental Protection Agency. As required by the Clean Air Act Amendment (CAAA), the Georgia Environmental Protection Division (GA EPD) has been conducting the attainment demonstration modeling for the 8-hour ozone to meet the National Ambient Air Quality Standards in the future. GA EPD adopted the Community Multi-scale Air Quality (CMAQ) model and the Comprehensive Air Quality Model with extensions (CAMx) for our chemical transport models. Emissions inputs were generated using the Sparse Matrix Object Kernel Emissions (SMOKE) and meteorological inputs were produced by the Fifth-Generation NCAR / Penn State Mesoscale Model (MM5). In this presentation, we will show the effects of high resolution (i.e. 4-km grid resolution) meteorological inputs choices on the future case ozone concentrations predicted by CMAQ and CAMx. For these simulations, two sets of meteorological inputs were prepared. The first set was generated by running MM5 at 4-km grid resolution using 12-km MM5 outputs from the Visibility Improvement State and

Tribal Association of the Southeast (VISTAS) regional haze modeling modeling as boundary conditions. The second set was generated by exercising the CAMx Flexi-nesting option to interpolate the VISTAS 12-km MM5 outputs to our 4-km grid. For the CMAQ 4-km counterpart, meteorological inputs were generated by using the Flexi-nesting algorithm outside CMAQ. Therefore, four sets of simulation will be compared: 1) CMAQ with true 4-km MM5 outputs, 2) CAMx with true 4-km MM5 outputs, 3) CMAQ with 4-km meteorological inputs interpolated from true 12-km MM5 outputs, and 4) CAMx with 4-km meteorological inputs interpolated from true 12-km MM5 outputs.

Gas-Phase and Aerosol Chemistry Interactions in South Europe and the Mediterranean Region

Marina Astitha and George Kallos
University of Athens, School of Physics, Division of Environment and Meteorology, Atmospheric Modeling and Weather Forecasting Group, University Campus, Bldg. PHYS-V, Athens 15784, Greece

The impacts of gas-phase and aerosol chemistry interactions in the atmosphere and climate have been studied extensively during the last years. The scientific basis of such interactions is rather wide, requiring the expertise and collaboration of major scientific fields to reach into some vital conclusions. The Euro-Mediterranean Region is considered an area sensitive to interactions between gas-phase and aerosol chemical processes due to the coexistence of anthropogenic and natural atmospheric pollutants and the morphology of the area. In several occasions such coexistence can create air quality conditions that exceed the imposed air quality limit values. The physico-chemical processes allowing the interactions between gas-phase and aerosol constituents will be the primary focus of the work presented herein. Dust particles affecting photochemical reactions and acting as surfaces for uptake of several gases are some of the processes discussed in the present work. These processes require extensive investigation since they are complex and uncertain and model development is needed to properly include the relevant physicochemical processes. The interactions are studied using atmospheric and air-quality modeling tools following the necessary development in the air quality model CAMx. The capabilities of the new model development and the first results obtained so far are discussed in this paper. The results have revealed interesting effects of the coexistence of natural and anthropogenic gases and particulate matter concerning the impacts on air quality and the environment in the Mediterranean Region.

Evaluation of boundary conditions, initial conditions, and model grid resolutions in CMAQ-Hg modeling

Pruek Pongprueksa, Che-Jen Lin, and Thomas Ho

In this study, we present model responses in terms of mercury concentration and net (dry and wet) deposition to boundary condition (BC), initial condition (IC) of mercury species, and model grid resolutions (12-km and 36-km). The variation of gaseous elemental mercury (GEM) concentration (0 - 2 ng m-3) in BC has a very strong influence to mercury wet deposition. Varying reactive gaseous mercury (RGM) or particulate mercury (PHg) in BC was found to be less significant. The variations of mercury species concentration in IC has weaker effects on concentration and deposition compared to the effects of BC. Comparisons of

simulation results at different grid resolution show excellent agreement (slope = 0.950-1.026, r = 0.816-0.973) in mercury concentration, dry deposition, and net deposition. However, the agreement in wet deposition is weaker (slope = 0.770-0.794, r = 0.685-0.892) due to aqueous-phase chemistry and the difference in simulated precipitation.

Innovative Methods for Evaluating Meteorological Model Performance during the Central California Air Quality Studies

Neil Wheeler, Kenneth Craig, and Clinton MacDonald Sonoma Technology, Inc. Petaluma, CA

The Central California Air Quality Studies (CCAQS) comprise two studies, the California Regional Particulate Air Quality Study (CRPAQS) and the Central California Ozone Study (CCOS). CCAQS is a multi-year effort of meteorological and air quality monitoring, emission inventory development, data analysis, and air quality simulation modeling. To assess the readiness of meteorological data and models to drive the air quality simulations models, the following issues were investigated: (1) the adequacy and validity of measurement methods; (2) the sufficiency of data precision, accuracy, bias, consistency, and time-resolution; and (3) the ability of models to represent important phenomena. In addition, new model evaluation techniques were developed and tested. This paper describes those techniques and how they can be used to understand biases in meteorological model estimates and improve the representation of meteorological phenomena that are important in air quality modeling.

Forest Growth and Fire Fuel Predictions from 2000 to 2050 for Air Quality Modeling

Limei Ran, Uma Shankar, Aijun Xiu, Steve McNulty, Jennifer M. Myers

Forest cover has important and substantial effects on air quality. In addition to biogenic emissions and CO2 uptake, forest fire emissions can greatly affect our air quality. In recent years forest fires happened more frequently and more severely across the North America due to drought and higher temperature. With global warming, the situation could get worse especially in the southeast region. The goal of this study is to predict dead and live biomass fuels to be used in fire emission calculation when fires occur in the southeast region in future years. The PnET model developed at the Southern Global Change Program (SGCP) of the USDA Forest Service (FS) Southern Research Station (SRS) is used to estimate live biomass growth from 2000 to 2050 at species level within the Forest Inventory and Analysis (FIA) plots with inputs of soil conditions, the Community Climate System Model (CCSM) data, and CO2 emission scenario. Future dead fuel will be estimated based on predicted live biomass and the relationship of current dead fuel and live biomass fuel obtained from FS SRS at Knoxville. The dead and live fuel data are estimated at county level. MODIS 1km landuse data will be used in fuel allocation within each county. Fire and biogenic emissions from future forests will be tested using the BlueSky emission model (BlueSky-EM) and the MEGAN biogenic emission model.

Assessing Contributions to Mercury Pollution in Northeastern US Using CMAQ-PPTM Mercury Tagging

Shan He, John Graham, Junghun Woo, Gary Kleiman

This modeling study is to evaluate previously developed northeastern states

mercury emission inventory, assess the behavior of mercury transport, reaction and deposition, and identify contributing sources of mercury pollution in northeastern US. The modeling domain covers northeastern US as well as high emission regions in central and southeastern US with 12km resolution and 21 vertical layers. This study relies on our previously developed regional 2002/2003 mercury inventory which is updated from the 1999 NEI Hg emission inventory for the six New England states, New York and New Jersey. The mercury emission inventory for region outside 8 northeast states is based on US EPA s Clean Air Mercury Rule (CMAR) inventory and 2000 Canadian mercury inventory. For criteria air pollutants, 2002 RPO inventory and the updated Canadian inventory are adopted. A four month period during the summer of 2004 is modeled using CMAQ-PPTM Hg Tagging. Evaluation is conducted through comparing model results with three sets of measurements, including ambient air measurements, weekly integrated samples, and rain event samples from AIRMAP and mercury deposition network. The study identifies facilities with significant Hg emissions and units with uniform stack parameters and speciation profiles, then tags each individual Hg species to model Hg transport, chemical transformation, and deposition. The output would help to understand the atmospheric lifetime of the different Hg species and the spatial impact of emission sources. The study also tags all coal burning EGUs and non-coal burning EGU within a 200km radius of the Steubenville measurement site. The total Hg emission within this circle is 10.6 tons/yr, representing about 10% of total US mercury point source emissions. In addition, this study tags all other emissions to distinguish their contribution from the aforementioned sources, as well as the boundary conditions to analyze the impact of emissions transported into the domain.

Diagnostic Study on Particulate Matter Predictions of CMAQ-MADRID in the Southern Ontario

M. Taghavi(1), J. Sloan(2), S. Nikzad(2), H. Zhuanshi(2), J. Arteta(2), F. Meng(2), (1)Hormozgan University, BandarAbbas, Iran (2)Waterloo Center for Atmospheric Science, Waterloo, ON, Canada

The size and composition of aerosols are two major parameters that define their effects on human health, visibility degradation, and climate change. For example, the effects of fine particulate matter (PM2.5) on human health are more significant than those of coarse PM due to its ability to penetrate the blood circulation system. To quantify and understand these impacts, the composition and size distribution of the aerosol must be known. The complicated physical and chemical processes associated with PM formation and its atmospheric transport, and fate makes its accurate representation difficult in air quality models. We have used the Community Multiscale Air Quality Model (CMAQ), coupled with the Model of Aerosol Dynamics, Reaction, Ionization, and Dissolution (MADRID), referred as CMAQ-MADRID to quantify the atmospheric behavior of PM. The CAMQ-MADRID model, which is configured with 8 size bins for this work, is being used to predict size and composition distributions for PM over southern Ontario for the period of June-August 2001. The results will be compared with field measurements carried out during the same time period by Environment Canada and the Ontario Ministry of the Environment. The model predictions will also be compared with measurements recorded by national and regional monitoring networks. There is also a focus on secondary aerosol formation and size distributions, especially for nitrate (NO3-), sulfate (SO4=) and the source-receptor relations between precursors and pollutants are also investigated.

Quantifying the response of atmospheric model predictions to surface properties at different grid resolutions
Maudood Khan, William Crosson, Arastoo Biazar, and Mohammad Al-Hamdan

Accurate characterization of the land surface and its physical state plays an important role in determining the distribution of the surface energy budget, and consequently the evolution of the planetary boundary layer. Since day-to-day variation in emissions is small, modeling of ozone and particle chemistry and transport is particularly susceptible to inadequate representation of boundary layer processes. This is especially true for atmospheric modeling applications (e.g., public exposure to excessive heat and/or pollution) that require special focus on processes that occur within the boundary layer in conditions of weak synoptic-scale forcing. The 24-category USGS Land Use Land Cover (LULC) dataset most commonly used in meteorological and air quality modeling applications has been found to be deficient in its characterization of the urban/suburban landscape. We have incorporated the new released version of the National Land Cover Database (NLCD-2001) within the MM5/CMAQ and ARW/CMAQ modeling systems. Annual simulations were conducted at 36-km grid resolution over the continental United States and at 12- and 4-km grid resolution over Houston, New York, and Phoenix. We present here meteorological and air quality model performance evaluation results. Spatiotemporal statistical analysis of simulated fields highlights the relative importance of various land surface properties under varying physical states and at different grid resolutions.

Examining the Influence of in situ Aircraft Emissions with CMAQ
Francis S. Binkowski and Saravanan Arunachalam

We will present results ofr a case study that compares boudary layer and tropospheric condentrations of ozone and pm2.5 from CMAQ simulations that were run with standard inputs with a run that included aircraft emissions.

EAKF-CMAQ: Theoretical justification, development, and evaluation of
Alexis Zubrow, Li Chen, V. R. Kotamarthi

An integrated approach to modeling atmospheric chemistry with trace gas data assimilation is a relatively new focus of the atmospheric chemistry modeling community. It is expected that the predictive capability of CTMs can be significantly improved by assimilating measurements of key trace gases from satellite-based platforms and surface monitors. Ensemble adjustment Kalman filter (EAKF) methods are simple to implement, don't need adjoints and backward integration, and are capable of handling non-Gaussian model errors. These factors have led to the adoption of EAKF methods for weather and climate simulations. Additionally, EAKF provides a measure of error resulting from the assimilation. We have combined EAKF data assimilation with a single-tracer version of CMAQ. The Data Assimilation Research Testbed (DART), developed by NCAR, was used to create an EAKF enabled CMAQ for assimilating CO. We present theoretical justification for EAKF as well as comparisons with other sequential data assimilation techniques. We argue that it is a viable approach for further data assimilation experiments and potentially can be used to improve air quality forecasting, estimate uncertain parameters, and adjust emission values. We will present results from a number of numerical experiments that explore the model performance under various methods used to generate the prior for the initial

conditions and emissions. Results from EAKF-CMAQ provided improvements over a standard CMAQ run. The generation of priors was shown to significantly impact the fidelity of the EAKF-CMAQ runs. In addition, generation and conversion of measurement data to the model domain had a substantial impact on the model performance.

Initial Applications of the Control Strategy Tool within the Emissions Modeling Framework

Authors: Alison Eyth: Institute for the Environment, University of North Carolina at Chapel Hill; David Misenheimer, Darryl Weatherhead, Larry Sorrels: US EPA OAQPS Jim Wilkinson, Gregory Stella: Alpine Geophysics

EPA is developing the Control Strategy Tool (CoST) to allow users to generate emission inventories with additional controls applied on top of a future-year base inventory. COST tracks information about control measures, their costs, and the types of emissions sources to which they apply. It also computes control strategies that match control measures to emission sources using algorithms such as maximum emissions reduction and least cost . The result of a control strategy contains information that specifies the estimated cost and emissions reduction achieved for each control measure-source combination. The resulting control strategy can be exported to a CSV file as a table; viewed in a graphical table that supports sorting, filtering, and plotting; or it can exported to an emissions inventory file that can be input to SMOKE. CoST is currently implemented as components within the within the Emissions Modeling Framework (EMF), which is under development by EPA to solve the many long-standing difficulties of complex emissions modeling. By providing this new tool integrated within the EMF, it facilitates a level of collaboration between control strategy development and emission inventory modeling that was not previously possible. CoST will replace AirControlNET, a software tool that EPA developed previously. The reasons for replacing AirControlNET are to provide a more flexible software platform, support multi-pollutant analyses (including criteria pollutants and precursors, HAPs, and climate change gases), improve transparency of the underlying data and assumptions, allow eased import/export and editing of the underlying data, and enhance connectivity with other related software tools and datasets. CoST is being applied in pilot studies during the summer of 2007. The results of these studies will be discussed.

The application of fine-scale Computational Fluid Dynamics simulations of pollutant concentrations in support of air quality studies and potential interfacing within the CMAQ system.

Alan H Huber Institute for the Environment University of North Carolina, Chapel Hill, NC

Fine-scale Computational Fluid Dynamics (CFD) simulations of pollutant concentrations within roadway and building microenvironments is feasible using high performance computing. CFD models are emerging as a promising technology for such assessments, in part due to the advancing power of computational hardware and software. Unlike currently used regulatory air quality models, CFD simulations are able to account rigorously for topographical details such as terrain variations and building structures. Applications using current state-of-art computing hardware at the University of North Carolina will be discussed. The results of CFD simulations can both be directly used to better

understand specific case studies as well as be used to support the development of better-simplified algorithms that may be generally applied. Evaluation for supporting air quality modeling and best-practice CFD methodologies will be discussed. A framework for potential interfacing of fine-scale CFD simulations with the CMAQ system will be discussed.

Results from Using EPA's Emissions Modeling Framework
Marc Houyoux, Alison Eyth, Madeleine Strum

The Office of Air Quality Planning and Standards (OAQPS) at EPA has built and is applying an Emissions Modeling Framework (EMF) for managing emissions modeling. The EMF was created to help solve many of the significant challenges of emissions modeling, including (1) preventing bottlenecks and errors caused by emissions modeling activities, (2) performing emissions modeling in a consistent way across multiple projects, (3) sharing emissions data in a multi-user environment, and (4) providing transparency to emissions modeling. This paper describes EPA's ongoing experiences using the EMF in support of its 2002-based air quality modeling efforts to manage its emissions modeling data, to share data across the organization, and to run the Sparse Matrix Operator Kernel Emissions (SMOKE) modeling system. We further describe how we have used the EMF to reduce overall runtime and quality assurance time needed for emissions modeling in support of annual air quality modeling runs for a national 36-km grid and two 12-km grids, which collectively cover the continental United States. This paper also provides an update on the status of EMF s development and release of the system to the modeling community.

Development of a new inorganic atmospheric aerosol phase equilibrium model (UHAERO) for CMAQ
Andrey V. Martynenko, Fang-Yi Cheng, Jiwen W. He, John H. Seinfeld

A variety of thermodynamic models have been developed to predict inorganic gas-aerosol equilibrium. The models can be distinguished based on three general features: (1) the method of computing activity coefficients of the aerosol-phase species, (2) the method of computing the aerosol water content, and (3) the numerical technique that is used to determine the equilibrium state. In this talk, the current state of the art of thermodynamic quilibrium models is reviewed, and a new inorganic atmospheric aerosol phase quilibrium model (UHAERO) is presented. UHAERO incorporates two mole fraction based multicomponent activity coefficient models, namely the PSC an the ExUNIQUAC model. UHAERO-PSC is benchmarked against predictions obtained with the Aerosol Inorganic Model (AIM) and proved to be identical in terms of accuracy over the entire range of compositions and relative humidity for the sulfate/nitrate/ammonium/water system. Based on the widespread application of ISSOROPIA, the examination of the model performance of UHAERO against that of ISSOROPIA over an extended composition, temperature, and RH domain is detailed. It is observed that the overall speed of UHAERO is comparable to that of ISSOROPIA. The accuracy in the prediction of thermodynamic properties of electrolyte solutions such as pH value is quantified. The potential error in using the ZSR mixing rule to estimate the aerosol water content at low RH is assessed. The model success or failure to accurately predict deliquescence point depression in the multi-phase aerosol growth is compared. At the end, the performance of UHAERO modules in conjunction with chemical transport models such as CMAQ is

assessed for a PM episode.

Effects of Liquid Water on Secondary Inorganic Aerosol Concentrations in Central and Northern California during a Winter Episode

Paul Livingstone (1), Ajith Kaduwela (1,2), Kemal Gurer (1), Paul Allen (1), and Bruce Jackson (1) 1. Planning and Technical Support Division, California Air Resources Board, Sacramento, CA 95814 2. Department of Land, Air and Water Resources, University of California, Davis, CA 95616

Meteorological parameters drive the distribution of tracers in the air, and are used in key components of chemical transport models such as CMAQ. One such parameter, the liquid water content, is especially important for simulating soluble components, such as secondary inorganic aerosol (SIA). A winter PM episode was captured in San Joaquin Valley during December 2000-January 2001, and comprehensive observations and analyses have been conducted on chemical and meteorological parameters. During the winter episode, San Joaquin Valley was rather stagnant and no significant rainfall was observed. We employed CMAQ to conduct fine-grid simulations for this episode using meteorological inputs from MM5 with and without observational constraints on liquid water content near the surface, respectively. The simulated SIA components were evaluated with observations. We will present detailed results of our findings.

Impacts of Ethanol Fuel on PM Concentrations in Northern California during a Winter Episode

Paul Livingstone (1), Ajith Kaduwela (1,2), Kemal Gurer (1), Paul Allen (1), and Luis Woodhouse (1) 1. Planning and Technical Support Division, California Air Resources Board, Sacramento, CA 95814 2. Department of Land, Air and Water Resources, University of California, Davis, CA 95616

The use of ethanol as an additive to dilute fossil fuel reduces emissions of NOx, primary PM, greenhouse gases, and primary air toxics compared to the unblended fossil fuel. But it increases emissions of ethanol and acetaldehyde as well as the price of corn-based food products. A recent study showed that the use of an ethanol blend known as E-85 (20% ethanol and 80% gasoline) instead of regular gasoline (5% ethanol and 95% gasoline) may slightly increase ozone exposure in Los Angeles air basin under certain meteorological conditions owing to the non-linearity of ozone photochemistry. Thus, the impact of ethanol blends on PM exposure warrants further investigation. We employed meteorological conditions of a winter PM episode captured in San Joaquin Valley during December 2000-January 2001, to evaluate impacts of emission changes owing to the potential use of ethanol blends on PM exposure in northern California. The simulated impacts of the use of ethanol blends on PM exposure for this scenario will be presented and discussed.

Comparison of CMAQ and CAMx for an annual simulation over the South Coast Air Basin

Jin Lu (1), Kathleen Fahey (1), and Ajith Kaduwela (1,2) 1. Planning and Technical Support Division, Air Resources Board, California Environmental Protection Agency, Sacramento, CA, USA; 2. Department of Land, Air, and Water Resources, University of California at Davis, CA, USA

The South Coast Air Basin is currently designated as nonattainment for PM2.5. Addressing this issue properly requires extensive and rigorous long-term

chemical transport modeling used in conjunction with detailed species observations to elucidate important seasonal and regional differences in PM concentrations. A complex interplay between meteorology and chemistry shapes the aerosol size and composition distribution, and both primary and secondary particles make up significant portions of the total PM2.5 levels in the South Coast Air Basin. Effectively understanding the PM2.5 problem in this region therefore requires that comprehensive modeling be supplemented with well characterized emissions, meteorology, and chemistry. CMAQ and CAMx are two such comprehensive chemical transport models, and both of these are commonly used in regulatory applications. There have not been many comparisons between the two modeling systems for long-term simulations, however, in spite of the fact that there is an increasing dependence on long-term regulatory modeling to develop State Implementation Plans for nonattainment areas like the South Coast Air Basin (Tesche et al., 2006). Here we apply both models to a 116 x 80 5-km2 cell domain covering the South Coast Air Basin and surrounding areas for a 12-month simulation during 2005. The results from the two models will be presented and compared with observations from speciation sites throughout the basin. Performance statistics and sensitivities for the two models will also be presented.
References: Tesche, T.W., Morris, R., Tonnesen, G., McNally, D., Boylan, J., Brewer, P., 2006. CMAQ/CAMx annual 2002 performance evaluation over the eastern U.S. Atmospheric Environment 40(26), 4906-4919.

A Multiscale Modeling Approach to Assess Aviation Impacts on Local Air Quality

Saravanan Arunachalam, B.H. Baek, Andrew Holland, Zachariah Adelman, Neil Davis, Binyu Wang, James Wallace, Francis Binkowski, and Adel Hanna: Institute for the Environment, University of North Carolina at Chapel Hill

Emissions from aviation sources typically represent a small portion of the total emissions in an air quality region. However, given the projected growth in aviation transport and the continued decrease of emissions from most other anthropogenic sources, the analysis of emissions from aviation is of increased importance to understand their impacts on air quality. The Federal Aviation Administration (FAA) Emissions and Dispersion Modeling System (EDMS) is the required model for performing air quality analysis of aviation sources in the United States and is typically used to analyze changes to local air quality in the vicinity of individual airports. In the public release, EDMS computes spatially and temporally allocated emissions for use with the American Meteorological Society/EPA Regulatory Model (AERMOD) for estimating pollutant concentrations. The EPA National Emission Inventory (NEI) is used to support local- and regional-scale air quality modeling. Currently, aircraft emissions are represented as surface-level emissions by county in the NEI. However, given that aviation sources, and their emissions, operate in a three-dimensional environment, air quality models can benefit from emissions data that are more realistically spatially allocated. To provide realistic three dimensional representations of all aviation emissions, we developed an interface to the Sparse Matrix Operator Kernel Emissions (SMOKE) modeling system called EDMS2Inv that accepts the AERMOD-ready spatially and temporally allocated (hourly) emissions inventory from EDMS for direct use in the Community Multiscale Air Quality (CMAQ) model. We then applied these emissions in CMAQ simulations at 36 and 12-km resolution to quantify the incremental effects of aviation emissions on air quality. Simultaneously, we also applied the AERMOD model using these emissions to

study the near-scale variability of concentrations due to these aviation emissions. This paper summarizes the implementation of this improved representation of aviation emissions from three airports (Atlanta - Hartsfield, Chicago - O'Hare and Providence - T.F. Green) using the new link from EDMS to CMAQ, and presents preliminary results from annual CMAQ and AERMOD simulations with an emphasis of the contribution of aircraft emissions below 3,000 meters on predicted ozone and PM2.5.

Functional Description and Demonstration of the National Urban Database and Access Portal Tools (NUDAPT)
David Williams, Torrin Hultgren, and Jason Ching

Urban air quality models are increasing in complexity, not only in the number and type of input parameters, but in the variety of data sources and methods required to derive those input parameters. A typical Geographic Information System (GIS) is well suited to managing and manipulating these datasets, but is inefficient to implement for a modeler who only requires a small subset of the available functionality. A new, web-based system has been developed using ESRI's ArcGIS Server that delivers geoprocessing functionality (clip, project, resample, reformat) on demand. By storing source data alongside derived Urban Canopy Parameters (UCPs) in a centralized repository for easy comparison, extraction, transformation, and downloading, this system facilitates data sharing and collaboration. This paper will describe and demonstrate the functionality of the portal site utilizing data from the city of Houston, and illustrate a path forward for integrating data from additional cities.

Utilizing the Mosaic Approach to Estimate Deposition Velocities in CMAQ Model
Jehn-Yih Juang, Donna Schwede, Jon Pleim

In the current version of CMAQ model, the dry deposition velocities are calculated using grid-averaged soil and vegetation parameters. In this paper, we investigate the use of the mosaic approach to aggregate the contributions of the sub-grid scale land use to the deposition velocities and fluxes within each CMAQ grid. Output of land use-specific deposition fluxes will improve the usefulness of CMAQ output in ecological assessments and will facilitate future process-based simulation of bi-direction chemical exchange across water, soil and vegetation surface. At present, aerodynamic and stomatal resistances are calculated within the meteorological model (using the PX land-surface model) based on the averaged parameters. In the mosaic approach, these parameters are re-calculated within CMAQ based on the sub-grid scale land use and the assumption of kinetic energy balance in each CMAQ grid. A box model is presented first to analyze the sensitivity of the CMAQ deposition velocities and fluxes to the use of the mosaic approach. Implementation of the mosaic approach in the full CMAQ model is then analyzed for several regions of the U.S. using simulated meteorology and emissions for 2001. Comparisons of fluxes from the mosaic scheme with the results based on the grid-averaged soil and vegetation parameters is presented.

Further developments and applications for the adjoint of CMAQ
Amir Hakami, Kumaresh Singh, Adrian Sandu, John H. Seinfeld

Results of our continued work on the recently developed adjoint model for CMAQ (CMAQ-ADJ) are presented. These include discussions and improvements for the adjoint of horizontal advection schemes, parallel implementation of CMAQ-ADJ,

detailed analysis of computational efficiency for adjoint calculations, and extension to aqueous and aerosol phase processes. Brief discussion of the potential applications in areas of policy support, climate variability, inverse modeling, and air quality forecasting will be included.

Evaluation of Emission Control Strategies for Regional Scale Air Quality: Performance of Direct and Surrogate Techniques

Sastry Isukapalli, Tayfun Kindap, Aparna Vemuri, Sheng-Wei Wang, and Panos Georgopoulos Environmental and Occupational Health Sciences Institute, Piscataway, NJ 08854

Evaluation of emissions control strategies often involves several variables such as region-specific and source category-specific controls, and requires several photochemical air quality model simulations for combinations of various potential controls. Different sensitivity analysis techniques that can be applied include direct techniques such as the Direct Decoupled Method (DDM) and the Automatic Differentiation (AD), as well as surrogate techniques such as the High Dimensional Model Representation (HDMR). These provide alternative means for assessing model response without requiring simulations for each combination of different variables. The DDM requires addition of equations for the sensitivity calculations to the original model source code, and relies on local gradients. The AD technique is based on automatic processing of the model source code and also relies on local gradients. In contrast, the HDMR technique can be applied without alteration to the model and relies on a global response spanning the ranges of different dimensions. In this study, these sensitivity methods are comparatively evaluated for assessing the model response in the context of emission reductions on air quality using the CMAQ model for selected states in the Mid-Atlantic and Northeast US regions. Sensitivity techniques are compared for different control strategy options with respect to the following criteria : (a) estimation of sensitivity metrics, (b) performance as surrogates for estimating model response, and (c) providing source apportionment information. Disclaimer: This work is funded in part by the USEPA (Cooperative Agreement CR-83162501) and the New Jersey Department of Environmental Protection (NJDEP, through base funding to the Ozone Research Center). This work has not been reviewed by and does not represent the opinions of the funding agencies.

Estimate of Mercury Emission from Natural Sources in East Asia

Suraj K. Shetty, Che-Jen Lin, David G. Streets, Thomas C. Ho and Hsing-wei Chu

East Asia is considered to be one of the largest source regions that contribute to mercury release into the atmosphere. Although extensive studies have been devoted to estimating the anthropogenic mercury emission, little is known about mercury emission from natural sources in that region. Recently there are several studies that developed formulations for estimating natural emission. In this study, we adept the algorithms developed previously, coupled with detailed GIS data and satellite LAI products, to estimate mercury emission from natural sources including vegetation, soils, and water surface in an East Asian domain containing 164´97 grid cells at a spatial resolution of 36 km. It was observed that emissions from natural sources showed strong seasonal variation due to meteorology and vegetation coverage variation. Seasonal simulations (4 months) were performed to project the annual emission. From the simulation results, we estimated that the annual natural GEM emission in the domain is 750 Mg, with 560 Mg contributed by

China. The estimated natural mercury emission from China is comparable to the estimated annual anthropogenic emission of 575 Mg for Year 2001 (Streets et al., 2005). Combining both anthropogenic and natural emission, the total estimated mercury emission from China is about 1135 Mg/yr. This value is similar to a recent estimate of total mercury emission (1100 Mg/yr) using an inverse modeling approach (Pan et al, 2007).

Person Oriented Exposure Modeling for Ambient Air Toxics: High Resolution Modeling for Local Scale Air Quality

Sastry Isukapalli, Pradeep George, Spyros Stamatelos, Sheng-Wei Wang, and Panos Georgopoulos Environmental and Occupational Health Sciences Institute, Piscataway, NJ, 08854

Person-oriented modeling for assessing individual and population exposures to air toxics requires ambient concentration estimates at high resolutions. However, due to theoretical constraints, the resolution of grid models is often limited to 2 km. Further limitations arise due to the complexity in developing meteorology and emissions inputs at high resolutions, thus resulting in typical simulations at 4 km resolution or coarser. Several approaches have been used in the past for incorporating photochemical grid model outputs into exposure modeling at the resolution of a census tract and a census block. These include statistical techniques such as the Spatio-Temporal Random Field (STRF) and the Bayesian Maximum Entropy (BME), and hybrid methods that use local atmospheric dispersion models in conjunction with outputs from grid models. For even finer scales, street canyon models or detailed Computational Fluid Dynamics (CFD) simulations can be used with outputs from grid models. This study presents a critical evaluation of techniques for estimating concentrations of air toxics at different scales using available estimates at the next coarser resolution. Evaluation criteria include: (a) performance as a surrogate for obtaining finer scale model outputs from coarser scale model outputs, evaluated through model outputs at different resolutions; and (b) performance w.r.t. estimating point concentrations at specific point locations, evaluated using available measurements. Case studies are presented using CMAQ simulations in conjunction with statistical techniques, local scale models, and CFD simulations. The corresponding estimates of population exposures and study-specific, individual exposures are comparatively assessed. Disclaimer: This work is funded in part by the USEPA (Cooperative Agreement CR-83162501) and the American Chemistry Council (ACC). This work has not been reviewed by and does not represent the opinions of the funding agencies.

Off-line Air Quality Coupling System: Study of WRF-CMAQ Simulations for the TexasAQS 2000 Episode

Fong Ngan and Daewon Byun

The Weather Research and Forecasting (WRF) modeling system was demonstrated to have accurate numeric and high quality mass conservation characteristics. WRF framework is closer to CMAQ than other meteorological models. The causes of mass inconsistency such as the disparities of meteorological and air quality modeling is reduced when CMAQ is linked to WRF/ARW because both are based on common governing set of equations. However, there are other issues such as detailed numerical implementations and the frequency of data communication that would deteriorate such quality. In order to perform the off-line air quality

modeling accurately, we have to prepare many parameters describing meteorological conditions properly. WRF is able to generated comparable meteorological fields as MM5 when similar physical options and inputs are used in the simulations. In the latest version of WRF/ARW, more updated physical options and nudging processes are included so that more accurate meteorological data for CMAQ modeling can be generated. In this study, the effects of temporal interpolation on the mass inconsistency in WRF-CMAQ coupling is examined. Usually, WRF output is updated hourly but CMAQ needs meteorological information every integration time step. Tracer and full CMAQ simulations were performed and evaluated with the WRF meteorological data at various output frequencies, such as hourly, every 15 minutes and 1 minutes. The WRF outputs simulating an eleven-day TexAQS 2000 episode with 3-nested domains were used in the CMAQ simulations to study a high ozone event in the Houston-Galveston area. By comparing the results with the extensive surface and aircraft measurements during the TexAQS 2000 experiment, we evaluated the efficacy of the coupling method of CMAQ with WRF and studied the weakness and limitations of such method to model air quality in the Houston-Galveston area.

Air Quality Assessment of the South Coast Air Basin and Transboundary Pollutant Impacts of Emissions in the Imperial Valley-Calexico Region and From Southern California

Santosh Chandru, Yongtao Hu, Armistead G. Russell, Ana Yael Vanoye García, Arturo Morán Romero, Alberto Mendoza

Air pollution continues to be an increasing problem with the socio-economic and industrial growth in both sides of the US-Mexico border. Earlier Studies in the region have primarily focused on analysis of primary PM and to certain extent on secondary PM. In the current study, the dynamics of O3 and PM is studied with a modeling perspective using the Models-3 framework (USEPA, 1999) over the US-Mexico border of the Mexicali- Imperial valley region and Southern California, including Los Angeles and San Diego areas, for pollution events in August 2001, where peak O3 concentrations reached 190 ppbv in the LA basin on August 26, 2001. The study also addresses the air quality impacts of two power plants located three miles south of the US-MX border on the Mexicali-Imperial region. Cross-boundary transport of pollutants and its resulting impacts is also studied. The Mesoscale Meteorological model (MM5) is utilized to simulate the meteorological fields. The BRAVO Emissions Inventory (USEPA, 2001) along with the NEI files (USEPA, 2001) and Mexico NEI 1999: Six Northern States is used for emissions modeling using SMOKE. The Chemical Transport Model of the Community Multiscale Air Quality (CMAQ v4.4) model simulated pollutant concentrations, including PM components. Several sensitivity analyses using the Direct Decoupled Method in CMAQ (Cohan et al., 2005) were conducted, including the impact of area and mobile sources of NOx and VOC on particulate matter and O3,and how SO2 impacts particulate matter levels. Sensitivities were also studied for perturbations in VOC, and NOx concentrations in the Los Angeles basin and Tijuana-San Diego regions. Mobile NOx emissions from Tijuana-San Diego region had impacts of upto 5 ppbv of O3 in the Mexicali area. The impacts of SO2 emissions from the two power plants on PM concentrations are also discussed.